

SL. No	Title	Page No.
IC18ME01	STRESS DISTRIBUTION AROUND HOLES IN PIEZO- LAMINATES BY STROH FORMALISM (Invited Paper)	01
	-- Dr. D.K.Nageswara Rao, M. Ramesh Babu, Dr. K. Raja Narendra Reddy	
IC18ME02	DISTINCT MODELS OF GEARS AND GEAR TRAINS - A REVIEW	11
	-- G. Tharanitharan, Dr. P. Tamilselvam, T. Tharoon	
IC18ME03	APPLICATION OF OPTIMIZATION ALGORITHM FOR COMPOSITE LAMINATE OPTIMIZATION	24
	-- A. Karthikeyan, Dr. A. Karthikeyan, Dr. K. Venkatesh Raja, S. Karth	
IC18ME04	TRAVELING SALESMAN PROBLEM FOR VISITING 10 TAMIL NADU CITIES USING GENETIC ALGORITHM	32
	-- A. Karthikeyan, Dr. A. Karthikeyan, Dr. K. Venkatesh Raja, S. Karth	
IC18ME05	EFFECT OF ALUMINIUM OXIDE NANOPARTICLE AS NANO-ADDITIVE ON THE OPERATING CHARACTERISTICS OF DIESEL ENGINE FUELLED WITH BLENDS OF DIESEL AND WASTE TYRE PYROLYSIS OIL	40
	-- Chinnasamy C, Prakash k, Vetrivel A, Tamilselvam P	
IC18ME06	IMAGE BASED VEHICLE SPEED DETECTING DEVICE TO AVOID ACCIDENTS IN STREET ROADS	48
	-- S. Hemnath, P. Sadasivam, U. Sangameswaran	
IC18ME07	POULTRY FARM MONITORING AND CONTROLLING USING PLC WITH INTERNET OF THINGS	52
	-- Mr. A Vishnu, Sheshagiri N, Joeresh Julius A, Sathish Kumar A, Satharth Noorul Hassan	
IC18ME08	STUDY THE MATERIAL BEHAVIOUR OF AA6063/WC/ZrO MMCs AND INVESTIGATION OF WIRE EDM PARAMETERS.	59
	-- Mr. P. Janagarathinam, V. Suriyanarayanan, S. Suresh	
IC18ME09	AUTONOMOUS SWARM ROBOTS	63
	-- T. Kousalya, Terrin J. Mario Pereria, K. M. Aarsha Suresh, Dilshad Bin Mohammed Iqbal, K. Nivethithaan	

IC18ME10	IMPACT OF CRYOGENIC TREATMENT ON THE FRICTION WELDED ALUMINIUM METAL MATRIX COMPOSITE	68
	-- <i>Sreenivasan KS, Satish Kumar S, Vignesh T, Subbramaniyan MS</i>	
IC18ME11	EFFECTS OF THE FRICTION STIR WELDING PARAMETERS ON THE CORROSION BEHAVIOR OF SIMILAR AND DISSIMILAR WELDED ALUMINIUM ALLOYS 6061-6061, 6082-6082, AND 6082-6061	75
	-- <i>Syed Khaja Naimuddin, Dr K.P. Vidhu</i>	
IC18ME12	IMPROVING THE HEAT TRANSFER RATE OF AC CONDENSER BY OPTIMISING THE MATERIAL	88
	-- <i>Mohd Abdul Raheem, Dr Ananth</i>	
IC18ME13	REDUCTION OF NOX AND PM WITH MULTIPLE INJECTION IN DIESEL ENGINE FUELED WITH COTTON SEED OIL BIODIESEL BLEND	97
	-- <i>Ramesh Babu Nallamothe, Anantha Kamal Nallamothe, Seshu Kishan Nallamothe, I N Niranjan Kumar, BV Appa Rao</i>	
IC18ME14	DESIGN AND OPTIMIZATION OF HIGH-SPEED MOTORIZED SPINDLE	103
	-- <i>A. Sandeep, A. Sravan, Dr. P. John Paul</i>	
IC18ME15	DESIGN AND ANALYSIS OF STEAM GENERATORS	109
	-- <i>M. Shravan Kumar, Mohd Tabraizuddin, Dr. P. Velmurugan,</i>	
IC18ME16	DOMESTIC OIL EXTRACTION MACHINE	115
	-- <i>Anand.M, Manimaran R, Praveen Kumar.M, Sujith Bhrathi.S</i>	
IC18ME18	BASIC DESIGN OF AN ANTHROPHOMORPHIC ROBOTIC ARM	119
	-- <i>Pradeep.S, Hari shankar.S.P, Nandha Kumar.M, Rajeshwaran.T, Karthik.V</i>	
IC18ME18	STUDIES ON RECYCLED ALUMINIUM (AA319) REINFORCED WITH RECYCLED GLASS	132
	-- <i>China Mahammad Bhasha, Naveen Kumar chebrolu, Venkataramana Murthy VP</i>	
IC18ME19	PRODUCTION OF METHYL ESTERS FROM MILK SCUM, PERFORMANCE AND EMISSION ANALYSIS ON CI ENGINE	137
	-- <i>Shashikumar S, Soujanya G, Ramya V</i>	

IC18ME20	PRODUCTION, PURIFICATION AND EVALUATION OF DIFFERENT PLASTIC BIO FUEL BLENDS FROM MUNICIPAL WASTE PLASTICS	143
	-- <i>Naveen Kumar P, Rajesh S, D Krishnaveni</i>	
IC18ME21	EVALUATION OF MECHANICAL PROPERTIES GLASS FIBER REINFORCED HEMATITE FILLED HYBRID COMPOSITES	147
	-- <i>Venkatesh, Rajesh S, P Naveen Kumar</i>	
IC18ME22	GOLDEN STARTUP” – A NEW BUSINESS HUB PROPOSAL	151
	-- <i>Elangovan Muniyandy, Indumathi A R, Nilesh J Sompura</i>	
IC18ME23	EVALUATION OF EVAPOTRANSPIRATION MODELS FOR PADDY CROPS USING METEOROLOGICAL DATA FOR KANCHEEPURAM DISTRICT, TAMILNADU	155
	-- <i>D.Soundar Rajan, P.Suresh, M.M.Vijayalakshmi</i>	
IC18ME24	ONBOARD DRIVER MONITORING SYSTEM WITH SAFETY ENHANCED BRAKE SYSTEM	164
	-- <i>Dineshkumar C, Subramanian M, Dinesh B</i>	
IC18ME25	OPERATING COST ANALYSIS OF MICROGRID INCLUDING RENEWABLE ENERGY SOURCES AND A BATTERY UNDER DYNAMIC PRICING	170
	-- <i>Hephzibah Jose Queen, J.Jayakumar, Narciss Starbell</i>	
IC18ME26	EVALUATION OF INFLUENCE OF THE PRINCIPLES INVOLVED IN CARBON FOOTPRINT IN THE PETROLEUM INDUSTRY USING TISM	176
	-- <i>S.P.Prasanna, S.Bathrinath, K.Rahul, S.Saravanasankar</i>	
IC18ME27	EFFECTS OF ROUGHNESS PARAMETERS ON INCLINED SPHERICAL BALL ROUGHENED SOLAR AIR HEATER	184
	-- <i>Ramesh Murmu, Dr. P. Kumar, Prof. H.N. Singh</i>	
IC18ME28	OPTIMIZATION OF RC ONE WAY SLAB USING GENETIC ALGORITHMS	195
	-- <i>Shaik Bepari Fayaz Basha, S.Mahaboob Basha, Y.Dasthagir</i>	
IC18ME29	WEAR BEHAVIOUR OF ALUMINIUM MATRIX COMPOSITES	199
	-- <i>Vijayakumar.K</i>	

IC18ME30	THERMAL ANALYSIS OF VARIOUS FRICTION SURFACING MATERIALS USING ANSYS	203
	-- <i>Sivanesh A R,Aravind Kumar R,Arivazhakan.D</i>	
IC18ME31	EFFECT OF IMMERSION DEPTH OF A SWIRLING FLOW TUNDISH SEN ON MULTIPHASE FLOW AND HEAT TRANSFER IN MOLD	207
	<i>Siddappa Nyamagoud, J Sudha pallavi,M Veerareddy</i>	
IC18ME32	VIBRATION ANALYSIS OF TWO WHEELER SUSPENSION SYSTEM UNDER VARIOUS LOADING CONDITIONS (AN ANALYTICAL APPROACH)	212
	-- <i>Mr. Vinodkumar Reddy.B, Mr J.Chandra sekhar, Mr. K.Venkat Siva</i>	
IC18ME33	THERMAL ANALYSIS OF DISC BRAKE TO MINIMIZING THE TEMPERATURE BY USING ANSYS	218
	-- <i>Praksh .D.Chavan Mahadev.Godamagave Abhishek kulkarni</i>	
IC18ME34	DESIGN AND EXPERIMENTAL STUDY ON SOLAR DISH COLLECTOR FOR STIRLING ENGINE	223
	-- <i>B. Simran, Dr.Vikash Kumar</i>	
IC18ME35	NATURAL CONVECTIVE HEAT TRANSFER FROM INCLINED NARROW PLATES	230
	-- <i>R.Swapna,Mr.V.Ravinder</i>	
IC18ME36	MODELING AND MANUFACTURING OF A CENTRIFUGAL BLOWER	238
	-- <i>Velpula.Srinu, N.Kishorekumar, K.Veerawamy</i>	
IC18ME37	DESIGN OF ABSORPTION REFRIGERATION SYSTEM DRIVEN BY ENGINE EXHAUST GAS FOR VEHICLES	245
	-- <i>P.Pavan Kumar,Dr. Ananth</i>	
IC18ME38	HEAT TRANSFER ENHANCEMENT	253
	-- <i>Md Nizam Raza,Vikas Kumar</i>	

IC18ME39	ANALYTICAL INVESTIGATION OF HEAT TRANSFER ENHANCEMENT IN A MICRO TUBE USING NANO FLUIDS	258
	-- <i>Sanketh m,Dr.Vikash Kumar</i>	
IC18ME40	HEAT TRANSFER ALONG VERTICAL CHIMNEY	264
	-- <i>K. Rajanikanth, D.r. T.V.Reddy.</i>	
IC18ME41	PERFORMANCE ANALYSIS OF BOILER IN POWER PLANT	271
	-- <i>P.Papi reddy Dr. Ananth</i>	
IC18ME42	IMPROVEMENT OF AN AUTOMOBILE RADIATOR USING THERMAL ANALYSIS	281
	-- <i>S.Vinay,Dr.Karthikeyan</i>	
IC18ME43	DESIGN AND CFD ANALYSIS OF HAIR PIN HEAT EXCHANGER AT DIFF NANO FLUIDS	285
	-- <i>M.Renuka Dr. Velmurugan</i>	
IC18ME44	ANALYSIS OF HEAT TRANSFER RATE BY VARYING COOLING FLUID FOR ENGINE CYLINDER FINS	293
	-- <i>Mr.Ranjith Aavula Mr.Vikash kumar</i>	
IC18ME45	DESIGN AND ANALYSIS OF HEAVY VEHICLE CHASSIS FOR DIFFERENT ALLOY MATERIALS	304
	-- <i>Md Akhil,Mohd Imran,A. Karthikeyan</i>	
IC18ME46	DESIGN AND ANALYSIS OF PRESSURE VESSEL WITH FRP MATERIAL	310
	-- <i>Sukruthi Priya, Ravi Chandra, V. Ravinder</i>	
IC18ME47	EVALUATION OF OVERALL HEAT TRANSFER COEFFICIENT FOR A COMPOSITE 3D PANEL USING FEM	313
	-- <i>D Shekhar, B. Sadanand,Dr. P. Velmurugan</i>	
IC18ME48	EFFECT OF WELDING SPEED AND GROOVE ANGLE ON STRENGTH OF BUTT WELD JOINT USING TIG WELDING	317
	-- <i>B. Dileep Kumar,Mr. Vikash Kumar,Dr. S. Ananth</i>	

IC18ME49	EXPERIMENTAL INVESTIGATION OF TUBE CONFIGURATION IN HORIZONTAL SURFACE CONDENSER	321
	<i>--Mr.N.Ragavan, Ms.L.priyanka, Mrs.B.Sai Deepika</i>	
IC18ME50	EFFECT OF GEOMETRIC AND ROUGHNESS PARAMETERS ON ARTIFICIALLY ROUGHENED SOLAR AIR HEATER	328
	<i>--Md. Ahmad Kamal Hassan, Dr.M.Muzaffarul Hasan</i>	
IC18ME51	ANALYSIS OF SINGLE STRAP HYBRID BUTT JOINT IN LAMINATED FRP COMPOSITES	340
	<i>--Mrs.I.Prasanna, Ms.A.HAppay, Mrs.K.Sandhya</i>	
IC18ME52	EFFECT OF BIODIESEL BLENDS AND NANO-PARTICLES ON ENGINE PERFORMANCE	347
	<i>--Md.Ashfaque Alam, Dr.A.K.Prasad</i>	
IC18ME53	COST AND TIME EFFECTIVENESS THROUGH SIX SIGMA'S ECRS TECHNIQUE – EXPERIMENTAL STUDY AT AN AUTOMOBILE ASSEMBLY PLANT	354
	<i>--Mr.R.Saravanan, Mr.T.Malyadri, Mr.Nagasrisaihari Sunkara, Mr.M.S.Srinivasa Rao</i>	
IC18ME54	STUDY ON SCOPE OF EMERGING TREND OF ORGAN PRINTING BY USING 3D PRINTING TECHNOLOGY	360
	<i>--Mr.K.Prakash, Mr.A.Vetrivel, Mr.L.Shri Hari, Mr.M.Sakthivel</i>	

# Stress Distribution around Holes in Piezo-Laminates by Stroh Formalism

Dr. D.K.Nageswara Rao  
Faculty of Mech. & Industrial Engg.  
Bahir Dar Institute of Technology  
Bahir Dar University  
BahirDar, Ethiopia.  
dr.dknrao@gmail.com

M. Ramesh Babu  
Dept. of Mech. Engg.  
Vaagdevi Engineering College  
Warangal, India  
rameshbabu060570@gmail.com

Dr. K. Raja Narender Reddy  
Dept. of Mech. Engg.  
Kakatiya Institute of Tech.& Sci.  
Warangal, India  
krajanr@rediffmail.com

**Abstract**—The general solution presented in this paper is based on the extended Stroh formalism by Hwu to address the problems of stress concentration in laminated plates embedded with piezo-electric layers with holes subjected to remotely applied coupled electromechanical loading. This surpasses the limitations of the existing solutions by virtue of generalities, such as generalized mapping function and arbitrary biaxial loading. The range includes variety of materials-anisotropic and isotropic; loading-inplane, bending, coupled mechanical and electromechanical loading; and shapes of holes from circular, polygonal and variety of irregular shapes. Thus the general solutions derived have come out as one-stop solutions for stresses, moments and electrical displacements around holes in piezo-electric or polymer composite laminates or isotropic plates. These solutions are also validated by Finite Element Method using ANSYS software and a good concurrence of the results has been noted for these two approaches. Results are presented for certain cases of inplane loading of piezolaminate.

**Keywords**—*Stress Concentrations, Stroh formalism, piezo-electric laminates, coupled electromechanical loading.*

## I. INTRODUCTION

Piezo-composites are essentially used as intelligent structures for control and actuation applications as well as for health monitoring of structures. Piezoelectric materials are most widely used in these structures because of their fast electromechanical response and low power requirements and ease of manufacturing. They have the ability to convert electrical energy into mechanical energy. The generated surface charge density is linearly proportional to the applied stress and this is called the piezoelectric effect. Piezo-composites comprise layers of piezoelectric ceramics and polymers. Stress concentration due to holes in laminated structures is unavoidable where holes are to be made deliberately for various functional reasons. Further, the structures when used in high technology applications may be subjected to various kinds of coupled loads. In order to assess the structural integrity and residual strength of such structures, it is essential to determine the stresses and related parameters around the hole for safety reasons.

Majority of the solutions have been produced using Lekhnitskii's [1] approach and very few solutions have adopted Savin's [2] method. These approaches do not address the inplane-bending coupled loading whereas, Becker's [3, 4] complex potential method has addressed

such problems. The stress concentration problems in piezoelectric plates containing either circular or elliptical holes or inclusions or arbitrary shaped holes with cusps and cracks by applying complex potential method [5-9]. Green's functions[10,11] have been applied to study the coupled elastic and electric fields in piezoelectric solids with arbitrary shaped defects like, cavities, inclusions, cracks, etc. under mechanical and electric loads. The simplicity of Stroh formalism lies in the fact that the eigen values and eigen vectors that are characteristic of the material considered are represented in terms of certain fundamental matrices. These matrices address the kind of material, type of laminate, etc. The solution by Stroh formalism has been more elegant due to the representation of the data in matrix form. Chung and Ting [12] have studied the two-dimensional problem of an elliptic hole in an anisotropic piezoelectric plate using Stroh formalism. However, the electromechanical coupling has been effectively addressed by the extended Stroh formalism given by Hwu and Hsieh [13]. They have applied this for directly solving many problems of electro-elastic composite laminates. The present solution has further enhanced the scope of Hwu's extended Stroh formalism [14] by incorporating into it the generalized mapping function and an arbitrary biaxial loading condition so that it can address the case of any shape of hole with given mapping function and several kinds of inplane and bending loads. Now, the solution derived is the most universal in terms of materials, holes, and loading. It can address isotropic, anisotropic including the piezoelectric plates, all shapes of holes and all kinds of inplane, bending, coupled loads, mechanical and electrical. Some of the results obtained for inplane loading on piezo-laminates are presented in this paper.

## II. PROBLEM STATEMENT

A centrally located arbitrary shaped cutout is considered in an infinite symmetric piezoelectric laminate. The boundary of the cut-out is free from loading and the laminate is subjected to remotely acting biaxial mechanical stresses and electrical displacements in an open circuit condition. It is required to determine the stresses and electrical displacements around the cutout.

### III. PROBLEM FORMULATION

A symmetric piezo-composite laminate with a hole defined by the mapping function (1) is considered under generalized plane stress condition acted up on by remote mechanical stresses  $\sigma_1^\infty, \sigma_2^\infty$  and electrical displacements  $D_1^\infty, D_2^\infty$  in open circuit condition about respective arbitrarily oriented axes  $x_1', x_2'$  as given by (3).

#### A. Generalized Mapping Function

The complex coordinate  $z_k$  in  $\zeta$ -plane becomes

$$z_k = \omega(\zeta) = x_1 + \mu_k x_2 \quad (k = 1, 2, 3, 4, 5, 6, 7, 8)$$

$$x_1 = \frac{R}{2} \left[ \left( \zeta + \frac{1}{\zeta} \right) + \sum_{j=1}^N m_j \left( \zeta^j + \frac{1}{\zeta^j} \right) \right]$$

$$x_2 = \frac{-iR}{2} \left[ \left( \zeta - \frac{1}{\zeta} \right) - \sum_{j=1}^N m_j \left( \zeta^j - \frac{1}{\zeta^j} \right) \right] \quad (1)$$

#### B. Remote Loading Boundary Conditions

The boundary conditions along  $x_1, x_2$  axes are given by

$$\sigma_{11}^\infty = \frac{\sigma}{2} [(\lambda+1) + (\lambda-1)\cos 2\beta]$$

$$\sigma_{22}^\infty = \frac{\sigma}{2} [(\lambda+1) - (\lambda-1)\cos 2\beta]$$

$$\sigma_{12}^\infty = \frac{\sigma}{2} [(\lambda-1)\sin 2\beta] \quad (2)$$

The following values of  $\beta$  and  $\lambda$  are taken for different cases of loading.

Tension along  $x_1$ -axis:  $\lambda = 0, \beta = \pi/2$

Tension along  $x_2$ -axis:  $\lambda = 0, \beta = 0$

Inclined uni-axial loading:  $\lambda = 0, \beta \neq 0$

Biaxial loading-arbitrary:  $\lambda = 1, \beta \neq 0$

Equi-biaxial loading:  $\lambda = 1, \beta = 0$

Shear loading:  $\lambda = -1, \beta = \pi/2$  or  $3\pi/4$

Electrical displacement along  $x_1$ -axis:  $\lambda = 0, \beta = \pi/2$

Electrical displacement along  $x_2$ -axis:  $\lambda = 0, \beta = 0$

Load vectors for mechanical loading (2) and electrical displacements are:

$$\mathbf{t}_1^\infty = \begin{bmatrix} \sigma_{11}^\infty & \sigma_{12}^\infty & 0 & D_1^\infty \end{bmatrix}^T$$

$$\mathbf{t}_2^\infty = \begin{bmatrix} \sigma_{12}^\infty & \sigma_{22}^\infty & 0 & D_2^\infty \end{bmatrix}^T \quad (3)$$

The coupled constitutive relations (4) for the electro-elastic problem are expressed in terms of stresses  $\sigma_{ij}$ ,

strains  $\varepsilon_{kl}$ , electric displacements  $D_j$ , electric field  $E_k$ , the elastic stiffness tensor [15] at constant electric field  $C_{ijkl}^E$ , piezoelectric stress tensor  $e_{kij}$  and dielectric permittivity tensor at constant strain  $\omega_{jk}^s$  as

$$\begin{cases} \sigma_{ij} = C_{ijkl}^E \varepsilon_{kl} - e_{kij} E_k \\ D_j = e_{jkl} \varepsilon_{kl} + \omega_{jk}^s E_k, \end{cases} \quad i, j, k, l = 1, 2, 3 \quad (4)$$

The equilibrium equations are given by

$$\sigma_{ij,j} = 0 \quad D_{i,i} = 0 \quad (5)$$

A generalized displacement function  $u_k$  as given in (6) is considered to satisfy all the basic equations in (4) and (5).

$$u_k = a_k f_k(z_k) \quad (6)$$

where,  $f_k(z_k)$ ,  $k = 1, 2, 3, 4, 5, 6, 7, 8$  are eight arbitrary analytical functions in terms of complex variable  $z_k = x_1 + \mu_k x_2$ . The eigenvalues are determined from the roots of the eigenrelation. The functions  $f_k(z_k)$  in (6) will be determined by applying the boundary conditions and eigenvalues and eigenvectors. Considering the eight eigenvalues  $\mu_k$  and their corresponding eigenvectors  $\mathbf{a}_k, \mathbf{b}_k$ , the generalized displacement function  $u_k$  in (6) is represented in vector form as (7).

$$\mathbf{u} = \sum_{k=1}^8 \mathbf{a}_k f_k(z_k) = \sum_{k=1}^4 [\mathbf{a}_k f_k(z_k) + \bar{\mathbf{a}}_k f_{k+4}(\bar{z}_k)] \quad (7)$$

Similarly, the corresponding generalized stress function is represented as

$$\Phi = \sum_{k=1}^8 \mathbf{b}_k f_k(z_k) = \sum_{k=1}^4 [\mathbf{b}_k f_k(z_k) + \bar{\mathbf{b}}_k f_{k+4}(\bar{z}_k)] \quad (8)$$

Representing each analytical function  $f_k(z_k)$  as a product of a constant  $q_k$  and  $f(z_k)$  and similarly applying the same simplification for the corresponding conjugate functions also, we have

$$f_k(z_k) = q_k f(z_k) \quad f_{k+4}(\bar{z}_k) = \bar{q}_k \bar{f}(\bar{z}_k) \quad (9)$$

Introducing (9) into the generalized displacements (7) and generalized stress functions (8), we have

$$\mathbf{u} = 2 \operatorname{Re} [\mathbf{A} \langle f(z_k) \rangle \mathbf{q}]$$

$$\Phi = 2 \operatorname{Re} [\mathbf{B} \langle f(z_k) \rangle \mathbf{q}] \quad (10)$$

$\operatorname{Re}$  stands for the real part of the complex number,  $\mathbf{q}$  is complex constant vector,  $\mathbf{A}$  and  $\mathbf{B}$  are material eigenvector

matrices of size 4x4. The components of **A**, **B** and **q** are given by

$$\mathbf{A} = [\mathbf{a}_1 \quad \mathbf{a}_2 \quad \mathbf{a}_3 \quad \mathbf{a}_4] \tag{11}$$

where, the components of displacement vector **u**, stress function vector **Φ** and analytical functions  $f(z_k)$  are given by

$$\mathbf{u} = \begin{Bmatrix} u_1 \\ u_2 \\ u_3 \\ u_4 \end{Bmatrix} \quad \Phi = \begin{Bmatrix} \phi_1 \\ \phi_2 \\ \phi_3 \\ \phi_4 \end{Bmatrix}$$

$$\langle f(z_k) \rangle = \text{diag} [f(z_1) \quad f(z_2) \quad f(z_3) \quad f(z_4)] \tag{12}$$

The eigenvectors **a<sub>k</sub>** and **b<sub>k</sub>** of fundamental elasticity matrix are non-singular and satisfy the orthogonality relation as

$$\begin{bmatrix} \mathbf{A} & \overline{\mathbf{A}} \\ \mathbf{B} & \overline{\mathbf{B}} \end{bmatrix} \begin{bmatrix} \mathbf{B}^T & \mathbf{A}^T \\ \overline{\mathbf{B}}^T & \overline{\mathbf{A}}^T \end{bmatrix} = \begin{bmatrix} \mathbf{I} & \mathbf{0} \\ \mathbf{0} & \mathbf{I} \end{bmatrix} \tag{13}$$

The eigenrelation formulated about  $x_1, x_2$  axes is taken about the rotated axes as

$$\mathbf{N}(\theta)\xi = \mu(\theta)\xi \tag{14}$$

where,

$$\mathbf{N}(\theta) = \begin{bmatrix} \mathbf{N}_1(\theta) & \mathbf{N}_2(\theta) \\ \mathbf{N}_3(\theta) & \mathbf{N}_4^T(\theta) \end{bmatrix}$$

$$\mathbf{N}_1(\theta) = -\mathbf{T}^{-1}(\theta)\mathbf{R}^T(\theta), \quad \mathbf{N}_2(\theta) = \mathbf{T}^{-1}(\theta) = \mathbf{N}_2(\theta) \tag{15}$$

where, **Q**(θ), **R**(θ) and **T**(θ) are transformed 4x4 material real matrices given in terms of **Q**, **R** and **T** as,

$$\mathbf{Q}(\theta) = \mathbf{Q} \cos^2 \theta + (\mathbf{R} + \mathbf{R}^T) \sin \theta \cos \theta + \mathbf{T} \sin^2 \theta$$

$$\mathbf{R}(\theta) = \mathbf{R} \cos^2 \theta + (\mathbf{T} - \mathbf{Q}) \sin \theta \cos \theta - \mathbf{R}^T \sin^2 \theta$$

$$\mathbf{T}(\theta) = \mathbf{T} \cos^2 \theta - (\mathbf{R} + \mathbf{R}^T) \sin \theta \cos \theta + \mathbf{Q} \sin^2 \theta \tag{16}$$

For distinct eigenvalues  $\mu_k(\theta)$  given by the corresponding column eigenvectors **a<sub>k</sub>**, **b<sub>k</sub>** are independent of each other.

$$\text{Im } \mu_k(\theta) > 0, \quad \mu_{k+3}(\theta) = \overline{\mu_k(\theta)} \tag{17}$$

$$\mathbf{a}_{k+3} = \overline{\mathbf{a}_k} \quad \mathbf{b}_{k+3} = \overline{\mathbf{b}_k} \tag{18}$$

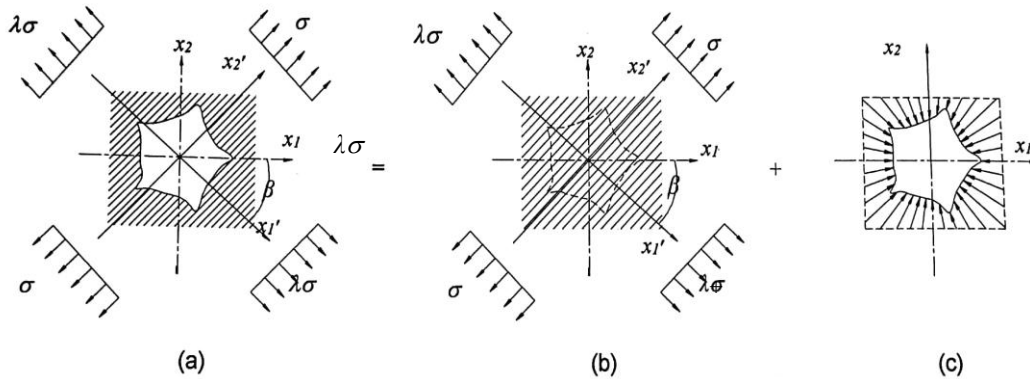


**Fig. 1** Scheme of solution (a) plate with hole, loading at infinity (b) uniform plate with loading at infinity (c) plate with no external loading and with negative loading on the edge of the hole.

#### IV.METHOD OF SOLUTION

The method of solution for the problem is illustrated in Fig.1. The solution is obtained by superposition of stress functions determined in two stages. In the first stage, the stress function has been obtained for the plate without hole due to remotely applied load by mechanical stresses and electrical displacements about the arbitrary axes  $x'_1, x'_2$ . In this stage, remotely applied load will develop the stress and electrical displacements that are same everywhere in the

plate as those applied at infinity. This stage of solution is called uniform stress field condition. A fictitious hole is assumed in this stage and the boundary conditions around the hole are obtained by satisfying the uniform stress field conditions. For the second stage solution, the plate with hole is applied by negative of boundary conditions those obtained from first stage on its hole boundary with absence of remote loading as shown in Fig. 1(b). The stress functions in this stage are considered with arbitrary analytical functions followed by certain unknown constants. These arbitrary analytical functions and unknown constants of the stress

functions are obtained by satisfying the boundary conditions in the second stage. The final stress function is obtained by superimposing the stress functions in the first and second stages that corresponds to the plate with a traction free hole and remote loading as shown in Fig. 1(a).

It is required to determine the constants in the final stress function for a traction free hole and remote mechanical and electrical loading. By taking the derivative of the final stress function with respect to tangential direction and equating it to zero, we will be able to determine the unknown constants existing in the stress function.

#### A. First Stage Solution

In the first stage of the solution, Fig.1 (b) shows the laminate with fictitious hole is considered and subjected to remotely applied mechanical and electrical loading about the arbitrary axes  $x'_1, x'_2$  and this produces the uniform state of stress. The stress functions around the fictitious hole which satisfy the uniform state stress condition due to loading at infinity are determined as given below.

$$\frac{d\phi_i}{ds} = \frac{\partial\phi_i}{\partial x_1} \frac{dx_1}{ds} + \frac{\partial\phi_i}{\partial x_2} \frac{dx_2}{ds} \quad (19)$$

The differentiation of stress function along the arc length  $s$  is called surface traction on the arc. It is given by

$$t_i = \frac{d\phi_i}{ds} \quad (20)$$

From (19) and (20) we obtain

$$t_i = \frac{d\phi_i}{ds} = \frac{\partial\phi_i}{\partial x_1} \frac{dx_1}{ds} + \frac{\partial\phi_i}{\partial x_2} \frac{dx_2}{ds} \quad (21)$$

$$t_i ds = d\phi_i = \phi_{i,1} dx_1 + \phi_{i,2} dx_2 \quad (22)$$

Substitute for  $\sigma_{i1} = -\phi_{i,2}$ ,  $\sigma_{i2} = \phi_{i,1}$  into (22), we get stress function as

$$d\phi_i = \sigma_{i2} dx_1 - \sigma_{i1} dx_2 \quad (23)$$

Integrating (23) along the arc we obtain stress function as

$$\begin{aligned} \phi_i &= \int d\phi_i = \int (\sigma_{i2} dx_1 - \sigma_{i1} dx_2) = \sigma_{i2} \int dx_1 - \sigma_{i1} \int dx_2 \\ \phi_i &= \sigma_{i2} x_1 - \sigma_{i1} x_2 \end{aligned} \quad (24)$$

Take  $i = 1, 2, 3$

$$\begin{aligned} \phi_1 &= \sigma_{12} x_1 - \sigma_{11} x_2 & \phi_2 &= \sigma_{22} x_1 - \sigma_{21} x_2 \\ \phi_3 &= \sigma_{32} x_1 - \sigma_{31} x_2 & \phi_4 &= \sigma_{42} x_1 - \sigma_{41} x_2 \end{aligned} \quad (25)$$

Take  $\sigma_{41} = D_1$  and  $\sigma_{42} = D_2$  into above equations and introducing (3) into (25), we obtain the stress function in vector form as

$$\Phi^I = (x_1 \mathbf{t}_2^\infty - x_2 \mathbf{t}_1^\infty) \quad (26)$$

where,

$$\begin{aligned} \Phi &= (\phi_1 \quad \phi_2 \quad \phi_3 \quad \phi_4)^T, \\ \mathbf{t}_1^\infty &= (\sigma_{11} \quad \sigma_{21} \quad \sigma_{31} \quad D_1)^T \text{ and} \\ \mathbf{t}_2^\infty &= (\sigma_{12} \quad \sigma_{22} \quad \sigma_{32} \quad D_2)^T \end{aligned} \quad (27)$$

Substituting for  $x_1$  and  $x_2$  from (1) into (26), we obtain the stress function around the fictitious hole

$$\Phi^I = \begin{bmatrix} R \left( \cos \psi + \sum_{j=1}^N m_j \cos j\psi \right) \mathbf{t}_2 \\ -R \left( \sin \psi - \sum_{j=1}^N m_j \sin j\psi \right) \mathbf{t}_1 \end{bmatrix} \quad (28)$$

From (28), we get

$$\begin{aligned} \Phi^I &= \begin{bmatrix} R \left( \sum_{j=1}^N m_j (\mathbf{t}_1 \sin j\psi + \mathbf{t}_2 \cos j\psi) \right) \\ -R (\mathbf{t}_1 \sin \psi - \mathbf{t}_2 \cos \psi) \end{bmatrix} \\ \Phi^I &= \text{Re} \left[ R (\mathbf{t}_2 - i\mathbf{t}_1) \left( \frac{1}{\zeta} \right) + \sum_{j=1}^N m_j R (\mathbf{t}_2 + i\mathbf{t}_1) \left( \frac{1}{\zeta^j} \right) \right] \end{aligned} \quad (29)$$

#### B. Second Stage Solution

In the second stage, the plate is considered with hole as shown in Fig. 1(c) and negative loading is applied on the surface of the hole with absence of loading at infinity. The stress function in this stage is considered in the following form with some arbitrary unknown constants  $\mathbf{q}, \mathbf{q}_j$

$$\Phi^{II} = 2 \text{Re} \mathbf{B} \langle f(z_k) \rangle \mathbf{q} + 2 \text{Re} \mathbf{B} \sum_{j=1}^N \langle f(z_k) \rangle \mathbf{q}_j \quad (30)$$

The first term in the above (30) represents the stress function relate to the circle hole boundary and the circle can be degenerated into various shapes of hole by introducing number of terms into the stress function. The stress functions for holes other circle will be represented by second term of above stress function. Finally the stress function for general shape of hole will be represented by (30). The unknown arbitrary constants  $\mathbf{q}, \mathbf{q}_j$  associated with the complex function are determined satisfying the traction free boundary condition.

For traction free boundary condition the tangential stress around hole exist and remaining normal and shear stress vanish. The unknown constants  $\mathbf{q}, \mathbf{q}_j$  in the stress function are obtained by equating the essential boundary conditions at hole with absence of remote loading from

second stage to negation loading condition which obtained from stage I.

$$\Phi'' = -\Phi' \quad (31)$$

Substituting for  $\Phi''$  from (30) into (31), we get

$$2\text{Re}\mathbf{B}\langle f(z_k) \rangle \mathbf{q} + 2\text{Re}\mathbf{B}\sum_{j=1}^N \langle f(z_k) \rangle \mathbf{q}_j = -\Phi' \quad (32)$$

To apply the boundary conditions of the given problem, it is not to possible in  $z$ -plane. It is easy to solve by transforming the region in  $z$ -plane to  $\zeta$ -plane using conformal mapping function. The physical region of the plate exterior to the hole is being transformed to the parametric plane  $\zeta$ -plane using the mapping function given by  $z_k = \omega(\zeta) = x_1 + \mu_k x_2$  in (1). After transforming region outside the hole in  $z$ -plane to  $\zeta$ -plane, the stress function  $\Phi$  in the  $\zeta$ -plane is given as

$$2\text{Re}\left\{ \mathbf{B}\langle f(\zeta_k) \rangle \mathbf{q} + \mathbf{B}\sum_{j=1}^N \langle f(\zeta_k) \rangle \mathbf{q}_j \right\} = -\Phi' \quad (33)$$

Substituting the stress function  $\Phi'$  from (29) into (33), we get

$$\begin{aligned} & 2\text{Re}\left\{ \mathbf{B}\langle f(\zeta_k) \rangle \mathbf{q} + \mathbf{B}\sum_{j=1}^N \langle f(\zeta_k) \rangle \mathbf{q}_j \right\} \\ & = -\text{Re}\left[ R(\mathbf{t}_2 - i\mathbf{t}_1) \left( \frac{1}{\zeta} \right) + \sum_{j=1}^N m_j R(\mathbf{t}_2 + i\mathbf{t}_1) \left( \frac{1}{\zeta^j} \right) \right] \\ & 2\text{Re}\left\{ \left[ \left[ \frac{R(\mathbf{t}_2 - i\mathbf{t}_1)}{2} \left( \frac{1}{\zeta} \right) + \mathbf{B}\langle f(\zeta_k) \rangle \mathbf{q} \right] \right] \right. \\ & \left. + \left[ \left[ \sum_{j=1}^N \frac{m_j R(\mathbf{t}_2 + i\mathbf{t}_1)}{2} \left( \frac{1}{\zeta^j} \right) + \mathbf{B}\sum_{j=1}^N \langle f(\zeta_k) \rangle \mathbf{q}_j \right] \right] \right\} = 0 \quad (34) \end{aligned}$$

As we know that  $\zeta$  becomes infinity i.e.,  $\zeta \rightarrow \infty$  when  $z \rightarrow \infty$  and the function  $f(\zeta)$  with negative powers of  $\zeta$  will make the stress function  $\Phi''$  equal to zero. After substituting  $\mathbf{f}(\zeta)$ ,  $\mathbf{f}_j(\zeta)$  are equal to  $\zeta^{-1}$  and  $\zeta^{-j}$ , where  $j=1$  to  $N$  into (34), we get

$$2\text{Re}\left\{ \left[ \left[ \frac{R(\mathbf{t}_2 - i\mathbf{t}_1)}{2} \left( \frac{1}{\zeta} \right) + \mathbf{B}\left\langle \frac{1}{\zeta} \right\rangle \mathbf{q} \right] \right] \right. \\ \left. + \left[ \left[ \sum_{j=1}^N \frac{m_j R(\mathbf{t}_2 + i\mathbf{t}_1)}{2} \left( \frac{1}{\zeta^j} \right) + \mathbf{B}\sum_{j=1}^N \left\langle \frac{1}{\zeta^j} \right\rangle \mathbf{q}_j \right] \right] \right\} = 0$$

$$2\text{Re}\left\{ \left[ \left[ \frac{R(\mathbf{t}_2 - i\mathbf{t}_1)}{2} + \mathbf{B}\mathbf{q} \right] \left( \frac{1}{\zeta} \right) \right] \right. \\ \left. + \left[ \left[ \frac{m_j R(\mathbf{t}_2 + i\mathbf{t}_1)}{2} + \mathbf{B}\mathbf{q}_j \right] \sum_{j=1}^N \left( \frac{1}{\zeta^j} \right) \right] \right\} = 0 \quad (35)$$

By simplifying (35) we get constants  $\mathbf{q}, \mathbf{q}_j$  as

$$\begin{aligned} \mathbf{q} & = -R \frac{\mathbf{B}^{-1}(\mathbf{t}_2 - i\mathbf{t}_1)}{2} \\ \mathbf{q}_j & = -R \frac{m_j \mathbf{B}^{-1}(\mathbf{t}_2 + i\mathbf{t}_1)}{2} \end{aligned} \quad (36)$$

After substituting the arbitrary constants  $\mathbf{q}, \mathbf{q}_j$  from (36) into (30) we may get stress function  $\Phi''$  as

$$\Phi'' = -2\text{Re}\left\{ \mathbf{B}\langle f(\zeta_k) \rangle \mathbf{B}^{-1} \frac{R(\mathbf{t}_2 - i\mathbf{t}_1)}{2} \right. \\ \left. + \sum_{j=1}^N \mathbf{B}\langle f(\zeta_k) \rangle \mathbf{B}^{-1} R \frac{m_j(\mathbf{t}_2 + i\mathbf{t}_1)}{2} \right\} \quad (37)$$

### C. Final Solution

The stress function for the given plate with a traction free hole boundary condition with loading at infinity is obtained by superposing the stress functions (20) and (37) from stage I and stage II solutions is given by

$$\Phi = \Phi' + \Phi'' \quad (38)$$

Substituting equation for  $\Phi'$  and  $\Phi''$  from (26) and (37) into (38), we get the stress function as

$$\begin{aligned} \Phi & = (x_1 \mathbf{t}_2 - x_2 \mathbf{t}_1) \\ & - 2\text{Re}\left\{ \mathbf{B}\langle f(\zeta_k) \rangle \mathbf{B}^{-1} \frac{R(\mathbf{t}_2 - i\mathbf{t}_1)}{2} \right. \\ & \left. + \sum_{j=1}^N \mathbf{B}\langle f(\zeta_k) \rangle \mathbf{B}^{-1} R \frac{m_j(\mathbf{t}_2 + i\mathbf{t}_1)}{2} \right\} \end{aligned} \quad (39)$$

### D. Boundary conditions

In this solution, the plate is considered with an arbitrary shaped hole and the size of the hole is very small as compared with plate dimensions. In order to evaluate the stresses around hole the plate is assumed to subject the loads at infinity and there in no stress along edge of hole. To satisfy the boundary conditions at infinity and the traction free condition for the hole, we have the conditions as

$$\begin{aligned} \Phi & \rightarrow \Phi' \text{ at infinity} \\ \mathbf{t}_n & = \Phi_{,s} = 0 \text{ along the hole boundary} \end{aligned} \quad (40)$$

To satisfy the first boundary condition in (40) i.e.,  $\Phi \rightarrow \Phi'$ , the stress function  $\Phi''$  in the final solution should become

zero at infinity. In order to make the stress function  $\Phi''$  equal to zero, the function  $f(\zeta)$  in (39) is considered as polynomial with negative powers.

After introducing the constants  $\mathbf{q}, \mathbf{q}_j$ , we get the stress function as

$$\begin{aligned} \Phi = & x_1 t_2^\infty - x_2 t_1^\infty - 2 \operatorname{Re} \left\{ \mathbf{B} \langle \zeta^{-1} \rangle \mathbf{B}^{-1} R \left( \frac{t_2^\infty - i t_1^\infty}{2} \right) \right\} \\ & - 2 \operatorname{Re} \left[ \sum_{j=1}^N m_j \mathbf{B} \langle \zeta^{-j} \rangle \mathbf{B}^{-1} R \left( \frac{t_2^\infty + i t_1^\infty}{2} \right) \right] \end{aligned} \quad (41)$$

### E. Stresses and Electrical Displacements around the Hole

The stresses and electrical displacements around the hole boundary in piezo-composites are obtained by taking the derivative of stress function  $\Phi$  with respect to the normal directions. The derivative of the stress function (41) with respect to the normal direction  $\mathbf{n}$  is written as

$$\Phi_{,n} = \left\{ \begin{array}{l} \left( \frac{dx_2}{dn} t_1^\infty - \frac{dx_1}{dn} t_2^\infty \right) \\ -2 \operatorname{Re} \left[ \mathbf{B} \langle f(\zeta_k)_{,n} \rangle \mathbf{q} + \mathbf{B} \sum_{j=1}^N \langle f(\zeta_k)_{,n} \rangle \mathbf{q}_j \right] \end{array} \right\} \quad (42)$$

Upon introducing the constants  $\mathbf{q}, \mathbf{q}_j$  from (36) into (42), we get

$$\begin{aligned} \Phi_{,n} = & -t_2^\infty \sin \theta - t_1^\infty \cos \theta + \\ & \frac{1}{\rho} \operatorname{Re} \left[ \{ \mathbf{G}_3(\theta) + i \mathbf{G}_1(\theta) \} (t_2^\infty - i t_1^\infty) \frac{1}{\zeta} \right] \\ & + \frac{1}{\rho} \operatorname{Re} \left[ \{ \mathbf{G}_3(\theta) + i \mathbf{G}_1(\theta) \} (t_2^\infty + i t_1^\infty) \sum_{j=1}^N j \frac{m_j}{\zeta^j} \right] \end{aligned} \quad (43)$$

The following identities are used in (42) to convert the complex numbers into real numbers.

$$\begin{aligned} \mathbf{B} \langle \mu_j(\theta) \rangle \mathbf{B}^{-1} &= \mathbf{G}_1(\theta) + i \mathbf{G}_3(\theta) \\ \mathbf{G}_1(\theta) &= (\mathbf{N}_1^T(\theta) - \mathbf{N}_3(\theta) \mathbf{S} \mathbf{L}^{-1}) \text{ and} \\ \mathbf{G}_3(\theta) &= \mathbf{N}_3(\theta) \mathbf{L}^{-1} \\ \mathbf{S} &= i(2\mathbf{A} \mathbf{B}^T - \mathbf{I}), \mathbf{H} = 2i\mathbf{A} \mathbf{A}^T, \mathbf{L} = -2i\mathbf{B} \mathbf{B}^T \end{aligned} \quad (44)$$

where,  $\mathbf{G}_1(\theta)$  and  $\mathbf{G}_3(\theta)$  are two real matrices defined by generalized fundamental matrices  $\mathbf{N}_1(\theta)$  and Barnett-Lothe tensors  $\mathbf{S}, \mathbf{H}$  and  $\mathbf{L}$ .

The tangential stress and electrical displacement around the hole are given by

$$\sigma_{ss} = -\mathbf{s}^T \Phi_{,n} \quad D_{ss} = -i_3^T \Phi_{,n} \quad (45)$$

$\mathbf{s}$  and  $\mathbf{n}$  denote the unit tangent and unit normal to the hole boundary respectively. The following transformation matrices  $\mathbf{n}^T, \mathbf{s}^T$  are used for evaluating the stresses in the normal and tangential directions. The  $i_3^T$  matrix is used to exclusively obtain the electrical displacement from the derivatives of the stress function.

$$\begin{aligned} \mathbf{n}^T &= [-\sin \theta \quad \cos \theta \quad 0 \quad 0] \\ \mathbf{s}^T &= [\cos \theta \quad \sin \theta \quad 0 \quad 0], \\ i_3^T &= [0 \quad 0 \quad 0 \quad 1] \end{aligned} \quad (46)$$

## IV. RESULTS AND DISCUSSION

### A. Circular Hole

The stresses and electrical displacements around a circular hole in PZT 4 piezoelectric plate are presented in Fig. 2 for remote loading along y-axis. The results exactly match with those of Liang [10].

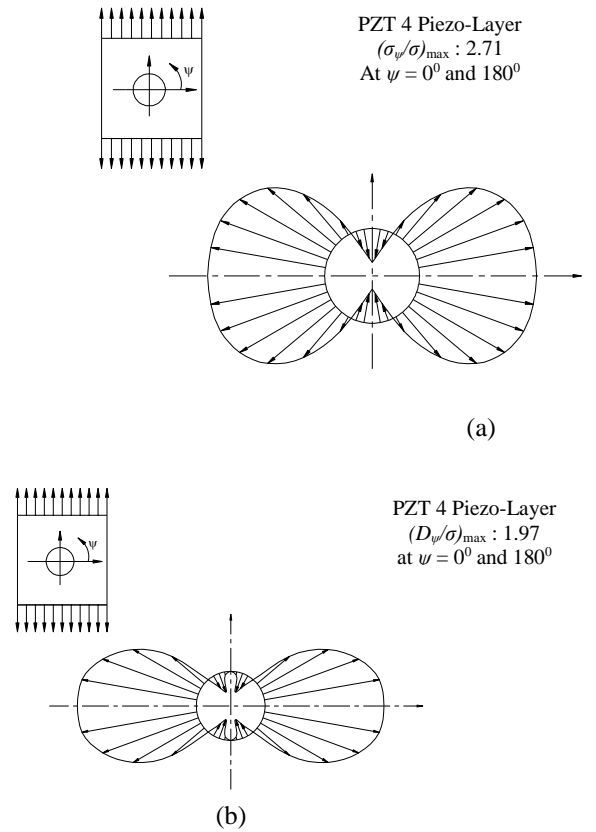


Fig. 2 Piezoelectric plate (PZT 4) with circular hole under remote Y-axis loading (a) hoop stress (b) electrical displacements, Liang [10]

### B. Elliptical Hole-Remote y-axis loading

Stresses and electrical displacements around elliptical holes ( $b/a = 0.2, 0.5, 1, 2,$  and  $5$ ) in piezoelectric plate PZT 4 under remote stresses along y-axis are presented in Fig. 3. Similarly, in Fig. 4, they are presented for remote electrical displacements. These results match exactly with those of Xu [11].  $a, b$  are semi major and minor axes respectively.

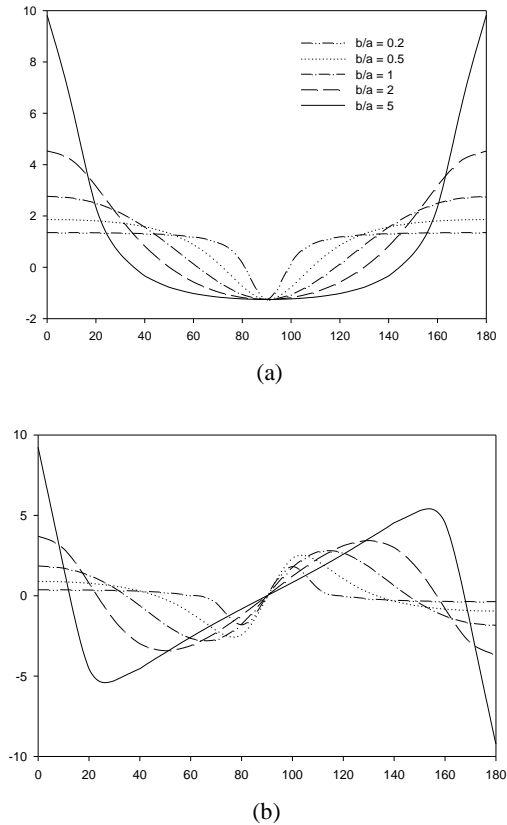


Fig. 3 Piezoelectric laminate (PZT 4) with elliptical hole under remote stress along y-axis (a) hoop stress (b) electrical displacements, Xu [11]

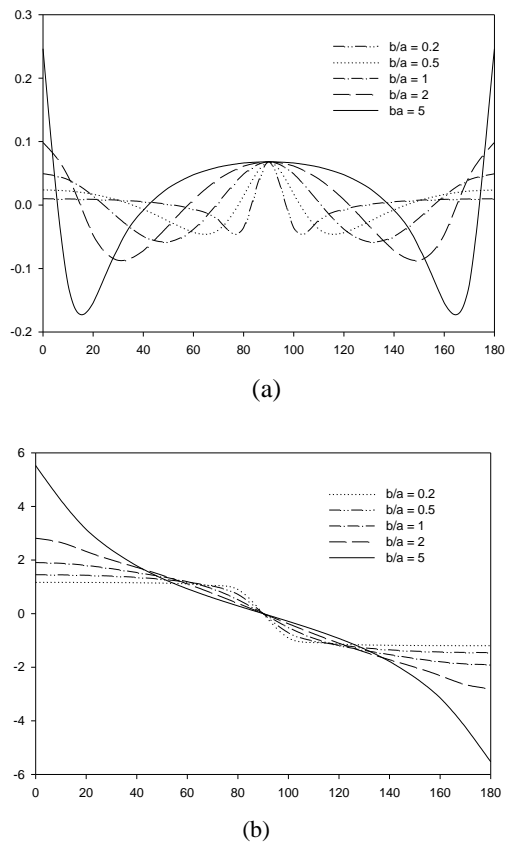


Fig. 4 Piezoelectric laminate (PZT 4) with elliptical hole under remote electrical displacement loading  $D_2$  (a) hoop stress (b) electrical displacements, Xu [11]

The nominal stresses are listed in Table 2 for other cases of elliptical holes ( $a/b = 3, 1, 1/3, 1/10$ ) in the same PZT 4 plate under remotely applied mechanical loading along  $x$ -axis. They match closely with those of Sosa [5] and Xu [11].

TABLE I. RESULTS FOR OTHER ELLIPTICAL HOLES IN PZT 4 PIEZOELECTRIC PLATE

$a/b$	Sosa [ 5 ]	X.-L.Xu [11]	Present solution
3	1.745	1.743	1.72
1	3.234	3.23	3.16
1/3	7.708	7.7	7.5
1/10	23.67	23.26	22.68

(a) Remote Shear and Electrical Loading  
Stresses around elliptical holes ( $b/a = 0.2, 0.5, 1, 2,$  and  $5$ ) in PZT 4 piezoelectric plate under remote shear and electrical displacements are presented in Fig. 5 (a) and (b) respectively. They are in concurrence with those of Zhou [8].

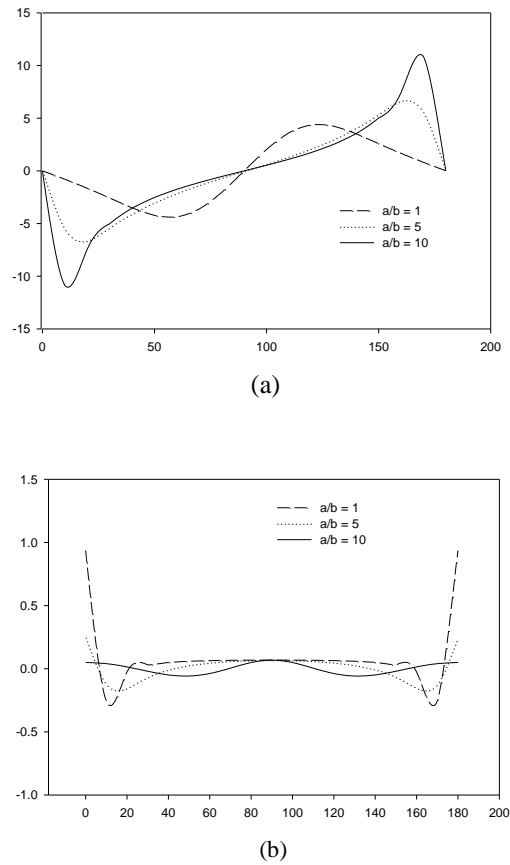


Fig. 5 Stresses around elliptical hole in Piezoelectric laminate (PZT 4) under (a) remote shear loading (b) electrical displacement loading  $D_2$ , Zhou [8]

### C. Irregular Shaped Holes

The stresses around various irregular shaped holes in symmetric piezo-laminate  $[PZT5H/45/-45/PZT5H]_s$  under mechanical and electrical loading are presented in the following.

#### Shape 1

The values of  $\sigma_{\psi}/\sigma$  around circular hole in piezo-laminate  $[PZT5H/45/-45/PZT5H]_s$  under equi-biaxial mechanical and electrical displacement loading are shown in Fig. 6. The maximum value of  $\sigma_{\psi}/\sigma$  is 2.47 at  $130^\circ, 310^\circ$  whereas for simple  $[45/-45]_s$  Graphite/epoxy laminate, it is equal to 3.06.

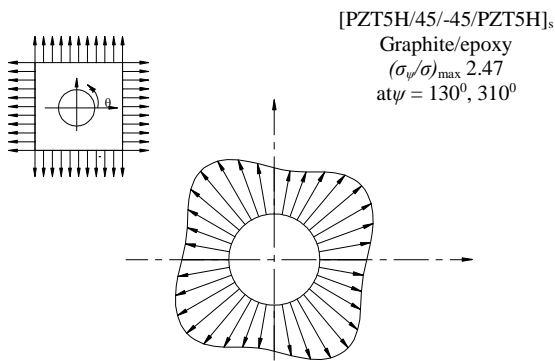


Fig. 6 Stress distribution around shape 1 hole in graphite/epoxy  $[PZT5H/45/-45/PZT5H]_s$  laminate under equi-biaxial mechanical and electrical displacement loading

#### Shape 2

The values of  $\sigma_{\psi}/\sigma$  around Shape 2 hole in  $[PZT5H/45/-45/PZT5H]_s$  under remote equi-biaxial mechanical and electrical displacements are as shown in Fig. 7. The maximum value of  $\sigma_{\psi}/\sigma$  is 38.13 at  $0^\circ$ , whereas in case of simple  $[45/-45]_s$  Graphite/epoxy laminate, it is equal to 28.13.

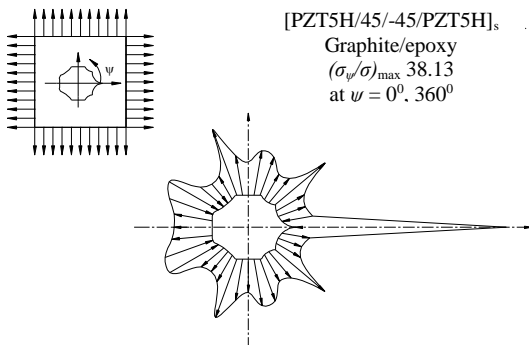


Fig. 7 Stress distribution around shape 2 hole in graphite/epoxy  $[PZT5H/45/-45/PZT5H]_s$  laminate under equi-biaxial mechanical and electrical displacement loading

#### Shape 3

The values of  $\sigma_{\psi}/\sigma$  around Shape 3 hole in  $[PZT5H/45/-45/PZT5H]_s$  laminate under equi-biaxial mechanical and electrical displacements are plotted in Fig. 8. The maximum value of  $\sigma_{\psi}/\sigma$  is 8.22 at  $50^\circ, 310^\circ$  whereas in case of the simple  $[45/-45]_s$  Graphite/epoxy laminate, it is equal to 12.04.

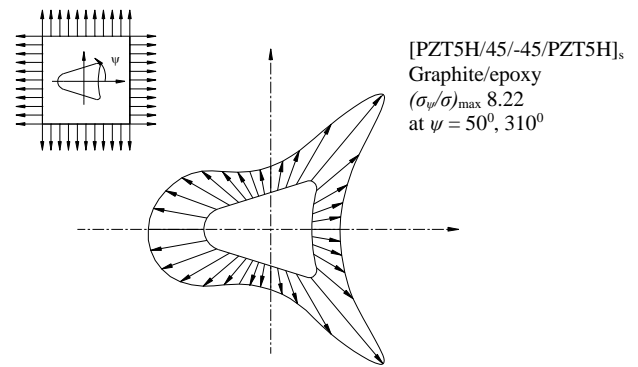


Fig. 8 Stress distribution around shape 3 hole in graphite/epoxy  $[PZT5H/45/-45/PZT5H]_s$  laminate under equi-biaxial mechanical and electrical displacement loading

#### Shape 4

The values of  $\sigma_{\psi}/\sigma$  around Shape 4 hole in  $[PZT5H/45/-45/PZT5H]_s$  laminate under equi-biaxial mechanical and electrical displacement are shown in Fig. 9. The maximum value of  $\sigma_{\psi}/\sigma$  is 7.03 at  $120^\circ, 300^\circ$  whereas in case of simple  $[45/-45]_s$  Graphite/epoxy laminate, it is equal to 7.63.

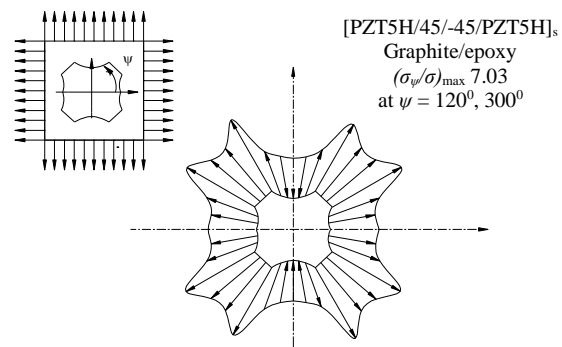


Fig. 9 Stress distribution around shape 4 hole in graphite/epoxy  $[PZT5H/45/-45/PZT5H]_s$  laminate under equi-biaxial mechanical and electrical displacement loading.

#### Shape 5

The values of  $\sigma_{\psi}/\sigma$  around shape 5 hole in  $[PZT5H/45/-45/PZT5H]_s$  laminate under equi-biaxial mechanical and electrical displacement are shown in Fig. 10. The maximum value of  $\sigma_{\psi}/\sigma$  is 6.59 at  $40^\circ, 320^\circ$ , whereas in case of simple  $[45/-45]_s$  Graphite/epoxy laminate, it is equal to 9.47.

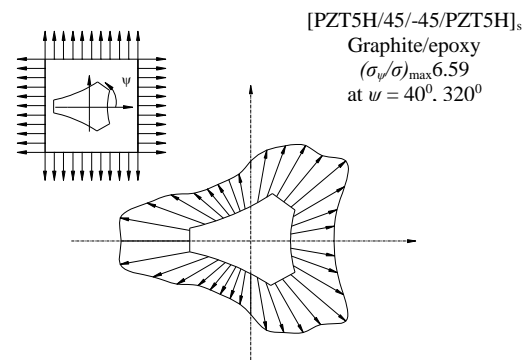


Fig. 10 Stress distribution around shape 5 hole in graphite/epoxy  $[PZT5H/45/-45/PZT5H]_s$  laminate under equi-biaxial mechanical and electrical displacement loading.

**Shape 6**

The values of  $\sigma_{\psi}/\sigma$  around shape 6 hole in [PZT5H/45/-45/PZT5H]<sub>s</sub> laminate under equi-biaxial mechanical and electrical displacement is shown in Fig. 11. The maximum value of  $\sigma_{\psi}/\sigma$  is 5.21 at 10<sup>0</sup>, 190<sup>0</sup> whereas in case of simple [45/-45]<sub>s</sub> Graphite/epoxy laminate, it is equal to 5.93.

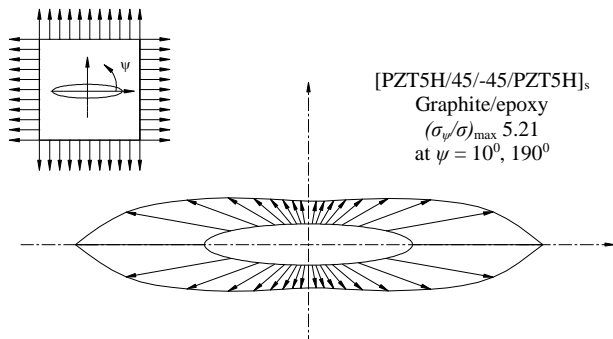


Fig. 11 Stress distribution around shape 6 hole in graphite/epoxy [PZT5H/45/-45/PZT5H]<sub>s</sub> laminate under equi-biaxial mechanical and electrical displacement loading.

**Shape 7**

The values of  $\sigma_{\psi}/\sigma$  around shape 7 hole in [PZT5H/45/-45/PZT5H]<sub>s</sub> laminate under equi-biaxial mechanical and electrical displacement are shown in Fig. 12. The maximum value of  $\sigma_{\psi}/\sigma$  is 8.07 at 0<sup>0</sup>, 360<sup>0</sup> whereas in case of simple [45/-45]<sub>s</sub> Graphite/epoxy laminate, it is equal to 9.83.

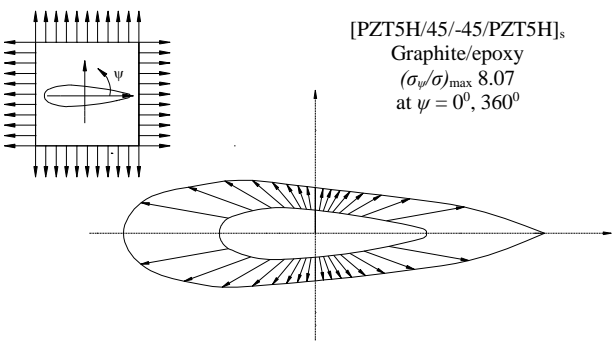


Fig. 12 Stress distribution around shape 7 hole in graphite/epoxy [PZT5H/45/-45/PZT5H]<sub>s</sub> laminate under equi-biaxial mechanical and electrical displacement loading.

**Shape 8**

The values of  $\sigma_{\psi}/\sigma$  around Shape 8 hole in [PZT5H/45/-45/PZT5H]<sub>s</sub> laminate under equi-biaxial mechanical and electrical displacement are shown in Fig. 13. The maximum value of  $\sigma_{\psi}/\sigma$  is 12.65 at 0<sup>0</sup>, 180<sup>0</sup> whereas in case of simple [45/-45]<sub>s</sub> Graphite/epoxy laminate, it is equal to 9.19.

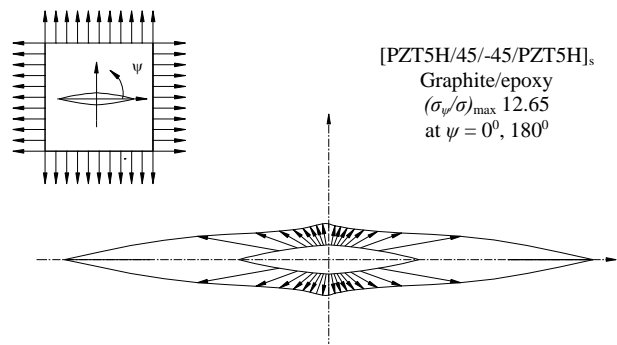


Fig. 13 Stress distribution around shape 8 hole in graphite/epoxy [PZT5H/45/-45/PZT5H]<sub>s</sub> laminate under equi-biaxial mechanical and electrical displacement loading.

**Shape 9**

The values of  $\sigma_{\psi}/\sigma$  around shape 9 hole in laminate [PZT5H/45/-45/PZT5H]<sub>s</sub> under equi-biaxial mechanical and electrical displacements are shown in Figure 14. The maximum value of  $\sigma_{\psi}/\sigma$  is 9.42 at 190<sup>0</sup>, 330<sup>0</sup> whereas in case of simple [45/-45]<sub>s</sub> Graphite/epoxy laminate, it is equal to 8.37.

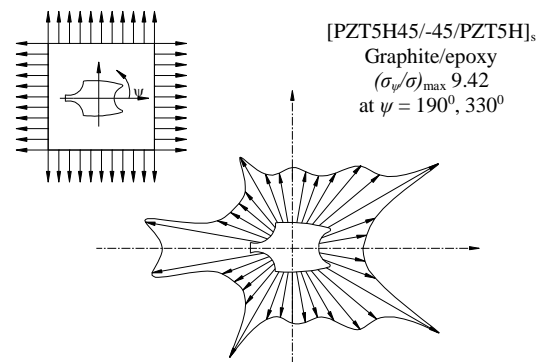


Fig. 14 Stress distribution around shape 9 hole in graphite/epoxy [PZT5H/45/-45/PZT5H]<sub>s</sub> laminate under equi-biaxial mechanical and electrical displacement loading.

**VI. CONCLUSIONS**

1. In case of piezo-composites, the pattern of stress distribution around the hole is exactly same as that of the polymer composite laminate. However all the values are reduced to a scale.
2. A lower values of stresses are observed in case of laminates with piezo-electric layers compared to the simple laminates. This may be due to the increased stiffness of the plates by the presence of piezo layers.
3. The solutions in the literature have addressed either circular or elliptical holes in single layered piezoelectric plates of PZT4 while the present solution considers the piezolaminates [PZT5H/45/-45/PZT5H]<sub>s</sub> with all kinds of regular and irregular shaped holes.

## REFERENCES

- [1] Lekhnitskii SG. Anisotropic plates. New York: Gordon and Breach, 1968.
- [2] Savin GN. Stress concentration around holes. New York: Pergamon Press, 1961.
- [3] W. Becker, "A Complex Potential Method for Plate Problems with Bending-Extension Coupling," *Archive of Applied Mechanics*, vol. 61, pp. 318-326, 1991.
- [4] W.Becker, "Complex Method for the Elliptical Hole in an Unsymmetric Laminate," *Archive of Applied Mechanics*, vol.63, pp.159-169, 1993.
- [5] H.Sosa, "Plane problems in piezoelectric media with defects," *Int J Solids Struct.*, vol. 28(4), pp. 491–505, 1991.
- [6] T.Sasaki, T.Suzuki, K.Hirashima, "Transversely isotropic piezoelectric materials with an arbitrarily shaped boundary," *Acta Mech.*, vol.184: pp.217–30, 2006.
- [7] L. Dai, W.L.Guo, X.Wang, "Stress concentration at an elliptic hole in transversely isotropic piezoelectric solids," *Int J Solids Struct.*, vol. 43 pp.1818–31, 2006.
- [8] M.Zhou, S.Duan, Y.Kong, S.Liu, "Stress distribution in a piezoelectric material with an elliptical hole subjected to remote uniform shear mechanical and electric loads," *Adv Mater Res.*, vols. 97-101, pp. 956-59, 2010.
- [9] D.Yanliang, L.Shuhong, D.Shijie, L.Yanqiang, "Electro-elastic fields of piezoelectric materials with an elliptic hole under uniform internal shearing forces," *Chinese J Mech Eng.*, vol. 26(3), pp. 539-44, 2013.
- [10] Y.C.Liang, C.Hwu, "Electromechanical analysis of defects in piezoelectric materials," *Smart Mater. Struct.*, vol. 5, pp. 314–20, 1996.
- [11] X.L.Xu, RKND.Rajapakse, "On a plane crack in piezoelectric solids," *Int J Solids Struct.*, vol. 38, pp. 7643-58, 2001;
- [12] MY.Chung, TCT.Ting, "Piezoelectric solid with an elliptic inclusion or hole," *Int J Solid Struct.*, vol. 33(23), pp. 3343-61, 1996.
- [13] C.Hwu, MC.Hsieh, "Extended Stroh-like formalism for electro-elastic composite laminates and its applications to hole problems," *Smart Mater Struct.*, vol. 14, pp. 6-682005.
- [14] C.Hwu, "Some explicit expressions of extended Stroh formalism for two-dimensional piezoelectric anisotropic elasticity," *Int J Solids Struct.*, vol. 45, pp. 4460–73, 2008.
- [15] Sokolnikoff IS. *Mathematical theory of elasticity*. New York: McGraw-Hill, 1956.

# DISTINCT MODELS OF GEARS AND GEAR TRAINS - A REVIEW

**G. Tharanitharan**<sup>1\*</sup>

<sup>1\*</sup>Department of Mechanical Engg.  
SNS College of Technology,

**Dr.P.Tamilselvam**<sup>2</sup>

Department of Mechanical Engg.  
SNS College of Technology,

**T.Tharoon**<sup>3</sup>

<sup>3</sup>Project Assistant, Department of  
Mechanical Engineering, Coimbatore  
Institute of  
Engineering and Technology,

**Ridon Bagra**<sup>4</sup>

<sup>4</sup>PG Scholar SNS College of Technology

## Abstract:

In this paper reviews the various models of gears such as Spur, Helical, Hypoid gears and gear trains such as Planetary gear train setup. The main intent of this paper is to understand the various models of Spur gear such as micro pitting model, mesh interface damping model, transient elasto-hydrodynamic lubrication model and load distribution model. Surface interpolation model, shell model for hypoid gears and also to attain influence of design parameters on mechanical power losses on Spur, Helical and Hypoid gears and also give valid information what are the factors considered while design of gears and gear train system in order to achieve desired quality. However the models are used to improve the performance of a gear system and also to diminish the failure of a gear system and also gear train. From that to understand which factor has major influence on efficiency and power loss of gear drive system and also to realize which factors are majorly considered while design of gear drive system. It can be indicated that the geometric dimensions, operating condition, lubricating conditions are major influencing factors on various models of gears and gear train set up. The lubricant properties such as density, geometric parameters such as face width, module, operating condition such as temperature, rotational speed are the factors influencing on not only power loss of spur gears but also influence on tribo-dynamic behaviour of spur gears. An assessment of future research is also recommended.

**Keywords:** *Micro pitting, EHL model, design parameters, spur, helical, hypoid gears, planetary gear train*

---

\*Corresponding author. Email: tharoonkvp@gmail.com;  
Tel: (+91) 7092395298

## 1. INTRODUCTION:

Gears are toothed wheels used for transmitting motion and power from one point to another point. A circular body of cylindrical shape or that of the shape of frustum of a cone and of uniform small width, having teeth of uniform formation, provided on its outer

circumferential surface is called a gear or toothed gear or toothed wheel. Gear drive have some advantages compared than flat, belt drive. They are i). There is no slip and velocity ratio remains constant, ii). Occupation of space or utilization of space is very less, iii). Whenever the larger power is transmitted where the gear drive is used and it is a positive drive. iv). the efficiency of the gear system is very high. Generally gears are used in automobiles, turbines, low speed applications and also high speed application. The classification of gears is as shown the Fig 1. Day by day application of gear drive system is increased because of their characteristics so essential to learn about gear drive system. In general, efficiency of the gear drive system depends upon the design parameters but not only depends on design parameters but also lubricant properties and operating conditions. A gear train contains more number of gears which are used to transmit power from the driving shaft to driven shaft and transmit motion in the form of chain manner. The types of gear trains are i). Simple gear train, ii). Compound gear train, iii). Reverted gear train, iv). Epicyclic gear train. Epicyclic gear train has more applications because of its designate it consist rotating gear is known as planet gear, unmovable gear is known as sun gear. The models are used to design a gear train such as Floquetlyapunor theory, newmark time integration scheme and lumped parameter dynamic model.. In this paper, the study of various models of spur gear such as micro pitting model, mesh interface model, transient elasto-hydrodynamic lubrication model and load distribution model. Surface interpolation model, shell model for hypoid gears and also to attain influence of design parameters on mechanical power losses and mechanical efficiency of Spur, Helical, and Hypoid gears and also to study of vital department of planetary gear train system.

## 2. SPUR GEARS

Spur gears have their teeth which are straight and parallel to the axis of the wheel. They are used to transmit power between two parallel shafts. They are simple in construction and have highest efficiency and precision rating is also high. Spur gears are used in household gadgets, motor cycle, automobiles and aircraft. It has maximum precision compared to other type of gears.

Mentioned all research papers may follow common methodology as shown in the Fig 2.

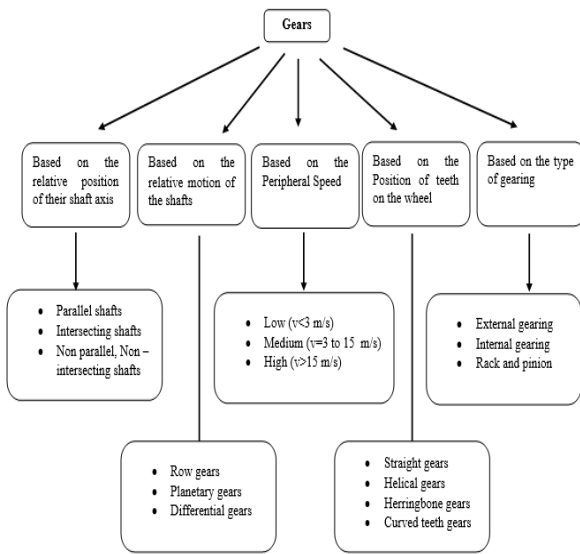


Fig 1. Classification of gears

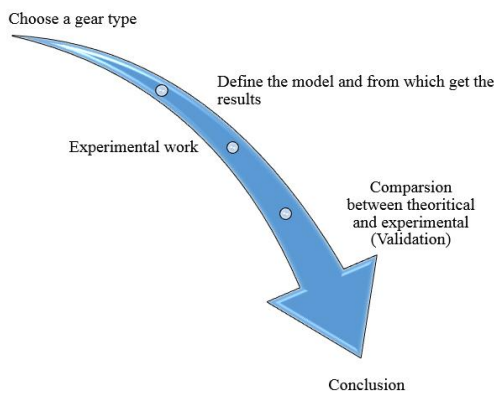


Fig 2.Common Methodology

### 2.1 Elastohydrodynamic lubrication model

S.Li and A Kahraman [1] has investigated “Influence of dynamic behaviour on elastohydrodynamic lubrication of spur gear”. In this study the behaviour of elastohydrodynamic lubrication of high speed spur gear contacts under dynamic condition was probed. A non-linear time varying vibratory model of spur gear is used to predict the steady state non-linear response in the form of tooth separation. In order to demonstrate the foremost influence of dynamic loading on gear lubrication, the EHL predictions under dynamic loading condition are compared to quasi static contact loads for gear sets having smooth and rough surfaces, In this paper three mathematical models were developed such as,  
 i). Purely torsional dynamic model of a spur gear (Fig 3)

In that prediction of dynamic gear tooth contact forces, the individual dynamic tooth force is given by

$$W_d(t) = W_s(t) \left( DMF(t) \left( \frac{T_1}{r \& l} \right) \right)$$

equ (1)

ii). The gear load distribution model

It referred to predict  $k(t)$ ,  $e(t)$ ,  $w_s(t)$ . It’s associated with tooth bending, shear deformation, base rotation and contact deformation.

iii). Transient mixed EHL model

This model contained the variations of radii of curvature, sliding velocities.

$$h(x,t) = h_0(t) + g_0(x,t) + v(x,t) - R_1(x,t) - R_2(x,t)$$

equ (2)

$$W'_d(t) = \int p(x,t) dx$$

equ (3)

The results of EHL are differ from static tooth load condition. In this model, the local contact pressure exceeds 1GPa. The load is one kind of factor which influence on  $h(x,t)$ ,  $p(x,t)$  and also surface roughness have influence on  $h(x,t)$ ,  $p(x,t)$ .

S.Li and A.Kahraman [2] has presented a paper on “A spur gear mesh interface damping model based on elastohydrodynamic contact behaviour”. In this study discrete gear dynamics model was developed and the instantaneous tribological behaviour of tooth contacts was probed. This paper formulate the EHL based gear mesh viscous damping and definition of an equivalent viscous damper along the line of action is given by,

$$\xi = \left[ (\tan^2 \phi) \sqrt{2km} \sum_{n=1}^N Dn \right]$$

equ (4)

The model was developed based on the following assumptions radii of curvature was represented by pitch point expression for damping ratio was derived along the line of action. The value of gear mesh damping is proportional to the torque but inversely proportional to the rotational speed and lubricant temperature. ( $D_n$ =Gear mesh damping for  $n^{\text{th}}$  contacting tooth pair) and they probed on “A mixed EHL model with asymmetric integrated control volume discretization” [3]. An asymmetric integrated control volume approach is employed to reduce the discretization errors. This approach is very efficient and accurate compared to other conventional approach. This method reduces the computational time and improves the efficiency of the system.

### 2.2 Wind age, Spin power loss and Micro pitting model of spur gear

SathyaSeetharaman and AhmetKahraman has developed a model of wind age power loss of spur gear [4]. Wind age power loss is combination of individual gear with air or air-oil mixture. The losses due to squeezing of the same medium at the gear mesh interface. Squeezing can occur under heavy loads and insufficient at this condition, the lubrication oil film breaks down and metal to metal contact occurs. Generally power losses are divided into

two categories one is load dependent (Mechanical) losses due to friction at gear mesh contact interfaces, another one load-independent (spin) power losses [5] due to lubrication method it can be occur zero torque.

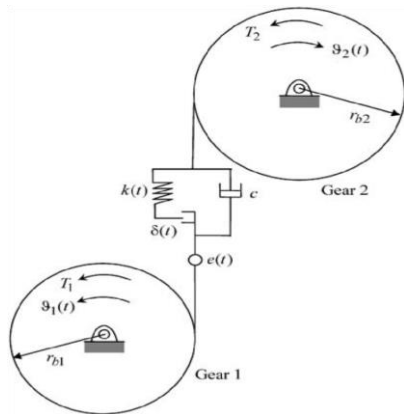


Fig. 3. A purely torsional dynamic model of a spur gear pair [1]

Wind age and Spin power loss model is given by,

$$P_w = P_p + P_{aequ} \quad (5)$$

$$P_d = P_{d1} + P_{d2} \quad \text{equ (6)}$$

$$P_{d1} = P_{dci} + P_{dfi} \quad \text{equ (7)}$$

The lubricant property (density), Geometric parameters (module, face width), Operating condition such as temperature, rotational speed are greatest influence factors on power loss.

The module, face width is directly proportional to the power loss, torque is inversely proportional to the power loss. In spin power loss model (Fig 4) Immersion parameter is directly proportional to the power loss.

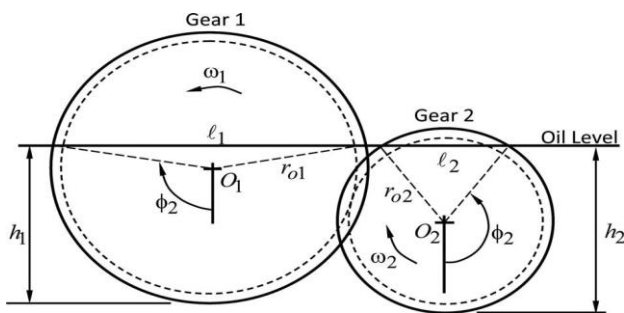


Fig 4. Definition of oil churning parameters for a gear pair immersed in oil [5].

Sheng Li and AhmetKahraman [6] has done a work on “Micro pitting model for spur gear under mixed lubrication condition” The objective of the study is to discuss about micro pitting severity index (MSI) and to divine the surface normal tangential tractions, contact radii, surface velocity and normal tooth force. Pitting is a surface fatigue failure which occurs when the load on the gear

tooth surface endurance strength of the material. Micro pitting severity index is ratio between micro pitted area and the entire contact area. Micro pitting formulation depends on  $A_s$  and the fatigue strength of the material. MIS increases between of 10 to 30 million contact cycles after that the value of MIS is decreased and they done a research work on “Micro pitting fatigue lives of lubricated point contacts: Experiment and model validation”. The aim of the experiment [7] is to find out the contribution factors on micro pitting formation. It can be mentioned that the contribution of contact pressure and rolling velocity on micro pitting formation significantly. The micro pit formation is decreased with high contact pressure and low rolling velocity. The slide to roll ratio and surface roughness amplitude is directly proportional to the micro pit formation.

### 2.3 Other models of spur gears

Sheng Li and AhmetKahraman [8] has probed on “Prediction of spur gear mechanical power losses using transient elastohydrodynamic lubrication model”. It can be noted that the mechanical losses are combination of sliding and rolling velocity for rough gear tooth surfaces. The instantaneous rolling and sliding velocity is calculated by means of predicated transient pressure and film thickness. The average gear mesh mechanical power loss is given by,

$$P_{\text{mesh}} = (1/N) \sum_{n=1}^N P_{\text{mesh}}(n\Delta\psi) \quad \text{equ (8)}$$

The gear module, surface roughness amplitude and operating conditions are factors influence on gear efficiency. The module, film thickness is directly proportional to the efficiency of gear system. Surface roughness is inversely proportional to the efficiency of ground and chemically polished gear 18% of loss due to asperity contact friction influence on total power loss, asperity actions are more sensitive with operating speed. Ultimately the substantial impact of rolling action on efficiency of gear drives system.

S.Li and A.Kahraman [9] has presented in his investigation paper on “A tribo-dynamic model of spur gear”. The aim of the investigation is to adopt the mixed EHL model of spur gear with transverse torsional dynamic model. This model indicates two relationship and quantity the influence of operating condition, surface roughness and lubrication properties on tribo-dynamic behaviour. The surface roughness amplitude is increased with increment of bearing force due to increase of friction. The bearing force is decreased because of reduction of lubricant viscosity at higher temperature and also reduces the viscous component of  $F_s$ .

Huali Ding, AhmetKahraman [10] the objective of this paper is to study the interaction between gear surface wear and gear dynamic response. The study consists of finite element based deformable body model, simplified discrete model, and wear model and to demonstrate two way interaction between wear and dynamic behaviour. Vibration amplitude and forced

frequency response influence on surface wear quantitatively and qualitatively. Smaller wear depths are divided at high speed because of increment of  $h_{min}$  and reduction of  $K$  with speed.

M.A. Hotait and A. Kahraman [11] has done research work on "Experiment on the relationship between the dynamic transmission error and the dynamic stress factor of spur gear pairs". In this study dynamic factor on dynamic transmission error measurement from unmodified and modified spur gear is demonstrated experimentally. The intention of this paper is to show the relationship between durability and noise metrics. There is a linear relationship between DF, DTE which means to predict the linear relationship durability and noise metrics. Dynamic tooth forces and dynamic stress factors influence on vibration of gear system.

Alessio Artoni, Massimo Guiggiani, Ahmet Kahraman and Jonny Harianto [12] has investigated on "Optimization of gear tooth surface modification within range of torque and misalignments". The objective function is peak contact stress, loaded transmission error amplitude (to be minimized) and this study using LDP, global optimization algorithm technique. Even if only robustness to torque and misalignment has been directly integrated.

M. Kolivand and A. Kahraman [13] has done work on "General approach to locate instantaneous contact lines of gears (any type of gears) by using surface roll angle. The surface roll angle is determined by the position and normal vectors of points on one of the mating surfaces and axes of both gears. The instantaneous contact lines are attained by a novel approach. This method has several advantages compared to the conventional method. It is much faster than conventional method, avoids several computational steps, the principle curvatures. It is more accurate model because of it needs only surface and normal gear axis vectors.

Rune Pedersen, Ilmar F. Santos, Iran A. Hede has investigated on "Advantages and Drawbacks of applying periodic time-variant model analysis to spur gear dynamics". The study [14] is proposed time variant modal for examining spur gear. It can be noted that this method is accurate and easy to handle compared to time-step integration method. It gives the solution for vibration problem also the parametric resonance frequency in elastic mode does not depend on the number of Fourier components. The parametric resonance area is depends on the number of Fourier components. More number of components increases the accuracy of the entire system.

Victor Roda – Casanova, Francisco T. Sanchez – Marin, Ignacio Gonzalez – Perez Jose L Iserte, Altonso Fuentes has done a research work [15] on "Determination of the ISO face load factor in spur gear drives by the finite element modelling of gears and shafts". The main intention of the work is to find out kinship between the mesh alignment and the face load factor by using FEA model. That model is compared with Method C. The length of gear shaft, face width, ratio of pitch radii of

gears to pitch radii of shafts are influencing factors on transmission motion done by gear system. The contribution of position of gear over shaft is not significant on the efficiency of the gear system.

Zaigang Chen, Yimin Shao has presented a paper on "Dynamic simulation of spur gear with tooth root crack propagating along tooth width and crack depth". The main intent of the work [16] is to study the contribution of tooth crack and vibration on mesh stiffness by using statistical indicators such as RMS and Kurtosis. The crack leads the noise so the prediction of kinship between tooth crack and vibration is necessary one. The tooth width and crack depth is independent of RMS and Kurtosis. RMS and Kurtosis is depends on the crack propagation. Crack propagation is directly proportional to the magnitude of frequency and sidebands. They investigated on "Mesh stiffness of an internal spur gear pair with ring gear rim deformation" by using Timoshenko beam theory [17]. It can be noted that type of ring support, ring thickness, number of supports and the mesh force affects the mesh stiffness of internal gear pair.

Fakher Charri, Walid Baaccar, Mohamed Slim Abbas, Mohamed Haddar has investigated on "Effect of spalling or tooth breakage on gear mesh stiffness and dynamic response of a one – stage spur gear transmission" by using analytical functions [18]. Tooth breakage and Spalling are factors directly proportional to the gear mesh stiffness. The gear mesh frequency, amplitude, modulation, sidebands of the gear system which are factors evaluate the stiffness of gear mesh.

R.G. Parker, S.M. Vijayakar, T. Imanjo has done work on "Nonlinear dynamic response of a spur gear pair: Modelling and experimental comparisons". The aim of the study [19] is to use the spur gear pair by using FEA model and contact mechanism. It can be noted that there is non-linear relationship exists between the contact loss and meshing teeth.

Yongjunshen, Shaopu Yang, Xiandong Liu has probed on "Nonlinear dynamics of a spur gear pair with time varying stiffness and backlash based on incremental harmonic balance method". The objective is to use the spur system by using IBHM including backlash, stiffness with respect to time, STE. This method is very useful to give accurate results [20]. The co-efficient ratio of gear system and excitation amplitude is the influencing factors on vital reply of gear system or manage the driving behaviour of gear system.

### 3. HELICAL GEARS

Helical gears are simple modification of spur gear. A helical gear has teeth in the form of helix around the gear so the new term "helix angle" is introduced in helical gears. This type of gears are used in automobiles, turbines, high speed applications. This gears have some following advantages than spur gear, i). Noise level is less, ii). Load carrying capacity is high.

#### 3.1 Models of helical gears

Sheng Li, AarthyVaidyanathan, Jonny Harianto and AhmetKahraman [21] has presented a paper on "Influence of design parameters on mechanical power losses of helical gears". In this study, a helical gear mechanical efficiency model was developed and EHL model was constructed. Varying amounts of tooth modifications have strong influence on losses as well as efficiency and also the basic design parameters such as pressure, helix angle, number of teeth, module, and major diameters. Power loss is directly proportional to the module, outer diameter, transmission error and  $A_{wd}$ . Power loss is inversely proportional to the  $\xi_f, \xi_t, \phi, \sigma_b, \sigma_c, N$ .

M.Hotait and A.Kahraman [22] has done research on "Experiments on root stresses of helical gear with lead crown and misalignment". The experiment concerns with shaft alignment and lead crown of helical gear influence on bending stress, load distribution. The root stresses was predicated by means of crown values. The amount of the lead crown influence on root stress along with the face width, misalignment of shafts. Immoderate lead crown, to increase at most root and contact stress.

A. Kahraman, P. Bajpai, N.E. Anderson has presented a paper on "Influence of tooth profile deviations on helical gear wear". The intent of the paper [23] is to estimate the contribution of tooth profile modification contained involute crown, lead crown, and involute slope on wear of helical gear. The wear rate depends on the involute mismatch and total involute crown majorly. The model approached the finite-element based in order to divine the contact pressure.

M. Kubur, A. Kahraman, D.M. Zini and K. Kienzle [24] has investigated on "Dynamic analysis of a multi-shaft helical gear transmission by finite elements Model and Experiment". The intent of the paper is to obtain the dynamic behaviour of multi shaft helical gear setup. Shaft angle, shaft dimensions, bearing stiffness, hand of the gear, other parameters with respect to bearings and shaft are the influencing factors on dynamic behaviour of gear setup.

#### 4. HYPOID GEARS

Hypoid gears are same in appearance to spiral bevel gears. They differ from spiral gears in that the axis of pinion is offset from the axis of gear and their pitch surfaces are hyperboloids rather than cones that type of gears are most desirable for those applications involving larger speed reduction ratios. They operate more smoothly and quietly.

##### 4.1 Models of Hypoid gears

A.Artoni, M.Kolivand and A.Kahraman [25] has done work on "An ease-off based optimization of the loaded transmission error of hypoid gears. The aim of the paper is to minimize the LTE and contact pressure because of LTE is one of the source of noise and vibration of gear systems. Effectiveness of this optimization is attained by using a face milled and face hobbled hypoid gear. However the face milled designs are cost effective.

D.Park, M.Kolivand and A.Kahraman [26] is probed on "An approximate method to predict surface wear hypoid gear using surface interpolation. The objective of the paper is to reduce the time required for wear computations. Surface interpolation model supports to dictate the surface velocity for sliding distance computation by means of differential geometry formulation contained surface normal curvature and their directions. This model shown that the time required for wear computations reduced 10 times, accurate model compared to semi analytical contact model.

M.A.Hotait, A.Kahraman and T.Nishino [27] has investigated on "Root stress of hypoid gears with misalignment". The intent of the paper is to study the effect of misalignment on root stresses of hypoid gear pair system. Stress associated with root is known as root stress. A novel methodology is used to measure the root stress under different loading and misalignment condition. This model included an automatic mesh generator that integrates actual tooth and blank surfaces.

M.Kolivand, S.Li.Kahraman [28] has presented a paper on "Prediction of mechanical gear mesh efficiency of hypoid gear pairs". The aim of the study is to predict what are the factors influencing on efficiency and also power losses. The model was developed under EHL model, Shell model. This study proposed a new model for both face milling and face hobbing cutting method. The temperature is directly proportional to the power loss and inversely proportional to the efficiency.  $\xi/P_t$  ratio is inversely proportional to lubricating temperature and  $T_{or}$ . Surface roughness and the pinion shaft offset are factors influence on mechanical efficiency of hypoid gears and also speed, torque, lubricant temperature are influence on efficiency and power losses.

M.Kolivand, A.Kahraman [29] has done a research work on "A load distribution model for hypoid gears using ease-off topography and shell theory". This model combines the ease-off model and Rayleigh-Ritz based shell model. The main intention of the paper is to predict the instantaneous contact curve through roll angle and to interpret the tooth compliance. This model is accurate compared to FE based model and tooth profile are optimized.

J.J. Yang, H. Zhang, X.Z. Deng, B.Y. Wei has probed on "Ultrasonic lapping of hypoid gear: system design and experiments". In this study [30] the ultrasonic lapping methodology is proposed which improves the efficiency of the system, accuracy and tooth profile of gear system than the traditional lapping system. This method has following advantages i). Increase the control area, ii). Decrease the noise level in terms of vibration, iii). Reduce the roughness, harmonics, acceleration of the system and amplitude of GMF, iv). Give the tooth regular pattern, v). Increase the quality of the entire system.

#### 5. OTHER MODELS OF GEARS

Ma Ru Kang and Ahmet Kahraman has probed on "Measurement of vibratory motions of gears supported by compliant shafts". The intension the study [31] is to measure the torsional, translational and rotational motion of parallel axis gears by using effective method. This study is proposed a method such that new accelerometer based measurement technique. This technique gives not only dynamic transmission error amplitudes but also the translational motion in LA and OLA directions. The results expressed in terms of shaft flexibility, gear type and input torque. The motions are directly proportional to low vibration amplitudes in helical gears. The motion values are inversely proportional to the vibration amplitudes in spur gears.

J.Hong, D.Talbot, A.Kahraman [32] has investigated on "A semi analytical load distribution model for side-fit involute splines". The objective of paper is to envisage load distribution of spline joints. The semi analytical model was developed and this method is accurate, having less calculation (computational) time and having different load conditions such as i).pure torsion, ii).combined torsion and radial load, iii).combined torsion radial loads and tilting moments. A new multistep discretization solution is developed to identify the effect of design variation and manufacturing errors.

Sheng Li and Ahmet Kahraman has investigated on "A fatigue model for contacts under mixed elastohydrodynamic lubrication condition". The objective of the research [33] is to estimate the fatigue concepts of the mating surfaces. A fatigue concept is developed and containing mixed EHL model, a potential theory, a multi-axial, fatigue criterion and also including Lagrangian-Eulerian scheme in order to evaluate the effect of the surface roughness.

Prashant Sondkar and Ahmet Kahraman has developed "A dynamic model of a double helical planetary gear set". The aim of the experiment [34] is to synthesis of a double helical planetary gear set including number of planets, torsional, transverse, axial, rotation motion. It can be noted that the dynamic load amplitudes are obtained depends upon the right to left stagger values.

H. Xu, A. Kahraman, N.E. Anderson, D.G. Maddock has probed on "Prediction of Mechanical efficiency of parallel-Axis gear pairs". The objective of the paper [35] is to predict power loss with respect to friction. However the mechanical efficiency of gear drive system depends on the geometric parameter operating condition and lubricating condition. The friction coefficient is estimated by using a multiple linear regression analysis.

J. Hong, D. Talbot, A. Kahraman has done research work on "Load distribution analysis of clearance-fit spline joints using finite elements". In this study [36] a combined finite element and surface integral contact analysis model under combined torsional load, radial load and tilting moment is proposed. The impact of spline misalignment is expressed in terms of spline lead crown. So the lead crown modification leads reduction of load

concentrations and increases the load distribution of splines. The pure to torsion loading is unequally shared because of indexing errors.

## 6. GEAR TRAINS

### 6.1 Models of Planetary gear train

A.Kahraman, H.Ligata, A. Singh [37] has presented a paper on "Influence of ring rim thickness on planetary gear set behavior". The intension of the paper is to estimate the contribution of ring gear rim thickness on the rim deflection and root and hoop stresses. It can be noted that rim thickness is an important factor it should considered while designing of gear train because of it can play major role on planet load sharing of gear sets.

H. Ligata, A. Kahraman and A. Singh has conducted on "An Experimental study of the influence of Manufacturing errors on the planetary gear stresses and planet load sharing". The intension of the experiment [38] is to study the contribution of manufacturing error such as pinhole position errors on planet load sharing and gear root stresses. It can be concluded that the contribution of manufacturing error, number of planets, torque level on planet load sharing and gear root stresses are quantitatively and significantly.

A AI-Shyyab and A Kahraman [39] has developed "A nonlinear dynamic model for planetary gear sets". This model is sufficient to study the sub harmonic resonance, bifurcation schemes, planet mesh phasing and planet load sharing. The model contained power flow configuration, number of planet, planet mesh phasing configuration and HBM (Harmonic balance method) formulation and they investigated [40] on nonlinear dynamic analysis of a multi-mesh gear train using multi term HBM. The HBM solution is very efficient methods compared to other methods and it is very accurate method.

M. Inalpolat, A. Kahraman has probed on "A theoretical and experimental investigation of modulation side bands of planetary gear sets". The intension of the study [41] is to probe the modulation side bands of planetary gear sets under unequal planet load sharing inquisitively and exploratory with respect to amplitude distributions. The model includes number of planets, planet position angles and the number of teeth of the stationary gear. Whatever the planetary gear sets which will come under following categories i). Equally spaced and in phase planets, ii). Equally spaced and sequentially phased planets, iii). Unequally spaced and in phase planets, iv). Unequally spaced sequentially phased planets, v). Unequally spaced and arbitrarily phase planets. This study indicates the following points i). The gear set is in phase and equally spaced that kind of gear sets have symmetric sidebands. ii). If the planet meshes are in phase, the harmonic amplitude will achieved. iii). The side bands are asymmetrically distributed in case of sequential phased planetary gear sets.

A. Kahraman and H. Ding has developed a methodology [42] to envisage surface wear of planetary gears under dynamic condition. The focus of the study is

to find out wear depths at ring planet meshes and the sun planet meshes. The method contains combination of torsional dynamic model and surface wear model from that to foretell the contribution of worn surface profiles motion transmission error and contribution of dynamic tooth force on wear model. The internal gear pair wear is considered because of the wear rate of ring planet meshes smaller than the wear depth or rate of sun planet meshes in order to reduce wear cycles. The dynamic forces and harmonic amplitude contributes on surface wear in both off-resonance and resonance condition. The wear depth is high in resonance region because of increment of dynamic mesh load.

C. Yuksel and A. Kahraman has investigated on “Dynamic tooth loads of planetary gear sets having tooth profile”. The objective of the paper [43] is to ascertain the contribution factors on wear model of planetary gear sets. The wear rate is dictated by archard’s wear model. This model is accurate and efficient. The wear rate is higher on the dedendum of the sun gear compared to others. The harmonic of the gear force is major factor influence on wear of planetary gear sets.

A Kahraman, H. Ligata, K. Kienzle, D.M. Zini has done a research work on “A Kinematics and Power flow analysis methodology for automatic transmission planetary gear trains”. The goal of the paper [44] is to scrutiny the any type of one degree of freedom transmission planetary gear train with help of a kinematic synthesis formulation, kinematic configuration search algorithm and power flow analysis formulation. This model is very efficient and gives the results accurate results. The components of automatic transmission PGT is as shown the Fig 5.

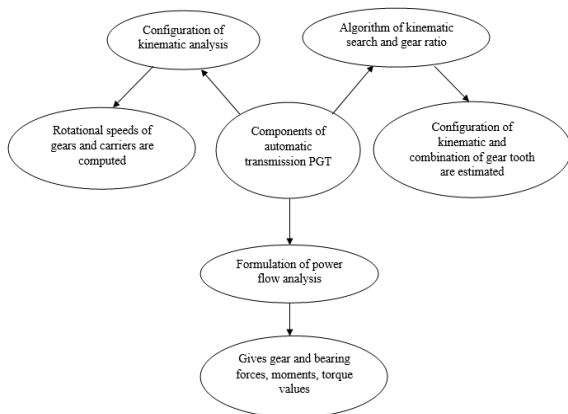


Fig 5. Components of automatic transmission PGT

Zaigang Chen, Yiminshao and Daizhong Su has probed on “Dynamic simulation of planetary gear set with flexible spur ring gear”. The intent of the work [45] is to find out influence factors on the dynamic behaviour of planetary gear by using Timoshenko beam theory. The flexibility of ring gear, ring thickness are the contribution factors on shape and value of the mesh stiffness of internal gear pair and driving deportment of planetary

gear system. DTE is inversely proportional to the ring thickness.

VijayakumarAmbarisha and Robert G. Parker has a presented a paper on “Nonlinear dynamics of planetary gears using analytical and FEA model”. The objective of the study [46] is to examine the dynamic behaviour of spur planetary gear system by using lumped parameter and FEA model. The dynamic behaviour depends on the tooth contact loss, multiple steady state solution, chaos stresses, mesh deflection, resonance condition. It can be noted that the lumped parameter model gives results accurately.

Tristan M. Ericson, Robert G. Parker has investigated on “Planetary gear model vibration experiments and correlation against lumped parameter and finite element models”. The aim of the work [47] is to signalize the vital deportment of planetary gear in terms of rotational, irrotational vibrations, natural frequencies, mode shapes by using lumped parameter model and FEA modal. The higher frequency modes are greatest influence factor on the tooth mesh deflection. The driving behaviour modal including highest planet bearing stiffness and radial stiffness gives accurate results than the modal contained PBSE because isotropic planet bearing stiffness assumption gives more error for entire gear system. The custom designed is obtained in 17<sup>th</sup> natural frequency in the case of lumped parameter modal and 9<sup>th</sup> natural frequency in case of FEA modal. Thepercentage of error is tabulated in table 1 and 2.

Table 1 Errors percentage in Lumped parameter model

S.NO	Model	Number of Natural frequency	Percentage of (%) error
1.	<b>Lumped parameter model</b>	13 <sup>th</sup> Natural frequency	Within 5% error
2		16 <sup>th</sup> Natural frequency	Within 10% error
3.		Remaining all Natural frequency	Within 13% error

Table 2 Errors percentage in FEA model

S.NO	Model	Number of Natural frequency	Percentage of (%) error
1.	<b>FEA model</b>	5 <sup>th</sup> Natural frequency	Within 5% error
2		7 <sup>th</sup> Natural frequency	Within 10% error
3.		9 <sup>th</sup> Natural frequency	Within 4% error
4.		Remaining all Natural frequency	Within 20% error

Zaigang Chen, Yimin Shao has done a work on "Dynamic simulation of planetary gear with root crack in ring gear". The intent of the research work [48] is to examine the dynamic response of planetary gear by using potential energy principle. It can be noted that the internal gear tooth root crack is inversely proportional to the mesh stiffness. The internal gear tooth root crack is the greatest influencing factor on dynamics response of planetary system. It changes the frequency system and produces more sidebands and proportional to the amplitudes of the gear system.

X. Gu and P. Velex [49] has developed "A model to study influence of planet position errors in planetary gears". The objective of the study is to peruse planetary in terms of errors and deflection by using classic lumped parameter model. The planet deflections and errors are contribution factors on expeditious gear geometry. The mesh stiffness is directly proportional to the contact length. The expeditious gear geometry is predicted in account of actual pressure angle, contact ratio, position of base planes, meshing areas.

Woohyung Kim, JiYeong Lee, Jintai Chung has probed on "Dynamics analysis for a planetary gear with time varying pressure angles and contact ratios". The objective of the paper [50] is to peruse the dynamic behaviour of planetary gear by using newmark time integration scheme. The model is proposed with change of pressure angles and contact ratio with respect to time. The amplitude of system inversely proportional to the bearing stiffness. This model gives highest radial displacements.

Zhonghong Bu, Geng Liu, Liyan Wu [51] has probed on "Modal analyses of herringbone planetary gear train with journal bearing". The objective of the study is to examine the herring bone planetary gear train by using analytical model including vibration studies also. The vibration mode contained rotational and axial, translational, planet, rotational and axial ring mode, translational ring mode. The mode shapes of TM are greatest influence factor on driving behaviour of journal bearing. The model strain and kinetic energy helps to scrutinize frequency without deviation.

X. Gu and P. Velex has done a research work on "The dynamic simulation of eccentricity errors in planetary gears". The intension of the study [52] is to examine the errors relevant eccentricity of planetary gear system by lumped parameter model. Errors affect the dynamic behaviour, transmission of motion and load sharing. Those kinds of errors are reduced by floating members. Centrifugal force is created by rotating carrier. It reduces sun gear-planet contact ratio and noise of the system in terms of vibration.

## 7. OTHER MODELS OF GEAR TRAIN

Avinash Sign has presented a paper [53] on "Load sharing behaviour in epicyclic gears: physical explanation and generalized formulation". The planet to planet load sharing is evaluated by closed form non dimensional equations included positional errors. The

floating system eliminates one portion of error. The remaining portions are eliminated by elastic deformation. The number of planets directly proportional to the position error. The quantity of float of system does not affect the load sharing significantly.

S. Theodossiadis and S. Natsiavas has probed on "Nonlinear dynamics of gear pair systems with periodic stiffness and backlash" by using response diagrams [54]. It can be noted that backlash, mesh stiffness are strongest contribution factors on driving department of gear system. Mesh stiffness is directly proportional to the dynamic response with nonzero backlash condition. Harmonic forcing is influence factor on amplitude type and periodic response. Damping is directly proportional to the driving reply and inversely proportional to the amplitude of the system.

Haidong Yu, Peter Eberhard, Yong Zhao, Haowang has probed on "Sharing behaviour of load transmission on gear pair systems actuated by parallel arrangements of multiple pinions". The objective of the study [55] is to analyse the gear pair system by multiple pinions which are arranged parallels. The ratio of gear to load sharing index meshing frequency, bearing stiffness pinions, mounting locations of pinions, gear configuration coefficients are the factors on the load transmission behaviour of gear pair system. These are predicted by Floquetlyapunor theory and lumped parameter dynamic model.

## 8. CONCLUSIONS

In this paper reviews the various models of gears such as Spur, Helical, Hypoid gears and gear trains such as Planetary gear train setup. The main intent of this paper is to understand the various models of Spur gear such as micro pitting model, mesh interface damping model, transient elasto-hydrodynamic lubrication model and load distribution model. Surface interpolation model, shell model for hypoid gears and also to attain influence of design parameters on mechanical power losses on Spur, Helical and Hypoid gears and also give valid information what are the factors considered while design of gears and gear train system in order to achieve desired quality. However the models are used to improve the performance of a gear system and also to diminish the failure of a gear system and also gear train. From that to understand which factor has major influence on efficiency and power loss of gear drive system and also to realize which factors are majorly considered while design of gear drive system. It can be indicated that the geometric dimensions, operating condition, lubricating conditions are major influencing factors on various models of gears and gear train set up. From the literature studies carried out, the following conclusions may be inferred:

- The lubricant properties such as density, geometric parameters such as face width, module, operating condition such as temperature, rotational speed are the factors influencing on not only power loss of spur gears but also influence on tribo-dynamic behaviour of spur gears.

- Micro pitting of spur gear is depends upon the specified number of contact cycles.
- The gear module, surface roughness amplitudes are the factors influence on spur gear efficiency.
- The vibration amplitude and forced frequency response influence on surface wear of spur gear quantitatively and qualitatively.
- Surface roll angle method is more accurate and faster approach compared to conventional method.
- The tooth modifications, design parameters, Lubricant properties, Operational conditions are influence factors on efficiency of helical gears.
- Surface interpolation method is more accurate compared to semi analytical contact model.
- Surface roughness and the pinion shaft offset are factors greater influence on mechanical efficiency of hypoid gears.
- More number of Fourier components increases the accuracy of the entire gear system.
- The transmission of motion done by gear system depends on the length of gear shaft, face width, ratio betwixt pitch radii of gears and pitch radii of shafts.
- The involute mismatch and total volume crown are contribution factors on wear rate of helical gears.
- Shaft angle, shaft dimensions, bearing stiffness, hand of the gear, dimensions relevant to shafts and bearings are greatest contribution factors on dynamic behaviour of gear system.
- The co-efficient ratio of gear and excitation amplitude is influencing factors to manage vital reply of gear system.
- The rim thickness is important factor, it has more contribution on efficiency of gear train system.
- Harmonic balance method is very efficient method and accurate method compared to traditional methods.
- The archard’s wear model is used to foretell the wear rate of gear train. This method is very efficient and accurate.
- The tooth contact loss, multiple steady state solution, chaos stresses, mesh deflection, resonance condition are contribution factors on dynamic behaviour of gear train.
- The floating members are used in gear train because which are used to disqualify the errors of gear train system.
- Floquetlyapunor theory, newmark time integration scheme and lumped parameter dynamic model are used in gear train to peruse the dynamic deportment of planetary gear train system.
- Backlash, mesh stiffness and damping are contribution factors on driving behaviour of planetary gear train system

S.No	Type of gear	Gear model / Outcome	Contribution Factors on the model / Outcome
1.	<b>SPUR GEAR SYSTEM</b>	Windage power loss model	<ul style="list-style-type: none"> <li>➤ Density</li> <li>➤ Face width (Direct proportional)</li> <li>➤ Rotational Speed</li> <li>➤ Module (Direct proportional)</li> <li>➤ Temperature (Inversely proportional)</li> </ul>
2.		Spin power model	<ul style="list-style-type: none"> <li>➤ Face width (Direct proportional)</li> <li>➤ Temperature (Inversely proportional)</li> <li>➤ Dimensionless immersion parameter (Direct proportional)</li> </ul>
3.		Micro pitting model	<ul style="list-style-type: none"> <li>➤ Contact pressure</li> <li>➤ Rolling velocity</li> <li>➤ MIS</li> <li>➤ Slide to roll ratio (Direct proportional)</li> </ul>
4.		Efficiency of gear system	<ul style="list-style-type: none"> <li>➤ Module (Direct proportional)</li> <li>➤ Film thickness (Direct proportional)</li> <li>➤ Surface roughness (Inversely proportional)</li> <li>➤ Rolling action</li> </ul>
5.		Tribodynamic model	<ul style="list-style-type: none"> <li>➤ Operating condition</li> <li>➤ Surface roughness (Direct proportional)</li> <li>➤ Lubricating properties</li> </ul>
6.		Surface wear	<ul style="list-style-type: none"> <li>➤ Vibration amplitude</li> <li>➤ Forced frequency response</li> </ul>
7.		Vibration	<ul style="list-style-type: none"> <li>➤ Dynamic</li> </ul>

Table 3. Consolidation of Contribution factors on model

		of the gear system	<ul style="list-style-type: none"> <li>➤ tooth forces</li> <li>➤ Dynamic stress factors</li> </ul>			<ul style="list-style-type: none"> <li>➤ proportional) Speed (Inversely proportional)</li> </ul>
8.		Periodic time-variant model	<ul style="list-style-type: none"> <li>➤ Parametric resonance</li> <li>➤ Fourier components</li> </ul>	14.		<ul style="list-style-type: none"> <li>➤ Root stresses of gear</li> <li>➤ Lead crown</li> <li>➤ Face width</li> </ul>
9.		Transmission of motion done by gear system	<ul style="list-style-type: none"> <li>➤ Length of gear shaft</li> <li>➤ Face width</li> <li>➤ Ratio between radii of pitch of gears and radii of pitch of shaft</li> </ul>	15.		<ul style="list-style-type: none"> <li>➤ Dynamic deformation of gear system</li> <li>➤ Shaft angle</li> <li>➤ Shaft dimensions</li> <li>➤ Bearing stiffness</li> <li>➤ Hand of the gear</li> <li>➤ Other parameters with relevant to bearings and shaft</li> </ul>
10.		Crack propagation	<ul style="list-style-type: none"> <li>➤ Magnitude of frequency (Direct proportional)</li> <li>➤ Sidebands (Direct proportional)</li> </ul>	16.	<b>HYPOID GEAR SYSTEM</b>	<ul style="list-style-type: none"> <li>➤ Power loss / Efficiency</li> <li>➤ Temperature (Direct proportional to power loss, Inversely proportional to efficiency)</li> <li>➤ <math>\xi/P_t</math> ratio, <math>T_{or}</math></li> <li>➤ Surface roughness</li> <li>➤ Speed</li> <li>➤ Torque</li> </ul>
11.		Gear mesh stiffness	<ul style="list-style-type: none"> <li>➤ Tooth breakage (Direct proportional)</li> <li>➤ Spalling (Direct proportional)</li> <li>➤ Gear mesh frequency</li> <li>➤ Modulation</li> <li>➤ Sidebands</li> <li>➤ Amplitude of the system</li> </ul>	17.		<b>PLANETARY GEAR TRAIN</b>
12.		Dynamic behaviour	<ul style="list-style-type: none"> <li>➤ Co-efficient ratio of gear</li> <li>➤ Excitation amplitude</li> </ul>			
13	<b>HELICAL GEAR SYSTEM</b>	Power loss	<ul style="list-style-type: none"> <li>➤ Module (Direct proportional)</li> <li>➤ Outer diameter (Direct proportional)</li> <li>➤ Transmission error (Direct proportional)</li> <li>➤ <math>A_{wd}</math>(Direct proportional)</li> <li>➤ <math>\xi_b, \xi_t, \phi</math> (Inversely proportional)</li> <li>➤ Contact stress (Inversely proportional)</li> <li>➤ Bending stress (Inversely</li> </ul>			

			<p>proportional to bearing stiffness)</p> <ul style="list-style-type: none"> <li>➤ Mode shapes of TM</li> <li>➤ Backlash</li> <li>➤ Harmonic forcing</li> <li>➤ Damping</li> <li>➤ Ratio of gear to load sharing index</li> <li>➤ Meshing Frequency</li> <li>➤ Bearing stiffness</li> <li>➤ Mounting locations of pinions</li> <li>➤ Gear configuration coefficient</li> </ul>
18.		Surface wear	<ul style="list-style-type: none"> <li>➤ Dynamic forces (Direct proportional</li> <li>➤ Harmonic amplitude</li> </ul>

9. FUTURE RECOMMEDIATIONS:

In this paper the different models were developed for spur, helical, hypoid gears and also gear train system in account of design parameters, lubricant properties, and operating conditions, vibration analysis. It is highly recommend that the various models will develop in account of contribution of materials properties such as fatigue strength, toughness, hardness from which to understand which properties of material, play an important role in efficiency and power loss of gear system and dynamic deportment of gear train system and also taken into contribution of composite materials because of now a days composite material play an important role in industry in order to their characteristics.

REFERENCES

[1]. S Li and A Kahraman. Influence of dynamic behaviour on elastohydrodynamic lubrication of spur gears. *Tribol. Int.*, 2011 DOI: 10.1177/1350650111409517.

[2]. S Li and A Kahraman. A spur gear mesh interface damping model based on elastohydrodynamic contact behaviour. *Int. J. Powertrains*, Vol.1 No.1, 2011.

[3]. S.Li and A.Kahraman. "A mixed EHL model with asymmetric integrated control volume discretization". *Tribology International* 42 (2009) 1163–1172. DOI: 10.1016/j.triboint. 2009.03.020.

[4]. SathyaSeetharaman and AhmetKahraman. A model of wind age power loss of spur gear. *Tribol. Int.*, 2014. ISSN: 1040-2004 print .DOI 10.1080/10402000903452848.

[5]. S.Seetharaman and A.Kahraman. Load-Independent Spin Power Losses of a spur gear pair: Model Formulation. *Journal of Tribology* 2009 Vol. 131/022201-1.

[6]. Sheng Li and AhmetKahraman. A micro-pitting model for spur gear contacts. *International Journal of Fatigue* (2014) 224-233.

[7]. Sheng Li and AhmetKahraman. "Micro pitting fatigue lives of lubricated point contacts: Experiment and model validation". *International Journal of Fatigue* 48 (2013) 9–18. <http://dx.doi.org/10.1016/j.ijfatigue.2012.12.003>.

[8]. Sheng Li and AhmetKahraman. Prediction of spur gear mechanical power losses using a transient elastohydrodynamic lubrication model. *Tribology Transactions*, 53:554-563, (2010) DOI: 10.1080/10402000903502279.

[9]. S Li and A Kahraman. A tribo-dynamic model of a spur gear pair. *Journal of Sound and Vibration* 332(2013) 4963-4978.

[10]. Huali Ding and AhmetKahraman. Interactions between nonlinear spur gear dynamics and surface wear. *Journal of Sound and Vibration* 307 (2007) 662-679.

[11]. M.A.Hotait and A.Kahraman. Experiment on the relationship between the dynamic transmission error and the dynamic stress factor of spur gear pairs. *Mechanism and Machine Theory* 70 (2013) 116-128.

[12]. AlessioArtoni, Massimo Guiggiani, AhmetKahraman and Jonny Harianto. Robust optimization of gear tooth surface modification within range of torque and misalignments. *Journal of Mechanical Design* 2013, Vol.135/121005-1.

[13]. M Kolivand and A Kahraman. A General approach to locate instantaneous contact lines of gears by using surface roll angle. *Journal of Mechanical Design* 2011, Vol.133/014503-1.

[14]. Rune Pedersen, IlmarF.Santos, Iran.A.Hede has investigated on "Advantages and Drawbacks of applying periodic time-variant modal analysis to spur gear dynamics". *Mechanical Systems and Signal Processing* 24 (2010) 1495–1508.

[15]. Victor Roda – Casanova, Francisco T. Sanchez – Marin, Ignacio Gonzalez – Perez Jose L Iserte, Altonso Fuentes. "Determination of the ISO face load factor in spur gear drives by the finite element modelling of gears and shafts". *Mechanism and Machine Theory* 65 (2013) 1–13.

[16].Zaigang Chen, Yimin Shao. "Dynamic simulation of spur gear with tooth root crack propagating along tooth width and crack depth". *Engineering Failure Analysis* 18 (2011) 2149–2164.

[17].Zaigang Chen, Yimin Shao. "Mesh stiffness of an internal spur gear pair with ring gear rim deformation" *Mechanism and Machine Theory* 69 (2013) 1–12.

[18].FakherCharri, WalidBaaccar, Mohamed Slim Abbes, Mohamed Haddar. "Effect of spalling or tooth breakage on gear mesh stiffness and dynamic response of a one – stage spur gear transmission" *European Journal of Mechanics A/Solids* 27 (2008) 691–705.

- [19]. R.G. Parker, S.M. Vijayakar, T. Imanjo. "Nonlinear dynamic response of a spur gear pair: Modelling and experimental comparisons". *Journal of Sound and vibration*(2000) 237(3), 435455 DOI: 10.1006/jsvi.2000.3067.
- [20]. Yongjunshen, Shaopu Yang, Xiandong Liu. "Nonlinear dynamics of a spur gear pair with time varying stiffness and backlash based on incremental harmonic balance method". *International Journal of Mechanical Sciences* 48 (2006) 1256–1263.
- [21]. Sheng Li, AarthyVaidyanathan, Jonny Harianto and AhmetKahraman. Influence of design parameters on mechanical power losses of helical gears. *Journal of Advanced Mechanical Design, Systems and Manufacturing* Vol 3, No. 2, 2009.
- [22]. M.Hotait and A.Kahraman. Experiments on root stresses of helical gear with lead crown and misalignment. *Journal of Mechanical Design* 2008, Vol.130/074502-1.
- [23]. A. Kahraman, P. Bajpai, N.E. Anderson. "Influence of tooth profile deviations on helical gear wear". *Transactions of the ASME* Vol 127 July 2005. DOI: 10.1115/1.1899688.
- [24]. M. Kubur, A. Kahraman, D.M. Zini and K. Kienzle. "Dynamic analysis of a multi-shaft helical gear transmission by finite elements Model and Experiment". *Journal of Vibration and Acoustics* JULY 2004, Vol. 126 DOI: 10.1115/1.1760561#.
- [25]. A.Artoni, M.Kolivand and A.Kahraman. An ease-off based optimization of the loaded transmission error of hypoid gears. *Journal of Mechanical Design* 2010, Vol.132/011010-1.
- [26]. D.Park, M.Kolivand and A.Kahraman. An approximate method to predict surface wear hypoid gear using surface interpolation. *Mechanism and Machine Theory* 71 (2014) 64-78.
- [27]. M.A.Hotait, A.Kahraman and T.Nishino. An investigation of root stress of hypoid gears with misalignment. *Journal of Mechanical Design* 2011, Vol.133/071006-1.
- [28]. M.Kolivand, S.Li.Kahraman. Prediction of mechanical gear mesh efficiency of hypoid gear pairs. *Mechanism and Machine Theory* 45 (2010) 1568-1582.
- [29]. M.Kolivand, A.Kahraman. A load distribution model for hypoid gears using ease-off topography and shell theory. *Mechanism and Machine Theory* 44 (2009) 1848-1865.
- [30]. J.J. Yang, H. Zhang, X.Z. Deng, B.Y. Wei. "Ultrasonic lapping of hypoid gear: system design and experiments". *Mechanism and Machine Theory* 65 (2013) 71–78.
- [31]. Ma Ru Kang and AhmetKahraman. "Measurement of vibratory motions of gears supported by compliant shafts". *Mechanical Systems and Signal Processing* 29 (2012) 391–403.
- [32]. J. Hong, D.Talbot, A.Kahraman. "A semi analytical load distribution model for side-fit involute splines". *Mechanism and Machine Theory* 76 (2014) 39–55.
- [33]. Sheng Li and AhmetKahraman. "A fatigue model for contacts under mixed elastohydrodynamic lubrication condition". *International Journal of Fatigue* 33 (2011) 427–436 DOI:10.1016/j.ijfatigue.2010.09.021.
- [34]. PrashantSondkar and AhmetKahraman. "A dynamic model of a double helical planetary gear set". *Mechanism and Machine Theory* 70 (2013) 157–174http://dx.doi.org/10.1016/j.mechmachtheory.2013.07.005.
- [35]. H. Xu, A. Kahraman, N.E. Anderson, D.G. Maddock. "Prediction of Mechanical efficiency of parallel-Axis gear pairs". *Journal of Mechanical Design* JANUARY 2007, Vol. 129 DOI: 10.1115/1.2359478.
- [36]. J. Hong, D. Talbot, A. Kahraman. "Load distribution analysis of clearance-fit spline joints using finite elements". *Mechanism and Machine Theory* 74 (2014) 42–57. http://dx.doi.org/10.1016/j.mechmachtheory.2013.11.007.
- [37]. A.Kahraman, H.Ligata, A. Singh. "Influence of ring rim thickness on planetary gear set behavior". *Journal of Mechanical Design* FEBRUARY 2010, Vol. 132 / 021002 DOI: 10.1115/1.4000699.
- [38]. H. Ligata, A. Kahraman and A. Singh. "An Experimental study of the influence of Manufacturing errors on the planetary gear stresses and planet load sharing". *Journal of Mechanical Design*. APRIL 2008, Vol. 130 / 041701. DOI: 10.1115/1.2885194.
- [39]. A AI-Shyyab and A Kahraman. "A nonlinear dynamic model for planetary gear sets" *Proc. IMechE* Vol. 221 Part K: J. Multi-body Dynamics JMBD92 © IMechE 2007 DOI: 10.1243/14644193JMBD92.
- [40]. A AI-Shyyab and A Kahraman. "Non-linear dynamic analysis of a multi-mesh gear train using multi-term harmonic balance method: period-one motions". *Journal of Sound and Vibration* 284 (2005) 151–172. DOI:10.1016/j.jsv.2004.06.010.
- [41]. M. Inalpolat, A. Kahraman. "A theoretical and experimental investigation of modulation side bands of planetary gear sets". *Journal of Sound and Vibration* 323 (2009) 677–696. DOI: 10.1016 /j.jsv. 2009.01.004.
- [42]. A. Kahraman and H. Ding. "A Methodology to Predict Surface Wear of PlanetaryGears under Dynamic Conditions". *Mechanics Based Design of Structures and Machines: An International Journal*, 38:4, 493-515, DOI:10.1080/15397734.2010.501312.
- [43]. C. Yuksel and A. Kahraman. "Dynamic tooth loads of planetary gear sets having tooth profile". *Mechanism and Machine Theory* 39 (2004) 695–715. DOI:10.1016/j.mechmachtheory.2004.03.001.
- [44]. A Kahraman, H. Ligata, K. Kienzle, D.M. Zini. "A Kinematics and Power flow analysis methodology for automatic transmission planetary gear trains". *Journal of Vibration and Acoustics* JULY 2004, Vol. 126 DOI: 10.1115/1.1760561#.
- [45]. Zaigang Chen, Yiminshao and Daizhong Su "Dynamic simulation of planetary gear set with flexible spur ring gear" *Journal of Sound and Vibration* 332 (2013) 7191–7204.
- [46]. VijayakumarAmbarisha and Robert G. Parker has a presented a paper on "Nonlinear dynamics of

planetary gears using analytical and FEA model”. Journal of Sound and Vibration 302 (2007) 577–595.

[47]. Tristan M. Ericson, Robert G. Parker. “Planetary gear model vibration experiments and correlation against lumped parameter and finite element models”. Journal of Sound and Vibration 332 (2013) 2350–2375.

[48]. Zaigang Chen, Yimin Shao. “Dynamic simulation of planetary gear with root crack in ring gear”. Engineering Failure Analysis 31 (2013) 8–18.

[49]. X. Gu and P. Velex, “A model to study influence of planet position errors in planetary gears”. Journal of Sound and Vibration 331 (2012) 4554–4574.

[50]. Woohyung Kim, JiYeong Lee, Jintai Chung. “Dynamics analysis for a planetary gear with time varying pressure angles and contact ratios”. Journal of Sound and Vibration 331 (2012) 883–901.

[51]. Zhonghong Bu, Geng Liu, Liyan Wu. “Modal analyses of herringbone planetary gear train with journal bearing” Mechanism and Machine Theory 54 (2012) 99–115.

[52]. X. Gu and P. Velex “The dynamic simulation of eccentricity errors in planetary gears”. Mechanism and Machine Theory 61 (2013) 14–29.

[53]. Avinash Sign. “Load sharing behaviour in epicyclic gears: physical explanation and generalized formulation”. Mechanism and Machine Theory 45 (2010) 511-530.

[54]. S. Theodossiades and S. Natsiavas. “Nonlinear dynamics of gear pair systems with periodic stiffness and backlash” Journal of Sound and vibration (2000) 229(2), 287310 Article No. jsvi.1999.2490.

[55]. Haidong Yu, Peter Eberhard, Yong Zhao, Haowang. “Sharing behaviour of load transmission on gear pair systems actuated by parallel arrangements of multiple pinions”. Mechanism and Machine Theory 65 (2013) 58–70.

## NONMENCLATURE

A	= Area
B	= Excluded area
b	= Gear face width
C	= Friction drag coefficient
c	= Specific heat
F	= Drag force
H	= Control volume
h	= Immersion depth
$\bar{h}$	= Dimensionless immersion parameter
L	= Length parameter along gear faces
M	= Gear rotational position index
m	= Gear module
n	= Number of teeth of gear
$\bar{n}$	= Unit normal vector
P	= Power loss
p	= Pressure
Q	= Cavity area
r	= Gear radius

T=Temperature

t=Time

U = Free-stream velocity

V = Volume

v =Velocity

x = Axis parallel to gear face

y = Axis perpendicular to gear face

$\delta$  = Boundary layer thickness

$\theta$  = Angle, tangential direction

$\mu$  = Viscosity

$\rho$  = Density

$\tau$  = Shear stress

$\varphi$  = Immersion angle

$\Omega$  = Rotational speed in rpm and rad/s

$\xi$  = Rolling power loss

## Subscripts

*b* = Backlash

*c* = Cavity, circumference

*d* = Drag

*e* = End

*f* = Face

*i* = Gear index

*m* = Rotational position

*o* = Outside

*p* = Periphery, pitch line or pocketing

*s* = Specified number of contact cycles

T = Total

v = Constant volume

w = Wind age

$\infty$  = Ambient

## Superscripts

*m* = Rotational position

*L* = Laminar

*T* = Turbulent

*r* = Radial

$\theta$  = Tangential

# Application of Optimization Algorithm for Composite Laminate Optimization

A.Karthikeyan, Asso. Prof., Department of Aeronautical Engineering, Excel Engineering College, Tamil Nadu, kas01@rediffmail.com

Dr.A.Karthikeyan, Professor, Department of Mechanical Engineering, Malla Reddy College of Engineering, Secunderabad, Telangana State, karthirajme@gmail.com

Dr.K.Venkatesh Raja, Asso. Prof, Department of Mechanical Engineering, VSA Group Of Institutions, Tamil Nadu, kvenkateshrraja@hotmail.com

S.Karthi, Asst. Professor, Department of Aeronautical Engineering, Excel Engineering College, Tamil Nadu, [kcg.karthi@gmail.com](mailto:kcg.karthi@gmail.com)

## Abstract

*In this project composite laminate optimization code was developed using genetic algorithm in ANSYS APDL code. Now a day's composite material widely used in many industries like aerospace, automobile, marine, structural industries and many more, due to high strength to weight ratio. The main objective of this research is economically use the composite material by optimization techniques. The strength of the Laminated structures is depends upon the fiber angle, thickness, material, sequence of layer and no of layer. To find the optimized combination of above parameter is very difficult by traditional methods, it may struck in to local optimum. To avoid the above difficulties global searching algorithm like genetic algorithm were used.*

## Keywords:

*Laminate optimization, Genetic algorithm, Structural optimization.*

## I. INTRODUCTION

Composite materials have received substantial attention as manufacturing materials. Although the high stiffness-to-weight and strength-to-weight properties of composite materials are attractive, their greatest advantage is their ability to be designed to satisfy directional strength and stiff nesses for any particular loading, or multi-loading, of the structure. In laminated composite structures, each ply has its greatest stiffness and strength properties, along the direction, through which the fibers are oriented in. By orienting each layer at different angles, the structure can be designed for a specific loading environment. Along with structural performance and weight, cost is an area of great interest when considering optimization studies in structural design. Obviously, reducing the amount of material required for the structure, minimizes the cost of a laminate composite. However, another method for cost reduction is to allow more than one material in the The design of optimal composite laminates has been shown to be well suited to the defining characteristics of genetic algorithms. Techniques for improving the efficiency of this methodology have been explored for several problems using local improvement, memory, migration, and varied selection schemes [13]. For large structures, such as the design of a wing or fuselage, the optimization is divided into smaller, tractable, sub problems using predefined local loads to constrain the optimization [13], [1], [9]. Isolated local optimization results in widely varying stacking sequence orientations between adjacent panels that causes serious manufacturing difficulties and, hence, generates the need for a globally blended solution. [7] Design of a fiber-reinforced composite laminate requires the specification of the stacking sequence, which is defined by the

stacking sequence. Thus, it is possible to use layers of low cost material at locations, in the structure, where performance is less important. In general, the problem of composite laminate stacking sequence optimization has been formulated as a continuous design problem, and solved using gradient based techniques. These methods of solution present several disadvantages: [2]Stacking sequence design often involves design variables, which are limited to small discrete sets of values of ply thickness, orientation angle or material type, due to manufacturing or cost limitations, therefore, these methods require the transformation of these variables into continuous variables, in order that a solution might be obtained,[3]Converting the continuous solutions back to discrete feasible values, often produces sub-optimal, or even infeasible designs,[4]Composite laminate design problems often have discontinuous objective functions, exhibiting multiple designs with similar performances, involving many local optimum designs. Genetic Algorithms are suitable optimization algorithms for problems with discrete design variables. Its implementation does not require any evaluation of gradients which, together with its easiness of implementation, make it worthwhile investigating. [5]Although, Genetic Algorithms require many function evaluations, which reflect in large computational costs, there are many reported applications of Genetic Algorithms to the design of composite structures. Genetic algorithms have been applied to stacking sequence optimization of composite plates, (Callahan and Weeks, 1992), to stiffened composite panel design (Nagendra et al., 1996), design of laminated composite panels (Hajela,1990) (Leung and Nevill, 1994) (Fernandes et al., 1998)(Haftka, 1998).

orientation and material type of each ply layer, creating a discrete optimization problem. It is computationally expensive to design an entire wing or fuselage structure with the panels optimized simultaneously. Instead, local panels are commonly optimized for the specified local loads by ignoring the possible continuity of some or all of the layers from one panel to another across the structure[8]. Soremekun et al. [18] introduced multiple elitist selection schemes that by nature aid in discovering alternative designs with similar fitness values. In a standard elitist selection strategy only a single member of a parent population can survive the selection process without being modified and be placed in the child population. [12] In a multiple elitist selection strategy the genetic algorithm allows a greater number of high fitness members to survive the selection process at each

generation. Application of GAs for optimization of composite structures was reported by Hajela (1989, 1990). Callahan and Weeks (1992) used a GA to maximize strength and stiffness of a laminate under in-plane and flexural loads. Labossiere and Turkkan (1992) used a GA and neural networks for optimization of composite materials. Haftka, Watson, Gurdal and their coworkers (Nagendra et al., 1992; Le Riche and Haftka, 1993; Nagendra et al., 1993a,b; Gurdal et al., 1994; Le Riche, 1994; Soremekun, 1997) have developed specialized GAs for stacking sequence optimization of composite laminates under buckling and strength constraints. Sargent et al. (1995) compared GAs to other random search techniques for strength design of laminated plates. [10] The applications of GA methods in the field of composite structure optimization include the weight minimization of stiffened panels and shells (Harrison et al., 1995, Nagendra et al., 1996; Kallassy and Marcelin, 1997; Jaunky et al., 1998, Kaletta and Wolf, 2000; Gantovnik et al., 2003b; Kang and Kim, 2005), the strength optimization of plates with open holes (Todoroki et al., 1995, Sivakumar et al., 1998), the improvement of the energy absorption capability of composite structures (Woodson et al., 1995, Averill et al., 1995; Crossley and Laananen, 1996), [11] the optimization of sandwich-type composite structures (Malott et al., 1996, Kodiyalam et al., 1996; Wolf, 2001; Gantovnik et al., 2002b; He and Aref, 2003; Lin and Lee, 2004), the optimization of dimensional and thermal buckling stability under hygrothermal loads (Le Riche and Gaudin, 1998; Spallino and Thierauf, 2000), the strain energy minimization of laminated composite plates and shells (Potgieter and Stander, 1998), maximizing the fundamental frequency of the laminated composite structure (Sivakumar et al., 1998), the stacking sequence blending of multiple composite laminates (Soremekun et al., 2001, 2002; Adams et al., 2003; Seresta et al., 2004; Adams et al., 2004), the optimization of electromagnetic absorption in laminated composite structures (Matous and Dvorak, 2003), the optimization of composite structures considering mechanical performance and manufacturing cost (Park et al., 2004), the optimization of composite tire reinforcement (Abe et al., 2004), [14] the optimization of composites against impact induced failure (Rahul et al., 2005). A GA is a powerful technique for search and optimization problems with discrete variables, and is therefore particularly useful for optimization of composite laminates. However, to reach an optimal solution with a high degree of confidence typically requires a large number of function evaluations during the optimization search. Performance of GAs is even more of an issue for problems with mixed integer design variables. [15] Several studies have concentrated on improving the reliability and efficiency of GAs. The proposed project is the extension of the study by Kogiso et al. (1994b,a), [16] where, in order to reduce the computational cost, the authors used memory and local improvements so that information from previously analyzed design points is utilized during a search. In the first approach a memory binary tree was employed for a

composite panel design problem to store pertinent information about laminate designs that have already been analyzed (Kogiso et al., 1994b). After the creation of a new population of designs, the tree structure is searched for either a design with identical stacking sequence or similar performance, such as a laminate with identical in-plane strains. Depending on the kind of information that can be retrieved from the tree, the analysis for a given laminate may be significantly reduced or may not be required at all. The second method is called local improvement

## II. GENETIC ALGORITHM OVERVIEW

Genetic algorithms are robust, stochastic and heuristic optimization methods based on biological evolution process. There are several optimization techniques that are used in the context of engineering design optimization. Genetic algorithm is one such technique and is a search strategy based on the rules of natural genetic evolution. The standard genetic algorithm proceeds as follows: an initial population of individuals is generated at random. Every evolutionary step, known as a generation, the individuals in the current population are decoded and evaluated according to some predefined quality criterion, referred to as fitness function. To form a new population (the next generation), individuals are selected according to their fitness. Selection alone cannot introduce any new individuals into the population, i.e. it cannot find new points in the search space. These are generated by genetically-inspired operators, of which the most well known are crossover and mutation. Crossover is performed with crossover probability between two selected individuals. The mutation operator is introduced to prevent premature convergence to local optima by randomly sampling new points in the search space. Genetic algorithms are stochastic iterative processes that are not guaranteed to converge; the termination condition may be specified as some fixed maximal number of generations or as the attainment of an acceptable fitness level.

### *Genetic operators*

Establishing the GA parameters is very crucial in an optimization problem because they greatly affect the performance of a GA [6]. The genetic algorithm contains several operators, e.g. reproduction, crossover and mutation.

#### *(a) Reproduction*

The reproduction operator allows individual strings to be copied for possible inclusion in the next generation. After assessing the fitness value for each string in the initial population, only a few strings with a high fitness value are considered in their production. There are many different types of reproduction operators including proportional selection, tournament selection, ranking selection, etc. In this study, tournament selection is selected, since it has better convergence and computational time compared to any other reproduction operator (Deb, 1999). In tournament selection, two individuals are chosen from the population at random,



3. Single crossover with left to right cross shifting
  4. Single crossover with right to left cross shifting
- The best results from above four operations are stored.

**(c) Mutation**

The best sequence from previous iteration was selected based on high fitness. In this process variables are randomly exchange in between the single sequence itself. It is shown in below

Sequence1		After Mutation
Before Mutation		1 3 <u>5</u> 2 <u>4</u>
1 3 4 2 5		

The above process is repeated for all best sequences and result was stored.

**(d) Addition**

The best sequence from previous iteration was selected based on high fitness. In this process variables are added randomly in the best sequence It is shown in below

Sequence1		After Addition
Before Addition		1 3 4 2 5 <u>2</u> <u>3</u>
1 3 4 2 5		

The above process is repeated for all best sequences and result was stored.

**(e) Deletion**

The best sequence from previous iteration was selected based on high fitness. In this process variables are deleted randomly in the best sequence It is shown in below

Sequence1		After Deletion
Before Deletion		1 3 2 5
1 3 4 2 5		

The above process is repeated for all best sequences and result was stored.

**(f) Alteration**

The best sequence from previous iteration was selected based on high fitness. In this process variables are altered randomly in the best sequence It is shown in below

Sequence1		After Alteration
Before Alteration		1 3 <u>2</u> 2 5
1 3 4 2 5		

The above process is repeated for all best sequences and result was stored. This is called one generations.

Finally the overall best result from above six operations was plotted and stored. The same process was repeated for 50 numbers of generations. The optimization algorithm is shown in following Fig 1.

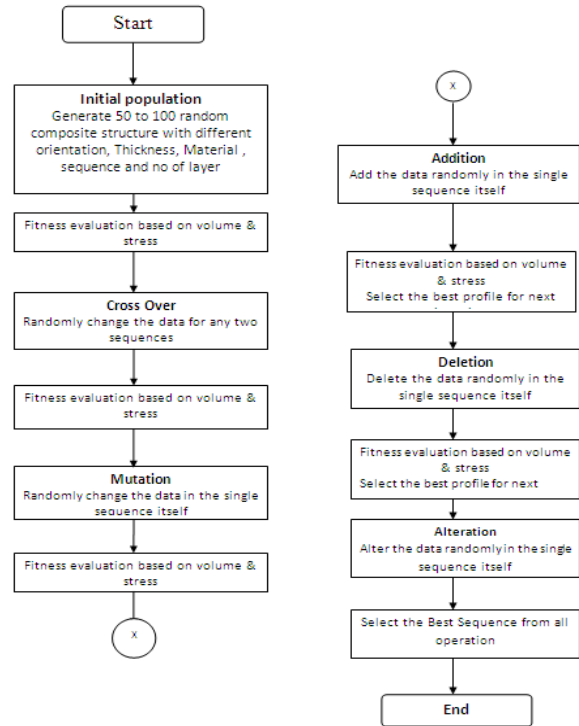


Figure 1. Genetic Algorithm for composite laminate optimization

**V. CASE STUDIES**

Genetic algorithm successfully implemented in following practical problems. The details of the inputs are shown below

1. Number of Material
2. Maximum Number of layer
3. Number of thickness
4. Number of angle
5. Loading & Boundary conditions
6. Model imported / created
7. Number of generations

All problems considered with following material properties  $E_1= 10,000 \text{ N/mm}^2$ ,  $E_2= 10,000 \text{ N/mm}^2$ ,  $E_3= 250,000 \text{ N/mm}^2$ ,  $\mu_{12}=0.25$ ,  $\mu_{23}=0.01$ ,  $\mu_{31}=0.25$ ,  $G_{12}=2000 \text{ N/mm}^2$ ,  $G_{23}=5000 \text{ N/mm}^2$ ,  $G_{31}=5000 \text{ N/mm}^2$ ,  $\rho=7850 \text{ Kg/mm}^3$

**4.1 Plate with hole**

A plate is subjected to biaxial load (1000 N) as shown in Figure 2. Following inputs were used

1. Number of Material =1
2. Maximum Number of layer (N) =8
3. Number of thickness =1 (2mm)
4. Number of angle =2 (45,-45)
5. Number of generations =50

The best results obtained in the 35<sup>th</sup> iteration as shown in below table 1

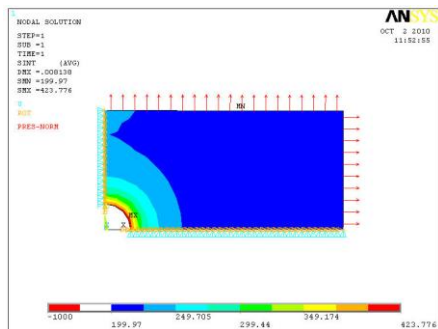


Figure. 2a

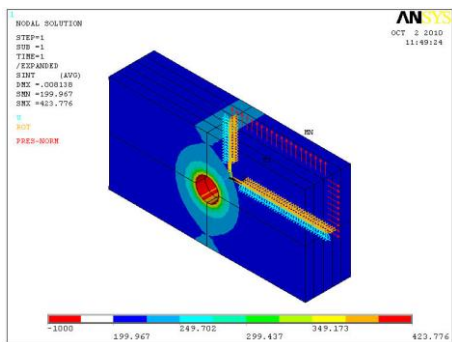


Figure. 2b

Figure 2a,b. Optimized stress distribution of plate with hole

4.2 Bumper with front & side load

A bumper is subjected to biaxial load (10000 N) as shown in Fig. 3. Following inputs were used

1. Number of Material =1
2. Maximum Number of layer (N) =4
3. Number of thickness =1 (3mm)
4. Number of angle =3 (0,45,90)
5. Number of generations = 50

The best results obtained in the 23<sup>rd</sup> iteration as shown in below table 2.

Table 1.Optimum results at 35<sup>th</sup> iteration

GA operators	Number Of Layer	Material	Thickness	Angle	Stress N/mm <sup>2</sup>	Volume mm <sup>3</sup>
Reproduction	4	1,1,1,1	2,2,2,2	45,-45,-45,45	528.77	10222.43
Cross over	5	1,1,1,1,1	2,2,2,2,2	-45,45,45,-45,-45	423.02	12303.65
Mutation	5	1,1,1,1,1	2,2,2,2,2	-45,45,45,-45,-45	423.02	12303.65
Addition	5	1,1,1,1,1	2,2,2,2,2	-45,45,45,-45,-45	423.02	12303.65
Deletion	5	1,1,1,1,1	2,2,2,2,2	-45,45,45,-45,-45	423.02	12303.65
Alteration	5	1,1,1,1,1	2,2,2,2,2	-45,45,45,-45,-45	423.02	12303.65

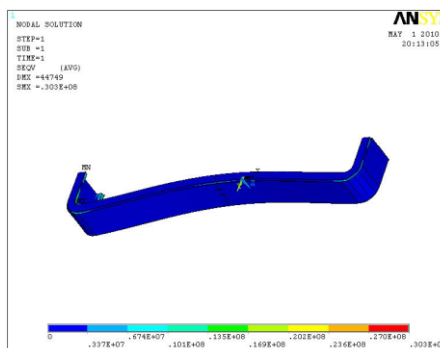
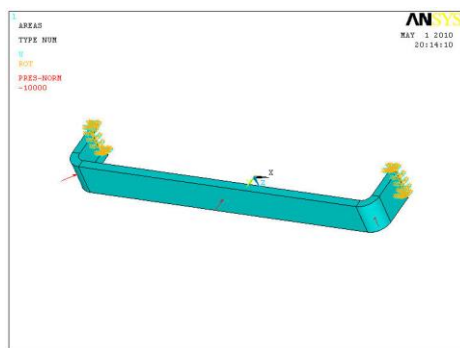


Figure 3a,b. Bumper Model and Optimized stress distribution of plate with hole

Table 2. Optimum results at 23<sup>rd</sup> iteration

GA operators	Number Of Layer	Material	Thickness	Angle	Stress N/mm <sup>2</sup>	Volume mm <sup>3</sup>
Reproduction	4	1,1,1,1	3,3,3,3	0,45,90,0	4.567e7	504323.33
Cross over	3	1,1,1	3,3,3	45,0,90	3.03e7	402442.22
Mutation	3	1,1,1	3,3,3	45,0,90	3.03e7	402442.22
Addition	3	1,1,1	3,3,3	45,0,90	3.03e7	402442.22
Deletion	3	1,1,1	3,3,3	45,0,90	3.03e7	402442.22
Alteration	3	1,1,1	3,3,3	45,0,90	3.03e7	402442.22

4.3 Hollow Shaft with Twisting Load

A hollow shaft is subjected twisting load of 1000 N as shown in Fig. 4. Following inputs were used

- Number of Material =1
- Maximum Number of layer (N) =6
- Number of thickness =1 (2mm)
- Number of angle =2 (45,-45)
- Number of generations =50

The best results obtained in the 45<sup>th</sup> iteration as shown in below table 3.

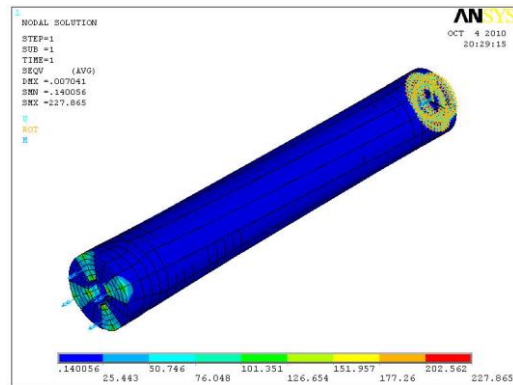


Figure. 4b

Figure 4a,b. Hollow shaft with twisting load and optimum Stress results

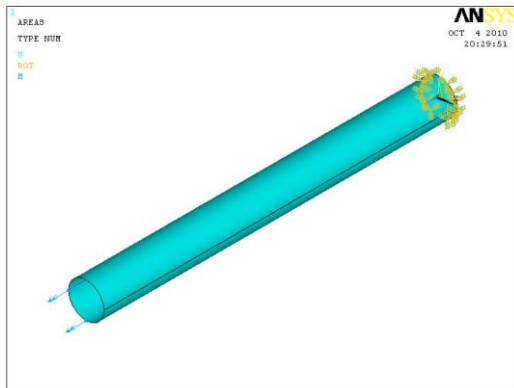


Figure. 4a

Table 3. Optimum results at 45<sup>th</sup> iteration

GA operators	Number Of Layer	Material	Thickness	Angle	Stress N/mm <sup>2</sup>	Volume mm <sup>3</sup>
Reproduction	6	1,1,1,1,1,1	2,2,2,2,2,2	45,-45,45,45,-45,45	354.44	7023432.43
Cross over	5	1,1,1,1,1	2,2,2,2,2	-45,45,-45,45,-45	227.645	6283185.154
Mutation	5	1,1,1,1,1	2,2,2,2,2	-45,45,-45,45,-45	227.645	6283185.154
Addition	5	1,1,1,1,1	2,2,2,2,2	-45,45,-45,45,-45	227.645	6283185.154
Deletion	5	1,1,1,1,1	2,2,2,2,2	-45,45,-45,45,-45	227.645	6283185.154
Alteration	5	1,1,1,1,1	2,2,2,2,2	-45,45,-45,45,-45	227.645	6283185.154

4.4 Plate with bending Load(M<sub>y</sub>)

A plate is subjected to bending load 1000 N in Y axis as shown in Fig. 5. Following inputs were used

- Number of Material =1
- Maximum Number of layer (N) =4
- Number of thickness=1 (2mm)
- Number of angle =2 (0,90)
- Number of generations =50

The best results obtained in the 33<sup>rd</sup> iteration as shown in below table 4.

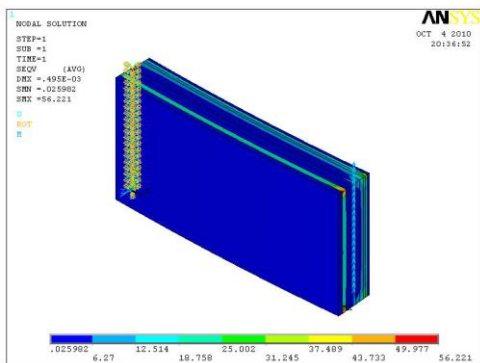


Figure. 5a

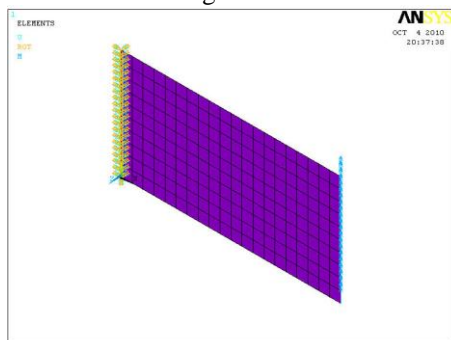


Figure. 5b

Figure 5a,b. Plate with bending load and optimum Stress results

4.5 Box with pressure Load

A Box is subjected to bending load 1000 N as shown in Fig. 6. Following inputs were used

1. Number of Material =1
2. Maximum Number of layer (N)=4
3. Number of thickness =2 (2mm,1mm)
4. Number of angle=2 (0,45)
5. Number of generations=50

The best results obtained in the 40<sup>th</sup> iteration as shown in below table 5.

Table 4.Optimum results at 33<sup>rd</sup> iteration

GA operators	Number Of Layer	Material	Thickness	Angle	Stress N/mm <sup>2</sup>	Volume mm <sup>3</sup>
Reproduction	4	1,1,1,1	2,2,2,2	0,90,90,0	75.33	6750000
Cross over	4	1,1,1,1	2,2,2,2	0,90,0,90	56.221	6250000
Mutation	4	1,1,1,1	2,2,2,2	0,90,0,90	56.221	6250000
Addition	4	1,1,1,1	2,2,2,2	0,90,0,90	56.221	6250000
Deletion	4	1,1,1,1	2,2,2,2	0,90,0,90	56.221	6250000
Alteration	4	1,1,1,1	2,2,2,2	0,90,0,90	56.221	6250000

Table 5.Optimum results at 40<sup>th</sup> iteration

GA operators	Number Of Layer	Material	Thickness	Angle	Stress N/mm <sup>2</sup>	Volume mm <sup>3</sup>
Reproduction	4	1,1,1,1	2,3,2,3	0,45,0,45	208322	10000000
Cross over	4	1,1,1,1	2,3,2,3	0,45,0,45	208322	10000000
Mutation	4	1,1,1,1	2,3,2,3	0,45,0,45	208322	10000000
Addition	4	1,1,1,1	2,3,2,3	0,45,0,45	208322	10000000
Deletion	4	1,1,1,1	2,3,2,3	0,45,0,45	208322	10000000
Alteration	4	1,1,1,1	2,3,2,3	0,45,0,45	208322	10000000

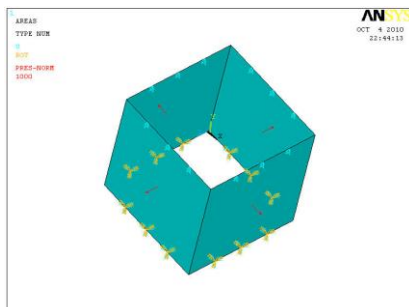


Figure. 6a

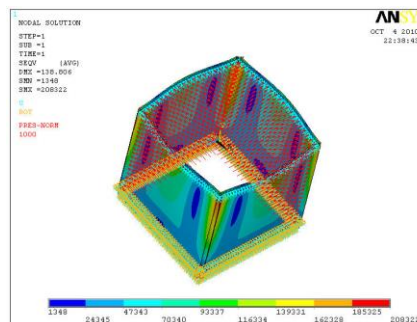


Figure. 6b

Figure 6a,b. Box subjected to pressure load and optimum Stress results

### CONCLUSION:

The global optimized genetic algorithm plays major role in composite optimization. The above algorithm can be applicable for any type of problems with known loading and boundary conditions. Further the computation time will be reduced by using cluster based optimization i.e. many computers simultaneously involved in optimization process. In future this work may be extended to failure criteria approach and dynamic problems.

### REFERENCES

- [1] Schmit LA, Farshi B". Optimum laminate design for strength and stiffness". *Int J Numer Meth Eng*,7(4),519–36, 1973
- [2] Fukunga H, Vanderplaats GN. "Strength optimization of laminated composites with respect to layer thickness and/or layer orientation angle". *Comput Struct* 40(6),1429–39, 1991.
- [3] Adali S, Richter A, Verijenko VE. "Optimization of shear-deformable laminated plates under buckling and strength criteria". *Compos Struct*, 39(3–4):,67–78, 1997.
- [4] Abu-Odeh AY, Jones HL. "Optimum design of composite plates using response surface method", *Compos Struct* 43(3),233–42, 1998,
- [5] Park JH, Hwang JH, Lee CS, Hwang W. "Stacking sequence design of composite laminates for maximum strength using genetic algorithms", *Compos Struct*,52(2):217–31,2001,
- [6] Sciava MD, Gherlone M, Lomario D. "Multiconstrained optimization of laminated and sandwich plates using evolutionary algorithms and higher-order plate theories", *Compos Struct*;59(1),149–54, 2003.
- [7] Farshi B, Herasati S. "Optimum weight design of fiber composite plates in flexure based on a two level strategy", *Compos Struct* ,73(4):,95–504. 2006.
- [8] Muc A, Gurba W. "Genetic algorithms and finite element analysis in optimization of composite structures", *Compos Struct* ,54(2–3),,275–81 ,2001.
- [9] Walker M, Smith RE. "A technique for the multiobjective optimisation of laminated composite structures using genetic algorithms and finite element analysis" *Compos Struct*,62(1),123–8, 2003.
- [10] Kere P, Lyly M, Koski J. "Using multicriterion optimization for strength design of composite laminates", *Compos Struct*,62(3–4),329–33, , 2003.
- [11] Ganguli R, Chopra I. "Aeroelastic optimization of a helicopter rotor with composite coupling", *J Aircraft* 32(6),1326–34,1995.
- [12] Ganguli R, Chopra I."Aeroelastic optimization of a helicopter rotor with two-cell composite blades", *AIAA J*,34(4),835–41, 1996.
- [13] Ganguli R, Chopra I. "Aeroelastic tailoring of composite couplings and blade geometry of a helicopter rotor using optimization methods" *J Am Helicopter Soc*, 42(3),218–28. 1997.
- [14] Murugan MS, Ganguli R. "Aeroelastic stability enhancement and vibration suppression in a composite helicopter rotor", *J Aircraft* ,42(4),1013–24, 2005.
- [15] Smith EC, Chopra I. "Formulation and evaluation of an analytical model for composite box-beams", *J Am Helicopter Soc* 36(3), 23–5, 1991.
- [16] Ferrero JF, Barrau JJ, Segura JM, Sudre M, Castanie B. "Analytical theory for an approach calculation of non-balanced composite box beams" *Thin-Walled Struct* , 39(8),709–29, 2001.

# Traveling Salesman Problem for Visiting 10 Tamil Nadu Cities Using Genetic Algorithm

A.Karthikeyan, *Asso. Professor, Department of Aeronautical Engineering, Excel Engineering College, Tamil Nadu,*  
kas01@rediffmail.com

Dr.A.Karthikeyan, *Professor, Department of Mechanical Engineering, Malla Reddy College of Engineering, Telangana State,*  
karthirajme@gmail.com

Dr.K.Venkatesh Raja, *Asso. Prof, Department of Mechanical Engineering, VSA Group Of Institutions, Tamil Nadu.*  
kvenkateshrraja@hotmail.com

S.Karhi, *Asst. Professor, Department of Aeronautical Engineering, Excel Engineering College, Tamil Nadu.*  
kcg.karhi@gmail.com

## Abstract

**The main objective of this paper is to find the shortest path for visiting 10 cities in Tamil Nadu using genetic algorithm. Genetic algorithms are an evolutionary technique that use crossover and mutation operators to solve optimization problems using a survival of the fittest idea. They have been used successfully in a variety of different problems, including the traveling salesman problem. In the traveling salesman problem we wish to find a tour of all nodes in a weighted graph so that the total weight is minimized. The traveling salesman problem is NP-hard but has many real world applications so a good solution would be useful.**

*Key words: Traveling Salesman problem, Genetic algorithm, cites.*

## I. INTRODUCTION

The origins of the Traveling salesman problem are unclear. A handbook for Traveling salesmen from 1832 mentions the problem and includes example tours through Germany and Switzerland, but contains no mathematical treatment. Mathematical problems related to the Traveling salesman problem were treated in the 1800s by the Irish mathematician W. R. Hamilton and by the British mathematician Thomas Kirkman. Hamilton's Icosian Game was a recreational puzzle based on finding a Hamiltonian cycle. The general form of the TSP appears to have been first studied by mathematicians during the 1930s in Vienna and at Harvard, notably by Karl Menger, who defines the problem, considers the obvious brute-force algorithm, and observes the non-optimality of the nearest neighbor heuristic. Richard M. Karp showed in 1972 that the Hamiltonian cycle problem was NP-complete, which implies the NP-hardness of TSP.

This supplied a scientific explanation for the apparent computational difficulty of finding optimal tours. Great progress was made in the late 1970s and 1980, when Grötschel, Padberg, Rinaldi and other managed to exactly solve instances with up to 2392 cities, using cutting planes and branch-and-bound. In the 1990s, Applegate, Bixby, Chvátal, and Cook developed the program Concorde that has been used in many recent record solutions. Gerhard Reinelt published the TSPLIB in 1991, a collection of benchmark instances of varying difficulty, which has been used by many research groups for comparing results. In 2005, Cook and others computed an optimal tour through a 33,810-city instance given by a microchip layout problem, currently the largest solved TSPLIB instance. For many other instances with millions of cities, solutions can be found that are provably within 1% of optimal tour.

The Traveling Salesman Problem is well-known among NP-hard combinatorial optimization problems[1]. It represents a class of problems which are analogous to finding the least-cost sequence for visiting a set of cities, starting and ending at the same city in such a way that each city is visited exactly once. The desire of economy, in which least time span or least distance are also significant for a decision maker, ultimately poses TSP as a multi-objective problem. In TSP as a Multi-Objective Combinatorial Optimization Problem, each objective function is represented in a distinct dimension. Of this form, to decide the multi objective TSP in the optimality means to determine the k-dimensional points that pertaining to the space of feasible solutions of the problem and that possess the minimum possible values according to all dimension.

The permissible deviation from a specified value of a structural dimension is also considerable because Amna Rehmat, Hina Saeed, Muhammad Shahzad Cheema Pak.j.stat.oper.res. Vol.88 1.III No.2 2007 pp87-98 traveling sales man can face a situation in which he is not able to achieve his objectives completely. There must be a set of alternatives from which he can select one that best meets his aspiration level. Conventional programming approaches does not deal with this situation however some researches have specifically treated the multi-objective TSP. Fischer and Richter (1982) used a branch and bound approach to solve a TSP with two (sum) criteria. Gupta and Warburton (1986) used the 2- and 3-opt heuristics for the maxordering TSP. Sigal (1994) proposed a decomposition approach for solving the TSP with respect to the two criteria of the route length and bottlenecking, where both objectives are obtained from the same cost matrix. Tung (1994) used a branch and bound method with a multiple labeling scheme to keep track of possible Pareto optimal tours. Melamed and Sigal (1997) suggested an e-constrained based algorithm for bi-objective TSP. Ehrgott (2000) proposed an approximation algorithm with worst case performance bound. Hansen (2000) applied the tabu search algorithm to multi objective TSP. Borges and Hansen (2002) used the weighted sums program to study the global convexity for multi-objective TSP. Jaszkiwicz (2002) proposed the genetic local search which combines ideas from evolutionary algorithms, local search with modifications of the aggregation of the objective functions. Paquete and Stützle (2003) proposed the two-phase local search procedure to tackle bi-objective TSP. During the first phase, a good solution to one single objective is found by using an effective single objective algorithm. This solution provides the starting point for the second phase, in which a local search algorithm is applied to a sequence of different aggregations of the objectives, where each aggregation converts the bi-objective problem into a single objective one. Yan et al (2003) used an evolutionary algorithm to solve multi objective TSP. Angel, Bampis and Gourvès (2004) proposed the dynasearch algorithm which uses local search with an exponential sized neighborhood that can be searched in polynomial time using dynamic programming and a rounding technique. Paquete, Chiarandini and Stützle (2004)

suggested a Pareto local search method which extends local search algorithm for the single objective TSP to bi-objective case. This method uses an archive to hold non-dominated solutions found in the search process. There are several practical uses for this problem [2], such as vehicle routing with the additional constraints of vehicle's route, such as capacity of vehicles (Laporte,1992), drilling problems (Onwubolu, 2004), minimize waste(Grafinkel,1977), clustering data arrays (McCormick et al.,1972),X-ray crystallography(Bland et al.,1989), Shot Sequence Generation for Scan Lithography (Shinano et al., 2008) and many others. This problem has also been used during the last years as a comparison basis for improving several optimization techniques, such as genetic algorithms (Affenzeller, 2003), simulated annealing (Budinich, 1996)), Tabu search (Liu, 2003), local search (Bianchi, 2005), ant colony (Chu, 2004) and Branch and Bound (B&B). The principal types of B&B used to solve the TSP are: The best known Development of an Innovative Algorithm for the Traveling Salesman Problem (TSP) 350 exact algorithms are based on either the B&B method for the Asymmetric TSP (ATSP) (Fischetti et al., 2002) or the Branch and Cut (B&C) method for the Symmetric TSP (STSP) using the double index formulation of the problem (Naddef, 2002).Currently, most algorithms for the TSP ignore high cost arcs or edges and save the low cost ones. In case of the ATSP, the Assignment Problem (AP) is a common choice

## II. OBJECTIVE

The main objective of our project is as follows:

- ✓ To find the shortest path for Tamil Nadu cities.
- ✓ To reduce the time for calculation
- ✓ To search each and every point in the dynamic search space.
- ✓ To get the global optimal solution for the given TSP problem.
- ✓ To accept any type of constraints (fixed constraints & Variable constraints)

## III. GENETIC ALGORITHM

“Survival of the fittest” (On the Origin of Species by means of Natural Selection) Charles

Darwin, 1859 A.D.[7,8,21]. This thesis studies the problems faced by the Genetic Algorithm in the area of vehicle routing and proposes solutions. The end product of those proposals comes in the form of a standardized model of a Genetic Algorithm for the Vehicle Routing, called the Localized Genetic Algorithm (LGA). A genetic algorithm (GA) is a search technique used in computing to find exact or approximate solutions to optimization and search problems[22]. Genetic algorithms are categorized as global search heuristics. Genetic algorithms are a particular class of evolutionary algorithms (also known as evolutionary computation) that use techniques inspired by evolutionary biology such as inheritance, mutation, selection, and crossover (also called recombination).

Genetic algorithms are used in search and optimization, such as finding the maximum of a function over some domain space.

- In contrast to deterministic methods like hill climbing or brute force complete enumeration, genetic algorithms use randomization.
- Points in the domain space of the search, usually real numbers over some range, are encoded as bit strings, called chromosomes.
- Each bit position in the string is called a gene.
- Chromosomes may also be composed over some other alphabet than  $\{0,1\}$ , such as integers or real numbers, particularly if the search domain is multidimensional.
- GAs are called "blind" because they have no knowledge of the problem.

An initial population of random bit strings is generated.

- The members of this initial population are each evaluated for their fitness or goodness in solving the problem.
- If the problem is to maximize a function  $f(x)$  over some range  $[a,b]$  of real numbers and if  $f(x)$  is nonnegative over the range, then  $f(x)$  can be used as the fitness of the bit string encoding the value  $x$ .

From the initial population of chromosomes, a new population is generated using three genetic

operators: reproduction, crossover, and mutation.

- These are modelled on their biological counterparts.
- With probabilities proportional to their fitness, members of the population are selected for the new population.
- Pairs of chromosomes in the new population are chosen at random to exchange genetic material, their bits, in a mating operation called crossover. This produces two new chromosomes that replace the parents.
- Randomly chosen bits in the offspring are flipped, called mutation.

The new population generated with these operators replaces the old population.

- The algorithm has performed one generation and then repeats for some specified number of additional generations.
- The population evolves, containing more and more highly fit chromosomes.
- When the convergence criterion is reached, such as no significant further increase in the average fitness of the population, the best chromosome produced is decoded into the search space point it represents.

Genetic algorithms work in many situations because of some hand waving called The Schema Theorem.

- Short, low-order, above-average fitness schemata receive exponentially increasing trials in subsequent generations.

Genetic Algorithms are a family of computational models inspired by evolution. These algorithms encode a potential solution to a specific problem on a simple chromosome-like data structures so as to preserve critical information. Genetic algorithms are often viewed as function optimizers, although the range of problems to which genetic algorithm have been applied is quite broad. The basic components of GA are illustrated in the Figure 3.1 gene, chromosome, and population. Usually the chromosome is represented as a binary string. The real trick of GA is on the encoding of problem domain, and the selection of next generation.

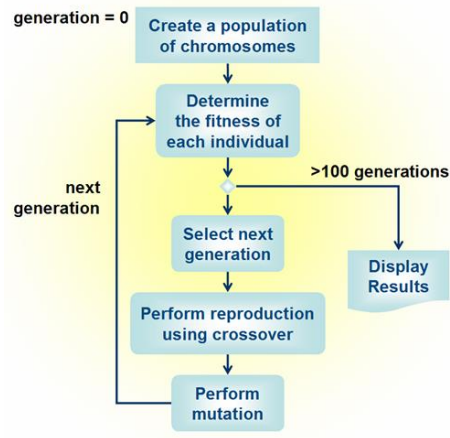


Fig 3.1 Genetic Algorithm flow chart

### 3.1 Input data's for TSP program

1. Distance Matrix for Tamil Nadu cities in the form of 2D array.
2. Number of cities
3. Number of Generations
4. Crossover probability
5. Mutation probability
6. Fixed constraints (Starting cities number)
7. Variable constraints or dynamic constraints

### 3.2 Output results

1. Best sequence (Shortest Route) in Genetic Algorithm with distance in Km.

### 3.3 Sample Inputs for 5 cities problems

- Enter the number of Generations ::>100
  - Allow mutation (1:: Yes/2::No) (1:: recommended) ::>1
  - Enter the number of fixed constraints : > 1
  - Enter the number of fixed in position 1:: > 2
  - Enter the number of variable constraints :: > 1
- Set 1
- Enter the value of constrain 1:: > 4
  - Enter the value of constrain 2:: > 5
  - Enter the probability of survival (0 to 1) :: > 0.6
  - Do you want to apply probabilities (y/n) :: >y
  - Enter the probability of cross over

(0 to 1) :: >0.8

- Enter the probability of mutation (0 to 1):: >0.8
- Do you the output to be printed (1: yes/2:No) :: >1

### Results from Genetic Algorithm:

Sequence :: > 24153  
 Distance ::> 718 KM  
 Generation:: > 5<sup>th</sup> Generation  
 Possibility :: > 120  
 Available :: > 105 sequences  
 Solution :: > 47<sup>th</sup> sequences

The program is executed for few numbers of times to get optimal solution having alternate feasible sequences for the same feature. The sequential problem took very few microseconds for the execution of population size of 10; the number of operations are 16; with the probability of survival 0.6. Eight sets of variable constrains and one set of fixed constrains are included in the program (as inputs) with reference to a specific part module

## IV. IMPLEMENTATION OF GENETIC ALGORITHM TO TSP PROBLEMS

For Example : 5 cites problems

General sequence is 1 2 3 4 5

Total No of cities N = 5

Possible combinations =  $2^{N-1}$

$$= 2^{5-1}$$

$$= 016 \text{ combinations}$$

### 4.1 Reproduction [stage I]

In reproduction operation city sequence are randomly generated and total distance was calculated for each sequence.

- 13452 [sequence]
- 23154
- 41235
- 32145
- 45123

At least 10 to 20 sequence are generated, this is called initial population. When population size is more, it produces more accurate answers. But it increases computation time.

After generating initial population fitness function was calculated for each sequence

$$f[i] = 1 - d[i]/d[\max]$$

Where

d-distance

i=1,2,.....each sequence

d[ $\max$ ]=max value

Then select the high fitness value [ie. less distance sequence] for next stage

#### 4.2. Cross over [stage II]

The best sequence was selected based on high fitness value  $f[i] > 0.7$ . Following are the some of the best sequences

32415  
31245  
12345  
32154  
43215

In crossover operation data's are exchange randomly between any 2 randomly selected sequences. For ex: 32415 and 12345 [parent] are the best sequence selected from above sequences.

After the crossover operation, two new sequences was created by exchanging data's randomly in parents

32 | 415 and 12 | 345  
32 145          12435 [Childs]

Then distance was calculated for new sequences [Childs].like this 10 to 20 cross over sequence is carried out for all the best sequence Again the Fitness was calculated for each sequence by using following formula.

$$f[ii] = 1 - d[ii]/d[\maxc]$$

Where

d-distance

ii=1,2,.....each sequence

d[ $\maxc$ ]=max value in crossover

Then select the high fitness value [ie less distance] sequence for next stage

#### 4.3. Mutation

The best sequence was selected from cross over operation ie fitness value  $f[i] > 0.8$ . Following are the some of the best sequence

21345  
32154  
42135  
45231

In mutation operation data exchange randomly in a single sequence. It is shown in following sequence.

Old sequence    new sequence

<u>2</u> 1 <u>3</u> 45	<u>3</u> 1 <u>2</u> 45
3 <u>2</u> 1 <u>5</u> 4	34 <u>1</u> 5 <u>2</u>

Then distance was calculated for new sequences. Like this 10 to 20 sequence was created for all the best sequence. Again fitness function is calculated for each sequence by using following formula.

$$f[ii] = 1 - d[ii]/d[\maxm]$$

Where

d-distance

ii=1,2,.....each sequence

d[ $\maxm$ ]=max value in mutation

Then select the high fitness value [ie less distance sequence] in mutation operator. Finally the overall minimum distance ie shortest path was selected from the all operations. This is called one generation.

#### Disadvantages of GA

It generates multiple local minimum

#### V. TSP FOR VISITING 10 CITIES

The main objective of this project is to implement the TSP problem to visit 10 Tamil Nadu cities. The distance (Km) between each cities are given below in table 5.1

Table 5.1.Distance Matrix for 10 Tamil Nadu cities (km)

city	1	2	3	4	5	6	7	8	9	10
1	0	230	354	47	263	247	262	330	181	552
2	230	0	492	183	307	398	400	307	71	689
3	354	492	0	350	225	164	89	321	438	469
4	47	183	350	0	259	252	244	283	134	543
5	263	307	225	259	0	300	133	96	236	531
6	247	398	164	252	300	0	143	322	312	305
7	262	400	89	244	133	143	0	229	346	530
8	330	307	321	283	96	322	229	0	236	627
9	181	71	438	134	236	312	346	236	0	617
10	552	689	469	543	531	305	530	627	617	0

First Row & First Column represent the cities Number & Name of cities are as follows 1.Chidambaram, 2.Chennai, 3.coimbatore, 4.Cuddalore, 5.Dharamapuri, 6.Dindugul, 7.Erode, 8.Hosur, 9.Kancheepuram, 10.Kanyakumari, Remaining values represents the distance between all cities.

In all case studies 0.8 cross over & mutation probability are considered and test is carried out for 100 iterations.

Shortest route for 10 cities (1.Chidambaram, 2.Chennai, 3.coimbatore, 4.Cuddalore, 5.Dharamapuri, 6.Dindugul, 7.Erode, 8.Hosur, 9.Kancheepuram, 10.Kanyakumari) without any constraints is 7 5 4 8 2 9 1 3 6 10 =1770 KM from genetic algorithm and 10 6 3 7 5 8 2 9 4 1=1324 KM is the best solution in the Simulated Annealing. If city 1 is starting location then 1 4 7 3 5 8 2 9 6 10 = 1696 KM is the best sequence from genetic algorithm and 1 4 9 2 8 5 7 3 6 10 =1324 KM is the best solution in the Simulated Annealing. Like this various cities are fixed as single (1) and multiple (123) starting sequence. The different combinations of sequence for various constraints are shown in table 5.2 and figure 5.1

Table 5.2 Shortest route for 10 cities for No Constraints

Fixed Constraints Staring cities	Best Sequence	Distance(K M)
		GA
No	75482913610	1770
No	10637582941	
No	14928573610	

1	147358296 10	1696
1	149285736 10	
2	241598736 10	1752
2	291485736 10	
3	382941756 10	1880
3	375892416 10	
4	498536712 10	2179
1 2	12461073589	2146
1 2	12948573610	
2 3	238571946 10	2176
2 3	237589416 10	
1 2 3	12376 10 584	2256
1 2 3	123758946 10	
15 10	15 10 673842	2205
15 10	15 10 637842	
10 9 8	10 985241367	2147
10 9 8	10 985736142	
1234	12349685710	2599
1234	12349857610	
12345	12345768910	2782



Fig.5.1 a) shortest path for 10 cities 1 4 9 2 8 5 7 3 6 10 =1324KM



Fig.5.1 b) shortest path for 10 cities starting from city 2, 291485736 10 =1369km

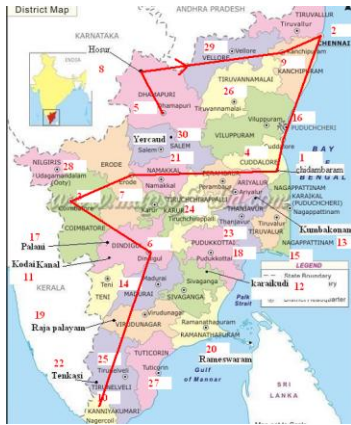


Fig.5.1 c) shortest path for 10 cities starting from city 5, 5 8 9 2 4 1 7 3 6 10=1453 km

Fig 5.1 a,b,c Shortest Path for 10 Cities

## VI. CONCLUSION AND FUTURE WORK

In this paper we have discussed the travelling salesman problem using Genetic Algorithm. Various techniques of genetic algorithm have been discussed in this paper to study travelling salesman problem which is a permutation problem in which goal is to find the shortest path between cities traversing each city at least once. This paper gives a solution to find an optimum route for traveling salesman problem using Genetic algorithm technique for visiting Tamil Nadu cities, in which cities are selected randomly as initial population. The new generations are then created repeatedly until the proper path is reached upon reaching the stopping criteria. The proposed approach can be applied for various advanced network models like logistic network, task scheduling models, vehicle navigation routing models etc. The same approach can also be used for allocation of frequencies in cells of cellular network.

## VII. REFERENCES

[1] ChetanChudasama, S. M. Shah and Mahesh Panchal, “Comparison of Parents Selection Methods of Genetic Algorithm for TSP”, International Conference on Computer Communication and Networks (CSI- COMNET), 2011.

[2] Dwivedi, TarunaChauhan,SanuSaxena and PrincieAgrawal, “Travelling Salesman Problem using

Genetic Algorithm”, International Journal of Computer Applications(IJCA), 2012, pp. 25-30.

[3] Naveen kumar, Karambir and Rajiv Kumar, “A Genetic Algorithm Approach To Study Travelling Salesman Problem”, Journal of Global Research in Computer Science, 2012, Vol. 3, No. (3).

[4] Adewole Philip, AkinwaleAdioTaofiki and OtunbanowoKehinde, “A Genetic Algorithm for Solving Travelling Salesman Problem”, International Journal of Advanced Computer Science and Applications, 2011, Vol. (2), No. (1).

[5] Ivan Brezina Jr.,Zuzana Cickova, “Solving the Travelling Salesman Problem using the Ant colony Optimization”, Management Information Systems, 2011, Vol. (6), No. (4).

[6] Buthainah Fahran, Al-Dulaimi, and Hamza A. Ali, “Enhanced Traveling Salesman Problem Solving by Genetic Algorithm Technique (TSPGA)”, World Academy of Science, Engineering and Technology, 2008, Vol. (14).

[7] Rong Yang, “Solving Large Travelling Salesman Problems with Small Populations”. IEEE 1997.

[8] Chiung Moon, Jongsoo Kim, Gyunghyun Choi ,YoonhoSeo,” An efficient genetic algorithm for the traveling salesman problem with precedence constraints”, European Journal of Operational Research 140 (2002) 606–617, accepted 28 February 2001.

[9] Shubhra Sankar Ray, Sanghamitra Bandyopadhyay and Sankar K. Pal,” New Operators of Genetic Algorithms for Traveling Salesman Problem”, 2004 IEEE.

[10] Lawrence V. Snyder a,\* , Mark S. Daskin ,” A random-key genetic algorithm for the generalized traveling salesman problem”, European Journal of Operational Research 174 (2006) 38–53, 2005.

[11] Milena Karova, Vassil Smarkov, Stoyan Penev,” Genetic operators crossover and mutation in solving the TSP problem”, International Conference on Computer Systems and Technologies – Comp Sys Tech’ 2005.

[12] Plamenka Borovska," Solving the Travelling Salesman Problem in Parallel by Genetic Algorithm on Multicomputer Cluster", International Conference on Computer Systems and Technologies - CompSysTech'06

# EFFECT OF ALUMINIUM OXIDE NANOPARTICLE AS NANO-ADDITIVE ON THE OPERATING CHARACTERISTICS OF DIESEL ENGINE FUELLED WITH BLENDS OF DIESEL AND WASTE TYRE PYROLYSIS OIL

*Chinnasamy C\**

Department of Mechanical Engineering, SNS College of Technology, Coimbatore, India- 641 035

Email: [chinnu18189@gmail.com](mailto:chinnu18189@gmail.com)

Mob: +91-9994866851

*Prakash k*

Department of Mechanical Engineering, SNS College of Technology, Coimbatore, India- 641 035

Email: [prakasktg@gmail.com](mailto:prakasktg@gmail.com)

*Vetrivel A*

Department of Mechanical Engineering, SNS College of Technology, Coimbatore, India- 641 035

Email: [vetri232@gmail.com](mailto:vetri232@gmail.com)

*Tamilselvam P*

Department of Mechanical Engineering, SNS College of Technology, Coimbatore, India- 641 035

## Abstract

*The experimental investigation was carried out to study the influence of adding aluminium oxide ( $Al_2O_3$ ) nanoparticles as nano-additive on diesel engine working characteristics fuelled with blends of diesel and waste tyre pyrolysis oil (WTPO). The WTPO is extracted in the pyrolysis process using automobile waste tyre as feedstock. The alumina nanoparticles were dispersed in the WTPO20 blend (20% of WTPO and 80% of diesel) in the proportion of 25 and 50ppm using ultrasonic stabilization. The physical properties of fuel blends with and without nanoparticles were measured and compared. The experimental results revealed that, the addition of alumina nanoparticles into WTPO20 blend enhances the performance and combustion characteristics of diesel engine and minimizes the emission constituents such as CO, HC and smoke opacity with an increase in EGT and NO emissions.*

**Keywords:** Alumina, nanoparticle, pyrolysis, combustion, engine performance, emission

## INTRODUCTION

The quest for alternative fuel for diesel engine has begun at the right time because of scarcity of fuel demand, successive rise in fossil fuel price, and increase in population. The biodiesel extracted from vegetable oil has attracted most of the researchers owing to its

biodegradability and renewability. The biodiesel powered diesel engine emits lesser carbon monoxide (CO), hydrocarbon (HC) and smoke opacity. However, due to higher oxidation nature of biodiesel, the NO<sub>x</sub> emission increased. The implementation of biodiesel as commercial alternative fuel requires large infrastructural requirement and huge capital investment. Another hurdle of commercializing the use of biofuel is its high production cost and about 70-85% of its production cost comes from its raw material. Therefore, the use of waste fried oil, waste cooking oil from food sectors and waste plastic oil made from Polyethylene, Polypropylene etc. Not only helps in minimizing the raw material cost, but also helps in effective waste utilization[1], [2]

Rubber is the main constituent in tyres. Both natural and artificial rubbers are used for tyre manufacturing [3]. The waste tyres consist of non-decomposed and non-biodegradable material. Therefore, waste tyres can cause serious issues on the environment if they are not recycled properly [4]. However, adding sawdust into rubber pyrolysis helps in improving the environmental conditions of pyrolysis oil by minimizing the contents of PAHs, nitrogen, and sulfur [5]. The waste tyre possesses high volatiles with less ash content and higher heating value than other solid fuels like coal and biomass. So, waste tyres can be used as a source of energy for propelling the internal combustion engines. Pyrolysis is the common method followed to derive the oil from waste tyres. There are two stages involved in pyrolysis: primary pyrolysis and secondary cracking. In the

primary stage, the vapour products are first produced from the waste tyres which are made up of a variety of hydrocarbons and then they encounter secondary reactions [6]. The most significant parameter influencing the yield of pyrolysis reaction is the reaction temperature [7].

Nanofluids having a stable suspension of nanoparticles with 1-100 nm, size, have emerged as motivating field of research in recent times. Nanofluids can be employed in most of the energy-related systems owing to their enhanced thermal conductivity [8]. The influence of alumina nano-additive in methyl ester of neem oil on the working characteristics of diesel engine was reported by Balaji, G., et al. [9]. They found the addition of alumina nanoparticles improves BTHE and minimizes BSFC owing to higher surface area to volume ratio. The emissions such as NO, CO, HC and smoke opacity were reduced by the addition of alumina nano-additives due to its oxidation nature. Seyyed Hassan Hosseini et al. [10] found that the addition of alumina in waste cooking oil-diesel blend enhances the engine torque and power by 5.36%. Sivakumar Muthusamy et al. [11] found that the addition of alumina nanoparticles in pongamia biodiesel-diesel blend resulted in marginal rise of BTHE and decrease in BSFC. Shiva Kumar, P et al. [12] found that the addition of ferrofluid as nano-additive in pongamia-diesel blend reduces CO, HC emissions by 35.8 and 22.9%. A Prabu et al. [13] studied the effect of nano particles such as Alumina ( $Al_2O_3$ ) and Cerium oxide ( $CeO_2$ ) as additives in Jatropha biodiesel and they found a considerable reduction in CO, HC, NO and smoke emissions owing to catalytic activity caused by nanoparticles because of their higher surface area to volume ratio and thermal conductivity. Naresh Kumar Gurusala et al. [14] studied the effects of alumina nanoparticles in waste chicken fat biodiesel and they concluded that, the combustion duration of the nanoparticle-blended fuel were decreased when compared to all other blends. C. Syed Aalam et al. [15] studied the addition of alumina nano-additives in zizipus jujube methyl ester blended fuel and they concluded that, the nanoparticles are very much effective in enhancing the properties of biodiesel. J. Sadhik Basha et al. [16] evaluated the use of Alumina and CNT (carbon nanotube) nanoparticles in jatropha biodiesel and they found that the peak pressure and heat release rate (HRR) were lower by the addition of nanoparticles compared to jatropha biodiesel. C. Syed Aalam et al. [17] reported a study in which aluminium oxide nanoparticles were added to Mahua biodiesel blend in different proportions to investigate its effects and they found an improvement in calorific value and a reduction in the flash point.

From the comprehensive literature reports, it is evident that, owing to potential properties such as higher thermal conductivity, surface area to volume ratio and superior catalytic activity, the nanoparticles were preferred as nano-additive in liquid fuels. There are numerous reports available on the use of alumina nano-additives in various

biodiesels with different fatty acid composition extracted from various vegetable oils. However, there are no reports available to study the influence of alumina as nano-additive in the blends of WTPO and diesel which has different composition from biodiesel. Therefore, the present study is attempted to study the working characteristics of single cylinder diesel engine operated with 25 and 50ppm of alumina nano-additives in WTPO20 blend.

## 2. MATERIALS AND METHODS

### 2.1 Pyrolysis Oil Extraction from Jatropha Biomass

The conversion of long chain polymers into less complex molecules in the absence of oxygen by the application of heat and pressure is called as pyrolysis. The WTPO extraction was carried out in a reactor containing a batch of heaters. The collected automobile waste tyres were fed into a reactor along with silica alumina catalyst of 2.5wt% through a hopper provided at the top of a reactor. The reaction was carried out for about 120 minutes at an operating temperature ranging from 400-500°C by applying the heat at a rate of 30°C/min. The vapors started coming out of reactor after 40 minutes and then condensed into a liquid fuel in a condenser and stored in a tank. The extract consists of 70-80% of pyrolysed oil, gas of 10-20% and solid coke residue of 5-10%. The schematic layout of pyrolysis process is given in fig 1.

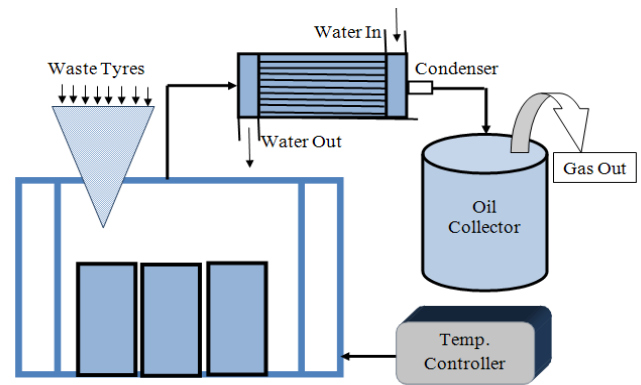


Figure 1 Schematic layout of pyrolysis process

### 2.3 Characterization of alumina nanoparticles

The scanning electron microscope (SEM) of alumina nanoparticles are shown in fig 2. The SEM morphology confined to the crystalline nature of agglomeration and aggregate formation. The average grain structure was found about 30nm. X-ray Diffraction (XRD) (Make: PANalytical) of  $Al_2O_3$  nanoparticles is shown in fig 3. The diffraction peaks with various planes confirm the crystalline structure of nanoparticles. Sharp peak was observed at  $2\theta = 25.26^\circ$ . The grain size calculation was made using Debye-scherer's formula as given below in eq (1).

$$D = (k \cdot \lambda) / (\beta \cdot \cos \theta) \quad (1)$$

Where, D represents the average grain size of nanoparticles, k- shape factor (taken as 0.89),  $\lambda$ -wavelength of nanoparticles ( $1.54 \cdot \text{\AA}$ ),  $\beta$ - Full width at half maximum ( $5.128 \cdot 10^{-2}$ ),  $2\theta$ - Bragg angle ( $25.26^\circ$ ).  $\theta$ - $12.36^\circ$  and D is calculated as 27.36nm. The  $\text{Al}_2\text{O}_3$  nanoparticles were further analyzed by Fourier Transform infrared (FT-IR) using Bruker- spectrum with a wavelength ranging from 1000-3500 $\text{cm}^{-1}$  to identify the functional groups and the bands corresponding to various vibrations as shown in fig. It is inferred that, the high broadband occurring in the range of 2500-3500 $\text{cm}^{-1}$  is due to various -OH groups. The bands below 1500 $\text{cm}^{-1}$  corresponds to Al-O vibrations.

**Table 1 Specifications of nanoparticle**

Item	Sample 1
Purity (%)	99.9
Average Particle Size (nm)	20
Appearance	Blackish grey
Bulk density ( $\text{g}/\text{m}^3$ )	0.06-0.18
Molecular weight (g/mol)	28.92
Specific Surface area ( $\text{m}^2/\text{g}$ )	40-50
Thermal Conductivity (W/mK)	0.26

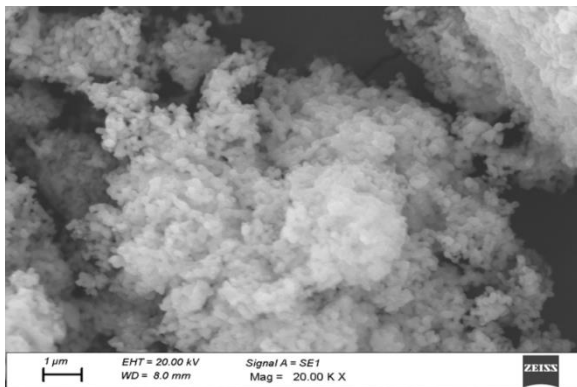


**Figure 2 SEM image**

## 2.4 Fuel blend preparation

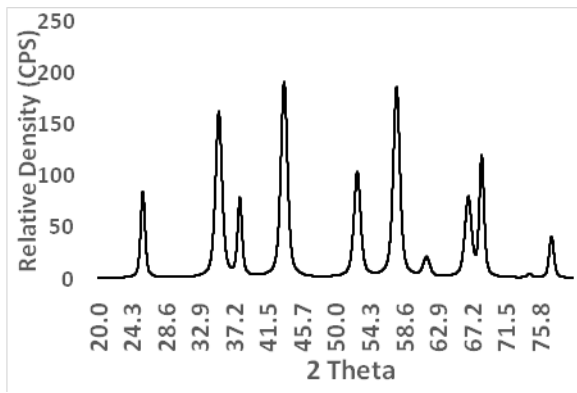
The alumina nanoparticles with a size range of 20-50nm were supplied by Sigma Aldrich, USA with a purity of

99.9%. The detailed specification of nanoparticles is given in table 1. The  $\text{Al}_2\text{O}_3$  nanoparticles were dispersed into WTPO20 blend containing 20% of WTPO and 80% of diesel in the mass fractions of 25 and 50ppm using ultrasonic vibrator (make: Hielscher, Model: UP400S) at a frequency of 24kHz for 20min. The resultant mixture is then symbolized as WTPO20+Al25ppm and WTPO20+Al50ppm. Each test mixture was kept in a tube under static conditions to observe the sedimentation of nanoparticles. The nanoparticles were found settled at the bottom of the tube after 12 hours. Therefore, to maintain the fuel blend from sedimentation of nanoparticles, surfactant Sorbitan monooleate (Span 80) was mixed with each fuel blend. The stability test was carried out again in addition with a surfactant which resulted in no nanoparticles settling down even after one week.

The alumina nanoparticles are having 30 times greater thermal conductivity than that of WTPO20 blend. Therefore, the WTPO20 blend with alumina nanoparticles are expected to exhibit higher thermal conductivity and evaporation rate compared to that of WTPO20 blend which in turn shortens the ignition delay. The surface area to volume ratio of alumina nanoparticles is higher than WTPO20 blend. Therefore, the WTPO20 blend with alumina nano-additives will have superior heat transfer properties compared to WTPO20 blend. The various physical properties of diesel, WTPO20 blend with and without  $\text{Al}_2\text{O}_3$  nanoparticles were measured and listed in table 2.

**Table 2 Fuel properties comparison**

Properties	Diesel	WTPO20	WTPO20+ Al25pm	WTPO20+ Al50ppm
Calorific value (MJ/kg)	44	42.8	42.1	42.4
Kinematic viscosity @ 40°C ( $\text{mm}^2/\text{S}$ )	3.5	4.23	4.26	4.28
Flash point (°C)	75	114	108	106
Density @ 15°C ( $\text{kg}/\text{m}^3$ )	832	843	845	846
Cetane number	53	49	50	52


**Figure 3 XRD analysis**

## 2.5 Experimental setup and conditions

A single cylinder four stroke water cooled direct injection diesel engine (Kirloskar made) was used in this study to conduct an experimental investigation. The schematic layout of experimental setup is shown in fig 4. The engine specifications are given in table 3. The engine was operated at a constant speed of 1500rpm through governor. The maximum power output of the engine is 3.5kW under maximum load condition. The injection pressure and timing were maintained as 210 bar and 23° BTDC respectively. The engine has hemispherical shaped chamber at the piston crown. The engine was cooled by passing the cold water around engine cylinder block and head. A piezoelectric pressure transducer (make: PCB Piezotronics) was mounted on the cylinder head to measure the combustion data. The performance attributes such as BTHE and BSFC are measured using labview based engine analysis software “EnginesoftLV”. The exhaust pollutants such as CO and HC were measured on dry basis and NO emission was measured using chemiluminescence method using a chemical sensor mounted in the four gas emission analyzer (make: HEPHZIBAH) and Smoke level was measured using an AVL made smoke meter. The exhaust gas temperature was measured using chromelalumel (K-type) RTD make PT 100 type thermocouple. The uncertainty analysis of various measuring instruments is given in table 4.

**Table 3 Engine specifications**

Parameter	Specification
Type of Engine	Kirloskar (Model: 240PE) Single Cylinder Variable Compression Ratio direct injection diesel Engine.
Bore & Stroke	87.5 × 100mm

Compression ratio	17.5
Cubic capacity	0.661 liters
Fuel Injection timing	23° BTDC
Rated power	3.5 KW @ 1500rpm
Injection pressure	210 bar
Piezo sensor Range	Up to 350bar Pressure
Crank angle encoder	Resolution of 1 Deg, Speed of 5500 RPM with TDC pulse
ECU	PE3 Series ECU, Model PE3-8400P
Type of Cooling	Water cooled
Type of Loading	Eddy Current Dynamometer with water cooling

**Table 4 Uncertainty analysis**

Instrument/Parameter	Type and manufacturer	Measuring Range	Accuracy	% of Uncertainty
Fuel flow	-	-	± 0.03L/hr	±0.5
Engine speed	-	-	±2 rpm	± 0.2
Exhaust gas analyzer	HG-540 & HEPHZIBAH	CO-0-9.999 % HC-0-15000 ppm NO- 0-10000 ppm	±0.01 % of Vol ±1 ppm ±2 ppm	±1.5 ±1.5 ±3
Smoke meter	AVL	0-100%	±0.1%	±1.25
Temperature sensors	RTD PT100 type K thermocouple	0-1200 °C	±1 °C	±0.1
Pressure sensor	PCB Piezotronics	0-200 bar	±1 bar	±2
Crank angle encoder	-	-	±0.1°	±0.03
BTHE	-	-	±0.5	±0.05
BSFC	-	-	±0.06kg/kW-hr	±1

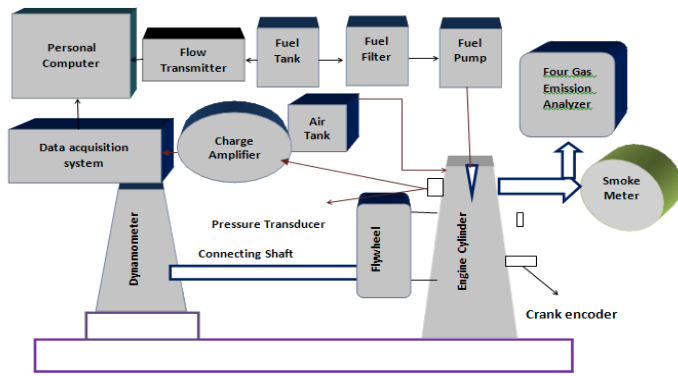


Figure 4 Schematic layout of experimental setup

### 3. Results and discussion

In this section, the variation of performance parameters such as BTHE and BSFC, emission constituents such as CO, HC, EGT, NO and smoke opacity were measured with respect to load. The variation of combustion parameters such as cylinder pressure and heat release rate was measured for various fuel blends with respect to varying crank angle. Each output parameter was measured five times and average of it was considered for the analysis.

#### 3.1 Performance characteristics

The variation of brake thermal efficiency with respect to varying load for diesel, WTPO20 and WTPO20 blend with nano-additives is depicted in fig 5. Replacing diesel with WTPO20 blend reduces the BTHE. This may be due to higher density, viscosity of WTPO leading to poor fuel-air mixture formation. However, the addition of 25 and 50ppm of alumina nanoparticles enhances the BTHE by 8.5 and 12.3% compared to that of WTPO20 blend. The enhancement may be attributed to enhanced combustion because of the catalytic activity caused by the presence of nanoparticles owing to its higher thermal conductivity and surface area to volume ratio.

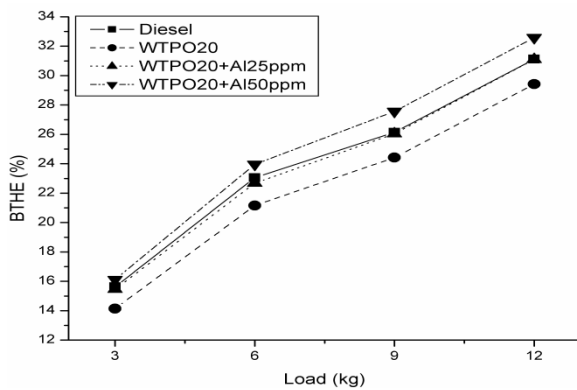


Figure 5 Variation of BTHE

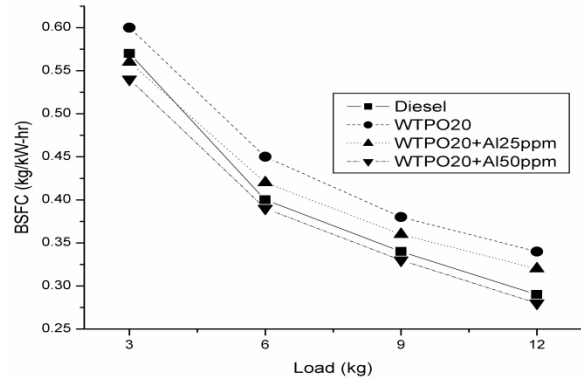


Figure 6 Variation of BSFC

The variation of BSFC with respect to varying load for various fuel blends under constant speed of 1500rpm is shown in fig 6. The increase in BSFC was observed for all loads for WTPO20 blend compared to that of diesel. This is attributed to higher density, viscosity and lower calorific value of WTPO. However, the addition of 25 and 50ppm of alumina nanoparticles minimizes the fuel consumption by 7.14 and 13.58% respectively. The presence of nanoparticle favors better burning characteristics owing to improved fuel-air mixing and evaporation rates.

#### 3.2 Emission characteristics

The variation of CO emission with respect to varying load condition is depicted in fig 7. There was a slight increase in CO emission compared to that of diesel at all loads which is due to insufficient propagation of mixtures nearer to burning zones causing incomplete combustion. The addition of 25 and 50ppm of alumina nano-additive into WTPO20 minimizes the CO emissions to a maximum of 11.11 and 17.64% respectively. This may be attributed to shortened ignition delay, accelerated combustion reaction and enhanced ignition characteristics by the addition of nano-additives.

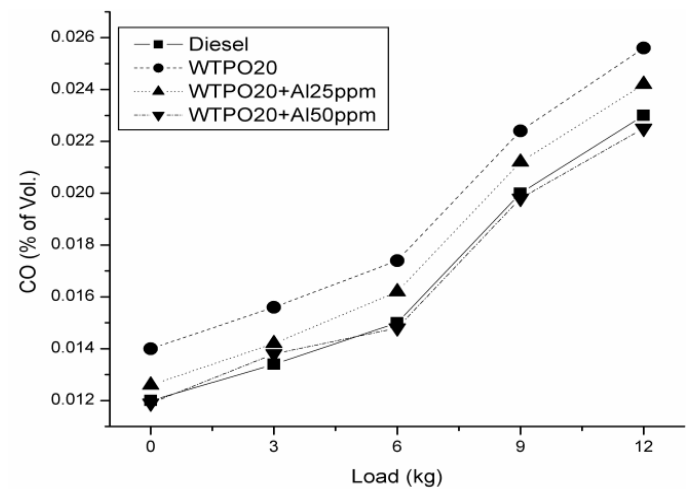


Figure 7 Variation of CO emissions

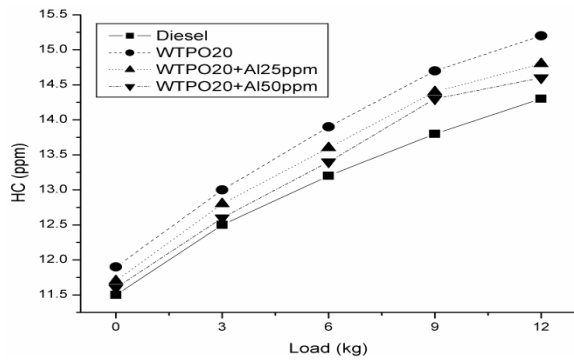


Figure 8 Variation of HC emissions

The variation of HC emissions with respect to varying load at a constant speed of 1500rpm for various fuel blends is plotted in fig 8. The HC emissions are mainly formed due to unburnt mixtures (or) incomplete combustion. The HC emission increases slightly for WTPO20 blend compared to diesel. This may be due to insufficient depth of fuel spray onto combustion chamber causing the incomplete combustion since all the incoming fuel mixture will not dwell in the burning zones to ignite. The addition of 25 and 50ppm of  $Al_2O_3$  accelerates the rate of combustion and reactivity between molecules owing to higher surface area to volume ratio and thermal conductivity and reduces the HC emissions slightly upto 2.27 and 4.1% respectively.

The variation of NO emissions with respect to varying load is presented in fig 9. The formation of NO is direct dependent factor of combustion flame temperature and stoichiometric conditions of the engine. The figure exhibits with an increase in load the NO emission increases due to increase in cylinder temperature. The increasing trend of NO emissions was observed for WTPO20 blend compared to diesel. This may be owing to prolonged ignition delay owing to higher viscosity and density of WTPO resulting in higher heat release rate and leading to higher cylinder temperature. Another possible reason could be due to the aromatic content of WTPO. The addition of 25 and 50 ppm of nano-additives further increases the NO emissions by 6.6 and 9.7% respectively compared to WTPO20. The rapid burning behavior caused by the catalytic activity of nanoparticle which increases the cylinder temperature and enhances the reaction between nitrogen and oxygen species.

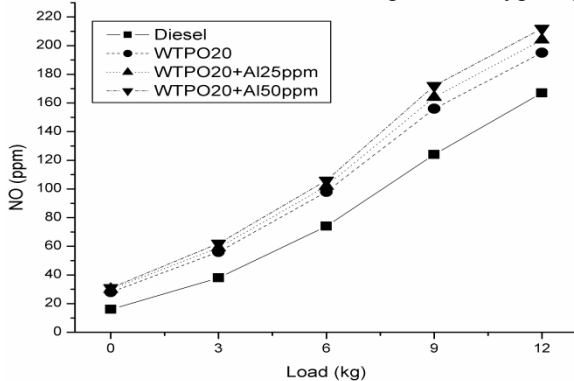


Figure 9 Variation of NO emissions

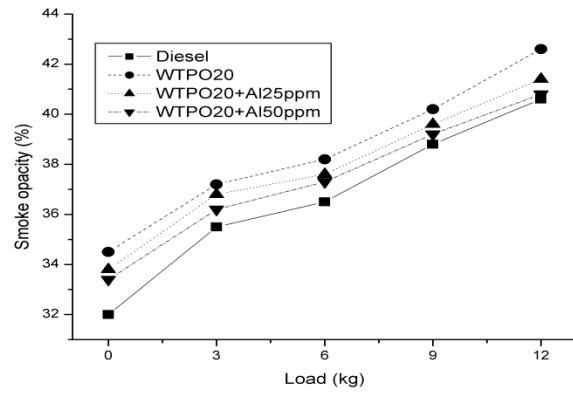


Figure 10 Variation of smoke opacity

The smoke opacity measured with respect to varying loads for all fuel blends is depicted in fig 10. The smoke is the soot particles present in the exhaust gas. The smoke opacity slightly increases for WTPO20 blend compared to that of diesel. This may be due to higher aromatic content of WTPO. However, the addition of 25 and 50ppm of alumina nanoparticles into WTPO20 blend minimizes the smoke emission upto 2.89 and 4.41% respectively owing to near complete combustion achieved by the catalytic action of nanoparticles because of higher surface area to volume ratio.

The variation of exhaust gas temperature with respect to load is presented in fig 11. The rise in EGT was observed for WTPO20 blend compared to diesel. This may be owing to higher viscosity and density of blend resulting in prolonged ignition delay and leading to higher flame temperature. The addition of 25 and 50ppm of nanoparticle further increases the EGT. This may be as a result of accelerated combustion and rapid burning caused by the catalytic activity of nanoparticles.

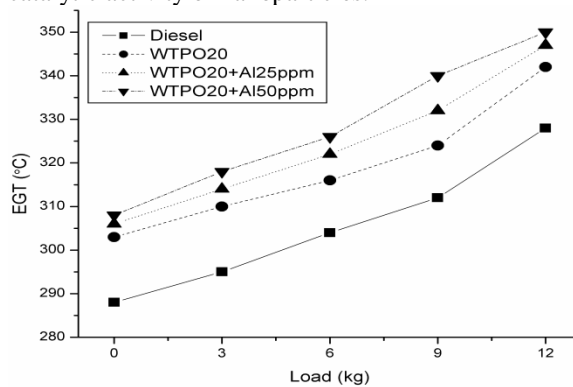


Figure 11 Variation of EGT

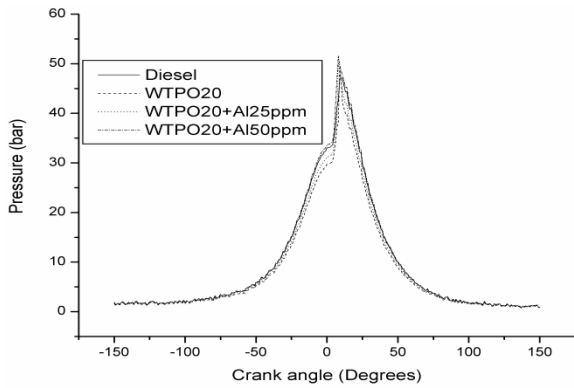


Figure 12 Variation of pressure

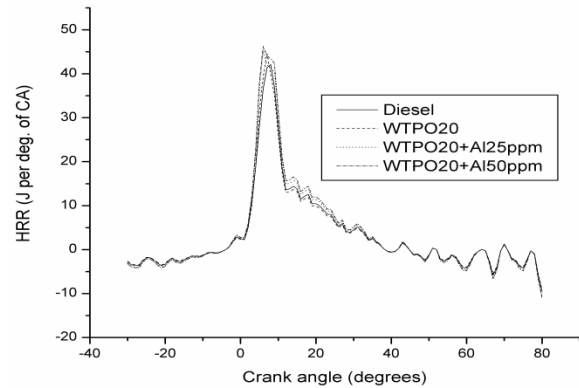


Figure 14 Variation of HRR

### 3.3 Combustion characteristics

Fig 12 represents the variation of In-cylinder pressure with respect to degrees of crank angle (CA) for different fuel blends at full load condition. It can be observed that, the peak pressure of WTPO20 is lesser than that of diesel. Peak pressure is a dependent factor of premixed combustion which is in turn depends on ignition delay (ID). By the addition of WTPO into diesel fuel the ignition delay was prolonged and increase in peak pressure was witnessed. However, the addition of 25 and 50 ppm of nano- additives into WTPO20 blend, improves the peak pressure and locates the point of peak pressure 2 degrees of CA earlier than that of WTPO20. The peak pressure for diesel, WTPO20, WTPO20+Al25ppm and WTPO20+Al50ppm was observed as 47.2, 49.3, 50.3 and 51.5 bar respectively. The rise in pressure could be due to higher surface area to volume ratio of nanoparticles and rapid rise of reaction rate caused by the catalytic activity of nanoparticles.

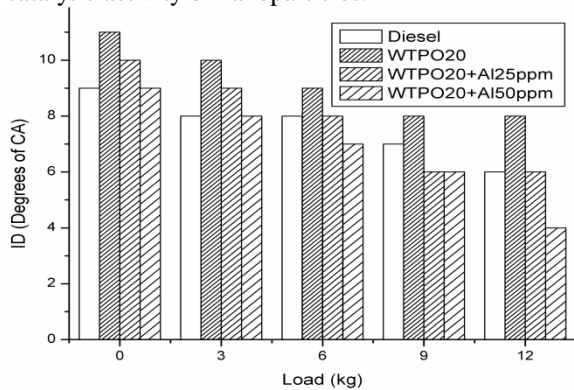


Figure 13 Variation of ID

The variation of ignition delay with respect to varying load is shown in fig 13. As the load increases, the ID was shortened owing to increased combustion temperature which in turn reduces the viscosity of fuel blend by breaking the bond between oil molecules resulting in rapid mixing and evaporation of air and fuel molecules. For WTPO20 blend, the ignition delay was prolonged to a maximum period of 2°CA at maximum load which indicates the poor ignition behavior of WTPO.

However, as the 25 and 50ppm of alumina nano-additives were added with WTPO20, the ignition delay is shortened owing to the enhanced surface area of heat transfer and enhanced reactivity between fuel and air molecules.

The variation of heat release rate with respect to crank angle for various blends at full load condition is shown in fig 14. The combustion process is initiated only when the negative heat release rate turns into positive. As we can observe due to longer ID by the addition of WTPO, the duration of combustion increases as more fuel gets accumulated inside the chamber with slower mixing rate of fuel and air resulting in lower heat release rate while comparing with diesel fuel. However, with an addition of nano-additives, the maximum heat release rate improved due to the action of nanoparticles acting as nano catalyst and thereby enhancing the heat conduction properties between air and fuel molecules.

### 4. Conclusion

The effect of adding alumina nanoparticles into WTPO20 blend was experimentally studied by investigating the performance, emission and combustion attributes of single cylinder diesel engine and the following conclusions were drawn.

- The increase in brake thermal efficiency upto 12.3% and decrease in brake specific fuel consumption upto 13.58% was observed by the addition of alumina nanoparticles into WTPO20.
- The emission constituents such as CO, HC and smoke opacity were reduced by the addition of alumina nanoparticles. However, an increase in EGT and NO emissions were witnessed.
- The cylinder pressure and heat release rate was increased along with decrease in ignition delay by the addition of alumina nanoparticles into WTPO20.
- Overall, the addition of alumina nano-additives in WTPO is an effective technique to boost the engine output characteristics.

### References

- [1] J. B. Hirkude and A. S. Padalkar, "Performance and emission analysis of a compression ignition. Engine operated on waste fried oil methyl esters," *Appl. Energy*, vol. 90, no. 1, pp. 68–72, 2012.

- [2] M. Mani, C. Subash, and G. Nagarajan, "Performance, emission and combustion characteristics of a DI diesel engine using waste plastic oil," *Appl. Therm. Eng.*, vol. 29, no. 13, pp. 2738–2744, 2009.
- [3] P. Parthasarathy *et al.*, "Influence of process conditions on product yield of waste tyre pyrolysis- A review," *Korean J. Chem. Eng.*, vol. 33, no. 8, pp. 2268–2286, 2016.
- [4] S. T. Kumaravel, A. Murugesan, and A. Kumaravel, "Tyre pyrolysis oil as an alternative fuel for diesel engines - A review," *Renew. Sustain. Energy Rev.*, vol. 60, pp. 1678–1685, 2016.
- [5] W. liang Wang, J. min Chang, L. ping Cai, and S. Q. Shi, "Quality improvement of pyrolysis oil from waste rubber by adding sawdust," *Waste Manag.*, vol. 34, no. 12, pp. 2603–2610, 2014.
- [6] A. Ayanoğlu and R. Yumrutaş, "Rotary kiln and batch pyrolysis of waste tire to produce gasoline and diesel like fuels," *Energy Convers. Manag.*, vol. 111, pp. 261–270, 2016.
- [7] C. İlkiliç and H. Aydin, "Fuel production from waste vehicle tires by catalytic pyrolysis and its application in a diesel engine," *Fuel Process. Technol.*, vol. 92, no. 5, pp. 1129–1135, 2011.
- [8] J. Sadhik Basha and R. B. Anand, "Performance, emission and combustion characteristics of a diesel engine using Carbon Nanotubes blended Jatropa Methyl Ester Emulsions," *Alexandria Eng. J.*, vol. 53, no. 2, pp. 259–273, 2014.
- [9] G. Balaji and M. Cheralathan, "Influence of alumina oxide nanoparticles on the performance and emissions in a methyl ester of neem oil fuelled direct injection Diesel engine," *Therm. Sci.*, vol. 21, no. 1, pp. 499–510, 2017.
- [10] S. H. Hosseini, A. Taghizadeh-Alisaraei, B. Ghobadian, and A. Abbaszadeh-Mayvan, "Effect of added alumina as nano-catalyst to diesel-biodiesel blends on performance and emission characteristics of CI engine," *Energy*, vol. 124, pp. 543–552, 2017.
- [11] M. Sivakumar, N. Shanmuga Sundaram, R. Ramesh kumar, and M. H. Syed Thasthagir, "Effect of aluminium oxide nanoparticles blended pongamia methyl ester on performance, combustion and emission characteristics of diesel engine," *Renew. Energy*, vol. 116, pp. 518–526, 2018.
- [12] S. Kumar, P. Dinesha, and I. Bran, "Influence of nanoparticles on the performance and emission characteristics of a biodiesel fuelled engine: An experimental analysis," *Energy*, vol. 140, pp. 98–105, 2017.
- [13] A. Prabu and R. B. Anand, "Emission control strategy by adding alumina and cerium oxide nano particle in biodiesel," *J. Energy Inst.*, vol. 89, no. 3, pp. 366–372, 2016.
- [14] N. K. Gurusala and V. A. M. Selvan, "Effects of alumina nanoparticles in waste chicken fat biodiesel on the operating characteristics of a compression ignition engine," *Clean Technol. Environ. Policy*, vol. 17, no. 3, pp. 681–692, 2015.
- [15] C. S. Aalam, C. G. Saravanan, and M. Kannan, "Experimental investigations on a CRDI system assisted diesel engine fuelled with aluminium oxide nanoparticles blended biodiesel," *Alexandria Eng. J.*, vol. 54, no. 3, pp. 351–358, 2015.
- [16] J. S. Basha and R. B. Anand, "The influence of nano additive blended biodiesel fuels on the working characteristics of a diesel engine," *J. Brazilian Soc. Mech. Sci. Eng.*, vol. 35, no. 3, pp. 257–264, 2013.
- [17] C. S. Aalam and C. G. Saravanan, "Effects of nano metal oxide blended Mahua biodiesel on CRDI diesel engine," *Ain Shams Eng. J.*, vol. 8, no. 4, pp. 689–696, 2017.

# Image Based Vehicle Speed Detecting Device to Avoid Accidents in Street Roads

S.Hemnath<sup>1</sup>

Dept. of Mechanical Engg

SNS College of Technology

Coimbatore, India

[hem.mech1992@gmail.com](mailto:hem.mech1992@gmail.com)

P.Sadasivam<sup>2</sup>

Dept. of Mechanical Engg

SNS College of Technology

Coimbatore, India

[u.sangamesh4@gmail.com](mailto:u.sangamesh4@gmail.com)

U.Sangameswaran<sup>3</sup>

Dept. of Mechanical Engg

SNS College of Technology

Coimbatore, India

[sadhasivam134@gmail.com](mailto:sadhasivam134@gmail.com)

## Abstract

Systems for vehicle detection and speed measurement play a vital role in enforcing speed limits. They also provide relevant data for traffic control. Those systems are divided into intrusive and nonintrusive. Intrusive sensors are usually based on inductive loop detectors which are widely used but have complex installation and maintenance, accelerate asphalt deterioration and will be damaged by wear and tear. Non-intrusive sensors are used to avoid these problems which include laser meters and Doppler radars but are usually more expensive and require frequent maintenance. As digital cameras become cheaper and able to produce images with higher quality image-based systems can become a lower cost alternative for non-intrusive speed measurement. In this project, it is proposed the pipeline for a non-intrusive image-based system for vehicle speed measurement in Street roads. Project main goal is to measure vehicle speed with accuracy comparable to the video based system on inductive loop detectors. The input image is captured by a single fixed overhead camera positioned so that the rear license plate of vehicles in three adjacent lanes are clearly visible. The captured image will be forwarded to the area station Incharge to track the Vehicle.

## Keywords

Raspberry PI, IR Sensor, USB Camera, Raspbian Jessie Lite

## I. INTRODUCTION

Human errors in particular drivers are the causes for the most of the road accidents. It is reported that over 80% of all major crashes on Street roads are caused from inconsiderate driving. The main causes of accidents are vehicle overspeeding, driving after consuming alcohol, distraction during driving, nonadherence to traffic signals, non-wearing of seat-belts and safety gears, tailgating, poor lane discipline etc.

However, in most of the countries speeding or excessive vehicle speed on the road is considered to be the single biggest factor for road accidents contributing to fatal injuries or even death and financial costs to society. In India, over 40% of fatal collisions are caused by excessive or inappropriate speed. Increasing traffic congestion and street accident due to over speeding of vehicle are critical issues to solve for the smart cities.

Thus, vehicle speed monitoring and controlling is one of the important issues in order to maintain a safe road. In this project it is done with the Raspberry PI 3, IR Sensor, USB Camera and Connecting Wires. Raspberry PI is a processor which acts as a CPU for the Computer. IR Sensor is used to detect the motion of the Vehicle. USB Camera captures the image of the Vehicle when it crosses the Speed Limit and Connecting wires are used to connect the IR Sensor to the Raspberry PI. This proposed project area focuses on the controlling of the speed if the vehicle crosses the minimum speed limit. If the vehicle crosses the speed limit, the message along with vehicle number and details will be sent to area police station incharge.

## II. LITERATURE SURVEY

In this paper, it is proposed a non-intrusive, videobased system for vehicle speed measurement in urban roadways. Our system uses an optimized motion detector and a novel text detector to efficiently locate vehicle license plates in image regions containing motion. Distinctive features are then selected on the license plate regions, tracked across multiple frames, and rectified for perspective distortion.[1]

This paper presents a device to detect rash driving on highways and to alert the traffic authorities in case of any violation. In past, lot of devices to detect rash driving on

highways has been made. Most of the approaches require human concentration and involve a lot of effort, which is difficult to implement. In this paper we intend to design a system aimed at early detection and alert of dangerous vehicle driving patterns related to rash driving.[2]

Different systems (Road-based and Vehicle-based) are used for monitoring vehicle speed. However, managing speed data in an efficient and intelligent way is an on-going issue in transportation system.[3]

### III. MODELLING

#### 1. BLOCK DIAGRAM OF PROPOSED MODEL

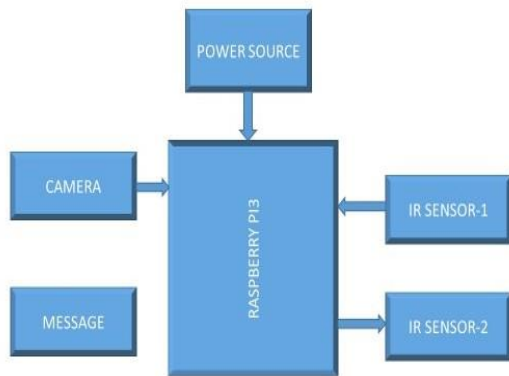


Fig.1 Block Diagram

#### 2. 3D DIAGRAM OF PROPOSED MODEL

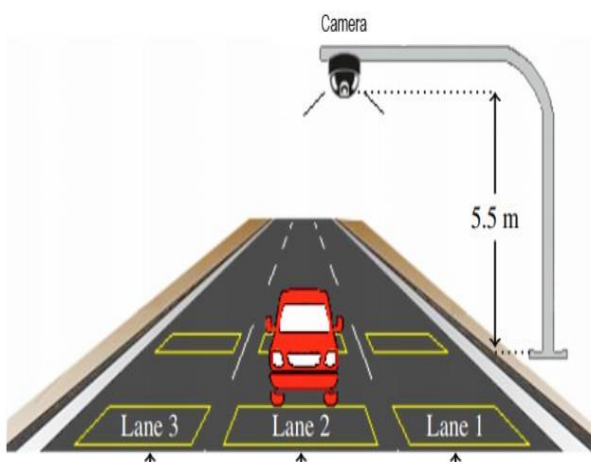


Fig.2 3D Diagram

### IV. COMPONENTS

The basic model of Image based vehicle speed detecting device basically consists of following components.

- Raspberry PI 3
- IR Sensor Module
- USB Camera
- Connecting Wires(Female-Female Port)

#### 1.RASPBERRY PI 3

A Raspberry Pi is a credit card-sized computer originally designed for education, inspired by the 1981 BBC Micro. Creator Eben Upton's goal was to create a low-cost device that would improve programming skills and hardware understanding at the pre-university level. But thanks to its small size and accessible price, it was quickly adopted by tinkerers, makers, and electronics enthusiasts for projects that require more than a basic microcontroller.

The raspberry pi board comprises a program memory (RAM), processor and graphics chip, CPU, GPU, Ethernet port, GPIO pins, Xbee socket, UART, power source connector. And various interfaces for other external devices. It also requires mass storage, for that we use an SD flash memory card. So that raspberry pi board will boot from this SD card similarly as a PC boots up into windows from its hard disk.[6]

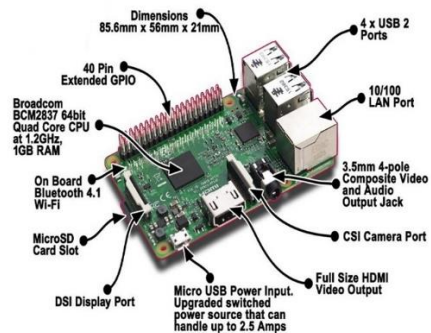


Fig.3 Raspberry PI 3

#### 2. IR SENSOR MODULE

IR sensor is very popular sensor, which is used in many applications in electronics, like it is used in Remote control system, motion detector, Product counter, Line follower Robots, Alarms etc.

IR sensor basically consist an IR LED and a Photodiode, this pair is generally called IR pair or Photo coupler. IR sensor work on the principal in which IR LED emits IR radiation and Photodiode sense that IR radiation. Photodiode resistance changes according to the amount of IR radiation falling on it, hence the voltage drop across it also changes and by using the voltage comparator (like LM358) we can sense the voltage change and generate the output accordingly.[5]



Fig.4 IR Sensor

### 3. USB CAMERA

A USB webcam is a camera that connects to a computer, usually through plugging it in to a USB port on the machine. The video is fed to the computer where a software application lets you view the pictures and also transfer them to the Internet.

The software you choose can be set to upload images on a time interval using FTP (file transfer protocol) to a website, or it can be set to provide a live feed for displaying on a remote machine or again in a website.



Fig.5 USB Camera

### 4. CONNECTING WIRES ( FEMALE-FEMALE PORT)

A Connecting wire (also known as jumper, jumper wire, jumper cable, DuPont wire, or DuPont cable – named for one manufacturer of them) is an electrical wire, or group of them in a cable, with a connector or pin at each end (or sometimes without them – simply "tinned"), which is normally used to interconnect the components of a breadboard or other prototype or test circuit, internally or with other equipment or components, without soldering.



Fig.6 Connecting Wires

## V. OPERATING SYSTEM

To use Raspberry PI on the Computer the Operating System RASPBIAN JESSIE LITE should be installed on the SD Card.

### RASPBIAN JESSIE LITE

Raspbian is a Debian-based computer operating system for Raspberry Pi. There are several versions of Raspbian including Raspbian Stretch and Raspbian Jessie. Since 2015 it has been officially provided by the Raspberry Pi Foundation as the primary operating system for the family of Raspberry Pi single-board computers. Raspbian was created by Mike Thompson and Peter Green as an independent project. The initial build was completed in June 2012. The operating system is still under active development. Raspbian is highly optimized for the Raspberry Pi line's low-performance ARM CPUs.

Raspbian uses PIXEL, Pi Improved Xwindows Environment, Lightweight as its main desktop environment as of the latest update. It is composed of a modified LXDE desktop environment and the Openbox stacking window manager with a new theme and few other changes. The distribution is shipped with a copy of computer algebra program Mathematica and a version of Minecraft called Minecraft Pi as well as a lightweight version of Chromium as of the latest version.[4]

### VI. ADVANTAGES

- Low cost
- It is portable
- Simple in construction
- It reduces accidents
- Saves Human Life

## VII. CONCLUSION

While driving on Street roads, drivers should not exceed the maximum speed limit permitted for their vehicles. However, accidents keep on occurring due to speed violations as drivers follow their speedometers and control their speed according to them, and reduce the speed if they find it to be exceeding and beyond their control. Since number of accidents on street roads increases day by day so it is necessary to check speed of the vehicles on street roads so as to remove accident cases and to provide a safe journey by controlling high speed of the vehicle. It also minimizes the difficulties of traffic police department and make ease to control the rash driving on highways. The police can perform their duties while sitting in control room and can provide their service with more ease and accuracy. To overcome this problem, we have implemented a circuit called as a Image Based Vehicle Speed Detecting Device to Avoid Accidents in Street Roads.

## VIII. REFERENCES

1. A Video-Based System for Vehicle Speed Measurement in Urban Roadways - Diogo C. Luvizon, Bogdan T. Nassu and Rodrigo Minetto.
2. Detection of Over Speeding Vehicles on Highways - Monika Jain, Praveen Kumar, Priya Singh, Chhavi Narayan Arora, Ankita Sharma.
3. Development of a Prototype Wireless Vehicle Speed Monitoring System - Md. Mominul Ahsan.
4. Overspeed Monitoring System - Joel Migwi, Kariuki S. Kairu.
5. Internet of Things for Intelligent Traffic Monitoring System - I Made Oka Widyantara, Nyoman Putra Sastra.
6. Development and Testing of Adaptive Vehicle Speed Monitoring System integrated with Alcoholic Detector for Public Buses - Farhan Ramju, Ramadhani S. Sinda, Shubi Kijage.
7. Solid Edge Software for 3D Drawing of Model

## **POULTRY FARM MONITORING AND CONTROLLING USING PLC WITH INTERNET OF THINGS**

Mr. A Vishnu<sup>1</sup>Sheshaghiri N<sup>2</sup> Joeresh Julius A<sup>3</sup> Sathish Kumar A<sup>4</sup> Satharth Noorul Hassan<sup>5</sup>

<sup>1</sup>Assistant professor, Department of Mechatronics Engineering, SNS College of Technology

<sup>2,3,4,5</sup> Final year student, Department of Mechatronics Engineering, SNS College of Technology

E-mail address: vishnu\_mechetro@yahoo.com, Tel.: +91 8056572812

### **1. INTRODUCTION:**

The poultry farm is one of the major contributions to the world economy. More than 50 billion chickens are raised annually as a source of food. An average human consumes 70 pound (appx) of chicken in a year. The consumption of the chickens is gradually increasing day by day. According to ICRA's estimate per capita meat consumption is around 3.6 kg per annum which puts total broiler meat market size at Rs.730 billion in terms of retail price. The egg production is at 84 billion eggs translating to a per capita egg consumption of 63 eggs per annum. One of the key roles involved in the development of human civilization is in the area of agriculture. With the continuing increase in the world's population, the demand for food supply is extremely raised. Applying engineering processes to poultry farming may help to maximize the benefit to human kind in terms of cheaper and plentiful availability as well as contribute to the growth of the economy. India is world's second largest emerging economy and along with it has rapidly growing poultry sector. Poultry is one of the fastest growing sectors in India with an average growth rate of 12 % for broiler production per annum. The environment

conditions of farms basically affect initial growth of livestock that means there is weight loss in birds, so farmers do not get appropriate weight of birds at the end which is not profitable for farmers. Especially farmers are lagging in field of automation and control conditions of farms. The most of scale poultry farms are situated in rural areas lagging in technology. So, the technology in the poultry automation would result in high production rate and increase in economy of the country. The labor for this humongous sector is a problem faced now a day so we decided to automate the complete process like egg hatching, feeding system, watering system, temperature control, medicine system. So, for this system we have proposed of using a Mitsubishi PLC and a HMI system collaborated with an IOT system. The PLC system is chosen because the of the input, temperature and life features of the PLC. The whole action can be single handedly controlled by the PLC. The IOT system is enabled for increasing the communication with the poultry owner. The wireless HDMI touch display system is used for continuous monitoring. The whole system can be stopped by using a google assistant voice control system.

Key words : Poultry farm , PLC , Iot

## **2. OBJECTIVE**

- To provide continuous monitoring and complete automation of the poultry farm which helps to avoid adverse effect on livestock
- Power consumption is being reduced as using of solar panel
- Every updates will be intimated to the user on the system being progressed through SMS.
- Using of Google assistant the entire process is also been controlled.

## **3. EXISTING METHODOLOGY**

### **3.1 SYSTEM ANALYSIS**

This chapter reviews the system and related studies in the world of poultry, Existing system and The Feature of poultry automation.

### **3.2 EXISTING SYSTEM**

In an existing temperature control system the most of the poultry farming uses the traditional method of heating like using boilers to heat up the farm. For the cooling system, water is sprayed inside the farm by using the fogger. Most of the time chicken died with external climatic conditions, the light or the boilers fixed inside the farm doesn't provide the sufficient heat to a farm. The death rate of chicken is high in the existing method of farming. The shortage of workers is also a problem faced by a poultry owner's. The workers works inside the farm get affected by many diseases and birds as well.

### **3.3 DEMERITS IN THE EXISTING SYSTEM**

- i. Death rate of chicken is high
- ii. Efficiency of the current system is very low
- iii. Lack of workers
- iv. Infection for both humans and chickens
- v. Maintaining the temperature is tedious process

### **3.4 CHALLENGES FACED BY THE POULTRY INDUSTRY**

Constraints have been identified in the areas of husbandry, feeding and health, availability of inputs, information and credit. The negative effects of the hot climatic conditions of the sub-region have also been a challenge. Adverse effects of excessive exposure to high temperatures include excessive panting, poor growth and development of birds and reduced egg production and size, and lower egg shell quality. It is very disappointing that the poultry industry has been plagued by large imports of day old chickens, eggs and feed despite the availability of local birds which are more sumptuous, nutritious and healthy.

### **3.5 DEMERITS OF EXISTING FARMING**

But despite its clear advantages in terms of profitability and affordability, the batter cage system and similar intensive farming techniques also come with disadvantages. Most notably, chickens and hens in intensive poultry farming often suffer from different conditions and pain. A lot of intensively reared chickens

suffer from lameness as a result of fast growth, a result of selective breeding and concentrated feed. In addition, the way the cages are designed and as the chickens grow, their droppings accumulate on the floor. When the droppings decompose, ammonia is released. The ammonia then fills the air with unhealthy fumes and this puts chickens at risk of incurring painful blisters, hock burns or ulcerated feet.

## 4. METHODOLOGY

### 4.1 PROPOSED SYSTEM

The labor for this humongous sector is a problem faced now a day so we decided to automate the complete process like egg hatching, feeding system, watering system, temperature control, medicine system. So for this system we have proposed of using a PLC and a HMI system collaborated with an IOT system. The IOT system is enabled for increasing the communication with the poultry owner. The wireless HDMI touch display system is used for continuous monitoring. The whole system can be stopped by using a Google assistant voice control system.

### 4.2 FEATURES OF THE FARM HOUSE AUTOMATION SYSTEM ARE:

- Automatic lighting
- Climate control
- Fire and smoke detection
- Humidity and moisture control
- Feeder control
- Remote mobile connectivity
- Instant alert system

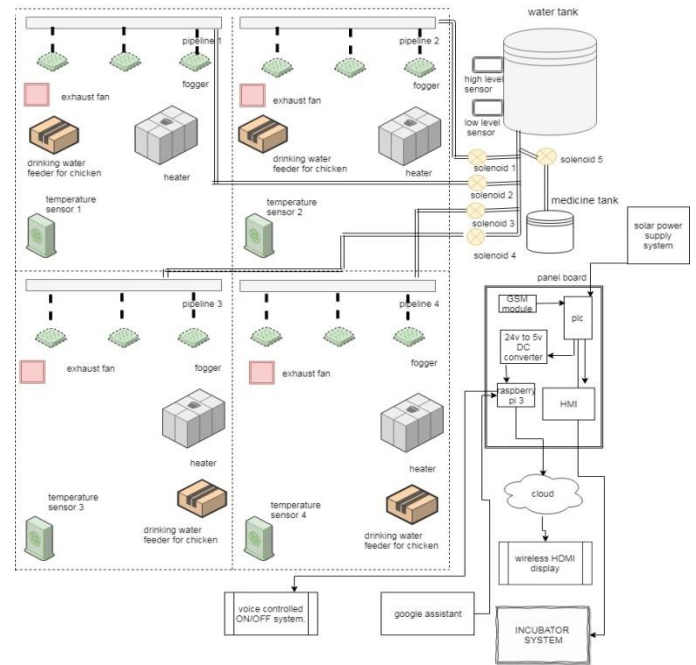


Figure 1 Conceptual diagrams for proposed system

## 5. COMPONENTS AND SYSTEM DESIGN

This section will discuss about the system design and the electronic components that had been used in the system process.

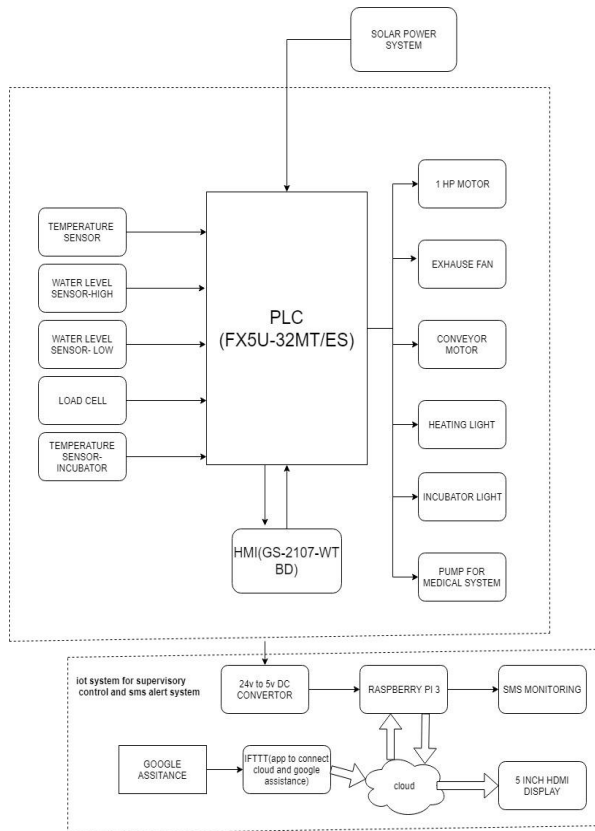


Figure 2 Functional block diagram

## 6. COMPONENTS

### 6.1 TOOLS REQUIRED

1. Languages
  - a. Ladder logic
2. GX WORK3 (fx series plc)
3. ESP8266.
4. F- Series PLC
5. HMI

### 6.2 FX5U-32MT/ES

The first model in the iQ-F series is the FX5U, offering high performance in a compact, cost effective package. The FX5U continues the FX tradition of total flexibility by offering a huge range of new and existing add-on options which further enhance the built-in functions of Ethernet, analogue I/O,

data logging, position control, security, communications and networking functions incorporated as standard.

The FX5U will provide users with the ability to specify more powerful systems but with fewer overall components, saving time and cost.

- FX5U CPU base units with very fast processing time
- Versions with up to 256 inputs and outputs
- Expanded input/output area for networks and complex applications
- Can be upgraded by combining with expansion modules
- Built-in SD card slot
- Run/Stop/Reset switch
- Built-in Ethernet port, RS485
- Displays the input and output states via LEDs
- Integrated real-time clock
- Programming software GX Works3

### 6.3 GS-2107-WTBD (HMI)

Mitsubishi Electric GOT2000 HMIs provide the user with a comprehensive range of options to ensure application or process is covered. Comes equipped with a high speed CPU for responsive HMI operation even under high load processes including logging and device data transmission. Supporting a wide variety of communication options including RS232, RS485/422 and Ethernet making this series of HMI very versatile

- Premium processor coupled with expanded memory
- Multi-touch operation

- Wide variety of communication functions to ensure your application is covered
- Double the speed for monitoring & booting of previous generation
- Simplified setup and debugging controls for simple setup
- Supports a wide variety of image formats, including PNG

#### **6.4 FR-D720S-255-EC (VFD)**

- Simple cabling, the integrated spring clamps connect control and power lines quickly which ensures reliability and simple cabling.
- Easy parameterization software FR-Configuration encourages easy functions such as graphical machine analysis to optimize the drive system.
- An integrated digital dial gives the user direct access to all of the important parameters.
- The integrated four digit LED display monitors and displays current operating values and alarm messages.
- Features a second transistor output which is sink selectable source logic safety input instead of sink logic.
- Directly connect to PLC's instead of safety relays.
- Features a Sensor-less vector control which enables exceptional speed and torque performance.
- Serial interface (RS485) as standard.

- Emergency safe stop input compliant to EN 61800-5-2.
- Maximum short-term overload capacity of 200% for 0.5s.
- Automatically restart after power failures.

#### **6.5 MR-JE-20A (SERVO DRIVE)**

- Advance one touch tuning
- Instantaneous power failure override
- Large capacity drive recorder
- Absolute position detection system
- Performance Features;
- SSCNET III/H
- Fast and accurate
- high resolution encoder
- Energy conservation

#### **6.6 ESP8266**

The ESP8266 Wi-Fi Module is a self-contained SOC with integrated TCP/IP protocol stack that can give any microcontroller access to your Wi-Fi network. The ESP8266 is capable of either hosting an application or offloading all Wi-Fi networking functions from another application processor. Each ESP8266 module comes pre-programmed with an AT command set firmware, meaning, you can simply hook this up to your Arduino device and get about as much Wi-Fi-ability as a Wi-Fi Shield offers.

The ESP8266 module is an extremely cost effective board with a huge, and ever growing, community. This module has a powerful enough on-board processing and storage capability that allows it to be integrated with the sensors and other application specific devices through its

GPIOs with minimal development up-front and minimal loading during runtime. Its high degree of on-chip integration allows for minimal external circuitry, including the front-end module, is designed to occupy minimal PCB area.

## **7. SOFTWARE SPECIFICATION**

### **7.1 GX WORKS 3**

- It is the latest generation of programming and maintenance
- Software offered by Mitsubishi Electric specifically designed for the
- MELSEC IQ-R Series control system.
- It includes many new features such as graphic-based system configuration, integrated motion control setup,
- Multiple language support, providing an intuitive engineering environment Solution.

### **7.2 ARDUINO IDE**

The Arduino integrated development environment (IDE) is a cross-platform application (for Windows, macOS, Linux) that is written in the programming language Java. It is used to write and upload programs to Arduino board. The source code for the IDE is released under the GNU General Public License, version 2. The Arduino IDE supports the languages C and C++ using special rules of code structuring. The Arduino IDE supplies a software library from the Wiring project, which provides many common input and output procedures. User-written code only requires two basic

functions, for starting the sketch and the main program loop, that are compiled and linked with a program stub main() into an executable cyclic executive program with the GNU toolchain, also included with the IDE distribution. The Arduino IDE employs the program avrdude to convert the executable code into a text file in hexadecimal encoding that is loaded into the Arduino board by a loader program in the board's firmware.

### **7.3 BLYNK**

Blynk is a Platform with iOS and Android apps to control Arduino, Raspberry Pi and the likes over the Internet. It's a digital dashboard where you can build a graphic interface for your project by simply dragging and dropping widgets. It's really simple to set everything up and you'll start tinkering in less than 5 mins. Blynk is not tied to some specific board or shield. Instead, it's supporting hardware of your choice. Whether your Arduino or Raspberry Pi is linked to the Internet over Wi-Fi, Ethernet or this new ESP8266 chip, Blynk will get you online and ready for the Internet Of Your Things.

## **9. CONCLUSION**

This project can be adapted to requests formed in the design process, updating the sensor information and reflecting the real factors of environmental poultry farming. Each node has been set to receive the environmental factors (temperature, water level and food level). If any of these observing conditions drops below the predefined threshold, the sensor node will intimate the farmer and automating heating

method, filling of water and filling of food takes place. This system will be labor-saving for the farmer and report environmental changes immediately, thereby enabling the farmer to prevent adverse strictly implemented throughout the redaction method and compiled into the feasible machine language once Consequences.

The first set is formed of various sensors dedicated to measure the environmental parameters in the farm building as temperature, humidity, airflow, and others. The sensors are connected to a local control unit that acquires the readings and sends the data. The main controller receives all the information, processes it, and responds according to predefined algorithms.

## REFERENCES

1. A Few Connectivity Technologies Involved in Internet of Things, Eswar Patnala, Rednam S.S. Jyothi,IJCA Vol. 10, No. 9 Jun 2017 (pp. 167-177).
2. A Study on Internet of Things Service Server Application for Provision of Automatic Service, Am-Suk Oh IJCA Vol. 11, No. 9 Jun 2018 (pp. 25-32).
3. A Dynamic Analysis Tool for Real-time Characteristics Related to Cache Hit-ratio of Real-time Applications, Hyang Yeon Bae IJCA Vol. 10, No. 9 Jun 2017 (pp. 177-190).
4. Sensor Query Control for IoT Data Monitoring, Siwoo Byun IJCA Vol. 11 No Jun 2018 (pp. 109-118).
5. A Poultry Farming Control System Using a ZigBee-based Wireless Sensor Network, Bilal Ghazal,IJCA Vol. 10, No. 9 Jun 2017(pp. 191-198).
6. A Study on the Control Problem of Driving DC Motor with Very-low speed in Automatic Door System for Home, Hyun-Chang Lee,IJCA Vol. 10, No. 9 Jun 2017 (pp. 199-208).
7. Precise Frost and Ice Detection for Defrost Scheme of Agricultural Refrigerator using Integrated Sensor Module based on Moving Window Method, Ji Hoon Seung, Young Baik Kim, IJCA Vol. 10, No. 9 Jun 2017 (pp. 209-216).
8. A Study of Network Infrastructure based Wireless Network Management Service across the Integrated Heterogeneous Networks, Ronnie D. Caytiles and Byungjoo Park IJCA Vol. 10, No. 9 Jun 2017(pp. 217-226).
9. Comparative Study of PLC and Arduino in Automated Irrigation System, Mechelle Grace Zaragoza and Haeng-Kon KimIJCA Vol. 10, No. 6 Jun 2017 (pp. 207-218).
10. Development of HID-Based Motion Recognition Device, Won-Hyuck Choi, Da-Un Kim and Min-Seok Jiev IJCA VOL. 10, No. 8 Jun 2017 (pp. 93-104).

## STUDY THE MATERIAL BEHAVIOUR OF AA6063/WC/ZrO MMCs AND INVESTIGATION OF WIRE EDM PARAMETERS.

Mr.P.Janagarathinam<sup>1</sup>

Assistant Professor  
Dept. of Mechanical engineering  
SNS College of Technology  
(Affiliated to Anna University)  
Coimbatore.

Janagan12345@gmail.com

V.Suriyanarayanan<sup>2</sup>

Dept. of Mechanical Engineering  
SNS College of Technology  
(Affiliated to Anna University)  
Coimbatore.

suriyanarayananv2011@gmail.com

S.Suresh<sup>3</sup>

Dept. of Mechanical Engineering  
SNS College of Technology  
(Affiliated to Anna University)  
Coimbatore.

ssureshssuresh64@gmail.com

**Abstract— The necessity and the importance of the new materials with superior properties in the modern and hi-tech industries have become inevitable. For many industrial applications and particularly in nuclear applications, a wide range of materials is being adopted. The selected materials should have high ductility, low density and high strength with better machinability. The present work is focused on the evaluation of machining studies of AA6063/WC/ZrO composite. The composite is fabricated through stir casting route. The uniform dispersion of the reinforcement particles in the matrix is ensured through scanning electron microscopic image. The machinability of the fabricated composites is evaluated by wire cut electrical discharge machining. The influence of electrode material on affecting the individual machining characteristics is determined. In addition, the ZrO and WC weight percentage (%) is also considered for the evaluation in order to identify its influence on affecting the responses such as surface roughness, material removal rate and electrode wear ratio. The Brass wire electrode has produced better machined surface compared to other electrode at various machining conditions. The influence of each parameter on affecting the surface roughness is plotted and the surface roughness is increased with the ZrO content and WC is added to maintain the hardness to sustainable limit. The surface morphology of the machined area at different input condition is examined through SEM.**

**Keywords—wire cut EDM, composites, stir casting, L27 orthogonal array (key words)**

### I. INTRODUCTION

Wire electrical discharge machining (WEDM) is a particular thermal non-contact technique of machining. Within the past decade, the WEDM process is a competitive and economical machining option fulfilling the demanding machining requirements from a mere tool to complex die making process [1]. Now a day's WEDM process is commonly used for

machining of materials conventional materials to nascent materials like Metal Matrix Composites, ceramic composites, which have vast applications in automobile, aircraft, railway sectors, defence, aerospace, micro systems industries, agriculture farm machinery, etc. Metal matrix composites (MMCs) are advanced materials having properties such as light weight, high specific strength, good wear resistance, a low thermal expansion coefficient, low density [7]. These materials can be machined by non-conventional methods like water jet, laser cutting but these processes are restricted to linear cutting only [6]. Wire Electrical discharge machining (WEDM) shows higher ability for cutting complex shapes with high precision for MMCs [2]. Conventional machining of MMC's causes serious tool wear due to greater hardness and the existence of abrasive reinforcement particles. Numerous studies and research are going on in modelling of WEDM since its inception [3]. Most of the researchers thoroughly worked on process modelling, process parameters, materials of electrodes/tool-work-piece, dielectric medium, etc [5]. The process modelling of WEDM is considered as prime objective. There is need to categorize the variety of research for better understanding of research done in this area. This paper reviews machining of MMCs, techniques used, responses, findings and summery of review. The paper also discusses the future trends of research work in the same area. W-EDM process is widely used in machining of alloys and hard metals in aerospace and die making industries. Its main applications are in punch dies, squeezing dies, injection mould, plastic mould and powder metallurgy [11].

It can also cut various sample plate, magnetic steel, Silicon Steel Sheet, semi-conductive material or precious metal [10].

Furthermore, it can do tiny machining, abnormal shape groove or machining of standard defect of sample parts, widely used in electrics, precious machine tools, light industry, army industry and so on.

The aluminium matrix composite prepared by using stir casting process is having improved mechanical properties. Conventional machining techniques are not so successful in such applications, since the occurrence of hard reinforcements in the matrix [7]. Amid the different non-traditional machining processes, WEDM is appropriate for machining composites having reinforcements in the form of particles [8].

An WEDM is apt for machining a material irrespective of their chemical and physical nature of the material, nevertheless limited with electrically conductive nature [9]. WEDM is also referred as spark erosion machining, which is a process of the cutting of metal particles from a work piece by using a wire electrode.

Wire Electric discharge machining (WEDM), also known as spark machining, spark eroding, burning, wire burning or wire erosion, is a manufacturing process whereby a desired shape is obtained by using electric discharges (sparks). Material is removed from the work piece by a series of rapidly recurring current discharge between wire electrode and workpiece, separated by a dielectric liquid and subject to an electric voltage.

One of the electrodes is called the Tool-electrode, or simply the electrode, while the other is called the work piece-electrode, or work piece [6]. The proceed depends upon the tool and work piece not making actual contact.

When the voltage between the two electrodes is increased, the intensity of the electric field in the volume between the electrodes becomes greater than the two electrodes of the dielectric, which breaks down allowing current to flow between the two electrodes. This phenomenon is the same as the breakdown of the capacitor. As a result, material is removed from the electrodes. Once the current stops, new liquid dielectric is usually conveyed into the inter-electrode volume, enabling the solid particles to be carried away and the insulating properties of the dielectric to be restored [4]. Adding new liquid dielectric in the inter-electrode volume is commonly referred as “flushing”. also, after current flow, the difference of potential between the electrodes is restored to what it is before the breakdown, so that a new liquid dielectric breakdown can occur.

## II. LITERATURE SURVEY

Hamid Reza Ezatpour et al. have investigated the influence of adding nano alumina particles to Al 6061 alloy produced by stir casting process with an objective to improve the mechanical properties of the composites and reported that the nano composites present a fine grain microstructure with high porosity.

Sahraeinejad et al. have examined the effect of Al<sub>2</sub>O<sub>3</sub>, SiC particle sizes from 130 nm to 4.3 μm on Al 5059 matrix, and with different process parameters to obtain a uniform distribution of particles within the stir zone. They reported that Nano-scale particles seem to be more effective to increase hardness by increasing the particle fraction in the produced composites.

Nassim Samer et al. investigated the microstructure and mechanical properties of an Al composite reinforced with nano sized TiC particles. The mechanical property of this composite behaves uncommon with regard to previous micrometer sized Al-TiC composites. The composite consists of high amount of reinforcement are having Young’s modulus of ~110 GPa, tensile strength of about 500 MPa and a maximum elongation about 6%.

Riaz Ahamed et al. have done the investigation on Al-SiC-B4C metal matrix composite and found an increase in the hardness, elongation, tensile strength and yield strength of the composite compared to the pure alloy.

Aykut Canakci et al. have fabricated AA2024-B 4C composite by stir casting process with varying volume fraction of 3, 5, 7 and 10 % and with sizes 29 and 71 μm. They have concluded that the raise in volume percentage, increases hardness of the composite, although the strength of the material is decreased with an addition of the particle volume percentage.

Saba Khoramkhorshid et al. have done an experimental analysis on the mechanical properties of Al composite reinforced with Al 84 Gd6 Ni7 Co3 powders and concluded that the presence of particles significantly enhances the mechanical properties compared to pure Al.

## III. EXPERIMENTAL PROCEDURE

### A. Material, Workpiece and tool

Aluminium Alloy (AA 6063):

The effective way to reduce the weight of any structure is to build it with the materials of low specific weight. Aluminium alloys are metallic materials. As they provide a various number of interesting mechanical and thermal properties, they are mostly used in various applications. In addition, shaping of aluminium is easy, especially in material removal, such as machining. In other words, aluminium alloys are considered as the group of materials which offers the highest levels of machinability, while comparing with other lightweight metal like magnesium and titanium alloys

	Si	Fe	Cu	Mn	Mg	Cr	Ti	other	Al
%	0.6	0.35	0.1	0.10	0.90	0.10	0.10	0.01	Bal

Tungsten Carbide (WC):

Tungsten Carbide is also known Tungsten (IV)carbide, and Tungsten Tetra Carbide. It is a chemical compound containing equal parts of Tungsten and Carbon atoms. In its most basic form Tungsten carbide is a, fine grey powder but it can be pressed and formed into shapes through a process called Sintering for use in industrial machinery, cutting tools, abrasives, Armor-piercing rounds, other tools and instruments, Jewellery. Its mechanical properties are as follows,

Density	-	15.63g/cm <sup>3</sup>
Boiling Point	-	6000oC
Thermal Conductivity	-	110W/mk
Melting Point	-	2785-2830oC
Molecular shape	-	TrigonalPrismatic.

Zirconium Oxide: (ZrO):

Zirconium Oxide sometimes known as Zirconia, is a White crystalline oxide of Zirconium. Its most naturally occurring form, with a monoclinic crystalline structure, is the mineral baddeleyite.

A dopant stabilized cubic structured zirconia, cubic zirconia is synthesized in various colours for use as a gem stone and a diamond simulant.

Zirconia is often more useful in its phase stabilized state. Upon heating, Zirconia undergoes disruptive phase changes. This phase transformation can then put the crack due to application of load into compression, retarding its growth and enhancing the fracture toughness.

Its properties are as follows

Density	-	5.68g/cm <sup>3</sup>
Melting Point	-	2715oC
Boiling Point	-	4300oC

Brass Wire Electrode:

The element Zinc is added to copper to form Brass EDM wire, which is the, most common EDM wire in use today. Brass wires for EDM are typically an alloy between 63/37 to 65/35, Cu/Zn ratio. Zinc has a lower melting/vaporization point which makes it a better electrode material than copper, so the

more the zinc into the surface of the EDM wire, the faster it will cut.

Brass wire began to be used in the late of the 1970s in WEDM machining. These conductive metal wires (diameter from 0.05mm to 0.35mm) are used in three-dimensional machining after programming the required shape and provide wires continuously. The most important properties to consider are: (i) electric discharge performance; (ii) heat resistance; (iii) low calorification; and (iv) heat release.

The machining of work piece is conducted on Wire Electrical Discharge Machine with variable current and voltage having following specifications:

Axis travel: 200x250 mm, speed: 1500 rpm, Range of current: 0 to 6 Amps, Voltage: 0 to 150 volts. The experiments were performed CNC-E3 (MCJ)-DK7720 CH high precision 4 axis CNC WEDM, which was manufactured by STEER corporation. It allows to choose input parameters according to the material and height of the workpiece.

The measurements of surface roughness (Ra) for each machining condition were obtained from a surface tester SJ210 Mitutoyo roughness meter. The material removal rate was calculated by using the following formula,

$$MRR = \frac{W \cdot l \cdot K}{t} \text{ mm}^3/\text{min} \quad (1)$$

Where,

- W = Width of the workpiece (5mm),
- l = Length of the cut in mm (25 mm),
- K = Kerf wire diameter + 2 times of sparking gap (0.20 mm),
- t = Time taken for the same length of cut in minutes.

### B. Experimental Design

Design of Experiments (DOE) is a powerful statistical technique which was used to study the effect of multiple variables simultaneously. An experimental plan is to set test parameter for each run of the test. The response is then measured for each run [5]. The method of analysis is to look for differences between response readings for different groups of the input changes.

In this study there are three controllable variables, namely current, pulse on time and pulse off time has been selected. The voltage is constant for 75 volts (Machining condition). The machining parameter design, three levels of machining parameters were selected, shown in Table 2.

TABLE 2. Machining process parameters

Parameter	Unit	Levels			Response
		1	2	3	
Current	Amps	3	4	5	<b>1. Material Removal Rate</b> <b>2. Surface Roughness</b>
Pulse on time	µs	25	30	35	
Pulse off time	µs	1	2	3	

### C. Taguchi's Design of Experiments

Taguchi method is a traditional approach applied to design the experiments. In the Taguchi design method the design parameters are controllable (factors to be controlled) and noise factors (factors can't controlled), which influence product quality, are considered [6]. Taguchi method is recommended for metal cutting problems to optimize the input parameters (factors).

### D. Experimental procedure

Based on the number of factors and levels, L<sub>9</sub> orthogonal array of "Taguchi method" has been selected for the

experiments using MINITAB 16. Each 9 experiments will carried out. Material removal rate and Surface roughness was selected as response (output) variables. All these data are used for the analysis and evaluation of the optimal parameters combination. The experimental procedure are, in the following order (1) Define input parameter levels and response variables, (2) Plan for design of experiments (3) Perform the Taguchi's experimental design using orthogonal array, (4) Calculate the statistical analysis of variance (ANOVA) for finding factors contribution(%), finally (5) Optimize and conduct conformation experiment to verify the performance of responses.

### III. MATERIAL PREPARATION

#### Stir Casting:

Stir casting is an economical process for the fabrication of aluminium matrix composites. There are many parameters in this process, which affect the final micro structure and mechanical properties of the composites. In this study, micron sized WC and ZrO particles were used as reinforcement to fabricate AA6063/WC/ZrO composites at a casting temperature (700-7500C) and stirring periods (120s). Factors of reaction at matrix or ceramic interface, porosity, ceramic incorporation and agglomeration of the particles were evaluated by scanning electron microscope (SEM) and high-resolution transition electron microscope (HRTEM) studies. From micro structural characterization, it is concluded that the shorter stirring period is required for ceramic incorporation to achieve metal or ceramic bonding at the interface. The higher stirring temperature (10000C) also leads to improve ceramic incorporation. In some cases, shrinkage porosity and intensive formation of Sic at the metal or ceramic interface are also observed. Finally, mechanical properties of the composites were evaluated, and their relation that the corresponding micro structure and processing parameters of the composites was discussed.

#### Casting Procedure and Timing:

Melting of AA6063,		
Melting Temperature	-	650-750oC
Melting Time	-	15-20mins
Pre-Heating of reinforcement powder:		
Pre-heat Temperature	-	500-540oC
Pre-heat Time	-	5-10mins
Stirring process:		
Stirring Time	-	1-2mins

The Al 6063 reinforced with tungsten carbide and zirconium oxide is prepared using the above stir casting method and the photocopy of the material is added below as fig.1

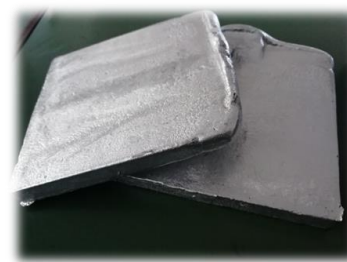
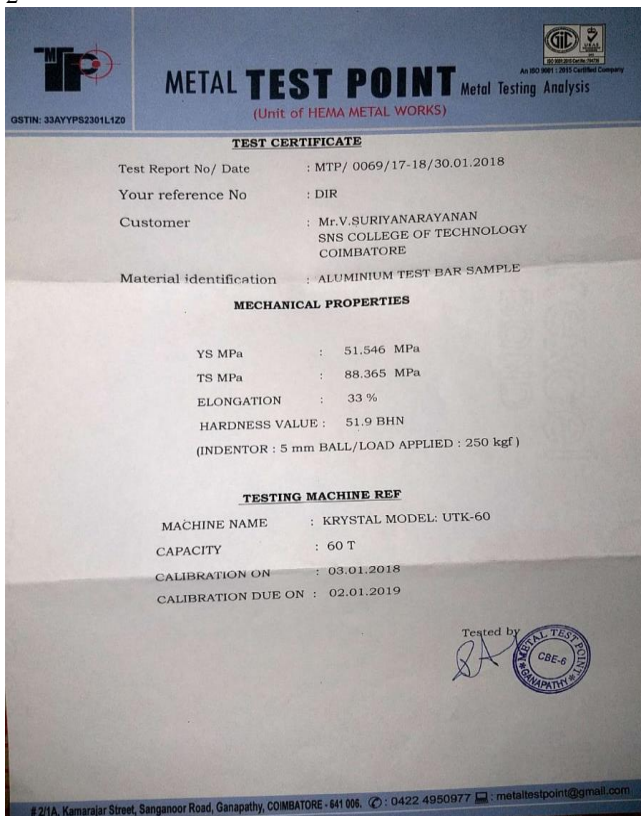


FIGURE 1 PHOTOGRAPH OF FINISHED METAL COMPOSITE.

#### IV TEST REPORT

The tensile and hardness test for the prepared nano material is taken and the report is added below as fig 2



**FIGURE 2 PHOTOGRAPH OF TENSILE AND HARDNESS TEST REPORT.**

#### V CONCLUSION

From the above experiment we can find the performance of AA6063/WC/ZrO when machined using Brass wire under various machining parameters. And it also focuses on both the material properties and also considering the machining parameters.

The material was prepared in the following composition

Al 6063	-	93% (450grams)
Tungsten Carbide	-	2% (9grams)
Zirconium oxide	-	5% (22.5grams)

As a result of the experiment the smoothness and ductility of the al material was increased by addition of zirconium oxide and it is favorable for machining under non-conventional machines ( Wire-EDM, EDM, etc.)

#### REFERENCES

- [1] Puri, A. B., & Bhattacharyya, B., “Modelling and analysis of the wire-tool vibration in wire-cut EDM”, Journal of Materials Processing Technology, Vol.141, pp.295–301, 2003.
- [2] Mohammadi, A., Tehrani, A. F., & Abdullah, A., “Introducing a new technique in wire electrical discharge turning and evaluating ultrasonic vibration on material removal rate”, Procedia - Social and Behavioral Sciences, Vol.6, pp.583–588, 2013.
- [3] Abdullah, A., & Shabgard, M. R., “Effect of ultrasonic vibration of tool on electrical discharge machining of cemented tungsten carbide ( WC-Co )”, International Journal of Manufacturing Technology, Vol.38, pp.1137–1147, 2008.
- [4] Prihandana, G. S., Mahardika, M., Hamdi, M., & Mitsui, K., “Effect of low-frequency vibration on workpiece in EDM processes”, Journal of Mechanical Science and Technology, Vol.25(5), pp.1231–1234, 2011.
- [5] Goswami, A., & Kumar, J., “Optimization in wire-cut EDM of Nimonic-80A using Taguchi’s approach and utility concept”, Engineering Science and Technology, an International Journal, pp.1-11,2014.
- [6] Durairaj, M., Sudharsun, D., & Swamynathan, N., “Analysis of Process Parameters in Wire EDM with Stainless Steel using Single Objective Taguchi Method and Multi Objective Grey Relational Grade”, Procedia Engineering, Vol.64, pp.868–877, 2013.
- [7] S.T.Mavhunga, E.T.Akinlabi, M.A.Onitiri, F.M.Varachia “Aluminium Matrix Composites for Industrial Use: Advances and Trends” 7(2017) 178-182.
- [8] Abhay S.Gore, Nilesh G.Patil , “Wire electro discharge machining of metal matrix composites: A Review” 20 (2018) 41-52
- [9] Punith Gowda K, Dr.J N Prakash, Dr.K Channakeshavalu.,“Evaluation of Wear Properties of AL2024 Reinforced with Tungsten carbide Particulate Metal matrix Composites”
- [10] Dharmesh M.Pantoliya, Sunil Sharma , “Preparation and Characterization of Zirconium Dioxide Reinforced Aluminium Metal Matrix Composites” Vol 4, Issue 5, May 2015.
- [11] Shreenivas Annigeri, Vishwanath Banakare, Dr.R.V.Kurahatti “The Effect on Mechanical Properties and Microstructure of LM6 Aluminium alloy reinforced with Tungsten carbide” Vol 6, Issue 6, June 2016.

# Autonomous Swarm Robots

T.Kousalya  
Assistant Professor  
Department of Mechatronics  
Engineering  
SNS College of Technology'  
Coimbatore-35  
[Kousalya.sae@gmail.com](mailto:Kousalya.sae@gmail.com)

K.M. Aarsha Suresh  
UG Scholar  
Department of Mechatronics  
Engineering  
SNS College of Technology  
Coimbatore-35  
[Aarsha97suresh@gmail.com](mailto:Aarsha97suresh@gmail.com)

K.Nivethithaan  
UG Scholar.  
Department of Mechatronics  
Engineering  
SNS College of Technology  
Coimbatore-35  
[Niverocker789@gmail.com](mailto:Niverocker789@gmail.com)

Terrin J. Mario Pereria  
UG Scholar  
Department of Mechatronics  
Engineering  
SNS College of Engineering  
Coimbatore-35  
[Terrinpereria@gmail.com](mailto:Terrinpereria@gmail.com)

Dilshad Bin Mohammed Iqbal  
UG Scholar  
Department of Mechatronics  
Engineering  
SNS College of Technology  
Coimbatore-35  
[Dilshadhadi@gmail.com](mailto:Dilshadhadi@gmail.com)

**Abstract— This paper aims to illustrate and a network of autonomous robots that can work and act together for performing various tasks and operations. Swarm-bots are a collection of mobile robots that can self-assemble and self-organize in order to solve problems that cannot be solved by a single robot. These robots combine the power of swarm intelligence with the flexibility of self-reconfiguration as aggregate swarm-bots can dynamically change their structure to match environmental variations. Swarm robots are more than just networks of independent agents, they are potentially reconfigurable networks of communicating agents capable of coordinated sensing and interaction with the environment. Robots are going to be an important part of the future. In the near future, it may be possible to produce and deploy large numbers of inexpensive, disposable, meso-scale robots. Although limited in individual capability, such robots deployed in large numbers can represent a strong cumulative force similar to a colony of ants or swarm of bees. Various methods of designing and fabrication is done to implement such bots. Once it's a success many of these will be developed for helping and improving the lifestyle of mankind.**

**Keywords—** *swarm robotics, autonomous robots, robotic communication, machine vision*

## I. INTRODUCTION

**AUTONOMUS SWARM ROBOTS:** In the 21st Century, robotics has become ubiquitous in all spheres of human activity. Ranging from industry to science to home care. Robots have heralded on

of the biggest changes to human life. Robots have taken over hundreds of tasks that humans find either repetitive or dangerous. From industrial welding to space exploration robots have enabled humans to achieve more with less. In industries, robots have completely supplanted humans in various fields including welding, machining etc. The concept of automatons performing dangerous or mundane tasks was even known to the ancient Greeks and Egyptians. In Greek mythology, the legend Cadmus refers to the man who was created of clay and was “breathed into life by man”. The most famous of all myths involving artificial humans was that of Pygmalion, in which a sculptor falls in love with a sculpture he had made and brings it to life. The ancient Greek inventor Hero of Alexandria is said to have made the earliest sketches for a fully working model of a mechanical automaton that was said to be powered by steam. But sadly, those sketches were said to have been destroyed when the Library of Alexandria was burned down in 5th Century AD. In China, the fabled metalsmith Yan Shi is said to have designed Mannequins that had the many human-like organs.

Despite the various advances in the field of robotics, robots in the modern day look very utilitarian and less like the robots as depicted in fiction. Modern robots are extremely efficient and fast in various tasks. But these robots tend to be task oriented than being universally i.e. they are made to fulfil one particular task say Welding or Assembly tasks. Modern robots are also employed in wide range of tasks and applications ranging from Education to Industry and Military to Space Exploration. Each robot created is unique and can do the tasks that they were built for in an exceedingly efficient way. Androids as depicted in Science fiction are still a dream, but many

researchers are finding ways to make that dream a reality.

Robots in the Information age come in many types and sizes. They range from extremely small such as nano-robots which are very small (typically 1 nanometre across) to automated excavators the size of skyscrapers. The main usage of robots is in industries where the work is quite risky and dangerous.

The main problems faced in robotic systems is the lack of communication among the robots, human intervention needed to carry out tasks, current limitation in software and hardware technology makes the robots primitive.

The solution to this problem can be addressed by the concept of swarm robots (Figure 1.1). This has helped us in developing better robots. The communication among the robots is brought about by using different wireless ways. Some of these wireless communications are:

- Wireless multi-hop communications
- Node mobility
- Networked robots
- Machine-to-machine communications

## II. LITERATURE REVIEW

### ➤ SWARM ROBOTICS

#### 1. Swarm robotics, a review from the swarm engineering perspective

(Manuele Brambilla et al. 2013)<sup>[22]</sup> suggested that swarm robotics could be an engineering field and that would help to tackle real-world applications. They also noted down the goals which are to be considered for modelling, designing, realizing, verifying, validating, operating, and maintaining a swarm robotic system.

#### 2. Research Advance in Swarm Robotics

(Ying Tan & Zhong-yang Zheng 2013)<sup>[21]</sup> differentiated elaborately between a single robot and a multi-individual robotic system. The descriptive differentiation underlines the advantages of a swarm robotics system. In their paper the main

emphasis is about the current research on the swarm robotic algorithms are presented in detail, including cooperative control mechanisms in swarm robotics for flocking, navigating and searching applications.

#### 3. Autonomous Self-Assembly in Swarm-Bots

(Roderich Grob et al. 2005)<sup>[14]</sup> observed the difference in performance of between single robot and of groups of robots self-assembling with an object or another robot. The robustness of the system with respect to different types of rough terrain were also assessed by them.

### ➤ SWARM INTELLIGENCE ALGORITHMS

#### 4. Robots, insects and swarm intelligence

(Amanda J. C. Sharkey 2006)<sup>[15]</sup> The relationships between robots and insects has been explained in two main areas of robotics research i.e., through the behavioral pattern of insects. The development in robotics has been brought by studying the working methodology and characteristics of the insects. It is concluded that bio-robotic modelling and biological inspiration have made important contributions to both insect and robot research, but insects and robots remain separated by the divide between the living and the purely mechanical.

#### 5. Ant Colony Optimization Algorithm for Robot Path Planning

(Michael Brand et al. 2010)<sup>[18]</sup> Path planning is an essential task for the navigation and motion control of autonomous robot manipulators. The ACO (Ant Colony Optimization) algorithm is an optimization technique based on swarm intelligence. Two different pheromone re-initialization schemes are compared and computer simulation results are presented.

## SPHERICAL ROBOTS

### ➤ A Literature Review on the Design of Spherical Rolling Robots

(Vincent A. Crossley 2006)<sup>[16]</sup> A spherical robot design is said to be holonomic, which means it can move in any direction. This increases the options for navigating around objects and prevents the robot from getting stuck in corners, but they cannot be over tuned. Stairs and ledges are not an issue for the spherical robots due their features. They have a great capability to recover from collisions with obstacles. This would be useful in a swarm application, where many spheres could be traveling in close proximity, and because of the design they would not interfere with each other's motion. They can be designed to be totally sealed and are also ideal for hazardous environments. The sensors, electronics, and mechanisms are all protected. This makes them capable of functioning in snow, mud, and even water. Spherical robots be assisted or powered by winds. They can also be smaller than wheeled vehicle, and can be made cheaper with fewer parts, or they could even be disposable.

### III. SYSTEM DESIGN

In the newly proposed system (*Figure 3.4*), the external shell is not connected to the central axis directly, instead the robot will be connected to the frame enabling the shell to move like a wheel. The use of 1 gyroscope instead of 2 and the use of high torque motors and drives will prevent the unwanted secondary boost. Along with this improvement there will also be a NRF Module will enable communication with other robots and it has an Arduino for automated movement and control. To put differently, the robot can move and interact with other robots on its own.

#### Advantages of the Proposed System

- The use of high torque motors will prevent the realignment of the gyroscopes and prevent unwanted boost in torque.
- It is autonomous and can communicate with other robots using nRF204L01 module (*Figure 2*)
- It is cheap to construct and has a simple design

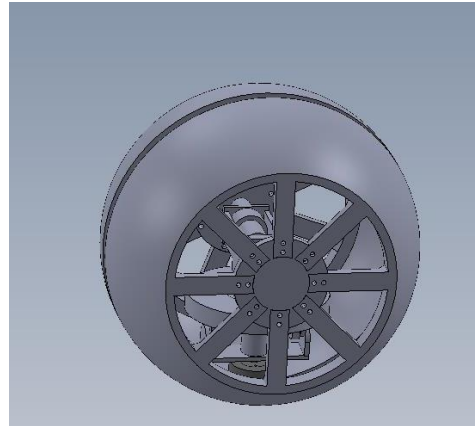


**Fig 1:**  
Proposed Model (Designed using SolidWorks 2016)

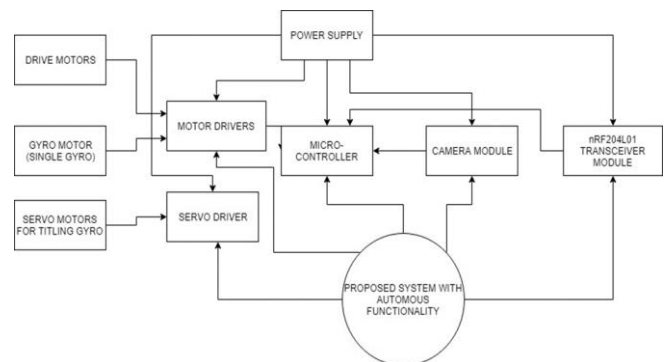


**Fig 2: Block Diagram of Proposed System**

### IV. DESIGN AND CONSTRUCTION OF THE ROBOT

Mathematical Calculation was done using the data from the CAD Model to find the Angular Momentum of the Gyro Rotor. So as to verify the selection of the servo motor which is responsible for tilting the spin axis of the gyro-rotor.

$$\text{Moment of Inertia of Gyro Rotor} = 6.58427 \times 10^{-3} \text{ Kg}\cdot\text{m}^2/\text{sec}.$$

<b>Angular momentum (L)</b>	
Formula: $L = I * \omega$ $\omega = 2618 \text{ rad/sec}$ $I = 2.515 \times 10^{-6} \text{ kg.m}^2$ $L = (2.515 \times 10^{-6}) * 2618$	
<b>L = 6.58427 x 10-3 Kgm2/sec.</b>	
<b>Moment of Inertia (I)</b>	
Formula: $I = 1/2 * M * R^2$ $M1 = 200\text{g Or } 0.200\text{kg}$ $R1 = 50\text{mm Or } 0.005\text{m}$ $I1 = 1/2 * M1 * [R1]^2$ $I1 = 1/2 * 0.200 * [0.005]^2$ $I1 = 2.5 \times 10^{-6} \text{ kg.m}^2$	Formula: $I = 1/2 * M * R^2$ $M2 = 30\text{g or } 0.030\text{kg}$ $R2 = 10\text{mm or } 0.001\text{m}$ $I2 = 1/2 * M2 * [R2]^2$ $I2 = 1/2 * 0.030 * [0.001]^2$ $I2 = 1.5 \times 10^{-8} \text{ kg.m}^2$
<b>I = I1 + I2</b>	
<b>I = 2.5x10-6 + 1.5x10-8</b>	

<b>Angular Velocity (ω)</b>
Formula: $\omega = (\theta_f - \theta_i) * t$ $\theta_f = 25000 \times 2\pi$ $\theta_i = 0$ $t = 60 \text{ sec}$
$\omega = (25000 * 2\pi) / 60$ $= 2618 \text{ rad/sec}$

Parameters	Formula	Description
<b>Angular Momentum of Gyro Rotor</b>	$L = I * \omega$	Where, L = angular momentum I = moment of inertia $\omega$ = angular velocity
<b>Moment of Inertia</b>	$I = 1/2 * M * R^2$	Where, M = Mass R = Radius
<b>Angular Velocity</b>	$\omega = (\theta_f - \theta_i) * t$ (in radsec-1)	Where, $\theta_f$ = final angle $\theta_i$ = initial angle t = time

## V. CONCLUSION

The Work plan for Project Phase – 1 was followed. The Literature Review and Component Identification was done successfully. Mathematical Calculations and Virtual Simulations were done with positive result. The Prototype was fabricated and was tested, there was some room for improvement to be made with the prototype as the outer hemispherical shell could not be manufactured properly. The prototype functioned successfully other than the earlier mentioned flaw.

## REFERENCES

1. Chemel, Brian, Edward Mutschler, and Hagen Schempf. "Cyclops: Miniature robotic reconnaissance system." *Robotics and Automation, 1999. Proceedings. 1999 IEEE International Conference on*. Vol. 3. IEEE, 1999. Rybski, Paul E., Dean F. Hougen, Sascha A. Stoeter, Maria Gini, and Nikolaos Papanikolopoulos.
2. Yim, M., Duff, D.G., Roufas, K.D.: PolyBot: a modular reconfigurable robot. In: *Proceedings of the 2000 IEEE International Conference on Robotics and Automation (ICRA 2000)*. Volume 1, IEEE Press, Piscataway, NJ (2000) 514–520
3. Castano, A., Shen, W.M., Will, P.: CONRO: Towards deployable robots with inter-robot metamorphic capabilities. *Autonomous Robots* 8 (2000) 309–324
4. Khosla, P., Brown, B., Paredis, C., Grabowski, B., Navarro, L., Bererton, C., Vandeweghe, M.: Millibot Report. Report on millibot project, DARPA contract DABT63-97-1-0003, Carnegie Mellon University, Pittsburgh, Pennsylvania, USA (2002)
5. S. Bhattacharya, S.K. Agrawal (Proceedings 2000 ICRA. Millennium Conference. IEEE International Conference on Robotics and Automation. Symposia Proceedings (Cat. No.00CH37065), 06 August 2002, DOI: 10.1109/ROBOT.2000.844763)

6. Mojabi, Puyan. (Robotics and Automation, 2002. Proceedings. ICRA'02. IEEE International Conference on. Vol. 4. IEEE, 2002)
7. Sahin, E., Labella T.H., Trianni, V., Deneubourg, J.L., Rasse, P., Floreano, D., Gambardella, L.M., Mondada, F., Nolfi, S., Dorigo, M.: SWARM-BOT: Pattern formation in a swarm of self-assembling mobile robots (2002). In: Proceedings of the IEEE International Conference on Systems, Man and Cybernetics, IEEE Press.
8. Camazine S, Deneubourg JL, Frank NR, Sneyd J, Theraulaz G, Bonabeau E. Self-organization in biological systems (2003). Princeton: Princeton University Press;.
9. Groß, R., Dorigo, M.: Cooperative transport of objects of different shapes and sizes. In Dorigo, M., Birattari, M., Blum, C., Gambardella, L.M., Mondada, F., Stützle, T., eds.: Proceedings of ANTS 2004 – Fourth International Workshop on Ant Colony Optimization and Swarm Intelligence. Volume 3172 of Lecture Notes in Computer Science., Springer Verlag, Berlin, Germany (2004) 107–118
10. Labella, T., Dorigo, M., Deneubourg, J.L.: Efficiency and task allocation in prey retrieval. In Ijspeert, A., Murata, M., Wakamiya, N., eds.: Proceedings of the First International Workshop on Biologically Inspired Approaches to Advanced Information Technology (Bio-ADIT2004). Volume 3141 of Lecture Notes in Computer Science., Springer Verlag, Heidelberg, Germany (2004) 32–47
11. Labella, T., Dorigo, M., Deneubourg, J.L.: Self-organised task allocation in a swarm of robots. Technical Report TR/IRIDIA/2004-6, Université Libre de Bruxelles, Belgium (2004) To appear in the 7th International Symposium on Distributed Autonomous Robotic Systems (DARS04), June 23-25, 2004, Toulouse, France.
12. Trianni, V., Nolfi, S., Dorigo, M.: Hole avoidance: Experiments in coordinated motion on rough terrain. In Groen, F., Amato, N., Bonarini, A., Yoshida, E., Kröse, B., eds.: Intelligent Autonomous Systems 8, IOS Press, Amsterdam, The Netherlands (2004) 29–36
13. Sahin E. Swarm robotics: from sources of inspiration to domains of application. In: Swarm robotics (2005), lecture notes in computer science, vol. 3342. Springer. p. 10-20.
14. Roderich Grob, Michael Bonani, Francesco Mondada, Marco Dorigo (Proceedings of the 3rd International Symposium on Autonomous Minirobots for Research and Edutainment (AMiRE 2005) pg. 314-322.)
15. Amanda J. C. Sharkey (Artificial Intelligence Review, December 2006, Volume 26, Issue 4, pp 255–268)
16. Vincent A. Crossley (Pittsburgh, Pa (2006): 1-6.)
17. Dervis Karaboga, Bahriye Akay (Artificial Intelligence Review, June 2009, Pg. 31:61)
18. Michael Brand, Michael Masuda, Nicole Wehner, Xiao-Hua Yu (2010 International Conference On Computer Design and Applications, 09 August 2010, DOI: 10.1109/ICCD.2010.5541300)
19. Park, G. D., Lee, H., Kim, K. H., & Lee, J. M. ((2011, November). Ubiquitous Robots and Ambient Intelligence (URAI), 2011 8th International Conference on (pg. 511-515). IEEE.)
20. Chase, R., & Pandya, A. (2012). A review of active mechanical driving principles of spherical robots. *Robotics*, 1(1), 3-23.
21. Tan, Y., & Zheng, Z. Research Advance in Swarm Robotics (2013). *Defence Technology*, 9(1), 18–39.
22. M. Brambilla, et al. Swarm Robotics: A Review from a Swarm engineering Perspective (2013), *Swarm Intelligence*, 7(1), 1-41.
23. Tamer Abukhalil, et al. Survey on Decentralized Modular Swarm Robots and Control Interfaces (2013). *International Journal of Engineering*, 7(2), 44-59.
24. Micheal Rubenstein et al. Programmable self-assembly in a thousand robot swarm (2014). *Science*, 345, 795-799.

# *Impact of Cryogenic Treatment on the Friction Welded Aluminium Metal matrix Composite*

Sreenivasan KS

*Department of Mechanical Engineering*

*Misrimal Navajee Munoth Jain Engineering College*  
Chennai, India

[kssreeni@gmail.com](mailto:kssreeni@gmail.com)

(Corresponding Author)

Satish Kumar S

*Department of Mechanical Engineering*

*Velammal Engineering College*  
Chennai, India

[satish\\_shan@yahoo.com](mailto:satish_shan@yahoo.com)

Vignesh T

*Department of Mechanical Engineering*

*Misrimal Navajee Munoth Jain Engineering College*  
Chennai, India

[vignesh.thangam98@gmail.com](mailto:vignesh.thangam98@gmail.com)

Subbramaniyan MS

*Department of Mechanical Engineering*

*Misrimal Navajee Munoth Jain Engineering College*  
Chennai, India

[subbramaniyan.ms@gmail.com](mailto:subbramaniyan.ms@gmail.com)

**Abstract**—Aluminum metal matrix composites have attracted its usage in the field of aerospace and marine applications in recent times. The aluminum metal matrix composite is subjected to welding process. Solid state welding process only will be effective to produce sound joints. Among the available solid-state welding process friction welding is the simplest and effective process to weld the aluminium metal matrix composite. To further improvise the strength and hardness of the friction welded joints they were subjected to cryogenic treatment. The research was about the effect of cryogenic treatment on parent metal and friction welded metal when exposed for different time periods (24, 36, 48 and 60 hours) at -196°C. Both Parent metal and welded metal shows improvement after cryogenic temperature in Ultimate Tensile Strength and Hardness. From the observation, it was found that the improvement in the Ultimate Tensile Strength and Hardness was seen up-to 48 hours of treatment. The percentage improvement of the strength and the hardness of friction welded samples were found to be more than the parent metal. The microstructural inspection showed fine dimples indicating the ductile mode of failure.

**Keywords**—Aluminium Metal Matrix Composite, friction Welding, Cryogenic Treatment, Ultimate Tensile Strength, Hardness

## I. INTRODUCTION

For a variety of applications, Aluminum is recognized as one of the most commonly used material. Mainly used for manufacturing aircrafts, Aluminum Alloys are known for its properties which include, light weight, high weight to strength ratio, corrosion resistance and ductility even at low temperatures.

Since the early 1960's, the demand for new and improved engineering materials grew with advancement of modern technology. Interests in the areas of aerospace, automotive industries had forced a rapid development of metal matrix composites. High demands on material for better overall performance has led to extensive research and development efforts in the field of composite. Among the composites field, the Aluminum based metal matrix composite materials are widely used [1].

The "Composite Material" is composed of a distributed and discrete reinforcement in a continuous phase of matrix [2]. In Aluminum metal matrix composite (AMMC), one constituent is Aluminum which forms network i.e. matrix phase and the other serves as a reinforcement which is generally ceramic or non-metallic hard materials. The main reason of reinforcing metals with ceramic particles or fibers is to improve the properties like strength, hardness etc.

Aluminum based metal matrix composites have been one of the key research areas in materials processing field in the last few decades. Most of the research work has been dealing with Aluminum matrix and Silicon Carbide (SiC) reinforcement as it results in the light weight combination of high strength and high hardness [3]. This is because Aluminum is lighter in weight and is preferred in most of the industries. Additionally, it provides greater improvement in strength and thermal expansion coefficient of Aluminum matrix composites.

Aircrafts and rocket propulsion systems require advanced metallic materials to reduce launch costs and enable extended space missions. Improved materials with higher strength-to-weight ratios, resistance to fuel environments at high pressures, and good ductility are required for further improvements in engine performance [4]. The reduction in weight can most efficiently be realized by the use of low-density alloys such as aluminum. Although several 7XXX series aluminum alloys show high strengths at room temperature none of the currently available commercial aluminum alloys can sustain its durability at cryogenic temperatures.

Aluminum metal matrix composites are now preferred as a substitute for commercial Aluminum alloys in the field of cryogenics. Though the strength impaired by the material itself maybe significantly high, it is not sufficient to sustain the versatile applications of modern technology at specific conditions such as at low temperatures [5]. To overcome this, the material is joined together by welding to provide required increase in strength. Welding of Aluminum is a tedious process as it is a ductile material. Normally Fusion welding is done to join materials of high strength together. As Aluminum alloys show more ductility, solid state welding process is effective for such materials. Friction welding is the most commonly used solid state welding process to join Aluminum Alloys. In this process the heat generated through mechanical friction between work pieces in relative motion to one another displaces and fuse the materials and joins them together [6]. Friction welding parameters like friction pressure of 99.8MPa, Spindle Speed of 1595.53 rpm, Burn-off-length of 2.15mm, Upset Pressure of 219.78 MPa are used in this process. Furthermore, when treated to cryogenic temperature the grain structure of the particle reduces enhancing the material properties of the metal matrix composite. Cryogenic enhancement of the composite material also results in the enhancement of joint efficiency and yield strength of the weld [7]. These enhanced material properties are perfectly suitable for the required application and are not extensively studied. This

project is mainly to study the enhancement of the optimized friction welded material under cryogenic conditions.

## II. MATERIAL PREPARATION

Aluminum alloy AA 7075 was selected as a matrix material whose chemical composition is given in the Table1. The reinforcement ceramic of 30 μm nominal diameter SiC particulate was selected particularly to prevent the reinforcement fracture as in the case of particulate size greater than 30 μm nominal diameter and also to prevent the interfacial debonding in the case of size lesser than 10 μm nominal diameter. Although many manufacturing processes are available, the stir casting process was employed to produce the AA 7075- 10% SiC<sub>p</sub> metal matrix composite because of its efficiency to produce metal matrix composite with uniform distributed reinforcement up to 10% volume of reinforcement.

Table 1. Chemical composition of AA 7075.

Element	Cr	Cu	Fe	Mg	Mn
Composition	0.20	1.8	0.4	2.5	0.12
Element	Si	Ti	Zn	Al	
Composition	0.025	0.05	5.5	Balance	

An electric arc tilting furnace had been used with the crucible material made of graphite with provision to melt the metal in an inert environment by blanketing with Argon gas shield. A three bladed stirrer with rotating speed ranging between 100 rpm to 600 rpm was used for the stirring of the molten aluminium and SiC abrasive particulate.

AA 7075 ingots were preheated to a temperature of 200°C before melting in order to remove the impurities like oxides and humidity. Similarly, the reinforcement abrasive SiC particulates were preheated to about 1 hour at a temperature of 900°C for eliminating surface impurities and also to form surface oxide layer to enhance wetting when added in the molten aluminium matrix

The preheated aluminium AA 7075 ingot is melted in the furnace for 3 hours and then the preheated 20 μm nominal diameter SiC particulates are added to the molten aluminium matrix at the rate of 20 gm per sec which is stirred at 300 rpm. The stirrer is placed at 0.65 of the crucible height to reduce the formation vortex and for having good distribution of the particulate. For improving the wettability of the SiC particulate Magnesium is added to the molten aluminium matrix before adding the SiC particulate. The molten aluminium matrix with SiC particulate is stirred at 400 rpm for 15 minutes and then it is poured into the mould for making the AA 7075 + 10 % SiC<sub>p</sub> cast rod of diameter 20 mm and length 75 mm.

Precipitation heat treatment of the AA 7075+ 10 % SiC<sub>p</sub> is done to improve its strength further. The cast rods are heated at 480°C temperature and maintained for 2 hrs to dissolve any precipitates and to ensure that the alloying elements remain in solid solution. The rods are quenched in water to form supersaturated solid solution. Then the rods are artificially aged by heating to a temperature of 121° C in a furnace for 24 hours and then air cooled to get the rods as AA7075 + 10 %SiC-T6 .

The microstructure of the specimen Fig 1 shows the uniform distribution of the composite particles in the metal matrix aluminium alloy AA-7075 + 10% SiC –T6 The metal matrix shows solution treatment and precipitation

hardened microstructure with the fine particles of eutectic precipitates in the grains. The precipitated particles are fine Mg<sub>2</sub>Si, Cu-Al<sub>2</sub> and Some Zn-Al<sub>2</sub>. The presence of the precipitates can be confirmed from the EDAX image as shown in figure 2. However, the SiC particles are bigger than the size of the precipitates and occupy the grain boundaries.

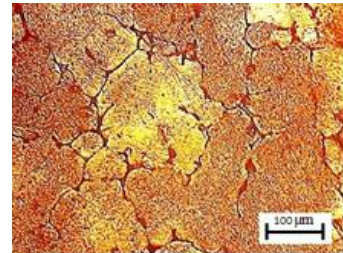


Fig. 1

### A. Heat treatment

Heat treatment process is the combination of both heating and cooling of alloys in solid phase. The main aim of the heat treatment process is to modify the mechanical properties of the alloy depending upon the requirement i.e. soft for forming operations or to attain a definite mechanical strength. The term heat treatment when associated with aluminium alloy it means for improving strength and hardness of the cast and wrought precipitation hardenable aluminium alloy [8]. Many aluminium alloys are existing which do not show any significant change in the strength and hardness when subjected to heat treatment process and they are broadly termed as non-heat treatable.

. As the aluminium alloy taken for consideration here in this investigation is AA7075 which is coming under heat treatable aluminium alloys that has to be subjected to precipitation hardening to get improved strength and hardness. The precipitation hardening process involves three steps,

1. Solution heat treatment
2. Quenching process
3. Aging

#### 1. Solution heat treatment:

For reaping maximum benefit out of the precipitation hardening process it is mandatory to develop a solid solution and this can be achieved by solution heat treating. The main objective of this process is to make the hardening elements present in the alloys to get soluble in the solid solution. The process is carried out at a particular high temperature called as soaking temperature. The soaking temperature ranges between 260°C to 480°C.

The time for which the soaking process is carried out is called as soaking time and it will be chosen to get homogeneous solid solution. The soaking time can vary from a minute (for thin sheets) to 20 hours (for large casting products) depending upon the type of manufacturing process and product size.

#### 2. Quenching Process:

. The moisture present in the environment when encounters the aluminium at high temperature hydrogen gets emerged and diffuses into the metal. The surface blistering and the formation of the voids are the main impact of the high temperature oxidation.

To avoid the detrimental effect of hydrogen the solution heat treated aluminium alloy should be quenched in

the cool water immediately without any delay. This process of immediate cooling of the hot aluminium alloy is called as quenching. Wit fast cooling supersaturated solution can be achieved which was very essential for the precipitation hardening process.

3. Ageing:

The aluminium alloys of 6xxx, 2xxx and copper content present 7xxx series can have their strength maintained after solution heat treatment and quenching. The temper at the room temperature are good enough to improve strength and fatigue life. The process of getting satisfying properties at this stage itself is called natural ageing. This type of aging is designated as T3 and T4 condition. However, in the 7xxx series of aluminium alloys the mechanical properties will not be stable after solution heat treatment and quenching process. It will keep on exhibiting significant change in mechanical properties every year. To have a stable mechanical property in this type of alloy artificial aging process is carried out and it is designated as T6.

B. Cryogenic Treatment

Cryogenics got its name from the combination of two Greek words ‘Kryo’ meaning freezing and ‘genic’ meaning produce. So, Cryogenics is the branch of engineering to study about generation of very low temperature environment and the material behaviour at that low temperature. From the definition it is evident that temperatures below the freezing temperature of water (0°C) i.e. lower than -180 ° C are considered as cryogenic temperature. The temperature below -180 °C was considered as the cryogenic temperature as the liquefied gases which are used to produce very low temperature such as liquid Nitrogen, Liquid Oxygen, Liquid Helium etc. has got their normal boiling point lesser than -180 ° C [8]. The liquefied gases which produce cryogenic temperatures are called as Cryogens or Cryogenics liquid. The normal boiling point of different gases are shown below in **Table 1**.

**Table 1:** Normal Boiling point of different cryogens

Cryogen	Normal Boiling Point	
	in ° C	In K
Helium (He)	-273.15	4.2
Hydrogen (H <sub>2</sub> )	-253	20.3
Nitrogen (N <sub>2</sub> )	-196	77.4
Oxygen (O <sub>2</sub> )	-183	90.2

1. Types of Cryogenic Treatment

The cryogenic treatment process shows effect on the bulk material unlike the coating process which have only impact on surface. In cryogenic treatment the material is cooled at required cryogenic temperature for a period of time and then heated back to the room temperature. The cryogenic treatment process can be conducted as one-time permanent process, as an additional process over the conventional type of heat treatment to improvise the material properties. It is broadly classified into two types depending upon temperature ranges and they are,

1. Shallow Cryogenic Treatment
2. Deep Cryogenic Treatment

In the case of shallow cryogenic treatment, the material is cooled in the range of -84° C and in the case of

deep cryogenic treatment the material will be treated in the temperature range of -196° C.

2. Need of Cryo-treatment

The materials subjected to manufacturing processes are susceptible to induced stress which affects the crystal structure of the material leading to be the prime reason for the failure of the materials during service. This induced stress will lead to the defects in the crystal lattice in the form of vacancies and dislocations [10]. Due to the increase in the stress level the magnitude of the defects increases causing the inter atomic distance to increase and when it exceeds the critical distance leads to crack initiation which further propagates to create failure in the material.

Recently aluminium alloys are preferred over stainless steel and nickel as a cryogenic material in ships and other offshore structures because of comparatively low cost, good strength to weight ratio, good corrosion resistance, and significant improvement in ultimate tensile strength and fatigue strength at cryogenic temperature. To further enhance the properties of aluminium alloys the abrasive particles are dispersed in the aluminium matrix to form aluminium metal matrix composite.

Aluminium metal matrix composites are the most preferred materials for altering aluminium alloys and stainless steel in different naval and aerospace applications. As the materials are used in the structural application it will be subjected to many manufacturing processes like riveting, welding etc. Among them the material failure predominantly occurs in the welded region produced by conventional fusion welding process. So, friction welding process is employed to join aluminium metal matrix composite as it operates near the recrystallisation temperature avoiding defects in the recrystallisation process.

To predict the behaviour of the Aluminium metal matrix composite of non-welded and friction welded samples in the cryogenic condition the temperature and time place a significant role. Deep cryogenic temperature of -196°C (77 K) is selected for cryo-treatment using liquid nitrogen as it produces well distributed and homogeneous microstructure [9].

Cryogenic Procedure:

In the case of Cryogenic treatment process the material to be treated will be kept in an insulated (Thermal) tank which will be supplied with liquid nitrogen or helium. The cryogenic treatment can be conducted in three different methods such as,

- i. Cryo-quench process in which the parts are directly immersed in the cryogenic fluid, liquid ways but supplying the cryogenic gas
- ii. Cryogenic treatment by cooling the air present in the tank containing the parts using the cryo- fluid.
- iii. Cryogenic treatment by creating a dry atmosphere inside the tank containing the parts by circulating the cryo- fluid with the help of fan.

During the cryo-quench process due to large temperature difference between the surface of the part and the bulk of the part will lead to development of harmful thermal stresses eventually leading to crack formation in the cryogenic treated parts. In the case of air cooling using the cryo-fluid process deposition of vapour ice on the parts had been witnessed which in turn interrupts the homogeneous effect of cryogenic treatment. Perhaps the third method in

which the cryogenic treatment with the help of fan circulating the cryo-fluid has no problems the other two method where as a controlled cryogenic treatment can be established. Consequently, the third method has been selected for the cryogenic treatment considering its merit over other two methods.

Cryogenic fluids like liquid nitrogen and liquid helium are used to produce cryogenic environment by producing temperature of -196°C and -268°C. As the earth’s atmosphere contains nearly 78% of nitrogen it is abundantly available while the liquid helium can be used for significantly specialised applications. Hence liquid nitrogen had been chosen as cryo-fluid in this work.

The **figure (2)** shows the schematic illustration of the cryogenic setup where the liquid nitrogen is kept in an external reservoir. The liquid nitrogen will be vaporised and pumped inside the insulated tank where the parts are kept.

To create a homogeneous cryogenic effect a fan is used which blows the vaporised nitrogen inside the thermally insulated tank in a uniform manner. The nitrogen flow is controlled based on the temperature inside the chamber.

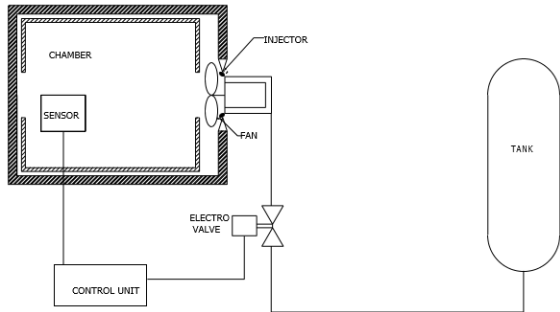


Fig. 2

The main cryogenic parameters which have significant impact are the cryogenic temperature and the soaking time. As deep cryogenic condition was preferred to reap the maximum benefit of cryogenic treatment a temperature of -196°C was maintained and the soaking period was varied as 24 hours, 36 hours, 48 hours and 60 hours [11]. The cooling rate was 2°C/min and the going back to the room temperature after the soaking period was also 2°C/min.

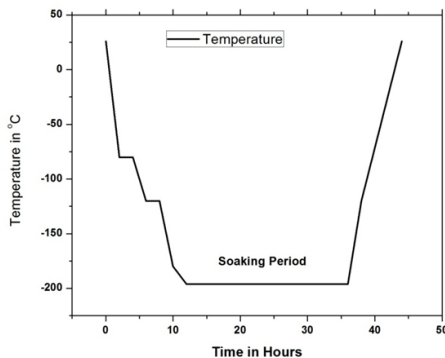


Fig. 3

### III. RESULT AND DISCUSSION

#### A. Impact of Cryogenic Treatment on Ultimate Tensile Strength

The comparison of ultimate tensile strength of AA 7075 +10% vol SiC -T6 metal matrix composite with the optimized friction welded specimen under

cryogenic conditions (-196°C) is shown in **Fig. 3**. The ultimate tensile strength value mainly depends upon the movement of the dislocation hindered by the precipitates present in the AA 7075 +10% vol SiC -T6 metal matrix composite. The coarse secondary phase eutectics Al<sub>7</sub>Cu<sub>2</sub>Fe, CuMgAl<sub>2</sub> and MgZn<sub>2</sub> formed as a result of quenching during the precipitate hardening process consumes more quantity of alloying elements and prevents the formation of more precipitates as said by Xu et al. These coarse secondary phases are found to have low strength and brittle in nature creating cracks in the material ultimately declining the strength [12]. When the aluminium metal matrix composite is subjected to deep cryogenic treatment the elements in the secondary phases get dissolved in the α-Al matrix because of which the size of the secondary phases gets reduced and the fine precipitates are evenly distributed in addition to grain refinement in the α-Al matrix. Due to the refinement of the grain the residual stress present in the metal matrix composite also gets reduced. The fine precipitates or dispersoids developed acts as the hindrance to the dislocation movement when the material is subjected to deformation.

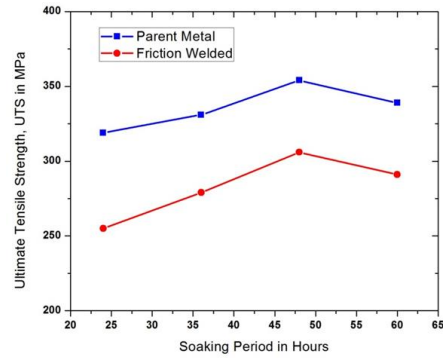


Figure 4 Soaking time Vs Ultimate Tensile strength of Parent and Friction welded sample

Table 2 Tensile Test Results after Deep Cryogenic Treatment

	UTS (MPa) for different soaking time				
	Room Temperature	24 hrs	36 hrs	48 hrs	60 hrs
Parent metal (PM)	314	319	331	354	339
Friction Welded (FW)	246	255	279	306	291
Difference in UTS	68	64	52	41	48
<b>Difference between UTS of the parent metal specimen and welded specimen in %</b>					
$\frac{(UTS_{PM} - UTS_{FW})}{UTS_{PM}} \times 100$	21.65	20.06	15.71	13.56	14.16

From the **Table (2)** it is clearly seen that the parent metal samples showed improvement in the UTS value as a result of the dissolution of the coarse secondary phases in the  $\alpha$ -Al matrix up to 48 hours of soaking time and the value starts reducing at 60 hours soaking time that might be because of the saturation of the dissolution. The UTS value of the deep cryogenic treated parent metal sample at soaking time of 48 hours from UTS value measured at the room temperature seems to have increased about 12% (i.e. increase from 314 MPa to 339 MPa).

The friction welded samples shown greater improvement in the UTS values after deep cryogenic treatment when compared with the deep cryogenic treated parent metal samples. The main reason for this improvement is during the friction welding process at optimum condition of high rotational spindle speed and friction pressure the SiC particulates and the secondary phases present in the AA 7075 +10% vol SiC -T6 gets broken down into smaller size and well distributed in the welded region, in addition to that grain refinement [13]. When the friction welded specimens are subjected to deep cryogenic treatment the secondary phase again breaks down to smaller sizes and continues to dissolve the secondary phases in the  $\alpha$ -Al matrix up to 48 hours of upon increase in the soaking time up to 48hours. The failure in the friction welded sample deep cryogenic treated at 48 hours took place in the parent metal side but in all other friction welded specimens failure occurred in the weld region. Due to the deep cryogenic treatment, the friction welded sample at 48 hours shown lesser difference from the parent metal treated in that condition [14]. The improvement in the UTS value of the deep cryogenic treated friction welded sample at soaking time of 48 hours and the UTS value of friction welded specimen at room temperature observed to be 20.33% (i.e. improved from 246 MPa to 296 MPa).

The fractured images of the tensile test specimens for both parent metal and friction welded, cryogenically treated for 48 hours, has been shown in the **fig. 5**. The parent metal fractured image **Fig. 5a** shows the improvement in the tensile strength at 48 hours soaking time and that can be clearly seen from the presence of dimples. Similarly, the fractured surface of the friction welded from **Fig. 5b** is also showing the presence of dimples indicating predominant ductile failure. Thus, the fractured surface of both the parent metal and the friction welded specimens cryogenically treated for 48 hours soaking time had shown improvement in the tensile strength by showing presence of dimples.

**B. Impact of Cryogenic Treatment on Hardness**

The hardness values of the cryogenic treated friction welded sample and the cryogenic treated parent metal are shown in the **Table 3**. The soaking temperature up to 48 hours has shown some improvement in the hardness value. The improvement in the hardness values for increased soaking period has no effect when compared with the UTS values

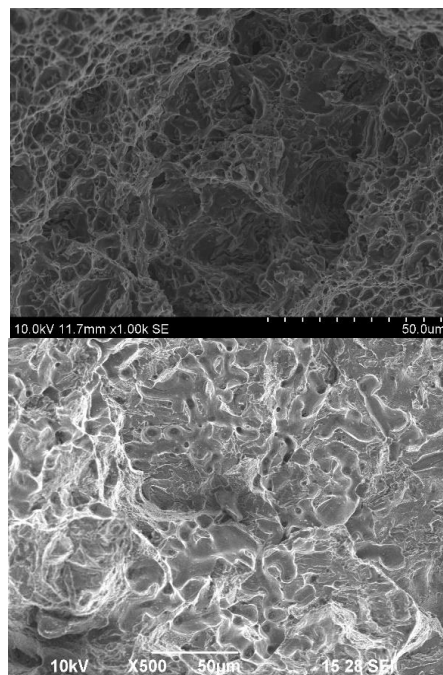
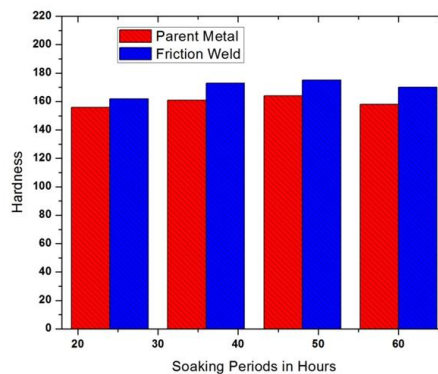


**Fig. 5** Fractured Surfaces **a.** Parent metal **b.** Friction welded for 48 hours soaking period

**Table 3** the hardness value of the cryogenic treated friction welded sample and the cryogenic treated parent metal.

	Hardness (HD)				
	Room Temperature	24 hrs	36 hrs	48 hrs	60 hrs
<b>Parent metal (PM)</b>	145	156	161	164	164
<b>Friction Welded (FW)</b>	151	162	173	175	175
<b>Difference in HD</b>	6	6	12	11	11
<b>Difference between HD of the parent metal specimen and welded specimen in %</b>					
$((HD_{PM} - HD_{FW}) / HD_{PM}) * 100$	4	3.8	7.4	6.7	6.7

**Fig. 6** Hardness Vs Soaking Periods in hours of Parent Metal and Friction welded metal



The hardness of the weld region in the friction welded specimen can be increased by soaking for about 48

hours at  $-196^{\circ}\text{C}$  and by further increasing the soaking time no effect is witnessed. The increase in the friction welded samples hardness value with respect to the hardness value of the friction welded sample at room temperature is 15.89% (i.e. increase in hardness from 151 to 175). Similarly, for the parent metal the increase in the hardness value is about 13.10%.

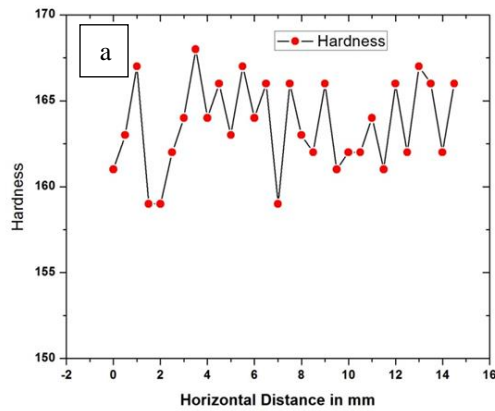


**Fig. 7a** Hardness of the parent metal sample for 48 hours soaking period

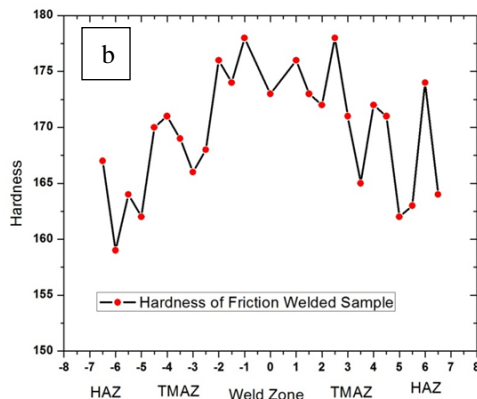


**Fig. 7b** Hardness of the cryogenic treated friction welded sample for 48 hours soaking period

From the hardness graph as shown in fig. 7a & 7b it would be clearly seen that the variation in the hardness values across the length of the parent metal specimen have not shown any drastic deviation after cryogenic distribution and this could be due to the distribution of dissolved fine precipitates in the aluminium matrix [15].

#### IV. CONCLUSION

1. comparison of the parent and friction welded aluminum metal matrix metal was done by using cryogenic treatment at different time periods.
2. Impact cryogenic treatment on hardness and ultimate tensile strength for both parent and friction welded metal was made.
3. From the result, friction welded metal has more improvement in hardness and ultimate tensile strength when compared to parent metal by 11% and 13.56%.
4. Also, the microstructure of friction welded metal when compared to parent metal had a refined grain structure.

#### REFERENCE

- [1] Aruri Devaraju & Kishan, V , ‘Influence of Cryogenic cooling (Liquid Nitrogen) on Microstructure and Mechanical properties of Friction stir welded 2014-T6 Aluminium alloy’, *Materials today: proceedings*, Vol.5, Issue 1, Part 1, pp.1585-1590, 2018.
- [2] Kaixuan Gu, Hong Zhang, Bing Zhao, Junjie Wang, Yuvan Zhou & Zhiqiang Li 2013, ‘Effect of Cryogenic treatment and aging treatment on the tensile properties and microstructure of Ti-Al-4V alloy’, *Materials Science & Technology A*, Vol.584, pp.170-176, 2013.
- [3] Ji Wang, Ruidong Fu, Yijun Li & Jiafeng Zhang , ‘Effects of deep cryogenic treatment and low-temperature aging on the mechanical properties of friction-stir-welded joints of 2024-T351 aluminium alloy’, *Materials Science & Engineering A*, Vol.609, pp.147-153, 2014.
- [4] Sarpeet Singh & Gaurav Dhuria , ‘Investigation of post weld cryogenic treatment on weld strength in friction stir weld dissimilar aluminium alloys AA2014-T651 and AA7075-T651’, *Materials Today: Proceedings*, Vol.4, Issue 8, pp.8866-8873, 2017.
- [5] Sarkari Khorrami, M, Kazeminezhad, M, Miyashita, Y, Saito, N & Kokabi, AH, ‘Influence of ambient and Cryogenic temperature of friction stir processing of severely deformed aluminium with SiC nanoparticels’, *Journal of Alloys and Compounds*, Vol.718, pp.361-372, 2017.
- [6] Shan Gao, Zisheng Wu, Pengfei Jin & Junjie Wang, ‘Study on Microstructure and Properties of 5A06 Aluminium Alloy Welded Joint by Deep Cryogenic Treatment’, *Advanced Materials Research*, Vol.314-316, pp.927-931, 2011.
- [7] Senthil Kumar, G & Beemkumar, N, ‘Experimental analysis of Mechanical properties of Aluminium Alloy weldments by Friction Welding Process under Cryogenic Treatment’, *International Journal of Ambient Energy*, Vol.40, Issue 1, pp.82-85, 2017.
- [8] Kamal babu, K, Paneerselvam, K, Sathiya, P, Noorul Haq, A, Sundarrajan, S, Mastanaiah, P, Srinivasa Murthy, CV, ‘Experimental Investigation on Friction Stir Welding of Cryorolled AA2219 Aluminium Alloy Joints’, Vol.24, No.1, pp.1750001(17 Pages), 2014.
- [9] Rasool Mohideen, S & Dan Sathiaraj, ‘Deep Cryogenic Treatment on Aluminum Silicon Carbide (Al-SiC) Composite’, *Advanced Materials Research*, Vol.383-390, pp. 3320-3324, 2012.
- [10] Pavan, KM, Sachin, LS, Mayur, RS, Chandrasekar, A & Ajaykumar, BS, ‘Effect of Cryogenic Treatment on the Mechanical and Microstructural Properties of AluminiumAlloys-A brief study’, *International Journal of Mechanical and Production Engineering*, Vol.2, Issue 5, pp.93-99, 2014.
- [11] Dilip Khedekar & Gogte, CL, ‘Development of the Cryogenic processing cycle for age hardenable AA7075 aluminium alloy and optimization of the

- process for surface quality using gray relational analysis', *Materials Today Proceedings*, Vol.5, pp.4995-5003, 2018.
- [12] Sotriov, N, Falkinger, G, Grabner, F, Schmid, G, Schneider R, Grant, RJ, Kelsch, R, Radlmay, K, Scheerer, M, Reich C, Sehrscho, H & Loipetsberger, M, 'Improved formability of AA5182 aluminium alloy sheet at cryogenic temperatures', *Materials Today: Proceedings*, Vol.2S, pp.S113-S118, 2015.
- [13] Zheng Liu, Pengfei Zhao, Yawei Li, Xianquan Jiang, "Effect of cryogenic treatment time on Microstructure and properties of 17CrNiMo6 Steel", *Materials Sciences*, volume 8, Issue 7, pp.828-836, 2018.
- [14] P. Poza, J. Llorca, "Fracture toughness and fracture mechanism of Al-Al<sub>2</sub>O<sub>3</sub> Composites at cryogenic and elevated temperatures", *Materials Science and Engineering: A*, volume 206, Issue 2, pp.183-193, 1996.
- [15] F.Bouzada, M.Cabeza, P.Merino, S.Trillo, "Effect of Deep Cryogenic Treatment on the Microstructure of an Aerospace Aluminium Alloy", *Advanced Materials Research*, volume 445, pp.965-970, 2012.

# Effects Of The Friction Stir Welding Parameters On The Corrosion Behavior Of Similar And Dissimilar Welded Aluminium Alloys 6061-6061, 6082-6082, And 6082-6061

**Syed Khaja Naimuddin,**

Research Scholar,  
Vignan University, Guntur, India,  
\*Email: sknaim2611@gmail.com.

**Dr K.P.Vidhu**

Professor, Dean of Research & Development, Vignan  
University, India,  
Email: dean\_res@vignanuniversity.org

**Abstract**— The process parameters of the Friction Stir Welding (FSW) effecting the metallurgical properties of similar and dissimilar aluminum alloys and the corrosion behavior are investigated. Similar aluminum alloys 6061-6061, & 6082-6082, and dissimilar alloys 6061-6082, are produced by varying the rotation speed of 1400 and 1120 rpm and traverse speed of 24 and 40mm/min with a hexagonal tool pin profile and constant axial load of 11kn. The microstructure of the welded joints with different parameters was observed in scanning electronic microscope (SEM). The corrosion behavior of friction stir welded joint and the base metal is studied with 5% NaCl, using Weight loss method and the rate of corrosion is measured by the salt spray test (FOG TEST). The microscopic views of the corroded joints were observed after corrosion by an optical microscope. It is observed that the welded joints 6082-6082 with a rotation speed of 1400rpm and 40mm/min traverse speed is more resistant to corrosion and has minimum weight loss, pits of the corrosion were observed in almost all the samples. Minimum pitting was observed on 6082-6082 and 6061-6082 at 1400rpm and 40mm/min speed.

**Keywords:** FSW (Friction Stir Welding); SEM (Scanning Electron Microscope)

## 1. INTRODUCTION

Aluminium, an important metal extensively used in structural engineering, Marine, Aerospace and Automobiles. Aluminium alloys oxidize whether in solid solution or intermetallic particles. Aluminium has lineament to oxygen, and is counteractive to variety of chemicals. Aluminium alloys represent excellent corrosion resistance by the defensive character of oxide film formation on its surface by passivity. Aluminium alloys which are difficult to join by conventional techniques are joined by Friction Stir Welding (FSW). FSW is a solid state welding which has a temperature

high enough to plasticize but not melt the material which reduces the solidification defects caused by melting and

chemical reactions. It drastically improves the mechanical and metallurgical properties of the material. FSW uses a non-consumable tool with pin (hexagonal, triangular and conical) and shoulder which is rotating in single direction with prefixed travel speed between the metals to be joined. The process parameters of the FSW like rotational speed, travel speed and pin profile have a great impact on the quality of welding mechanical properties, metallurgical properties and corrosion resistance. FS welded aluminium alloys have application especially in Marine atmosphere, which is very aggressive to most metals. 6000 series aluminium alloys are used in Marine applications. FSW techniques are widely used in joining the similar and dissimilar materials and are proved to give quality welds. Microstructure characterization of the material in the scanning electronic microscope reveals the grain size, sediments and distinct zones formed in the welding process like Nugget zone (NZ), thermo-mechanically affected zone (TMAZ), heat affected zone (HAZ). The Tunnel defects on the advancing side and retreating side recrystallize between the base metal and weld metal.

The Salt Spray Test also known as fog test is a common test to evaluate resistance of material to corrosion. Material is exposed continuously to an elevated temperature a closed chamber of salt spray or fog of salt. Specimen to be tested or placed in the closed salt chamber where in the material is exposed to spray of salt water or fog of salt continuously to fix time duration of the test.

## 1.1. REVIEW OF LITERATURE

Various researchers have described the corrosion behavior of similar and dissimilar materials joined by Friction Stir Welding. Welded joints of FSW for

aluminium alloys have not exhibited enhanced corrosion. Aluminium alloys of 2219, 2124, 7075, and 6013 are more resistant to corrosion than the parent material [R.W. Fonda et al., (2009) Jariyaboon M et al., (2007) & Satheesh K et al., (2013)]. Intergranular corrosion is observed mostly in the weld nugget, and enhanced in the grain boundary sediments. Coarse sediments and wide sediment-free area increased by the thermal effect during the FSW process are linked with the corrosion in Intergranular. Parameter of FSW effecting the corrosion behaviour of weldment of FSW is reported by many researchers [Surekha K et al., (2009) W. M. Thomas et al.,(1991-1995) Matrukanitz and RP (1990),

& J.B.Lumsden]. Process parameters affecting the corrosion behaviour of FS Welded high strength sedimentation, hardenable AA2219-T87 was studied by surekha et al [Surekha K et al, S Vijayan and. R. Raju, Hirata T., Oguri T, & Lombard H]. Results have proved that rotation of tool influenced the corrosion rate attributing the break down and dissolution of particles [AO Mosieh et al., (2015)].

[Qin, h, Zhang,H, sun,d et al., ] corrosion behavior of friction stir welded joints of 2A14-T6 aluminium alloy, international journal of minerals, metallurgy and materials concluded that the weldment of FSW joint is better and is more resistant to corrosion than parent metal.[ Aline .f.s.Bugrian, Hong-fengWang et al., (2016)]

Jerriyaboon et al investigated the parameters of FSW viz rotation of tool and travel speed effecting the corrosion behaviour on aluminium alloy AA2024-T351. Concluded that rotation speed has a major effect on corrosion attack NZ has intergranular attack at lesser speed rotation welds, at higher speed welds the HAZ has corrosion attack. [GD'UrsoaC et al.,(2017) Govindraj Elatharsan et al., (2014)]

Ahmed S Hassan et al.,(2010) has studied aluminium alloys A319 and A356 cast alloys for corrosion. His observation is resistance to corrosion of weldment is decreasing with increase in speed of rotation of the tool. [K.Surekha et al., (2009)]

Friction Stir Welding compared with MIG welding and TIG welding of aluminium alloys is investigated by number of researchers concluding that the welded joints of Friction Stir Welding are resistant to corrosion more than Tungsten Inert Gas weld and Metal Inert Gas welded joints. [Anjaneya Prasad B. and Prasanna P (2013), Ashwani Kumar et al.,(2014) Navyashree, V and Sivaramakrishna (2015)]

Harmith singh et al has compared 6066 welded by Metal Inert Gas and Friction welding to compare the

mechanical properties and microstructure; Concluded that welded joints of FSW are more strong as compared to Metal Inert Gas welded joints.

Farhad Gharavi et al investigated 6061 welded joint by fsw in 0.6% mol L<sup>-1</sup> NaCL solution indicated process of welding has major effect on resistance to corrosion [D.A. WadesonaX et al., (2015)]

Vincant Protan et al investigated the FSW joint 2050-T3, For corrosion in NaCl solution. He has found that most of corrosion resistance is carried on wrought Aluminium alloy [R.W. Fonda et al., (2009) Ahmed s Hassan and tamer s mahmood (2010) , and Jilan Yang et al.,(2018)].

Elangovan.k and Balasubramaniam.v (2008) has studied the tool pin and the speed of the welding influencing fsw processing zone. [S Vijayan and. R. Raju,(2008) Elangovan K et al.,(2008) & Buffa G. et al.,(2006)]

Peel M.J. et al., (2003) proved that microstructure, residual stresses and mechanical properties are the functions of speed of welding in friction stir welding. [Hirata T et al.,(2006) Lombard H et al.,(2008)]

M. Dehghanis et .al. Investigated for aluminium alloy 3003H18 for welding parameters on microstructure, confirmed strength of weld and good results. [ M.Dehghanis. A.A.Akbarimousavia. Amadeh, R.S Coelho,A.Kostka et al., H.I.Dawoo et al.,]

In this work investigation is being done on how the FSW welded similar and dissimilar alloys AA6061-AA6082 controlled by welding parameters effect the corrosion behaviour of Aluminium Alloys.

## 2. MATERIAL AND METHODOLOGY

In this investigation, joints of aluminium alloys AA6082-AA6061 are welded by FSW process. The 6mm thick plates of similar and dissimilar aluminium alloys 6082-6082, 6061-6061, and 6082-6061 were cut into the required size (200mm×100mm) by cutting

& grinding and joined by friction stir welding on the vertical milling machine. The parameters taken into consideration are traverse speed of the tool (40mm /min and 24mm/min), a tool rotational speed of the tool (1400 rpm and 1120 rpm) tilt angle of 1<sup>0</sup> as in Table 1.

Friction stir welding is selected mainly because the processing temperature falls below the Melting point, thereby eliminating the solidification defects and other undesirable chemical reactions, as compared to all welding processes.

TABLE 1. FSW Parameters Used

Aluminium	Rotational	Travel
6082-6082	1120	24
6082-6082	1120	40
6082-6082	1400	24
6082-6082	1400	40
6061-6082	1120	24
6061-6082	1120	40
6061-6082	1400	24
6061-6082	1400	40
6061-6061	1120	24
6061-6061	1120	40
6061-6061	1400	24
6061-6061	1400	40

The welding is done in the rolling direction by Single pass welding procedure to make the butt joint. A hexagonal tool pin made of die steel is used for this welding. The tool pin geometry used in this work as shown in the Figure1. Shows tool pin geometry of the tool used in FSW. The process parameters used in this investigation are 1120 and 1400 rpm welding traverse speed of 40 and 24mm/min tool depth of 5.2mm and tit angle of 1°.

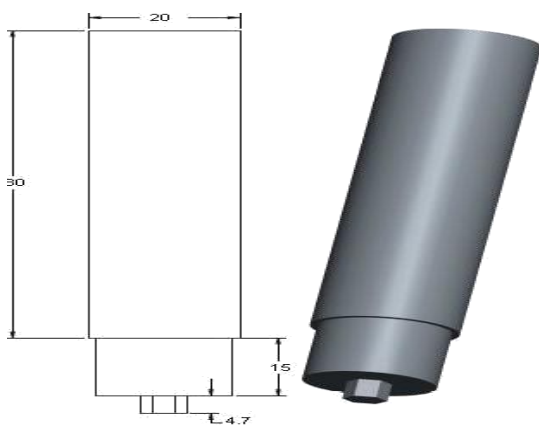


Figure1. Pin profile geometry of the tool used.

2.1. MICRO STRUCTURAL ANALYSIS

Friction stir welded aluminium alloy samples of similar and dissimilar alloys are prepared as per ASTM E3-01, the test method used for micro itching is ASTM E407-07 and samples are polished to mirror finish figure 2. The Etchant used is Kellar’s reagent. The samples are scanned in Optical Microscope NEOPHAT-32, in LUCID Laboratories.

The Micro structural images are taken for the base alloys 6061,6082 and the friction stir welded joints

12 samples of similar and dissimilar alloys by varying the parameters like rotational speed (1400 rpm & 1120 rpm ) traverse speed (40mm/min & 24mm/min).

The images of the microstructure of similar and dissimilar aluminium alloys of 6061-6082 with different parameters are as shown in the figures. The samples are scanned in the optical microscope for topography and external morphology, chemical composition and crystalline structure.



Figure2. FSW welded samples

2.2 CORROSION TEST

2.2.1 SALT SPRAY TEST

Salt spray test is conducted in CMENVIRO system silver-fog corrosion test chamber as per ASTM- B117 in LUCID Laboratories. The corrosion test in the above equipment is conducted on the weldment and the base metal of the friction steel welded zone in 5% NaCL solution for 96 hours. To determine corrosion parameters, to analyze the uniform and localized corrosion of the base metal and the weldments and the pitting potentials for characterizing the parameters influencing the uniform corrosion rates the corrosion test id performed.

The macrostructure of the corroded samples are observed in the Optical Microscope the images are as shown in the figure.3(a), Five cm sq. area of the weldment of each sample consisting of nugget zone(NZ) thermo-mechanically affected zone (TMAZ) and heat effected zone (HAZ), and parent metal were exposed to 5% NaCl solution.

To convert corrosion rate the corrosion rate can be calculated in metric equivalent millimeter per year (mm/yr) or mills per year in British equivalent using the following formula.

To calculate rate of corrosion and loss of metal  

$$\text{mm/yr} = 87.6 \cdot (W/DAT).$$

$$\text{Mpy} = 25.4 \text{ microns.}$$

Where W= loss of metal in mg.

D= density in mg/ cm<sup>3</sup>\*cm<sup>3</sup>.

A= Sample area (Cm<sup>2</sup>)

T= exposure Time in hours

### 3.2 Micro structural Evolution for weldment

## 3. RESULTS AND DISCUSSIONS

### 3.1 MICROSTRUCTUR EVOLUTION BY SEM

The experiment is conducted by changing the rotation of tool 1400 & 1120 rpm and traverse speed of 24 & 40 mm/min with a hexagonal tool pin profile and a constant axial load of 11kn for the purpose of investigating the weld parameters effecting the microstructure and metallurgical properties of the aluminum alloy AA6082-AA6082, AA6061-AA6061, AA6082-AA6061. The aluminium alloy plates of thickness 6mm are cut to the required size and were ground to finish. The but-joints were prepared in the vertical milling machine by friction stir welding. The samples were secured by mechanical clamps in the position. Single pass procedure for welding is used in the direction of rolling using hexagonal pin tool by changing the rotation speed and traverse speed to fabricate different samples.

The specimen were cut from the fabricated FSW joints for metallography and polishing is done by grinding wheels using abrasive disks and clothes to get a mirror finish. Kellar's reagent is the chemical etchant used. The specimen was tested as per ASTM E3-01, E407-07. The experiment was conducted in LUCID laboratories Hyderabad. The microstructures were observed on SEM (scanning electronic microscope) NEOPHOT-32 the microstructure of the base alloys AA 6061 and AA6082 is in image figure 3(a) and 3(b). In the microstructure of 6061, particles of Si and Mg are sediment evenly distributed in solid solution, un dissolved (Fe, Mn) also are present in the matrix. It has well solutionised matrix and hardened precipitation.

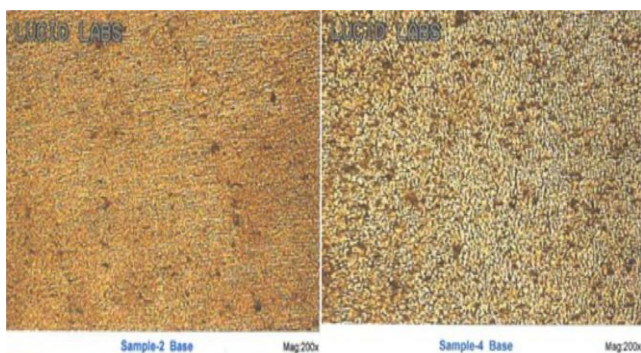


Figure 3(a) microstructure of base alloy AA6061 3(b) microstructure of base alloy AA6082

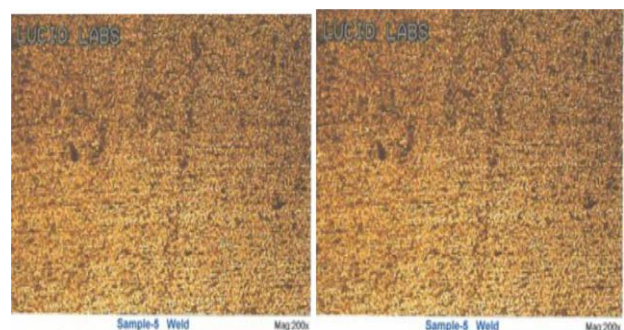
The microstructure of AA6082 has higher Cu content and lower manganese, hardening occurs through precipitation of very fine scale precipitates; impurities are mainly Fe and Si as seen in the image 3(b).

The micro structural characterization from the SEM images of the weldment, three distinct zones is identified, the NZ, the TMAZ and HAZ. The Microstructures of the base metal (BM), the weldment of similar alloys and weldment of dissimilar alloys are shown in the figures. A dynamically re crystallized zone are seen in the grains and the sediments of the weldment. Micro structure of the FSW joint exhibits a clear distinction between the different rotational speeds and different travel speeds. The upper part of the weldment is influenced by the hexagonal tool pin.

The NZ comprises the strong effect by the rotational speed of the tool, which is subjected to a high level of frictional heating to plastic deformation. NZ upper part is influenced by stir pin. The highest strain and strain rates take place in NZ [Harmeet singh et al, Vincent proton et al]. Frictional heating during FSW and intense plastic deformation results re crystallized fine grained microstructure with stir zone(SZ).Figure observation shows that considerable amount of consistent particles are distributed. randomly in the base material. The tunnel defects forms on the advancing side of the FSW tool.

In the weldment AA6082-AA6082 there a very few particles of the second phase compared to the base material of 6082. The second particles are more intense and uniform. The TMAZ has highly deformed and homogeneous, coarser aluminium grains because of stirring of the tool. This region has lesser plastic deformation and re crystallization than the NZ. The TMAZ has larger recrystallized grains than NZ. Variation in the grains structure and the grain size is observed in the HAZ, as it is away from the center line. The grain size is decreasing with increase in the distance to the weld center line.

In the examination at 1120 rpm rotational speed and 40mm/min as in figure 4© and at 1120 rpm and 24mm/min fig 4(d), the TMAZ has more highly deformed and inhomogeneous coarser alumina grains. Whereas 1400 rpm and 24mm/min in fig 4(b) the TMAZ is comparatively less deformed coarser alumina grains. And for 1400 rpm at 40mm/min fig 4(a) has lesser coarser aluminium grains less intense and uniform and TMAZ and has larger re crystallized grain than NZ. The HAZ region has less variation in all 4 samples of 6082-6082.



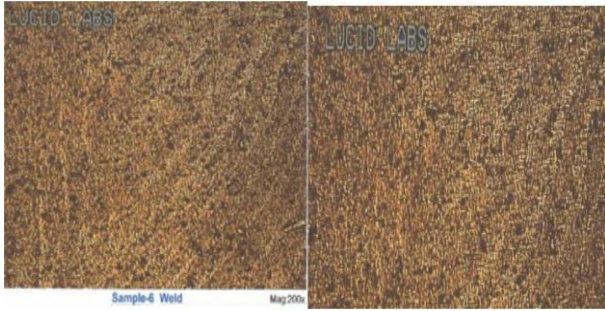


Figure 4(a): Micro structure of weldment AA6082 - AA6082 at 1400 rpm and 40m/min

Figure 4(b): Microstructure of weldment AA6082 - AA6082 at 1400 rpm and 24m/min

Figure 4(c): Microstructure of weldment AA6082 - AA6082 at 1120rpm and 40mm/min

Figure 4(d): Microstructure of weldment AA6082 - AA6082 at 1120rpm and 24 mm/min

AA6061-AA6061 the FSW creates the micro structural changes in HAZ and NZ of 6061 aluminium alloy. The HAZ grains are fine than the parent metal. The sediment size in the weldment of FSW is smaller compared to the base metal and the distribution of constituent particles is also wider than the base alloy. In the weldment grain boundary phases can be seen similar to parent alloy.

Examination at 1120 rpm rotational and 40mm/min fig 5(c) and at 1120 rpm at 24mm/min fig 5(a), the TMAZ has less deformed and inhomogeneous coarser alumina grains; whereas 1400 rpm and 24mm/min fig 5(b) the TMAZ is comparatively less deformed coarser alumina grains. In the 1400 rpm at 40mm/min fig 5(d) micro structural evolution HAZ grains are finer than the base alloy. NZ consistent particles are fine. The grain boundary phases are almost same as the base alloy. This Proves to be the best combination of the FSW process.

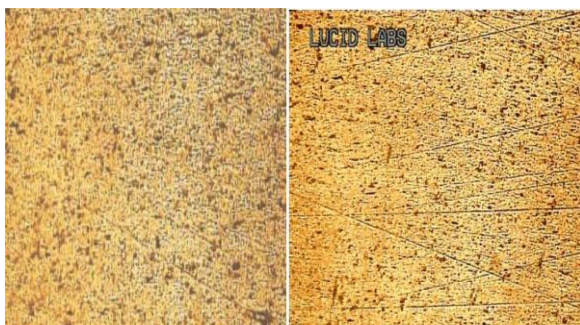


Figure 5(a): Microstructure of weldment AA6061 - AA6061at 1120rpm at 24mm/min

Figure 5(b): Microstructure of weldment AA6061 - AA6061at 1400rpm 24 mm/min



Figure5(c): Microstructure of weldment AA6061 - AA6061at 1120rpm 40 mm/min

Figure5(d) : Microstructure of weldment AA6061 - AA6061at 1400 rpm 40mm/min

In AA6061-AA6082 There are very less second phase particles in the NZ compared to the base materials of 6061 and 6082. The frictional heating during the process and plastic deformation results re crystallized fine-grained microstructure within the SZ. TMAZ has larger re crystallized grains than NZ. Variation in the grain structure and grain size is observed in HAZ as seen in the images in fig 6(a), 6(b), 6(c), 6(d).

Micro structural changes induced by the FSW were clearly identified in the analysis of the weldment of dissimilar alloys. The mixture of different alloys can be easily identified by different etching response to both alloys. 1400 rpm at 40mm/min fig 6(b) has best SZ of all 4 samples of 6061-6082 with lesser variation in HAZ. The NZ has fine consistent particles with respect to all samples, The TMAZ having no much difference.

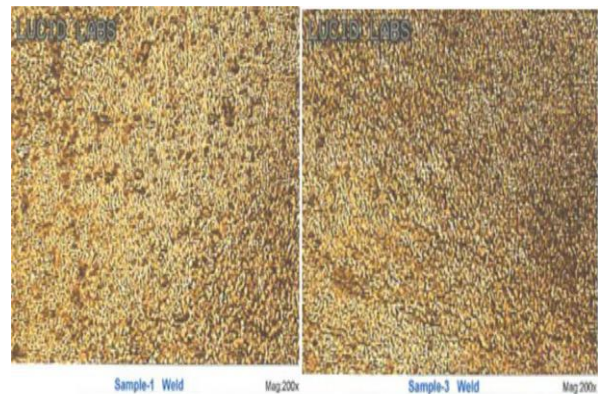




Figure 6(a): Micro structure of weldment AA6061 -AA6082 at 1120 rpm 40mm/min

Figure 6(b): Micro structure of weldment AA6061 -AA6082 at 1400 rpm 40mm/min

Figure 6(c): Micro structure of weldment AA6061 -AA6082 at 1120 rpm 24mm/min

Figure 6(d): Micro structure of weldment AA6082 -AA6061 at 1400 rpm 24mm/min

### 3.3. Corrosion Behavior

#### 3.3.1 Optical micrograph

The corrosion rate for the base alloy and FSW samples produced, by varying the process parameters is tested in 5% NaCl Salt spray test conducted in CMENVIRO system silver-fog corrosion test chamber as per ASTM- B117 for 96 hours (4 days).

**BASE ALLOY** The corrosion behavior of the weldment varies significantly from the base metal. Various samples tested with different process parameters gives clear indication of better corrosion resistance of weldment than the base metal.

From the micrograph it is concluded that a poor resistance to pitting corrosion of the weldment is due to different pitting potentials in all the weld regions, sediments present can be seen in the images figure 7(a) and 7(b).

#### WELDMENT OF THE WELDED JOINTS

The micrographs indicate that in the weldment, at 1120 rpm rotational speed the poor pitting corrosion resistance of welded joints is due to difference in pitting potentials across the weld regions, because of in homogeneity of microstructure in

these regions. At 1400 rpm the dimensions of the constituent particles in the welded joints are smaller than the parent alloy and are more homogeneous, thereby less chance of pitting potentials and are more corrosion resistant to the weldment. Corrode surfaces of all the samples in the figures show the surface is rough and bumpy, this indicate a general corrosion exception with significant change is observed with the changed travel speed and rotational speed.

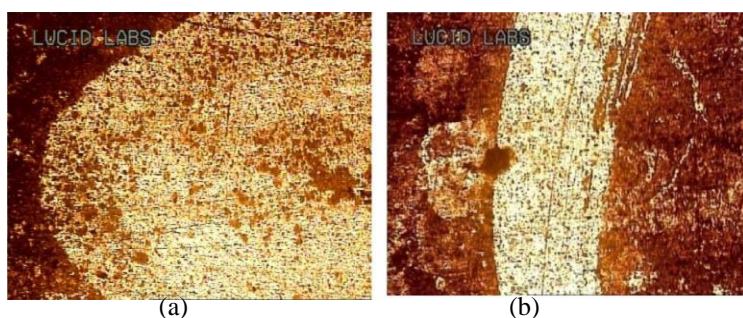


Figure 7(a): Optical micrograph after corrosion AA6061 base metal

Figure 7(b): Optical micrograph after corrosion AA6082 base metal

AA6082-AA6082 the micrographs, indicate that this welded joint is more resistant to corrosion than the other under investigation. The resistance to corrosion is increasing as rotational speed is increasing from 1120rpm to 1400rpm and travel speed from 24mm/min to 40 mm/min. At 1120rpm the highly deformed coarser alumina grains in TMAZ are more subjected to corrosion than the

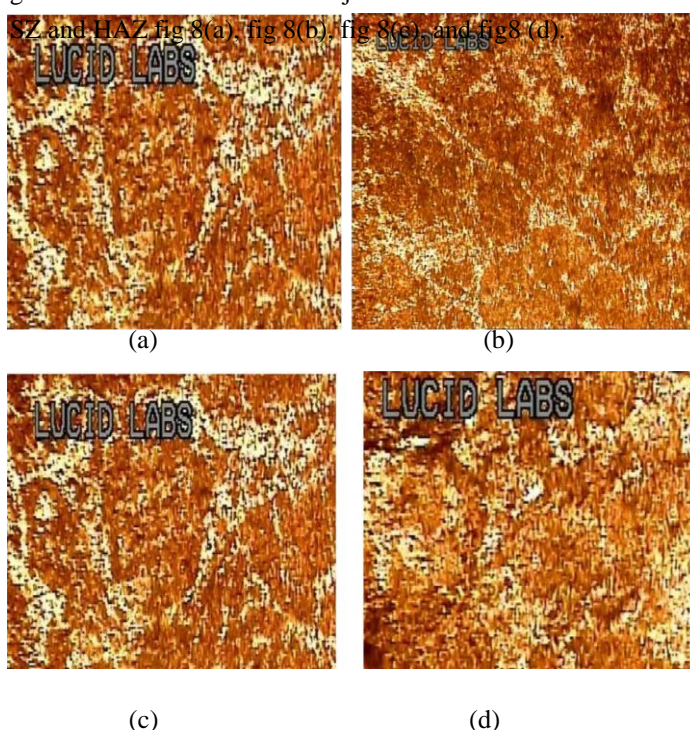


Figure 8(a): Optical micrograph after corrosion AA6082 –AA6082 at 1120 rpm and 24mm/min. Figure 8(b): Optical micrograph after corrosion AA6082 – AA6082 at 1120 rpm and 40mm/min. Figure 8(c): Optical micrograph after corrosion AA6082 –AA6082 at 1400rpm and 24 mm/min. Figure 8(d): Optical micrograph after corrosion AA6082 – AA6082 at 1400 rpm and 40mm/min.

AA6082-AA6061 A longer exposure to corrosion media has shown passivity to all samples of 6082-6061 at 1120rpm and 24mm/min has the highest corrosion. The active corrosion increased by increasing the welding speed. Poor resistance to corrosion is due to the difference in the pitting potentials across the welded region. The image of the corrode sample shows the degradation of alloy with more or less uniform attack of NaCl figure 9(a), 9(b), 9(c), 9(d).

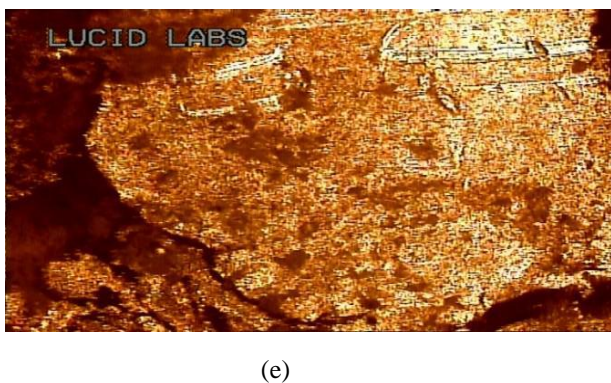
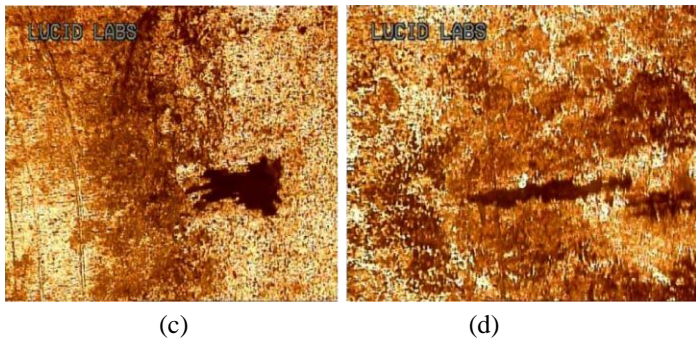
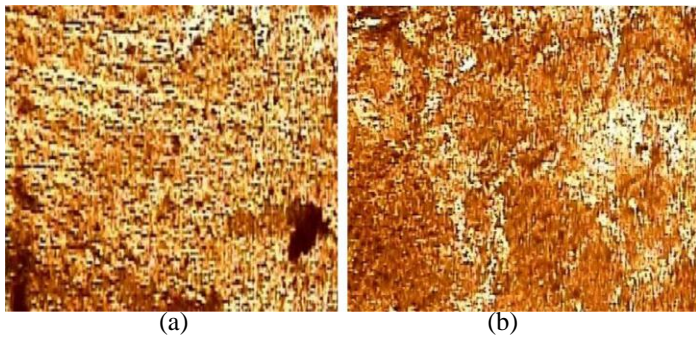


figure 9(a): Optical micrograph after corrosion AA6082 -AA6061at 1400 rpm and 24mm/min. Figure 9(b): Optical micrograph after corrosion AA6082 -AA6061 at 1400 rpm and 40 mm/min. Figure 9(c): Optical micrograph after corrosion AA6082 -AA6061

at 1120 rpm and 40 mm/min. Figure 9(d): Optical micrograph after corrosion AA6082 – AA6061 at 1120rpm and 24mm/min. Figure 9(e): Optical micrograph after corrosion AA6082-AA6061 at 1120 and 24mm/min.

AA6061-AA6061 the TMAZ and HAZ regions have less deformed coarser alumina, therefore corrosion rate is found lesser in these areas compared to NZ. Micrographs, of 1400rpm at 40 mm/min travel speed indicate a higher resistance than the lower rotational and travel speeds. Figures: 10(a), 10(b), 10(c), & 10(d).

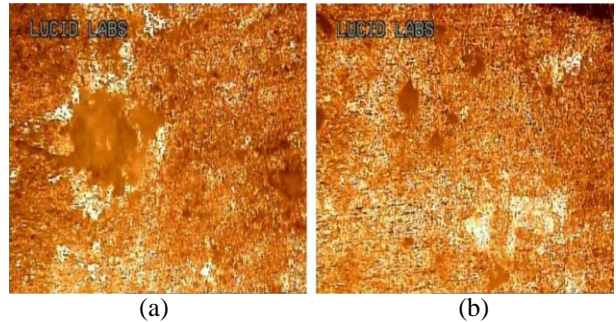


Figure 10(a): Optical micrograph after corrosionAA6061-AA6061 at 1120 rpm and 24mm/min. Figure 10(b): Optical micrograph after corrosion AA6061-AA6061 at 1120 rpm and 40mm/min. Figure 10(c): Optical micrograph after corrosion AA6061-AA6061 at 1400 rpm and 24 mm/min

#### Weight loss method

The corrosion curves are plotted based on weight loss during corrosion test conducted for 96 hours in CMENVIRO system silver-fog corrosion test chamber as per ASTM-B117. Corrosion curves are plotted in the software MINITAB-17; between the weight loss in mm/yr. vs. time in hours.

Then specimen were weighed before starting the experiment and after every 12 hours, the specimen has been taken and cleaned with acetone & distilled water and then weight loss in the specimen are noted. Rate of corrosion of specimens were measured with the weight loss using the formula

To calculate rate of corrosion and loss of metal

$$\text{mm/yr} = 87.6*(W/DAT).$$

$M_{py} = 25.4$  microns.

Where  $W$  = loss of metal in mg.

$D$  = density in  $mg/cm^3$ .

$A$  = Sample area ( $cm^2$ )

$T$  = exposure Time in hours

The experimental data obtained by weight loss measurements were recorded to obtain various corrosion parameters, viz, corrosion rate, rotational speed and travel speed these are summarized in tables.

Results obviously show the corrosion has taken place with the evidence of weight loss.

It is interesting to see that the rate of corrosion is varied with change in parameters.

Weight loss is small in general especially when the rotational speed increased from 1120 rpm to 1400rpm and travel speed, from 24mm/min to 40mm/min. The rate of corrosion is proportional to the exposure time. Low rotational speed at lesser travel speed has shown more weight loss as compared to higher speed at high travel speed.

Similar alloys 6082-6082 showing more resistance to corrosion and less weight loss followed by 6061-6061, for same parameters. Dissimilar alloys 6082-6061 is less resistant to corrosion.

Whereas lower rotational speed and traverse speed resulted in more weight loss, especially in dissimilar aluminium alloys as shown in figure 11, 12, 13 and 14. Increase in rotational speed and traverse speed, has proved to be less weight loss proving to be resistant to corrosion.

All experiments results obtained from measurements are interpreted in Table: 2 and

Table: 3

Table 2. Weight loss in time for similar and dissimilar alloys with varying Parameters in terms of rotational speed and travel speed.

Specimen	Rotation speed	Travel speed	Weight loss in mm/yr Time in hours							
			12	24	36	48	60	72	84	96
6082-6082	1120	24	0.54	0.54	0.81	0.94	1.01	1.29	1.31	1.35
6061-6061	1120-	24	0.54	0.81	0.87	0.94	1.08	1.08	1.15	1.28
6082-6061	1120-	24	0	0.54	0.72	1.08	1.29	1.43	1.54	1.61
6082-6082	1120	40	0	0.27	0.36	0.4	0.43	0.45	0.61	0.74s
6061-6061	1120	40	0	0.54	0.54	0.67	0.75	0.81	0.92	1.01
6082-6061	1120	40	0	0.27	0.54	0.54	0.65	0.72	0.77	0.87
6082-6082	1400	24	0	0.54	0.54	0.54	0.61	0.75	0.81	0.94
6061-6061	1400	24	0	0.27	0.54	0.54	0.65	0.81	0.85	0.85
6082-6061	1400	24	0	0.54	0.54	0.67	0.86	1.08	1.15	1.28
6082-6082	1400	40	0	0.27	0.36	0.4	0.43	0.45	0.46	0.47
6061-6061	1400	40	0	0.27	0.36	0.4	0.54	0.54	0.61	0.61
6082-6061	1400	40	0	0.27	0.18	0.27	0.43	0.45	0.54	0.61

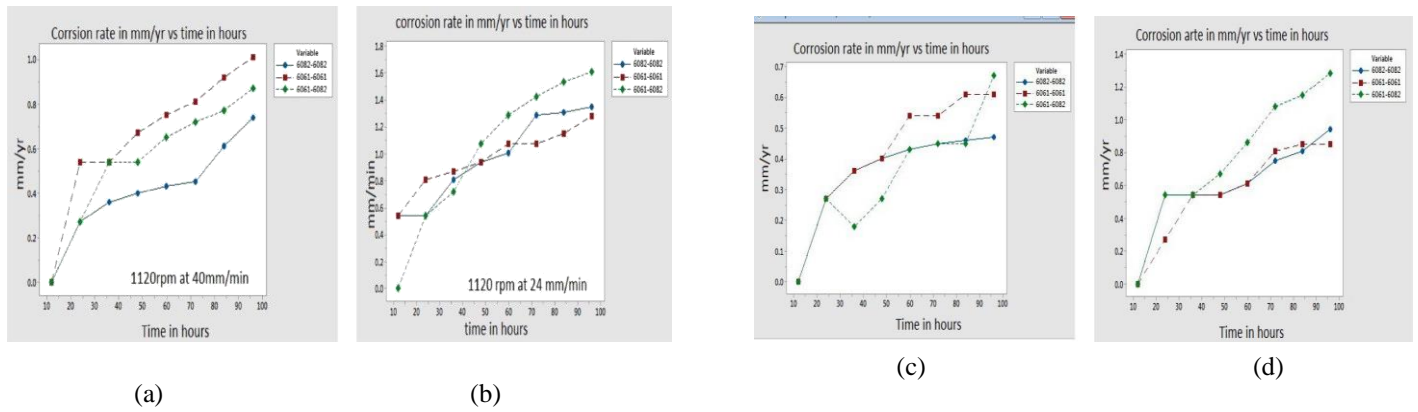


Figure 11(a): Weight Loss vs. time at 1120rpm and 40mm/min travel speed.  
 Figure 11(b): Weight Loss vs. time at 1120 rpm and 24mm/min travel speed.

Figure 11(c): Weight Loss vs. time at 1400rpm and 40 mm/min travel speed.  
 Figure 11(d): Weight Loss vs time at 1400rpm and 24 mm/min travel speed.

Table 3: Weight loss in time, for similar and dissimilar alloys with varying welding Parameters

Specimen	Rotation speed	Travel speed	Weight loss in mm/yr Time in hours							
			12	24	36	48	60	72	84	96
6082-6082	1120	24	0.54	0.54	0.81	0.94	1.0	1.29	1.31	1.35
6082-6082	1120	40	0	0.27	0.36	0.4	0.43	0.45	0.61	0.74
6082-6082	1400	24	0	0.54	0.54	0.54	0.61	0.07	0.81	0.94
6082-6082	1400	40	0	0.27	0.36	0.4	0.43	0.45	0.46	0.47
6061-6061	1120	24	0.54	0.81	0.87	0.94	1.08	1.08	1.15	1.28
6061-6061	1120	40	0	0.54	0.54	0.67	0.75	0.81	0.92	1.01
6061-6061	1400	24	0.	0.2	0.54	0.54	0.65	0.81	0.85	0.85
6061-6061	1400	40	0	0.27	0.36	0.4	0.54	0.54	0.61	0.61
6082-6061	1120	24	0	0.54	0.72	1.08	1.29	1.43	1.54	1.61
6082-6061	1120	40	0	0.27	0.54	0.54	0.65	0.72	0.77	0.87
6082-6061	1400	24	0	0.54	0.54	0.67	0.86	1.08	1.15	1.28
6082-6061	1400	40	0	0.27	0.18	0.27	0.43	0.45	0.54	0.61

CONCLUSION

Weld parameters of FSW viz, travel speed and rotational speed of the tool which decides the quality of weld has a great effect on Microstructure and corrosion character of FSW welded similar and dissimilar aluminium alloys. The effect of the welding parameters is observed as follows.

1. Microstructure of welded joints revealed that the 6061-6061 with a 1400rpm at 40mm/min travel speed and hexagonal tool head, the HAZ grains are finer than the base alloy, in NZ consistent particles are fine.

In the weldment of 6082-6082 variation in grain size and grain structure is observed in HAZ, grains are decreasing with the increase in the distance from center line. In 6082-6082 the TMAZ has not much difference with the base metal and has lesser variation in the HAZ region.

2. Optical Micrograph of welded joints exposed to salt spray chamber for 96 hours. Corrosion behavior of 6082-6082 and 6061-6061, is similar but the difference in solidification changed the mechanism of corrosion attack. The strengthening precipitates dissolution has made a clear softened region in the FSW joints. The effect of the parameters chosen, the rotational speed, travel speed and the tool pin geometry has great effect on the corrosion behavior. Corrosion resistance increased with the increase in the rotational speed and travel speed within the parameters chosen. The pitting corrosion resistance of the weldment is better compared to the base material. Corrosion resistance is higher in weldment than the base metal in similar alloys 6082-6082 at 1400rpm and travel speed of 40 mm/min.

The FSW of 6061-6061 alloys at 1400 rpm and 40mm/min improve the corrosion resistance and HAZ has better corrosion resistance than the other region. Dissimilar alloy 6082-6061 the corrosion resistance is very poor in the weldment due to the pitting potentials difference across the weld region.

3. In Weight loss method of corrosion test, the corrosion rate is proportional to exposure time corrosion resistance in the base metal is better than the weldment.

Minimum weight loss is observed in similar alloy 6082-6082 at 1400rpm at 40mm/min.

6061-6061 showing corrosion on an advancing side for same parameters.

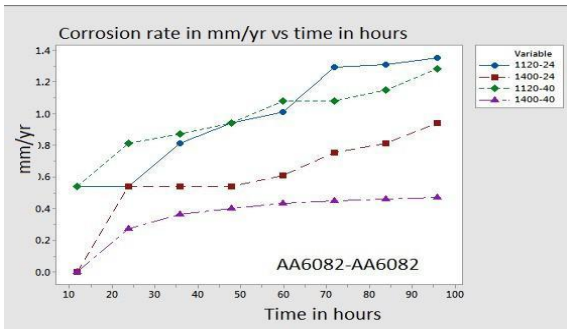


Figure 12: Weight Loss Vs time AA6082-AA6082

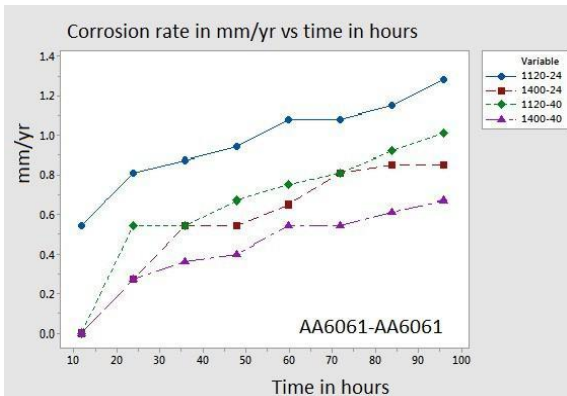


Figure 13: Weight Loss vs. time AA6061-AA6061

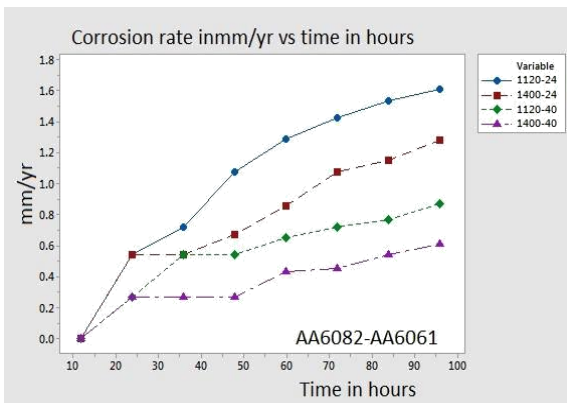


Figure: 14 Weight Loss Vs time 6061-6082

Twelve different specimens have been taken for the test; all specimens were corroded mostly in weld zone this result shows that metals were subjected to the intergranular corrosion. For the Constant transverse feed (24 mm/min) and varying rotational speed of tool (1120, 1400, rpm), the 1400rpm rotational speed attains the high corrosion resistance as shown in Fig.9

For the Constant transverse feed of tool (40 mm/min) and varying rotational speed (1120 and 1400 rpm), the maximum traverse feed 40mm/min attains the high corrosion resistance as shown in Fig.10.

Scope of future work

1. Corrosion resistant materials can be applied and make further tests.
2. Potentiostatic / potentiodynamic corrosion testing can be done for pitting corrosions.

REFERENCES

- [1] R.W. Fonda, P.S. Pao, H.N. Jones, C.R. Feng, B.J. Connolly, A.J. Davenport, Microstructure, mechanical properties, and corrosion of friction stir welded Al 5456, *Material Science Engineering A*, vol. 519, 2009, pp.1-8.
- [2] Surekha K., Murty B.S., Prasad Rao K., Effect of processing parameters on the corrosion behaviour of friction stir processed AA 2219 aluminium alloy, *Solid State Sciences*, 11, 2009, pp.c907-917.
- [3] Qin, h, Zhang,H, sun,d et al corrosion behavior of friction stir welded joints of 2A14-T6 aluminium alloy, *international journal of minerals, metalurgy and materials*
- [4] W. M. Thomas, E. D. Nicholas, J. C. Needham, M. G. Nurch, P. Temple-Smith, C. Dawes, Patents on Friction Stir Butt Welding, International: PCT/GB92/02203; British: 9125978.8; USA: 5460317, (1991-1995).
- [5]Matrukanitz, R.P. (1990). Selection and weld ability of heat-treatable aluminium alloys. *ASM Handbook-Welding, Brazing andSoldering*,vol.6, p. 528-536.
- [6] Jariyaboon M, Davenport AJ, Ambat R,Connolly BJ, Williams SW, Price DA. The effect of welding parameters on the corrosion behaviour of friction stir welded AA2024–T351. *CorrosSci* 2007; 49:877–909.
- [7] Satheesh K, Manikkavasagan, Rajamurugan. G, "Effect of process parameters on friction stir welding of dissimilar Aluminium Alloy ",*IOSR J MechCiv Eng*. 2013;49-53
- [8] Muruganandam.D,Sreenivasan.K.S,RaviKumar.S, Sushilal Das VSR,"StudyOf Process Parameters InFriction Stir",*Int Conf Ind Eng Oper Manag Kuala Lumpur*. 2011 ;( Jan 22-24):22-27.
- [9] Madhusudhan R, Sarcar M, Ramanaiah N, Prasadarao K,"An Experimental Study on the Effect of Weld Parameters on Mechanical and Micro structural Properties of Dissimilar Aluminium Alloy FSWelds",*Int J Mod Eng Res*. 2012;2(4):1459-1463.
- [10] Mars.G, Fontana and ELLS. Mitra, "Eight Forms Of Corrosion" in *Corrosion Science And Engineering Text book*.
- [11] Ahmed s Hassan ., tamer s mahmood, foud s mehmoed in corrosion behavior of dissimilar alloy a319 an da356 joined by friction stir welding in proceeding of the world congress on engineering 2010 vol II WCE 2010 LONDON U.K.
- [12] Harmeet singh, Harish kumar, Chandra shekar, gaurav jain, in comparative study of friction stir welding and MIG welding, in *international journal of mechanical engineering and technology*.
- [13] Vincent proton, j o el Alexia Eric Andneu et al. nugget in 2050 aluminium alloy friction stir welding; *International journal series*.
- [14] M.Dehghanis.A.A.Akbari mousavia. Amadeh - Effects of welding parameters and tool geometry on properties of 3003-H18 aluminium alloy to mild steel friction stir weld in *transactions of non ferrous metals society CHINA- ELSEVIER*
- [15] R.S Coelho,A.Kostka, J.F Dos Santos, A. Kaysser- in *Friction dissimilar welding of aluminium alloys to high strength steels: Mechanical properties and their relation to microstructure- Material science and engineering -ELSEVIER*
- [16] H.I.Dawood, Kahtan.S, Rahmat, B.Uday In Effect of small tool pin profiles on microstructures and mechanical properties of 6061 aluminium alloy by friction stir welding-*Transactions of non ferrous metals society China-ELSEVIER*
- [17] Jilan Yang, Yufei Lua, Zhenhong Guo, Jianfeng Gub- Corrosion behaviour of a quenched and partitioned medium carbon steel in 3.5wt% NaCl solution- *science Direct January 2018*
- [18] S Vijayan and. R. Raju, "Process Parameter Optimization and Characterization of Friction Stir Welding of Aluminum Alloys," *International Journal of Applied Engineering Research*, Vol. 3, No. 10, 2008, pp. 1303-1316.
- [19] Hirata T., Oguri T., Hagino H., Tanaka T., Chung S.W., Takigawa Y. and Higashi K. (2006), 'Influence of Friction Stir Welding Parameters on Grain Size and Formability in 5083 Aluminum Alloy', *Materials Science and Engineering A*, Vol. 456, pp. 344-349.
- [20] Lombard H., Hattingh D.G., Steuwer A. and James M.N. (2008), 'Optimising FSW process parameters to minimise defects and maximise fatigue life in 5083-H321 aluminium alloy', *Engineering Fracture Mechanics*, Vol. 75, pp. 341-354.
- [21] Balasubramanian V. (2008), 'Relationship between base metal properties and friction stir welding process parameters', *Materials Science and Engineering A*, Vol. 480, pp. 397-403.
- [22] Peel M.J., Preuss M. and Withers P.J. (2003), 'Microstructure, mechanical properties and residual stresses as a function of welding speed in AA 5083 Friction Stir Welds', *Acta Materialia*, Vol. 51, pp. 4791-4801.
- [23] Elangovan K., Balasubramanian V. and Babu S. (2008), 'Developing an Empirical Relationship to Predict Tensile Strength of Friction Stir Welded AA2219 Aluminum

- Alloy', *Journal of Materials Engineering and Performance*, Vol. 17, No. 6, pp. 820-830.
- [24] Buffa G., Hua J., Shivpuri R. and Fratini L. (2006), 'A continuum based FEM model for friction stir welding –model development', *Materials Science and Engineering*, Vol. 419, pp. 389-396.
- [25] Ouyang J.H. and Kovacevic R. (2002), 'Material flow during friction stir welding (FSW) of the same and dissimilar aluminum alloys', *Journal of Material Engineering and Performance*, Vol. 11, No. 1, pp. 51-63
- [26] Elangovan.k & Balasubramanium. (2008), Influence of tool pin profile and welding speed on the formation of friction stir processing zone in AA2219 aluminium alloy, *journal of material processing technology*, vol200, pp. 163-175
- [27] Anjaneya Prasad B. and Prasanna P. "experimental comparison of the MIG and FSW Processes for AA6061 Aluminium alloys" *International journal of Mining, Metallurgy and Mechanical engineering*, vol 1, pp137-140, 2013.
- [28] Ashwani Kumar, Shakti Singh Gautam and Alok kumar, "heat input & joint efficiency of three welding processes TIG, MIG & FSW using AA6061". *International journal of mechanical engineering Research*, vol 1, pp89-94 jan 2014.
- [29] Amerdeep,S.N Sunil Mangshetty, "Comparison of mechanical and microstructural behaviour of Tig welded and Friction stir welded dissimilar AA6063 and AA7075", *International journal for scientific research & development*, vol3, june 2015.
- [30] Navyashree, V.Sivaramakrishna,"Experimental Investigation of Friction stir Welding and TIG Welding for AL-6082" *International journal of Innovative Research in science, Engg. & Technology*, vol 4, july 2015.
- [31] D.A. WadesonaX, ZhouaG.E thompsonP, Skeldonal,DjapicOosterkampG, Scamansc in *Corrosion behaviour of friction stir welded AA7108T79 aluminium alloy. In Corrosion science volume 48, issue4, april 2006.-Elsevier*
- [32] Farad Gharavi,Khamirul AminMatori, Robiah younus, Norisoan KamilOthman, FirouzFadaeifard "Corrosion behaviour of Al6061 alloy weldment produced by friction stir welding process" *journal of material research and technology- science direct. Sept-2015*
- [33] Aline .f.s.Bugrian, Fernanda Martins Queiroz, Maysa Terada, Isolda Costa "localized corrosion resistance of dissimilar Aluminium alloys joined by friction stir welding"
- [34] GD'UrsoaC, GiardiniaS, LorenzibM, CabrinibT, Pastoreb "the effects of process parameters on mechanical properties and corrosion behaviour in friction stir welding of aluminium alloys" in *Procedia engineering-Elsevier-2017*
- [35] K.surekha,B.SMurty, K.Prasad Rao. "Effect of process parameters on the corrosion behaviour of friction stir processed AA2219 aluminium alloy".*solid state sciences-Elsevier-April-2009*
- [36] Hong-fengWang, jian-li Wang, WeiSong, Dun-wenZuo,Ding-lin Shao "Analysis on the corrosion Performance of friction stir welding joint of 7022 Aluminium alloy" *International journal of Electrochemical science- july2016*
- [37] Govindraj Elatharsan,Velukkudi Santhanam, Senthil kumar " corrosion Analysis of friction stir welded AA7075 Aluminium alloy" *journal of mechanical engineering-2014.*
- [38] J.B.Lumsden, M.W.Mahoney, G. Pollock, C.G.Rhodes "intergranular Corrosion Following friction stir welding of aluminium alloy 7075-T651", *CORROSION journal of science and engineering*
- [39] Farhad Gharavi, Khamirul Amin Matori, Robiah Yunus, Norisan Kamil othman, Firouz Fadaeifard "corrosion behavior of AL6061 alloy weldment produced by friction stir welding process- *journal of materials research and Technology-2014*
- [40] AO Mosieh, FH Mahmoud, TS mahoud." *Microstructure and static immersion corrosion behaviour of AA7020-o Al plates joined by friction stir welding"* *proceedings of instotution of mechanical engineering journal of materials; design and applications-2015*

# IMPROVING THE HEAT TRANSFER RATE OF AC CONDENSER

## BY OPTIMISING THE MATERIAL

Mohd Abdul Raheem  
Mechanical Engineering  
Malla reddy College of Engg  
Hyderabad, India  
Email:mohdraheem931@gmail.com

Dr Ananth  
Mechanical Engineering  
Malla reddy College of Engg  
Hyderabad,India  
Email:ananthsir@gmail.com

**Abstract—** Air conditioning systems have condenser that removes unwanted heat from the refrigerant and transfers that heat outdoors. The primary component of a condenser is typically the condenser coil, through which the refrigerant flows. Since, the AC condenser coil contains refrigerant that absorbs heat from the surrounding air, the refrigerant temperature must be higher than the air.

In this thesis heat transfer by convection in AC by varying the refrigerants are determined by CFD and thermal analysis. The assessment is out on an air-cooled tube condenser of a vapour compression cycle for air conditioning system. 3D modeling is done in CREO and analysis is done in ANSYS.

**Keywords—**Condenser, CREO, CFD, Refrigerant, ANSYS, Condenser unit.

### I. INTRODUCTION

In systems involving heat transfer, a condenser is a device or unit used to condense a substance from its gaseous to its liquid state, by cooling it. In so doing, the latent heat is given up by the substance, and will transfer to the condenser coolant. Condensers are typically heat exchangers which have various designs and come in many sizes ranging from rather small (hand-held) to very large industrial-scale units used in plant processes. For example, a refrigerator uses a condenser to get rid of heat extracted from the interior of the unit to the outside air. Condensers are used in air conditioning, industrial chemical processes such as distillation, steam power plants and other heat-exchange systems. Use of cooling water or surrounding air as the coolant is common in many condensers.

### Examples of condensers

A surface condenser is an example of such a heat-exchange system. It is a shell and tube heat exchanger installed at the outlet of every steam turbine in thermal power stations. Commonly, the cooling water flows through the tube side and the steam enters the shell side where the condensation occurs on the outside of the heat transfer tubes. The condensate drips down and collects at the bottom, often in a built-in pan called a *hotwell*. The shell side often operates at a vacuum or partial vacuum, produced by the difference in specific volume between the steam and condensate. Conversely, the vapor can be fed

through the tubes with the coolant water or air flowing around the outside.

In chemistry, a condenser is the apparatus which cools hot vapors, causing them to condense into a liquid. See "Condenser (laboratory)" for laboratory-scale condensers, as opposed to industrial-scale condensers. Examples include the Liebig condenser, Graham condenser and Allihn condenser. This is not to be confused with a condensation reaction which links two fragments into a single molecule by an addition reaction and an elimination reaction.

Larger condensers are also used in industrial-scale distillation processes to cool distilled vapor into liquid distillate. Commonly, the coolant flows through the tube side and distilled vapor through the shell side with distillate collecting at or flowing out the bottom.

- A condenser unit used in central air conditioning systems typically has a heat exchanger section to cool down and condense incoming refrigerant vapor into liquid, a compressor to raise the pressure of the refrigerant and move it along, and a fan for blowing outside air through the heat exchanger section to cool the refrigerant inside. A typical configuration of such a condenser unit is as follows: The heat exchanger section wraps around the sides of the unit with the compressor inside. In this heat exchanger section, the refrigerant goes through multiple tube passes, which are surrounded by heat transfer fins through which cooling air can move from outside to inside the unit. There is a motorized fan inside the condenser unit near the top, which is covered by some grating to keep any objects from accidentally falling inside on the fan. The fan is used to blow the outside cooling air in through the heat exchange section at the sides and out the top through the grating. These condenser units are located on the outside of the building they are trying to cool, with tubing between the unit and building, one for vapor refrigerant entering and another for liquid refrigerant leaving the unit. Of course, an electric power supply is needed for the compressor and fan inside the unit.

### Equation

- For an ideal single-pass condenser whose coolant has constant density, constant heat capacity, linear enthalpy over the temperature range, perfect cross-sectional heat transfer, and zero longitudinal heat transfer, and whose tubing has constant perimeter, constant thickness, and constant heat conductivity, and whose condensible fluid is perfectly mixed and at constant temperature, the coolant temperature varies along its tube according to:

$$\Theta(x) = \frac{T_H - T(x)}{T_H - T(0)} = e^{-NTU} = e^{-\frac{hPx}{mc}} = e^{-\frac{Gx}{mCL}}$$

where:

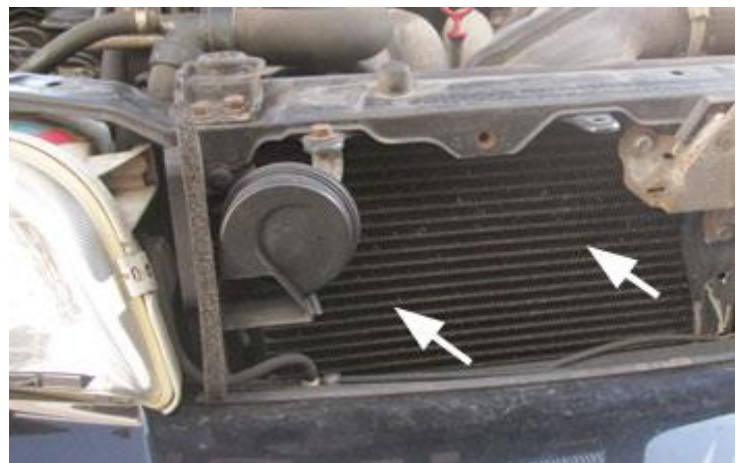
- $x$  is the distance from the coolant inlet;
- $T(x)$  is the coolant temperature, and  $T(0)$  the coolant temperature at its inlet;
- $T_H$  is the hot fluid's temperature;
- $NTU$  is the number of transfer units;
- $m$  is the coolant's mass (or other) flow rate;
- $c$  is the coolant's heat capacity at constant pressure per unit mass (or other);
- $h$  is the heat transfer coefficient of the coolant tube;
- $P$  is the perimeter of the coolant tube;
- $G$  is the heat conductance of the coolant tube (often denoted  $UA$ );
- $L$  is the length of the coolant tube.

## II. AIR CONDITIONER CONDENSER



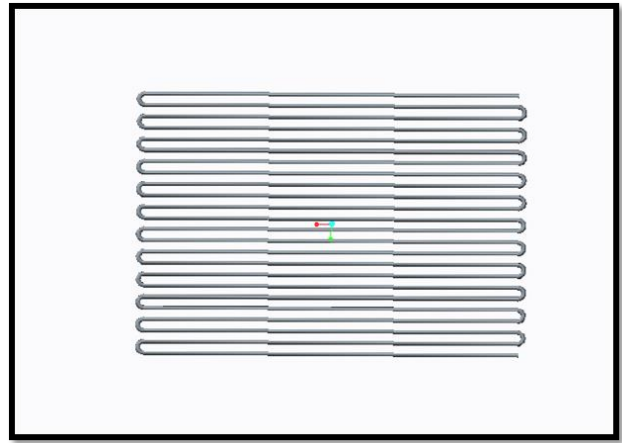
Air conditioner (A/C) condenser is an essential part of a car air conditioning system. Let's review how the vehicle A/C system works: The A/C system is a closed loop filled with refrigerant (typically R134) under pressure. The A/C compressor circulates the refrigerant through the system. The evaporator is a small heat exchanger installed inside the vehicle ventilation system. The cabin air flows through the evaporator fins. The condenser is a larger heat exchanger installed in front of the vehicle, typically, beside or right in front of the radiator. The ambient air is pushed through the condenser fins by an electric fan and by natural flow during driving. The system is based on a simple effect: the cabin heat is absorbed when the refrigerant vaporizes inside the evaporator. The heat is released outside when the refrigerant turns from a vapor into a liquid state inside the condenser. Through this continuous process, your cabin is kept cool even on a hot sunny day.

### A. A/C condenser problems

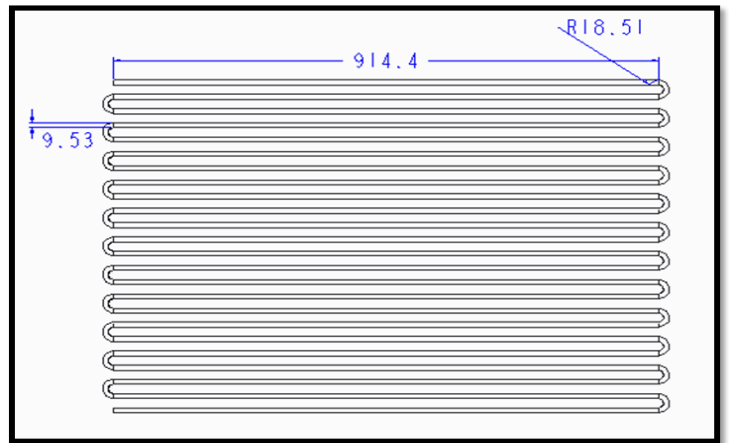


The A/C condenser is installed in front of the vehicle, so it often gets damaged in a frontal collision or by rocks or other

objects on the road. Corrosion is another enemy of an A/C condenser, especially in the places where salt is used on roads in winter months. If a condenser is damaged, the refrigerant leaks out and the air conditioning system stops working. A damaged A/C condenser cannot be repaired and must be replaced. One of the signs of a leaking A/C condenser is an oily greenish residue around the impacted area. Sometimes a leak might be at the place of connection with one of the air conditioning system lines. Automotive repair shops use special equipment to find refrigerant leaks in an air conditioning system. Another issue with the A/C condensers is when the fins get clogged up with leaves and other debris. This reduces the air flow through the condenser fins and affects the efficiency of an air conditioning system.



### B. A/C condenser replacement



There are two types of replacement parts, the OEM (original) and A/M (aftermarket). An OEM A/C condenser can be ordered from a dealer but it's usually more expensive (\$250-850). An aftermarket part is cheaper (\$70-\$320) and can be purchased online or from an auto parts supplier. The labor is more expensive, since in many cars, the front bumper and many other parts might need to be removed in order to get to the A/C condenser. Also the air conditioning system refrigerant must be recovered before and recharged after the A/C condenser is replaced. This is not something that can be done in your driveway. To perform this repair, automotive repair facilities use a special A/C service machine. For this reason, we strongly advise to have any air-conditioner repairs done at a dealer or a reputable auto repair shop.

To ensure good A/C system performance, it's a good idea to keep your A/C condenser clean and free of debris. If salt is used on the roads in winter months in your area, washing your car regularly will help keep the salt from accumulating on the condenser and causing corrosion.

### 3D Modelling Of Condenser

**THE MODEL IS DESIGNED FROM BASED ON JOURNAL OF PLATE-FIN-AND-TUBE CONDENSER PERFORMANCE AND DESIGN FOR REFRIGERANT R-410A AIR-CONDITIONER**

### CFD Analysis For Condenser

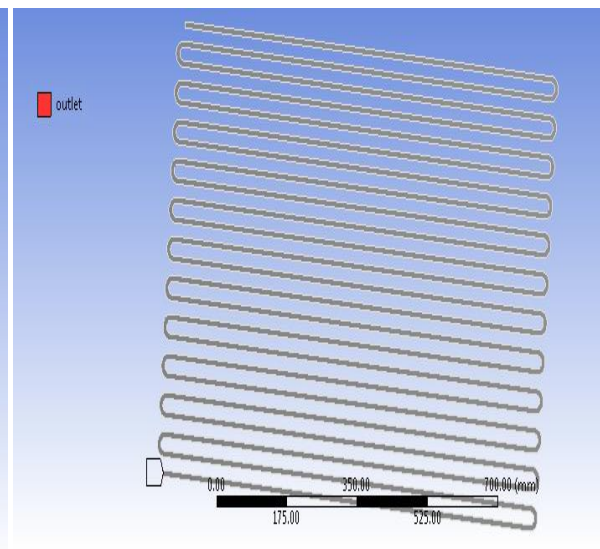
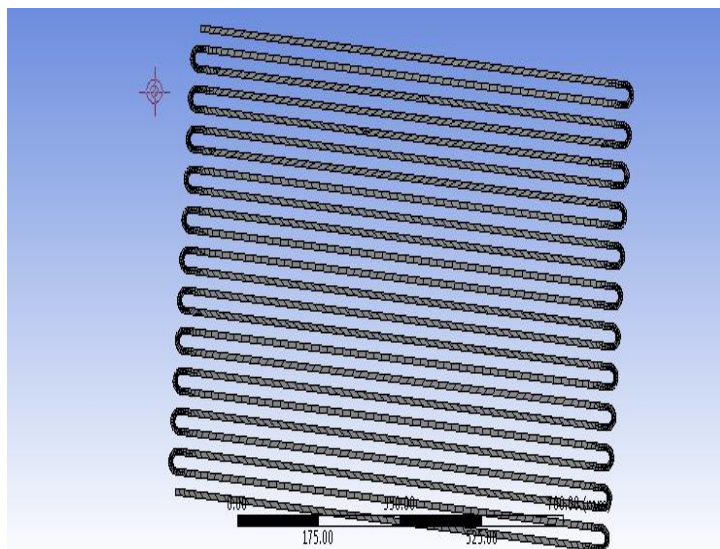
#### Save Creo Model as .iges format

→ Ansys → Workbench → Select analysis system → Fluid Flow (Fluent) → double click

→ → Select geometry → right click → import geometry → select browse → open part → ok



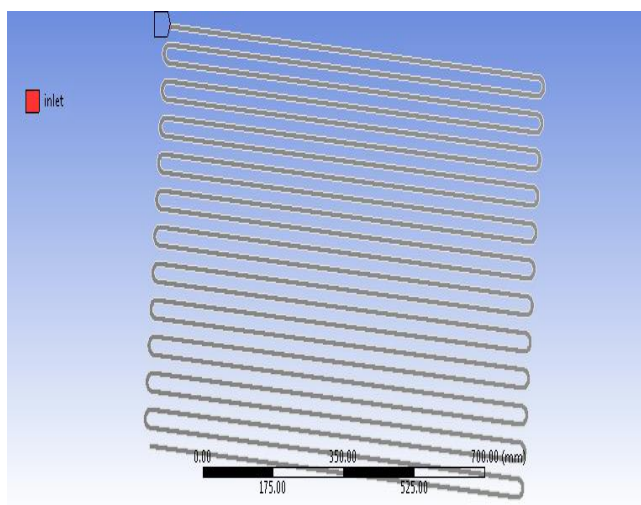
→ → Select mesh on work bench → right click → edit  
 Select mesh on left side part tree → right click → generate mesh →



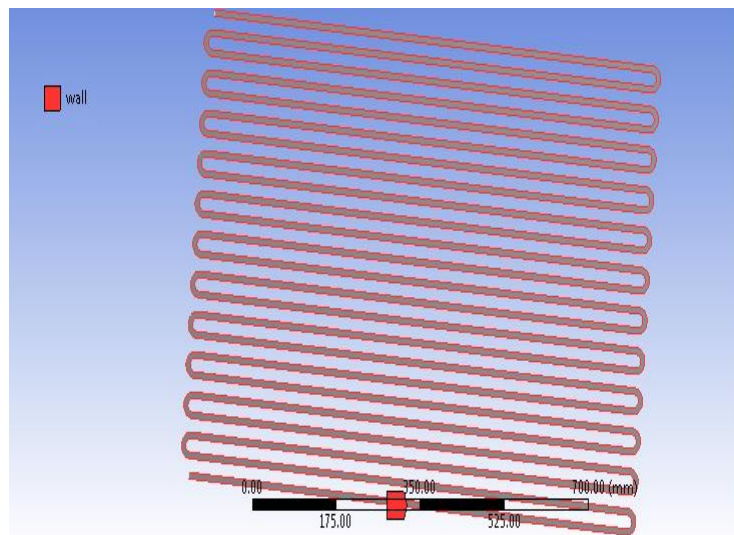
**SPECIFYING BOUNDARIES FOR INLET AND OUTLET**

**Inlet**

Select edge → right click → create named section → enter name → inlet



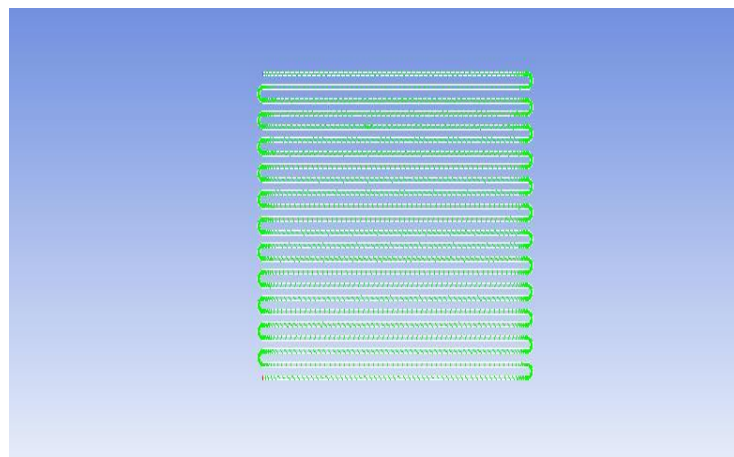
**Wall**



**Outlet**

Select edge → right click → create named section → enter name → outlet

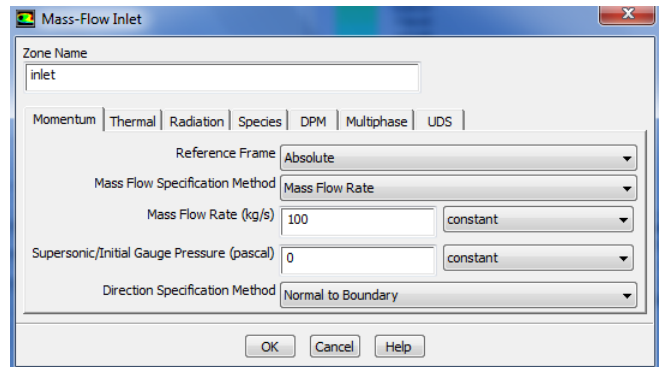
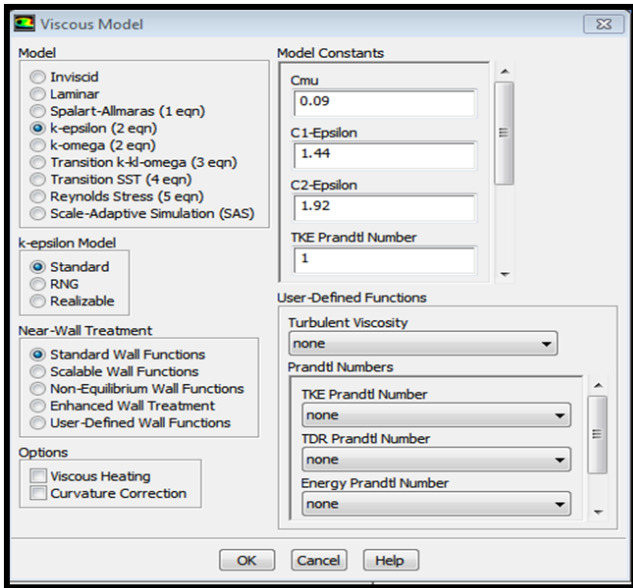
**File export** → fluent → input file (mesh) → save required name → save.  
 →→ Ansys → fluid dynamics → fluent → select working directory → ok  
 →→ file → read → mesh → select file → ok.



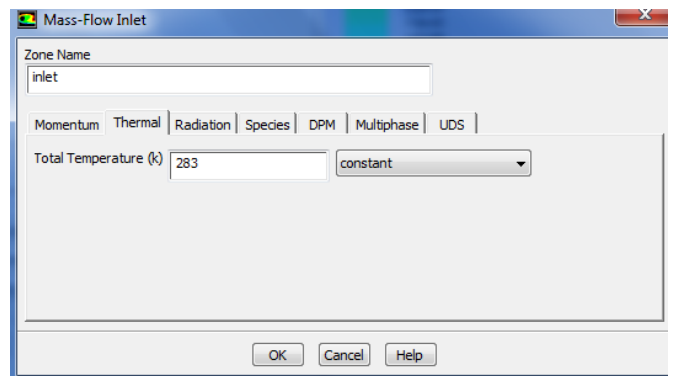
General → Pressure based  
 Model → energy equation → on.  
 Viscous → edit → k-epsilon

## INLET BOUNDARY CONDITIONS

### Inlet



### Inlet Temperature

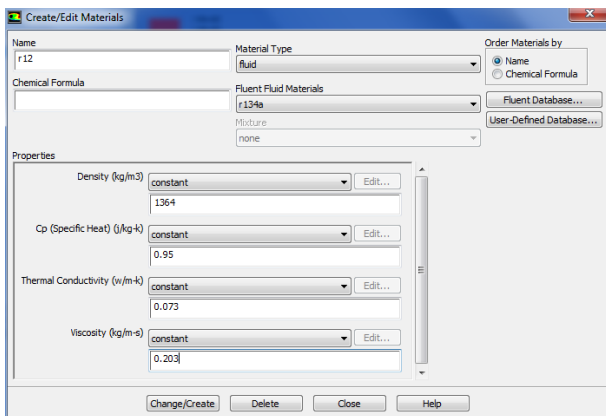


Materials → new → create or edit  
 → specify fluid material or specify properties  
 → Ok

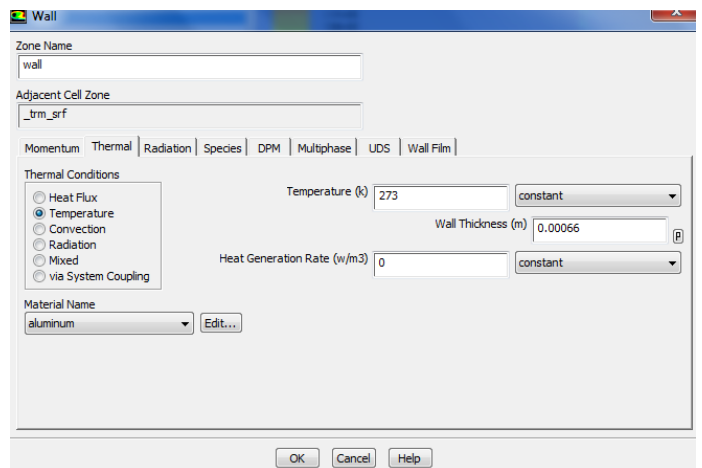
## FLUID - R22

Temperature - T - (°C)	Density - ρ - (Kg/m <sup>3</sup> )	Specific Heat Capacity - Cp - (10 <sup>3</sup> J/Kg.K)	Thermal Conductivity - k - (W/m K)	Kinematic Viscosity - ν - (10 <sup>-6</sup> m <sup>2</sup> /s)	Prandtl Number - Pr -
-50	1547	0.875	0.067	0.310	6.2
-40	1519	0.885	0.069	0.279	5.4
-30	1490	0.896	0.069	0.253	4.8
-20	1461	0.907	0.071	0.235	4.4
-10	1429	0.920	0.073	0.221	4.0
0	1397	0.935	0.073	0.214	3.8
10	1364	0.950	0.073	0.203	3.6
20	1330	0.966	0.073	0.198	3.5
30	1295	0.984	0.071	0.194	3.5
40	1257	1.002	0.069	0.191	3.5
50	1216	1.022	0.069	0.190	3.5

## R22 PROPERTIES



### Wall

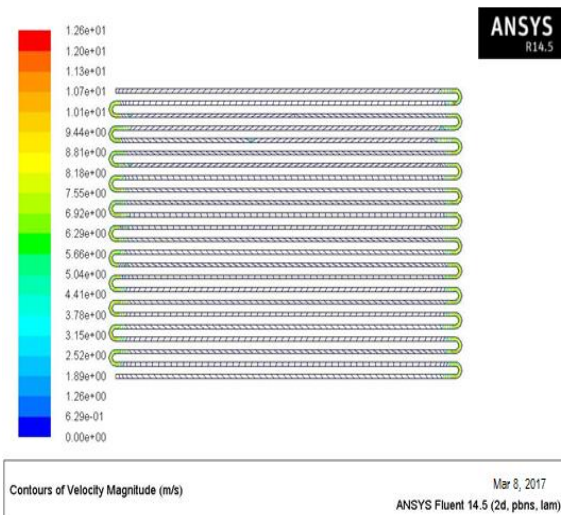
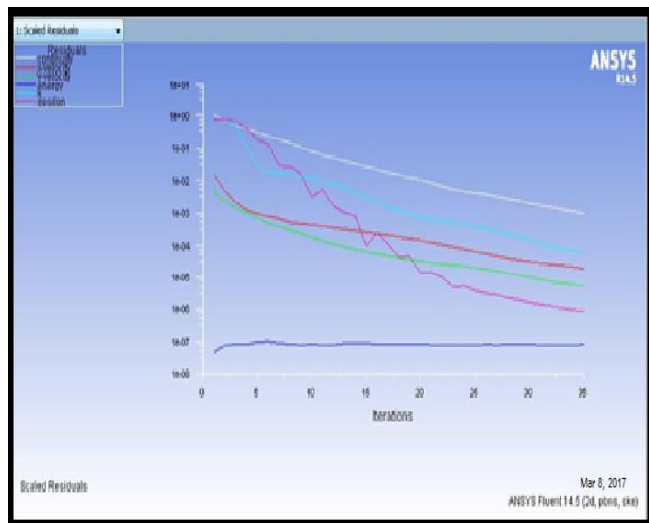


Solution → Solution Initialization → Hybrid Initialization → done

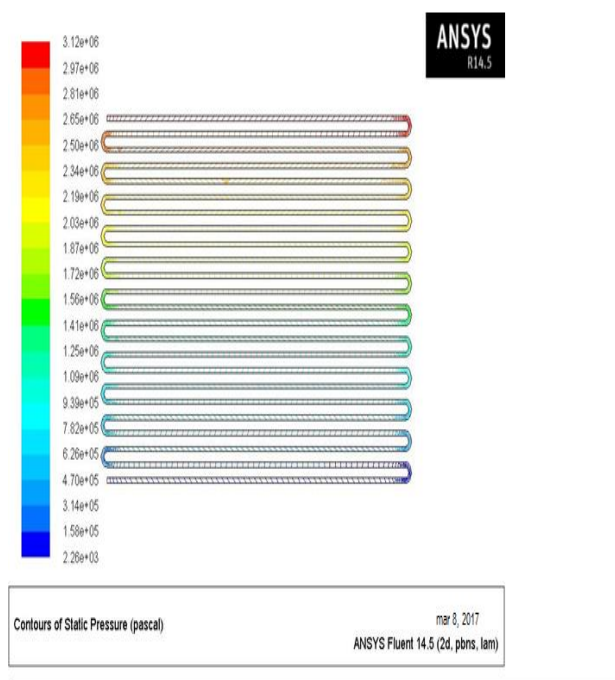
Run calculations → no of iterations = 100 → calculate → calculation complete

→→ Results → graphics and animations → contours → setup

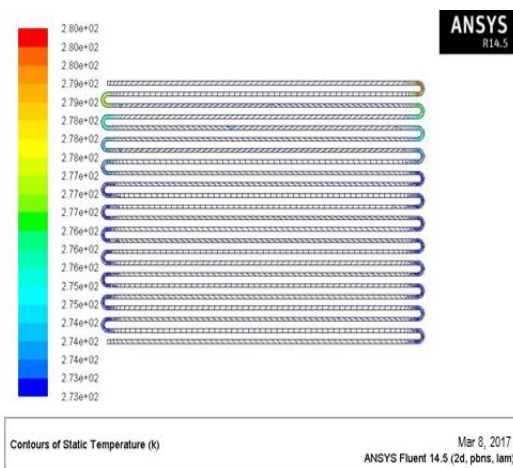
### Iterations



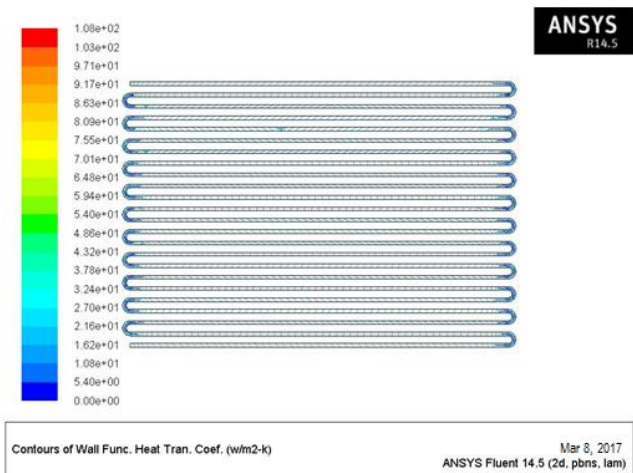
### Contours of Velocity Magnitude



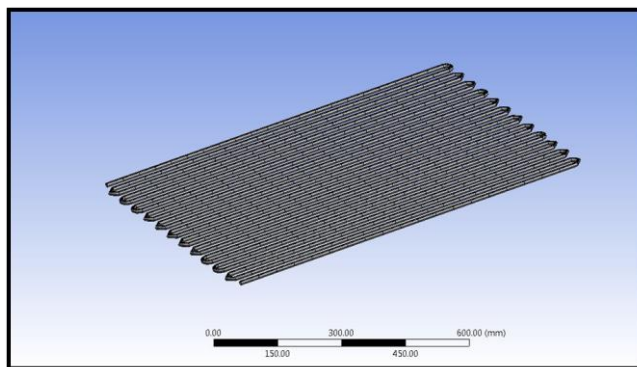
### Contours of Static Pressure



### Contours of Static Temperature



**Meshed model**



**Contours of Wall function Heat Transfer Coefficient**

**Mass Flow Rate (kg/s)**

-----

inlet	100
interior-_trm_srf	-35415.109
outlet	-100.02785
wall	0

-----

Net -0.02784729

**Total Heat Transfer Rate (w)**

-----

inlet	-1439.2496
outlet	2389.7905
wall	-94.993591

-----

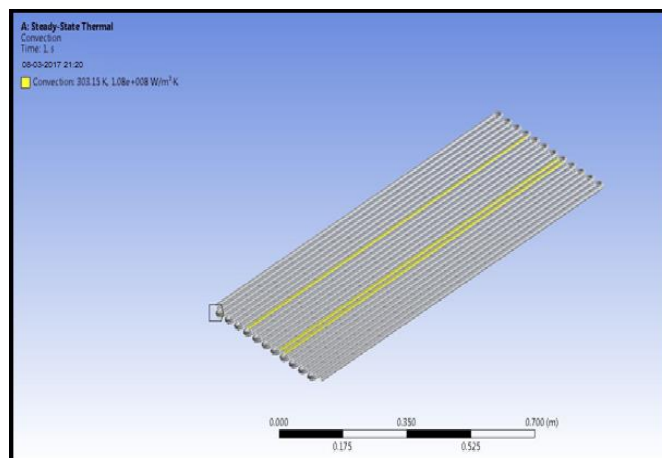
Net 855.549

**Boundary conditions**

Select steady state thermal >right click>insert>  
 Select steady state thermal >right click>insert>select heat flux  
 Select steady state thermal >right click>solve

Solution>right click on solution>insert>select temperature

**Convection**

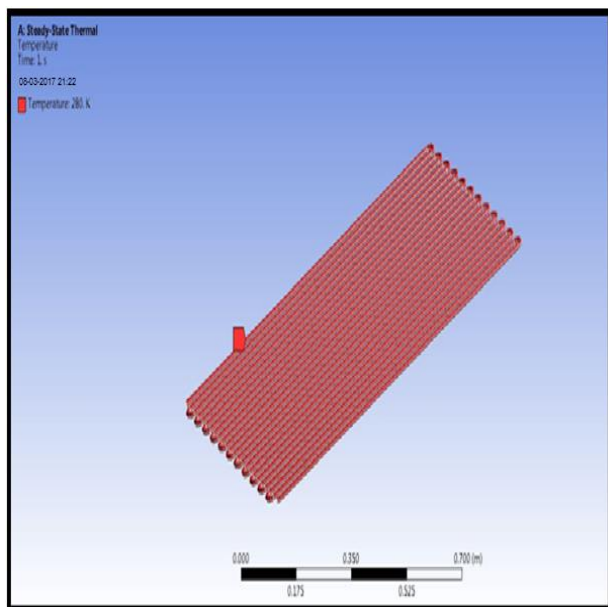


**Temperature**

**ALUMINIUM 6061 MATERIAL**

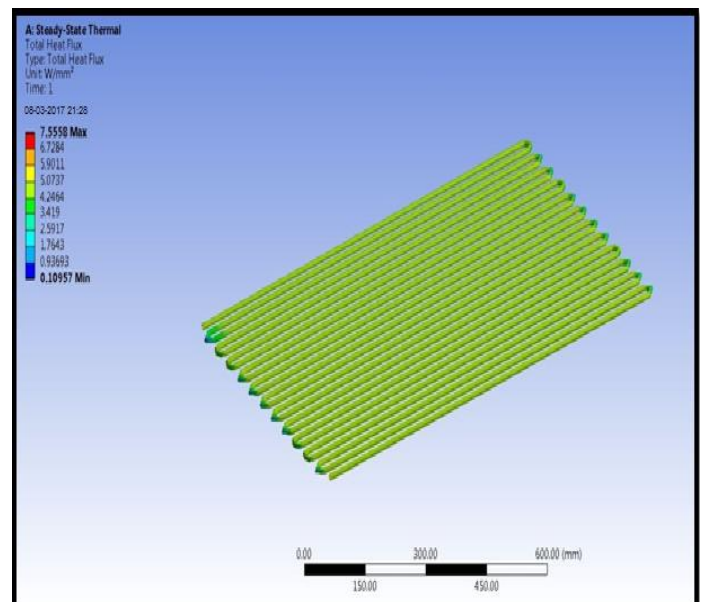
**PROPERTIES**

Thermal conductivity of aluminum = 15.1W/mk  
 Specific heat =356J/Kg K  
 Density = 0.00000412 Kg/mm<sup>3</sup>  
 Model >right click>edit>select generate mesh



## Results

### Temperature

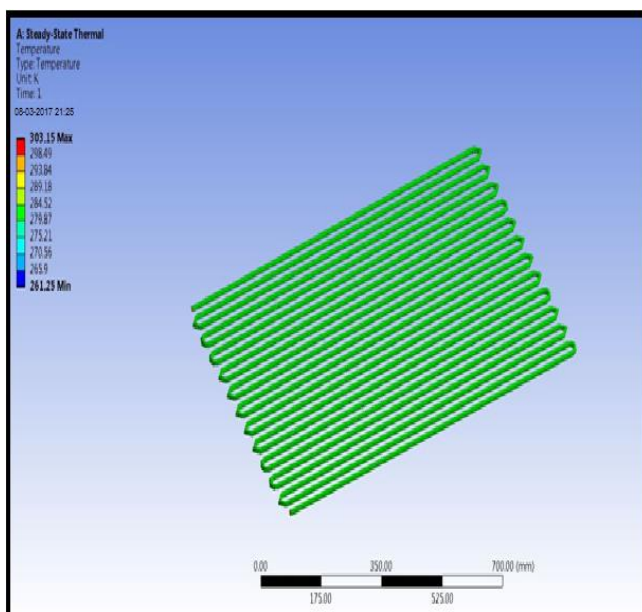


## CONCLUSION

In this thesis heat transfer by convection in AC are determined by CFD and thermal analysis. The assessment is out on an air-cooled tube condenser of a vapour compression cycle for air conditioning system. The materials considered for tubes are Copper and Aluminum alloys 6061. The refrigerants will be R22.

## REFERENCES

- [1]. Experimental Investigation of Split air Conditioning System by liquid Based Cooling System by Balaji N, Suresh Mohan kumar P
- [2]. EFFICIENT USAGE OF WASTE HEAT FROM AIR CONDITIONER by M. Joseph Stalin, S. Mathana Krishnan, G. Vinoth Kumar
- [3]. Comparitive analysis of an automotive air conditioning systems operating with CO2 and R134a by J. Steven Brown a, Samuel F. Yana-Motta b, Piotr A. Domanski c
- [4]. Performance Enhancement of Air-cooled Condensers by M. M. Awad , H. M. Mostafa , G. I. Sultan , A. Elbooz
- [5]. S.H. Noie-Baghban, G.R. Majideian, "Waste heat recovery using heat pipe heat Exchanger (HPHE) for surgery rooms in hospitals", Applied Thermal Engineering, Vol. 20, (2000) 1271-1282.
- [6]. P.Sathiamurthi, R.Sudhakaran "Effective utilization of waste heat in air conditioning. Proc. (2003) 13-14.



### Heat flux

- [7]. P. Sathiamurthi, PSS.Srinivasan, design and development of waste heat recovery system for air conditioner, European Journal of Scientific Research ISSN 1450-216X Vol.54 No.1 (2011), Pp.102- 110.
- [8]. N.Balaji, P.Suresh Mohan Kumar, Eco friendly Energy Conservative Single window Air Conditioning System by Liquid Cooling with helical inter cooler ISSN 1450-216X Vol.76 No.3 (2012), pp.455-462
- [9] S.C.Kaushik, M.Singh. "Feasibility and Refrigeration system with a Canopus heat exchanger", Heat Recovery Systems & CHP, Vol.15 (1995)665 - 673.

# ***Reduction of NO<sub>x</sub> and PM with multiple injection in diesel engine fueled with cotton seed oil biodiesel blend***

**Ramesh Babu Nallamothu**

Marine Engineering Department, Andhra University,  
Visakhapatnam, India. (ASTU, Adama, Ethiopia)  
[rbnallamothu@gmail.com](mailto:rbnallamothu@gmail.com)

**Anantha Kamal Nallamothu**

Mechanical Engineering Department,  
Vellore Institute of Technology, Vellore, India

**Seshu Kishan Nallamothu**

Automobile Engineering Department, SRM  
SRM Institute of Science and Technology, Chennai, India

**I N Niranjan Kumar, BV Appa Rao**

Marine Engineering Department,  
Andhra University, Visakhapatnam, India.

**Abstract—** Diesel engines are successful in commercial applications both on road and off road due to their higher thermal efficiency and fuel economy. CO and HC emissions are less from diesel engines compared to its counterpart gasoline engine. But NO and PM (smoke) emissions are higher due to heterogeneous combustion. Simultaneous reduction of NO<sub>x</sub> and smoke became a tough task faced by researchers to comply with the stringent emission regulations imposed upon. On the other hand biodiesel as a replacement of petro-diesel in diesel engine applications is found to be a good means of solving the problems like depletion of fossil fuel and environmental degradation. High temperature in combustion chamber causes formation of NO<sub>x</sub> and heterogeneous mixing causes smoke formation. In this work an attempt is made to study the influence of splitting injection on NO<sub>x</sub> and smoke in CRDI diesel engine operated with cotton seed oil biodiesel blend (B20). Injection was split into three pulses, namely pre, main and post. The dwell between pre and main was varied and dwell between main and post was fixed at 3° CAD. Fixed quantity of 0.5mg/cycle fuel was injected in post, whereas the fuel injection in pre is 10% of the main injection. The dwell between pilot and main was varied at different main injection timing. The post injection is closely coupled with main injection with a dwell of 3 CAD. The main injection timing along with pilot and post was retarded from the recommended 23° bTDC in steps of 3 degrees. Base line data was obtained with petrodiesel single injection and B20 single injection at recommended 23° bTDC. At all main injection timing the dwell of 10 CAD observed to be the best for smoke reduction, where as 20 CAD is better for NO<sub>x</sub> reduction. In overall Dwell 10 CAD is better for trade off between NO<sub>x</sub> and Smoke. It is found that splitting injection is very much helpful in simultaneous reduction of harmful emissions like NO<sub>x</sub> and smoke from diesel engines.

**Keywords—** Pilot injection, post injection, Biodiesel, blends, dwell

## I. INTRODUCTION

Depletion of fossil fuels due to heavy usage of fossil fuels like gasoline and diesel to meet ever growing energy demand world over became a prime concern of the world at the moment. In addition the environmental degradation

caused by the harmful pollutants emitted by burning of petroleum fuels is also haunting the world. With the growth of the population the usage of Diesel increasing in transportation and industrial applications to meet the energy requirements causing the release of tons and tons of dangerous pollutants adding to the atmospheric air. These emissions are the main reasons for the consequences like global warming, acid rains and various ailments of human beings. In an effort to minimize the damage caused to the environment, the countries world over imposed a stringent regulations on the emissions from usage of petroleum fuels and other fossil fuels. Complying with stringer environmental regulations became a big challenge for industries, automobile manufactures and the researchers in the field. Different ways and means are being explored to conserve the conventional fuel resources, reduce the dependence on petroleum fuels and reduce the environmental degradation.

One way is to look for biobased alternative fuels like biodiesel, bio-ethanol etc which are renewable, eco-friendly and home grown. It gives the solution to the problems like depletion of petroleum resources, environmental damage and dependence on oil importation. Another way which is tried with is improvement of combustion process by improving the design of combustion chamber, modifying the fuel injection system etc which improves the fuel economy, efficiency of combustion process, reduces the green house gases and other harmful emissions.

Vegetable oils, having features of renewability, biodegradability, eco-friendly etc are promising replacement for conventional petroleum diesel. Higher viscosity is the major drawback of straight vegetable oils which hinder its usage directly in unmodified diesel engines. Direct usage of straight vegetable oils may cause deposits in combustion chamber and damages the engine. Transesterification process is the well established procedure which can be used to produce biodiesel by bringing down the viscosity. Tri-

glycerids present in vegetable oil get converted into mono alkyl esters of long chain fatty acids (Biodiesel) when vegetable oil reacts with alcohol in the presence of catalyst. Glycerine comes out as a byproduct [1].

Therefore, explorations to find Biodiesel are one of the most promising alternative fuels to replace or to reduce dependency on the conventional petroleum-based fuels with multiple environmental advantages and application in compression ignition (CI) engines with no modification. Biodiesel is nonexclusive, biodegradable, non flammable, renewable, nontoxic, environment friendly, and similar to diesel fuel [2]. The main advantages of biodiesel include the following: it can be blended with diesel fuel at any proportion; it can be used in a CI engine with no modification; it does not contain any harmful substances; and it produces less harmful emissions to the environment than diesel fuel. Biodiesel, popularized as the mono alkyl esters are derived from triglycerides (vegetable oils or animal fats). Transesterification is the most convenient process to convert triglycerides to biodiesel. Transesterification process involves a reaction of the triglyceride feedstock with light alcohol in the presence of a catalyst to yield a mixture of mono alkyl esters currently, using hydroxides of sodium or potassium, is the common route for industrial production of biodiesel [3].

The minimization of fuel consumption and the reduction of emissions have been two driving forces for engine development throughout the last decades. The first objective is in the financial interest of the vehicle owners. The second is imposed by legislation, sometimes also supported by excise reductions or customers' demands for clean engines. The ongoing emission of NO<sub>x</sub> is a serious persistent environmental problem due to; it plays an important role in the atmospheric ozone destruction and global warming [4]. NO<sub>x</sub> is one of the most important precursors to the photochemical smog. Component of smog irritate eyes and throat, stir up asthmatic attacks, decrease visibility and damages plants and materials as well. By dissolving with water vapor NO<sub>x</sub> form acid rain which has direct and indirect effects both on human and plants. An SCR (Selective Catalytic Reduction) exhaust gas after treatment system which uses urea solution as a reducing agent has a high NO<sub>x</sub> reduction potential and is a well-known technique for stationary applications [5]. The idea of using urea SCR systems for the reduction of NO<sub>x</sub> emissions in diesel engines is two decades old. Since then, many applications have been developed, some of which have reached commercialization [6]. But, it is still a challenge for researchers.

With the recent development of common rail direct injection system, it became possible to reduce NO<sub>x</sub> and other emissions by adopting multiple injection strategy [7,8].

Split fuel injection involves reducing splitting the injection as two or more events which can lead to a reduction in the ignition delay in the initial fuel pulse. This leads greater

fraction of combustion to occur later in the expansion stroke. As majority of NO<sub>x</sub> occurs during premixed stage, the net amount of NO<sub>x</sub> formed during the split fuel injection is lowered [9]. Multiple injections method is found to be very effective at reducing particulate emissions at high load, and combined technique of multiple injections with EGR is effective at intermediate and light loads. However, increased particulate emissions due to EGR causes increased engine wear due to degradation of lubricant. Increased Brake Specific Fuel Consumption (BSFC) is another concern. Split injection up to 5 splits, are experimented in combination with EGR[10]. Proper dwell between injections was significant as small dwell led to situation of single injection while long reduced the effect of pre-mix combustion. For pilot injection dwell around 10 CAD reduces emission efficiently. Around 21 CAD bTDC injection timing of first injection was observed to be optimum for simultaneous reduction of NO<sub>x</sub> and soot [11]. The rapid depletion of petroleum fuels and ever increasing price of them has led to an intensive search for alternative fuels. Biofuels being renewable and ecofriendly are attracting growing interest around the world [12]. The findings indicate the level of pollution is high and will continue to grow if left unabated. Tailpipe emission findings estimated the highest level of NO<sub>x</sub> emissions at 3.44 g/km, HC emissions at 6.53 g/km, CO at 13.9 g/km, PM<sub>2.5</sub> at 1.3 g/km and 35.96 g/km of CO<sub>2</sub>. These amount of emission exceed the proposed draft NEMA ambient air quality emission data and the World Bank ambient air quality guidelines. This implies that persons exposed to these emissions on a daily basis are likely to develop health complications over time as the concentration levels increase. Several mitigation methods can be applied to reduce the emission level such as reduce consumption of fossil fuels and increase efficiency in transport usage of energy [13].

## II. METHODOLOGY

The main objective of this work is to study the effect of multiple injection strategy on reduction of NO<sub>x</sub> and smoke with retardation of injection and varying the dwell between pre and main. A novel scheme of experiments was adopted in the work to understand the influence of multiple injections by varying different parameters on the emissions from the engine. The used injection strategy is pilot (pre)-main-post. The pilot is fixed at 10% and post fuel quantity is fixed as 0.5mg/cycle. The retardation was done from 23° to 11° in 3° interval. The dwell is varied from 10 CAD to 20 CAD in three steps. Long term consumption of cotton seed oil is very much detrimental to human health in many aspects. Cotton seed oil which is nonedible is used for the preparation of biodiesel. Biodiesel is prepared using transesterification process.

The steps followed in this work are as given below:

- Extraction of oil from cotton seeds using mechanical press

- Preparation of biodiesel using transesterification process.
- Characterization of biodiesel.
- Preparation of B20 blend
- Testing the performance of CRDI diesel engine with diesel and B20 in single injection for base data and B20 with multiple injection strategy varying injection timing.
- Comparing the emissions from multiple injection and single injection



Fig 1. Experimental setup

A. Engine setup

The setup consists of single cylinder, four stroke, CRDI VCR (Variable Compression Ratio) engine connected to eddy current dynamometer. It is provided with necessary instruments for combustion pressure, crankangle, airflow, fuel flow, temperatures and load measurements. These signals are interfaced to computer through high speed data acquisition device. The set up has stand-alone panel box consisting of air box, twin fuel tank, manometer, fuel measuring unit, transmitters for air and fuel flow measurements, process indicator and piezo powering unit. Rotameter are provided for engine cooling water flow measurement. CRDI VCR engine works with programmable Open ECU for Diesel injection, fuel injector, common rail with rail pressure sensor and pressure regulating valve, crank position sensor, fuel pump and wiring harness. The setup enables study of CRDI VCR engine performance with programmable ECU at different compression ratios and with different EGR. Engine performance study includes brake power, indicated power, frictional power, BMEP, IMEP, brake thermal efficiency, indicated thermal efficiency, Mechanical efficiency, volumetric efficiency, specific fuel consumption, Air fuel ratio, heat balance and combustion analysis.

Table 1. Specification of the CRDI Engine

Engine	Kirloskar, single cylinder, four stroke water cooled, VCR
Stroke	110 mm
Bore	87.5 mm
Capacity	661 cc
Power	3.5 kW
Speed	1500 RPM
Compression Ratio	12-18
Injection system	Common rail direct injection with open ECU
Injection pressure	300 bar
Dynamometer	Eddy current dynamometer
Dynamometer arm length	185 mm

A novel scheme of experiments is adopted in the work to understand the influence of multiple injections by varying different parameters on the emissions from the engine.

The injection is split into pilot(pre)-main-post. After different trials the quantity of Pilot injection is fixed as 10% and post fuel quantity is fixed as 0.5 mg/cycle. The dwell between main and pilot is maintained as 10 degrees. Closely coupled post injection is used with 3 degrees after main injection. Main injection timing is retarded from recommended injection timing of 23° to 11° bTDC. The influence of this retardation on NOx emission and smoke is measured. B20P10M20P3 stands for Biodiesel blend 20, pilot injection with dwell of 10° , Main injection at 20° and post injection with dwell of 3°

III. RESULTS AND DISCUSSIONS

A. Biodiesel characteristics

The properties of prepared cotton seed oil biodiesel is given in table 1, given below.

Table 2. Properties of biodiesel (Eta Laboratories)

Properties	B100
Density@15 °C,(gm/cm <sup>3</sup> )	0.8865
Kinematics viscosity@40 °C	4.85
Flash point, °C	149
Fire Point, °C	160
Cloud point, °C	+1
Gross Calorific Value, kJ/kg	40,695
Cetane number	50.8
Copper strip corrosion @ 50oC for 3 hrs	Not worse than no 1
Acid value as mgof KOH/gm	0.063
Carbon Residue	0.041%
Sulphur	0.0043%

B. NOx Emission

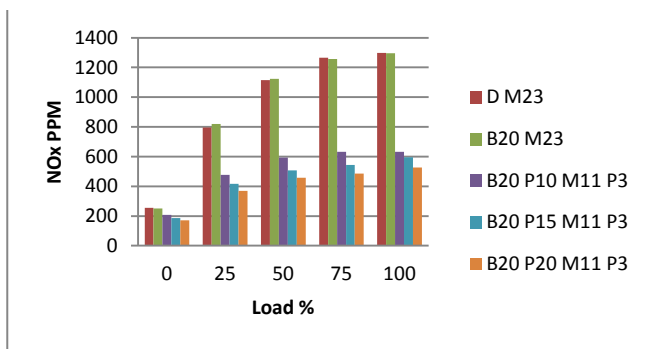


Fig 2. NOx emission at M11

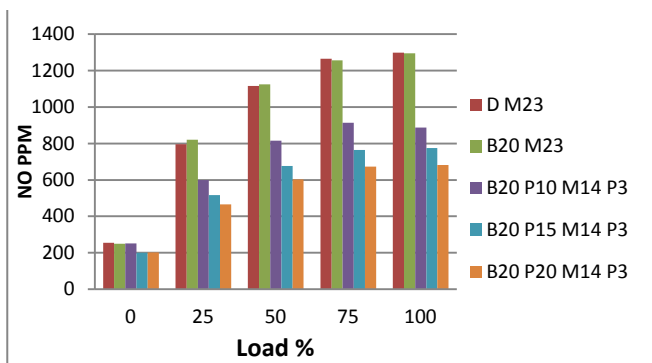


Fig 3. NOx emission at M14

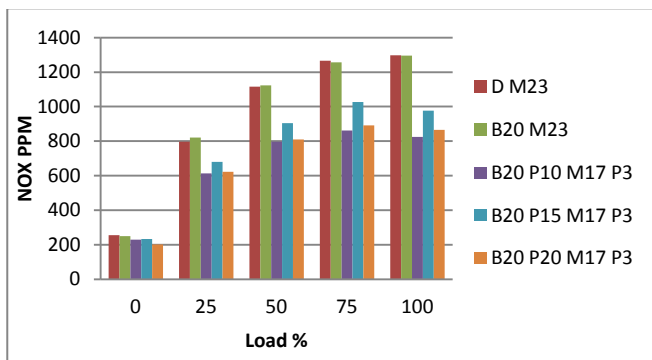


Fig 4 . NOx emission at M17

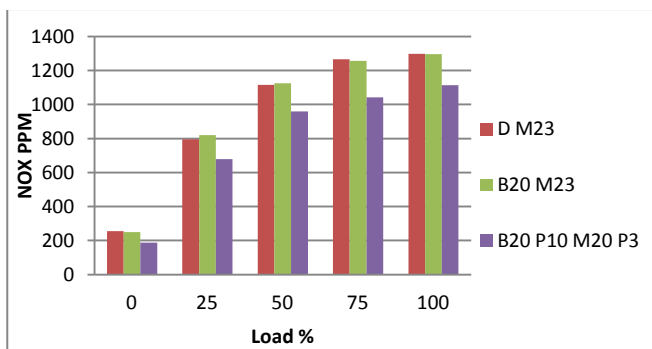


Fig 5. NOx emission at M20

It is observed from the above figures that with multiple injection the NOx emission reduced considerably. From Fig 2, it is noted that at M11 the NOx emission is reducing as the dwell between pilot and main increasing from 10 CAD to 20 CAD. There is a maximum reduction of 56.91% with dwell of 20 CAD compared to single injection M23.

At M14 also similar trend of reducing NOx emission with increase in the dwell period. Maximum reduction of 49.75% is noted with a dwell of 20CAD compared to single injection with a load of 6kg.

At M17, Fig 4, dwell 10 CAD found to be better than others. The maximum reduction in NOx emission is 33.58% with a load of kg. It is observed that the effect is more influential at the load of kgs. As the main injection timing is retarded the NOx emission observed to be reducing due to reduction in the peak temperatures developed in the combustion chamber. Multiple injection strategy is observed to be more effective in reducing NOx at part load condition. There is a increment in NOx with P10 M23 P3 . In overall the dwell of 20 CAD is observed to be better for NOx reduction. At M17.

It is observed that the rate of rise in NOx reducing with increasing the load. At M20 with the dwell of 15 and 20 CAD, the engine didn't work smoothly. The dwell of 10 CAD is better.

### C. Opacity

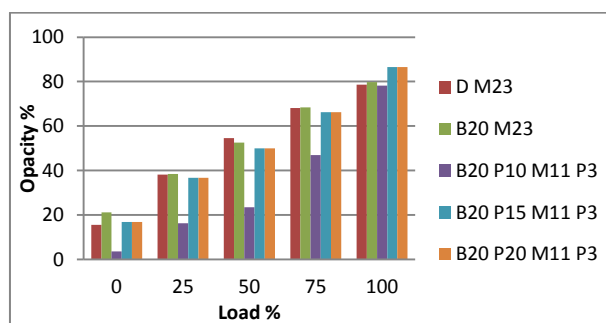


Fig 6. Opacity at M11

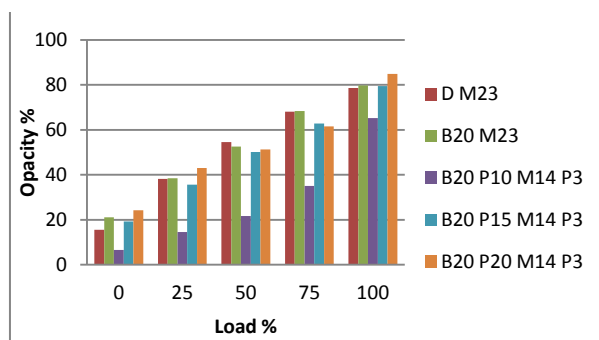


Fig 7. Opacity at M14

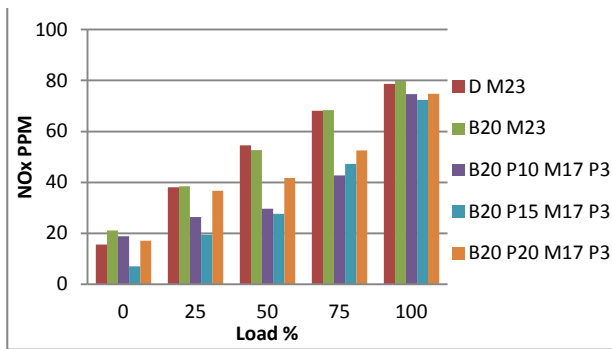


Fig 8. Opacity at M17

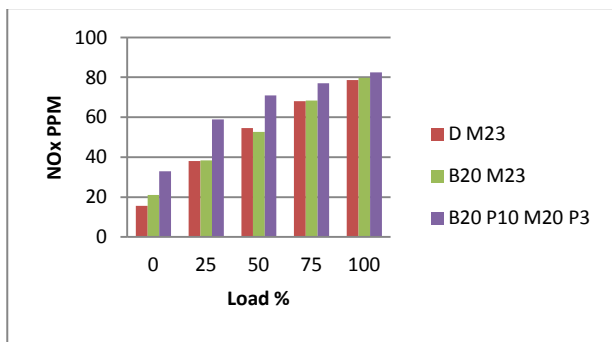


Fig 9. Opacity at M20

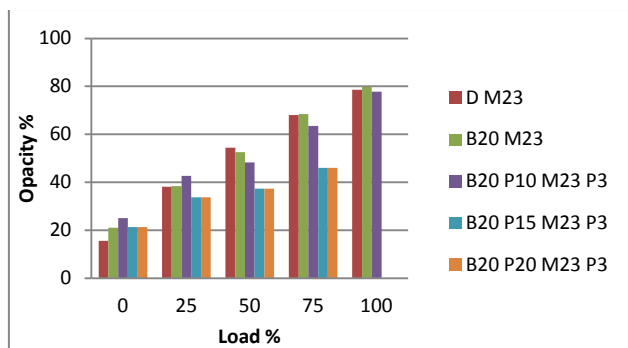


Fig 10. Opacity at M23

From the above figures it is observed that splitting the fuel injection has considerable effect on smoke emission. Maximum reduction of smoke is noted at M14 with dwell of 10 CAD with 6 kg load. At this condition the reduction in smoke is 58.93%. The reduction of smoke at M11 with a dwell of 10 CAD 55.32% with load of 6 kg.

It is observed that the engine is hesitating at higher load with higher dwells of 15 and 20 CAD at M23 and M20. At all main injection timing the dwell of 10 CAD observed to be the best.

The retardation of multiple injection with main injection retardation from 23° bTDC to 11° bTDC, smoke emission is considerably effected. Smoke opacity reduced gradually up to main injection 14° and then starts increasing with further retardation. The reduction is 69.1%, 62.23%, 58.93%, 48.68%, 18.29%

with load of 0%, 25%, 50%, 75%, 100% respectively at P10 M14 P3.

At retarded injection timing higher dwell caused more smoke at higher loads.

#### IV. CONCLUSIONS

- It is observed that multiple injection is a good means of having tradeoff between smoke and NOx emissions.
- Retardation of multiple injection upto M11 helped in reducing both NOx and smoke. Further retardation caused rise in smoke.
- P10 M11 P3 is better for smoke and NOx tradeoff.
- At all main injection timing the dwell of 10 CAD observed to be the best for smoke reduction, where as 20 CAD is better for NOx reduction. In overall Dwell 10 CAD is better for trade off between NOx and Smoke.
- Further combustion related analysis is required to understand completely the influence of multiple injection
- Multiple injection strategy seems to be more efficient than conventional in reducing emission due to their capability in controlling heat release rate and hence peak temperature. Multiple injection is better than single injection in optimising tradeoff between NOx and smoke due to their efficiency in reducing initial high temperatures and supporting combustion of late injection.
- Reduction in emissions was improved with multiple pre-main-post injection strategy, as pre injection supports main injection combustion and reduced delay while post combustion helps in oxidation of soot particles without impact on NOx.
- Proper dwell between injections was significant as small dwell led to situation of single injection while long reduced the effect of pre-mix combustion. For pilot injection dwell around 10 CAD reduces emission efficiently.
- Around 21 CAD bTDC injection timing of first injection was observed to be optimum for simultaneous reduction of NOx and smoke.

#### Acknowledgment

We are thankful to Marine engineering department, Andhra University, for giving this opportunity to work on biodiesel applications in diesel engines. We are also thankful to sri venkateswara research center, Kanchipuram for providing necessary research facilities.

#### References

- [1] Pankaj S. Shelkea, Nitin M. Sakharea, Subhash Lahanea, "Investigation of Combustion Characteristics of a Cottonseed Biodiesel Fuelled Diesel Engine", Global Colloquium in Recent

Advancement and Effectual Researches in Engineering, Science and Technology (RAEREST 2016), Procedia Technology 25 (2016)

- [2] YanuandriPutrasar, ArifinNur, AamMuharam, (2013), "Performance and emission characteristic on a two cylinder DI diesel engine fuelled with ethanol -diesel blends," in *International Conference on Sustainable Energy Engineering and Application[ICSEEA]* Energy Procedia 32.
- [3] A.S.A.E.Atabani, (2013),"Non-ediblevegetable oils: A critical evaluation of oil extraction, fatty acid compositions, biodiesel production, characteristics, engine performance and emissions production'," *Renewable and Sustainable Energy Reviews journal*,pp. 211-245.
- [4] T. Pushparaj, S. Ramabalan,(2013),"Green fuel design for diesel engine combustion,performance and emission analysis'," in *International Conference On DESIGN AND MANUFACTURING IConDM .research scholar.*, Tamil Nadu, india , .
- [5] Busca G., Lietti L., Ramis G., and Berti F., Chemical and mechanistic aspects of the selective catalytic reduction of NOx by ammonia over oxide catalysts: A review, *Applied catalysts B: environmental*, 18(1-2), 1998, 1-36
- [6] H. Bosch, F. J. J. G. Janssen: Catalytic Reduction of Nitrogen Oxides: A Review on the Fundamentals and Technology, *Catalysis Today*, 2(369), 1988.
- [7] Perry, R. A. and Siebers, D. L. Rapid reduction of nitrogen oxides in exhaust gas streams. *Nature*, 324, 1986, 657–658.
- [8] Imarisio, R, et al.: " Multiple injection, a cost effective solution for emission reduction of common-rail DI Diesel Engines", *Aachener Kolloquium Fahrzeug-und Motorentechnik*, 9(2000), 1047-1062.
- [9] Badami, M, et al.: " Influence of Multiple injection strategies on emissions, combustion noise and BSFC of a DI common rail diesel engine", *SAE Tech. Ser.*, No.2002-01-0503, (2002)
- [10] Gao Z and Schreiber W (2001), "The Effects of EGR and Split Fuel Injection on Diesel Engine Emission", *InternationalJournal of Automotive Technology*, Vol. 2, No. 4, pp. 123-133.
- [11] Ramesh Babu Nallamotheu, Anantha Kamal Nallamotheu, Seshu Kishan Nallamotheu, I N Niranjan Kumar, BV Appa Rao, " Emission Analysis of CRDI Diesel Engine fueled ith cotton seed oil biodiesel with multiple injection strategy", *International Journal of Emerging Technologies and Innoativve Research*, ISSN: 2349-5162, Vol.5, Issue9, Page no.707-712, September-2018.
- [12] Ramesh Babu Nallamotheu , Geleta Fekadu , & Prof B.V. Appa Rao "comparative performance evaluation of gasoline and its blends with ethanol in gasoline engine", *G.J.B.A.H.S.*,Vol.2(4):100-106, October –December, 2013, ISSN: 2319 – 5584.
- [13] Solomon Neway, Ramesh Babu Nallamotheu, Seshu Kishan Nallamotheu, Anantha Kamal Nallamotheu"Investigation on Pollution Caused by Gasoline and Diesel fuelled Vehicles", *International Journal of Engineering Trends and Technology (IJETT)*, V36(7),376-381 June 2016. ISSN:2231-5381.

# DESIGN AND OPTIMIZATION OF HIGH-SPEED MOTORIZED SPINDLE

A. Sandeep

Department of Mechanical Engg.  
Malla Reddy College of Engineering,  
Maisammaguda, Dhulapally, Kompally,  
Secunderabad, Telangana-500100, India  
Email: [areboinasandeep@gmail.com](mailto:areboinasandeep@gmail.com)

A. Sravan

Department of Mechanical Engg.  
Malla Reddy College of Engineering  
Maisammaguda, Dhulapally, Kompally,  
Secunderabad, Telangana-500100, India  
Email: [sravanalugala6@gmail.com](mailto:sravanalugala6@gmail.com)

Dr. P. John Paul

Principal  
Professor, Department of ECE.  
Malla Reddy College of Engineering  
Maisammaguda, Dhulapally, Kompally,  
Secunderabad, Telangana-500100, India  
Email: [principal@mrce.in](mailto:principal@mrce.in)

**Abstract:**The geometric quality of high-precision parts is highly dependent on the dynamic performance of the entire machining system, which is determined by the interrelated dynamics of machine tool mechanical structure and cutting process. This performance is of great importance in advanced, high-precision manufacturing processes. The state-of-the-art in machine tool main spindle units is focus on motorized cutting. In this thesis, high speed motorized spindle is designed and analyzed under the given load conditions. The spindle used in this thesis is that used in a milling machine. The 3D modeling of spindle is designed in Pro/Engineer. The material used for spindles is Steel. In this thesis, different materials are analyzed for spindle. Aluminum alloy 6061 and 7075 are replaced with steel. By replacing the steel with aluminum alloys, the weight of the spindle decreases. Structural and Dynamic analyses is done using Ansys software. Modal analysis also is done to determine the frequencies.

**Key Words:** FEA, ANSYS, Thermal Deformation, Failure.

## 1. INTRODUCTION TO SPINDLE

In machine tools, a spindle is a rotating axis of the machine, which often has a shaft at its heart. The shaft itself is called a spindle, but also, in shop-floor practice, the word often is used metonymically to refer to the entire rotary unit, including not only the shaft itself, but its bearings and anything attached to it (chuck, etc.).

A machine tool may have several spindles, such as the headstock and tailstock spindles on a bench lathe. The main spindle is usually the biggest one. References to "the spindle" without further qualification imply the main spindle. Some machine tools that specialize in high-volume mass production have a group of 4, 6, or even more main spindles. These are called multi spindle machines. For example, gang drills and many screw machines are multi spindle machines. Although a bench lathe has more than

one spindle (counting the tailstock), it is not called a multi spindle machine; it has one main spindle.

Examples of spindles include:

On a lathe (whether wood lathe or metal lathe), the spindle is the heart of the headstock.

In rotating-cutter woodworking machinery, the spindle is the part on which shaped milling cutters are mounted for cutting features (such as rebates, beads, and curves) into mouldings and similar millwork.

Similarly, in rotating-cutter metalworking machine tools (such as milling machines and drill presses), the spindle is the shaft to which the tool (such as a drill bit or milling cutter) is attached (for example, via a chuck).

Varieties of spindles include grinding spindles, electric spindles, machine tool spindles, low-speed spindles, high speed spindles, and more.



Fig: 1. Lathe headstock: H4 - Spindle



Fig: 2. Lathe tailstock: T5 - Spindle



Fig: 3. Multi spindle lathe

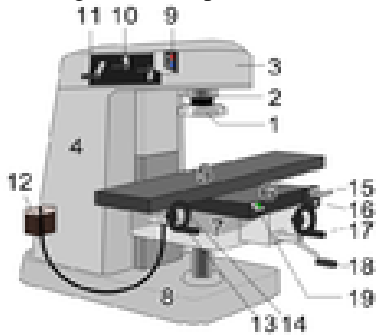


Fig: 4. Vertical milling machine (single spindle): #2 – Spindle

### High Speed Spindles

A high speed spindle that will be used in a metal cutting machine tool must be designed to provide the required performance features. The major performance features include:

- Desired Spindle Power, Peak and Continuous
- Maximum Spindle Load, Axial and Radial
- Maximum Spindle
- Speed Allowed
- Tooling Style, Size and Capacity for ATC
- Belt Driven or Integral Motor-Spindle Design

In addition to the high speed spindle system design, maintenance and reliability issues will also be discussed.

### High Speed Spindle Design: Major Component List

The major components required for a high speed milling spindle design include:

- Spindle Style; Belt Driven or Integral Motor-Spindle
- Spindle Bearings; Type, Quantity, Mounting, and Lubrication Method
- Spindle Motor, Belt-Type, Motor-Spindle, Capacity, Size
- Spindle Shaft; Including Tool Retention Drawbar and Tooling System Used
- Spindle Housing; Size, Mounting Style, Capacity

## 2. LITERATURE SURVEY

In this paper by Deping Liu, Hang Zhang, Zheng Tao and YufengS [1], presents a method to investigate the characteristics of a high-speed motorized spindle system. This paper taking the high-speed milling motorized spindle of CX8075 produced by Anyang Xinsheng Machine Tool Co. Ltd. As an example, a finite element model of the high-

speed motorized spindle is derived and presented. The results show that the maximum rotating speed of the motorized spindle is far smaller than the natural resonance region speed, and the static stiffness of the spindle can meet the requirements of design. The static and dynamic characteristics of the motorized spindle accord with the requirements of high-speed machining. The thermal deformation of spindle is  $6.56\mu\text{m}$ , it is too small to affect the precision of the spindle. The results illustrate the rationality of the spindle structural design. In the paper by LanJin, Zhaoyang Yan, Liming Xie, Weidong Gou, LinhuTang [2], a method is described in this paper for measuring the spindle rotation error and a technique for separating the eccentric error caused by setup error of the master cylinder. The system consists of two non-contact capacitance sensors used to measure the radial displacement of the rotating master cylinder and an LMS Test. Lab used to collect the measurement data. LMS Test. Lab offers a complete engineering solution for rotating machinery. Based on our experimental research, it indicates that this system can be used to measuring the spindle rotary error at different speeds. It is also verified the feasibility of the error separation methods developed in this paper. In the paper by R. Radulescu, S. G. Kapoor and R. E. DeVor [3], a mechanistic dynamic model is used to simulate a face milling process during constant and variable speed machining. The model can be used to predict the optimum speed trajectory that can provide a low level of vibration and consequently a large productivity rate and a small surface error. The model is used to investigate the vibration of face milling processes that have one, or multiple coupled modes of vibration acting throughout the cut. For cutting processes having one dominant mode of vibration, the model predicts that variable speed machining is especially effective over constant speed machining when the tool-work system changes its dominant mode of vibration throughout the cut, or when the tool-work system has several modes of vibration coming from component parts that are cut in the same time. For cutting processes having multiple dominant modes of vibration, the model predicts that variable speed machining is especially effective over constant speed machining when the tool-work modes of vibration are unequal and moderately coupled to each other. Also, the model suggests that for tool-work systems having complex geometries with dynamics hard to predict, variable speed machining is safer to use than constant speed machining when trying to achieve high productivity rates. This is due to the fact that variable speed machining is robust with respect to the dynamics of the tool-work system. Finally, the model predictions are in good agreement with the experiment. In the paper by Sébastien SEGUY, Gilles DESSEIN, Lionel ARNAUD, TamásNSPERGER<sup>[4]</sup>, the aim is to analyze the effect of spindle speed variation on machine tool chatter in high-speed milling. The stability analysis of triangular and sinusoidal shape variations is made numerically with the semi-discretization method. Parametric studies show also the influence of the frequency

and amplitude variation parameters. This modeling is validated experimentally by variable spindle speed cutting tests with a triangular shape. Stable and unstable tests are analyzed in term of amplitude vibration and surface roughness degradation. This work reveals that stability must be considered at period variation scale. It is also shown that spindle speed variation can be efficiently used to suppress chatter in the flip lobe area.

#### Design and analysis of high speed motorized spindle

Motorized spindle is one of the core parts of high-speed machine tool to a great extent, its thermal characteristics determine the thermal stress and thermal deformations and therefore the research on thermal characteristics is of great significance to increase the accuracy of high-speed machine tool. The motorized spindle is modeled, its thermal and dynamic characteristics analysis are carried out by finite element method using ANSYS software. It provides a powerful theoretical basis for reducing temperature-rise, calculating thermal deformations and improving working conditions of the high speed spindle. The results of temperature rise are used to determine the working speed of the spindle without bearing failure. The modal analysis was conducted for finding natural frequency, corresponding stress and displacement of the motorized spindle.

Dynamic and thermal analysis of high speed motorized spindle Modern technology to a great extent relies on the use of High speed 3 ntroduc spindle is a competent technology for significantly ever-increasing productivity and plummeting production costs. On the one hand, high precision is essential for the ongoing trend of manufacturing activity, a striking example of which is found in electronics industry, automobile industry and machine tool industry .On the other hand, high precision is essential for leading-edge research. Compared to conventional spindles, motorized spindles

are equipped with built-in motors for better energy consumption, balancing to achieve high-speed operation and good quality of product. However, the built-in motor 3ntroducing a great amount of heat into the spindle system as well as additional mass to the spindle shaft, thus complicating its thermo-mechanical- dynamic behaviors. This paper presents thermal characteristics and dynamic characteristics of High speed motorized spindle were analyzed experimentally. Numerical analysis [4]was done and results were validated with experimental results.

#### Finite Element Analysis of High-Speed Motorized Spindle Based on ANSYS

This paper presents a method to investigate the characteristics of a high-speed motorized spindle system. The geometric quality of high-precision parts is highly dependent on the dynamic performance of the entire machining system, which is determined by the interrelated dynamics of machine tool mechanical structure and cutting process. This performance is of great importance in advanced, high-precision manufacturing processes. The

state-of-the-art in machine tool main spindle units is focus on motorized spindle units for high-speed and high performance cutting. This paper taking the high-speed milling motorized spindle of CX8075 produced by Anyang Xinsheng Machine Tool Co. Ltd. As an example, a finite element model of the high-speed motorized spindle is derived and presented. The model takes into account bearing support contact interface, which is established by spring-damper element COMBIN 14. Furthermore, the static analysis, modal analysis, harmonic response analysis and thermal analysis were done by means of ANSYS commercial software. The results show that the maximum rotating speed of the motorized spindle is far smaller than the natural resonance region speed, and the static stiffness of the spindle can meet the requirements of design. The static and dynamic characteristics of the motorized spindle accord with the requirements of high-speed machining. The thermal deformation of spindle is 6.56 $\mu\text{m}$ ; it is too small to affect the precision of the spindle. The results illustrate the rationality of the spindle structural design.

#### Dynamic characteristics analysis of high Speed motorized spindle

high speed machining (hsm) is a capable technology for drastically increasing productivity and reducing production costs. Development of high-speed spindle technology is strategically critical to the implementation of hsm. Compared to conventional spindles, motorized spindles are equipped with built-in motors for better power transmission and balancing to achieve high-speed operation. However, the built-in motor introduces a great amount of heat into the spindle system as well as additional mass to the spindle shaft, thus complicating its thermo-mechanical- dynamic behaviors. This paper presents a finite element analysis of dynamic characteristics of high speed motorized spindle using ansys. It includes the finite element selection, boundary condition, numerical formulae for finding input parameters to the ansys. This analysis is used to extract natural frequencies and mode shapes of the high speed motorized spindle including gyroscopic and centrifugal effects. The dynamic characteristics and modal characteristics of motorized spindles were analyzed experimentally. Numerical analysis was done and results were validated with experimental results

### 3. INTRODUCTION TO CAD

Computer-aided design (CAD), also known as computer-aided design and drafting (CADD), is the use of [computer](#) technology for the process of design and design-documentation. Computer Aided Drafting describes the process of drafting with a computer. CADD software, or environments, provide the user with input-tools for the purpose of streamlining design processes; drafting, documentation, and manufacturing processes. CADD output is often in the form of electronic files for print or machining operations. The development of CADD-based software is in direct correlation with the processes it seeks to economize; industry-based software (construction, manufacturing, etc.)

typically uses vector-based (linear) environments whereas graphic-based software utilizes raster-based (pixelated) environments[5].

4. INTRODUCTION TO PRO/ENGINEER  
 Pro/ENGINEER Wildfire is the standard in 3D product design, featuring industry-leading productivity tools that promote best practices in design while ensuring compliance with your industry and company standards. Integrated Pro/ENGINEER CAD/CAM/CAE solutions allow you to design faster than ever, while maximizing innovation and quality to ultimately create exceptional products. Customer requirements may change and time pressures may continue to mount, but your product design needs remain the same – regardless of your project’s scope, you need the powerful, easy-to-use, affordable solution that Pro/ENGINEER provides[6].

The main modules are  
 Assembly  
 Drawing  
 Sheet Metal

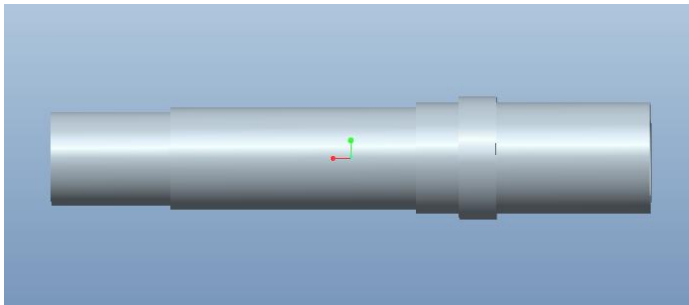


Fig:5 Part Design

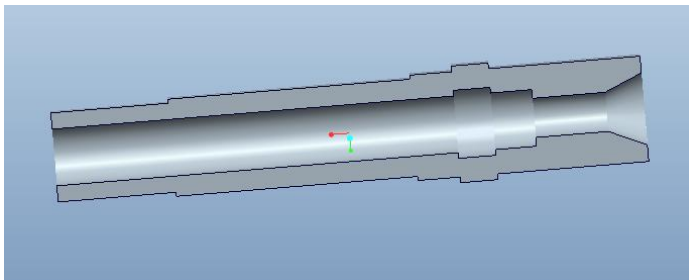


Fig:6 Cut section

#### 5. STATIC ANALYSIS OF HIGH SPEED MOTORIZED SPINDLE

Spindle speed 10000rpm, 13000rpm and 16000 rpm  
 Used materials aluminum alloy 6061, aluminum alloy 7075 and steel

Material properties of aluminum alloy 6061

Aluminum alloy 6061  
 Young’s modulus=68900Mpa  
 Poisson’s ratio=0.33  
 Density=0.000027kg/mm<sup>3</sup>

Material properties of aluminum alloy 7075

Aluminum 7075  
 Young’s modulus=71700Mpa

Poisson’s ratio=0.33  
 Density=0.000028kg/mm<sup>3</sup>  
 Material properties of steel  
 Steel for cutting tool  
 Young’s modulus=205000Mpa  
 Poisson’s ratio=0.3  
 Density=0.00000785kg/mm<sup>3</sup>  
 Carbon fiber material properties  
 Young’s modulus=70000Mpa  
 Poisson’s ratio=0.3  
 Density=0.00000160kg/mm<sup>3</sup>

Used software for this project work bench  
 Open work bench in Ansys 14.5  
 Select static structural>select geometry>import IGES model>OK

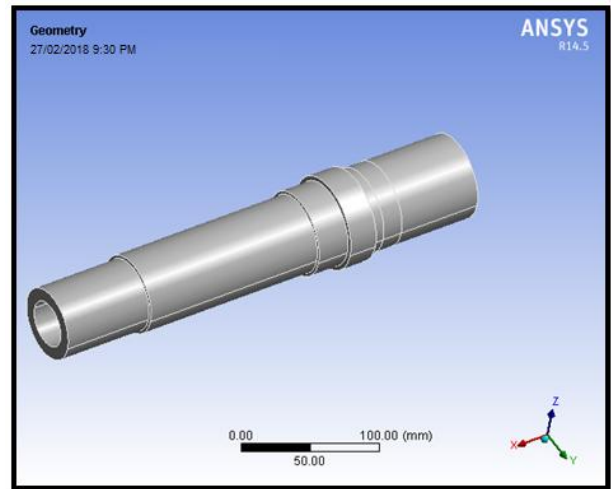
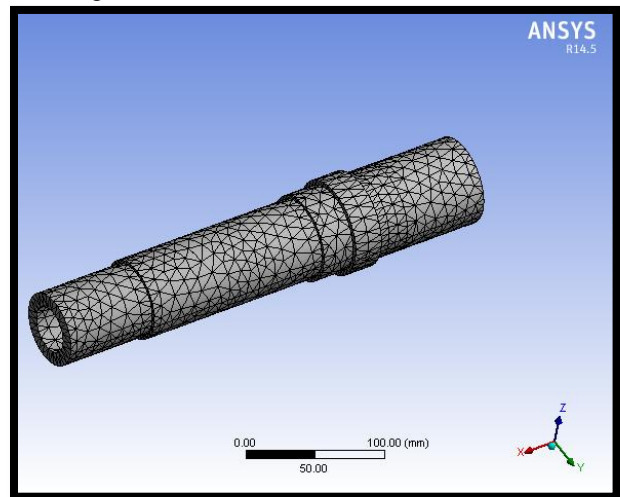


Fig:7 strain

Click on model>select EDIT  
 Select model >apply materials to all the objects (different materials also)  
 Mesh> generate mesh>ok



CASE: 1 Spindle Speed 10000rpm  
 Fig:8 Stress

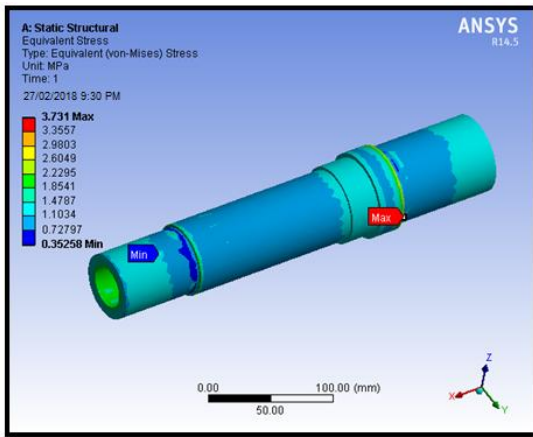


Fig:9 Strain

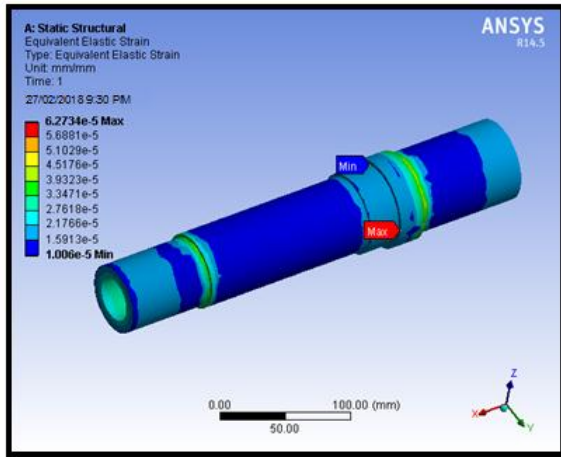


Fig:10 Material- Aluminum Alloy 6061 Deformation

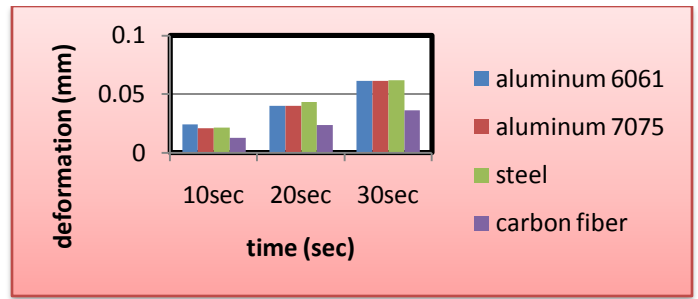


Fig:12 Stress plot

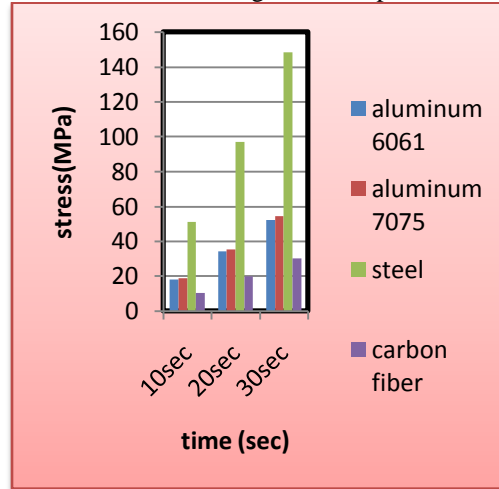


Fig:13 Strain plot

6. CONCLUSION

The geometric quality of high-precision parts is highly dependent on the dynamic performance of the entire machining system, which is determined by the interrelated dynamics of machine tool mechanical structure and cutting process. This performance is of great importance in advanced, high-precision manufacturing processes. The state-of-the-art in machine tool main spindle units is focus on motorized spindle units for high-speed and high performance cutting.

In this thesis, different materials are analyzed for spindle. Aluminum alloy 6061 and 7075 are replaced with steel. By replacing the steel with aluminum alloys, the weight of the spindle decreases. Structural and Dynamic analyses is done using Ansys software. Modal analysis also is done to determine the frequencies.

By observing the static and dynamic analysis, the stress increase by increasing spindle speed and stresses decreasing for carbon fiber than aluminum 7075, aluminum 6061 and steel.

By observing the modal analysis, the stress increase by increasing spindle speed and stresses decreasing for aluminum 7075 then aluminum 6061 and steel.

MATERIAL- STEEL DEFORMATION

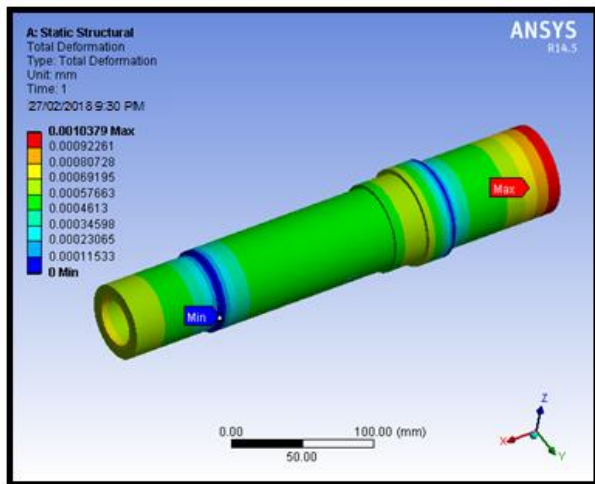


fig:11 STRES

Speed at 13000 rpm  
Deformation plot

By observing the modal analysis, the deformation increases and frequency increasing for carbon fiber than aluminum 7075, aluminum 6061 and steel.

So we conclude the suitable material for high speed motorized spindle is carbon fiber.

#### 7. REFERENCES

- 1.Design and analysis of high speed motorized spindle.
  - 2.Syath Abuthakeer.S 1 , Mohanram2.P.V 1 , Mohan Kumar G 3 1- Department of Mechanical Engineering, PSG College of Technology, Coimbatore 3- Park college of Engineering and Technology, Coimbatore
  - 3.Deping Liu\* Hang Zhang, Zheng Tao and Yufeng Su
  - 4.Finite Element Analysis of High-Speed Motorized Spindle Based on ANSYS
  - 5.Dynamic and thermal analysis of high speed motorized spindle.
  - 6.Dynamic characteristics analysis of high Speed motorized spindle
- 1,2. department of mechanical engineering, psg college of technology, coimbatore – 641 004, india 3 park college of engineering and technology, coimbatore, india

# DESIGN AND ANALYSIS OF STEAM GENERATORS

M. Shraavan Kumar  
Department of Mechanical Engg.  
Malla Reddy College of  
Engineering, Maisammaguda,  
Dhulapally, Kompally,  
Secunderabad, Telangana-500100,  
India  
Email: [sraavanmusham88@gmail.com](mailto:sraavanmusham88@gmail.com)

Mohd Tabraizuddin  
Department of Mechanical Engg.  
Malla Reddy College of  
Engineering Maisammaguda,  
Dhulapally, Kompally,  
Secunderabad, Telangana-500100,  
India  
Email: [tabraizuddin\\_8@hotmail.com](mailto:tabraizuddin_8@hotmail.com)

Dr. P. Velmurugan, Prof.  
Department of Mechanical Engg.  
Malla Reddy College of  
Engineering Maisammaguda,  
Dhulapally, Kompally,  
Secunderabad, Telangana-500100,  
India  
Email: [velmurugan\\_mech@mrce.in](mailto:velmurugan_mech@mrce.in)

**Abstract:-Steam boiler is a closed vessel in which water or other fluid is heated under pressure and the steam released out by the boiler is used for various heating applications. The main considerations in the design of a boiler for a particular application are Thermal design and analysis, Design for manufacture, physical size and cost. Thermal analysis to determine the temperature distribution, heat flux for both models steam boiler without baffles and steam boiler with baffles. Finding which model is best one. 3D modeled in parametric software CREO and analysis done in ANSYS.**

**Keywords:** *Finite element analysis, steam boiler, CREO, ANSYS.*

## 1. INTRODUCTION

Boilers are pressure vessels designed to heat water or produce steam, which can then be used to provide space heating and/or service water heating to a building. In most commercial building heating applications, the heating source in the boiler is a natural gas fired burner. Oil fired burners and electric resistance heaters can be used as well. Steam is preferred over hot water in some applications, including absorption cooling, kitchens, laundries, sterilizers, and steam driven equipment.

Boilers have several strengths that have made them a common feature of buildings. They have a long life, can achieve efficiencies up to 95% or greater, provide an effective method of heating a building, and in the case of steam systems, require little or no pumping energy show below fig. However, fuel costs can be considerable, regular maintenance is required, and if maintenance is delayed, repair can be costly[1].

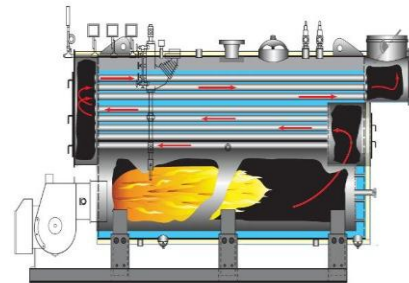


Fig:1How Boilers Work

### Fire tube Boiler

The burner mixes the fuel and oxygen together and, with the assistance of an ignition device, provides a platform for combustion. This combustion takes place in the combustion chamber, and the heat that it generates is transferred to the water through the heat exchanger. Controls regulate the ignition, burner firing rate, fuel supply, air supply, exhaust draft, water temperature, steam pressure, and boiler pressure.

## Types of Boilers

Boilers are classified into different types based on their working pressure and temperature, fuel type, draft method, size and capacity, and whether they condense the water vapor in the combustion gases. Boilers are also sometimes described by their key components, such as heat exchanger materials or tube design. These other characteristics are discussed in the following section on Key Components of Boilers.

Two primary types of boilers include Firetube and Watertube boilers. In a Firetube boiler, hot gases of combustion flow through a series of tubes surrounded by water. Alternatively, in a Watertube boiler show below fig,

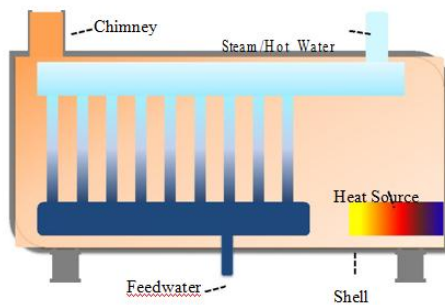


**Fig:2** Water tube boiler

Firetube boilers are more commonly available for low pressure steam or hot water applications, and are available in sizes ranging from 500,000 to 75,000,000 BTU input (5). Watertube boilers are primarily used in higher pressure steam applications and are used extensively for comfort heating applications. They typically range in size from 500,000 to more than 20,000,000 BTU input (5).

The combustion chamber, usually made of cast iron or steel, houses the burners and combustion process. Temperatures inside the combustion chamber can reach several hundred degrees very quickly.

Heat exchangers may be made from cast iron, steel tube bundles, or, in the case of some smaller boilers, copper or copper-clad steel. The exhaust stack or flue is the piping that conveys

the hot combustion gasses away from the boiler to the outside. Typically this piping is made of steel, but in the case of condensing boilers it needs to be constructed of stainless steel to handle the corrosive condensate. Another consideration is whether the exhaust stack will be under a positive or negative pressure. This can determine how the joints of the exhaust stack must be sealed.

## Best Practices for Efficient Operation Efficiency

The percentage of the heat energy contained in the fuel that is captured by the working fluid (e.g. water) in the boiler is defined as the combustion efficiency of the boiler. Combustion efficiencies of 80% or higher are usually possible for hot water boilers and low pressure steam boilers for commercial buildings. Complete combustion results when a hydrocarbon fuel such as natural gas or oil burns and produces only carbon dioxide, water and heat. If there is insufficient oxygen and/or poor mixing of fuel and oxygen, then incomplete combustion will occur resulting in other products of combustion including carbon monoxide and unburned fuel.

When incomplete combustion occurs, the chemical energy of the fuel is not completely released as heat and the combustion efficiency is reduced.

For high overall boiler efficiency, the heat released by combustion must be efficiently transferred into the working fluid. Any heat not transferred into the fluid will be lost through the boiler shell or the flue gas. The temperature of the flue gasses in the boiler stack is a good indicator of this heat transfer and thus the efficiency. There are practical limits to how low the stack temperature can be. The temperature will be higher than the working fluid in the boiler. In non-condensing boilers, it must be high enough so that the water vapor in the exhaust gas does not condense and bathe the heat transfer surface in the corrosive condensate. Condensing natural gas boilers are designed and built with materials designed to resist corrosion. As such, they may have exhaust temperatures

less than 150°F. Capturing the heat from the condensate can result in combustion efficiencies of greater than 90%

### Sample Maintenance Logs & Boiler Checklists

Boiler O&M best practices begin with maintaining regularly scheduled inspection logs and checklists to ensure proper equipment operation. Pressure, water temperature, and flue gas temperatures should be recorded daily, as they can serve as a baseline reference for system operation and troubleshooting problems. More detailed inspections and checks should be performed to document system performance, which can be very important since a gradual change in system operating conditions over time may not be readily apparent without the use of such documentation. The Federal Energy Management Program O&M Best Practices Guide to Achieving Operational Efficiency (5) contains example Daily, Weekly, and Monthly Maintenance and Inspection Logs that can be adapted to your facility. The following Maintenance Checklists have been assembled based on the recommended best practices found in this document as well.

### STEAM BOILER

Steam boilers heat water to produce steam, which is then used to generate energy or heat for other processes show below fig.



Fig:3 Steam boiler

Boilers are used to generate steam that then provides heat or power. Water is converted to steam in the boiler. This steam travels through the heating apparatus which can be any piece of equipment that requires steam for operation. The cooled steam is then condensed into water and returns to the boiler to start the cycle again.

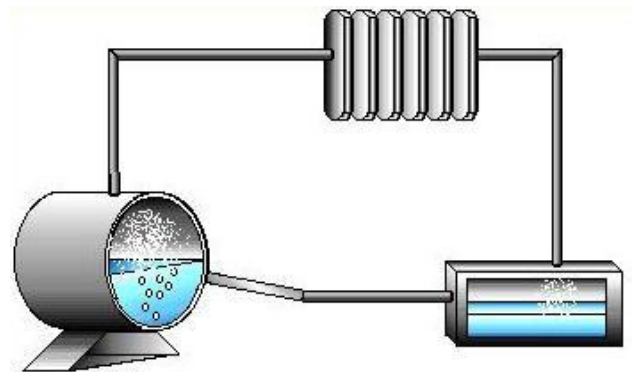


Fig:4 Boiler Diagram

### EQUIPMENT DESIGN

There are three main types of steam boilers: Fire tube, water tube, and cast iron.

In fire tube boilers, the combustion gases travel within the tubes to heat the surrounding water.

In water tube boilers, on the other hand, the water travels inside the tubes and the heat on the outside, as shown above fig.

Cast iron boilers are similar to water tube boilers, but the water is contained in cast iron sections instead of in tubes.

The diagram below shows the components of a fire tube boiler[2].

All steam boilers have four independent systems. The feed water system supplies water to the boiler, the fuel system transports the fuel, the draft system controls air flow for fuel combustion, and the steam system collects and controls the produced steam.

## 2.LITERATURE REVIEW

### Finite Element Analysis of Steam Boiler Used In Power Plants

A boiler or steam generator is a closed vessel used to generate steam by applying heat energy to water. During the process of generating steam, the steam boiler is subjected to huge thermal and structural loads[3]. To obtain efficient operation of the power plant, it is necessary to design a structure to withstand these thermal and structural loads. Using CAD and CAE software is the advanced methodology of designing these structures before constructing a prototype. In this project finite element analysis of the steam boiler was carried out to validate the design for actual working conditions. The main tasks involved in the project are performing the 3D modeling of the boiler and finite element analysis[4]. In this project, design optimization of the

Boiler is also done based on the results obtained from the thermal and structural analysis. NX CAD software is used for design and 3D modeling. ANSYS software is used for doing finite element analysis.

## 3. INTRODUCTION TO FINITE ELEMENT METHOD:

Finite Element Method (FEM) is also called as Finite Element Analysis (FEA). Finite Element Method is a basic analysis technique for

resolving and substituting complicated problems by simpler ones, obtaining approximate solutions Finite element method being a flexible tool is used in various industries to solve several practical engineering problems. In finite element method it is feasible to generate the relative results[5]

## Structural and Thermal Analysis of a Boiler Using Finite Element Analysis

Steam boiler is a closed vessel in which water or other fluid is heated under pressure and the steam released out by the boiler is used for various heating applications. The main considerations in the design of a boiler for a particular application are Thermal design and analysis, Design for manufacture, physical size and cost. In the present work a fire tube boiler is analyzed for static and Thermal loading. The geometric model of boiler is created in CATIA V5 software as per the drawing. This model is imported to HYPERMESH through IGES format and FEA model with converged mesh is developed using shell elements. To this FEA model various loading conditions like design pressure, thermal loads and operating conditions are applied. One of the supporting legs is arrested in all the directions and the other one is arrested only in X, Z-directions and all rotations. All these are created by using HYPERMESH and it is exported to ANSYS for solution to obtain the deflections, stresses. Those values are correlated with material allowable values as per the ASME Section VIII Division 2[6]

## 4. PROBLEM DESCRIPTION

The objective of this project is to make a 3D model of the steam boiler and study the CFD and thermal behavior of the steam boiler by performing the finite element analysis.3D modeling software (PRO-Engineer) was used for designing and analysis software (ANSYS) was used for CFD and thermal analysis.

**The methodology followed in the project is as follows:**

Create a 3D model of the steam Boiler assembly using parametric software pro-engineer.

Convert the surface model into Para solid file and import the model into ANSYS to do analysis.

Perform thermal analysis on the steam Boiler assembly for thermal loads.

Perform CFD analysis on the existing model of the surface steam boiler for Velocity inlet to find out the mass flow rate, heat transfer rate, pressure drop.

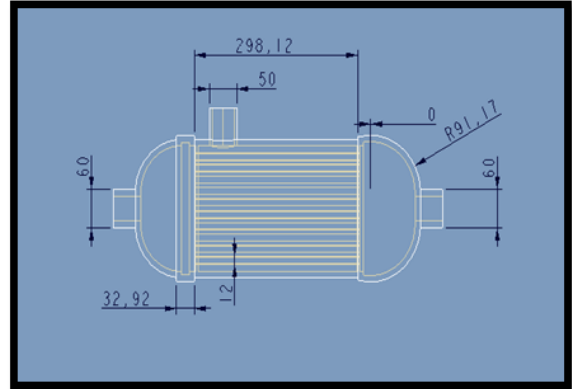


Fig:6 Steam boiler 2D model

## 5. MODELLING AND ANALYSIS MODELS OF STEAM BOILER USING CREO

The steam boiler is modeled using the given specifications and design formula from data book. The isometric view of steam boiler is shown in below figure. The steam boiler outer casing body profile is sketched in sketcher and then it is revolved up to  $360^{\circ}$  angle using revolve option and tubes are designed and assemble to in steam boiler using extrude option show below fig.

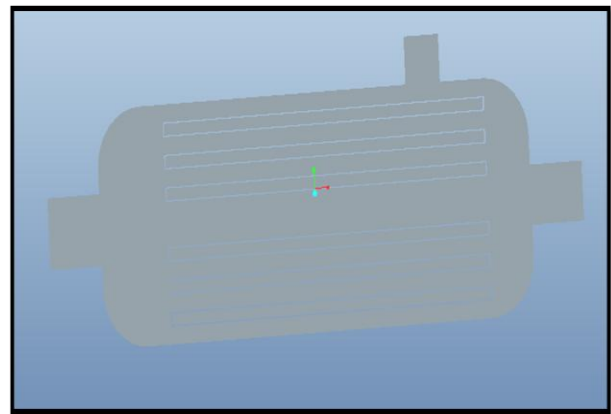


Fig:7 Steam boiler surface model

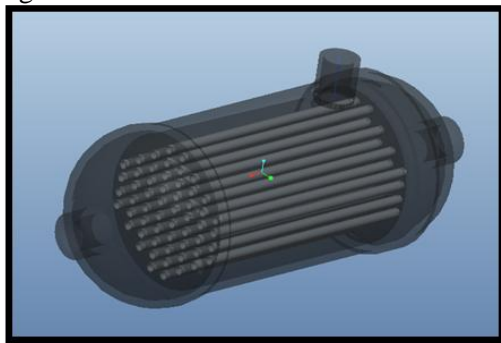


Fig:5 Steam boiler 3D model

## CONCLUSION

In this thesis the steam flow in steam boiler tubes is modeled using PRO-E design software. The thesis will focus on design and analysis with different velocities (25, 30, 35 & 40 m/s). design and analysis done for the steam boiler by steel, stainless steel & brass at different heat transfer coefficient values. These values are taken from analysis at different velocities. By observing the analysis the pressure drop, velocity, heat transfer coefficient, mass flow rate & heat transfer rate increases by increasing the inlet velocities. By observing the thermal analysis, the taken different heat transfer coefficient values are from analysis. Heat flux value is more for brass material than steel & stainless steel. So we can

conclude the brass material is better for steam boiler.

## REFERENCE

- 1.Design and analysis of the prototype of boiler for steam pressure control 1Akanksha Bhoursae, 2 Jalpa Shah, 3Nishith Bhatt Institute of Technology, Nirma University, SG highway, Ahmedabad382481,India 3Essar steels limited,Hazira,Surat-394270,India
2. Lou Roussinos, P. E., “Boiler Design and Efficiency”[online], Available: <http://www.forestprod.org/drying06williamson.pdf>, Accessed: September 1, 2010.
3. Analysis of New Boiler Technologies Dr Mike Inkson
4. 5.A Study Analysis and Performance of High Pressure Boilers With its Accessories J. Suresh babu<sup>1</sup>,R.Latha<sup>2</sup> ,B.Praveen<sup>3</sup>,V.Anil kumar<sup>4</sup>,R Rama kumar<sup>5</sup>,s.peerulla<sup>6</sup> 1 Assistant Professor in MED, K.S.R.M College of engineering, AP, India 2 3 4 5 6 Student, mechanical department, K.S.R.M College of engineering, AP, India
- 5.Bathe, K. J., Finite Element Procedures in Engineering Analysis, Prentice Hall, 1982
- 6.Structural and thermal analysis of a boiler using finite element Analysis

# Domestic Oil Extraction Machine

(Anand.M<sup>1</sup>, Manimaran R<sup>2</sup>, Praveen Kumar.M<sup>3</sup>, Sujith Bhrathi.S<sup>4</sup>)

<sup>1</sup>Assitant Professor, Department of Mechatronics Engineering,SNS College of Technology, Coimbatore, Tamilnadu-641035

<sup>2,3,4</sup>UG-Student, Department of Mechatronics Engineering,SNS college of Technology, Coimbatore, Tamilnadu-641035

## Abstract:

For years and times, we have been using the Edible oil from various vegetable seeds like coconut, groundnut, mustard and various other seeds. In modern days the oils which we are using are mostly got from the petroleum extract called as paraffin. It is being very unsafe using all extracted from petroleum products which leads to various health problems like cancer, heart problems, paralysis and other problems associated with other health issues. In olden days our ancestors have used the oil extracted from the traditional oil extraction machines. The process of extracting oil from seeds using traditional oil extraction machine requires a large number of seeds to process the oil. It is good being used oil which is been extracted by traditional oil extraction machine and also it gives an assurance that it is been produced only using oil seeds not by any other Petroleum products. The cooking tradition of each and every home mainly depends upon the edible oils without the oil no cooking process could be carried down and also it is not also affordable for every home to have seeds in large numbers to crush seeds that could not be affordable to spend money for oilseeds in a middle-class family where 1kg of oilseeds costs around Rs 100 and daily salary of an individual is Rs 400 per day. But the usage of edible is a mandatory in Indian Cooking style and a person to live.

## Keywords:

*Oil expeller, Screw type method, Domestic purpose, Good for health.*

## Introduction:

For years and times, we have been using the Edible oil from various vegetable seeds like

coconut, groundnut, mustard and various other seeds. In modern days the oils which we are using are mostly got from the petroleum extract called as paraffin. It is being very unsafe using all extracted from petroleum products which leads to various health problems like cancer, heart problems, paralysis and other problems associated with other health issues. In olden days our ancestors have used the oil extracted from the traditional oil extraction machines. The process of extracting oil from seeds using traditional oil extraction machine requires a large number of seeds to process the oil. It is good being used oil which is been extracted by traditional oil extraction machine and also it gives an assurance that it is been produced only using oil seeds not by any other Petroleum products.

## Method:

This project deals with a different method of oil extraction by using twin screw expeller mechanically. Mechanical pressing is the most popular method of oil separation from vegetable oilseeds in the world (Mrema& McNulty, 1985). In India, nearly 90% of the total 24 million tonnes of produced oilseeds are crushed using this method. The main reason for popularity of mechanical oil expellers in India as well as in other developing countries is that these equipments are simple and sturdy in construction, can easily be maintained and operated by semi-skilled supervisors, can be adapted quickly for processing of different kinds of oilseeds, and the oil expulsion process is continuous with product obtained within a few minutes of start of the processing operation.

## System Analysis:

### **Existing System:**

The current existing wooden oil extraction machine and other industrial oil expeller machine cost very high and only can be used in large scale operation with a capacity of 10-20kg only. Also, the cost of machine is too expensive so that it can be bought only for professional use and it is large in size also so that it occupies large place. This type of machine is widely used all over places only in industries this wooden oil extraction machine uses 3 phase electricity power supply so that it needs industrial power supply. It has a large size drum so that it is hard to rotate it uses a 35HP gear box at time of carelessness in operating the machine it leads to breakage of bones by misplacing the hand inside the drum. It also comes with wooden drum and Crushing roller which had a drawback makes the oil get expired soon without proper cleaning. The wood has a drawback of breaking down at time of heavy load.

### **Disadvantages in The Existing System:**

- 1.The current existing wooden oil extraction machine and other industrial oil expeller machine cost very high
- 2.The system can only be used in large scale operation with a capacity of 10-20kg.

### **Proposed System:**

This project deals with a different method of oil extraction by using twin screw expeller mechanically. Mechanical pressing is the most popular method of oil separation from vegetable oilseeds in the world (Mrema& McNulty, 1985). In India, nearly 90% of the total 24 million tonnes of produced oilseeds are crushed using this method. The main reason for popularity of mechanical oil expellers in India as well as in other developing countries is that these equipments are simple and sturdy in construction, can easily be maintained and operated by semi-skilled supervisors, can be adapted quickly for processing of different kinds of oilseeds, and the oil expulsion process is continuous with product obtained within a few minutes of start of the processing operation

Extraction efficiency was better with Lot II. Tests also involved preheating the sunflower seeds of Lot II to 50, 60, and 75 °C before extraction. There was a large improvement in expeller capacity and oil output compared to seeds processed at room temperature. One source of renewable energy currently being investigated around the world for use in internal combustion engines is vegetable oil. Oil-type sunflower and the oil obtained from this seed has been shown to be a possible alternative to diesel fuel. If sunflower oil does become a practical alternative energy source, the farmer may not only grow his own fuel source, but also extract the oil from the sunflower seed. Figure 1 shows the steps involved in a small processing system.

Most of the hulls are removed in a large commercial operation because they speed machine wear, contain little oil, and the processed meal with hulls is high in fiber. Extraction efficiency was better with Lot II sunflower seeds than with Lot I sunflower seeds at room temperature (22 °C). Overall expeller capacity and oil output were 40% greater with Lot I than with Lot II sunflower seeds. Preheating the sunflower seeds had a dramatic impact on expeller performance.

This system totally helps all individuals in to this machine in every home. Every machine will be provided at a cheap cost affordable for all peoples. The minimum quantity of seeds required in this machine is 250 Grams to 500 Grams. So that all peoples are affordable in crushing oil and using it for daily needs. Our innovation is going create a revolution the edible oil industry. Our machine will be placed in all homes like as mixture grinder and other home appliances to extract oil from seeds.

### **Advantages of proposed system:**

- 1.The proposed system uses domestic motors and other small household size components
- 2.This intern reduces the size and cost of the product and capacity could be reduce to 1-2 kg.

### **Project Description:**

In olden days our ancestors have used the oil extracted from the traditional oil extraction machines. The process of extracting oil from seeds using traditional oil extraction machine requires a large number of seeds to process the oil. It is good being used oil which is been extracted by traditional oil extraction machine and also it gives an assurance that it is been produced only using oil seeds not by any other Petroleum products.

Speaking in terms of efficiency Expeller processing cannot remove every last trace of liquid (usually oil) from the raw material. A significant amount remains trapped inside of the cake left over after pressing. In most small-scale rural situations this is of little or no importance, as the cake that remains after the oil has been removed finds uses in local dishes, in the manufacture of secondary products, or for animal feed. Some raw materials, however, do not release oil by simple expelling, the most notable being rice bran. In order to remove oil from commodities that do not respond to expelling or to extract the final traces of oil after expelling, it is necessary to use solvent extraction.

The cooking tradition of each and every home mainly depends upon the edible oils without the oil no cooking process could be carried down and also it is not also affordable for every home to have seeds in large numbers to crush seeds that could not be affordable to spend money for oilseeds in a middle-class family where 1kg of oilseeds costs around Rs 100 and daily salary of an individual is Rs 400 per day. But the usage of edible is a mandatory in Indian Cooking style and a person to live.

### **Conclusion and Result:**

Thus, the proposed system on “Automated Domestic Oil Expeller” is successfully completed its phase I with a complete literature survey. Also, in accordance with the survey made and with the idea on the proposed system the design and the component selection of the product is done and verified successfully.

By adopting this project into use delay will be reduced and process will be speed up. The price that is invested can be reduced.

### **REFERENCES**

- N. Prakash Babu, P. Pandikumar, S., Anti-inflammatory activity of *Albizia lebbek* Benth., an ethnomedicinal plant, in acute and chronic animal models of inflammation: 9 March 2009 *Journal of ethnopharmacology*, 2009 – Elsevier.
- Isaac Bamgboye and A.O.D. Adejumo., Development of a Sunflower Oil Expeller, September, 2007, *Agricultural Engineering International: the CIGR Journal*.
- Soto, R. Chamy, M.E. Zuñiga \* Escuela de., Enzymatic hydrolysis and pressing conditions effect on borage oil extraction by cold pressing., January 2006; *Journal of ethnopharmacology*, 2006 - Elsevier
- Hasan h. ALI dr. Roger fales., Inlet metering pump analysis and experimental evaluation with application for flow control., 12 July 2018, *Renewable Energy*, 2018 – Elsevier.
- Chokchai mueanmas, ruamporn L., Extraction and esterification of waste coffee grounds oil as non-edible feedstock for biodiesel production., 7 september 2018 *Renewable and Sustainable Energy Reviews*, 2009 – Elsevier.
- Lahai koroma, T.B.R. Yormah, L.M. Kamara, G.M.T. Robert., Extraction, utilization, characterization and confirmation of the structure of gorli oil from the dry seeds of the traditional medicinal plant *caloncoba echinata* in sierra leone, Volume 2 issue 8, august 2018, *Journal of ethnopharmacology*, 2009 – Elsevier.
- Adeeko, K. A. and Ajibola, O.O. (1980). “Processing Factors Affecting Yield and Quality of Mechanically Expressed Groundnut Oil”. *Journal of British Society of*

Research in Agricultural Engineering.  
Vol.45. No. 1. pp31

- Ajibola, O.O., Eniyemo, S.E, Fasina, O.O and Adeeko, K.A. (1990). Mechanical Expression of Oil from Melon Seeds. Journal of British Society of Research in Agricultural Engineering. Vol.45. No. 1. pp 45.
- Akinoso, R., Igbeka, J.C., Olayanju, T. and Bankole, L. (2006). “Modeling of Oil Expression from Palm Kernel ( *Elaeis guineensis* Jacq.)”. Agricultural Engineering International: the CIGR Ejournal. Manuscript FP 05 016. Vol. VIII. October, 2006.
- Canˆeque, V., Velasco, S., Sancha, C., Manzaneres, O., & Souza, O. (1998). Effect of moisture and temperature on the degradability of fiber and on nitrogen fractions in barley straw treated with urea. Animal Feed Science Technology, 74, 241–258.
- Berti, M., Wilckens, W., Fischer, S., & Araos, R. (2002). Borage. A new crop for Southern Chile. In J. Janick & A. Whipkey (Eds.), Trends in new crops and new uses (pp. 501–505). Alexandria: ASHS Press.
- Bocevaska, M., Karlovic, D., Turkulov, J., & Pericin, D. (1993). Quality of corn germ oil obtained by aqueous enzymatic extraction. Journal of American Oils Chemists’ Society, 70, 1273–1277.

# Basic Design of An Anthropomorphic Robotic Arm

Pradeep.S<sup>1</sup>, Hari shankar.S.P<sup>2</sup>, Nandha Kumar.M<sup>3</sup>, Rajeshwaran.T<sup>4</sup>, Karthik.V<sup>5</sup>

<sup>1</sup>Assistant professor, Department of Mechatronics Engineering, SNS College of Technology, Coimbatore

<sup>2,3,4,5</sup>UG Student, Department of Mechatronics Engineering, SNS College of Technology, Coimbatore

**Abstract**—The project is concerned with the design and fabrication of writing bot using the Mechatronics system. As per today's status robotics is a key technology in the modern world and it is an emerging technology in the modern world. It is a bot which automatically writes regarding the voice recognized from the user. The physically challenged people suffer a lot to write the exam, in all the possible way the world improves the technology, it is not useful for the physically challenged people. So that this would help the physically challenged people with an anthropomorphic writing bot. The main components of the project are Arduino, servo motor, voice recognition module, and motor drive. Three micro servo motors are employed to manipulate the motion of the end effector. Two servo motors are used to control the movement of the base and joints of the arm. Thus, the voice recognition module is used to recognize the voice. When the user's voice is recognized by the module it sends a command to the Arduino, and then the Arduino control the servo motor according to the voice the bot will write. This task can be used socially like in the field of industries, court and teaching and it can be as well applied for local purposes, commercial enterprise. The benefit of this writing bot gives more accuracy, less cost, and negligible risks to the people and has a diverse scope in future battlefields.

**Keywords**—*Arduino, Servo motor, Voice module, Robotic arm*

## I. INTRODUCTION

In this chapter, technologies in developing a writing bot based on the Mechatronics system are discussed. One of the most functional system of automation is robotics. This robotic system combined with Mechatronics engineering, mechanical engineering, electrical engineering, and computer engineering to form a complete robotic system. The primary feature of this project is speech recognition i.e., Making the system to understand and interpret human voices. Speech recognition is a technology where the system understands the words (irrespective of the meaning) given through speeches. Speech is an ideal method for robotic control and communication. The speech recognition functions individually and independently from the robot's Processor [Central Processing Unit (CPU)]. This has a positive advantage, because it does not occupy the robot's CPU processing power for word recognition. The CPU must merely poll the speech circuit recognition lines occasionally to check if the command has been sent to the robot.

Robotics is an evolving technology where there are many approaches in building a robot and no one can be certain which method or technology may be used in the far future. Robotics is a converging science which employs the

advancement of mechanical engineering, material science, sensor fabrication, manufacturing techniques, and advanced algorithms. The study of robotics will expose an amateur or a professional to hundreds of different fields of study.

Writing bots are robots that implement the writing character of human hand with the help of suitable controlling devices. In the early 1920s, machine recognition came into existence. The first machine to recognize speech to any significant degree was commercially named as Radio Rex. As the developments were made in the field of machine recognition and robotics, many methods are now available to create a writing bot. IoT being one of the most used tools in today's era. Many writing bot are equipped for making it easy accessible by the users.[1]

The writing bots are created with the prime motto of helping the physically challenged people. The physically challenged people face much problems in writing, especially at the time of examinations. The writing robots help the physically challenged people in a much efficient way than the scribe writers. Moreover, the problem for the need of scribe writers during the exam times can be overcome by using the voice-controlled writing robots.

The writing bots provide a good and satisfactory writing quality. Different writing bots have different writing quality and this writing quality depends on the design, components and the material used for the development of the writing bot.

The word Anthropomorphic is derived from two Greek words Anthropos meaning human and morpheme meaning form. In other words, Anthropomorphic refers to the attribution of human traits, emotions or intention to non-human entities. Since writing is a characteristic subjected only to humans, the writing bots which implement this human character may be called as anthropomorphic writing bots Anthropomorphic Robot arms are programmable manipulator with similar functions of the human arm. Several kinds of technology prostheses are available for basic function of a human arm. The aim of the project is to develop a robotic arm which helps the physically challenged person to write with the help of voice commands.

## II. OBJECTIVE

- To design and develop a voice-controlled Anthropomorphic Robotic Arm to write exams for the physically challenged.
- To design a robot to achieve a satisfactory writing quality of characters with simple structures

### A. Problem statement

The physically challenged people are unable to write their exam without any human aid.

Lack of Volunteers during the exam times, so that the physically challenged students are unable to focus on exam preparation and also the timetable and the exam venues are decided so late. Older writers are barred because they may know the subject matter better than the candidate and this could result in an unfair advantage. New Writers are mostly busy preparing for their own exams or having personal works. The entire process of documentation is tedious.

## III. LITERATURE REVIEW

In this paper, a detailed study of existing methodologies has been gained, based on both kinds of literature.

[2]M. A. Anusuyadiscussed a review of the speech recognition by a machine. The author says that even when there are many developments in the field of robotics, the accuracy of the automatic speech recognition still remains a challenge for the developers". Her paper stresses the importance of the definition of various types of speech classes, speech representation, feature extraction techniques, speech classifiers, database, and performance evaluation. The paper deals with the basic model of speech recognition, types of speech recognition, application of speech recognition and problems faced during the ASR design. This paper also suggests the approaches to speech recognition like Acoustic phonetic approach, Pattern recognition approach, approach, and Artificial Intelligence approach. The author has also given a description of Dynamic Time Wrapping, Vector Quantization, feature extraction, and classifiers. The paper discusses the major themes and advances made in the past 60 years of research, so as to provide a technological perspective[3]. Some of the key methods in the development of speech recognition like Hidden Markov Model, DARPA program, Noisy speech recognition etc., were given in a detailed manner.

[4]M. Balaganesh discussed the Robotic arms showing writing skills by speech recognition. The author has given a clear description of the speech recognition software and hardware part. The software part consists of the speech signal, Mel's cepstral coefficient, Dynamic time wrapping and recognition of isolated words. Speech signals refer to the speech sounds produced due to the airflow from the lungs. Mel's coefficient and dynamic time wrapping are the

parameters used for speech recognition. The hardware part of the speech recognition consists of MAX 232 interface, PIC 16F628A, and stepper motors. The MAX 232 is an integrated circuit that converts signals from an RS-232 serial port to signals suitable for use in TTL compatible digital logic circuits. The PIC 16F628A is an 18-Pin Flash-based member of the Versatile PIC16CXX family. The author has also given the algorithm for the working of the robotic arm by speech recognition. The microphone is fitted to the robotic arm. The input is given via the microphone which converts the voice into an electrical signal. A PC sound cord transfers this signal to a MATLAB TOOL BOX where the signal acquisition process takes place. The microcontroller unit converts the text signal from the MATLAB toolbox into mechanical action.

### *Robotic Motion and Control:*

[5]Oussama Khatib has discussed the motion and force control of robotic manipulators. This paper deals with the control of manipulator motions and active forces based on the operational space formulation. The fundamentals of operational space formulation have been discussed by the author. The end effector motion control, active force control and force control compensator have been given in a detailed manner along with the necessary equations and diagrams. The behavior of the end effector during any impact has also been discussed by the author. The author has highlighted the COSMOS system along with its architecture. The results of using the COSMOS system along with the other parameters have been given briefly by the author. The author has also added the graph of Contact Force Time Response using Force Sensing Fingers and the graph of Contact Force Time Response using Force Sensing Wrist. The author has concluded that a higher level of performance can only be achieved by a new design of mechanisms based on the requirements of manipulator force control.

[6]GianlucaMasserahas discussed Developing a Reaching Behavior in a simulated Anthropomorphic Robotic Arm Through an Evolutionary Technique. The paper deals with an evolutionary technique for developing a neural network-based controller for an anthropomorphic robotic arm with 4 DOF able to exhibit a reaching behavior. The author has given a detailed explanation about the arms reach. The redundancy potentially allows anthropomorphic arms to reach a target point by circumventing obstacles or by overcoming problems due to the limits of the DOF. The author has also compared the robotic arm with the human hand. The sensors used in the robotic arm has also been discussed. The previous attempts of Bianco and Nolfi (2004) to use evolutionary techniques to develop the controller for a robotic arm has also been discussed. The experimental setup and the angles of simulation of the robotic arm have also been given. The author has also highlighted the importance of the neural controller in the robotic arm. The

evolutionary algorithm of the robotic arm has also been given in the paper. The results showing the Performance on reaching a fixed target, Performance on reaching a random positioned target along with the suitable diagram has been given by the author.

[7]Thorsten Stein has discussed the Guidelines for the motion control of Humanoid robots: Analysis and Modelling of Human Movements. This paper deals with the analysis of trajectories of limbs and develops guidelines for motion planning based on task-specific characteristics. Also, a new algorithm is provided to compose these elementary models into large models. The author has given information about complex functionalities like humanoid shape, multimodality, ability to learn etc, For the analysis of human movements, the author suggests the concept of motion patterns. The process of data acquisition and processing of human motion data has also been discussed in the paper. The intro and inter-individual variations of the humans along with the graph has been given by the author. The author has also suggested ways for modeling the characteristics of human movements along with the necessary equations. Classification of phases in human motion and motion control of the humanoid robot has also been discussed by the author.

[8]VeljkoPotkonjak has discussed the Redundancy Problem in Writing: From Human to Anthropomorphic Robot Arm. This paper deals with the analysis of the motion of a redundant anthropomorphic arm during the writing. The Distributed Positioning allows a unique solution of the inverse kinematics of redundant mechanisms such as human arm and anthropomorphic robot arm. The paper shows the reasons why the new approach is adopted from the previous results. The author has shown that a strict relationship exists between the form of trajectory and the (tangential) velocity at which it is executed in handwriting. The author has also shown the Seven-DOF's arm in writing task: three for shoulder, two for the elbow, and two for the wrist. The works of previous authors have also been discussed. The author has shown the different angles and working of different joints of the human arm while writing along with the related diagrams and graphs. The model of the arm-hand complex in writing has been discussed briefly by the author along with the required graphs and calculations. The concept of inclination and legibility, which is an important factor to be considered, has been given in a detailed manner by the author.

[9]Tsuneo Yoshikawa has discussed the Analysis and Control of Robot Manipulators with redundancy. This paper deals with the quantitative measurement of manipulability which is applicable to both redundant and nonredundant manipulators. The Control problems of redundant manipulators have also been discussed in this paper. The measure of manipulability has been explained in a detailed manner by the author with the help of calculations and

diagrams. Other topics like Subtasks with Order of Priority, Utilization of Redundancy for Optimizing Given Performance Criterion, Singularity Avoidance and Obstacle Avoidance have also been discussed by the author.

*Character Recognition:*

[10]AdlinaTaufikSyamlan has discussed the Character Recognition for Writing Robot Control Using ANFIS. Image processing, character recognition, path planning, and theta deduction are dealt with in this paper. Letters are restricted to uppercase and in a form of an image. The image is converted into binary, which then letters are separated to form an image matrix. Image matrix will serve as training data for the neural network. Performances of a neural network are evaluated using test set prepared, to determine the scope of font recognizable using the neural network. The author has discussed the problems like Effect of size in the neural network, Effect of fonts in the neural network, misclassification, and Feature Boundaries in this paper[11].

[12]Salman Yussof has discussed the Algorithm for Robot Writing using Character Segmentation. The paper deals with a flexible algorithm that can allow a robot to write. This algorithm is based on character segmentation, where the main idea is to store character information as segments and the segment information can then be used by the robot to write. The author has developed a sample application using the proposed algorithm to allow a Mitsubishi RV-2AJ robotic arm to write English characters and numbers. The concepts of character segmentation and character storage has been explained in a detailed manner in this paper. The examples of the character table, segment table, and point table have also been added. The implementation of the algorithm along with the block diagram has also been highlighted.

[13]G. Nagydiscussed the Self-Corrective Character Recognition System. The paper deals with a simple statistical categorizer are used to improve recognition performance on a homogeneous data set. This experimental study of the effect of the various parameters in the algorithm is based on ~30 000 characters from fourteen different font styles. The experimental setup and the algorithm of the self-corrective character recognition system have been discussed briefly. The related graphs were very much helpful in analyzing the errors. The tabular column of different machines provided further knowledge on character recognition.

[14]S.Batmavady has discussed about the Segmentation, Recognition and Synthesis of Tamil characters for Robotic Writing. This paper deals with the two important phases namely, recognition of characters and writing of characters. Recognition is done via polynomial fitting. Each character is probed in a graphical sense and equations are obtained.

Basic figures like cycloid, circle, spiral, ellipse, etc are studied and their features are utilised in developing equations. The concepts of character recognition like character recognition, feature extraction and character identification has been discussed clearly by the author. For writing, parametric equations and synthesis of characters has been explained clearly in detail along with the related diagrams. The author has concluded that in this robotic writing, pure equations are employed, it is easy to change the size of the characters and change the direction of characters with minor modifications in the equations.

[15]Herbert Gish discussed about the Segregation of speakers for speech recognition and speaker identification. This paper deals with the method for segregating speech from speakers engaged in dialogs. The method employs a distance measure between speech segments used in conjunction with a clustering algorithm, to perform the segregation. The paper gives detailed information about the distance between speech utterances and theoretical distribution of the distances in a detailed manner along with the related equations. The result of the papers deals with the distributions as a function of duration. The method of segregating speech application in clustering has also been discussed in this paper.

#### *Arduino Recognition:*

[16]Dr. AbdellatifBabachas discussed the Robot Arms Control with Arduino. The robot arm in this paper has the ability to move in 4 axis directions with 5 servo motors. The robot control is provided by connecting to the Android application via Bluetooth module connected to Arduino Nano microcontroller. Researches have been done by the author and implemented in order to have knowledge about mechanics and software during the operations carried out by the robot arm which is designed to fulfill the tasks determined in accordance with predetermined commands. Arduino Nano microcontroller written in Java language is programmed and servo motor control is provided. The servomotor is preferred in order to be able to perform these operations properly since the motor to be selected must operate precisely and must be at high torque. Thus, it is possible to perform the desired operations by means of the elements located on the Arduino without any circuit construction other than the circuit where the servo motor inputs are located.

[17]KeerthiPremkumar discussed the Smart Phone-Based Robotic Arm Control Using Raspberry Pi, Android, and Wi-Fi. This paper proposes a method for controlling a Robotic arm using an application build in the Android platform. The Android phone and raspberry pi board is connected through Wi-Fi. The android application is the command center of the robotic arm. The program is written in the Python language

in the raspberry board. The different data will control the arm rotation. The hardware and software components of the smartphone-based robotic arm along with its architecture has been given in detail by the author. The driver circuit architecture (Raspberry PIE) has been given by the author. The author has concluded that in smartphone technique, the delay and server problems are reduced as the Wi-Fi is used which is the fastest usage of internet.

#### *Methodology:*

[18]Boren Li has discussed the Human-like Robotic Handwriting and Drawing. The paper deals with the three strategies of trajectory planning are considered: the basic stroke method, the Bezier Curve method and the non-gradient numerical optimization method. A nonlinear three-link three-dimensional arm, similar to the human arm, tracks the planned trajectories. The feasibility of these methods is demonstrated by simulation. The basic stroke method and the Bezier curve method have been clearly discussed in this paper along with the diagrams and calculations.

[19]Katrin Franke has discussed the Ink-Deposition Model: The relation of writing and ink deposition processes. The paper describes the studies on the influence of physical and biomechanical processes on the ink trace and aims at providing a solid foundation for enhanced signature analysis procedures. Since the robot is able to take up different writing instruments like a pencil, ball pointer fine line pen, the type of inking pen was also varied in the experiments. The methodology includes the synthesis of ink traces and analysis of ink deposition. The related calculations and the graphs were also given in this paper. The author concluded that the better understanding and analytical modeling of the interaction processes of writing movements, physical ink properties, and ink deposition will allow for the design of appropriate algorithms.

[20]Marius-Florin Crainicdiscusses the Secure handwriting using a robot arm for educational purpose. The paper presents a different approach to facilitate and secure the writing of certificates or traditional grade books. This system uses a robot arm, RV-2AJ, which has a pen attached. After the calibration, the robotic arm can write even if the writing surface is on an inclined plane, or the paper is rotated. This system is more secure than the one that uses the ink printer because the movement of the robot arm to reproduce the font on the paper is unique. Another secure element is the embossing stamp. The embossing stamp is created by changing the pen with a needle. The needle creates small closed holes using a pattern in which the information used for writing is encrypted. The author has highlighted the mathematical concepts for the robot calibration with suitable equations. The author has also given the MATLAB algorithm for the robotic arm. The

paper has presented another type of handwriting using a robotic arm. In order to write the pen must gently touch the paper. For this thing, a calibration was made. So by reading 3 points from the writing plane the equation of the plane can be determined and the Z-axis value calculated in order to compensate the writing plane tilt.

[21]Alejandro Acero has discussed about the Environmental Robustness In Automatic Speech Recognition. This paper deals with the initial efforts to make SPHINX, the CMU spectral estimates across frequencies. The author proposes novel methods based on additive corrections in the cepstral domain. In the first algorithm, the additive correction depends on the instantaneous SNR of the signal. In the second technique, EM techniques are used to best match the cepstral vectors of the input utterances to the ensemble of based on additive corrections in the cepstral domain. The author has given detailed information about the Model of the Environment, SNR-Dependent Cepstral Normalization and Codeword-Dependent Cepstral Normalization. The Codeword-Dependent Cepstral Normalization has been further discussed further which includes MMSE Estimator of the Cepstral Vector, ML Estimation of Noise and Spectral Tilt and Implementation. The related graphs has also been given which was very useful.

*Design:*

[22]Ashraf Elfasakhany has discussed the Design and Development of a Competitive Low-Cost Robot Arm with Four Degrees of Freedom. The paper deals with the design, development, and implementation of a competitive robot arm with enhanced control and stumpy cost. The robot arm is equipped with several servo motors which do links between arms and perform arm movements. The servo motors include encoder so that no controller was implemented. To control the robot we used LabVIEW, which performs inverse kinematic calculations and communicates the proper angles serially to a microcontroller that drives the servo motors with the capability of modifying the position, speed, and acceleration. The robotic design along with the inverse kinematics have been briefed by the author with suitable diagrams and calculations. The selection of components like material to be used, servo motors, end effector selection etc., were also discussed in the paper.

[23]Jamshed Iqbal discussed the Modeling and Analysis of a 6 DOF Robotic Arm Manipulator. This paper deals with the kinematic models a 6 DOF robotic arm and analyzes its workspace. the end-effector of the robotic arm can point to the desired coordinates within the precision of  $\pm 0.5\text{cm}$ . The approach presented in this work can also be applied to solve the kinematics problem of other similar kinds of robot

manipulators. The kinematic model, which includes forward, and inverse kinematics has been discussed in a detailed manner by the author along the related calculations. The workspace analysis has also been discussed briefly

*Existing system*

The Existing system is a speech recognizing system. Speech recognition is the process of capturing spoken words using a microphone or telephone and converting them into a digitally stored set of words. The quality of a speech recognizing the system is assessed according to two factors: Its accuracy (Error rate in converting spoken words to digital data) and speed (How well the software can keep up with the human speaker. The Existing methodology is shown in Fig 1

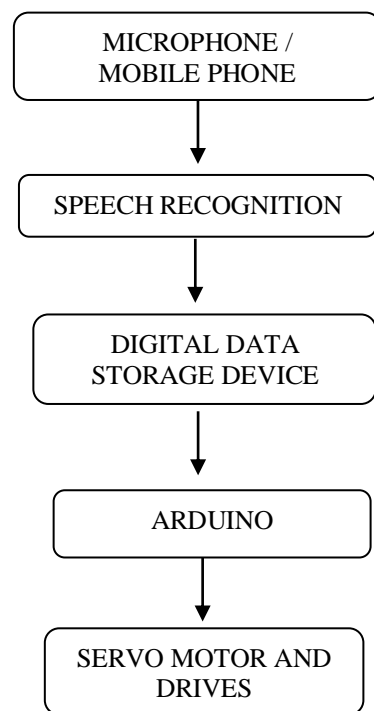


Figure 1

A. *Disadvantage of existing system:*

1. Even the best speech recognition sound in the room (Ex. Television or Radio), the no. of error will be increased.
2. Speech recognition works best if the microphone is close to the user (Ex. In a phone or if the user is wearing a microphone). More distant microphones (Ex. On a table or Wall) will tend to increase the no. of errors. system sometime makes error. If there is a noise or some other
3. In speech recognition system there is a possibility of unauthorized usage. Since this does not depend upon which person is speaking.

- 4. No password protection.

- Servo motor drive
- Mechanical links for robot arm

The detailed description for selecting components below

*Proposed system*

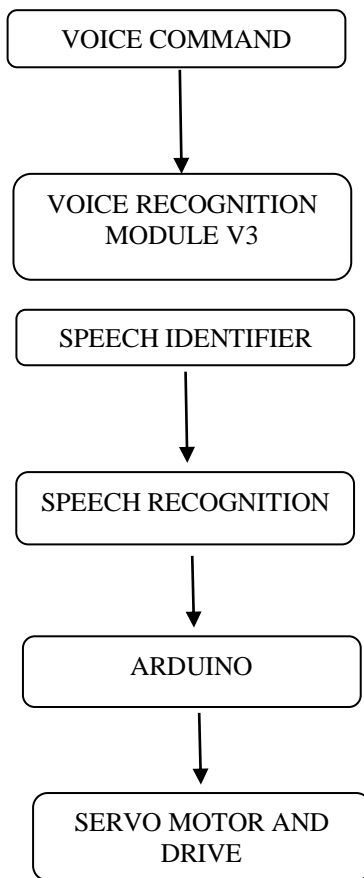


Figure 2 Proposed System

#### IV. COMPONENTS

The selection of materials involves the study of their Characteristics, advantages, availability, cost, user friendly property of components that we want to use.

##### A. Selection of components:

The selection of materials involves the study of their Characteristics, advantages, availability, cost, user friendly property of components that we want to use. In our project, we select each and every component, by study thoroughly about them. By proceeding like that only, we have done our selection.

- The software and device chosen to program the execution of our idea is Arduino microcontroller.
- Servomotors
- Elechouse voice recognition module

##### B. Arduino:

The Arduino mega 2560 is a microcontroller board based on the ATmega2560. It has 54 digital input/output pins (of which 14 can be used as PWM outputs), 16 analog inputs, 4 UARTs (hardware serial ports), a 16MHz crystal oscillator, a USB connection, a power jack, an ICSP header, and reset button. It contains everything needed to support the microcontroller; simply connect it to a computer with a USB cable or power it with an AC-to –DC adapter or battery to get started. The Mega is compatible with most shields designed for the Arduino Duemilanove or Diecimila. The Arduino board is shown in Fig 3

Arduino can sense the environment by receiving input from a variety of sensors and can affect its surroundings by controlling lights, motors, and other actuators. The microcontroller on the board is programmed using the Arduino programming language (based on wiring) and the Arduino development environment (based on processing). Arduino projects can be stand-alone or they can communicate with software on running on a computer (e.g. flash, processing, MaxMSP).



Figure 3 Arduino Mega 2560(www.arduino.cc)

The board can operate on an external supply of 6 to 20 volts. If supplied with less than 7V, however, the 5V pin may supply less than 5V and the board may be unstable. If using more than 12V, the voltage regulator may overheat and damage the board. The recommended range is 7 to 12 volts.

**C. The Five Major Benefits of Using Arduino Starter Kits:**

**Inexpensive:** - Arduino boards are relatively in expensive compared to other microcontroller platforms. The least expensive Version of Arduino module can be assembled by hand, and even the pre-assembled Arduino modules cost less than Rs. 1000.

**Cross platform:** -The Arduino software runs on Windows, Macintosh OSX, and Linux operating systems. Most Microcontrollers systems are limited to windows.

**Simple, clear programming environment:** - The Arduino programming environment is easy-to-use for beginners, yet flexible enough for advanced users to test advantage of as well. For teachers. It's conveniently based on the processing programming environments. So students learning to program in that environment will be familiar with the look and feel of Arduino.

**Open credits and extensible software:** - The Arduino software is published as open credits tools available for extension by experienced programmers. The language can be expanded through C++ libraries, and people wanting to understand the technical details can make the leap from Arduino to the AVR C programming languages on which it's based. Similarly, you can add AVR-C code directly into Arduino program if you want to.

**Open credits and extensible hardware:** - The Arduino is based on Atmel's ATMEGA8 and ATMEGA168 microcontroller. The plans for the modules are published under a creative common license, so experienced circuit designers can make their own version of the module, extending it and improving it. Even relatively inexperienced users can build the breadboard version of the module in order to understand how it works and save money.

**D. DC SERVO MOTOR:**

A servo is a device, electrical or mechanical or electro-mechanical, that upon receipt of stimulus or input, will employ feedback for velocity and/or position control, creating a closed loop.

**1) Servo Motor:**

There are three micro servos are used to control the movement of end effector such as "pitch" control servo motor, "yaw" control servo motor, and "roll" control servo motor. Pitch servo motor control the up and down movement. Yaw servo motor control the side to side movement. Roll servo motor control the rotating movement.

Two servo motors are used to control the movement of joints and base. Thus, the base and joint servo motors control the rotational movement.

**Working Principle of DC Servo Motor:**

A DC servo motor is an assembly of four major components, namely a DC motor, a position sensing device, a gear assembly, and a control circuit. Shown in fig 4.



Figure IV(www. robu.in)

The below figure shows the parts that consisting in RC servo motors in which small DC motor is employed for driving the loads at precise speed and position.

**Internal diagram:**

A DC reference voltage is set to the value corresponding to the desired output. This voltage can be applied by using another potentiometer, control pulse width to voltage converter, or through timers depending on the control circuitry. The dial on the potentiometer produces a corresponding voltage which is then applied as one of the inputs to error amplifier. In some circuits, a control pulse is used to produce DC reference voltage corresponding to desired position or speed of the motor and it is applied to a pulse width to voltage converter. In this converter, the capacitor starts charging at a constant rate when the pulse high. Then the charge on the capacitor is fed to the buffer amplifier when the pulse is low and this charge is further applied to the error amplifier. So the length of the pulse decides the voltage applied at the error amplifier as a desired voltage to produce the desired speed or position. In digital control, microprocessor or microcontroller are used for generating the PWM pluses in terms of duty cycles to produce more accurate control signals. Thus the internal diagram of servo motor is shown in figure 5.

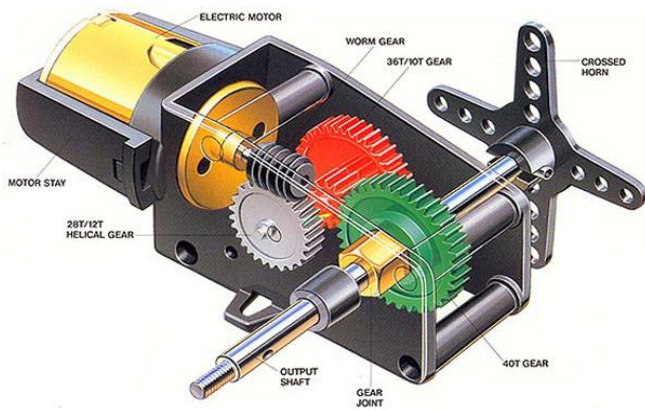


Figure 5 Servo Motor (www. visualgasin.wordpress.com)

The feedback signal corresponding to the present position of the load is obtained by using a position sensor. This sensor is normally a potentiometer that produces the voltage corresponding to the absolute angle of the motor shaft through gear mechanism. Then the feedback voltage value is applied at the input of error amplifier (comparator). The error amplifier is a negative feedback amplifier and it reduces the difference between its inputs. It compares the voltage related to current position of the motor (obtained by potentiometer) with desired voltage related to desired position of the motor (obtained by pulse width to voltage converter), and produces the error either a positive or negative voltage. This error voltage is applied to the armature of the motor. If the error is more, the more output is applied to the motor armature. As long as error exists, the amplifier amplifies the error voltage and correspondingly powers the armature. The motor rotates till the error becomes zero. If the error is negative, the armature voltage reverses and hence the armature rotates in the opposite direction.

*Fundamental characteristics:*

- The motor output torque should be proportional to the voltage applied to it
- The direction of torque developed by the servo-motor should be dependent upon the instantaneous polarity of the control voltage

*Specification:*

- Weight: 55g
- Dimension: 40.7 × 19.7 × 42.9 mm
- Operating Speed (4.8V no load): 20sec / 60 deg
- Operating Speed (6.0V no load): 16sec / 60 deg (no load)
- Stall Torque (4.8V): 10kg/cm
- Stall Torque (6.0V): 12kg/cm
- Operation Voltage: 4.8 - 7.2Volts
- Gear Type: All Metal Gears
- Stable and shock proof double ball bearing design
- Dead band width: 5 μs
- Temperature range: 0 °C – 55 °C.
- Control System: Analog
- Operating Angle: 120degree

- Required Pulse: 900us-2100us

*E. Why we select the servo motor?:*

There are two types of motors that primarily stand out. These choices are a standard DC motor and a signal-controlled servomotor, both of which have their own advantages and disadvantages. Advantages to the DC motor include a full 360-degree range of motion, one input, and the availability of high torque. However, there are large drawbacks when used in a controlled environment. The largest of these drawbacks is the low precision. The motor is either ON or OFF where speed can be adjusted based on the input. In order to accurately control the position a highly accurate microcontroller will most likely be needed. Another large drawback is the significant cost of higher torque motors.

Advantages to the signal-controlled servos include a lower cost when compared to DC motors, a signal-controlled position, and multiple similarly previous projects to be the starting point of research. Like DC motors, the signal-controlled servos have drawbacks. The largest drawback to servo motors is quickly increasing cost for the increase in torque. Another large drawback is that most stock servo motors only have a 90-degree range of motion. To gain a 180-degree, range of motion additional charges may apply.

In order to keep the low cost, low torque and simplicity high, servo motors were chosen to control the pitch, yaw, and roll of the wrist.

*F. Servo Control Method:*

Most standard servos have three leads, position power, negative, and signal. The power lead not only acts as the power source for the servo but can also be utilized to turn the servo either on or off. The typical input voltage for power is between 4.8 volts and 6.0 volts. The negative power lead should be common ground. The signal lead will control the direction of the servo.

The primary method of controlling the servo is to send a pulse-width modulation along the signal lead. This pulse-width modulation signal is a fifty hertz square width, the length of each pulse of the square wave controls how far the servo will rotate. For example, a pulse of 600 microseconds will rotate the servo arm -90 degrees and a 2400 microsecond pulse will rotate the arm positive 90 degrees.

*G. Open Loop Versus Closed Loop:*

For a servo motor, there is a significant difference in an open loop and closed loop control system. In an Open

loop control servo control system, the pulse widths control how far the servo rotate in a specified amount of time. In other words, the length of the pulse width modulation controls how fast the servo rotates, not position. For example, a 600-microsecond pulse may rotate the servo 90 degrees counter-clockwise in 0.15 seconds while a 1000 microsecond pulse may rotate the servo 45-degree counter-clockwise in the same 0.15.

In a close loop servo control system, the length of each pulse controls the position, instead of how fast the servo rotates. For example, a 600-microsecond pulse may rotate the servo to the 90 degrees' counter-clockwise position in 0.15 seconds while a 1000 microsecond pulse may rotate the servo to the 45-degree counter-clockwise position in 0.075 microseconds

Most standard servo motor can only rotate 90 degrees and can be stretched to 180 degrees for an additional cost. These rotational limitations are placed by a potentiometer built into the servo motor. As the potentiometer rotates with the servo, the voltage across the potentiometer changes allowing this voltage change to be used for feedback to control the position. The potentiometer can be disconnected to achieve a full 360-degree continuous rotation, however the feedback to control the position is lost and an external circuit will be required. Since it was specified that the base will rotate below 180 degrees, a continuous rotation is unneeded; this allow for the utilization of the built-in closed loop system.

*H. Digital versus Analog Servos:*

Like many components in the electronics world, servo motors come in standard analog and digital varieties. Functionally speaking, a digital servo is a standard analog motor with a built-in microprocessor that analysis incoming signals to control the motor. Digital servos have two distinct advantages over their analog counter parts. With the built-in microprocessor, the servo performance can be better optimized depending on servos function. Also because of the built-in microprocessor, the pulse width modulation sent from the microprocessor operates at a higher frequency than the standard 50Hz used for analog servos. This leads to higher accuracy, smoother acceleration, and the availability to hold higher torque. However, because of the addition of the microprocessor the servo comes with disadvantages. Since the digital servo operates at a higher frequency for higher accuracy, the power consumption also increases. The price of digital servos is also significantly higher than their analog counter parts.

*I. PSU:*

A power supply unit (or PSU) converts mains AC to low voltage regulated DC power for their internal

components of a computer. Modern personal computers universally use switched-mode power supplies. Some power supplies have a manual switch for selecting input voltage, while others automatically adapt to the mains voltage. The components that supplies power to a computer. Most personal computers can be plugged into standard electrical outlets. The power supply then pulls the required amount of electricity and converts the AC current to DC current. There are three major kinds of power supplies; unregulated (also called brute force), linear regulated, and switching. A fourth type of power supply circuit called the ripple-regulated, is a hybrid between the “brute force” and “switching” designs and merits a subsection to itself. The PSU board as shown in Fig 6

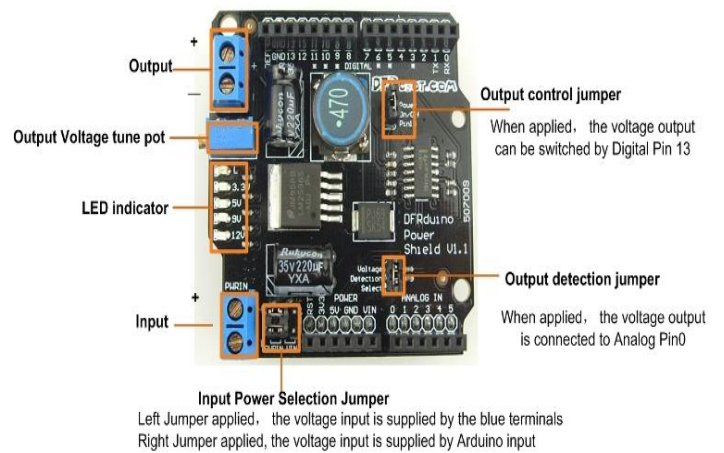


Figure 6 Power Supply Unit(www.robotshop.com)

*J. Voice Recognition Module:*

Voice recognition is a technique that facilitates natural and convenient human machine interface using the voice recognition module. It extracts and analyses voice features of human and delivered to machine or computer through Mic. Voice recognition technique is classified into many types based on different criteria such as scope of the users, number of words used for recognition, naturalness of speaking. If the voice recognition level is more than 95%, then only the voice recognition is practically used.

*K. Voice recognition module V2:*

Voice recognition module V2 supports 50 commands in all and only 5 commands at the same time. On V2, voice commands are separated into three groups while you training it. And only one group (5 commands) could be imported into recognizer. It means only five voice commands at the same time.

*L. Voice recognition module V3:*

Elechouse voice recognition module (Fig.7) is compact and easy control speaking recognition board. It

Arduino compatible. This product is a speaker dependent voice recognition module support up to 80 voice command in all. Maximum seven voice commands could work at same time. Any sound could be trained as a command. User need to train the module first before let it recognizing any voice command.



Figure 7 Elechouse Voice Recognition Module V3 (www.potentiallabs.com)

This board has two controlling ways: serial port (full function), general input things (part of function). General output pins on the board could generate several kinds of waves while corresponding voice command is recognized. On V3, voice commands are stored in large group like a library any seven voice commands in the library could be imported into recognizer. It means seven commands are effective at the same time.

It works under voltage 5.5 volts and less than 40 milliamps. It has both analog and digital interface. In digital interface has five volts TTL level for UART interface and GPIO. In analog interface has 3.5 mm mono channel microphone connector + microphone pin interface. It supports maximum 80 voice commands, it each voice 1500 milliseconds (one or two words speaking). It has seven voice command at a same time. It supports Arduino library. It is easy to control the UART and GPIO, it has user control general pin output. Its accuracy level is 99% under ideal environment.

*M. Why we choose the voice recognition module V3:*

It supports 80 voice commands and are stored in one large group and easy to control the UART, GPIO and recognize seven voice command at same time. Its accuracy level is high compared with V2.

*N. Servo Motor Drive:*

Driving servo motor with the Arduino servo library is pretty easy in servo drive PCA 9685 (Fig 8), but each one consumes a precious pin-not to mention some Arduino

processing power. The Adafruit 16 channel 12-bit PWM/servo driver will be drive up to 16 servos over I2C with only 2 pins. The on-board PWM controller will drive all 16 channels simultaneously with no additional Arduino processing overhead. What's more, you can chain up to 62 of them to control up to 992 servos -all with the same two pins.

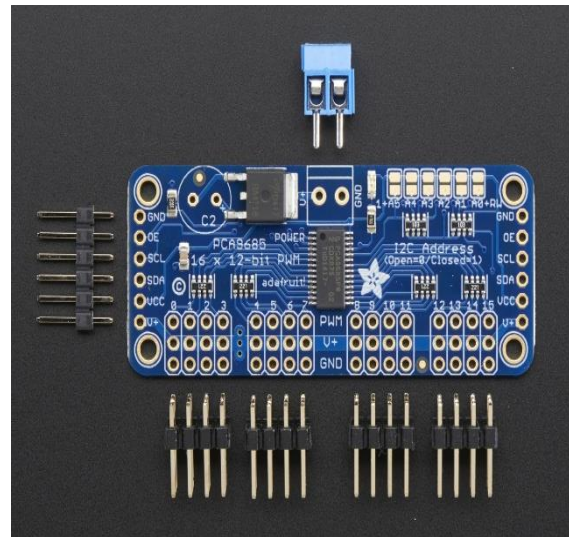


Figure 8 Adafruit PCA9685 Servo Drive (www.adafruit.com)

The Adafruit PWM/servo driver is the perfect solution for any project that requires a lot of servos. The pin diagram is shown in fig 9.

*O. Pin outs:*

There are two set of control input pins on either side. Both sides of the pins are identical. Use whichever side you like, you can also easily chain by connecting up two side-by-side.

*P. Power pins:*

**GND-**This the power and signal ground pin, must be connected.

**VCC-**This is the logic power pin, connected this to the logic level you want to use for the PCA 9685 output, should be 3 to 5 volts maximum. It also used for the 10 k pullups on SCI/SDA so unless you have your own pullups, have it match the microcontroller's logic level to do.

**V+-** this is an optional power pin that will supply distributed power to the servos if your not using for servos you can leave disconnected. It is not used at all by the chips. You can also inject power from the 2-pin terminal block at the top of the board. You should provide 5-6 volt DC if your using servos. If you have to, you can go higher to 12volt

DC, but if you mess up and connect VCC to V+ it would damage your board.

independently but they must all have the same PWM frequency. There are 220ohm resistors in series with all PWM pins and the output logic is the same as VCC.

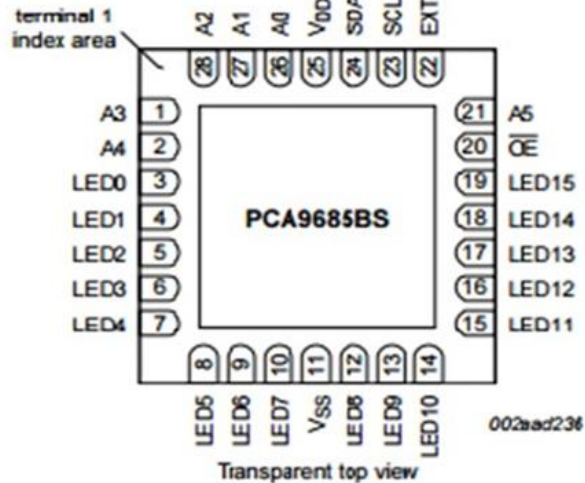
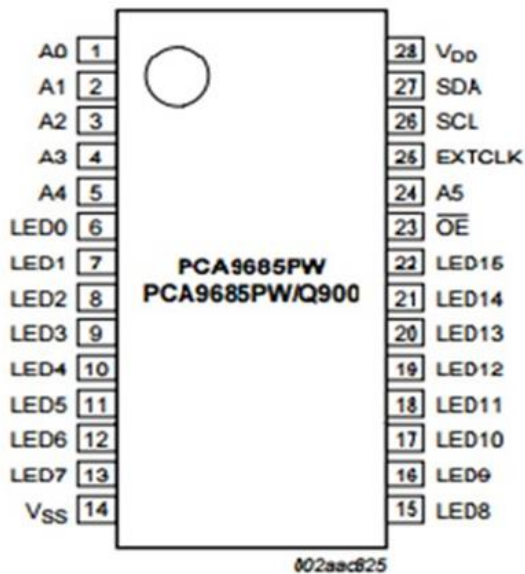


Figure 9 Pin Diagram of PCA9685(www.adafruit.com)

The PCA9685 is a 16-channel I2C-bus controlled LED controller optimized for Red/Green/Blue/Amber (RGBA) colour backlighting applications. Each LED output has individual 12-bit resolution (4096 steps) PWM controller with a fixed frequency. The controller operates at a programmable frequency from a typical 24 Hz to 1526 Hz with a duty cycle that is adjustable from 0% to 100% so the LED can be set to output a specific brightness. All outputs are set to the same PWM frequency.

With the PCA9685 as the master chip, the 16-channel 12-bit PWM Servo Driver only needs 2 pins to control 16 servos, thus greatly reducing the occupant I/Os. Moreover, it can be connected to 62 driver boards at most in a cascade way, which means it will be able to control 992 servos in total. The pin diagram is shown in Fig 4.7

**Q. Control pins:**

SCL-I2c clock pin, connect to your microcontrollers I2C clock line. Can use 3v or 5v logic, and has a weak pullup to VCC

SDA-I2Cdata pin, connect to your microcontrollers I2C data line. Can use 3v or 5v logic and has a weak pullup to VCC.

OE-output enable. It can be used to quickly disable all outputs. when this pin is low all pins are enabled. When the pin is high the outputs are disabled.

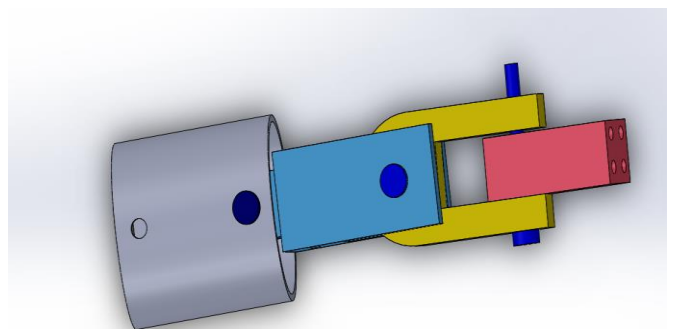
**R. Output Ports:**

There are 16 output ports. Each pot has 3 pins: V+, GND and the PWM output. Each PWM runs completely

After the text edit has been completed, the paper is ready for the template. Duplicate the template file by using the Save As command, and use the naming convention prescribed by your conference for the name of your paper. In this newly created file, highlight all of the contents and import your prepared text file. You are now ready to style your paper; use the scroll down window on the left of the MS Word Formatting toolbar.

*Design*

The design of the robotic arm is fully based on the SCARA type. Its full form is "SELECTIVE COMPLIANCE ASSEMBLY ROBOT ARM". It is similar in construction to the jointed arm robot is shown in fig 10, except the shoulder and elbow rotational axis are vertical. It means that the arm is very rigid in a vertical direction and complicated in horizontal direction. Its arm was rigid in Z the axis pliable in the XY- axes, which allowed it to adapt to holes in the XY- axes.



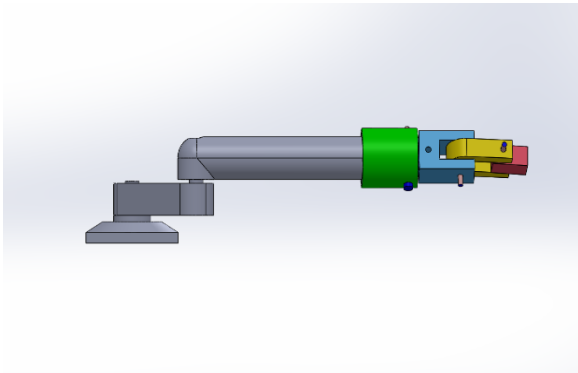


Figure 10 Wrist Design (UP) & Arm (DOWN)

By virtue of the SCARA's parallel-axes joint layout, the arm is compliant in the X-Y direction but rigid in the Z direction, hence the term: selective compliant. This is advantageous for many types of assembly operations, i.e., inserting a round pin in a round hole without binding.

#### S. Solid Works:

Solid works software is solid modeling computer aided design (CAD) and computer aided engineering (CAE). Solid works programs for calculations, error, structure, and failure analysis, the premium package is a verifiable autonomous collective. Specifically, SWIFT technology (solid works intelligent future technology) allows the user to automate various time-consuming task and techniques, "diagnosing and resolving problems related to future order, mates, sketch relationship and application of dimensions". Seemingly becoming a trend in a quality CAD software, solid works premium offers a variety of add-ons and additional programming asides from its traditional drawing capabilities. One such program is simulationXpress, a design validation tool that is included within every box of solid works ("how can be design better products using solid works?" 1). This program incorporates real world physics into an easy functional early detection design flaw widget. Research suggest that solid works is a company on the rise. Engineering placement agencies denote that the demand for solid work tool and skills is over twice that of comparable design pack

#### Conclusion

The Anthropomorphic writing bot has been designed in the type of modified SCARA by using the software SolidWorks. The selection of components for the writing bot has also been completed. The ideologies which are like the proposed system are studied carefully and the merits, demerits are taken into consideration. However, the general procedure for taking care of design will need extra caution during the time of implementation.

#### REFERENCES

1. Pradeep, S., et al., *Iot and its connectivity challenges in smart home*, in *International Research Journal of Engineering and Technology*. 2016. p. 1040-1043.
2. Anusuya, M. and S.K.J.a.p.a. Katti, *Speech recognition by machine, a review*. 2010.
3. Yasodharan, R., R. Sivabalakrishnan, and P. Devendran, *Trusted Routing with an Efficient Certificate Revocation for Mobile Ad Hoc Network*.
4. Balaganesh, M., et al. *Robotic arm showing writing skills by speech recognition*. in *Emerging Trends in Robotics and Communication Technologies (INTERACT), 2010 International Conference on*. 2010. IEEE.
5. Khatib, O. and J. Burdick. *Motion and force control of robot manipulators*. in *Robotics and Automation. Proceedings. 1986 IEEE International Conference on*. 1986. IEEE.
6. Massera, G., A. Cangelosi, and S. Nolfi. *Developing a reaching behaviour in a simulated anthropomorphic robotic arm through an evolutionary technique*. in *Artificial Life X: Proceeding of the Tenth International Conference on the simulation and synthesis of living systems (Cambridge, MA, MIT Press)*. 2006.
7. Stein, T., et al., *Guidelines for motion control of humanoid robots: Analysis and modeling of human movements*. 2006. **5**: p. 15-30.
8. Potkonjak, V., et al., *Redundancy problem in writing: from human to anthropomorphic robot arm*. *IEEE Trans Syst Man Cybern B Cybern*, 1998. **28**(6): p. 790-805.
9. Yoshikawa, T. *Force control of robot manipulators*. in *Robotics and Automation, 2000. Proceedings. ICRA'00. IEEE International Conference on*. 2000. IEEE.
10. Syamlan, A.T., H. Nurhadi, and B. Pramujati. *Character recognition for writing robot control using anfis*. in *Advanced Mechatronics, Intelligent Manufacture, and Industrial Automation (ICAMIMIA), 2015 International Conference on*. 2015. IEEE.
11. Kousalya, T., et al., *Study and Implementation of Fault Diagnosis in Induction Motor Using MCSA*.
12. Yussof, S., A. Anuar, and K. Fernandez. *Algorithm for robot writing using character segmentation*. in *Information Technology and Applications, 2005. ICITA 2005. Third International Conference on*. 2005. IEEE.
13. Nagy, G. and G.J.I.T.o.I.T. Shelton, *Self-corrective character recognition system*. 1966. **12**(2): p. 215-222.
14. Batmavady, S., K. Manivannan, and P.C. Janvier. *Segmentation, Recognition and synthesis of tamil characters for robotic writing*. in *Conference on Computational Intelligence and Multimedia Applications, 2007. International Conference on*. 2007. IEEE.

15. Gish, H., M.-H. Siu, and R. Rohlicek. *Segregation of speakers for speech recognition and speaker identification*. in *Acoustics, Speech, and Signal Processing, 1991. ICASSP-91., 1991 International Conference on*. 1991. IEEE.
16. Mohamed Ahmed Ghiet, A. and A. Baba, *ROBOT ARM CONTROL WITH ARDUINO*. 2017.
17. Premkumar, K. and K.G.J. Nigel. *Smart phone based robotic arm control using raspberry pi, android and Wi-Fi*. in *Innovations in Information, Embedded and Communication Systems (ICIIECS), 2015 International Conference on*. 2015. IEEE.
18. Li, B., et al. *Human-like robotic handwriting and drawing*. in *Robotics and Automation (ICRA), 2013 IEEE International Conference on*. 2013. IEEE.
19. Franke, K. and S. Rose. *Ink-deposition model: The relation of writing and ink deposition processes*. in *Frontiers in Handwriting Recognition, 2004. IWFHR-9 2004. Ninth International Workshop on*. 2004. IEEE.
20. Crainic, M.-F., et al. *Secure handwriting using a robot arm for educational purpose*. in *Methods and Models in Automation and Robotics (MMAR), 2014 19th International Conference On*. 2014. IEEE.
21. Acero, A. and R.M. Stern. *Environmental robustness in automatic speech recognition*. in *Acoustics, Speech, and Signal Processing, 1990. ICASSP-90., 1990 International Conference on*. 1990. IEEE.
22. Elfasakhany, A., et al., *Design and development of a competitive low-cost robot arm with four degrees of freedom*. 2011. **1**(02): p. 47.
23. Iqbal, J., et al., *Modeling and analysis of a 6 DOF robotic arm manipulator*. 2012. **3**(6): p. 300-306.

# Studies on recycled aluminium (AA319) reinforced with recycled glass

China Mahammad Bhasha<sup>1\*</sup>  
Research scholar, Department of  
Mechanical Engineering  
VFSTR (deemed to be University)  
A.P-522213, India.  
bash.chinna6@gmail.com

Naveen Kumar chebrolu<sup>2</sup>  
Assistant Professor, Department of  
Mechanical Engineering  
Malla Reddy College of Engineering &  
Technology  
T.S-500100, India  
chebrolu.naveenkumar@gmail.com

Venkataramana Murthy VP<sup>3</sup>  
Professor, Department of Mechanical  
Engineering  
Narsimha Reddy Engineering College  
T.S-500100, India  
vpvrmurthy@gmail.com

**Abstract.** Present work investigates the mechanical, thermal, & tribological properties of recycled glass strengthened with recycled AA319 matrix to form aluminum metal matrix composite (AMMC) by powder metallurgy (PM). Fabricated AMMCs widely use in automobile applications. Particle sizes of AA319 & glass 250 $\mu$ m, 75  $\mu$ m respectively. The weight fractions of glass content (10%, 20%, & 30%) in this manner the sintering temperature (600-660.4°C) and sintering time six hours individually. Mechanical, tribological & thermal behaviors tensile strength, hardness, density, wear, thermal conductivity were tested accordingly ASTM standards. Hardness increases with increases in weight fractions of glass content, higher hardness value 92.44BHN at AA319 (70%) - recycled glass (30%). Tensile strength and density decrease with increases in wt% of glass content as a result of brittleness & porosity increases. Wear properties are good. Thermal conductivity increases in the glass content increase because compares to glass AA319 have higher thermal conductivity.

**Key words:-** aluminum metal matrix composite, powder metallurgy, recycled glass

## 1. Introduction

Aluminum Matrix Composites (AMCs with scrap A356) strengthened with Nano iron compound created by metallurgy were investigated with low value producing of sunshine and efficient multifunctional materials for natural philosophy applications. AMCs strengthened with particles tend to supply improvement of properties processed in a different manner. Over the previous few decades, high-performance AMCs are wide developed with high strength, high stiffness, denseness, and sensible wear resistance capability [1-5]. Among them, A356 aluminum was broadly utilized as a network. A356 is an intriguing choice for military and car applications as the amalgam has imperative properties of high quality, lightweight and great limit with regards to the foundry (fluidity). This combination can likewise be effectively utilized as a network from the reused crisp piece (chips) to create fantastic metal grid composites in a monetary way [6-11]. Presently a day, reused glass can be substituted for up to 95% of crude materials; glass is 100% recyclable and can be reused perpetually without misfortune in quality or immaculateness. Assembling profits by reusing in a few different ways: reused glass decreases discharges and utilization of crude materials, broadens the life of the plant, for example, heaters, and spares vitality, and aluminum combination reusing is likewise assuming basic part car industry.

Planning of aluminum / glass network composites with method of powder metallurgy The composites have more glass content, square with conveyance and great scraped area opposition [12]. Powder metallurgy(PM) course is one of the alluring techniques for metallic froths generation since it takes into account preparing of wide range segments and close net molded geometries froths and in addition the froths with necessary sandwich structure. Broad scientists have been completed to create Al combination froths by the PM course [13]. Lightweight has turned into a critical perspective with a specific end goal to decrease CO<sub>2</sub> outflows in the car and enhancing range in electric vehicles thus lightweight materials, for example, aluminum, magnesium or composite materials are in effect broadly examined for car applications [14]. The sinter capacity of Al combination powder metallurgy PM amalgam was explored. Financially accessible Aluminum alloy319 has been uniaxial squeezed compacts in the scope of 100– 500 MPa were sintered at temperatures in the scope of 610– 660°C. The explored composite demonstrates a decent sintering reaction and 98% hypothetical thickness was accomplished. An ideal sintering profile has been chosen and the mechanical properties were estimated, for example, hardness, elasticity esteems acquired were near the modernly distributed qualities. Notwithstanding the sintering and warmth treatment, the microstructure of sintered material has been inspected and portrayed utilizing optical and filtering electron microscopy [15]. In, for the most part, the further developed basic composites utilize fiberglass, carbon/graphite, boron, Kevlar (aramid) and other natural materials, which stressed the principal properties as light weight, higher solid and solidness. These fortifying impacts of fiber fortifications in composites are getting by the level of strands (fiber-sap proportion), kind of filaments and fiber introduction regarding the course of burdens [16]. In particulate composites crack start is related to molecule break, interfacial-network disappointment, and incorporation break, contingent upon the specific composite and lattice condition. [17]. Al–319 alloys have been used as the reinforcement material in the present investigation with different mesh sizes 100 to 120 [18].

The objective of this work is to compare properties such as wear resistance, hardness, strength..etc of AA319 and AA356’.





Fig.2: Universal machine and Tensile test specimen

### 2.3. Hardness test

In those strategies, Brinell hardness test is utilized for the hardness testing shown in Fig.3 and applying load is 600kgf, 10mm steel ball utilizing to the infiltration after 15 sec evacuate the heap and measure the entrance gap distance across by utilizing the magnifying lens.



Fig.3: Brinell hardness testing machine

### 2.4. Density test

Thickness is the mass per unit volume of a material. Particular gravity is a measure of the proportion of the mass of a given volume of material at 23°C to a similar volume of deionized water. Particular gravity and thickness are particularly applicable on the grounds that plastic is sold on a cost for every pound premise and a lower thickness or particular gravity implies more material per pound or fluctuated part weight.

### 2.5 Thermal Conductivity Testing and Procedure:

Thermal conductivity in "thin" materials that are often described as "thermal interface materials. "Thin" materials are roughly those less than 1-2 cm thick.

### 2.6 Wear test

This test method describes a laboratory procedure for determining the wear of materials during sliding using a pin-on-disk apparatus were tested as pairs with nominally non-abrasive conditions. The principal need of experimental attention to use this type of apparatus to measure wear were described. The coefficient of friction may also be determined.

## 3. Results and discussion

S.no	Test Parameters	100% Al + 0% Glass	90% Al + 10% Glass	80% Al + 20% Glass	70% Al + 30% Glass
1	Tensile Strength in N/mm <sup>2</sup>	100.51	80.39	60.82	31.66
		105.76	90.85	66.36	31.03
2	Hardness ,BHN	84.88	86.24	88.42	92.44
3	Density, g/mm <sup>3</sup>	0.00261	0.00243	0.00221	0.00191
4	Thermal Conductivity, W/ (mm.K)	0.51	0.53	0.54	0.55

### 3.1 Tensile test

The Fig 4 shows that an increment in the amount of glass content while decreases the tensile strength of the composite because of the density of material decreases, brittleness increases & porosity increases.

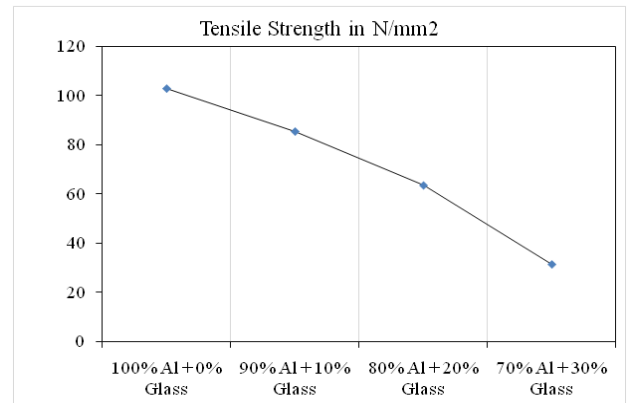


Fig 4 Tensile strength v/s with weight % of glass

### 3.2 Hardness test

From Fig 5 shows that, the hardness increases correspondingly with the glass content because of internal energy increases due to porosity.

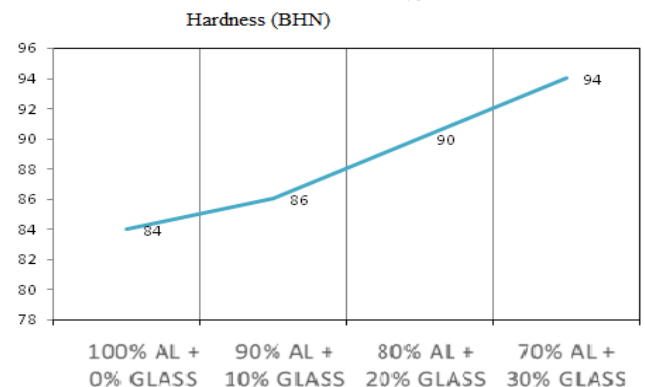


Fig 5 Hardness v/s with weight % of glass

### 3.3 Thermal conductivity test

From Fig 6 shows that, increase in the glass content, increases the thermal conductivity because the thermal conductivity is higher than to the Al-319, the thermal conductivity of the composites increases with the corresponding increase in the porosity.

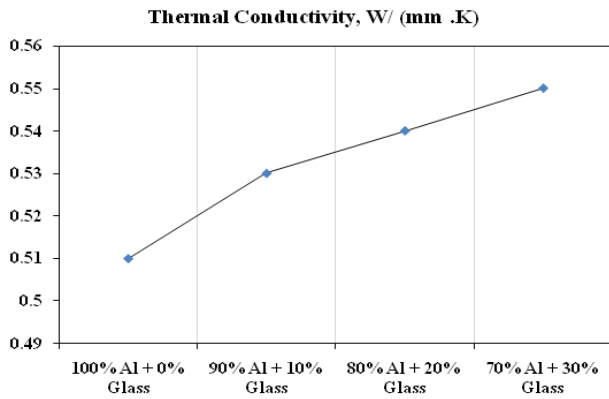


Fig 6 Thermal conductivity v/s with weight % of glass

### 3.4 Density test

The Fig 7 shows that increasing the glass content in samples, decreases the density of the samples respectively because the glass density is less compared to the density of the aluminum alloy 319.

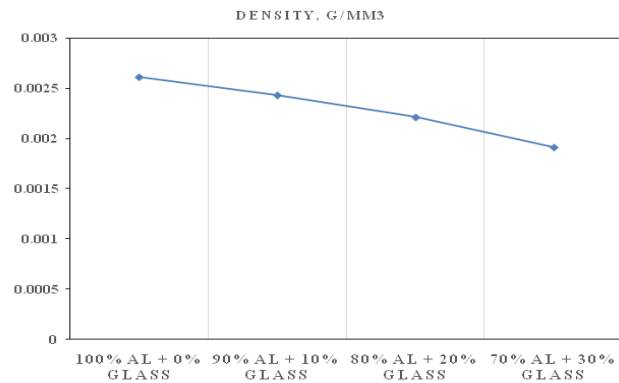


Fig 7 Density vs. weight % of glass

### 3.5 Wear behavior

The wear rate of the produced composite with recycled glass is shown in Fig 8 to 11. The wear rate decreases with increases recycled glass. It was found that minimum wear rate at 90% Al + 10% glass.

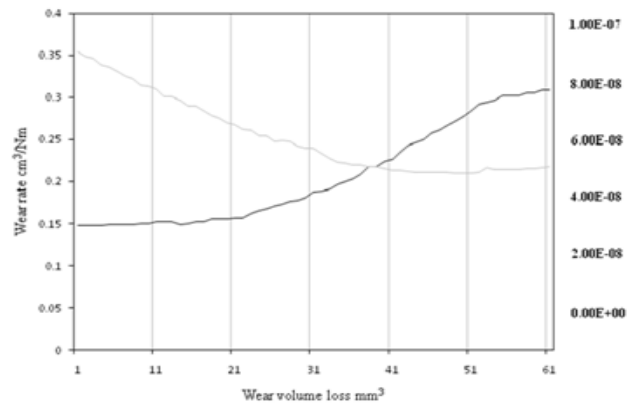


Fig 8 wear rate of pure aluminum sliding distance constant

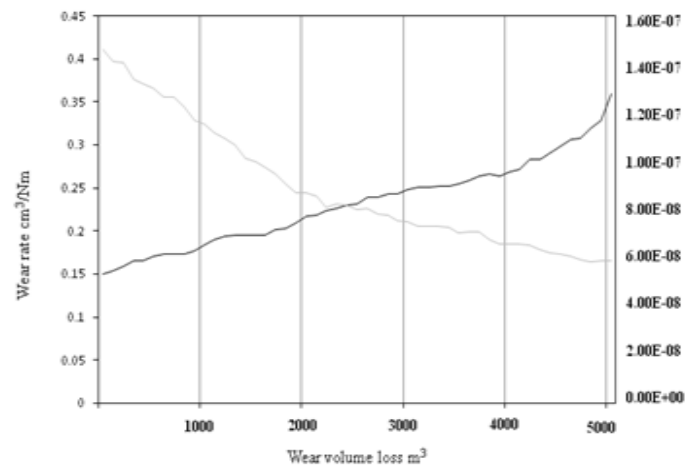


Fig 9 wear rate of sample (90% Al + 10% Glass) applied load constant

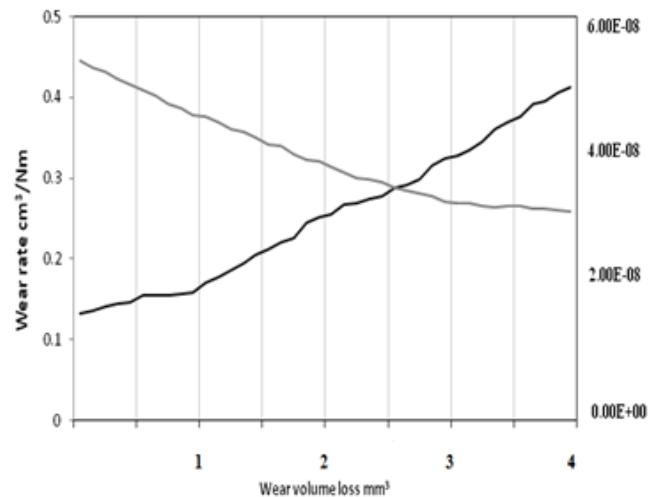


Fig 10 wear rate of sample (90% Al + 10% Glass) sliding distance constant

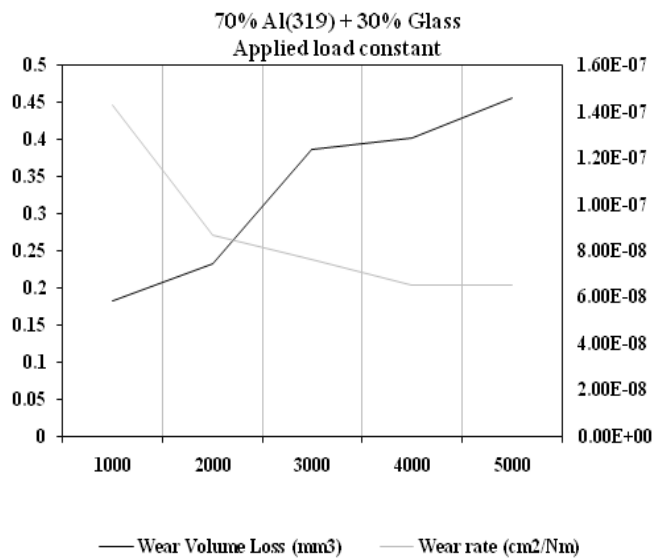


Fig 11 wear rate of sample (70% Al + 30% Glass) sliding distance constant

#### 4. Conclusion

- After the results the following conclusions were made with the addition of the glass reinforcement increases the hardness of A319 because the load penetration is less and internal energy is more.
- Thermal conductivity increases compared to the pure aluminium because glass is used as reinforcement.
- Wear properties are good because of the hardness increases and for the glass; there is the low coefficient of friction.
- The density decreases since the glass density is less than the aluminium density
- The tensile strength compared to the pure aluminium 319 alloy decreases due to porosity and the brittleness due to the glass.
- The above results and graphs the best properties are obtained at the 20% glass content.

#### REFERENCES

1. Rebba, B., Ramanaiah, N.: Evaluation of mechanical properties of aluminum alloy (Al-2024) reinforced with molybdenum disulphide (MOS<sub>2</sub>) metal matrix composites. *Procedia Mater. Sci.* 6, 1161–1169 (2014)
2. Majumdar, S., Kale, G.-B., Sharma, I.-G.: A study on preparation of Mo–30W alloy by alumina thermic co-reduction of mixed oxides. *J. Alloys Compd.* 394, 168–175 (2005)
3. Cannillo, V., Manfredini, T., Montorsi, M., Boccaccini, A.R.: Investigation of the mechanical properties of Mo-reinforced glass-matrix composites. *J. Non-Cryst. Solids* 344, 88–93 (2004)
4. Zhou, Y., Wang, Q., Han, X.-L., Sun, D.-L.: Fabrication and properties of continuous unidirectional Mo fiber reinforced TiAl composites by slurry casting and vacuum hot pressing. *Compos. Sci. Technol.* 83, 72–78 (2013)
5. Chen, L.-G., Lin, S.-J., Chang, S.-Y.: Tensile properties and thermal expansion behaviors of continuous molybdenum fiber reinforced aluminum matrix composites. *Compos. Sci. Technol.* 66, 1793–1802 (2006)
6. Din, T., Campbell, J.: High strength aerospace aluminum casting alloys a comparative study. *Mater. Sci. Technol.* 12, 644–650 (1996)
7. Choi, D.-H., et al.: Microstructure and mechanical property of A356 based composite by friction stir processing. *Trans. Nonferrous Met. Soc. China* 23, 335–340 (2013)
8. Srinivasu, R., Sambasiva, A., Madhusudhan, G., Srinivasa, K.: Friction stir surfacing of cast A356 aluminum end silicon alloy with boron carbide and molybdenum disulphide powders. *Def. Technol.* 11, 140–146 (2015)
9. Santella, M.-L., Engstrom, T., Storjohann, D., Pan, T.-Y.: Effects of friction stir processing on mechanical properties of the cast aluminum alloys A319 and A356. *Scripta Mater.* 53, 201–206 (2005)
10. Chainarong, S., Muangjumburee, P., Suthummanon, S.: Friction stir processing of SSM356 aluminium alloy, 12th global congress on manufacturing and management, GCMM 2014. *Procedia Eng.* 97, 732–740 (2014)
11. Ma, Z.-Y., Sharma, S.-R., Mishra, R.-S.: Effect of friction stir processing on the microstructure of cast A356 aluminum. *Mater. Sci. Eng.* A433 (1), 269–278 (2006)
12. Xu, B., et al.: Preparation and properties of sintered molybdenum doped with La<sub>2</sub>O<sub>3</sub>/MoSi<sub>2</sub>. *Int. J. Refract. Met. Hard Mater.* 28, 150–154 (2010)
13. Chawla, N.: Industrial paper, “Metal Matrix Composites in automotive applications”, advanced materials and processes, pp. 26–31 (2006)
14. Yao Guinia, b\*, Sun Keweia, Research on preparation of recycled glass / aluminum matrix composites with powder metallurgy, International Conference on Computer Distributed Control and Intelligent Environmental Monitoring (2011)
15. Frederick T. Wallenberger, James C. Watson, and Hong Li, PPG Industries, Inc. *Glass Fibers*, © 2001 ASM International. All Rights Reserved. *ASM Handbook*, Vol. 21: Composites (#06781G).
16. 1Arivazhagan.K, 2Mahalashmi.S, 3Dr.L. Boopathi1 , Evaluation on Recycling of E-waste Aluminum in Metal Matrix Composite , International Research Journal of Engineering and Technology (IRJET) e-ISSN: 2395 - 0056 www.irjet.net p-ISSN: 2395-0072(6Apr-2016) .
17. J.Jenix Rino1, D.Chandramohan2, K.S.Sucitharan3, An Overview on Development of Aluminium Metal Matrix Composites with Hybrid Reinforcement, international journal science and research(USR),India online ISSN:2319-7064 (December 2012).
18. Hieu Nguyen, Manufacturing Processes and Engineering Materials Used in Automotive Engine Blocks (April 8, 2005).
19. Petruadian, manufacturing process and applications of composite materials,(January2010).

## “PRODUCTION OF METHYL ESTERS FROM MILK SCUM, PERFORMANCE AND EMISSION ANALYSIS ON CI ENGINE”

**SHASHIKUMAR S**  
Assistant professor  
Dept. of Mechanical Engineering  
[Solur.shashi@gmail.com](mailto:Solur.shashi@gmail.com)  
Malla Reddy College of  
Engineering  
Secunderabad-500100

**SOUJANYA G**  
Assistant professor  
Dept. of Mechanical Engineering  
[Soujanya921@gmail.com](mailto:Soujanya921@gmail.com)  
Malla Reddy College of  
Engineering  
Secunderabad-500100

**RAMYA V**  
Assistant professor  
Dept. of Mechanical Engineering  
[ramyavishwagna99@gmail.com](mailto:ramyavishwagna99@gmail.com)  
Malla Reddy College of  
Engineering  
Secunderabad-500100

### ABSTRACT

The present scenario of world fuel consumption is massive and still increasing. The main source of fuel is fossil fuel. Today with the rise in prices of crude oil, petroleum products are becoming increasingly difficult for a average man to reach, also with alarming levels of pollution and the fear of depletion of petroleum products it's become inevitable to explore new possibilities in fuel production sector. Initiating from this view point various sources were looked at for production of alternative fuels .Most of the raw materials like seeds, grass, bio mass have been in the line of successful experimentation. Hence a unique raw material that is the milk dairy wash water scum has been selected. By trans-esterification methyl ester can be obtained from the scum which can be blended with diesel to get a new form of bio diesel and the further study of its properties and performance on IC engines can be obtained.

**Keywords:** Biodiesel, milkscum, transesterification

### 1. INTRODUCTION

Due to decrease in petroleum resources and increase in pollution problems there is a need in increasing the fuels like electricity, natural gas, and biodiesel. As there is a Continuous reduction in the fossil fuel day by day it has become more attractive to trap renewable energy sources. Currently biodiesel is prepared from oil like palm, sunflower soybean, canola, etc. throughout the world, which results in the food crisis of using food crops for producing biodiesel. In India around 150 million tons of Scum oil is produced per year. Thousands of large dairies are engaged in handling this milk across the country. Generally, a large diary process 5 lakh litres of milk per day, which produce approximately 200-350 kg of scum per day.

### 2.METHODOLOGY

#### 2.1 TRANS-ESTERIFICATION PROCESS

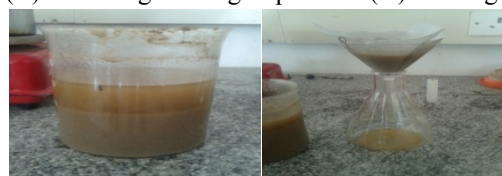
The 5 kg of scum collected and first purified by hand picking of coarse and floating impurities from milk dairy. Later heated till it reaches 100<sup>0</sup>C to lose all it moisture contents and was strained which in turn filtered it. After the filtration process 3.9kgs of purified scum/clarified butter obtained. Figure 1 shown the Stages Of Scum Filtration and one kg of purified scum was used for experimentation.



(A)Raw milk scum (B)Heating



(C)Removing floating impurities (D) Heating



(E) Separation of oil & solid waste (F)Filtering



(E) Pure milk scum (G)Heated refined milkscum

Figure 1: Stages Of Scum Filtration

The Trans-esterification process was carried out for the purified scum by a 2 stage process which involves that is Acid catalyzed esterification and Base catalyzed esterification.

### 2.1.1 ACID CATALYZED ESTERIFICATION

In acid catalyzed esterification initially 750 ml of scum is heated to 50°C, Added 263ml of methanol ,9ml of sulphuric acid and 2ml of Iso-propyl alcohol into a beaker. Transfer the heated scum to the round bottom flask of the esterification set up. Pour the methanol and acid mixture to the other beaker in the set up and slowly allowed the methanol acid mixture by opening the valve into the flask containing scum. The magnetic stirrer stirs the mixture of scum, methanol and acid, there by does not allow the mixture to solidify. The stirring is carried on for 60 to 120 minutes. In a test tube a sample of mixture is taken and kept aside for few minutes to check if the FFA's are forming a separate layer on top. If the FFA's form a separate layer the process is complete. Pour the mixture in the flask to the settling flask and allow settling for 15 minutes for the FFA's to form a separate layer. Separate the FFA's layer from the remaining



Figure 2: scum, Methanol & acid mixture and Separation of FFA layer

### 2.1.2 BASE CATALYZED ESTERIFICATION

In this stage, the product of acid catalyzed esterification obtained from is heated for 55°C, In a beaker added 123ml of methanol and 1.5 grams of KOH pellets and allowed it to dissolve. Transfer the heated scum to the round bottom flask of the esterification set up and Poured the methanol and KOH mixture to the other beaker in the set up. Slowly allow the methanol KOH mixture by opening the valve into the flask containing scum. 6. The magnetic stirrer stirs the mixture of scum, methanol and KOH, thereby does not allow the mixture to solidify. The stirring is carried on for 60 to 150 minutes. In a test tube a sample of mixture is taken and kept aside for few minutes to check if the glycerol is forming a separate layer in the bottom. If the glycerol forms a separate layer the process is complete and Pour the mixture in the flask to the settling flask and allow settling for 15 minutes for

the glycerol to form a separate layer. Separate the glycerol layer from the remaining biodiesel.



Figure 3: Formation Of Glycerol Layer

### 2.1.3 WATER WASH

The biodiesel obtained was washed 4 times with water to remove the catalyst. If clear wash water is got back it indicates that the catalyst is not present in the biodiesel. This is later heated to 100°C to get dry biodiesel which is free from moisture .Thus neat bio diesel is obtained.



Figure 4: Water washing of Bio Diesel and Heating Bio Diesel

### 2.2 PROPERTIES OF SCUM BIODIESEL

The blended fuel samples and biodiesels were tested for different chemical and physical properties. The first test conducted was the flame test for the produced biodiesel to make sure that it is in an hydrous form. This test was conducted with the help of a spirit lamp to check whether it burns without sparks and with a blue flame. Second test was to find out calorific values of the blended fuel samples and also for regular diesel. This is done by testing 50 grams of fuel in a bomb calorimeter and directly obtaining the calorific value of the fuel. The next test conducted was the viscosity test with the help of a Red Wood Viscometer for the blended fuel samples as well as regular diesel to check whether they hold good for ASTM fuel standards. The fuel samples were also tested for the flash points. The results have been furnished below

FUEL BLEND S	FLASH POINT °C	FIRE POINT °C	Specific gravity	CALORIFIC VALUE (kJ/kg)	VISCOSITY (CP)
DIESEL	46	53	0.820	43125	3.5
B10	48	56	0.825	42591	3.3
B20	50	61	0.830	42057	3.35
B30	56	67	0.835	41523	3.38

### 2.3 EXPERIMENTAL SETUP FOR ENGINE PERFORMANCE TEST

The experimental setup of the present work with various components is shown in the figure.5 parts are (1) Engine, (2) Dynamometer, (3)Shaft, (4) Flywheel, (5) Exhaust pipe, (6) Dynamometer control unit, (7) Gas analyzer, and (8) Fuel measurement system.

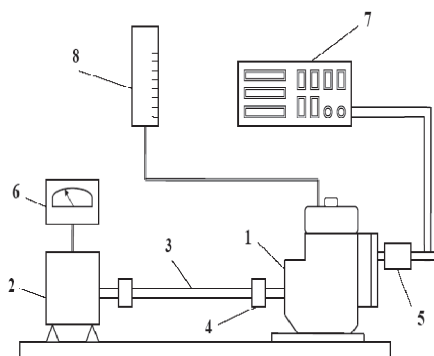


Figure 5: The schematic diagram of the experimental set-up of Diesel fuel Engine test rig..



Figure 6 Kirloskar Diesel Engine with sensing exhaust gas temperature

#### ENGINE AND DYNAMOMETER SPECIFICATION FOUR STROKE SINGLE CYLINDER DIESEL ENGINE TEST RIG

Make	Kirloskar
Capacity	3.7Kw
Compression Ratio	16.5:1
Cylinder Bore	80mm
Stroke	110mm
Cylinder capacity	553cc
Cooling	Water cooling
Electrical dynamometer	
Loading	Eddy current Dynamometer
Make	POWERMAG
Speed	1500rpm
Excitation Voltage	80v

### 3. RESULTS AND DISCUSSION

#### 3.1 CHARACTERIZATION OF DIESEL, BIODIESEL BLENDS.

The fuel characterization includes the fuel properties like viscosity, calorific value, flash and fire point etc. In this experiment some of the fuel properties were analyzed and were discussed below.

##### 3.1.1. SPECIFIC GRAVITY

The specific gravities Diesel , Biodiesel and blends are shown in graph. This test was carried at a temperature of 250 °C (ASTM standard). From the graph we can conclude that the specific gravities of the blends increase with the percent volume of biodiesel. The specific gravity of biodiesel is 0.880 and it is more than fossil diesel (0.820).

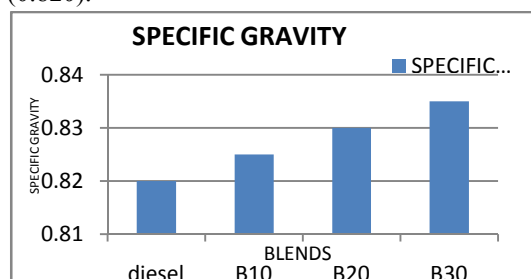


Figure 7: Specific Gravity Of Different Blends

##### 3.1.2. Density

The density of Diesel, Biodiesel and blends are shown in graph. This test was carried at temperature of 150°C (ASTM standard). From the graph we can conclude that the densities of the blends were less compared with fossil diesel as percentage of biodiesel increases the density increases slightly. The density of biodiesel is 0.880kg/m<sup>3</sup> and it is more than fossil diesel (0.855kg/m<sup>3</sup>).

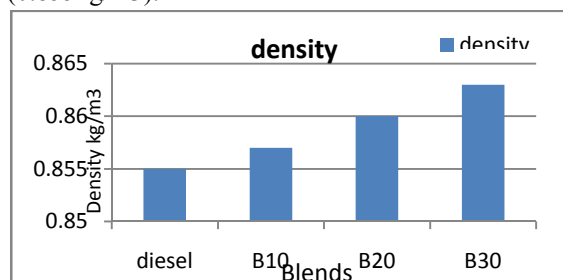


Figure 8: Density of Different Blends

##### 3.1.3. Calorific Value

The calorific Diesel, Biodiesel and blends are shown in graph The CV of B100 was found to be 37785.216 KJ/Kg and the CV of different blends were also determined according to ASTM standards. The CV of blends was found to be less than the fossil diesel (43125 KJ/KG).

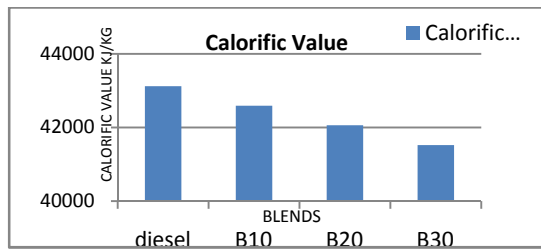


Figure 9: Calorific Value Of Different Blends

### 3.2. ENGINE PERFORMANCE AND EXHAUST EMISSION ANALYSIS

#### 3.2.1. PERFORMANCE CHARACTERISTICS

##### 3.2.1.1. BRAKE SPECIFIC FUEL CONSUMPTION

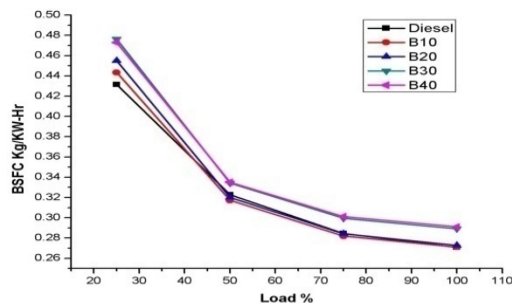


Figure 10: Variation of Brake Specific Fuel Consumption with Load

The variation of specific fuel consumption with respect to load is presented in Figure for different diesel–biodiesel blends. As the load increases, BSFC decreases for all fuel blends. At full load, B10 shows the lowest fuel consumption and at higher percentage of blends, the BSFC increases. This may be due to fuel density, viscosity and heating value of the fuels. B10 has higher energy content than B20, B30 and B60, but lower than Diesel. Lesser values of BSFC are apparently desirable.

##### 3.2.1.2 BRAKE SPECIFIC ENERGY CONSUMPTION

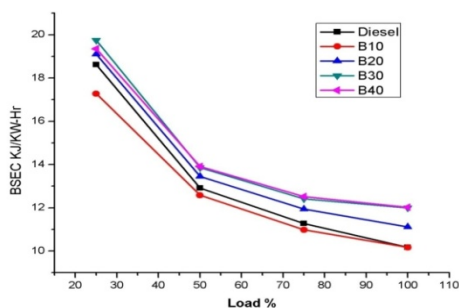


Figure 11: Variation of Brake Specific Energy Consumption with Load

The variation in BSEC with load for all fuels is presented in Fig.11. In all cases, it decreased sharply with increase in percentage of load for all fuels. The main reason for this could be

that the percent increase in fuel required to operate the engine is less than the percent increase in brake power, because compare to other things less amount of the heat is lost at higher loads. The BSEC for B20,B30 and B40 blends was higher than that of diesel. This trend was followed due to lower calorific value, with increase in biodiesel percentage in blends. Here maximum BSEC was found in B40. The brake specific energy consumption for B10 was low for the lower blends as compared with the diesel. As the blend increases the BSEC will also get increases with decrease in the load.

##### 6.2.1.3 BRAKE THERMAL EFFICIENCY

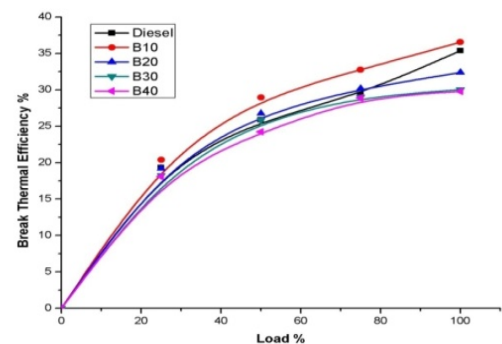


Figure 12: Variation of brake thermal efficiency with Load

The variation of brake thermal efficiency with load for different fuels is presented in Fig.12. In all cases, it increased with increase in load. This was due to reduction in heat loss and increase in power with increase in load. It is observed that the maximum efficiency for B10 blend was higher BSEC as compared to diesel. It shows an comparable Performance with biodiesel addition of 10%. The brake thermal efficiency obtained for B20, B30, and B40 were less than that of diesel. The decrease in brake thermal efficiency for higher blends may be due to the combined effect of its lower heating value and increase in fuel consumption. This drop in thermal efficiency with increase in proportion of mixed biodiesel can be attributed to the poor combustion characteristics of the blends due to their relatively high viscosity and poor volatility that overcomes the excess oxygen present in the biodiesel and due to coarse spray formation and poor atomization and mixture formation of biodiesel during blending. This lower brake thermal efficiency obtained could be due to reduction in calorific value and increase in fuel consumption as compared to B10.

### 3.3 EMISSION CHARACTERISTICS

#### 3.3.1 CARBON MONOXIDE EMISSIONS

The variation of Carbon monoxide Emissions with load for diesel fuel, biodiesel and blends B10, B20, B30 and B40 is shown in the Fig

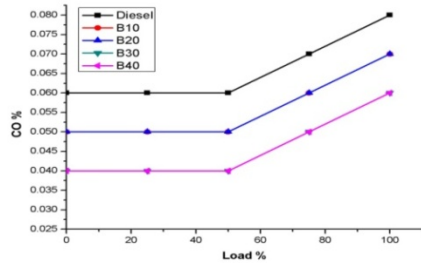


Figure 13: Variation of CO with Load

Variation of CO emissions with engine loading for different fuel is compared in Fig. The minimum CO produced was found by increasing blends of milk scum Biodiesel and it was observed that a reduction order as compared to diesel. Also It is observed that the CO emissions for biodiesel and its blends are lower than for diesel fuel. These lower CO emissions of biodiesel blends may be due to their more complete oxidation as compared to diesel. Some of the CO produced during combustion of biodiesel might have converted into CO<sub>2</sub> by taking up the extra oxygen molecules present in the biodiesel chain and thus reduced CO formation. It can be observed from Fig. that the CO initially decreased with load and later increased sharply up to full load. This trend was observed in all the fuel blend tests.

#### 3.3.2 HYDROCARBON EMISSIONS

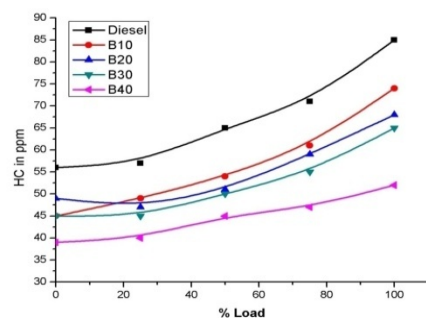


Figure 14: Variation of Hydro-carbon with Load

The hydrocarbons (HC) emission trends for blends of methyl esters oil and diesel are shown in Fig. B40 has least HC emission in all cases and in blends, B10 shows the lower HC emission compared to neat diesel at full load. The reduction in HC was linear with the addition of biodiesel for the blends tested. A reason for the reduction of HC

emissions with biodiesel is the oxygen content in the biodiesel molecule; these reductions indicate a more complete and cleaner combustion. The presence of oxygen in the fuel was thought to promote complete combustion. There is a reduction from 70 ppm to 45 ppm was obtained resulting in B40, as compared to diesel at the maximum load.

#### 3.3.3 CO<sub>2</sub> EMISSIONS

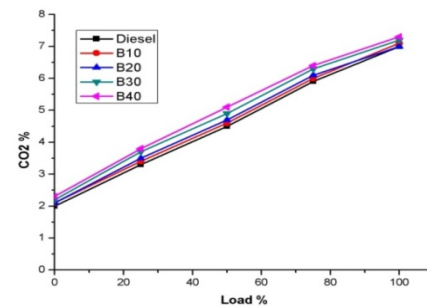


Figure 15: Variation of CO<sub>2</sub> v/s load

The carbon dioxide emission from the diesel engine with different blends is shown in Fig. CO<sub>2</sub> emission increases linearly as the load increases, which were higher than in case of diesel. the maximum CO<sub>2</sub> emission was found in B20 at full load because of complete combustion of fuel as compared to fossil diesel. The CO<sub>2</sub> emissions of all other blends were also higher than the conventional fossil diesel this is due to because of unburnt gases.

#### 3.3.4 O<sub>2</sub> EMISSIONS

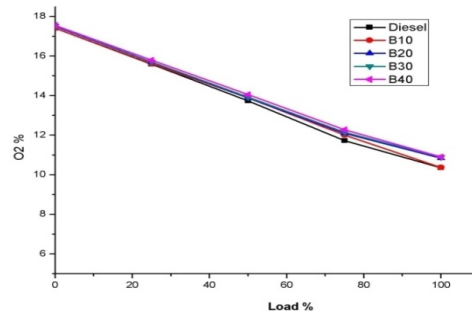


Figure 16: Variation of O<sub>2</sub> v/s load

For methyl ester and its blends, the graph indicated that the O<sub>2</sub> level is comparatively higher in all blends compared to diesel. At all load condition, B40 shows increasing trend with diesel fuel. Level O<sub>2</sub> of for blends of was slightly in increasing order as blend ratio increased. This may be due to the fact that fuels are oxygenated. The fuel have more oxygen content inherent in itself may be the cause of higher O<sub>2</sub> level, compared to diesel. The higher O<sub>2</sub> level in fuel blends is always preferred.

### 3.3.5 NOX EMISSIONS

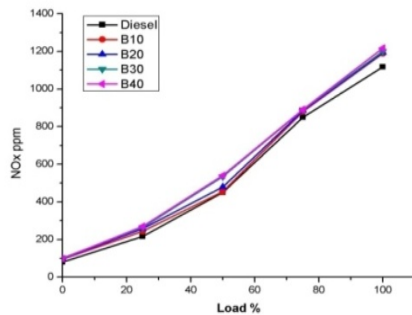


Figure 17: Variation of oxide of nitrogen with Load

In the Figure 17 indicates the NO<sub>x</sub> emission based on temperature trends for mixed biodiesel blends and diesel at different engine loads. The increase in the local temperature and the oxygen concentration within the fuel spray envelope at increasing power level favours the increase in NO<sub>x</sub> emissions. The NO<sub>x</sub> emissions of the blend were slightly higher than those of the diesel fuel at both full and partial loads. The higher temperatures of combustion and the presence of fuel oxygen with the blend caused higher NO<sub>x</sub> emissions. The nitrogen oxides emissions formed in an engine are highly dependent on combustion temperature, along with the concentration of oxygen present in combustion products. By comparing all the Blends B10 was emit less oxide of nitrogen.

### CONCLUSION

The overall studies based on the production, fuel characterization, engine performance and exhaust emission of Scum biodiesel and its blends B10, B20, B30 and B40 were successfully carried out. The following conclusions can be drawn, the production of Scum biodiesel methyl esters is a two stage transesterification process approximately 150 ml of methanol can be recovered. The time required to produce 860ml of biodiesel is 7 hrs and the blending stability time is 24 hours. Cost of one litre scum biodiesel = 44 rupees. The CV of blends was found to be less than the fossil diesel. The specific gravity of biodiesel B100 and it is more than fossil diesel. The maximum BSFC was found in B40 and it is 23% higher than the diesel. The heat content of pure B40 was lower than diesel. Due to these reasons, the BSFC for blends, namely B10, B20 and B30 were also higher than that of diesel. The BSEC for all blends was higher than that of diesel. This trend was observed due to lower

calorific value, with increase in biodiesel percentage in blends. The maximum BSEC was found in B40. Minimum BSEC was B10. The maximum thermal efficiency is for B10 (2.7%) was higher than that of diesel. The brake thermal efficiency obtained for B20, B30, and B40 were less than that of diesel. The blend of 10% also gave minimum brake specific energy consumption. Hence, this blend was selected as the optimum blend for further investigations and long-term operation. The minimum CO emission produced was found in B40 and it was observed that are reduction of 50%, as compared to diesel. The HC emission shows a reduction from 70 ppm to 45 ppm was obtained resulting in B40 and it is 35%, as compared to diesel at the maximum load. CO<sub>2</sub> emission increases linearly as the load increases, the maximum CO<sub>2</sub> emission was found in B40 because of complete combustion of fuel as compared to fossil diesel and The biofuel have more oxygen content inherent in itself may be the cause of higher O<sub>2</sub> level, compared to diesel. The higher O<sub>2</sub> level in fuel blends is always preferred. The amount of NO<sub>x</sub> produced for B40 was found to be little higher when compared to diesel.

### REFERENCE

1. "Opportunities And Challenges For Biodiesel Fuel" By Lin Lin , Zhou Cunshan , Saritporn Vittayapadung , Shen Xiangqian , Dong Mingdo, 28 September 2010, Applied Energy Volume 88, Issue 4, 88 (2011) 1020–1031 Sciencedirect.
2. "Performance And Emission Studies On Port Injection Of Hydrogen With Varied Flow Rates With Diesel As An Ignition Source" Applied Energy 87 (2010) 2218–2229 Sciencedirect.
3. "Biodiesel: An Eco-Friendly Alternate Fuel For The Future" – A Review By Lakshmanan Singaram Review Paper Udc: 662.756:547.1-326 Doi: 10.2298/Tsci0903185s, Thermal Science: Vol. 13 (2009), No. 3, Pp. 185-199
4. "Impact of using B100 Biodiesel in Ship Engines" by Kamolpatara Limratana, Sompong Pichetpinyo, Tanet Aroonsrisopon, Kasetsart J. (Nat. Sci.) 44 : 1191 - 1200 (2010)

# PRODUCTION, PURIFICATION AND EVALVATION OF DIFFRERNT PLASTIC BIO FUEL BLENDS FROM MUNICIPAL WASTE PLATICS

Naveen Kumar P  
 Dept Of Mechanicale Engg  
 (Affiliationof JNTUH)  
 Narsimha Reddy Engg College  
 (Affiliationof JNTUH)  
 Hyderabad Telangana, India  
 naveenmtpbiet@gmail.com

Rajesh S  
 Dept Of Mechanicale Engg  
 (Affiliationof JNTUH)  
 Narsimha Reddy Engg College  
 (Affiliationof JNTUH)  
 Hyderabad Telangana, India  
 rajesh.sc32@gmail.com

D Krishnaveni  
 Dept Of Mechanicale Engg  
 (Affiliationof JNTUH)  
 Narsimha Reddy Engg College  
 (Affiliationof JNTUH)  
 Hyderabad Telangana, India  
 krishnaveni.mechanical@gmail.com

**Abstract—** As we know that world getting modernizing and industrializing day by day. Plastics have been one of the materials with the fastest growth because of their wide range of applications due to versatility and relatively low cost. The duration of life of plastic products is relatively small, there is a vast plastics waste stream that reaches each year to the final recipients creating a serious environmental problem. Environmental concerns and fast depletion of petroleum fuels have caused the search for alternate fuels for internal combustion engines. Waste plastics are indispensable materials in the modern world and application in the industrial field is continually increasing. In this context, waste plastics are currently receiving renewed interest. As an alternative, non biodegradable, and renewable fuel, waste plastic oil is receiving increasing attention. The waste plastic oil was compared with the petroleum products and found that it can also be used as fuel in compression ignition engines.

Increase in energy demand, stringent emission norms and depletion of oil resources have led the researchers to find alternative fuels for internal combustion engines. On the Other hand waste plastic poses a very serious environment challenge because of their disposal Problems all over the world. In this paper an attempt has been made to investigate the production of waste plastic into liquid fuel by using pyrolysis process, a pyrolysis unit is designed, fabricated and evaluated for various kinds of plastic wastes, properties of liquid Fuels obtained are determined. Blending with diesel fuel is done.

**Keywords—** Biofuel, Diesel fuel, Low density polyethylene (LDPE), Plastic fuel (PF)

## I. Introduction

Plastic were invented in 1860, but have only been widely used in the last 30 years .Plastic are light, durable, modifiable and hygienic. Plastic are made of long chain of molecule called polymers. Polymers are made when naturally occurring substance such as crude oil or petroleum are transformed into other substance with completely different properties. These polymers can then be made into granules, powders and liquids, becoming raw materials for plastic products.

Plastics have become an indispensable part in today's world. Due to their lightweight, durability, energy efficiency, coupled with a faster rate of production and design flexibility, these plastics are employed in entire gamut of industrial and domestic areas. Plastics are produced from petroleum derivates and are composed primarily of hydrocarbons but also contain additives such as antioxidants, colorants and other stabilizers. Disposal of the waste plastics poses a great hazard to the environment and effective method has not yet been implemented. Plastics are non-biodegradable polymers mostly containing carbon, hydrogen, and few other elements like nitrogen. Due to its non biodegradable nature, the plastic waste contributes significantly to the problem of waste management. According to a nationwide survey which was conducted in the year 2000, approximately 6000 tonnes of plastic waste were generated every day in India, and only 60% of it was recycled, the balance of

40% could not be disposed off. Today about 129 million tonnes of plastics are produced annually all over the world, out of which 77 Million tones are produced from petroleum.

In India alone, the demand for plastics is about 8 million tonnes per year. More than 10,000 metric tonnes per day of plastics are produced in India and almost the same amount is imported by India from other countries. The per capita consumption of plastics in India is about 3 kg when compared to 30 kg to 40 kg in the developed countries. Most of these come from packaging and food industries. Most of the plastics are recycled and sometimes they are not done so due to lack of sufficient market value. Of the waste plastics not recycled about 43% is polyethylene, with most of them in containers and packaging. Continuous innovation explains that, plastics production has increased by an average of almost 10% every year on a global basis sinc1950

## II. Types of plastics

The types of the waste plastics are LDPE, HDPE, PP, PS, and PVC [10]. The problems of waste plastics can't be solved by land filling or incineration, because the safety deposits are expensive and incineration stimulates the growing emission of harmful greenhouse gases like COx, NOx, SOx and etc. These types of disposal of the waste plastics release toxic gas; which has negative impact on environment.

plastic wastes can also classified as industrial and municipal plastic wastes according to their origins, these groups have different qualities and properties and are subjected to different management strategies. Plastic wastes represent a considerable part of municipal wastes; further more huge amounts of plastic waste arise as a by-product or faulty product in industry and agriculture. the total plastic waste, over 78% weight of this total corresponds to thermoplastics and the remaining to thermosets [10]. Thermoplastics are composed of polyolefins such as polyethylene, polypropylene, polystyrene and polyvinyl chloride and can be recycled. On the other hand thermosets mainly include epoxy resins and polyurethanes and cannot be recycled.

## II.Objectives of the paper

- collection and washing of plastic waste
- drying and storing of plastic waste
- design and fabrication of pyrolysis unit.
- production of plastic liquid bio fuel from municipal waste plastics
- evaluation of produced liquid fuel properties.
- evaluation of produced liquid fuel properties such as
  1. flash point.
  2. fire point
  3. viscosity.
  4. density.
  5. calorific value

## III. METHOD AND METHODOLOGY

Following two major methods are used to converting plastic wastes into useful products such as fuels

- A. Thermal pyrolysis
- B. Catalytic pyrolysis

**A. Thermal pyrolysis**

The non-catalytic or thermal pyrolysis of plastic is a high energy, endothermic process requiring temperatures of at least 350° C–500° C. Thermal cracking or Pyrolysis, involves the degradation of the polymeric materials by heating in the absence of oxygen [1]. The process is usually conducted at temperatures between 350° C and 500° C and results in the formation of a carbonized char (solid residues) and a volatile

**B. Catalytic pyrolysis**

Addition of catalyst enhances the conversion and fuel quality. As compared to the purely thermal pyrolysis, the addition of catalyst in pyrolysis. Significantly lowers pyrolysis temperatures and time. A significant reduction in the degradation temperature and reaction time [1] under catalytic conditions results in an increase in the conversion rates for a wide range of polymers at much lower temperatures than with thermal pyrolysis. Narrows and provides better control over the hydrocarbon products distribution in Low density polyethylene (LDPE), High density polyethylene (HDPE), polypropylene [5] and polystyrene pyrolysis. While thermal pyrolysis, results in a broad range of hydrocarbons ranging from C5 to C28, the selectivity of products in the gasoline range (C5, C12) are much more enhanced by the presence of catalysts. Again, oils obtained by catalytic pyrolysis contain less olefins and more branched hydrocarbon and aromatic content. Increases the gaseous product yields. Under similar temperatures and reaction times, a much higher gaseous product yield is observed in the presence of a catalyst for plastic wastes [3].

In this papers going to use catalytic pyrolysis method to convert waste plastic into bio fuel. Mainly two catalysts are used such as dry ash powder and dry wood powder. Dry ash powder mainly consists of carbon content that accelerate the chemical reaction and dry powder helps to catch the fire easily and enhance the conversion of plastic waste into bio fuel compounds.

**C. RAW MATERIALS USED TO PRODUCE PLASTIC LIQUID FUELS**



Fig.1: Different municipal waste plastics

**C. Fabrication of plastic pyrolysis unit.**

Pyrolysis unit developed from MS materials with 5mm thickness. By using arc and gas welding technology. The experiments carry out with high temperature and atmospheric pressure so unit must be withstanding to high temperature. Professional thermocouples, pressure gauge and safety valves are provided to reactor. Reactor welded by using gas welding to prevent the leakage of vapours. The safe and efficient pyrolysis unit is shown in the above Fig.2.



Fig 2: Pyrolysis unit



Fig.3.Gaseous product

Reactor welded by using gas welding to prevent the leakage of vapours. The safe and efficient pyrolysis unit is shown in the above Fig.2.

**D. Steps involved in process**

1. **Feeding-** Feed the feedstock's to reactor through feeder and closes the feeder inlet.
2. **Heating-** To increase the temperature of reactor, heat the product of reactor inside by using heating source.
3. **Condensing-** The plastic get evaporated at high temperature, this vapor is condensed to atmospheric temperature by using straight and spiral tube condensers.
4. **Liquid collection-** Out coming product from the condenser is collected at liquid collector. At the end of condenser provide a cyclone separator to separate the plastic liquid fuel and non condensible gases. These non condensible gases are reuses to heat the pyrolysis unit.
5. **Water wash, Purification and pH test-** This involves many purification processes. In this method we take equal proportion of plastic fuel and water in a container and shake well, allow it for 5-7 hours to settle down. Now water along with some crystals is collected at bottom and pure plastic fuel is collected at the top container.
6. **pH Test-** After purification measure the pH value of plastic fuel by using pH meter. If the pH is less than 7, the fuel is acidic in nature. It is needed to wash with water many times to bring pH value of oil to 7.

**IV. PUIFICATION AND FILTRATION OF RAW PALSIC FUELS**

**A.PURIFICATION SETUP**

In this method we are going to take equal proportion of plastic fuel and water in a container and shake well, allow it for 5-7 hours to settle down



Fig.4. purification setup



Fig 5: Waste Carbon Residue

After this water along with some crystals is collected at bottom and pure plastic fuels are collected at the top container. In mean time check the pH value of plastic oil by using pH meter if it is in acidic in nature it is needed to many times wash with water to bring the pH of oil to 7. Water washing tank along with control valve and water collection unit is shown in figure

**V.RESULTS AND DISCUSSION**

A. Following bio fuel yields are obtained for waste plastic by using a catalytic paralysis process.

Table: 1. Liquid fuel yields by using catalytic pyrolysis process

Type of condenser	Types of feedstock	Yield of liquid product	Residue
Straight Tube condenser	Plastic covers	45% – 58%	4.5% – 5%
	Medicine bottles	36% - 45%	4.5% - 6%
	Edible oil cover	66% - 70%	5.6% -6 %

**B. PLASTIC LIQUID FUEL AND ITS DIFFERENT BLENDS**



Fig.6: Plastic fuel



Fig.7: Different Plastic fuel blends

Shows the plastic liquid fuel obtained from the pyrolysis of waste plastics by catalytic pyrolysis process and different blends with diesel fuel.

**C. Evaluation of Fuel Properties**

Table.2: Properties of different blends with plastic liquid fuel and diesel.

All properties of plastic liquid fuel and its blends are tabulated in above table Properties of plastic liquid fuel and its blends satisfy the ASTM standards of fuel properties. By considering these factors we can use this plastic liquid fuel blends as a fuel for diesel engines.

PARAMETERS	PFO	PF10	PF20
------------	-----	------	------

Flash point (°C)	57	59	63
Fire point (°C)	59	62	66
Kinematic viscosity at 40°C (mm <sup>2</sup> /s)	2.83	4.585	4.782
Density at 40°c (kg/m <sup>3</sup> )	812	815.6	817.4
Calorific value (MJ/kg)	44.81	43.07	42.71

**VI. Conclusion**

The Polymer Energy system uses a process called pyrolysis to efficiently convert plastics into liquid fuel compounds. The conversion of municipal waste plastics to liquid hydrocarbon fuel was carried out in thermal and catalyst degradation. This method is superior in all respects (ecological and economical). By adopting this technology, efficiently convert weight of municipal waste plastics into 65% of useful liquid hydrocarbon fuels without emitting any pollutants. It would also take care of hazardous plastic waste and reduce the import of crude oil. Depletion of non-renewable source of energy such as fossil fuels at this stage demands the improvements of this technique.

1. The properties of the blends PF20, PF40 and PF60 and others blends are determined by various tests and experiments shows that it can be a good source of alternative for diesel.
2. Since it is waste raw material it can be used without extra cost.
3. Biodiesel fuel and their different blends burn clearly and completely as that of the pure diesel.
4. The biodiesel obtained from different plastics will clear and satisfactory.
5. Plastic fuel and their different blends produce about lesser carbon monoxide and unburnt hydrocarbon emissions than diesel fuel, while nitrogen oxide emissions are higher than diesel fuel.
6. The production of plastic fuel from different plastics on a large scale can be beneficial economically.

**REFERENCES**

[1] Achyut K. Panda R.K. Singh D.K. Mishra [et al.]. Thermolysis of waste plastics to liquid fuel .A suitable method for plastic waste management and manufacture of value added Products A world prospective, 2009;1-6:1011

[2] Adriana L. Clementz, Nora R. Aimaretti, Debora Manuale, Agustin Codevilla, Juan C. Yori, Optimization of ethanol fermentation from discarded carrots using immobilized *Saccharomyces cerevisiae*, IN J Energy Environ Eng, 9 December 2014.

[3] A. Lopez I. de Marco, B.M. Caballero, M.F. Laresgoiti, A. Adrados [et al.]. Pyrolysis of plastic packaging waste: A comparison of plastic residuals from material recovery facilities with simulated plastic waste.

- [4] *N. Miskolczi , A. Angyal , L. Bartha , I. Valkai [et al]*,done the experiments on fuels by pyrolysis of waste plastics from agricultural and packaging sectors in a pilot scale reactor.
- [5] *Scott DS, Czernik SR, Piskorz J, Radlein[et al.]*.Fast pyrolysis of plastic. Energy and Fuels 1990
- [6] *Mohammad NahidSiddiquia, Halim Hamid Redhwi[et al.]*.Pyrolysis of mixed plastics for the recovery of useful products
- [7] *Muralidhar PawarHarshal R. and LawankarShailendra M.[et.al]*.done the experiments on Waste plastic Pyrolysis oil Alternative Fuel for CI Engine.

# EVALUATION OF MECHANICAL PROPERTIES GLASS FIBER REINFORCED HEMATITE FILLED HYBRID COMPOSITES

Venkatesh  
 Dept Of Mechanical Engg  
 (Affiliation of JNTUH)  
 Narsimha Reddy Engg College  
 (Affiliation of JNTUH)  
 Hyderabad Telangana, India  
 venkat.rs416@gmail.com

Rajesh S  
 Dept Of Mechanical Engg  
 (Affiliation of JNTUH)  
 Narsimha Reddy Engg College  
 (Affiliation of JNTUH)  
 Hyderabad Telangana, India  
 rajesh.sc32@gmail.com

A.YV Ravikumar  
 Dept Of Mechanical Engg  
 (Affiliation of JNTUH)  
 Narsimha Reddy Engg College  
 (Affiliation of JNTUH)  
 Hyderabad Telangana, India  
 ravikumar.ssit@gmail.com

**Abstract**—As we know that today world developed technically. In current trend most of the organizations focusing on preparing the objects by higher strength, hard materials for getting more life. Metals, Alloys Steels are the answer for the High Strength materials utilize for the preparing the useful things. But metals and alloys etc. has some disadvantages such as cost and weight etc. Composite materials are the answer for the other high strength materials at less weight with superior property.

In case of composites glass fiber reinforced composites (GFRP) are played crucial role due to its versatility. In this paper experiment investigation were conducted on four GFRP laminates. These laminates were prepared by adding hematite filler in different volume fraction during preparations. Then comparisons are made between these laminates according to tensile, impact and hardness strength found by testing the specimen mechanically.

**Keywords**—Glass fiber, polymer matrix, filler, laminates.

## I. Introduction

In current trends lot of innovations are made in case of preparing the materials for getting high strength materials at less weight and easy cost. Composites are the answer for that problem.

Composites are the materials are become an indispensable part in today's world. Due to their lightweight, durability, energy efficiency etc. These Composites are employed in entire world like plastics. Composites has been utilized from B.C. In the present era the composite raises its concentration among users due to its plenty of applications. The composite materials formed by the addition of multiple materials that gave the extraordinary properties such as low heaviness, tough rigidity etc. it have two main parts. That is matrix phase and reinforcement phase. The matrix is continues phase which surrounds the reinforcement phase.

**Matrix phase:** it is the main phase which poured on the reinforcement to give proper strength to the fibers. matrix has mainly three types that is polymer, ceramic, metallic matrix.

**Reinforcement:** it is also the main phase which provides the strengthening of composite material. The variety of fibers used in composites used, such as carbon fiber reinforcement and glass fiber reinforcements.

## II. Types of composites

### Polymer Matrix Composites (PMC)

It is more well-known class of composite than the other material as compared to the other matrix composites. This composite prepared by using polymer resin as matrix. This composite can survive elevated temperature. PMC has two types thermosetting and thermo plastic materials.

### Metal Matrix Composites (MMC)

As the name indicates it is formed by the metal matrix like aluminum, magnesium, copper ferrous etc. these are huge strength, low density and excellent stiffness. These materials can sustain high temperature than other matrix materials. Due to these properties it creates broad attention among people.

### Ceramic Matrix Composites (CMC)

Ceramic composites are fabricated by ceramic matrix and fixed fibers of additional ceramic fibers. These composites strong ionic bonding. It has decay resistance, high steadiness of temperature good strength. These are all the majorly use in elevated temperature applications. The news trends in industrialization, new techniques, require of excellence products are increased the expansion of ceramic products.

### Based on Reinforcement

Multi-layer composite consist several layers of fibrous composites bounded together by organic adhesives. After the joining of several look like layers the laminate can formed. The constituent materials in each layer are called laminates. If multi-layer composite is made up of layers of different constituent materials. They are called hybrid composites.

### Particulate reinforced composite

These composites are of particle in character. It has the irregular or regular shapes. Here size of particle varies from 1mm or more and volume concentration varies from 20 to 40% volume. Because of slightly bigger size particle, they can't interfere with dislocation and exhibit strengthens effect by hydrostatically restraining the movement of matrix close to it. In this category particle filler utilize in composites broadly used in minimizes contraction, get better machinability, get quality products, and also reduce friction and wear.

### Fiber Reinforcement

Fibrous composites this can be utilize for prime reason is little cross sections. In this case the matrix helps to join the fibers, transfer the loads, provides defense against ecological barriers and devastation due to improper handling. fibers are extremely influential in enhancing the break resistance of the material. fibers due to their little cross-sectional size, are not straight forwardly usable in engineering applications.

These FRC can be utilized as bullet proof jackets, automobile

### Laminates

Laminates or Multi-layer composite consist several layers of fibrous composites bounded together by organic adhesives. When many such same or different layers are bound jointly, constitutes multi-layer composites. The constituent materials in each layer are called laminates. If multi-layer composite is made up of layers of different constituent materials. They are called hybrid composites.

## II. Objectives of the paper

- Preparation of the hybrid composite by using glass fibre and polymer matrix and filler in various proportions in laminates.
- Conducting delamination tests in UTM for evaluation of mechanical properties. such as
  1. Hardness.
  2. Tensile strength.
  3. Impact strength.

## III. MATERIALS

- i. Polymer Resin (Matrix)
- ii. E-Glass fibre
- iii. Hematite ore
- vi. Methyl ethyl cobalt catalyst

**III.METHOD AND METHODOLOGY**

Following two major methods are used to preparing laminates of the composite materials from hand lay-up method.

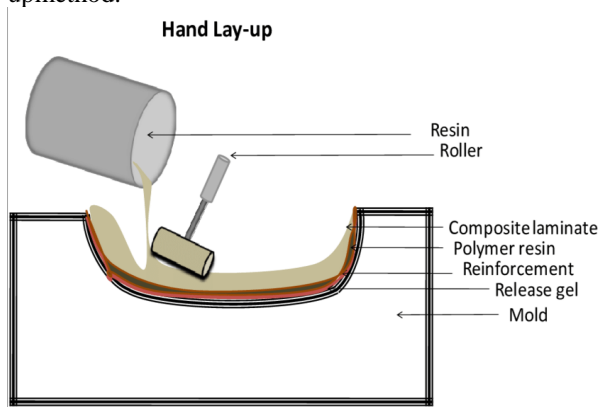


Fig III.1 hand layup method

Hand lay-up is the simplest method of preparing the composite materials due to less maintenance easy methods along with flexibility in preparation of different shapes. Steps involved in this process

- i) First apply the get coating on the mould.
- ii) A coat of Polymer resin mixed with catalyst is applied on the mould by using brush.
- iii) Then place the one set of E-glass fiber on the fibers on mould in 90° orientation.
- iv) Then polymer resins are applied to the reinforcement fibers and also remove the trapped air between the fibers and resin combination by using the roller.
- iv) Then place another set of fiber in 45° orientations. Repeat the same procedure for applying the resin.
- v) After that repeat the fibers placing and repeat the applying the resin up to getting required thickness.
- vi) After getting required thickness allow the resin to cool to become perfect solid.
- vii) Finally demould the product from the mould. Then trimmed it according to the size.
- viii) Reinforce material should be used i.e. base material as E-glass fiber(mesh type) and matrix material as GP resin by the varying volume fraction of the GP resin (matrix material) and adding the filler material as iron ore. The proportionate of varying as show in the table below.

composites ±90°	Composites± 45°	% of filler	Matrix volume %		Reinforcement volume %	
A	A1	0	Polymer resin	50	Glass fiber	50
B	B1	6	Polymer resin	44	Glass fiber	50
C	C1	9	Polymer resin	41	Glass fiber	50
D	D1	12	Polymer resin	38	Glass fiber	50

TABLE III.1 THE PROPORTIONATE CONSTITUTES OF THE LAMINATES.

The cured materials are cut to yield test specimens in accordance of ASTM standards. Tensile test has been carried out according to

ASTM D 3039, Impact test has been conducted ASTM E23 and Hardness has been measured in terms of B.H.N. value accordance of ASTM E10.

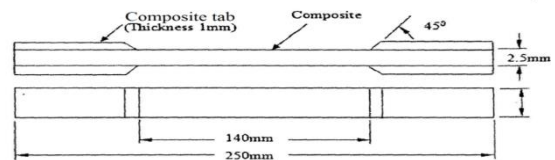
In this present work the three variables are varied.

- 1) Orientation of fiber material (90°, 45°)
- 2) Volume fraction of filler material.
- 3) Matrix volume.

Totally the eight laminates are prepared by varying above variables and designated as (A, B,C,D) for 90° and (A1,B1,C1,D1) for 45°.

**EXPERIMENTATION  
TENSILE TEST**

Tensile test was conducted on according to ASTM D3039, under displacement control using an UTM/E-40. Test specimen were well filed to attain overall length and gauge length of 250 and 140mm respectively and an appropriate cross sectional area of 25×3 mm<sup>2</sup> and aluminum tabs with dimensions of 55×25×2 mm with 45deg filing is done at the one end is glued as shown in Fig 5.1



FigIV.1 tensile test specimen as per ASTM D3039 standards.

**BRINELL HARDNESS TEST**

Hardness is firmly identified with quality. It is the property of a material to avoid scratching, dispersion. It is straight forwardly hardness measuring machines. the resistance of the material against indentation of an indenter of extraordinary shape and material under a given load. Through using Vickers, brinell, rockwell machines we can easily get hardness. The test led on Brinell hardness machine, according to the ASTM models the specimen readied according to ASTM E10. A weight of 100 kg was apply on the example for half minute utilizing ball indenter. the dia of indenter mark across was measured by utilizing a magnifying instrument. The hardness was measured at three unique areas of the example and the mean was calculated. The indentation was measured and hardness was computed utilizing equation.

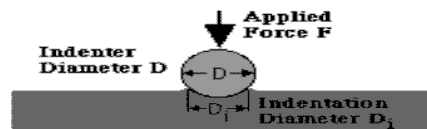
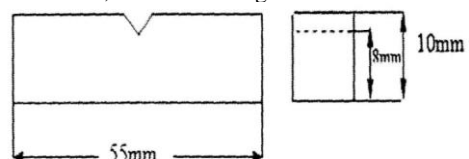


Fig.IV.2 Brinell hardness test

$$BHN = \frac{2P}{\pi D [D - \sqrt{D^2 - d^2}]} \dots\dots\dots (5.1)$$

**IMPACT TEST**

Impact test specimens are tested as per specification of ASTM 32 Standards, the dimensions of the specimen are 10mmx10mmx55m m of size, on one side surface of the specimen a V-notch is been made at an angle of 45de g with root depth of 2mm, as shown in Fig



**Fig IV.3 charpy impact test specimens as per ASTM E23 standards**

The test piece is simply supported at each end on anvils 40mm apart. A large pendulum is supported toward one side in a direction on the casing of the machine, and a striker is arranged at the other end. The pendulum in its at first raised position has an available energy of 300J and on discharge swings down to strike the example quickly behind the notch, bending and cracking in between the backings . A scale and pointer show the energy required during impact on specimen.

**V.RESULTS AND DISCUSSION**

In the wake of accomplishing eight different sorts of Hybrid overlays were fabricated, four of the Hybrid were  $\pm 45^\circ$  arranged composites and other four were  $\pm 90^\circ$  situated composite. Among four one laminate was fabricated without filler and rest other with varying filler. Various characterization test were conducted and their results are depicted in table and are discussed in the following sections.

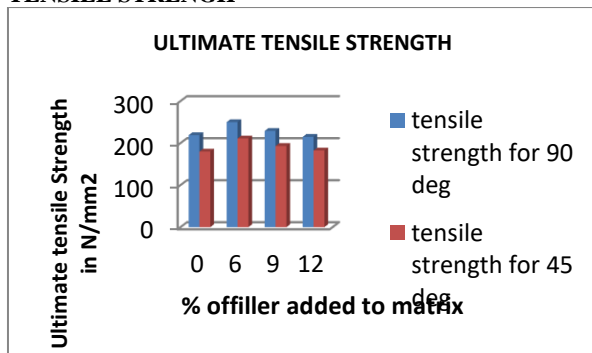
Sl.No	% of filler	Composites description for $\pm 90^\circ$	$\pm 90^\circ$ composites Mechanical properties		
			Uts (N/mm <sup>2</sup> )	BHN	IS (J/mm <sup>2</sup> )
01	0	A	219	73	2.15
02	6	B	250	83	2.40
03	9	C	229.10	80	2.19
04	12	D	215.	72	2.13

Table5.1 mechanical properties fo 90 deg oriented laminates

Sl.No	% of filler	Composites description for $\pm 90^\circ$	$\pm 90^\circ$ composites Mechanical properties		
			Uts (N/mm <sup>2</sup> )	BHN	IS (J/mm <sup>2</sup> )
01	0	A1	180.01	64	1.7
02	6	B1	211.11	74	2.21
03	9	C1	193.21	69	1.80
04	12	D1	182.46	65	1.65

Table 5.2 mechanical properties fo 90 deg oriented laminates

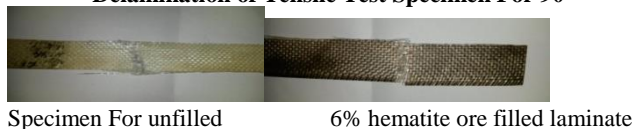
**TENSILE STRENGTH**



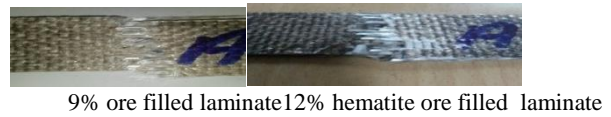
Graph V.1 tenile strenth by referring the above graph v.1

The composite developed with  $\pm 90^\circ$  oriented E-glass fiber reinforced and 6wt% of Fe<sub>2</sub>O<sub>3</sub> filled and polyester resin matrix shows more Tensile strength compared to other composites. The composite developed with  $\pm 90^\circ$  oriented E-glass fiber reinforced and 6wt% of Fe<sub>2</sub>O<sub>3</sub> filled and polyester resin matrix shows more Tensile strength compared to other composites.

**Delamination of Tensile Test Specimen For 90°**

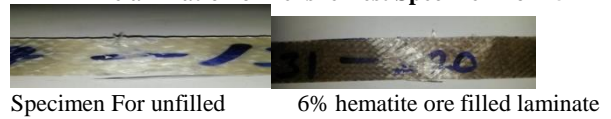


Specimen For unfilled 6% hematite ore filled laminate

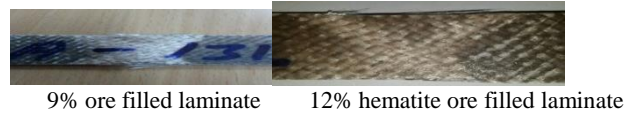


9% ore filled laminate 12% hematite ore filled laminate

**Delamination of Tensile Test Specimen For 45°**

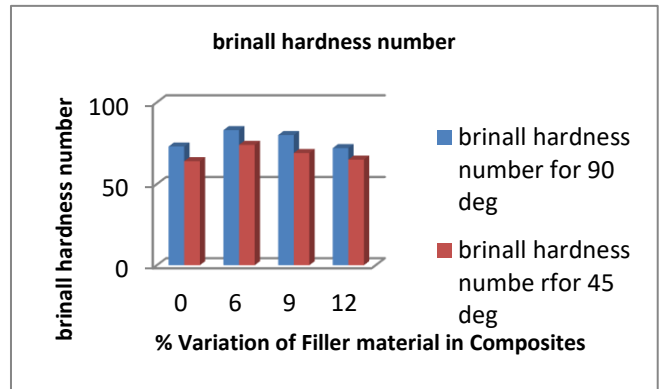


Specimen For unfilled 6% hematite ore filled laminate



9% ore filled laminate 12% hematite ore filled laminate

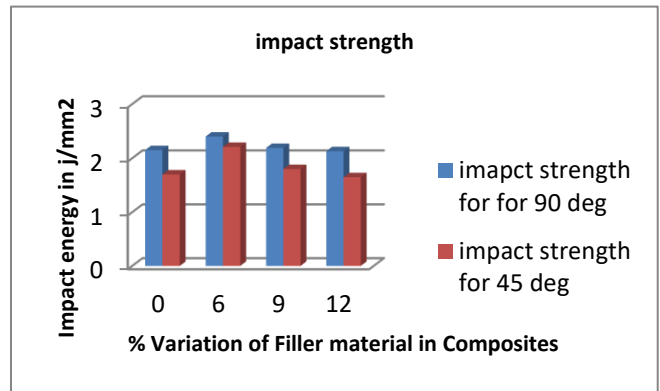
**BRINALL HARDNESS NUMBER**



Graph V.2 hardness number by referring the above graph v.2

The composite developed with  $\pm 90^\circ$  oriented E-glass fiber reinforced and 6wt% of Fe<sub>2</sub>O<sub>3</sub> filled and polyester resin matrix shows more Hardness Number compared to other composites.

**IMPACT STRENGTH**



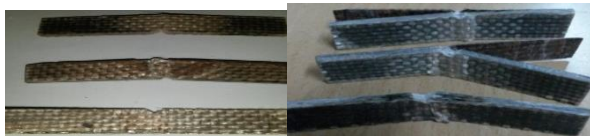
Graph V.3 impactstength by referring the above graph v.3

Thecompositedeveloped with  $\pm 90^\circ$  oriented E-glass fiber reinforced and 6wt% of Fe<sub>2</sub>O<sub>3</sub> filled and polyester resin matrix shows more Impact Strength compared to other composites

**Delaminationomn of impactImpact Test Specimen For 90°**



Specimen For unfilled 6% hematite ore filled laminate



9% ore filled laminate 12% hematite ore filled laminate

**Delamination of impact Impact Test Specimen For 45°**



Specimen For unfilled

6% hematite ore filled laminate



9% ore filled laminate

12% hematite ore filled laminate

**VI CONCLUSION**

In the current experimentation attempt, different categorization test were conducted over GFR-polyester-Hematite ore filled Hybrid composites. In general the expansion of fillers prompts cost and weight decrease of the general glass fiber fortified composites. The impact of the expansion of regular filler has been contemplated and it is reasoned that, the Tensile Strength, Hardness, Impact Strength of the composite B is better compared to other composites and at the 6wt% of filler content in both the orientations exhibits the good mechanical characterization.

**REFERENCES**

- 1) Rawlings 1999: Reid & Zhou 2000
- 2) Nakamura et al. 1991 a, Nakamura et al 1992
- 3) Katz HS & Milewski J V (eds) 1987 Handbook of fillers for plastics(Reinhold: on Nostrand)
- 4) Nikhil Gupta, Balraj Singh Brar & Eyassu Woldesenbet.
- 5) Maulida, M. Nasir, & H.P.S.A. Khalil, "Hybrid Composite Based on Natural Fiber" Proceedings of symposium on polymeric Materials, Penang, 1-2 June 2000 (Published by USM Press, Penang, 2000), pp
- 6) Manish Tewari, V.K Singh, P.C Gope & Arun k. Chaudhary
- 7) Satnam Singh, Pardeep Kumar, S.K. Jain.
- 8) Guu YH, Hocheng H Tai NH, Liu SY (2001) Effect of electric discharge machining on the characteristics carbon fiber reinforced carbon composites. J Mater science 36:2037-2043
- 9) Sonbaty EI, Khasaba UA, Machaly T (2004) factors affecting the machinability of GFR Epoxy composites. Composite structures 63:329-338

# “Golden Startup” – A New Business HUB Proposal

Elangovan Muniyandy  
Associate Prof., Mech. Engg.  
Vel Tech Rangarajan Dr Sagunthala  
R&D Institute of Sci. and Technology  
Chennai, India  
drmelangovan@veltech.edu.in

Indumathi A R  
Director, R & D  
GreenSHIP Research and Technology  
Bangalore, India  
admin@greenship.in

Nilesh J Sompura  
Director, Operation  
Shallow Waterways Shipping  
Gujarat, India  
info@3ewaterways.in

**Abstract**—Business is a technology based driven in this era. Fast development in the technologies leads to the automation of design, operation and manufacturing process. New generation are filled with technologies and bring more competition among the industries. Skilled man powers are involved in creative development using technologies in the companies and educational institutions. To increase the job opportunity, Government introduces a startup scheme to generate new entrepreneur by supporting finance and it provide a platform to reach market easily. These businesses are short term goal or achievement which is easily funded by private funding agencies. Here, Authors introduce a new business proposal to support creative idea which can produce a profit in a long term basis and getting fund needs more time and patient for the creator of product idea. Based on the experience, two cases have been studied in marine industry company and importance of “Golden Startup” is explained and can be taken for next level.

**Keywords**—business model, new approach, startup, micro model, young entrepreneur

## I. INTRODUCTION

“Startup” is category of new company to bring the idea or imaginary thought into a reality by innovation and development. This Government scheme supports validating a reliable product, improving process or services, and it can be a scalable business model with high potential of employment generation [1]. This is a new business model to meet the market needs with minimum investment and creates an opportunity to become young entrepreneur without business background. Startup India was initiated by Government of India on 15<sup>th</sup> August 2015, and this action plan for this initiative is based on i). Simplification and hand handling ii). Funding support and incentives and iii). Industry-academic partnership and Incubations. Based on certain conditions, “Startup” certificate is issued by the Department of Industrial Policy and Promotion (DIPP) for the registered company, and this certificate helps to get income tax exemption, trademark and patent application filing, public procurement, credit limit guarantee and self-certification compliance for the period of seven years.

Central government has initiated many incubation centers and encouraged private sector to establish a incubation centre to motivate a startup companies who are in need of infrastructure to place a team and need recognition in the market to reach customer. In most of the state, separate startup centre is created to provide an opportunity from the college students to young entrepreneur in terms of financial support in development of product and reaching the market with good support from an incubation centre. There are many private companies formed as

funding companies, which takes fund from various individuals and companies and this amount is provided to a potential company who has strong innovative ideas and thoughts for the development of product/service.

Presently, most of the incubation centre and funding agency/companies are extended their support to multimedia companies, Internet-based development for online shopping & market. Government has taken joined approach with different countries on development of agriculture, medical treatment and rural development field as seed funding for the development of innovative ideas to reach people and improve their standard of life. When it comes to marine industry, authors do not find companies coming forward to encourage this kind of initiative. Marine industry is a unique field which does not connect directly to human life and marine indirectly supports human society in transportation and petroleum products development. When compare to other industries, marine industry needs more development to use latest technology like cloud, the Internet of things and artificial intelligence from design to operation of ship. Similar study can be extended for other domain so that needy development can be identified.

## II. STARTUP IN INDIA

This startup is promoted for the easy start of companies with less investment which encourage non business background people can do business. To start a a small business, steps were given in report [2] which might help every new entrepreneur. From the government policy, It is possible to get an foreign investment and it creates job creation and skill development. Government of India has created a platform to communicate among startup companies, incubators, mentors, corporate and investors as “Startup HUB”. Under this startup umbrella, financial support is split into different channel/stages based on the entrepreneur idea/product status. IN General, most of the business can be categorized as design, manufacturing and service. For the design startup companies, factor affecting the design startup are discussed [3].

### A. Incubator(s)

Incubator is a company who support in providing space to setup an office and to execute minimum services at the initial period for the startup companies. Some incubator can support in financially but depends on the future of that business. In addition to that support is offered for marketing, material preparation for services, helping in strategy to grow the business by providing free consultancies. This business incubator help for the period of maximum three years and after the development, separate office will be provided outside the incubation centre.

### B. Mentor(s)

Mentor is an expert in particular domain who is ready to support start-up companies for the development. Incubator companies request for registration of mentor from different domain expert and are used for the consultancy to offer start-up companies business meeting. Getting a mentor is difficult task for start-up companies and that has been taken care by incubator by adding as a mentor. Mentor can be anywhere from India and outside India also. Maximum support is assured that start-up companies reaching to the targeted business growth.

### C. Corporate(s)

Corporate have been linked with start-up platform to have easy communication among all stakeholder. Recently many corporates have come out with requirements to improve the corporate business technology development using start-up companies talent. Business development talks are provided from corporate to enrich the startup companies in business development and supporting in critical issues during the development. It is also pointed that to compete with many companies, changing from individual to collaborative can bring more success [4]. This has been observed in current business strategy and most of the cases, small companies are bought big companies.

### D. Accelerator(s)

This is another kind of support for the startup companies who have the product ready at the initial stage. In that case, an accelerator helps from marketing material preparation to reaching the market and achieving the set target.

### E. Pitching

This is a program organized by an investor to support financially for the selected start-up companies. Invitation is sent to all start-ups who are all willing to take financial support for the development of their products or services. Here investor comes with an expert in different domain and based on the idea or innovation of the product, considering the need in market, start-ups are selected to provide a financial support. Many state governments also organize similar programs to create a job opportunity and economic development to the society.

## III. NEED OF GOLDEN STARTUP

It is observed that many startup companies are started in recent years and many startups are given financial & space support by incubation centres. Many projects are supported because of the return period to get revenue. It is expected to get the revenue in three to six months which does not involve in any research period. In some cases, it is necessary to validate the concept by adopting different technologies. Student can become employee and entrepreneur by understanding the incident, relationships and process in business development cycle [5]. There are some concepts that need more development time in which the revenue comes after one or two years. This kind of projects are not supported or given some reason to improve the concept to the next level of completion to proceed further.

Recently, it is observed that most of the research works are done using software and this software is purchased from other countries. Our companies/institutions are ready to buy and

not ready to develop by ourself. Is it not possible to develop in India. Yes it is possible but it cannot work in India because immediate revenue is expected after the investment. Indian investor is looking for quick return of money. Though, the product/software is good for long term. It is observed in many domains, same situation exists and this needs to be eradicated by our country. Otherwise each and every product or software, India needs to depend on other countries.

In the marine industry, all software is purchased from other countries paying few lakhs dollar every year. Same way, development of idea into product. To support this kind of long term based development, Government can take initiative to support. Two companies were studied on this need and observed that without funding, there is development for last two years. Owner has invested for two years to run with minimum people expecting investor. Now that companies are in a position to close that idea and look for some other business.

## IV. WORKING OF GOLDEN STARTUP

Presently each application is scrutinized by incubation centres and it is accepted if it is within their budget. All incubation centres are under control of central government department. When the proposal is based on long term and it is surely competitive to the world, this can be recommended to government. Government can have another seed fund called as "Golden Startup". This kind of project / proposal / idea / product can be supported from this fund which can be used for any domain.

## V. STARTUP IN MARINE INDUSTRY

Many schemes are introduced by government of India to support and encourage startup companies through different ministries and corporates. Most of the domains are related to information technology, internet of things, electronics, agriculture, technology hardware, automotive, renewable energy, non renewable energy, clean energy, green energy, telecommunication, health care, life science and rural development. In authors knowledge, very few companies are started in marine industry under start-up. Author had an opportunity to meet two marine start-up companies (i) GreenSHIP Research and Technology and (ii) Shallow waterways Shipping but the practical situation is different from the paper news. For other industry, there are many corporate support and incubator from big companies to utilize the new idea and innovation. Whereas for the marine industry, incubator and financial support needs to be improved in India.

### A. Need of Marine Incubation Center

Recently, Indian Register of Shipping (IRCLASS) in partnership with Siemens and Ministry of Shipping, to build competency in the field of maritime & shipbuilding start-up is started as "Centre of Excellence in Maritime & Shipbuilding (CEMS)". This start-up is mainly targeted to provide training in more than 24 labs under one roof and it is good opportunity to get trained for better quality experience in marine industry. Marine/shipping is an international business and small development can be utilized all over the world. When compared to other domains like satellite, telecommunication, system hardware and software development, marine industry development is less. There are

opportunity to improve the design and operation using latest technology but it happens in locally within company. It is not easy to accommodate all expert in one company for any development. Current world, everyday new technology or improvement which needs to be updated to get the full strength of development.

To improve the marine design and operation, authors recommend to have incubation centre to accommodate start-up companies by providing space for office and easy to provide mentor service because of enormous experts in every companies. Technology is going to lead the world and by adopting the latest technologies in marine industry, marine services can be offer best price and whole world can get benefit.

### VI. CASE (I) GREENSHIP RESEARCH AND TECHNOLOGY

This company was started in 2015 to provide the ship operation solution to operate the ship more economically by providing trim curve services to operate the vessel with optimum trim and provide route optimization and speed optimization services. As the company has an expert on this services but financially not strong enough. They approached few corporate to offer a service and ask for financial support for the development of new products. Company is ready to accept the trim curve service because of technical competency and fuel saving from the solutions. At the end, sservices was not accepted because of insufficient network (Office) all over India in a short period.

As a startup company, it is not easy to have an office entire India. Though solution is useful and can be benefitted, startup company is not able to get that services from the big company. If that is under some marine incubation centre, this issue must have been resolved and company must have grown well. Having knowledge, does not fetch business in India but needs financial support and infrastructure to reach customer.

This company has prepared for the development of three products as (i) GeoFLEET (ii) GeoPMS and (iii) GeoTRACK and three trade mark has been registered.

#### A. GeoFLEET

This product is aimed to reduce the operational cost of the ship. This product includes eight modules which are shown in Fig.1. This kind of services is provided only few companies internationally. Though this tool is more competitive, due to financial support, this has been kept idle now. If this is the situation for this kind of international product, how can expect more product in marine industry without support of corporate.

# GeoFLEET

- (i) Fleet Management
- (ii) Engine Performance
- (iii) Fuel Management
- (iv) Energy efficiency operational index (EEOI)
- (v) Hull Condition Monitoring
- (vi) Trim Optimisation
- (vii) EU MRV
- (viii) Reporting

Fig 1: GeoFLEET Product.

#### B. GeoPMS

This is mainly used for maintenance purpose. Due to the development of technology, this product is easy to develop and same time, using the cloud, monitoring and maintenance is much easier than any tool. This product stake holders are ship owner, charterer and management company.



Fig 2: GeoPMS Product.

#### C. GeoTRACK

This is product aimed to support fisher man community in India. More than 3 lakhs fishing boats are running in everyday in Indian costal. Every year, due to natural disaster or international borer issue, few boats and fishers are disappearing. This is a loss for the country as we lost human and big loss for the fisherman family. India is well developed in technology but this happens every year. To over this issue, this product was imed to develop, but not completed due to financial issue. Though this product can be developed for fisher man community, need support from government or corporate which can benefit to company and society. Schematic is provided in Fig 3.

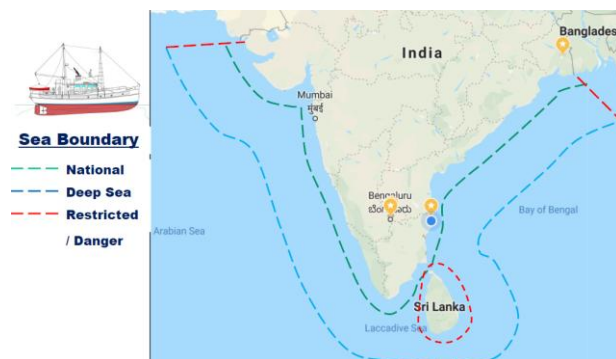


Fig 3: GeoTRACK Product.

## VII. CASE (II) SHALLOW WATERWAYS

This is also start-up company in marine industry. India has longest inland waterways and now there are many project from Central Government to utilize for commercial purpose to reduce the transportation. It has taken initiative to utilize the inland water ways for domestic transport as shipping transport is the cheapest mode of transport when compare other mode. Keeping the business opportunity in mind, eBarge has been designed by this company with Green container which can be used in shallow water ways. This design was patented “eBarge Green Container” and skeleton design was completed and showed fuel & cost saving for one voyage.

### A. EbARGE Green Container

As a startup company, able to reach many ship owner and big companies but it was asked for detail construction drawing which need minimum of 10 lakhs and need more man power. Due to various reason, this patent has been kept idle without financial support.



Fig. 4: eBarge Green Container

### B. JUMPO Barge

This is another concept to move the large amount of cargo from one country to another country. In this project, engine power require for higher loading capacity does not proportional to cargo. Considering the international demand of shipping, this JUMPO barge is designed in a concept level. This company is trying to get an investor to make it practical. This JUMPO barge is anchored in inside the sea and small barge will be used to supply the cargo to local cities in that country through inland waterways.

## VIII. CONCLUSIONS

India has highest percentage of young generation and startup helps to some extend to register a company. Each company has started with an new idea targeting a group of customer. Medium level expense products and short term return projects are going well. To support the long term development and long term return idea/concepts are not supported by current market which was explained with two case studies. It is recommended that of “Golden Startup” needs to be formed to support long term development project. Presently, only marine industry this study was done and this needs to be done in other industry as well. Working on this new business model, can bring more startup companies to develop their product and brings more job opportunity for future generation.

## ACKNOWLEDGMENT

The author would like to thank the management of Vel Tech Group for the opportunity to write a paper on this new business proposal. In this paper, technical data are shared from M/s GreenSHIP and M/s Shallow waterways. Special thank for both the company Director for allowing us to share the data in this paper.

## REFERENCES

- [1] <https://www.startupindia.gov.in/>
- [2] “Guide to Starting and Operating a msall Business”, MSDC, USA, 2016
- [3] “Startup Guide”, Harvard University, Office of Technology Development,
- [4] Boyoung Kim, “Critical Success Factors of a Design Startup Business”, Sustainability 2018, 10, 2981.
- [5] Yi-Chen Lin\*, et. al, “Research on Business strategy on business and performance evaluation in collaborative design”, International Journal of Electronic Business Management, Vol. 6, No. 2, pp. 57-69 (2008)
- Juha Saukkonen et. al. “From a Student of Startup Business to a Startup Employee or Entrepreneur: Study on Career Narratives of Students in Entrepreneurial Programs in a University”, Journal of Educational Issues, ISSN 2377-2263, Vol. 3, No. 1, 2017.

# *Evaluation of evapotranspiration models for paddy crops using meteorological data for kancheepuram district, tamilnadu*

D.Soundar Rajan

*Department of Civil Engineering  
St.Martin's Engineering College  
Dhulapally, Secunderabad -500 100,  
Telangana, India.  
dsr\_j@yahoo.co.in*

P.Suresh

*Department of Mechanical Engineering  
St.Martin's Engineering College  
Dhulapally, Secunderabad -500 100,  
Telangana, India.  
psuresh7@gmail.com*

M.M.Vijayalakshmi

*Department of Civil Engineering  
St.Martin's Engineering College  
Dhulapally, Secunderabad -500 100,  
Telangana, India.  
vnat12345@gmail.com*

**Abstract**— Evapotranspiration (ET) is the most important component of the hydrologic cycle. Accurate estimation of Evapotranspiration is essential for all the water management practices such as reservoir operation, agricultural water management models. Preliminary analysis for estimation of ET for the selected study area of Karunguzhi station of Maduranthagam taluk, in Kancheepuram district, Tamilnadu were more realistic to the estimated ET values and therefore the same station was used for identifying best ET models.

Four models were selected for estimating and evaluating the components of water balance during evapotranspiration for Karunguzhi. The evapotranspiration at Karunguzhi, located at latitude of 12°32'35" and longitude of 79°54'16" and altitude of 22.92 meter above mean sea level in Madhuranthagam taluk of Kancheepuram district, Tamilnadu was analyzed and the measured values were compared with the estimated values of the models.

The aim is to estimate ET by the Penman-Monteith, Blaney - Criddle, Priestley-Taylor and Penman model on daily basis for a multiyear period for a station at Karunguzhi and to estimate the ET by using the above mentioned four empirical models involving original constants for the above period of 2000-2014 (fifteen years) during Kharief, Rabi, and Summer seasons at Karunguzhi station. It is also aimed to evaluate the empirical models by comparing the estimated ET with available and experimental data to identify the better model and to identify suitable empirical model which can be applied to the entire region of Kanchipuram District Tamilnadu for estimating evapotranspiration. The constant of the selected model is recalibrated so that it can be applied to Karunguzhi, Kanchipuram district region. The result of the above study can help agricultural scientists and farmers to understand the water demands for development of agriculture activities.

**Keywords**— *Evapotranspiration, Field Measurement, Paddy Irrigation, crop coefficient, Penman Monteith Model.*

## I. INTRODUCTION

ET is the atmospheric demand of moisture that occurs through evaporation (moisture loss from the soil, standing and transpiration (biological use and release of water by vegetation) (Hansen *et al.*, 1980). ET can also be measured accurately by flux related methods. But can be difficult and are generally used in research settings (Allen *et al.*, 1998, Geiger *et al.*, 2003). The measurements of ET can be difficult, the methods are expensive, well trained research personnel's are required for accurate measurement. These measurement methods are required to evaluate ET estimation and are obtained by indirect methods.

The evaporation rate from pans filled with water is easily obtained. In the absence of rain, the amount of water evaporated during a period (mm/day) corresponds with the decrease in water depth in that period. Pans provide a measurement of the integrated effect of radiation, wind, temperature and humidity on the evaporation from an open water surface. Furthermore studies examined ET for Tamilnadu, that too only for few places in Tamilnadu state. No published studies have examined the spatial variability of ET models across Tamilnadu state. Monsoon season of Tamilnadu is October and November. During monsoon period rice is being cultivated. Traditional crops are sugarcane, sorghum, cotton, onion and other vegetables. Seventy percent of population lives on agriculture. Because of this, an assessment of the performance of ET models across space is required to allow proper monitoring of water use in Tamilnadu state's agriculture industry.

Most of the ET models were developed elsewhere and in varying environment such as US (Thornwaite, 1948), Europe (Penman, 1948, Makkink, 1957 and Turc, 1961), and Australia (Priestley and Taylor, 1972, Linacre, 1977). No published report is available about any model specifically developed for Tamilnadu state, India.

This study will compare several  $ET_0$  models in the reference to the  $ET_0$  model recommended by the Food and Agriculture Organization of United nations (FAO 56 Penman-Monteith and Allen *et al.*, 1998).

Hargreaves (1994) emphasized the importance of standardization of the reference evapotranspiration ( $ET_0$ ) calculation. Evapotranspiration  $ET_0$  measured by Lysimeters of various grasses has been used as the standard for developing the estimation equations. International organizations wish to use a single equation. The research center of the European communities and ASCE committee on Irrigation requirements has evaluated various equations for estimating  $ET_0$ . Due to its simplicity and accuracy of estimates, the Hargreaves *et al.* (1985) equation is recommended for general use. Perennial rye grass or Alta fescue grass is proposed as the standard reference crop. A penman combination equation is recommended as a reference for calibrating or evaluating other models for computing  $ET_0$ . It also emphasized the standardization of site conditions for collecting weather data and the quality of

data used are as important as the choice of reference equation used. The Hargreaves *et al.* (1985) equation uses only measured values of maximum and minimum temperatures and correlates well with the results from the Penman combination equations.

Solaiman *et al.* (1987) have selected 23 models for estimating consumptive use in the conditions of Saudi Arabia. The results from these models have been evaluated with reference to actual measurements performed in the same area in two separate 12 months periods and then ranked using five different rating criteria,  $R^2$ , (ET%), RMS, the smallness of intercept of correlation line and the standard deviation of the ratios of measured to estimated value.

Allen *et al.* (1998) studied and calibrated the FAO Blaney-Criddle (B-C) evapotranspiration equation and tested against Penman equation with local wind function and daily Lysimeter measurement of  $ET_0$  of alfalfa. Reports prove an excellent agreement between the calibrated FAO-BC model and Lysimeter observed values for daily, weekly and monthly estimates of  $ET_0$ . The study suggested that the  $ca$  (T) and evaporation (E) were assessed following a 39 minute irrigation event in semi-arid grassland in Southeastern Arizona, USA. Keeling plots (isotope mixing relationship) estimates of the isotopic composition of soil evaporation (SE) in bare plots closely matching the modeled values, lending to strong support for the validity of chamber approach.

Bellochi *et al.* (2003) studied the magnitude of error in estimating  $ET_0$  using estimated daily solar radiation data from air temperature. Reported finding was that the estimates of solar radiation are affected by both an overall error and seasonal patterns, which propagate in either  $ET_0$  estimates or derived outputs.

Monica Gupta and Raj Vir Singh (2004) developed monthly stochastic models using data obtained from Bikaner and Bellary stations, located in Arid regions of India. The autoregressive model developed for each station was then validated two years in advance, and predicted values were then compared with the observed evaporation data. Higher value of correlation coefficient (0.996) between predicted and observed evaporation series were found for both stations.

Medeiros *et al.* (2005) in this work made a comparison was made of  $ET_0$  estimates by Penman – Monteith, class A pan evaporation data and measured water consumption of grass, to generate crop curves corrected by leaf area to manage irrigation of the field beans, in a particular location in Brazil. The best crop curves were obtained based on the Penman – Monteith  $ET_0$  model, followed by class A pan evaporation data, method and by the grass compensation lysimeter. Also noted that the result reported in the literature indicates a good correlation between the crop coefficients and the leaf area index for different crops (Bandyopthay and Mallick 2003; and Medeiros *et al.*, 2001). The researchers use and several performance criteria that include

determination coefficient ( $R^2$ ), the agreement index ( $A_x$  and Percent relative error ( $R_e$ ).

Xu and Singh (2005) reported with three evapotranspiration models using the complementary relationship approach for estimating areal actual evapotranspiration these were evaluated and compared in three study region having large climatic diversity. The study reported was performed in two steps. First the three ET models with their original parameters were applied to test their general applicability. Second the parameter values were locally calibrated based on the water balance study.

Isikwue *et al.* (2014) evaluated the reference evapotranspiration by Penman-Monteith Method, for effective irrigation planning and management. The climatic data used were obtained from International Institute for Tropical Agriculture, Ibadan. The results showed that the lowest ET (60.406 mm/day), was obtained in rainy season (August) due to the high humidity of the air and the presence of clouds, while the highest ET (125.08 mm/day) was obtained in dry season (February) as a result of hot dry weather due to the dryness of the air and the amount of energy available.

Edebeatu *et al.* (2015) used four empirical evapotranspiration equation models to compare with the Penman-Monteith model. Modified model, provided a better value of evapotranspiration when compared with the FAO – 56 Penman-Monteith Model among other ET within the ambit of the applied statistical method used in their work. The present study employs four less demanding data requirement models for a region of Karunguzhi in Kanchipuram District of Tamilnadu state, India.

Penman-Monteith model requires meteorological data such as radiation, humidity, wind speed, maximum and minimum temperature and dew point temperature. Models that have less demanding data requirement are Blaney-criddle, Priestley-Taylor and Penman estimated by these models is compared with that of Penman-Monteith model and linear regression was performed for all the stations. From the result, few models were identified for use in estimation of ET, over the district of Kancheepuram and it is shown in figure 1. Identified model were suitably modified by recalibrating the constant without affecting the model form.

The Literature review shows that, for evaluating  $ET_0$  model for data short environment, the FAO PM model can be considered as a standard reference model.



Fig 1. Full Climatic Station at Karunguzhi in Kancheepuram District

## II. CASE STUDY AREA

Kancheepuram, the temple town is the District headquarters. The District Kancheepuram is situated on the northern East Coast of Tamil Nadu and is adjacent by Bay of Bengal and Chennai city and is bounded in the west by Vellore and Thiruvannamalai district, in the north by Thiruvallur district and Chennai district, Tamilnadu, India in the south by Villuppuram district in the east by Bay of Bengal. It lies between 11° 00' to 12° 00" North latitudes and 77° 28' to 78° 50' East longitudes and it is shown in Figure. 2. It has a total geographical area of 4393.37 Sq.Kms and coastline of 57 Kilometers. Agriculture is the main occupation of the people, 47% of the total population engaged in the District. The major crop cultivated in this District is Paddy with other crops like Millets, Cereals, Pulses, Sugarcane and Groundnuts,. The north east monsoon rainfall is almost uniform throughout the district. The existing maximum temperature is 21<sup>0</sup>C to 43<sup>0</sup>C and the minimum temperature ranges from 21<sup>0</sup>C to 25<sup>0</sup>C. The study area is highlighted in figure 2.

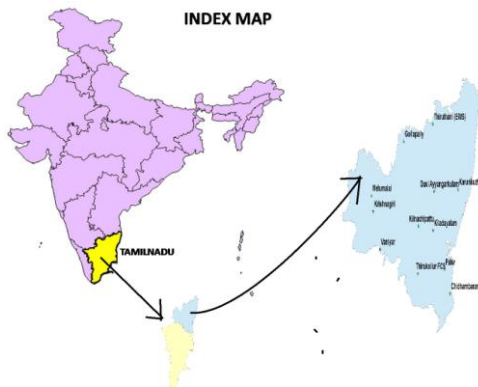


Figure 2. study area of Kancheepuram and surrounding Meteorological station of Tamilnadu

## III. METHODOLOGY

This study considers the following four models, namely, are FAO Penman-Monteith, Blaney-Criddle, Priestley-Taylor and Penman model.

### A. FAO Penman-Monteith Model

Chiew *et al.* (1995) estimated ET<sub>0</sub> using Penman – Monteith and FAO-24 methods and class A pan data for 16 Australian locations with wide range of climatic conditions were compared. Comparison was made by applying regression technique. The study also reveals that the FAO-24 Radiation model can be used as a surrogate for Penman-Monteith to estimate daily ET<sub>0</sub> for areas where wind speed data are not available and recommended FAO-24 Blaney-Criddle model, as it was found to yield similar monthly ET<sub>0</sub> estimates as Penman-Monteith model. Also noted that the correlation between class-A Pan data and Penman-Monteith ET<sub>0</sub> for evaporation totals over three or more days is satisfactory. However, the pan coefficient is very dependent on local climate and physical conditions, and it should be determined by comparing the pan data with either the Penman-Monteith or FAO-24 Radiation ET<sub>0</sub> estimates.

From the original Penman-Monteith equation and the equations of the aerodynamic resistance and surface resistance the FAO Penman-Monteith method to estimate ET<sub>0</sub> can be derived as

$$ET_0 = \frac{[0.408]\Delta(R_n - G) + \gamma[900/(T + 273)]u_2(e_s - e_a)}{\Delta + \gamma(1 + 0.34u_2)} \quad (1)$$

Where,

- ET<sub>0</sub> - Reference crop evapotranspiration (mm day<sup>-1</sup>)
- R<sub>n</sub> - Net radiation at the crop surface (MJ m<sup>-2</sup> day<sup>-1</sup>)
- G - Soil heat flux density (MJ m<sup>-2</sup> day<sup>-1</sup>)
- T - Mean daily air temperature at 2m height (°C)
- U<sub>2</sub> - Wind speed at 2 m height (m s<sup>-1</sup>)
- e<sub>s</sub> - Saturation vapour pressure (kPa)
- e<sub>a</sub> - Actual vapour pressure (kPa)
- Δ - Slope of vapour pressure curve (kPa°C<sup>-1</sup>)
- γ - Psychometric constant (kPa°C<sup>-1</sup>)

The equation uses standard climatological data of solar radiation (sunshine), air temperature, humidity and wind speed. To ensure the integrity of computations, the weather measurements are used at 2m (or converted to that height) above an extensive surface of green grass, shading the ground and not short of water.

### B. FAO 24 Blaney – Criddle Model

Blaney-Criddle model is one of the other models available to estimate evapotranspiration. Blaney and Criddle were working as consultant Engineers for the soil conservation services (SCS). To use in arid farmlands of western U.S, the Blaney-Criddle (1950) model was developed for estimating ET (Hanson *et al.*, 1980).The models relationships were derived from Experimental data for a variety of crops over the western U.S. (Blaney- Criddle, 1950).Balakrishnan (2000) reported that the monthly climatological data of Bhemanarayanagudi was analysed by computing ET<sub>0</sub> using modified PM, and also by Blaney-Criddle (1950), Hargreaves (1956) and Pan evaporation methods (Anonymous, 1988).

Blaney-Criddle model is one of the other models available to estimate evapotranspiration. Blaney and Criddle were working as consultant Engineers for the soil conservation services (SCS). The original model as described by Blaney and Criddle (1950) is

$$ET = kf \quad (2)$$

where PET is in mm per unit time, k is a crop-specific coefficient and f is a consumptive use factor given by:

$$f = \frac{T \times P}{100} \quad (3)$$

With T being the mean monthly temperature (°F) and P the monthly percentage of the actual daytime hours (Blaney and Criddle, 1950).

Several revisions of the Blaney-Criddle model have been proposed, but the one used in this study was originally described in the FAO 24 manual (Doorenbos and Pruitt, 1977) and modified by Frevert *et al.* (1983). The FAO 24 version introduces the grass reference elements into the equation, allowing the later use of crop coefficients (Doorenbos and Pruitt, 1977 and Jensen *et al.*, 1990). The model used in the study is as follows:

$$ET_o = A + Bf \quad (4)$$

$$f = p (0.46 T_m + 8.13) \quad (5)$$

Where,

p - Mean daily percent of annual daily daylight

Hours for given latitude

T<sub>m</sub> - mean air temperature in degree Celsius.

A & B - are calibration factors

Where,

$$A = 0.0042 \times RH_{\min} - n/N - 1.41 \quad (6)$$

$$B = 0.82 - (0.0041 \times RH_{\min}) + (1.07 \times n/N + (0.06 \times u_2) - (0.006 \times RH_{\min} \times n/N) - (0.0006 \times RH_{\min} \times u_2) \quad (7)$$

Where

RH<sub>min</sub> - Minimum daily relative humidity [%]

n - Actual duration of sunshine [hour]

N - Maximum possible duration of sunshine or daylight

Hours [hour]

u<sub>2</sub> - Day time wind speed at 2 m height [m s<sup>-1</sup>]

ET<sub>o</sub> - Reference evapotranspiration (mm day<sup>-1</sup>),

p - Mean percentage of annual daytime hours (defined as the percentage of the total annual daylight hours that occur in the time period being examined, such as daily or monthly (Doorenbos and Pruitt, 1977), T is the mean air temperature (°C), RH<sub>min</sub> is the minimum relative humidity (percent), n/N is the ratio of possible to actual sunshine hours, and U<sub>d</sub> is the daytime wind speed at 2 m (ms<sup>-1</sup>).

#### C. Priestley-Taylor Model

The ET process was controlled by available energy and the ability of evaporated water to be transferred from the surface. The transfer process was a function of the wind speed and the amount of water vapor in the air closest to the surface.

Priestley and Taylor (1972) demonstrated that for a well-water surface that extends over a large surface area, the ET process was well described by net radiation, air temperature and pressure.

The Priestley-Taylor model (Priestley and Taylor, 1972) for the calculation of daily ET (mm d<sup>-1</sup>) replaces the aerodynamic term of Penman-Monteith equation by a dimensionless empirical multiplier (a, Priestley-Taylor coefficient)

$$ET_o = \frac{L S (R_n - G)}{\lambda (S + \gamma)} a$$

where L (MJ kg<sup>-1</sup>) is the latent heat of vaporization, R<sub>n</sub> (MJ m<sup>-2</sup> d<sup>-1</sup>) is the net radiation, G (MJ m<sup>-2</sup> d<sup>-1</sup>) is the soil heat flux, s (kPa°C<sup>-1</sup>) is the slope of the saturation vapour pressure-temperature relationship, g (kPa°C<sup>-1</sup>) is the psychometric constant, λ latent heat of vaporization [MJkg<sup>-1</sup>], a is the Priestley-Taylor coefficient

The Priestley-Taylor equation is useful for the calculation of daily ET for conditions where weather inputs for the aerodynamic term (relative humidity, wind speed) are unavailable.

#### D. Penman Model

The Penman Model describes evaporation (E) from an open water surface, and was developed by Howard Penman in 1948. Penman's equation requires daily mean temperature, wind speed, air pressure, and solar radiation to predict E. Simpler Hydro meteorological equations continue to be used where obtaining such data is impractical, to give comparable results within specific contexts, e.g. humid vs. arid climates. Numerous variations of the Penman equation are used to estimate evaporation from water, and land. The equation for evaporation given by Penman is:

$$E_{mass} = \frac{mR_n + \rho_a c_p (\delta e) g_a}{\lambda_u (m + \gamma)}$$

Where: m = slope of the saturation vapor pressure curve (Pa K<sup>-1</sup>)

R<sub>n</sub> = net irradiance (W m<sup>-2</sup>)

ρ<sub>a</sub> = density of air (kg m<sup>-3</sup>)

c<sub>p</sub> = heat capacity of air (J kg<sup>-1</sup> K<sup>-1</sup>)

g<sub>a</sub> = momentum surface aerodynamic conductance (m s<sup>-1</sup>)

δ<sub>e</sub> = vapor pressure deficit (Pa)

λ<sub>v</sub> = latent heat of vaporization (J kg<sup>-1</sup>)

γ = psychometric constant (Pa K<sup>-1</sup>)

Which (if the SI units in parentheses are used) will give the evaporation ET<sub>o</sub> in units of kg/(m<sup>2</sup>·s), kilograms of water evaporated every second for each square meter of area.

## IV. RESULTS AND DISCUSSIONS

In the present study, four models for which the required data are meteorological with temperature and relative humidity, were selected and output of all the models were obtained by using daily meteorological data for a period of 15 years (2000-2014). These results are compared based on regression parameters and percentage error values. The constants of the selected models are recalibrated for the Kancheepuram District, India is by suitable approach for a location and suitable value of the constants determined

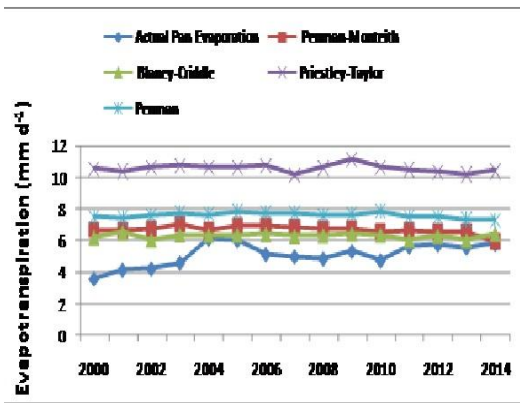


Figure 3. Average Performance of Pan Evaporation vs. Time for Actual and various ET Models for Karunguzhi Kancheepuram District for the Year of 2000 - 2014.

It is seen from the data of figure 3 for the year 2000 to 2014, the models over predicts the values of ET. In both the cases the over prediction is very high in the case of priestly-tailor Model (PTM). Hence it is decided to find the average values for the period of 15 years, 2000 to 2014, to study the performance of the models.

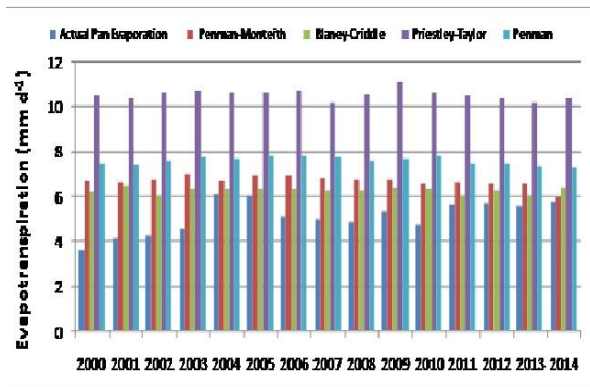


Fig 4. Yearly Evapotranspiration at Karunguzhi Kancheepuram District for the Period 2000 - 2014.

Figure 4 shows the yearly evapotranspiration (ET) at Karunguzhi Kancheepuram District for the Period 2000 - 2014. The highest ET is predicted by PTM in the year 2009. The lower ET is observed by PMM in the year 2014. The over-prediction of ET is noticed in all the models because the models are based on only a set of certain assumptions and all the real factors could not be included in the model. Moreover, these modes are of more generic in nature and not developed for the Indian Climate.

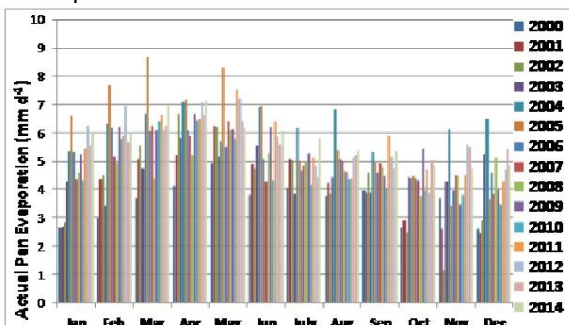


Fig 5. Monthly Actual Pan Evaporation at Karunguzhi, Kancheepuram for the Period of 2000 - 2014

Figure 5 shows the monthly actual pan evaporation at Karunkuzhi Kancheepuram for the period from 2000 to 2014. It indicates the wide monthly variation of actual pan evaporation over the period of consideration 2000 – 2014. There is no consistent trend for the above period. However, it can be noticed that the actual pan evaporation is found to be relatively high in the recent years.

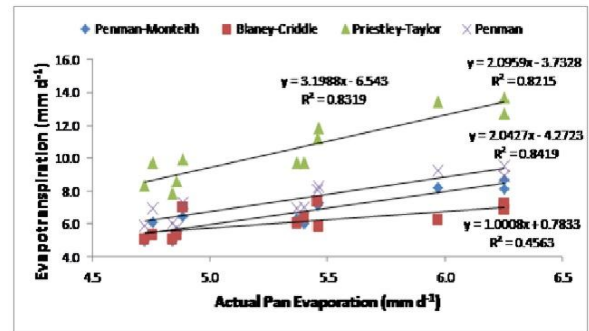


Fig 6. Correlation between Actual Pan Evaporation and various Models for Karunguzhi Kancheepuram for the Period 2000 - 2014.

The correlation coefficient between actual pan evaporation and various models for Karunkuzhi Kancheepuram for the period 2000 – 2014 shown in Figure 6, indicates that Penman – Monteith Model has the highest value of 0.8419.

#### A.MODIFIED FAO PENMAN-MONTEITH EQUATION

The analysis of the above data indicates that the Penman-Monteith Model is the best model among the four models analysed. However, the Penman-Monteith Model has the average R<sup>2</sup> value of only 0.63. Hence, various combinations of the coefficients of the model are verified for the better prediction. Based on the detailed analysis, the conventional Penman-Monteith Model is modified as follows with the new coefficients of 0.912 and 0.246, instead of 0.408 and 0.34 respectively.

$$ET_o = \frac{[0.912]\Delta(R_n - G) + \gamma[900/(T + 273)]u_2(e_s - e_a)}{\Delta + \gamma(1 + 0.246u_2)}$$

where,

ET<sub>o</sub> - Reference crop evapotranspiration (mm day<sup>-1</sup>)

R<sub>n</sub> - Net radiation at the crop surface (MJ m<sup>-2</sup> day<sup>-1</sup>)

G - Soil heat flux density (MJ m<sup>-2</sup> day<sup>-1</sup>)

T - Mean daily air temperature at 2 m height (°C)

u<sub>2</sub> - Wind speed at 2 m height (m s<sup>-1</sup>)

e<sub>s</sub> - Saturation vapour pressure (kPa)

e<sub>a</sub> - Actual vapour pressure (kPa)

Δ - Slope of vapour pressure curve (kPa°C<sup>-1</sup>)

γ - Psychrometric constant (kPa°C<sup>-1</sup>)

Table 1. R<sup>2</sup> value for Modified Penman Monteith Model for the Period 2000-2014. Karunkuzhi, Kancheepuram District .

Year	ET (mm day <sup>-1</sup> )	
	Conventional	Modified
2000	0.3139	0.6802
2001	0.8441	0.8944
2002	0.8984	0.9124
2003	0.1752	0.6681
2004	0.3086	0.6873
2005	0.8033	0.8433
2006	0.666	0.8213
2007	0.7243	0.8712
2008	0.2891	0.6411
2009	0.7736	0.8231
2010	0.8635	0.8921
2011	0.8101	0.8811
2012	0.5802	0.7843
2013	0.6138	0.8641
2014	0.8889	0.9266
<b>Average</b>	<b>0.6368</b>	<b>0.8127</b>

The R<sup>2</sup> value of the conventional and modified Penman Monteith model for various years are shown in the Table 1. When the average R<sup>2</sup> value of conventional model is 0.6368 the same is 0.8127 for the modified Penman Monteith Model.

In spite of the vagaries of nature, the predictability of the modified Penman Monteith Model with R<sup>2</sup> value of 0.8127 is considered to be very good. The predictability of modified Penman Monteith model in the recent past years such as 2013 and 2014 are considerably high at 0.8641 and 0.9266 respectively.

Table 2. R<sup>2</sup> Value by Conventional and Modified Penman Monteith Model for the year 2014. For Various locations

Meterological Station		ET (mm day <sup>-1</sup> )	
		Conventional	Modified
Location	Districts		
Dusi Ayyangar Kulam	Thiruvannamalai	0.691	0.552
Gollapally	Vellore	0.440	0.684
Karunkuzhi	Kancheepuram	0.878	0.915
Kiladayalam	Villupuram	0.639	0.530
Kilanchipattu	Thiruvannamalai	0.311	0.735
Krishnagiri Reservoir	Krishnagiri	0.753	0.093
Chidambaram	Cuddalore	0.330	0.449
Melumalai	Krishnagri	0.577	0.676

Palur (Panruti)	Cuddalore	0.764	0.681
Thirukoilur Fcs	Villupuram	0.503	0.577
Vaniyar Reservoir	Dharmapuri	0.532	0.491
Thiruthani (Ews)	Thiruvallur	0.662	0.762

The R<sup>2</sup> value of the conventional and modified Penman Monteith Model for various locations are shown in the Table 2. The best value of R<sup>2</sup> value by modified Penman Monteith Model is 0.915 for Karunguzhi Kancheepuram district (study area), while that is only 0.878 by conventional Penman Monteith Model. The predictability of modified Penman Monteith model in Kilanchipattu in Thiruvannamalai district and Thiruthani in Thiruvallur district are considerably moderate at 0.735 and 0.762 respectively.

### B. DATA ANALYSIS FROM GIS

GIS is a geographic information system for working with maps and geographic information. It is used for creating and using maps, compiling geographic data, analysing mapped information, sharing and discovering geographic information. It has been addressed with interpolation method. Each of the interpolation methods available in the ArcGIS Spatial Analyst extension uses a different approach for determining output cells. Choose a method based on the distribution of sample points and the phenomenon being studied. Krige, Spline, IDW, Distance Z-value.

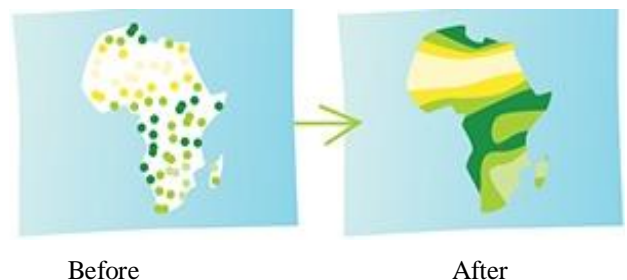


Fig 7. Performance of interpolation image

Figure 7 shows Mathematics the estimation of surface values at unsampled points based on known surface values of surrounding points. Interpolation can be used to estimate elevation, rainfall, temperature, chemical dispersion, or other spatially-based phenomena. Interpolation is commonly a raster operation, but it can also be done in a vector environment using a TIN surface model. There are several well-known interpolation techniques, including spline and kriging.

The performances of Penman-monteith, Blaney-Criddle, Priestley-Taylor and Penman models of various neighbouring location of Karunkuzhi Kancheepuram District Tamilnadu was analysed with mapped information resolution by GIS Geographic Information System is shown in figures 8,9 and 10.

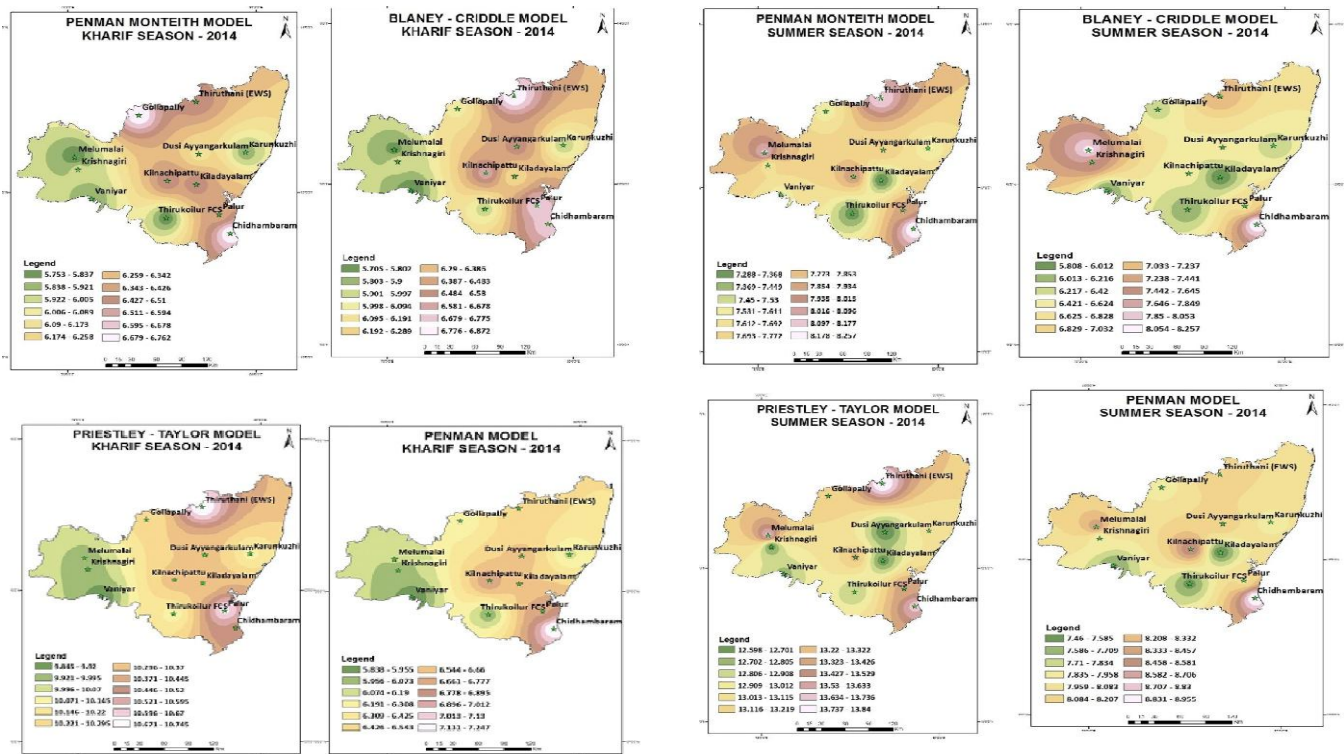


Fig 8. Performance of Penman-Monteith, Blaney-Cridde, Priestley-Taylor and penman models mm/day for the Kharif season year 2014

Figure 10. Performance of Penman-Monteith, Blaney-Cridde, Priestley-Taylor and penman models mm/day for the Summer season year 2014

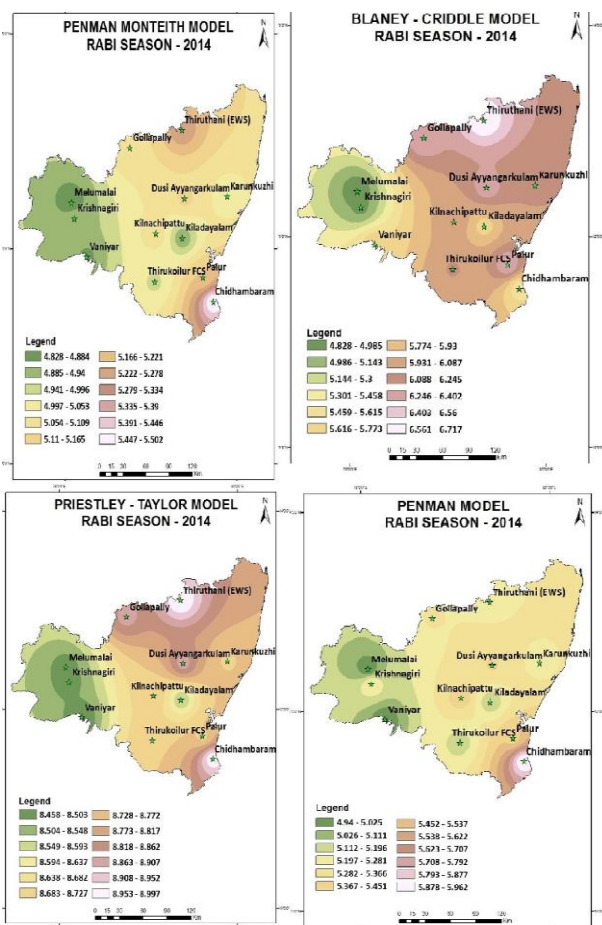


Fig 9. Performance of Penman-Monteith, Blaney-Cridde, Priestley-Taylor and penman models mm/day for the Rabi season year 2014

It is observed from the performance of various models by using GIS, Penman monteith model is more suitable for entire region of northern district of tamilnadu. Moreover, the ET values obtained from kharif season, rabi season and summer season are 5.72 to 6.7 mm/day, 4.8 to 5.5 mm/day and 7.28 to 8.2 mm/day respectively by using Penman monteith model has better accuracy compare to other models.

### V.CONCLUSION

This study evaluated that, the Penman Monteith Model is considered to be better suitable, compared to other model, for Karunkuzhi in Kancheepuram Districk. The modified Penman Monteith Model has better accuracy for the prediction with improved correlation coefficient. The prediction from the improved model can be used for the determination of crop pattern suitable for the locality. It can pave way for the improved productivity and hence better national wealth.

The Penman Monteith model is identified as the best model among the four and it is modified with a recalibrated constant. If the available meteorological variable is only maximum and minimum temperature, Penman Monteith model is more suitable for Kancheepuram District in daily ET<sub>0</sub> estimation.

Based on the detailed analysis, the conventional Penman-Monteith Model is modified as follows with the new coefficients of 0.912 and 0.246, instead of 0.408 and 0.34 respectively.

$$ET_0 = \frac{[0.912]\Delta(R_n - G) + \gamma[900/(T + 273)]u_2(e_s - e_a)}{\Delta + \gamma(1 + 0.246u_2)}$$

The best value of  $R^2$  value by modified Penman Monteith Model is 0.9150 for Karunguzhi Kancheepuram district (study area), while that is only 0.878 by conventional Penman Monteith Model. The predictability of modified Penman Monteith model in Kilanchipattu in Thiruvannamalai district and Thiruthani in Thiruvallur district are considerably moderate at 0.735 and 0.762 respectively.

Thus the Penman Monteith Model is considered to be better suitable, compared to other model, for Karunkuzhi in Kancheepuram District. The modified Penman Monteith Model has better accuracy for the prediction with improved correlation coefficient. The prediction from the improved model can be used for the determination of crop pattern suitable for the locality. It can pave way for the improved productivity and hence better national wealth.

We can also introduce horticultural crops (fruit crops) which need less water. Conservation of rain water through construction of many barriers, farm ponds and providing protective irrigation wherever possible can also be adopted. Based on the rainfall pattern, two crops can be taken (millet, pulses) Ex: Black gram, Green gram, Ground nut at least in about 35 to 40% of the dry land areas.

Poly – culture of traditional agriculture / land equivalent ratio (LER) can be used to increase the land use efficiency by introducing organic (farming) methods. Dry land farmers have various methods to reduce their exposure to crop production risk. Cultural practices play an important risk-reducing role; they include planting different crops with relatively low covariate yield (either in an intercrop or on separate fields). India's rain fed agricultural sector provides livelihoods for hundreds of millions of people, and it is the source of nearly half of the value of the country's agricultural production.

#### ACKNOWLEDGMENT

I wish to express my sincere thanks to Centre for Remote Sensing and Geo-informatics, Sathyabama University, Chennai for providing necessary resources to carry out this work and I would like to thank Centre for Institute of Energy Studies, Anna University, Chennai for providing valuable guidance to complete this research work.

#### REFERENCES

- [1] Hansen, V.E., Isrealson, O.W. and Stringham, G.E. (1980). "Irrigation Principles and Practices". 4<sup>th</sup> ed., John Wiley and Sons, Inc., New York., 417.
- [2] Allen, R.G., Periera, L.S., Raes, D. and Smith, M. (1998). "Crop evapotranspiration: Guidelines for computing crop requirements". Irrigation and Drainage Paper No.56, FAO, Rome, Italy, 300.
- [3] Geiger, R., Aron, R.H. and Toddhunter, P. (2003). "The climatic Near the Ground". 6<sup>th</sup> Ed. New York: Rowman and Littlefield.
- [4] Thornthwaite, C.W. (1948). "An approach toward a rational classification of climate". The Geographical Rev., 38(1): 55-94.
- [5] Penman, H.L. (1948). "Natural evaporation from open water, bare soil and grass". Proc., Royal Soc., London, London, U.K., A193, 120-146.
- [6] Makkink, G.F. (1957). "Testing the Penman formula by means of lysimeters". Journal of the Institution of Water Engineering, 11(3): 277-288.
- [7] Turc, L. (1961). "Evaluation des besoins en eau d'irrigation, evapotranspiration potentielle, formule climatique simplifiée et mise a jour. (in French)". Ann. Agron., 12:13-49.
- [8] Priestley, C.H.B. and Taylor, R.J. (1972). "On the assessment of the surface heat flux and evaporation using large-scale parameters". Monthly Weather Review, 100:81-92.
- [9] Linacre, E.T. (1977). "A simple formula for estimating evaporation rates in various climates, using temperature data alone". Agricultural Meteorology, 18: 409-424.
- [10] Hargreaves, G.H. (1994). "Defining and using Reference Evapotranspiration". Journal of Irrigation and Drainage Engineering, 120(6): 1132-1139.
- [11] Hargreaves, G.H. and Samani, Z.A. (1985). "Reference crop evapotranspiration from temperature". Appl. Engg. in Agric., 1(2):96-99.
- [12] Solaiman, A.A. and Abdin, M.A. (1987). "Evapotranspiration estimates in Extremely Arid Areas". Journal of Irrigation and Drainage Engineering, 113(4).
- [13] Bellochi, G., Donatelli, M. and Fila, G. (2003). "Evaluation of estimated radiation data for calculating Evapotranspiration and crop Biomass". Ital. J. Agron., 7(2): 95-102.
- [14] Monica Gupta.and Raj Vir Singh. (2004), developed monthly stochastic models using data obtained from Bikaner and Bellary stations, located in Arid regions of India.
- [15] Medeiros. G.A. Arruda. F.B. Sakai. E. and Fujiwara. M. (2001), "The influence of crop canopy on evapotranspiration and crop coefficient of beans (Phaseolus vulgaris L.)". Agric. Water Manage, 49:211-224.
- [16] Bandyopadhyay, P.K. and Mallick, S. (2003). "Actual evapotranspiration and crop coefficients of wheat (Triticum aestivum) under varying moisture levels of humid tropical canal command area". Agric. Water Manage., 59: 33-47.
- [17] Medeiros. G.A. Arruda. F.B. Sakai. E. and Fujiwara. M. (2001), "The influence of crop canopy on evapotranspiration and crop coefficient of beans (Phaseolus vulgaris L.)". Agric. Water Manage, 49:211-224.
- [18] Xu. C.Y. and Singh. V.P. (2005), "Evaluation of three complementary relationship evapotranspiration models by water balance approach to estimate actual regional evapotranspiration in different climatic regions". Journal of Hydrology, 308: 105-121.
- [19] Chiew. F.H.S. Kamaladasa. N.N. Malano. H.M. and McMahon. T.A. (1995), "Penman-Monteith, FAO-24 reference crop evapotranspiration and class-A pan data in Australia". Agricultural Water Management, 28: 9-21.
- [20] Hanson. V.E. Isrealson, O.W. and Stringham. G.E. (1980), "Irrigation Principles and Practices", 4<sup>th</sup> ed., John Wiley and Sons, Incd, New York, 417.
- [21] Blaney. H.F. and Criddle. W.D. (1950). "Determining Water Requirements in Irrigated Areas from Climatological Irrigation Data". Technical Paper No.96, US Department of Agriculture, Soil Conservation Service, Washington, D.C, 48.
- [22] Balakrishnan. P. (2000), "Climatological Data Analysis for Potential Evapotranspiration and crop Coefficient for Upper Krishna Project Command Area". Karnataka Journal of Agricultural Sciences, 13(1): 97-102.
- [23] Hargreaves, G.H. (1956). "Irrigation requirements based on climatic data". Paper 1105, Proceedings of American Society of Civil Engineers Irrigation and Drainage Division, 82(IR-3): 1-10.
- [24] Anonymous (1988). "Crop water requirements", Publication No.30. Water and Land Management Institute, Aurangabad, Maharashtra, 59-143.
- [25] Doorenbos. J. and Pruitt, W.O. (1977), "Crop Water Requirements, Irrigation and Drainage Paper 24". Food and Agriculture Organization of the United Nations, Rome, Italy: 144.
- [26] Frevert. D.K. Hill. R.W. and Braaten. B.C. (1983). "Estimation of FAO Evapotranspiration Coefficients". Journal of Irrigation and Drainage Engineering, ASCE, 109: 265-270.
- [27] Jensen, M.E., Burman, R.D. and Allen, R.G. (1990). "Evapotranspiration and irrigation water requirements". ASCE Manual and Reports on Engineering Practices No. 70., ASCE, New York, 1-360.

[28] Isikwue. C. Bernadette. Audu. O. Moses (2014), "Martin. Evaluation of Evapotranspiration using FAO Penman-Monteith Method in Kano Nigeria", International Journal of Science and Technology, ISSN 2049-7318.

[29] Edebeatu, Chinedu, Callistus (2015). "Comparison of four empirical evapotranspiration models against the penman – montieith in a mangrove zone". Int. Journal of Applied Sciences and Engineering Research,ISSN 2277-9442.

# Onboard Driver Monitoring System with Safety Enhanced Brake System

<sup>1</sup>Dineshkumar C

Automobile Engineering  
BSA Crescent institute of science and  
technology,  
Chennai-India.  
contactdinesh90@gmail.com

<sup>2</sup>Subramanian M

Automobile Engineering  
BSA Crescent institute of science and  
technology,  
Chennai-India.  
ramani@crescent.education

<sup>3</sup>Dinesh B

Mechanical Engineering  
Mepco Schlenk Engineering College,  
Virudhunagar-India.  
dhineshbala91@gmail.com

**Abstract**—Recent automobile vehicles require additional safety features to enhance the active safety. Due to lack of safety systems in vehicles road accidents are on the rise. The major cause of collision for 80% of accidents is drivers fault as cited by the ministry of road accidents of India. The current research work is carried out to analyze the fault of the driver and to measure the health condition of the driver by placing throb sensor and temperature sensor in steering wheel so as to slow down the vehicle by using Jake brake during abnormal health issue. The proposed systems were analyzed for different category of the condition of driver to improve the safety system technology. When triggered the exhaust valve is opened after the compression stroke enable to escape of compressed air from the cylinders to slowdown the vehicle which prevents the accidents in emergency situations.

**Keywords**— Throb sensor, Temperature sensor, Jake brake.

## I. INTRODUCTION

The brake system is designed to slow down and halt the motion of the vehicle. The automotive braking system had been developed in present days due to large number of accidents happened during health issues. The coordination of sensor technology developed to reduce the speed of the vehicle during emergency. The luxury vehicles had imposed by sensors to park the vehicle, stop the vehicle automatically, steer the vehicle automatically etc. In present day most of the vehicles depends on safety and features to enhance the customer satisfaction. The vehicle to vehicle communication technology had been developed in many countries and in the event of Indian vehicles no proper communication technology is improved. The vehicle communication is important parameter to enhance the safety to driver and pedestrian. The collision occurs due to high speed and health issues are the main criteria for vehicle industry to improve the vehicle safety. The automotive barking system used in many luxury vehicles not in Indian vehicles due to high cost of the vehicle [1]. The research is concentrate mostly on the drivers who undergo heart attack while driving. Because a recent census shows the more number of accidents occur due to heart failure. The drivers lose the control of the vehicle during the heart attack and it may lead to accidents. The proposed research planned to monitor the heart beat rate of the driver of the age group above 40 years onboard using a pulse sensor. The pulse sensor senses the heart beat rate and sends the data to the arduino board which interprets the data already fed in the board and gives out a signal when the heart beat rate falls or increases with the set limit. By monitoring the heart beat, the on board passengers can be prevented from the greater impact of accidents. The arduino board sends out the

warning signal to the dash board and also gives out a buzzing sound from the buzzer. As the health related issues are increasing day today and the need of enhance active safety system for an accurate and affordable heart rate measuring device or heart monitor is essential to ensure quality of health. Commonly most health related measuring tools and atmosphere are expensive and they do not follow the safety and ergonomics. The accidents are the unpleasant event that no one ever wants to occur in their life and it ruins the life of much people causing tremendous losing the life of people. Preventing the accident (accident prevention) refers to activities designed to foresee and avoid accidents. There has been an increase of 17.4% in the total number of death rate caused by road accidents during the period of 2011-2014. This percentage has raised eyebrows and caught the attention of many to curb the growing rate. It is found that 80% of the times it is the fault of the driver [2]. Much prevention system has been so far suggested and some were successful to a few percentages. But unfortunately still the accident rate remains a mysterious and very serious problem yet to be solved. So we suggest a technique to prevent accident by alcohol sensor since most of the accident occurring today is mainly because of drunk and drive. In order to avoid rash driving we go for a new technique of speed reduction system which uses the ultrasonic waves fitted to the vehicle to detect the obstacles and the distance they are apart from which we could reduce the speed of the vehicle automatically if the obstacles are present mere closer. In recent times automobile accidents are increasing day by day. This mainly happens when the driver is, drowsy or if he is alcoholic or if he is physically ill [4]. Prevention of accidents remains on one side as a huge question mark but rather on the other we look up for something as a life saving measures to safeguard our self in case of occurrence of any accidents. Many lives would have been saved if the emergency service could get the crash information in time. According to WHO (World Health Organization) reports, age of 35+ people will face Myocardial infarction [Heart attack] at anytime. Unfortunately we've that 8% of road accidents because of the drive health issues "Reported by NSC [National Safety council], so we plan to monitor the drive health (mode) biologically with help of drive's pulse rate. The below table 1 and figure 1. Shows the factors responsible for road accidents on Indian roads during the year 2016. The percentage of drivers fault is 41% and 12% of health issues fatal accidents in India and the different cause of road accidents leads to fatality is shown below [5].

TABLE 1. Factors responsible for Road Accidents on Indian roads in 2016

S.No	causes	% of Fatality	Persons killed
1	Fault of Driver	41	1,21,126
2	Fault of Pedestrian	1.01	3091
3	Mechanical Defect	0.96	2823
4	Health issues	12	30246
5	Stray Animal	0.25	629
6	Exceeding lawful speed	30	73896
7	Intake of Alcohol	2.58	6131
8	Overtaking	3.95	9462
9	Mobile phones	0.91	2138
10	Asleep or fatigued	0.75	1796
11	Other improper actions	7.2	17943

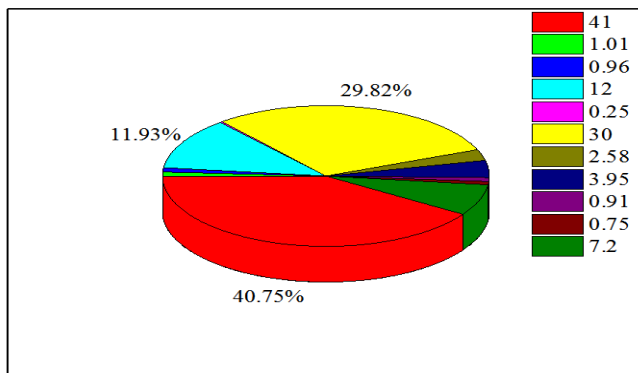


Fig 1. Shows the causes of road accidents in 2016

## II. PROPOSED SYSTEM

### A. POSITIONING OF HANDS

The positioning of throb sensor in steering wheel by representing survey using 200 peoples for positioning of hand in the steering wheel. The steering wheel is considered as wall clock position. The positing of hand on steering wheel is "4 and 8" and "3 and 9" are the two major used positions. These different hand positions refer to visualizing the steering wheel as the clock face and positioning the left hand at the 9 or 8 and the right hand at the 3 or 4 o'clock position. Today the National Highway Traffic Safety Administration recommends drivers put their hands at the 3 and 9 o'clock positions.

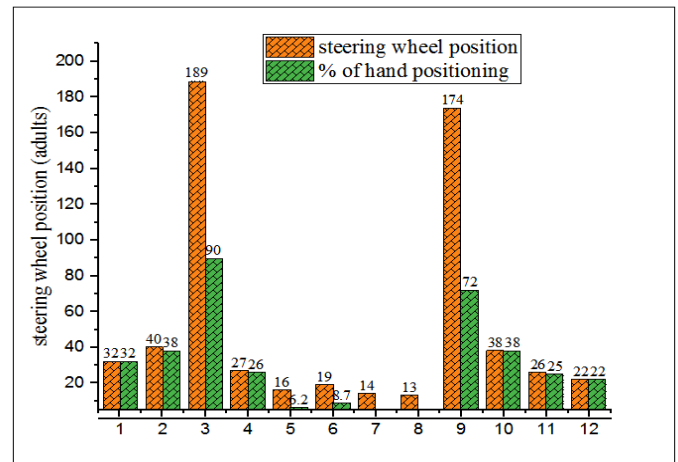


Fig 2. Percentage of Adult position of hands in steering wheel.

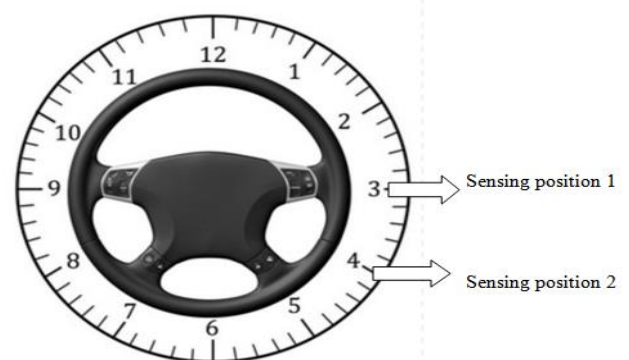


Fig 3. shows the steering wheel sensor position

From the above survey the major holding position of steering wheel is 3 & 9 (82%) and balance positions are 1 or 2% depends on situations, still this 1 or 2% are makeable because we have to monitor every single second. "The age group of above 35+ year's people can be affected by heart issues. The reports by National Safety council [NSC] say 8% of road accidents happened because of drive health issues. The 8% of drivers is affected and this 8% had tones of human, so we have to solve these problems and we planned to place the heart monitoring sensor in steering wheel. Steering wheel is the part which having maximum attention of driving and direct skin contact of drive. So this is the perfect place for heart rate sensor and we did survey with 100+ drivers on different situations.

### B. Control System

The function of control system of a vehicle can be operated by using an electronic control unit by using heartbeat pulse sensor and temperature sensor which links to steering wheel. The block diagram of a control system of a vehicle is shown in fig 4. The system composed of throb sensor which is used for sensing the pulse rate of the driver during driving the vehicle. The signal from the control unit which is coupled to the controller unit which is used to sense the abnormal pulse rate of the driver. The abnormal pulse rate is measured and this sensor which offers the signal to the electronic control unit. The LM324 IC chip is used for detecting the pulse rate by using IR sensor and it is used for sensing the volume of

blood and light is absorbed by the blood and the signal pulse are equivalent to the throb pulse. The heartbeat rate is measured by the pair of LED, LDR and a microcontroller. When the heart pumps the blood pressure varies certainly the infrared light gets reflected back to the detector and the change in voltage pulse. The components are used for the sensing device is resistors, intercom wire, transistor, IR LED emitter and detector, Arduino Uno, ceramic capacitor, tantalum capacitor. Quad op-amp. The completed system is a three wire connection system from sensing part is connected to arduino board. The system consists of two modes and this mode used to set the range of maximum and minimum pulse rate by manually. The driver who suffered already by health issue or heart attack and he knows the maximum and minimum pulse range as prescribed by doctors already. The control system consists of two modes which are used to measure the abnormal pulse rate and low pulse rate. The pulse range will be displayed in the dashboard during normal health condition of the driver. The pulse rate will be displayed continuously and even co passengers can know the pulse rate of the driver. During abnormal rate the system warns the driver and if he won't response the system gives the signal to the braking system. The output signal from the control unit offers to the solenoid control system to activate the Jake brake. The speed sensor is used to sense the speed of the vehicle and is used to offer the speed of the vehicle during critical situations. The Jake brake is activated depends upon the output signal from the sensor and control unit. The analysed pulse signal from the controller output is linked with the solenoid switch to activate the brake which is used to offer the brake force to apply during emergency situations. The controller consists of display which is used to display the driver's health pulse in the event of danger or emergency situations. The controller system is activates the Jake brake and the Jake brake is controlled by the controller which is placed on the engine head to compress the exhaust valves to open and the compressed air in the cylinder is removed from the cylinders. The air trapped in the cylinder is escaped and this device is operated by the electronic controller module when demand.

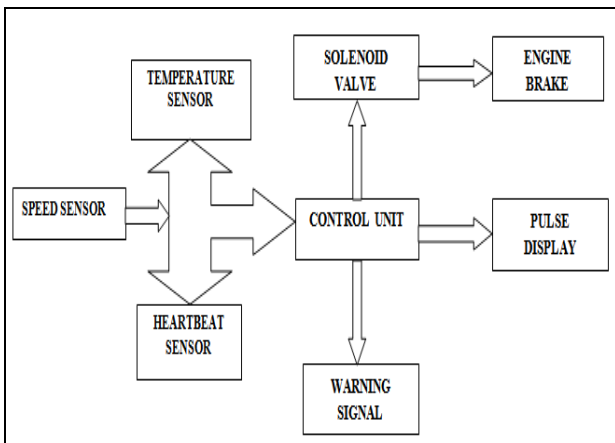


Fig 4. Layout of the controller unit

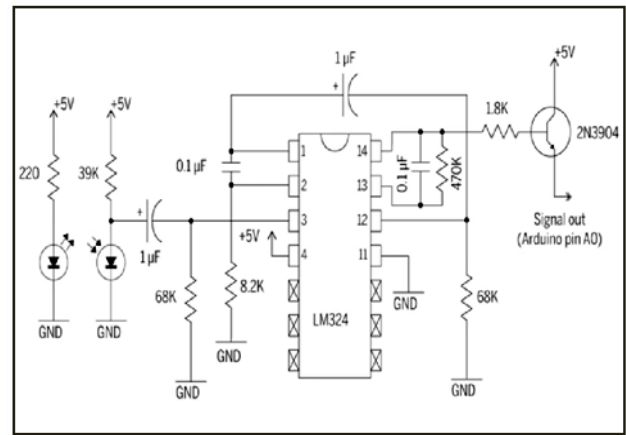


Fig 5. Simplified circuit of a pulse sensing system.

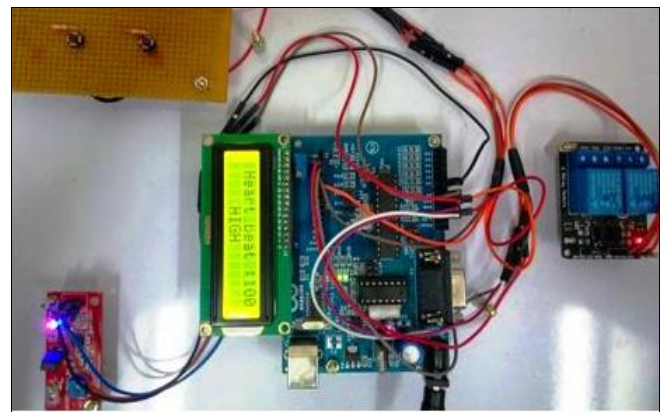


Fig 6. Prototype model of sensing system

TABLE 2. Average pulse rate of the human.

S.No	Age Group	Avg.Pulse rate
1	New born baby	140
2	10 years	85-90
3	18 years	80-90
4	Athletes	40-60
5	≥40(adults)	70-100

The above table 1. Reveals the average heart beat of the different groups of human. The adult pulse rate of age group people have focused for this research most commonly heartache problems have occurred generally in adults. In individuals the heart rate and pulse rate have varied due to panic, exercise, excitement, irregular respiration, and mental stress. The common safe heart rate for the individuals can be monitored by using the mathematical relationship. The performance of throb heartbeat sensor is calculated with the output of common usage of ECG [18].

The dignified error rate is -

$$\text{Error [E]} = \frac{[D-C] \times 100}{D}$$

Here,

- D- Defined heart rate
- C- Calculated heart rate
- E- Error rate

During compression stroke the compressed air fuel mixture is released Jake brake and it is normally called as Jacobs brake or Jake brake in an engine a braking mechanism is installed on engines. When the Jake brake is released during compression stroke and it opens the exhaust valves in the cylinders, it enables the compressed air trapped in the cylinders and makes the vehicle to slowdown during emergency situation. If the vehicle running on a low speed gear the engine rpm is high and then initiate Jake braking the result won't be that good. The process will cause wear on your clutch and transmission. This process is also known as clutch braking and is bad for your car. Often Jake braking is confused with clutch braking. This Jake brake can extend the life of friction brakes and help health issue drivers during critical conditions, maintain better control of their vehicle. For an example it might be an advantage during driving down a steep or long slope. A Jake brake creates braking force by enabling the compressed air inside the cylinders. In contrast, an exhaust brake blocks the path of the exhaust causing an increased pressure in the exhaust manifold. Engine retarders are also known as Jake brakes helps to save the conventional braking system during emergency stopping. Engine brake takes precautions in wear on brakes and supports the driver to keep alive in the event of collision and stability vehicle is increased in the emergency situations. Vigorous use of engine braking by shifting into a lower gear can support to the control speed while driving down very steep and long slopes saving the brakes from overheating and excessive wear. When legalize the engine brake changes the working principle of the engine exhaust valves. The retarding or slowdown the vehicles live axle wheels and allow you to have improved vehicle control without using a service brakes. It is often gossiped that the Jake brake is bad for your car but it can actually proven beneficial by Fenske. Jake brake is more efficient to engine brake because once the throttle is not longer pressed the fuel consumption is decreased. The research is carried out not only to enhance the braking system and to reduce the percentage of the fatality of the fault and health issue of the driver and to improve the braking performance and to supports the service brake of the vehicle.

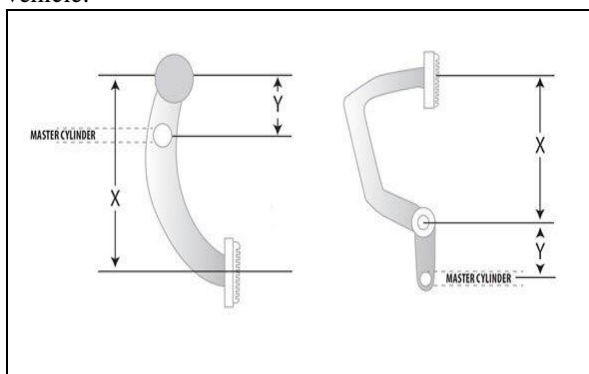


Fig 7. Pedal ratio calculation Pedal Ratio = X is divided by Y

Pedal Ratio is one of the most overlooked parts of a brake system. One of the main reasons and causes of a hard brake pedal is simply due to incorrect pedal ratio. When a brake pedal gets modified to fit in a vehicle or a booster or master cylinder gets installed where it fits in the car, the pedal ratio is rarely taken into consideration. Proper pedal ratio is a must when installing and operating a brake system. The below diagram show how to measure and figure the pedal ratio. In a manual brake system the pedal ratio will be between 5:1 and 6:1 and a power system will be between 4:1 and 5:1. In the above illustration of the hanging pedal on the left. Let we assume the overall length of “X” is 12” and “Y” measures 3”. That puts the pedal ratio at 4:1 which is perfect for a power system. To make this function as a manual system, the “Y” measurement would need to change to 2” giving a 6:1 ratio.

### III. RESULTS AND DISCUSSIONS

The sensor offers to measure the health condition of the driver and it depends upon the position of the hand is placed in the steering wheel of the vehicle. The hand position can be varied depends upon the comfort of the driver and sensor senses the pulse rate of the driver during critical condition. The below table shows the different heart rate readings obtained from ECG and proposed system throb sensor for the adult group  $\geq 40$ . The below table 3. Shows the different heart beat readings for different age groups which can be obtained from electrocardiogram by measuring the number of different adults under the same age group of 40. The accuracy level of the throb sensor has maximum error rate of 0.027 shown in the table 3.is compared with electrocardiogram when measured in normal condition. The pulse variation from the control unit make the vehicle tends to slow down by using solenoid control braking which is connected to engine brake. The engine brake is controlled by the control unit of the output signal. The pulse sensor input and health sensor input is monitored and the speed of vehicle is measured and reduced. The solenoid which is coupled with Jake brake in the vehicle and it is activated when the throb sensor offers the signal to the solenoid switch. The braking is activated and triggered depends on the pulse rate and speed sensor.

TABLE 3. Effect of measured heart rate on accurate heart rate

Age group	Pulse rate (bpm)	Actual rate (Defined ECG (bpm))	Measured rate (Calculate d) (bpm)	Error rate (%)	Abnormal Pulse rate (bpm)
40	110	74	75	0.013	122
41	110	72	72	0	122
42	110	73	75	0.027	125
43	110	71	72	0.014	128
44	110	72	73	0.013	121
45	110	73	75	0.027	120
46	110	74	73	0.013	123

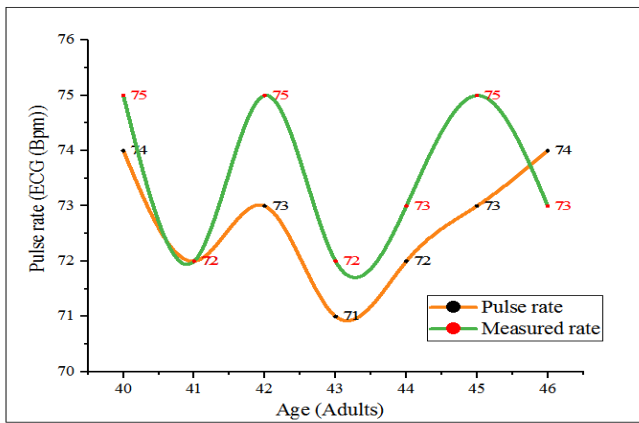


Fig 8.Effect of Adult Age group on pulse rate

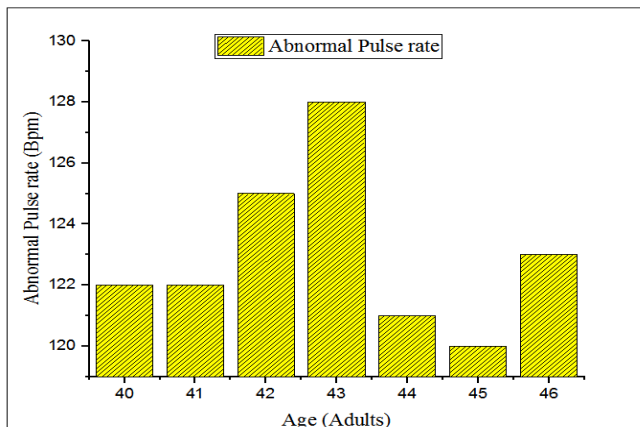


Fig 9.Effect of Adult Age group on abnormal pulse rate

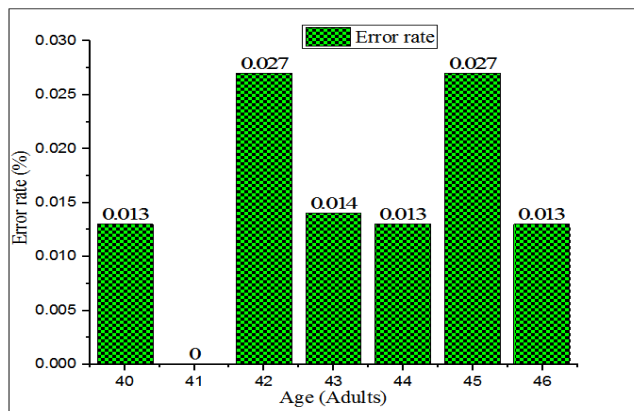


Fig 9.Effect of Adult Age group on Error rate

At the end of the compression cycle the exhaust valve releases brake most commonly confused with real engine braking and used mainly in heavy vehicle. The system works when opening the exhaust valves at the end of the compression cycle the amount of air fuel mixture stored in the engine cylinders and the compressed air is not offers to the engine crankshaft but it is liberating into the ambience. Normally at the end of the compression stroke the energy is used as the piston travelling towards top end compresses the charge inside the cylinder and the compressed charge it acts as a compressed spring and pushes the piston downward. Commonly when the engine brake in operation the compressed charge enables and released the piston towards downward. After removal of the energy stored within the cylinder the compressed charge is not returned the spring

back so the engine must expands more energy pulling the piston back down again. The below table 3.shows the comparison of proposed stopping distance and conventional stopping distance with an error rate of the vehicle. The speed of the vehicle is sensed during dynamic condition when the abnormal health is measured the control module offers the signal to the Jake brake to activate. The Jake brake releases the trapped air in the engine cylinder and makes the vehicle to slow down. The braking distance is measured and calculated by the speed of the vehicle. The stopping distance is calculated by considering the reaction distance and thinking distance for the particular vehicle speed. The stopping distance is compared with conventional stopping distance and the error rate is calculated. The error rate shows the vehicle distance covered than the conventional vehicle stopping distance. The maximum error rate is 1.05m than the conventional vehicle braking distance and the proposed systems objective is to reduce the vehicle speed than the maximum speed. The reduce speed vehicle impact will be lower than the maximum speed impact during abnormal health condition of the driver while driving the vehicle. The below table shows the comparison of proposed stopping distance and conventional stopping distance with error rate. The vehicle tends to slow down depends upon the speed of the vehicle by using Jake brake. The brake pedal is connected by the hydraulic piston is activated by the controller and which is used to stop down the vehicle. The proposed system activates the engine brake and hydraulic piston linked brake pedal.

TABLE 4.Comparison of proposed automatic vs. conventional manual stopping distance

Vehicle Speed	Proposed system (Automatic)	Conventional (Manual)	Error rate
km/hr	stopping distance (m)	stopping distance (m)	(m)
10	4.10	2	1.05
15	6.30	4	0.58
20	8.30	6	0.38
25	10.30	8	0.28
30	13.70	11	0.24
35	16.60	14	0.19
40	21.70	17	0.27

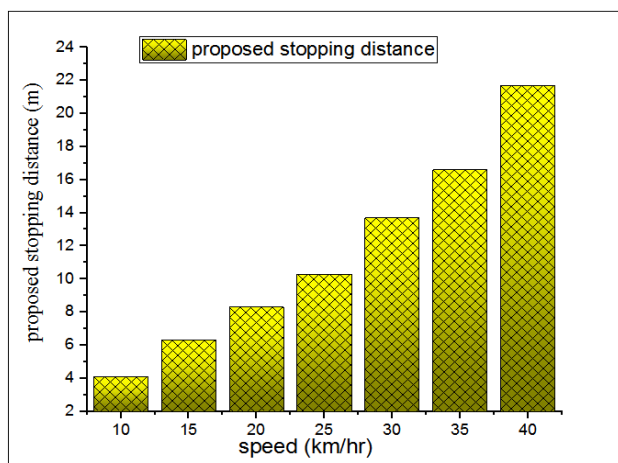


Fig 11. Effect of stopping distance on speed

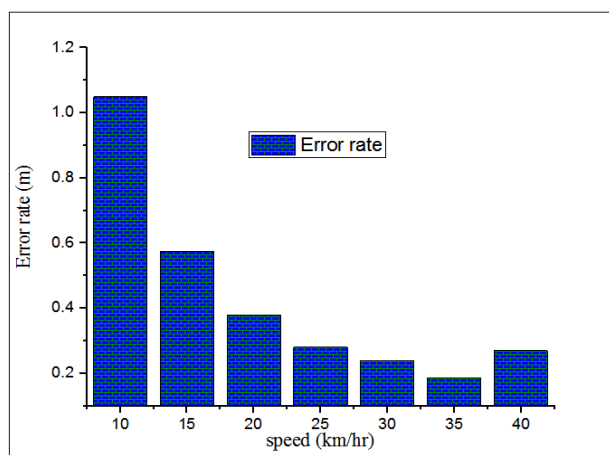


Fig 12. Effect of stopping distance on error rate

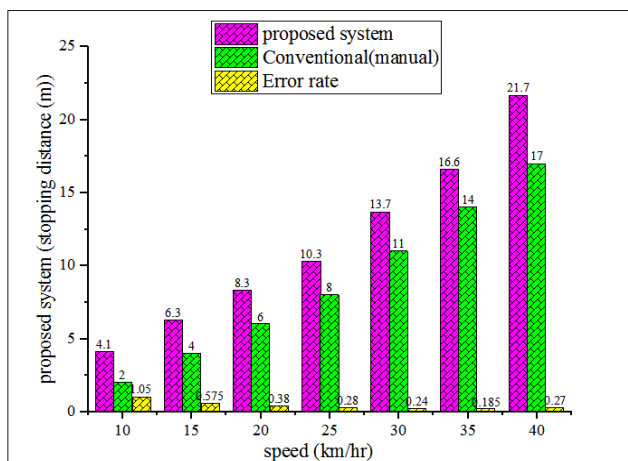


Fig 13. Comparison of proposed (automatic) vs. conventional (manual) stopping distance.

#### IV. CONCLUSION

The proposed research monitors the health condition the driver in all critical and normal condition of the driver. The drivers pulse rate is measured by using throb sensor which is displayed in dashboard and everyone can know the pulse range of the driver while driving the vehicle. In the event of any changes in driver health condition the throb sensor shows the fluctuation of the heartbeat range and monitors the pulse rate and displayed in dashboard. The signal from the throb sensor confirms the health issue of the driver and

gives the signal to the solenoid switch to activate the engine brake or Jake brake. The Jake brake enables the compressed air in the cylinder and releases the compressed air to the atmosphere. The vehicle speed is controlled or slows down without applying the service brake. The hydraulic piston connected with brake pedal to compress gradually. The vehicle tends to slow down and reduces the impact of the vehicle during the critical situation. The proposed system of this research is measured the abnormal health condition of the driver controlled the vehicle speed during driving in the event of collision. The engine brake enhanced the vehicle control, greater fuel economy and reduced the service brake maintenance.

#### REFERENCES

- [1] R. Punitha, G. Suchithra, A. Sujitha. Automatic car control during heart attack with an emergency messaging and comprehensive health monitoring system. Volume 6, Issue 1, January-2015.
- [2] Ministry of road transport & highways transport research wing. New Delhi, Road accidents in India – 2015.
- [3] Dineshkumar C, Subramanian M “Automotive braking system for passenger vehicle to enhance safety”. International Journal of Pure and Applied Mathematics Volume 117 No. 20 2017, 1011-1020 ISSN: 1311-8080 ISSN: 1314-3395 (on-line version). (2018).
- [4] B.Praveen Kumar, K. Mahendrakam, “Prevention of Accident due to Drowsy by using Eye blink, International Journal of Innovative Research in Science, Engineering and Technology. Volume 3, Issue 5, May 2014.
- [5] Road Accidents in India –Government of India Ministry of Road Transport & Highways Transport Research Wing New Delhi. 2016.
- [6] Sales K. Jose, X. Anitha Mary, Namitha Mathew, “ARM-7 Based Accident Alert and vehicle Tracking System, International Journal of Innovative Technology and Exploring Engineering (IJITEE), Volume 2, Issue 4, March 2013.
- [7] Highlights of 2009 Motor Vehicle crashes, Traffic Safety Facts, Research Notes, NHTSA (National Highway traffic Safety Administration). [Online] Accessed on 16 October 2011.
- [8] Veena.S.L1, R.Subhashini2 Driver Alertness Based on Eye Blinking and Bio-signals. International Journal of Advanced Research (2014), Volume 2, Issue 3, 666-670.
- [9] Andreas Meiera, Mark Gontera, Rudolf Kruse “Pre-crash classification of car accidents for improved occupant safety systems”.2014.
- [10] Herman A. Hamersma P. Schalk Els- Improving the braking performance of a vehicle with ABS and a semi-active suspension system on a rough road. 28 September 2014.
- [11] Rajiv Ranjan Singha, Sailesh Conjetia, Rahul Banerjeeb- “A comparative evaluation of neural network classifiers for stress level analysis of automotive drivers using physiological signals”. Biomedical Signal Processing, Elsevier Volume 8, Issue 6, November 2013, Pages 740-754.
- [12] V. Deepan, M. Subramanian, C. Dineshkumar “Motorcycle rider fatigue analyse: Results of an Online Survey” International Journal of Mechanical and Production Engineering Research and Development (IJMPERD) ISSN (P): 2249-6890; ISSN (E): 2249-8001 Vol. 8, 2018.
- [13] M.M.A. Hashem, Rushdi Shams, Md. Abdul Kader, and Md. Abu Sayed. “Design and Development of a Heart Rate Measuring Device using Fingertip” (KUET) Khulna 9203, 2015 Bangladesh.
- [14] Dineshkumar C, Subramanian M “Experimental Investigation of Onboard Driver Condition Monitoring System for Passenger Vehicles” International Journal of Mechanical Engineering and Technology (IJMET) Volume9, Issue6, June 2018, pp.01-09. Article ID: IJMET\_06\_07\_001.
- [15] Lori Mooren,Raphael Grzebieta, Ann Williamson, Jake Olivier Rena Friswell “Safety management for heavy vehicle transport: A review of the literature” Volume 62, February 2014, Pages 79-89.
- [16] Herman A. Hamersma, P. Schalk Els “Improving the braking performance of a vehicle with ABS and a semi-active suspension system on a rough road” Journal of Terra mechanics Department of Mechanical and Aeronautical Engineering, University of Pretoria, South Africa. Volume 56 (2014) 91–101.

# Operating cost analysis of Microgrid including Renewable energy sources and a battery under Dynamic Pricing

Hephzibah Jose Queen, *Research scholar, Karunya University*. J.Jayakumar, *Professor, Karunya University*. Narciss Starbell Assitant Professor, *Karunya University*

**Abstract—** In the course of the energy revolution the development of microgrids might play an important role to solve the upcoming problems to guarantee a stable power supply. This report deals with the potential of renewable energy sources and batteries to reduce the operating costs in a microgrid under dynamic pricing. For this purpose, three cases with different energy generating units and storage possibilities are compared to each other.

**Index Terms—**Microgrid, Solar power, wind turbine,.

## I. INTRODUCTION

THE upcoming energy revolution entails the integration of various distributed energy sources. This means an integration of renewable energy sources like solar and wind power. The establishment of microgrids is one option to integrate these new distributed energy sources in an effective way. A microgrid is an almost autonomous working, low voltage electricity network including different residential loads and generating units. To guarantee a stable operation of the microgrid, there is one connection point to the utility grid. If the energy generation in the microgrid is higher than the demand, electrical energy is feed in the utility grid respectively if the energy generation in the microgrid is lower than the required demand, additional energy is needed from the utility grid. To minimize the operating costs of the system, a battery storage unit can be added to the grid. Furthermore, dynamic pricing represents a good opportunity to minimize the total operating costs for a specific time period (here: 24 hours). Dynamic pricing means that the electricity price varies depending on supply and demand instead of being fed.

The following calculations show the cost benefit of the integration of renewable energy sources and the effect of a battery storage unit added to the microgrid. To simplify the optimization model, the microgrid is reduced to an one-bus-system with several units. Therefore, the line losses can be neglected and no power flow calculation is needed. Thus, the line losses are not considered in the optimization model of the

operating costs. In a second step, the line losses of an electricity network with the same units are determined and the costs for the losses are added to the total operating costs of the grid.

The available units are a solar panel, a wind turbine, two residential loads, a battery and the connection point to the utility grid. The input data are the same in systems, the one-bus-system and the six-bus-system. To run the load flow calculation, the results of the optimization model of the one-bus-system are used as input values for the battery. The one-bus-system represents a DC bus, whereas the six-bus-system are an ac network. Therefore, the load flow calculations are also calculated for an AC system.

## II. INPUT DATA

### A. Solar Panel

The available solar power is dependent on the direct solar radiation  $\text{sun}_{\text{direct}}$ , the diffuse solar radiation  $\text{sun}_{\text{diffuse}}$ , the size of the solar panel area  $A$  and the efficiency of the solar panel  $\eta_{\text{solar}}$ . This relation is described by equation (1)

$$P_{\text{Solar}} = \eta_{\text{solar}} \cdot A \cdot (\text{Sun}_{\text{direct}} + \text{Sun}_{\text{diffuse}}) \quad (1)$$

$$\eta_{\text{solar}} = 19.2\%$$

$$A = 80\text{m}^2$$

A monocrystalline solar cell has an average efficiency of 20%. The solar panel is connected to the grid via an DC/DC converter which has an efficiency of approximately 96%. Thus, the overall efficiency of the solar panel is 19:2%. The solar radiation values are measured values published by the Federal Office for Building and Regional Planning in Germany. The German weather service measured weather data in 15 different climate regions in Germany. Data used in this study case belongs to the first climate region which is located at the north sea coast. The measuring station is Bremerhaven, Germany. Table 1 lists the measured sun radiation values of region one for the 1<sup>st</sup> September. The results of the calculated solar power by equation 1 are shown in Table 2. There is one specific value for every hour.

TABLE I  
SOLAR RADIATION DATA

hour	Sun <sub>direct</sub> (W/m <sup>2</sup> )	Sun <sub>diffuse</sub> (W/m <sup>2</sup> )	Hour	Sun <sub>direct</sub> (W/m <sup>2</sup> )	Sun <sub>diffuse</sub> (W/m <sup>2</sup> )
1:00	0	0	13:00	54	284
2:00	0	0	14:00	49	265
3:00	0	0	15:00	39	228
4:00	0	0	16:00	131	238
5:00	0	0	17:00	40	159
6:00	0	2	18:00	14	67
7:00	13	77	19:00	0	0
8:00	45	171	20:00	0	0
9:00	112	256	21:00	0	0
10:00	203	298	22:00	0	0
11:00	249	332	23:00	0	0
12:00	109	348	24:00	0	0

TABLE II  
SOLAR POWER

hour	Sun power (kW)	Hour	Sun power (kW)
1:00	0	13:00	5.19168
2:00	0	14:00	4.82304
3:00	0	15:00	4.10112
4:00	0	16:00	5.66784
5:00	0	17:00	3.05664
6:00	0.03072	18:00	1.24416
7:00	1.38240	19:00	0
8:00	3.31776	20:00	0
9:00	5.65248	21:00	0
10:00	7.69536	22:00	0
11:00	8.92416	23:00	0
12:00	7.01952	24:00	0

B. Residential Loads

Table 3 shows the residential load data. There is one fixed value for each hour of the day. The load data is in accordance with the values from paper [2].

TABLE III  
RESIDENTIAL LOAD DATA

hour	load 1 kW	load 2 [kW]	hour	load 1 [kW]	load 2 [kW]
1:00	10.84	20.39	13:00	12.98	24.30
2:00	9.35	17.74	14:00	12.60	23.39
3:00	8.78	16.67	15:00	12.44	23.40
4:00	8.67	16.36	16:00	13.28	25.05
5:00	8.61	16.26	17:00	16.50	30.51
6:00	9.24	17.30	18:00	22.77	41.35
7:00	12.03	21.76	19:00	26.50	47.42
8:00	15.58	28.59	20:00	26.02	46.42
9:00	15.07	27.64	21:00	24.17	43.41
10:00	13.00	24.41	22:00	22.11	40.27
11:00	13.14	25.43	23:00	18.31	33.90
12:00	13.41	25.83	24:00	14.60	27.52

C. Wind Power

The wind turbine is connected to the bus via a generator and a rectifier. Due to mechanical (e.g. gearbox and bearings) and electrical (e.g. generator, rectifier and cables) losses and the coefficient of power (max.  $\frac{16}{27}$ ) of a wind turbine, the overall efficiency  $\eta_{wind}$  of the turbine, the generator and the rectifier is assumed to be 33%. Furthermore, the generated power is dependent on the air density  $\rho_{air}$ , the swept area of the blades A and the wind speed v. The wind power can be calculated by equation 2.

$$P_{wind} = \eta_{wind} \cdot \frac{1}{2} \cdot \rho_{air} \cdot A \cdot v^3 \quad (2)$$

$\eta_{wind}=33\%$   
 $\rho_{air}=1.225 \text{ kg/m}^3$   
 $A=2827 \text{ m}^2$

The wind speed data is taken from the same data base as the solar radiation data [1]. The used wind speed data is displayed in Table 4 and the resulting wind power values are listed in Table 5.

TABLE IV  
WIND SPEED

hour	Wind speed (m/s)	Hour	Wind speed(m/s)
1:00	5.1	13:00	2.0
2:00	4.3	14:00	5.0
3:00	3.7	15:00	7.0
4:00	3.6	16:00	5.0
5:00	3.3	17:00	3.0
6:00	3.0	18:00	3.0
7:00	2.0	19:00	3.0
8:00	1.0	20:00	2.0
9:00	2.0	21:00	3.0
10:00	4.0	22:00	2.0
11:00	4.0	23:00	3.0
12:00	4.0	24:00	3.0

TABLE V  
WIND POWER

hour	Wind power (kW)	Hour	Wind power(kW)
1:00	75.80937974	13:00	4.571959789
2:00	45.43785087	14:00	71.4368717
3:00	28.9479349	15:00	196.0227759
4:00	26.66366949	16:00	71.4368717
5:00	20.53781487	17:00	15.43036429
6:00	15.43036429	18:00	15.43036429
7:00	4.571959789	19:00	15.43036429
8:00	0.571494974	20:00	4.571959789
9:00	4.571959789	21:00	15.43036429
10:00	36.57567831	22:00	4.571959789
11:00	36.57567831	23:00	15.43036429
12:00	36.57567831	24:00	15.43036429

D. Battery Storage

The technical data of the battery storage are in accordance with the Tesla Powerwall 2.0. The maximum power is 3.3kW and the DC energy is 13.5kWh [4]. The assumed efficiency

for the charging ( $\eta_{charge}$ ) and discharging ( $\eta_{discharge}$ ) process is 93% each. The Tesla Powerwall is a lithium-ion battery pack with an integrated DC/DC converter. Therefore, the system is very easy to install. Moreover, this battery type is mainly used as a residential storage system in combination with solar panels.

E. Electricity prices

The electricity prices are in accordance with the prices  $price_t$  publish by the Euro-pean Energy Exchange for the 1<sup>st</sup> September 2017 [3]. The prices are listed in Table 6.

TABLE VI  
WIND POWER

Hour	Price (EUR/MWh)	hour	Price (EUR/MWh)
1:00	33.09	13:00	44.87
2:00	31.07	14:00	43.09
3:00	29.89	15:00	39.91
4:00	29.64	16:00	38.93
5:00	29.65	17:00	38.56
6:00	31.71	18:00	40.36
7:00	36.04	19:00	42.2
8:00	43.46	20:00	43.74
9:00	45.83	21:00	43.95
10:00	45.12	22:00	39.4
11:00	44.90	23:00	36.21
12:00	45.02	24:00	34.51

III. SIX –BUS-SYSTEM WITHOUT LINE LOSSES

A. Structure of the system

Simplify the optimization problem, the line losses of the microgrid are neglected. Therefore, the grid, can be reduced to a simple one-bus-system which is shown in figure 1. The wind turbine is connected at bus one, the solar panel at bus two and the battery at bus six. The connection point of the microgrid and the utility grid is at bus three. Bus four and five represent the two residential loads.

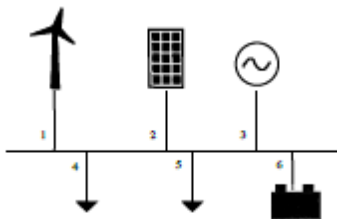


Fig 1 Structure of the one bus system

B. Mathematical Model

The optimization problem of minimizing the operating

costs of the microgrid can be modeled by the following equations. The objective function (see equation 3) is just dependent on the electricity price and the power used from the utility grid. The operating costs of the renewable energy sources are assumed to be zero. All parameters are defined from the perspective of the micro grid. Power that is feed into to the system (here: bus) is positive. Power that is drawn from the system is negative. Thus, the power values of the two loads have a negative sign and the generated power at the wind turbine and solar panel has a positive sign. Equation 4 symbolizes the power balance. Due to the reduction of the system to one bus with several connected units, there are no line losses in the system. At every time step, the stored energy in the battery has to be within the limits of 0kWh and the maximum capacity of the battery  $energy_{max}$  modeled in equation 6. Therefore, the power values from the point of view of the battery are needed. Therefore, the power of the battery has to be divided into the charging power and the discharging power (see equation 5). According to equation 7 and 8 the charging and discharging power as to be within the technical limits of the battery.

Objective function:

$$\min \sum_{t=0}^T price_t P_{utility,t} \tag{3}$$

Constraints:

$$0 = P_{utility,t} + P_{load1,t} + P_{load2,t} + P_{solar,t} + P_{wind,t} + P_{battery,t} \tag{4}$$

$$P_{battery,t} = P_{charge,t} + P_{discharge,t} \tag{5}$$

$$0 \leq \sum_{t=0}^{dT} (-P_{charge,t} \cdot \eta_{charge} - P_{discharge,t} / \eta_{discharge}) \cdot period < energy_{max} \tag{6}$$

$$P_{batterymin} \leq P_{charge,t} \leq 0 \tag{7}$$

$$0 \leq P_{discharge,t} \leq P_{batterymax} \tag{8}$$

C. Case studies

To evaluate the cost structure of the microgrid, three different cases are considered. The first case considers the micro grid without any renewable energy sources or battery storage. The residential loads are just supplied by the utility grid. In the second case, the solar panel and the wind turbine are added to the system and in the third case, the system is enhanced by a battery. In the simulation, the input data of the disconnected units is set to zero. The structure of the three cases are illustrated in figure 2, 3 and 4.

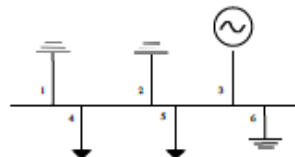


Fig 2 Case 1: Loads

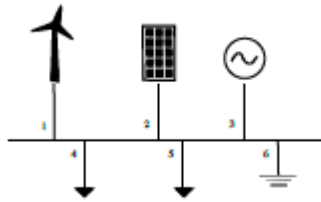


Fig 3 Case 2: Loads, solar panel and wind turbine

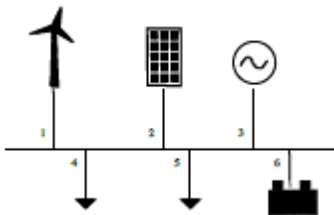


Fig 4 Case 3: Loads, Solar panel, wind turbine and battery

D. Results

The results of the optimization model for the three cases are listed in Table 7, 8 and 9. The operating costs can be seen in Table 6.

TABLE VII  
OPERATING COSTS OF THE ON BUS SYSTEM

CASE 1	CASE 2	CASE3
40.84 EUR	8.41 EUR	8.29 EUR

TABLE VIII  
CASE 1: LOADS

HOUR	P <sub>UTILITY</sub> (KW)	HOUR	P <sub>UTILITY</sub> (KW)
1:00	31.23	13:00	37.28
2:00	27.09	14:00	35.99
3:00	25.45	15:00	35.84
4:00	25.03	16:00	38.33
5:00	24.87	17:00	47.01
6:00	26.54	18:00	64.12
7:00	33.79	19:00	73.92
8:00	44.17	20:00	72.44
9:00	42.71	21:00	67.58
10:00	37.41	22:00	62.38
11:00	38.57	23:00	52.21
12:00	39.24	24:00	42.12

TABLE IX  
CASE 2: LOADS, SOLAR PANEL AND WIND TURBINE

HOUR	P <sub>UTILITY</sub> (KW)	HOUR	P <sub>UTILITY</sub> (KW)
1:00	-44.57937974	13:00	27.51636021
2:00	-18.34785087	14:00	-40.2699117
3:00	-3.497934898	15:00	164.2838959
4:00	-1.633669488	16:00	-38.7747117
5:00	4.332185134	17:00	28.52299571
6:00	11.07891571	18:00	47.44547571
7:00	27.83564021	19:00	58.4896357
8:00	40.28074503	20:00	67.86804021
9:00	32.48556021	21:00	52.14963571
10:00	-6.86103831	22:00	57.80804021
11:00	-6.92983831	23:00	36.77963571
12:00	-4.35519831	24:00	26.68963571

TABLE X

Case 2: Loads, Solar Panel, Wind turbine and Battery

HOUR	P <sub>UTILITY</sub> (KW)	P <sub>BATTERY</sub> (KW)	HOUR	P <sub>UTILITY</sub> (KW)	P <sub>BATTERY</sub> (KW)
1:00	-44.57937974	0	13:00	27.51636021	0
2:00	-18.34785087	-3.3	14:00	-40.2699117	0
3:00	-3.497934898	-3.3	15:00	-164.283895	0
4:00	-1.633669488	-3.3	16:00	-38.7747117	0
5:00	4.332185134	-3.3	17:00	28.52299571	0
6:00	11.07891571	-1.316	18:00	47.44547571	0
7:00	27.83564021	0	19:00	58.4896357	0
8:00	40.28074503	0	20:00	67.86804021	0
9:00	32.48556021	3.3	21:00	52.14963571	0
10:00	-6.86103831	3.3	22:00	57.80804021	0
11:00	-6.92983831	2.655	23:00	36.77963571	0
12:00	-4.35519831	3.3	24:00	26.68963571	0

E. Conclusion

The integration of renewable energy sources provides the opportunity to reduce the operating costs. In this case the operating costs are reduced to less than a fourth of the original operating costs. This shows, that there is a high potential of saving money and reducing the power drawn from the utility grid. The integration of a battery does not reduce the costs by a significant value. Although the battery has a very small impact in this study case, it could have a bigger influence by using another electricity price profile.

IV. SIX BUS SYSTEM WITH LINE LOSSES

A. Structure of the system

In a next step, the line losses in a six-bus-system with the same generating units and loads are calculated. The input data are the same as the input data for the one-bus-system. The input data for the battery power are in accordance with the results of the optimization calculation of the one-bus-system. The structure of the system is illustrated in figure 5

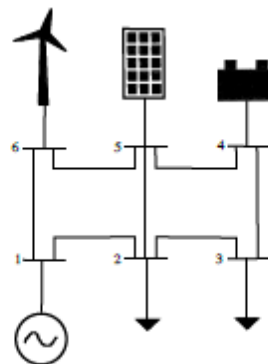


Fig 5 Structure of the Six-bus-system

B. Mathematical Model

The load buses and the battery bus are modeled as PQ buses and the wind turbine and the solar panel are modeled as

PV buses. Thus, the connection point to the utility grid represents the slack bus. The bus types are also listed in Table X. By means of the load flow calculation, the required power from the utility grid can be identified. Therefore, the following equations 9 and 10 must be satisfied. Although the input data is selected according to a DC network, the power flow is calculated for an AC network. The variable  $p_{b,t}$  describes the injected active power into the b-th bus of the system and the variable  $q_{b,t}$  describes the injected reactive power into the b-th bus of the system. The variable  $v_{b,t}$  describes the voltage at bus b at the time t. The power angle

$\theta_{b,k}$  represents the phase difference between bus b and bus k

and  $\theta_b$  the phase angle at bus b. The parameter  $Y_{b,k}$  is the admittance between the buses b and k and is calculated with the values  $R_{b,k}$  and  $X_{b,k}$  of the system [6]. The original values of R and X are listed in Table XII and the values for the parameter Y are shown in Table XIII. The MVA Base is 100MV A, the system frequency 50Hz and the nominal voltage 11kV.

TABLE XI  
BUS TYPES

BUS NUMBER	DESCRIPTION	BUS TYPE
1	UTILITY GRID	SLACK
2	LOAD	PQ
3	LOAD	PQ
4	BATTERY	PQ
5	SOLAR PANEL	PV
6	WIND TURBINE	PV

TABLE XII  
RESISTANCE AND REACTANCE OF THE SIX BUS SYSTEM

BUS TO BUS	DESCRIPTION	BUS TYPE
1-2	0.05	0.20
2-3	0.10	0.50
3-4	0.20	0.80
4-5	0.10	0.30
5-6	0.20	0.40
6-1	0.10	0.15
2-5	0.20	0.50

TABLE XIII  
ADMITTANCE MATRIX

BUS	1	2	3	4	5	6
1	4.3-9.3i	-1.2+4.7i	0+0i	0+0i	0+0i	-3.1+4.6i
2	-1.2+4.7i	2.3-8.4i	-0.4+1.9i	0+0i	-0.7+1.7i	0+0i
3	0+0i	-0.4+1.9i	0.7-3.1i	-0.3+1.2i	0+0i	0+0i
4	0+0i	0+0i	-0.3+1.2	1.3-4.2i	-1.0+3.0i	0+0i
5	0+0i	-0.7+1.7i	0+0i	-1.0+3.0i	2.7-6.7i	-1.0+2.0i
6	-3.1+4.6i	0+0i	0+0i	0+0i	-1.0+2.0i	4.1-6.6i

Subsequently, the line losses  $p_{loss,t}$  at the time t are the difference between the injected power into the system and the power drawn from the system (see equation 4.3). Simply said the difference between generation and demand. The parameter  $p_{b,t}$  symbolizes the power injected or drawn from the system at bus b at the time t. For instance, this value is negative for all load buses and positive for all buses with generating units.

The missing power in the system, respectively the line losses, are drawn from the utility grid. Therefore, the costs for the losses can be calculated. The parameter dt symbolizes the time period of 1 hour.

C. Case Studies

The cases for the six-bus-system are in accordance with the cases of the one-bus-system.

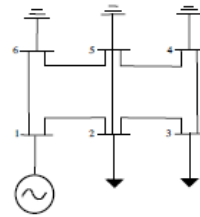


Fig 6. Case 1: Loads

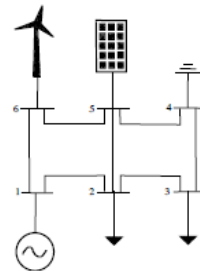


Fig 7. Case 2: Loads, Solar panel and Wind turbine

D. Results

The calculated line losses of the system and the associated costs for the losses are shown in Table 4.4 to 4.6. The line losses are very small in comparison to the load and the generated power by the solar panel and the wind turbine.

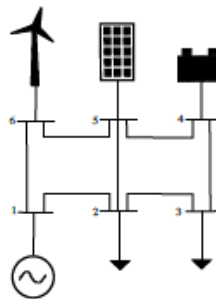


Fig 8 Case 3: Loads, Solar panel, wind turbine and Battery

TABLE XIV  
LINE LOSSES AND COSTS IN CASE I

HOUR	LOSSES (kW)	COSTS(EUR)	HOUR	LOSSES (kW)	COSTS(EUR)
1:00	0.99	0.000033	13:00	1.29	0.000058
2:00	0.82	0.000025	14:00	1.22	0.000053
3:00	0.76	0.000023	15:00	1.22	0.000049
4:00	0.74	0.000022	16:00	1.36	0.000053
5:00	0.74	0.000022	17:00	1.92	0.000074
6:00	0.80	0.000025	18:00	3.44	0.000139
7:00	1.10	0.000040	19:00	4.55	0.000192
8:00	1.71	0.000074	20:00	4.37	0.000191
9:00	1.61	0.000074	21:00	3.80	0.000167
10:00	1.30	0.000059	22:00	3.26	0.000128
11:00	1.38	0.000062	23:00	2.33	0.000084
12:00	1.42	0.000064	24:00	1.59	0.000055

TABLE XV  
LINE LOSSES AND COSTS IN CASE 2

HOUR	LOSSES (KW)	COSTS(EUR)	HOUR	LOSSES (KW)	COSTS(EUR)
1:00	4.29	0.000142	13:00	1.13	0.000051
2:00	1.95	0.000061	14:00	4.14	0.000178
3:00	1.17	0.000035	15:00	23.53	0.000939
4:00	1.08	0.000032	16:00	4.22	0.000164
5:00	0.91	0.000027	17:00	1.77	0.000068
6:00	0.86	0.000027	18:00	3.21	0.000130
7:00	1.03	0.000037	19:00	4.33	0.000183
8:00	1.58	0.000069	20:00	4.42	0.000193
9:00	1.40	0.000064	21:00	3.62	0.000159
10:00	1.88	0.000085	22:00	3.18	0.000125
11:00	1.95	0.000088	23:00	2.24	0.000081
12:00	1.95	0.000088	24:00	1.56	0.000054

TABLE XVI  
LINE LOSSES AND COSTS IN CASE 3

HOUR	LOSSES (KW)	COSTS(EUR)	HOUR	LOSSES (KW)	COSTS(EUR)
1:00	4.29	0.000142	13:00	1.13	0.000051
2:00	1.97	0.000061	14:00	4.14	0.000178
3:00	1.22	0.000036	15:00	23.53	0.000939
4:00	1.13	0.000033	16:00	4.22	0.000164
5:00	0.97	0.000029	17:00	1.77	0.000068
6:00	0.88	0.000028	18:00	3.21	0.000130
7:00	1.03	0.000037	19:00	4.33	0.000183
8:00	1.58	0.000069	20:00	4.26	0.000186
9:00	1.29	0.000059	21:00	3.62	0.000159
10:00	1.88	0.000085	22:00	3.18	0.000125
11:00	1.94	0.000087	23:00	2.24	0.000081
12:00	1.93	0.000087	24:00	1.56	0.000054

TABLE XVII  
OPERATING COSTS OF THE ONE BUS SYSTEM AND SIX BUS SYSTEM

HOUR	LOSSES(KW)	COSTS(EUR)	OPERATING COSTS WITHOUT LOSSES(EUR)	OPERATING COSTS WITH LOSSES(EUR)
1	43.72	0.001765	40.80	40.8018
2	77.40	0.003080	8.41	8.4131
3	77.30	0.003072	8.29	8.2931

E. Conclusion

The results verify the assumption of neglecting the line losses in the first calculations of the one-bus-system are reasonable. Especially, considering the additional costs shows that the line losses have almost no impact on the operating costs in this case studies. The results displays in Table XVII emphasis this. The total additional costs due to the line losses are less than 1Cent.

REFERENCES

[1] F.C Chendan Li, Federico de bosio,“Economic Dispatch for operating cost minimization under real- time pricing in droop-controlled dc microgrid ,”in *IEEE Journal of*

*Emerging and Selected topics in Power Electronics*,vol 5, pp.587-595, 2016.

[2] Hephzibah Jose Queen and J.Jayaakumar, “Operating cost analysis of a Microgrid including renewable energy sources without considering the losses”, in *International Journal of Pure and Applied Mathematics*, vol 118, no.20, pp.745-750, 2018

[3] Federal oce for building and regional planning in germany."http://www.bbsr.bund.de/EnEVPortal/DE/Regelungen/Testreferenzjahre/Testreferenzjahre/03\_ergebnisse.html?nn=436654. Accessed: 2017-10-04.

[4] eex."https://www.eex.com/de/marktdaten/strom/spotmarkt/auktion#!/. 2017/09/01. Accessed: 2017-10-06.

[5] tesla powerwall 2.0 dc." https://www.solahart.com.au/media/2849/powerwall-2-dc\_datasheet\_english.pdf. Accessed: 2017-10-07.

[6] D. Boroyevich, I. Cvetkovic, R. Burgos, and D. Dong, “Intergrid: A Future Electronic Energy Network,” *IEEE J. Emerg. Sel. Top. Power Electron.*, vol. 1, pp. 127–138, 2013.

[7] K. Strunz, E. Abbasi, and D. N. Huu, “DC Microgrid for Wind and Solar Power Integration,” *Emerg. Sel. Top. Power Electron. IEEE J.*, vol. 2, pp. 115–126, 2014.

[8] Y. Xu, W. Zhang, G. Hug, S. Kar, and Z. Li, “Cooperative control of distributed energy storage systems in a microgrid,” *IEEE Trans. Smart Grid*, vol. 6, pp. 238–248, 2015.

[9] A. J. Conejo, J. M. Morales, and L. Baringo, "Real-Time Demand Response Model," *IEEE Trans. Smart Grid*, vol.1, no.3, pp.236,242, Dec. 2010

[10] Open Energy Information (OpenEI), website: <http://en.openei.org>.

[11] L Barelli, G.Bidini, F.Bonucci, “A Microgrid operation analysis for cost effective battery energy storage and RES plants integration”, *Journal of Energy*, Elsevier, vol 113, pp 831-844, 2016

[12] Mallol poysto, sacedo-sanz, Jimenez Fernandez, “Optimal discharge scheduling of energy storage systems in Micro grids based on hyper-heuristics”, *Journal of Renewable Energy Elsevier*, Vol 83, pp 13-14, 2015

[13] J.D.P Kothari, “Power system optimization”, 2004.

## ***EVALUATION OF INFLUENCE OF THE PRINCIPLES INVOLVED IN CARBON FOOTPRINT IN THE PETROLEUM INDUSTRY USING TISM***

S.P.Prasanna  
Department of Mechanical  
Engineering

Kalasalingam Academy of  
Research and Education  
Krishnankoil, India  
prasanna@klu.ac.in

\*S.Bathrinath  
Department of Mechanical  
Engineering,

Kalasalingam Academy of  
Research and Education  
Krishnankoil, India  
bathri@gmail.com

K.Rahul  
Department of Mechanical  
Engineering,

Rajalakshmi Engineering  
College, Chennai,India  
rahulkishore0306@gmail.co  
m

S.Saravanasankar  
Department of Mechanical  
Engineering,

Kalasalingam Academy of  
Research and Education  
Krishnankoil, India  
ssaravanasankar@klu.ac.in

***Abstract***— Petroleum is the main source of energy in the world. But the process of extraction and use of petroleum products affects the environment adversely. To overcome the carbon footprint, 10 crucial factors including Human Resource quality, Technological Development, Geographical Factors, Market, Operational Factors, Functional Factors, By-products, Government Regulations, Disasters and Financial Support were analyzed. The ten factors were modeled using Total Interpretive Structural Modeling (TISM) which demonstrates the driving and dependence of factors related to the carbon footprint in the petroleum industry. This paper paves the way for future research and attempts to contribute to a sustainable extraction and usage of petrol in energy industries. Functional factors have a very influential role in this regard.

**Keywords**— Carbon footprint; TISM; Petroleum industry; Environment;

### I. INTRODUCTION

Petroleum and its by-products have different applications including providing fuel for various forms of transportation, industry and domestic electricity use. Essential daily products like plastics are manufactured from petrol. Hence, consumption of petroleum products has a major effect on the environment including gases released from petrol and oil industries contributing to global warming as an expanding ozone area being harmed due to emanations in the investigation, extraction, refining, transport and utilization stages in the petroleum industry. Nitrous oxides, Sulphur dioxide and carbon dioxide, the by-products of fuel combustion react with the atmosphere and deplete the ozone layer thereby increasing greenhouse gases. To offset this, countries have designed various subsidies, policies, sustainable manufacturing techniques, effective communication and technical developments. The policies include development in the transportation, scheduling process and nature of work in production (Panwar et al., 2016). Alternatives to petroleum include renewable energy (Solar, Wind energy) and biodiesel. Implementing 4.0 principles in the industry will impact the carbon footprint. Developing hydrogen as vehicle fuel also reduces carbon emissions (Momirlan and Veziroglu, 2005). Organizations should act to offset the safety and health risks in the petroleum industry. Improving safety measures can reduce oil spills, false floors preventing gasoline dripping into the water table in double-hulled tanker ships. Billions of dollars

are on research to reduce the carbon footprint. But such developments do not reduce the carbon percentage. In the future, we believe these ten factors will reduce carbon percentage and develop the petroleum industry to be self-sustaining.

### II. LITERATURE REVIEW

Literature review is divided into two sections namely, (A) Factors of carbon footprint in the petroleum industry and (B) Adopting a soft computing tool to identify the prior factors related to the carbon footprint.

#### A. Carbon footprint factors in the petroleum industry

- Quality of Human Resource

In the industry's 4.0 revolution, workers must be aware of all problems and the way to solve them. Many reports show that certain practices such as employee training, employee involvement, and process improvement enhance industry profitability (Mokhtar and Yusof, 2010). Practices like developing communication between managers and workers, successful service delivery teams, rewards and recognition motivate workers to perform better (Wirtz et al., 2008).

- Technological Development

To minimize environmental impact and produce minimum secondary waste, Renewable source are the solution as it is considered a clean source of energy. A renewable resource is a natural resource which replenishes and overcomes resource depletion caused by usage and consumption, either through biological reproduction or other naturally recurring processes in a finite amount of time on a human time scale. Renewable energy technologies can overtake the conventional energy sources, as it provides better opportunities for alleviation of greenhouse gases and reducing climate change (Panwar et al., 2016).

- Geographical Factors

Settling on area choices for creation of items is a key part and a calculated basic leadership trait for assembling firms. Ideal areas may offer upper an hand and add to the accomplishment of an endeavor. Firms considering location as the main factor on a global basis continue to increase (Flaherty, 1996). A range of factors may potentially influence firms in deciding to locate production facilities across national boundaries. A great deal of attention is paid in research literature to critical factors in industrial location decisions for over a century (Jungthirapanich and Benjamin, 1995). However, specific literature on international location decisions is limited. (Atthirawong and MacCarthy, 2001).

- Market Policy

Market policies have increased renewable energy use. The Renewable Energy Production Incentive created under the 1992 Energy Policy Act, has helped reduce fuel prices and

the gap between conventional and non –conventional energy sources (Bird et al., 2005).

**Operational Factors**

Operational efficiency improvement is based on deciding efficient transportation routes and is achieved by choosing less congested routes. Fuel consumption which increased in recent years, leads to frequent deliveries to retail outlets. This makes it difficult for companies to match load and vehicle capacity efficiently. It has been predicted that night time delivery is more efficient as freight vehicles are able to achieve efficient speeds. (Piecyk and Mckinnon, 2010).

- **Functional Factors**

Functional factors, the reason for carbon emission consists of four processes: exploration, extraction, refining and transportation. Organizations are expected to be more involved in partnership initiatives to improve their fleet utilization by increasing back loading and achieve greater integration of production and distribution operations (Piecyk and Mckinnon, 2010).

- **By-Products**

Petroleum products were commonly used in households. People all around the world still exist without the knowledge that they are the reason behind carbon footprint. The average annual household emission was found to be 16.55 t CO<sub>2</sub>e y<sup>-1</sup>, equal to an average personal emission of 5.70 t CO<sub>2</sub>e Ca<sup>-1</sup> y<sup>-1</sup>, 35.1% to transport, 20.6% for air travel and other fuel intensive leisure activities, and just 2.1% was associated with household waste disposal. Occupancy rate is the main reason for household energy consumption increase. A natural gas heating systems is more efficient than oil fueled one (Kenny and Gray, 2009).

**Government Policies**

Climate change has resulted in the government implementing new policies to curb emissions. Carbon taxes were introduced globally (Bruvoll and Larsen, 2004). Bio-fuel policy relies on carbon emission reduction which decreases petroleum product market demands (Thompson et al., 2011).

- **Disaster**

Over a billion years, the earth has faced various natural disasters but after the industrial revolution mankind created new types of disasters. The petroleum industry’s major disaster are oil spills caused by oil tankers. According to various reports, most spills are due to human error and technical malfunctioning which results in less than 7 metric tons per spill. But spills due to mishaps like impacts, grounding, frame disappointments, and blasts are significantly bigger, recording more than 700 metric tons. Oil businesses and its items lead to monetary advancement and also result in much perilous waste (Silva et. al., 2014).

- **Financial Support**

Modern industries need high capital investment. To stimulate growth and increase recovery from financial crises investment in renewable technologies is needed. (Masini & Menichetti, 2012). Financial support is the main pillar for development of industrial equipment.

(B)Soft computing tool for carbon footprint in the petroleum industry

Neural computing, Fuzzy reasoning, and evolutionary computing are increasing powerful tools for uncertainty analysis, risk assessment, data fusion, mining etc. These

tools are cost efficient and can be used to reduce exploration risk, extending life of wells and increasing production efficiency (Nikraves et al., 2003). Soft computing tools are set to play an important role in exploration as we lack specific models to determine this geological and physical phenomenon precisely. This also needs strong data and expert interpretation (Wong et.al, 2013).

### III. PROBLEM DESCRIPTION

A case evaluation of the proposed model was conducted in a petroleum unit which extracts and produces petroleum products, mainly fuel for vehicles. The petroleum industry rules the world by being the power source. The industry desires to assess its risk profile and expand their risk management practices. Since environment is polluted, flexibility is the only way to survive in the world and to increase their eco-friendly products. Before developing their management system, the industry needs to know whether they are technologically and financially capable of adopting and expanding practices to reduce the carbon footprint. This research was conducted to assess the factors of carbon footprint and to identify the most influential factors affecting carbon of petroleum industry. The results of the proposed model could enable and improve managerial decision through identifying, analyzing and improving ambience of the petroleum industry for adopting sustainability in the industries. The table 1 represents factors affecting carbon footprint.

TABLE I. FACTORS AFFECTING CARBON FOOTPRINT

S.NO	FACTORS	FACTORS CODE	REFERENCES
1	Quality of human resource	F1	Parast et al., 2011; Parast and Fini 2011; Mokhtar and Yusof, 2010.
2	Technological development	F2	Panwar et al., 2011; Huisingh et.al., 2015;
3	Geographical factors	F3	Maccarthy and Atthirawong 2003;
4	Markets	F4	Matthews et.al., 2008; Bird et.al.,2005;
5	Operational factors	F5	Sgouridis et.al., 2011; Piecyk and Mckinnon, 2010;
6	Functional factors	F6	Piecyk and Mckinnon 2010; Andres et.al., 2011;
7	By products	F7	Kenny and Gray 2009; Grunewald et.al., 2012
8	Government policies	F8	Bruvoll and Larsen 2004; Thompson et.al., 2011;
9	Disasters	F9	Silva et al., 2014; Kadafa, 2012.
10	Financial support	F10	Masini and Menichetti, 2012.

### IV. METHODOLOGY

A Total Interpretive Structural Modeling (TISM) is used to evaluate important influential relations among factors affecting the carbon footprint in the petroleum industry. Interpretive structural modeling (ISM) is a tool to establish prominent relations among factors (Rajesh 2017).

Interpretive Structural Modeling (ISM) is an effective methodology to deal with complex issues and has been in use for over a quarter century to help an organization's clients understand complex situations and evaluate solutions to unusual problems while implementing new developments in their works. It is a computer assisted learning process that allows individuals or groups to develop an overview chart of complex relationships between factors involved in complex situations. It establishes interrelationship amongst factors and discusses the managerial implications of research. Link interpretations are comparatively weak in ISM. Also, dealing with qualitative criteria is a serious task which has obscurities and vagueness. To offset this, ISM is modified to TISM where inter-linkage of factors are identified by following these steps (Agarwal 2015; Rajesh 2017).

*A. Fuzzy TISM*

This paper proposes TISM for carbon impression in oil ventures. Fuzzy TISM is multi-criteria basic leadership strategy and a powerful technique to recognize connections between various criteria by making far reaching methodical model link through a roundabout way to related criteria. TISM changes fuzzy sets into a reasonable efficient set. TISM with fuzzy sets ensures adaptability to clients to comprehend the impact of one factor over another. Client can display numbers in parallel codes (0, 1). '0' has no impact while '1' notices impact. The level of impact does not matter. Aided by fuzzy numbers, it manages the issue and ensures superior adaptability to express the impact level. Table 2 represents the applications of TISM.

TABLE 2. APPLICATIONS OF TISM

S.NO	APPLICATIONS	REFERENCE
1	Modeling enablers of TQM to improve airline performance	Singh and Sushil, 2013;
2	Modeling enablers to provide a flexible control system for industry	Jayalakshmi and Pramod, 2015;
3	Strategic performance management for Indian telecom service providers	Yadav, 2014;
4	Modeling post disaster challenges in humanitarian supply chains	Yadav and barke, 2016;
5	Strategic technology management in the automobile industry	Kedia, 2013;
6	Factors affecting customer loyalty in cloud computing	Sagar et.al., 2013
7	Revealing enablers and barriers to flexible green supply chain management	Shibin et.al., 2016
8	Modeling strategic performance management in automobile manufacturing enterprises	Yadav and Sagar, 2015;
9	Factors for smartphone manufacturing ecosystem in India	Jena et.al., 2016
10	A framework to enhance agile manufacturing systems	Sindhvani and Malhotra 2017;

The basic steps of TISM are briefly outlined as follows. (Jayalakshmi and Pramod, 2015) and (Agarwal and Vrat, 2015).

*Step I: Identify factors*

The first step in a TISM demonstration is distinguishing components whose connections are displayed. Variables for the demonstration in the investigation are components of carbon impression in oil enterprises as identified through writing and a specialist survey.

*Step II: Define logical relationship*

To build a format, it is necessary to define relevant links between the factors of enthusiasm as given in table 3. Here, logical relationships identified between variables is that "factor A will affect or upgrade factor B". An illustration might be in the "nature of a human asset will which will affect or improve the nature of work generation".

*Step III: Interpretation of relationship*

Each factor has a specific relationship translation. In TISM the elucidation will be "In what way will factor A affect or upgrade factor B?"

*Step IV: Pair - insightful correlation*

From different master audits and reports, the connection between each combination of factors a grid exhibiting nearness or nonattendance of relationship is done by putting either 'Yes (1) or 'No (0)' for every i-j interface.

*Step V: Reachability grid and transitivity check*

The interpretive rationale base has been deciphered as starting a reachability framework wherein '1' is doled out for a 'Yes' and '0' for 'No' as shown in table 4. At that point, beginning reachability lattices confirmed the transitivity lead to accomplish the final reachability framework as seen in table 5.

*Step VI: Partitioning the reachability network*

The final reachability network from step V is then isolated into various levels based on reachability and precursor sets for each factor through a progression of cycles called an apportioned level. The final levels are seen in table 6.

*Step VII: Developing digraph*

The elements are orchestrated graphically according to the levels in progression VI and coordinated connections are drawn according to connections in the reachability framework.

*Step VIII: Interaction grid*

The final digraph is converted to a double association network frame linked to all entomb activities through a '1' entry. Cells with '1' passage are translated by choosing from the learning base as an interpretive framework revealed in table 7.

*Step IX: Total interpretive auxiliary technique display*

Finally, TISM which, interfaces is reached and a clarification is composed at the edges of the separate connections. TISM display is checked for theoretical divergence and necessary modifications are made.

TABLE 3. FACTORS, CONTEXTUAL RELATIONSHIP AND INTERPRETATION

Factors	Quality of human resource	Technological Development	Geographical Factors	Market	Operational Factor	Functional Factor	By products	Govt. Reg.	Disaster	Financial support
Quality of human resource						Worker is the pillar of function	Employees consume by-products			
Technological Development	Technology equipment will affect employee job					Equipment can speed up the process				
Geographical Factors						Location can affect transportation			Resource extracted from nature	
Market					Delivery time should not be delayed					
Operational Factor										New method of travelling must be deployed
Functional Factor			Refining process affects location				Produces by-products		Causes environment pollution	Initial investment required
By Products						Non-use of by-products affects the functional process				
Government Regulations	Beneficial to workers	Forced to adopt new tech products	Regulations affect location and resource utilization							
Disaster							Avoiding fuel based vehicles for transportation			
Financial support	Salary for workers					Processes cannot be undertaken without financial support				

TABLE 4. INITIAL REACHABILITY MATRIX

FACTORS	F1	F2	F3	F4	F5	F6	F7	F8	F9	F10
F1	1	0	0	0	0	1	1	0	1	0
F2	1	1	0	0	0	1	0	0	1	0
F3	0	1	1	0	0	1	1	0	1	0
F4	0	0	0	1	1	0	0	0	0	0
F5	0	0	0	0	1	0	0	0	0	1
F6	0	0	1	0	0	1	1	0	1	1
F7	0	0	0	0	0	1	1	0	0	0
F8	1	1	1	0	0	0	0	1	1	0
F9	0	0	0	0	0	0	1	0	1	0
F10	1	0	0	0	0	1	0	0	0	1

TABLE 5. FINAL REACHABILITY MATRIX

FACTORS	F1	F2	F3	F4	F5	F6	F7		F8	F9	F10
F1	1	0	1*	0	0	1	1		0	1	1*
F2	1	1	1*	0	0	1	1*		0	1	0
F3	1*	1	1	0	0	1	1		0	1	1*
F4	0	0	0	1	1	0	0		0	0	1*
F5	1*	0	0	0	1	1*	0		0	0	1
F6	1*	1*	1	0	0	1	1		0	1	1
F7	0	0	1*	0	0	1	1		0	1*	1*
F8	1	1	1	0	0	1*	1*		1	1	0
F9	0	0	0	0	0	1*	1		0	1	0
F10	1	0	1*	0	0	1	1*		0	1*	1

TABLE 6. PARTITIONING OF THE REACHABILITY MATRIX

Iterations	Factors	Reachability set	Antecedent set	Intersection	Level
ITERATION 1	F1	1,3,6,7,9,10	1,2,3,5,6,8,10	1,3,6,10	
	F2	1,2,3,6,7,9,10	2,3,6,8	2,3,6	
	F3	1,2,3,6,7,9,10	1,2,3,6,7,8,10	1,2,3,6,7,10	
	F4	4,5,10	4	4	
	F5	1,5,6,10	4,5	5	
	F6	1,2,3,6,7,9,10	1,2,3,5,6,7,8,9,10	1,2,3,6,7,9,10	I
	F7	3,6,7,9,10	1,2,3,6,7,8,9,10	3,6,7,9,10	I
	F8	1,2,3,6,7,8,9	8	8	
	F9	6,7,9	1,2,3,6,7,8,9,10	6,7,9	I
	F10	1,3,6,7,9,10	1,2,3,4,5,6,7,10	1,3,6,7,10	
ITERATION 2	F1	1,3,10	1,2,3,5,8,10	1,3,10	II
	F2	1,2,3,10	2,3,8	2,3	
	F3	1,2,3,10	1,2,3,8,10	1,2,3,10	II
	F4	4,5,10	4	4	
	F5	1,5,10	4,5	5	
	F8	1,2,3,8,10	8	8	
	F10	1,3,10	1,2,3,4,5,10	1,3,10	II
ITERATION 3	F2	2	2,8	2	III
	F4	4,5	4	4	
	F5	5	4,5	5	III
	F8	2,8	8	8	
ITERATION 4	F4	4	4	4	IV
	F8	8	8	8	IV

TABLE 7. FINAL LEVEL OF ELEMENTS IN TISM

Factors codes	Factors	Levels
F1	Quality of human resource	II
F2	Technological development	III
F3	Geographical factors	II
F4	Market Policy	IV
F5	Operational factors	III
F6	Functional factors	I
F7	By products	I
F8	Government regulations	IV
F9	Disaster	I
F10	Financial support	II

V. VALIDATION OF TISM

A TISM display is more important than other models as each logical relationship among between factors is defined by specialists. Due to shortage of time, it is difficult to find specialists for the entire procedure. Thus, it is necessary to take the master supposition for the rationale behind the relationship as seen in Fig. 1 regarding TISM connections.

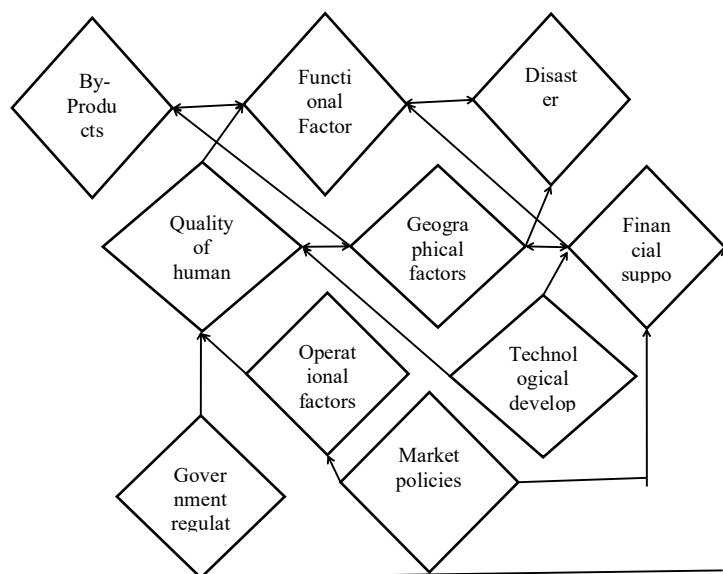


Fig .1 Validation of TISM

VI. RESULTS AND DISCUSSIONS

This paper attempts new ideas and different methods through which industries can reduce carbon emissions from the petroleum industry. With inputs from literature and expert reviews factors are partitioned into four levels. The

TISM model has been analyzed in terms of driver power and dependence between factors in the model.

- The petroleum industry has a global process of exploration, extraction, refining and transportation and any problem in these processes can cost the company a fortune. If production stops, the organization faces loss in stocks and in the market. Hence, industrial organizations should take precautions for the safety of workers and machines. Routine maintenance of the machines can prevent such incidents. Pollution and the effects of gaseous emission must be below levels indicated by government regulations. Petroleum by-products like plastics are a major issue to the environment. Dumping of plastics must be controlled. It is also necessary to totally eschew plastics. Disasters in the petroleum industry has more repercussions compared to other industries.
- Manpower plays a big role in increasing industrial productivity. If workers are not adequately qualified or not properly motivated by managers, then all steps toward technological development will lead to improved productivity. For an industry to be successful, individual work performance and attitude have an immense effect. Effective communication will influence individuals and groups to collaborate and contribute skills and expertise, which will lead to innovation. Workers must be provided adequate knowledge about carbon footprint and also newly developed technology. An added advantage to Industry 4.0 is that workers homes are controlled through cloud computing leading to SMART HOMES. Smart home provided to workers consume less fuel/energy. Such concepts must be implemented as it motivates workers to perform better. Geographical factors like power, transport, water and work site affect the petroleum industry. Regular power supply is imperative for industrial localization.
- Currently, technology products influence industrial productivity. The application of motive power and mechanical improvement to production processes has accelerated the pace of industrialization to an unprecedented degree, providing a vision of unexplored areas still ahead in applied science and technology. Introducing new technology to the petroleum industry in the refining process can overcome the effect of carbon emissions. Renewable energy is the successful technological advancement that the world has seen. Renewable energy is eco-friendly and does not release carbon gases. As the petroleum industry tends to concentrate more on the source of power, they need to move to renewable energy. Scheduling of product flows is based on transport facilities. The petroleum industry usually adopts pipeline, rail or barge transport methods as it is cheap and easy to transport products. Pipeline transportation does not need any fuel source, is eco-friendly and does not emit carbon gases into the environment. Organizations are trying to use battery trucks, a far more convenient way of transportation. Transporting through freight trucks consumes fuel, which is not cost efficient while fuel combustion releases carbon gases. In the future, automobiles will be battery

powered and controlled by cloud computing. Battery powered vehicles will lower petrol prices. Resources with skilled personnel, appropriate equipment, right infrastructure, proper maintenance and operation are needed. Financial support from the central government, interest of municipal leaders on carbon footprint issues, participation of services users and proper administration of funds are essential for a modern, sustainable system.

- Government arranging industry locations to reduce territorial variations, reducing air and water pollution is necessary in urban communities. There is a pattern to set up varied enterprises in a zone, where provision of water and power is assured. The most recent improvement is the increased number of mechanical units. The procedure of assembling is futile until the completed merchandise enters a market. Proximity to markets is fundamental for speedy transfer of merchandise as it reduces vehicle cost and empowers clients to receive items at little cost. Less travel prompts less use of fuel. Burning of fuel leads to discharge carbon gases.

## VII. CONCLUSION

Climate change, depletion of fossil fuels, emissions of carbon gases greatly impact the petroleum industry. India's oil consumption grew 8.3 percent year-on-year to 212.7 million tons in 2016 as against the global growth of 1.5 percent, which makes India, the third largest oil consuming country in the world. These numbers increase the percentage of carbon emission. This research paper attempts at providing a better vision concerning the factors behind carbon footprint. Subsequently, these factors were subjected to confirmation by reviewing their relevance in current development and future plans as well taking recourse to experts and research scholars opinions. Total Interpretive Structural Modeling (TISM) was used to link the proposed factors of carbon footprint with the coal industry. The model based on TISM is named EVALUATION OF INFLUENCE OF THE PRINCIPLES INVOLVED IN CARBON FOOTPRINT IN THE PETROLEUM INDUSTRY USING TISM. Factors involved in the TISM model are based on a vision for the betterment of organizations. These factors are based on theoretical assumptions and it requires enhancement. The model demonstrates key parameters and their interplay to reduce carbon emissions from the petroleum industry. Factors analyzed by research scholars and experts needs endorsement for wider acceptance. It is hoped that this study will help to develop a cleaner and sustainable environment. This in turn may help organizations achieve set goals and objectives, which will lead to their growth and expansion.

The results of this study help understand the relationship between carbon footprint and implementation of sustainable processes in the petroleum industry. The theoretical framework developed in this study will be a guideline for organizations to implement a new approach that incorporates sustainability in their priorities with confidence based on current developments. TISM is the most effective way to identify the success or failure of a project. This paper identified ten different factors of carbon footprint in the petroleum industry. The TISM model provides additional knowledge of the factors, rather than

focusing on all of them. TISM helps managers find the factors that drive others. This can also be used to achieve an organization's goals and objectives. There are several limitations to this study. First, this study, where the objective is to analyze and evaluate influential factors for the carbon footprint in the petroleum industry, is relatively new and usually factors influence values can change dynamically. Secondly, despite the fact that the consequences of this research study provide a decent estimate of the proposed model, different factors should be added to enhance the expectations of the proposed model including functional factors, operational factors and human resource quality. Lastly, it is worthy to conduct a comparative analysis of sustainable processes for the development of the petroleum industry in future works. The ten factors from various reports serve as a foundation to discover their sub variables. These can be explored further and validated. Adoption of these factors can pave the way for improved organizations and help industries reach new levels of performance.

## REFERENCES

1. Agarwal, A., & Vrat, P. (2015). A TISM based bionic model of organizational excellence. *Global Journal of Flexible Systems Management*, 16(4), 361-376.
2. Bird, L., Bolinger, M., Gagliano, T., Wiser, R., Brown, M., & Parsons, B. (2005). Policies and market factors driving wind power development in the United States. *Energy Policy*, 33(11), 1397-1407.
3. Bruvoll, A., & Larsen, B. M. (2004). Greenhouse gas emissions in Norway: do carbon taxes work?. *Energy policy*, 32(4), 493-505.
4. Grunewald, N., Harteisen, M., Lay, J., Minx, J., & Renner, S. (2012, August). The carbon footprint of Indian households. In *32nd General Conference of The International Association for Research in Income and Wealth* (p. 6A).
5. Huisingh, D., Zhang, Z., Moore, J. C., Qiao, Q., & Li, Q. (2015). Recent advances in carbon emissions reduction: policies, technologies, monitoring, assessment and modeling. *Journal of Cleaner Production*, 103, 1-12.
6. Jayalakshmi, B., & Pramod, V. R. (2015). Total interpretive structural modeling (TISM) of the enablers of a flexible control system for industry. *Global Journal of Flexible Systems Management*, 16(1), 63-85.
7. Jena, J., Fulzele, V., Gupta, R., Sherwani, F., Shankar, R., & Sidharth, S. (2016). A TISM modeling of critical success factors of smartphone manufacturing ecosystem in India. *Journal of Advances in Management Research*, 13(2), 203-224.
8. Kadafa, A. A. (2012). Oil exploration and spillage in the Niger Delta of Nigeria. *Civil and Environmental Research*, 2(3), 38-51.
9. Kedia, P. K. (2013, July). Total interpretive structural modelling of strategic technology management in automobile industry. In *Technology Management in the IT-Driven Services (PICMET), 2013 Proceedings of PICMET'13*: (pp. 62-71). IEEE.
10. Kenny, T., & Gray, N. F. (2009). A preliminary survey of household and personal carbon dioxide emissions in Ireland. *Environment international*, 35(2), 259-272.
11. MacCarthy, B. L., & Atthirawong, W. (2003). Factors affecting location decisions in international operations—a Delphi study. *International Journal of Operations & Production Management*, 23(7), 794-818.

12. Masini, A., & Menichetti, E. (2012). The impact of behavioural factors in the renewable energy investment decision making process: Conceptual framework and empirical findings. *Energy Policy*, 40, 28-38.
13. Matthews, H. S., Hendrickson, C. T., & Weber, C. L. (2008). The importance of carbon footprint estimation boundaries.
14. Mokhtar, S. S. M., & Yusof, R. Z. (2010). The influence of top management commitment, process quality management and quality design on new product performance: A case of Malaysian manufacturers. *Total Quality Management*, 21(3), 291-300.
15. Momirlan, M., & Veziroglu, T. N. (2005). The properties of hydrogen as fuel tomorrow in sustainable energy system for a cleaner planet. *International journal of hydrogen energy*, 30(7), 795-802.
16. Nikravesh, M., Zadeh, L. A., & Aminzadeh, F. (Eds.). (2003). *Soft computing and intelligent data analysis in oil exploration* (Vol. 51). Elsevier.
17. Panwar, N. L., Kaushik, S. C., & Kothari, S. (2011). Role of renewable energy sources in environmental protection: a review. *Renewable and Sustainable Energy Reviews*, 15(3), 1513-1524.
18. Parast, M. M., & Fini, E. H. (2011). Investigating the effect of productivity, quality, and safety on profitability in the US airline industry. *International Journal of Logistics Systems and Management*, 10(1), 70-89.
19. Piecyk, M. I., & McKinnon, A. C. (2010). Forecasting the carbon footprint of road freight transport in 2020. *International Journal of Production Economics*, 128(1), 31-42.
20. Sagar, M., Bora, S., Gangwal, A., Gupta, P., Kumar, A., & Agarwal, A. (2013). Factors affecting customer loyalty in cloud computing: A customer defection-centric view to develop a void – in-customer loyalty amplification model. *Global Journal of Flexible Systems Management*, 14(3), 143-156.
21. Sgouridis, S., Bonnefoy, P. A., & Hansman, R. J. (2011). Air transportation in a carbon constrained world: Long-term dynamics of policies and strategies for mitigating the carbon footprint of commercial aviation. *Transportation Research Part A: Policy and Practice*, 45(10), 1077-1091.
22. Shibin, K. T., Gunasekaran, A., Papadopoulos, T., Dubey, R., Singh, M., & Wamba, S. F. (2016). Enablers and barriers of flexible green supply chain management: A total interpretive structural modeling approach. *Global Journal of Flexible Systems Management*, 17(2), 171-188.
23. Silva, R. D. C. F., Almeida, D. G., Rufino, R. D., Luna, J. M., Santos, V. A., & Sarubbo, L. A. (2014). Applications of biosurfactants in the petroleum industry and the remediation of oil spills. *International journal of molecular sciences*, 15(7), 12523-12542.
24. Sindhvani, R., & Malhotra, V. (2017). A framework to enhance agile manufacturing system: A total interpretive structural modelling (TISM) approach. *Benchmarking: An International Journal*, 24(2), 467-487
25. Singh, A. K., & Sushil. (2013). Modeling enablers of TQM to improve airline performance. *International Journal of Productivity and Performance Management*, 62(3), 250-275.
26. Thompson, W., Whistance, J., & Meyer, S. (2011). Effects of US biofuel policies on US and world petroleum product markets with consequences for greenhouse gas emissions. *Energy Policy*, 39(9), 5509-5518.
27. Wong, P., Aminzadeh, F., & Nikravesh, M. (Eds.). (2013). *Soft computing for reservoir characterization and modeling* (Vol. 80). Physica.
28. Yadav, D. K., & Barve, A. (2016). Modeling post-disaster challenges of humanitarian supply chains: A TISM approach. *Global Journal of Flexible Systems Management*, 17(3), 321-340.
29. Yadav, N. (2014). Total interpretive structural modelling (TISM) of strategic performance management for Indian telecom service providers. *International Journal of Productivity and Performance Management*, 63(4), 421-445.
30. Yadav, N., -, S., & Sagar, M. (2015). Modeling strategic performance management of automobile manufacturing enterprises: An Indian context. *Journal of Modelling in Management*, 10(2), 198-225.
31. Rajesh, R. (2017). Technological capabilities and supply chain resilience of firms: A relational analysis using Total Interpretive Structural Modeling (TISM). *Technological Forecasting and Social Change*, 118, 161-169.
32. Agarwal, A., & Vrat, P. (2015). A TISM based bionic model of organizational excellence. *Global Journal of Flexible Systems Management*, 16(4), 361-376.

# Effects of Roughness Parameters on Inclined Spherical Ball Roughened Solar Air Heater

Ramesh Murmu<sup>1</sup>

<sup>1</sup>Research Scholar, Mechanical Engineering Department, NIT Jamshedpur Jharkhand-831014 India  
Mobile no- 7739336085  
Email: [murmunitjsr@gmail.com](mailto:murmunitjsr@gmail.com)

Dr. P. Kumar<sup>2</sup> Assistant Professor

<sup>2</sup>Associate Professor, Mechanical Engineering Department, NIT Jamshedpur Jharkhand-831014 India  
Email: [murmunitjsr@gmail.com](mailto:murmunitjsr@gmail.com)

Prof. H.N. Singh<sup>3</sup>

<sup>3</sup>Professor, Mechanical Engineering Department, NIT Jamshedpur Jharkhand-831014 India  
Email: [murmunitjsr@gmail.com](mailto:murmunitjsr@gmail.com)

## Abstract

An elaborative experimental investigations result in terms of heat transfer and frictional losses for an inclined spherical ball roughened solar air heater has been presented in a very precise way in the present paper with an objective to visualize the effects of roughness parameters on heat transfer and frictional losses. Experimentation was conducted under actual outdoor condition at the test rig designed and fabricated at the terrace of the Mechanical Engineering Department, NIT Jamshedpur, India. To show the effect of ever changing environmental variables like solar radiation, wind velocity, ambient temperature, etc, on the heat transfer results, the readings were noted for every 15 minutes in the experimental hours 10:00 to 15:00 hours. The present paper deals with the experimental results drafted in the form of rise in Nusselt number (Nu) and friction factor (f) for spherical ball roughened solar air heater (SAH) over those of smooth ones. Flow and roughness geometrical parameters have been varied as relative roughness pitch (p/e) 9-18, relative roughness height (e/D<sub>h</sub>) 0.024-0.040, ball's height to diameter ratio (e/d<sub>b</sub>) 0.5-2, angle of attack (α) 35°-75° and Reynolds no (Re) 2500-18500. Parametric analysis has also been made and the effects of these parameters on Nu and f characteristics have been shown. This article reveals that maximum augmentation in 'Nu' & 'f' for varying 'p/e', 'e/D<sub>h</sub>' & 'e/d<sub>b</sub>' and 'α' was respectively found to be of the order of 2.1 to 3.54 times, 1.87 to 3.21 times and 2.89 to 3.27 & 1.74 to 3.56 times for 'Nu' and 0.84 to 1.79 times, 1.46 to 1.91 times, 1.67 to 2.34 times & 1.21 to 2.67 times for 'f' in compared to non-roughened duct. The optimum roughness parameters found under present investigation is p/e = 15, e/D<sub>h</sub> = 0.036, e/d<sub>b</sub> = 1 and α = 55°.

**Keywords:** Artificially roughened solar air heater, relative roughness pitch, relative roughness height, Nusselt number, friction factor, angle of attack

## 1. INTRODUCTION

Sun is the ultimate source of most of the sources of energy. The UNDP in its 2000 World Energy Assessment found that annual potential of solar energy was 1,575–

49,837 exajoules (EJ), several times larger than total world energy consumption, which was 559.8 EJ in 2012 [1-2]. With about 300 clear and sunny days in a year, the calculated solar energy incidence on India's land area is about 5000 trillion KWh per year. The solar energy available in a single year exceeds the possible energy output of all of the fossil fuel energy reserves in India [3]. Frequent rise in energy prices have motivated many researchers to shift their thrust towards renewable sources of energy. Artificially roughened SAH is an effective method to harness solar heat energy to heat fluids (air & water) used for domestic & industrial applications. A solar collector is a type of heat exchanger which transfers the radiant energy of the incident sunlight to the sensible heat of a working fluid; air or liquid. A solar thermal collector collects heat by absorbing sunlight. The quantity of solar energy striking the Earth's surface (solar constant) averages about 1,000 W/m<sup>2</sup> under clear skies. Different types of solar collectors have been designed and developed in the last few years as a result of increased utilization of solar energy [4]. Solar air heating is a renewable energy heating technology used to heat or condition air for buildings or process heat applications. It is typically the most cost-effective out of all the solar technologies, especially in commercial and industrial applications, and it addresses the largest usage of building energy in heating climates, which is space heating and industrial process heating [5]. The value of heat transfer coefficient and heat capacity for air is low which reduces the heat transfer rate and thus increases the heat loss to the surroundings. A large number of researchers have used solar air heaters of different configurations to remove these drawbacks associated with solar air heaters to better serve the purpose of air heating [6]. Using artificial roughness of various shape geometry and orientation has been proven to be the most effective method to harness solar energy. Han et al. [7] investigated the effect of rib pitch to height ratio, and rib height to equivalent hydraulic diameter on friction factor and heat transfer coefficient for Reynolds number range of 7,000 to 90,000, relative roughness pitch range of 10 to 40, and relative roughness height range of 0.021 to 0.063 and found that the maximum values of friction factor and the Stanton number occur at a relative roughness pitch of 10. Saini and Saini [8] experimentally investigated the effect of arc shaped ribs on 'Nu & f' of rectangular ducts of

SAHs. Enhancement of 'Nu & f' was reported to be of order 3.6 and 1.75 times respectively over smooth. Lau et al. [9] continued their comparison studies on full and staggered discrete ribs arrays and reported that for a constant pumping power, 60° and 45° discrete ribs enhance the ribbed wall heat transfer by about 5 to 19 percent and 11 to 32 percent respectively compared to the corresponding full ribs case. Karwa et al. [10] carried out an experimental investigation on the integral transverse chamfered rib roughened absorber plate and found two-fold increase in the Stanton number and three-fold increase in the friction factor as compare of that of the smooth duct. Mahmood et al. [11] studied 45° angled rib turbulators and found that thermal performance is lower in the ribbed channel than in channel with dimples and/or protrusions. Ridouane and Campo [12] investigated computationally the heat transfer and pressure drop of laminar air flow in a parallel-plate channel with transverse hemi-cylindrical cavities and found enhancement in heat transfer by 30 % relative to smooth duct and pressure loss increments by 19 %. Gupta et al. [13-14] investigated 90° continuous, 60° broken ribs and 90° saw tooth profiled & established that the mean heat transfer for square channel with 60° V-broken ribs are more eminent than that of 90° saw tooth profiled rib and 90° continuous ribs. Momin et al. [15] investigated the heat transfer and friction characteristics of V-shaped rib roughness with relative roughness height range of 0.02 to 0.034, angle of attack range of 30°-90° and Reynolds number in the range of 2,500 to 18,000. The maximum enhancement in the heat transfer and friction factor was observed as 2.30 and 2.83 times of that of smooth duct for an angle of attack of 60°. Wongcharee et al. [16] investigated the effects of different shaped ribs like cylindrical, rectangular, triangular, concave-concave, convex-concave, on heat transfer and friction factor and found that the cylindrical ribs provided the highest value of thermo-hydraulic performance and minimum enhancement in Nusselt number was for rectangular ribs. Skullong and Promvong [17] performed experimental study on the heat transfer and friction characteristics in a solar air heater channel fitted with delta-winglet type vortex generators (DWs). The experimental result reveals that in the first case, the 60° DW-E at  $R_p=1$  provides the highest heat transfer and friction factor while the 30° DW-E at  $R_p=1$  performs overall better than the others. Pandey et al. [18] studied heat transfer and friction factor in rectangular channel with multiple-arc shaped with gaps as roughness element. The maximum increment in Nusselt number (Nu) and friction factor (f) was 5.85 and 4.96 times in comparison to the smooth duct. The maximum enhancement for Nu takes place at Reynolds number ( $Re$ ) = 21,000,  $g/e=1$ ,  $d/x=0.65$ ,  $W/w=5$ ,  $e/D_h=0.044$ ,  $p/e=8$  and  $\alpha/60=1$ . Kumar et al. [19-22] has used three sides instead of one side roughened duct & found that augmentation in Nu & f was respectively to be 21-86 % & 11-41 %. They also reported augmentation in thermal efficiency of three sides over one side roughened duct to be 44-56 % for varying  $p/e$  and 39-51 % for varying  $e/D_h$ . The

literature reveals that considerable amount of experimental & analytical work has been done to investigate the effect of turbulence promoters on 'Nu & f' characteristics of roughened flow passages. Roughness geometries of many shapes in different orientations like transverse rib, angled rib, inclined rib with gap, v-shaped rib, discrete or broken v-shaped rib, discrete v-shaped rib with pieces, w-shaped rib, wedge or chamfered shaped rib, dimpled shaped rib, rib-groove, Multi v-shaped rib, z-shaped rib, etc has already been used. However no study has been reported on SAH roughened with inclined spherical ball of different height and diameter soldered upon collector's face. Such roughness geometry has the advantage of inclined pattern as well as discrete roughness that could lead to rise in useful heat gain of air with reduction in propelling power of blower. More improvement can be expected in local heat transfer by using spherical ball roughened SAH, as such geometry can increase the number of secondary flow stream due to variation in angle of attack and geometrical dimension. The present research has been taken up with an objective to conduct experimentation under actual outdoor condition to visualize the effects of roughness parameters on heat transfer and frictional losses.

## 2. EXPERIMENTATIONS

Investigation is conducted to obtain the experimental values of 'Nu<sub>r</sub> & f<sub>r</sub>' in the spherical ball roughened collectors. The test rig was fabricated and calibrated properly before taking data for roughened and non-roughened ducts. The test rig had two ducts capable of accommodating roughened and non-roughened ducts simultaneously. The various sets of data recorded from the test rig included: inlet and outlet air temperatures, plate temperatures, pressure drop across the duct and the orifice and solar insolation.

### 2.1 Test Rig

The experimental set-up has been designed and fabricated as per the ASHRAE standards [23]. Fig. 1 & 2 respectively shows the schematic and actual photograph of experimental set-up. A 5 HP Centrifugal blower with a 3.5 kW Electric motor has been provided in the set-up to suck air from atmosphere through the test sections. The rectangular duct is having dimensions of 2150 mm × 330 mm × 30 mm in which the length of test section is 1200 mm and lengths of entry and exit sections are 650 mm and 300 mm respectively. The aspect ratio (W/H) of the duct is 11. The entry section is made a bell-mouthed shape at the inlet side to avoid losses at the entry. Each test section contains a glass cover of 4 mm thickness at the top and a back plate of 3 mm thick G.I sheet in the bottom. A Control valve was provided to control the flow in both the ducts. Calibrated orifice meter was installed to measure the flow rate of air through the roughened ducts. A copper constantan thermocouple has been provided at various locations to measure the plate temperatures. A digital pyranometer system was used to measure solar radiation, wind velocity, ambient temperatures. Fig. 3 & 4 shows the actual and schematic diagram of the spherical ball roughened plate

used under present study. Fig.5 shows the schematic diagram of roughened and non-roughened ducts. Fig. 6 shows the positioning of thermocouples on the absorber plates. A photograph of digital pyranometer system has been shown in Fig 7 & 8.

2.2 Roughness Parameters Range

SAH roughened passage has an L = 1200 mm, H = 30 mm and W = 300mm, the hydraulic diameter,  $D_h = 54.54$  mm. The spherical ball roughness geometry has been provided under various sets of dimensionless parameters under varying relative roughness pitch (p/e) 9-18, relative roughness height (e/D<sub>h</sub>) 0.024-0.040, ball height to diameter ratio (e/d<sub>b</sub>) 0.5-2 and relative angle of attack (α/55) 35°-75°. The flow Reynolds number has been varied from 2500-18500 to generate the best result in terms of 'Nu<sub>r</sub> & f<sub>r</sub>'. Table 1 shows the range of experimental set-up and operating roughness parameters.

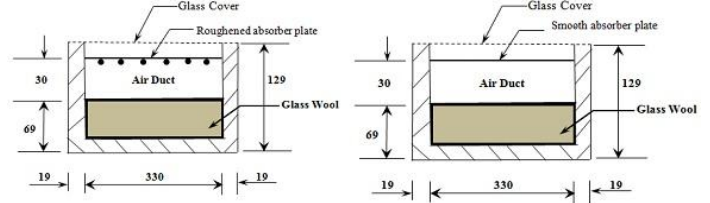


Fig. 5 Schematics of roughened and non-roughened ducts

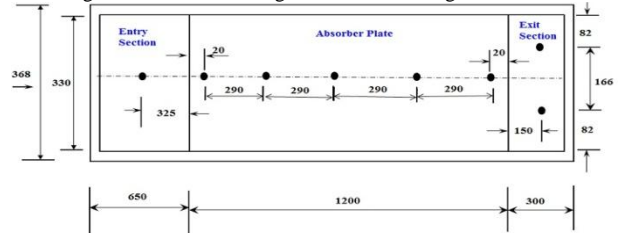


Fig. 6 Positioning of thermocouples on absorber

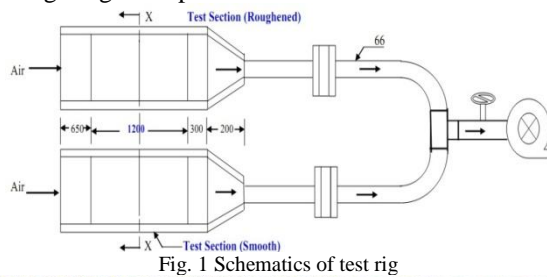


Fig. 1 Schematics of test rig



Fig. 7 Photograph of Pyranometer



Fig. 2 Photograph of test-rig



Fig. 8 Photograph of digital pyranometer system

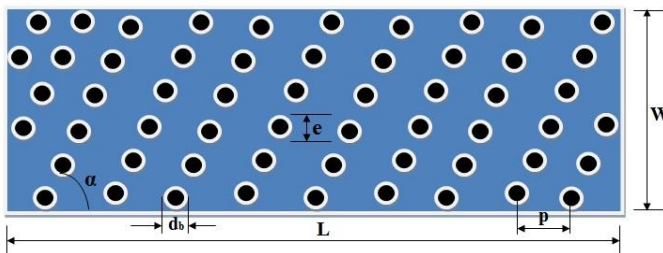


Fig. 3 Schematics of spherical ball roughened absorber



Fig. 4 Photograph of spherical ball roughened absorber

The values/range of geometrical parameters of solar air heater duct, roughness parameters and experimental conditions e.g. mass flow rate, wind velocity, insolation etc used during experimentation have been given in Table 1.

2.3 Data Reduction

The mean temperatures,  $T_{pm}$  &  $T_{fm}$  are simply the arithmetic mean of the noted values of temperatures at different locations in between the inlet & exit of the test section. Thus:

$$(T_{pm})_r = \frac{T_1 + T_2 + \dots + T_6}{6} \tag{1}$$

$$(T_{fm})_r = \frac{T_1 + T_6}{2} \tag{2}$$

Table 1 Details of Experimental Set-up and Operating conditions

S. No	Parameter	Values/R ange
1	Entry length	650 mm
	Test section length (L)	1200 mm
	Exit length	300 mm
	Width (W)	330 mm
	Height (H)	30 mm
	Duct aspect ratio (W/H)	11 mm
	Hydraulic diameter (D <sub>h</sub> )	54.54 mm
	Glass cover thickness (t <sub>g</sub> )	4 mm
	Distance between top glass cover and absorber plate (L <sub>1</sub> )	30 mm
	Relative roughness pitch (p/e)	9-18
2	Relative roughness height (e/D <sub>h</sub> )	0.024-0.040
	Ball height to diameter ratio (e/d <sub>b</sub> )	0.5-2
	Angle of attack (α)	35°-75°
3	mass flow rate (ṁ)	0.0104-0.05126 Kg/s
	Reynolds number (Re)	2500-18500
	Ambient temperature (T <sub>a</sub> )	21-41 °C
4	Solar radiation	674-986 W/m <sup>2</sup>
	Wind velocity (W <sub>v</sub> )	0.7-3.1 m/s

### 2.3.1 Mass flow rate measurement

Using the pressure drop measurement across the orifice, the flow rate of air under roughened plate is calculated as:

$$\dot{m} = C_d A_o \left[ \frac{2\rho\Delta p_o}{1-\beta^4} \right]^{0.5} \quad (3)$$

### 2.3.2 Friction Factor

The 'f' value is calculated using pressure drop ( $\Delta p$ )<sub>d</sub>, across test section length, L of 1200 mm and the mass flow rate,  $\dot{m}$  as:

$$f = \frac{(\Delta p)_d D_h}{2\rho L v_d^2} \quad (4)$$

where, D<sub>h</sub>: hydraulic diameter for the duct and is evaluated as:

$$D_h = \frac{4WH}{2(W+H)} \quad (5)$$

and, v<sub>d</sub> is the flow velocity of air flowing inside the roughened duct.

### 2.3.3 Reynolds Number

The 'Re' is calculated using:

$$Re = \frac{v_d D_h}{\nu} \quad (6)$$

### 2.3.4 Heat Transfer Coefficient

Useful heat gain of air is given by:

$$Q_u = \dot{m} C_p (T_6 - T_1) \quad (7)$$

The heat transfer coefficient for the heated test section has been calculated from:

$$h = \frac{Q_u}{A_p (T_{pm} - T_{fm})} \quad (8)$$

where, A<sub>p</sub> is the heat transfer area, assumed corresponding one side roughened plate area.

### 2.3.5 Nusselt Number

The heat transfer coefficient is used to determine the 'Nu' and is determined as:

$$Nu = \frac{h D_h}{k} \quad (9)$$

where, 'k': thermal conductivity of the air

### 2.4 Validation of Experimental Data

Alongside roughened ducts, data were also recorded for non-roughened duct for validating the experimental set-up. The data of 'Nu<sub>s</sub> & f<sub>s</sub>' obtained from experimentation have been compared with those of data obtained from the correlation of 'Nu<sub>s</sub> & f<sub>s</sub>' as per Dittus-Boelter equation and modified Blasius equation respectively.

Nu<sub>s</sub> for non-roughened surface as per Dittus-Boelter equation is given by:

$$Nu_s = 0.023 Re^{0.8} Pr^{0.4} \quad (10)$$

f<sub>s</sub> for non-roughened surface as per modified Blasius equation is given by:

$$f_s = 0.085 Re^{-0.25} \quad (11)$$

The data for 'Nu<sub>s</sub> & f<sub>s</sub>' of non-roughened ducts so obtained from experimentation and the correlations suggested above compared well with a mean deviation in experimental & estimated values of 'Nu<sub>s</sub> & f<sub>s</sub>' as ± 3.5 % for 'Nu<sub>s</sub>' & ± 4.4 % for 'f<sub>s</sub>'.

Fig. 9 (a & b) indicates the comparison of experimental values 'Nu<sub>s</sub> & f<sub>s</sub>' with 'Nu<sub>s</sub>' & 'f<sub>s</sub>' obtained from the correlations above.

### 2.5 Uncertainty Analysis

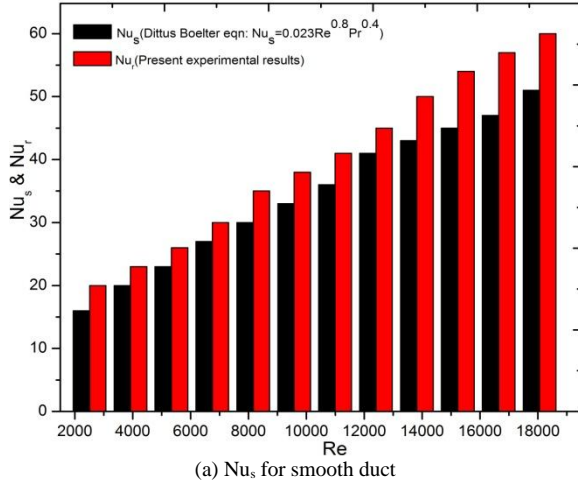
Based on the method of Kline and McClintock [24] of the uncertainties associated with various parameters, the uncertainties have been discussed and the elaborated form is given in Appendix-A. Uncertainties values of various parameters are given in Table 2:

Table 2 Uncertainties in measurement of various parameters

S.No.	Name of parameter	Uncertainty range (%)
1.	Area of absorber plate (A <sub>p</sub> )	0.08
2.	Cross sectional area of air flow duct (A <sub>c</sub> )	0.16
3.	Area of orifice meter (A <sub>o</sub> )	0.26
4.	Hydraulic diameter	0.37
5.	Density	0.106
6.	Mass flow rate	0.84
7.	Velocity of air through test section	0.76
8.	Reynolds Number (Re)	0.8
9.	Heat transfer co-efficient	3.724
10.	Nusselt number (Nu)	4.357
11.	Friction factor (f)	4.871
12.	Useful heat gain	3.753

### 3. Results and Discussions

The present investigation is aimed at examining how the 'Nu<sub>r</sub>' & 'f<sub>r</sub>' is affected by spherical ball roughness element and their varying roughness parameters. The literature of artificially roughened SAH reveals that introducing roughness on the surface of absorber enhances the heat transfer coefficient but the matter of concern is that it is



also increases frictional losses; consequently the pumping power required to ensure the continuous flow inside roughened duct also increases which results in higher power consumption, consequently reducing the net energy gain. Thus, the roughness parameters should be selected in such a way that maximum heat transfer can be obtained at the cost of minimum rise in pressure drop.

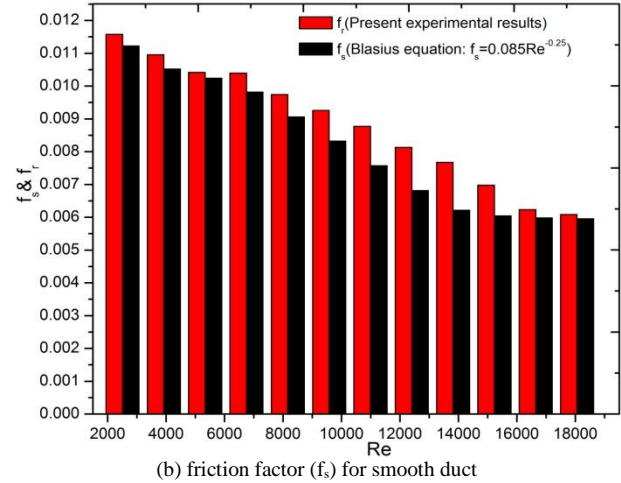


Fig. 9 Comparison of experimental and calculated values of 'Nu<sub>s</sub>' & 'f<sub>s</sub>'. Under present experimental studies, effects of spherical ball roughness element parameters such as 'p/e', 'e/D<sub>h</sub>', 'e/d<sub>b</sub>' & 'α' on 'Nu<sub>r</sub>' & 'f<sub>r</sub>' has been studied exhaustively and presented as rise in 'Nu<sub>r</sub>' & 'f<sub>r</sub>' with mass flow rate of air (Reynolds number).

#### 3.1 Heat Transfer Results

This section deals with the effects of spherical ball roughness element parameters as 'p/e', 'e/D<sub>h</sub>', 'e/d<sub>b</sub>' & 'α' on 'Nu<sub>r</sub>' has been studied exhaustively and presented as rise in 'Nu<sub>r</sub>' with mass flow rate of air (Reynolds number).

Fig. 10 shows the variation of 'Nu<sub>r</sub>' as a function of 'p/e' & 'Re' for fixed 'e/D<sub>h</sub>'=0.036, 'e/d<sub>b</sub>'=1 & 'α'=55°. The maximum & minimum value for 'Nu<sub>r</sub>' is obtained at 'p/e' of 15 & 9 respectively for the entire values of 'Re' investigated. Likewise, Fig. 12 shows the variation of 'Nu<sub>r</sub>' as a function of 'e/D<sub>h</sub>' & 'Re' for fixed 'p/e'=12, 'e/d<sub>b</sub>'=1 & 'α'=55°. The maximum & minimum value for 'Nu<sub>r</sub>' is obtained at 'e/D<sub>h</sub>' of 0.036 & 0.024 respectively for the entire values of 'Re' investigated. Fig 14 shows the variation of 'Nu<sub>r</sub>' as a function of 'e/d<sub>b</sub>' & 'Re' for fixed 'e/D<sub>h</sub>'=0.036, 'p/e'=12 & 'α'=55°. The maximum & minimum value for 'Nu<sub>r</sub>' is obtained at 'e/d<sub>b</sub>' of 1 & 2

respectively for the entire values of 'Re' investigated. Likewise, Fig. 16 shows the variation of 'Nu<sub>r</sub>' as a function of 'α' & 'Re' for fixed 'p/e'=12, 'e/d<sub>b</sub>'=1 & 'e/D<sub>h</sub>'=0.036. The maximum & minimum value for 'Nu<sub>r</sub>' is obtained at 'α' of 55° & 35° respectively for the entire values of 'Re' investigated. Maximum augmentation in 'Nu<sub>r</sub>' for varying 'p/e', 'e/D<sub>h</sub>' & 'e/d<sub>b</sub>' and 'α' was respectively 2.1 to 3.54 times, 1.87 to 3.21 times, 2.89 to 3.27 & 1.74 to 3.56 times compared to non-roughened duct. The presence of maximum Nusselt number at some particular roughness parameter signifies the presence of maximum shear layer and number of re-attachment point at that particular geometrical value. Air under roughened duct is heated because of heat absorbed by collector' surface and the roughness provided on its surface. Primary flow (flow of air in contact with absorber) and secondary flow (flow of air in contact of roughness) has the maximum opportunity to meet each other at relative roughness pitch of 15, relative roughness height of 0.036, spherical ball height to diameter ratio of 1 and angle of attack of 55°, causing maximum heat rise of air at such values.

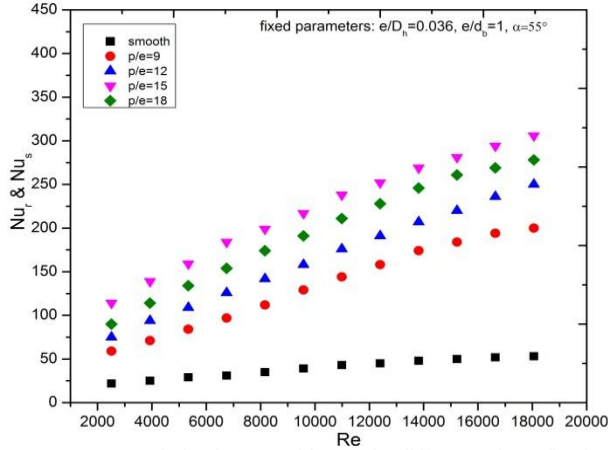


Fig. 10 Variation in 'Nu' with 'Re' for different 'p/e' & fixed 'e/D<sub>h</sub>'=0.036, 'e/d<sub>b</sub>'=1 & 'α'=55°

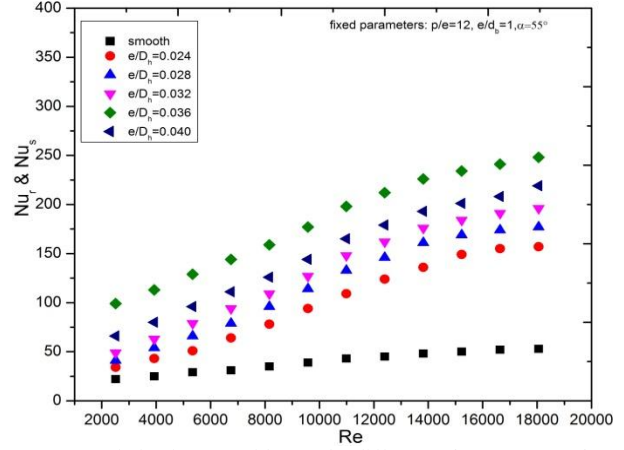


Fig. 11 Variation in 'Nu' with 'Re' for different 'e/D<sub>h</sub>' & fixed 'p/e'=12, 'e/d<sub>b</sub>'=1 & 'α'=55°

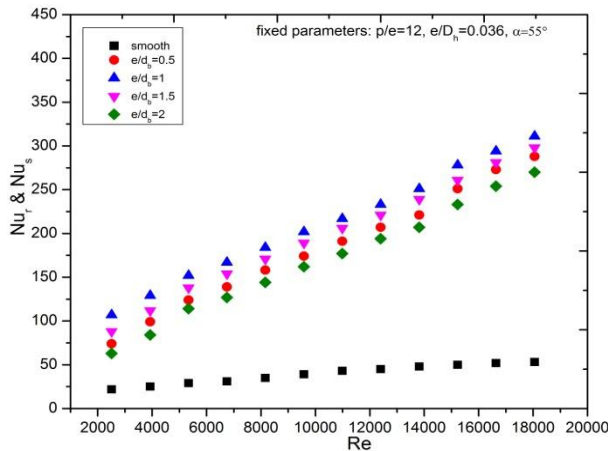


Fig. 12 Variation in 'Nu' with 'Re' for different 'e/d<sub>b</sub>' & fixed 'p/e'=12, 'e/D<sub>h</sub>'=0.036 & 'α'=55°

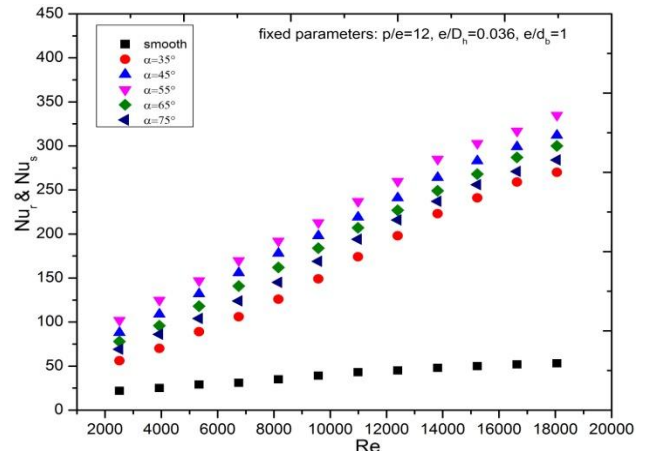


Fig. 13 Variation in 'Nu' with 'Re' for different 'α' & fixed 'p/e'=12, 'e/D<sub>h</sub>'=0.036 & 'e/d<sub>b</sub>'=1

### 3.2 Friction Factor Results

Providing artificial roughness on the collector surface results in rise in useful heat gain of air but that rise is obtained at slight increase in frictional losses compared to smooth duct. The roughness element helps in increasing heat transfer characteristics but these also offer resistance to flow that increases power requirement to propel air through roughened ducts. Geometrical dimensions of roughness is selected such that maximum Nu rise is obtained at minimum frictional losses. This section presents the effect of roughness geometrical parameter on rise in frictional losses of roughened duct compared to smooth ones. Fig. 14 shows variation of 'f<sub>r</sub>' as a function of 'p/e' & 'Re' for fixed 'e/D<sub>h</sub>'=0.036, 'e/d<sub>b</sub>'=1 & 'α'=55°. The maximum & minimum value for 'f<sub>r</sub>' is obtained at 'p/e' of 9 & 18 respectively for the entire values of 'Re' investigated. The occurrence of maximum friction factor at 'p/e' of 9 signifies that this geometrical parameter offers maximum resistance to the flow causing maximum propelling power requirement. Likewise, Fig. 15 shows the variation of 'f<sub>r</sub>' as a function of 'e/D<sub>h</sub>' & 'Re' for fixed 'p/e'=12, 'e/d<sub>b</sub>'=1 & 'α'=55°. The maximum & minimum value for 'Nu<sub>r</sub>' is

obtained at 'e/D<sub>h</sub>' of 0.040 & 0.024 respectively for the entire values of 'Re' investigated. At 'e/D<sub>h</sub>' of 0.040, maximum friction is obtained because of maximum height of spherical ball under constant hydraulic diameter. Air need more power to overcome the resistance offered by each spherical ball and move forward. Fig 16 shows the variation of 'f<sub>r</sub>' as a function of 'e/d<sub>b</sub>' & 'Re' for fixed 'e/D<sub>h</sub>'=0.036, 'p/e'=12 & 'α'=55°. The maximum & minimum value for 'f<sub>r</sub>' is obtained at 'e/d<sub>b</sub>' of 1 & 2 respectively for the entire values of 'Re' investigated. The presence of maximum and minimum value of friction factor at particular 'e/d<sub>b</sub>' value signifies that at 'e/d<sub>b</sub>' of 1, i.e. when the diameter of ball is equivalent to its height, more resistance is offered by roughness element. For minimum rise in friction, the favorable condition is ball's height should be twice its diameter. Likewise, Fig. 17 shows the variation of 'f<sub>r</sub>' as a function of 'α' & 'Re' for fixed 'p/e'=12, 'e/d<sub>b</sub>'=1 & 'e/D<sub>h</sub>'=0.036. Angle of attack is key parameter deciding rise in frictional losses value. If the arrays of spherical ball are oriented at such angle relative to flow which can result in tremendous rise in resistance offered by roughness element, such orientation should be

discarded. In the present investigation, it was found that maximum frictional losses are obtained at an angle of attack  $55^\circ$ . The maximum & minimum value for  $f_r$  is obtained at  $\alpha$  of  $55^\circ$  &  $35^\circ$  respectively for the entire values of  $Re$  investigated. It was found that the maximum augmentation

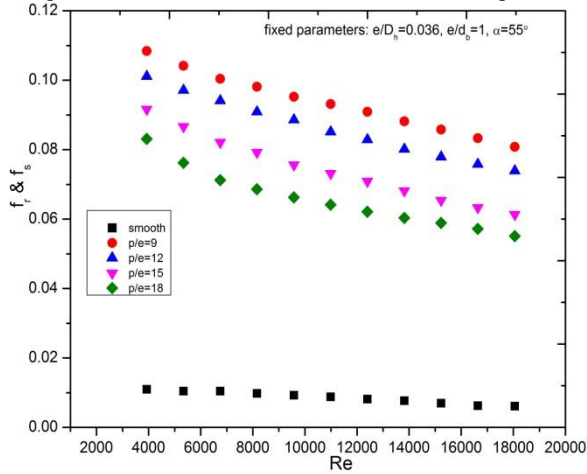


Fig. 14 Variation in ' $f_r$ ' with ' $Re$ ' for different ' $p/e$ ' & for fixed ' $e/D_h=0.036$ , ' $e/d_b=1$ ' & ' $\alpha=55^\circ$ '

in ' $f_r$ ' for varying ' $p/e$ ', ' $e/D_h$ ', ' $e/d_b$ ' and ' $\alpha$ ' was respectively found as of 0.84 to 1.79 times, 1.46 to 1.91 times, 1.67 to 2.34 times & 1.21 to 2.67 times compared to non-roughened duct.

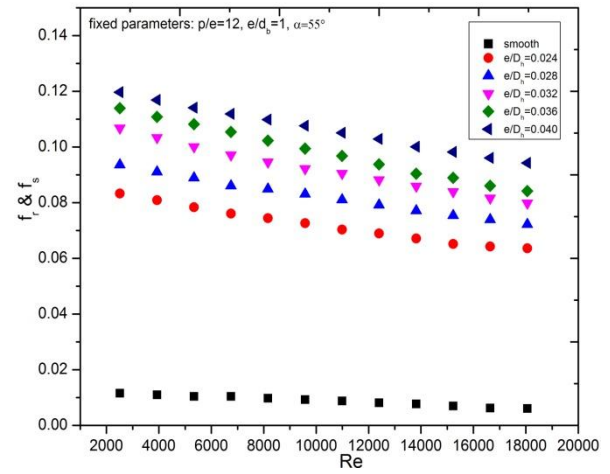


Fig. 20 Variation in ' $f_r$ ' with ' $Re$ ' for different ' $e/D_h$ ' & for fixed ' $p/e=12$ , ' $e/d_b=1$ ' & ' $\alpha=55^\circ$ '

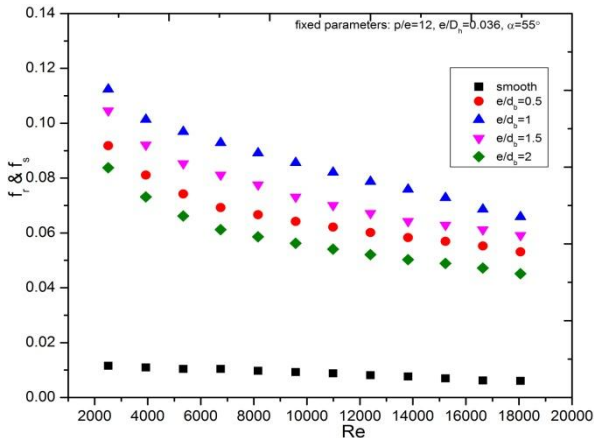


Fig. 22 Variation in ' $f_r$ ' with ' $Re$ ' for different ' $e/d_b$ ' & for fixed ' $p/e=12$ , ' $e/D_h=0.036$ ' & ' $\alpha=55^\circ$ '

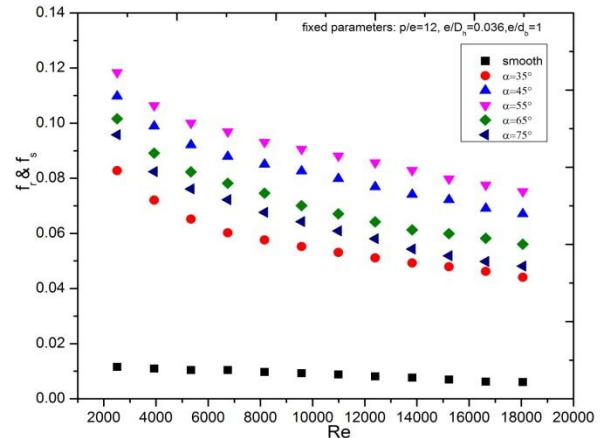


Fig. 24 Variation in ' $f_r$ ' with ' $Re$ ' for different ' $\alpha$ ' & for fixed ' $p/e=12$ , ' $e/D_h=0.036$ ' & ' $e/d_b=1$ '

It is clearly evident from this study that heat transfer is a very strong function of flow and geometrical parameters of roughness geometry. Varying the distances between spherical balls exhibited heat transfer augmentation only up to certain value beyond which any further increment in pitch resulted in heat transfer decrement. The inclination of spherical ball arrangement also shows that maximum heat transfer occur at an angle of attack of  $55^\circ$ .

#### 4. CONCLUSIONS

Exhaustive experimentation under actual outdoor conditions was conducted to generate experimental data for heat transfer and frictional losses. To increase the experimentation accuracy, data for absorber and air temperature, pressure drop across test section and orifice, wind velocity, solar radiation, etc, were recorded at every

15 minutes interval during experimentation from 1000 hours to 1500 hours. The results have been shown in the form of rise in ' $Nu_r$ ' & ' $f_r$ ' for roughened duct over those of non-roughened ones.

Nusselt number and friction factor for roughened duct varied as ' $p/e$ ', ' $e/D_h$ ', ' $e/d_b$ ' & ' $\alpha/55^\circ$ ' were varied under the given operating range. In the entire range of ' $Re$ ' studied, ' $Nu_r$ ' increased as ' $p/e$ ' was increased from 9 to 15. On further increasing the value of ' $p/e$ ', ' $Nu_r$ ' decreased. Nusselt number for roughened duct increased as the ' $e/D_h$ ' was increased from 0.024 to 0.036, beyond this, Nusselt number started decreasing with increase in  $e/D_h$  value. An increase in ball height to diameter ratio ' $e/d_b$ ' resulted in an increase in  $Nu_r$  from 0.5 to 1. Upon increasing  $e/d_b$  from 1 to 2, it was found ' $Nu_r$ ' decreased. ' $Nu_r$ ' increased as angle

of attack was increased from 35° to 55°. On further increment, 'Nu<sub>r</sub>' started decreasing. Maximum augmentation in 'Nu<sub>r</sub>' for varying 'p/e', 'e/D<sub>h</sub>', 'e/d<sub>b</sub>' and 'α/55' was respectively found as 2.1 to 3.54 times, 1.87 to 3.21 times, 2.89 to 3.27 & 1.74 to 3.56 times compared to non-roughened duct. The optimum roughness parameters yielding best result is 'p/e' = 15, 'e/D<sub>h</sub>' = 0.036, 'e/d<sub>b</sub>' = 1 and α = 55°. Friction factor decreased monotonously as the 'p/e' increased from 9-18. With the variation of 'e/D<sub>h</sub>' from 0.024 to 0.04, the values of 'f<sub>r</sub>' increased monotonously. As 'e/d<sub>b</sub>' varied from 0.5 to 1, friction factor increased and as 'e/d<sub>b</sub>' varied from 1 to 2, friction factor decreased for the entire 'Re' range investigated. The 'f<sub>r</sub>' increased as the angle of attack 'α' was increased from 35° to 55°. For further increment in angle of attack from 55° to 75°, 'f<sub>r</sub>' decreased. The maximum augmentation in 'f<sub>r</sub>' for varying 'p/e', 'e/D<sub>h</sub>', 'e/d<sub>b</sub>' and 'α' was respectively found as 0.84 to 1.79 times, 1.46 to 1.91 times, 1.67 to 2.34 times & 1.21 to 2.67 times compared to non-roughened duct.

**REFERENCES**

1. "Energy and the challenge of sustainability" (PDF). United Nations Development Programme and World Energy Council. September 2000. Retrieved 17 January 2017.
2. Sukhatme, S.P., Solar Energy Engineering, Prentice Hall Inc., New Jersey, 1986.
3. Muneer, T., Asif, M., Munawwar, S., "Sustainable production of solar electricity with particular reference to the Indian economy". Renewable and Sustainable Energy Reviews. 9 (5): 444. 2005.
4. Duffie, J.A. Beckman, W.A., Solar Engineering Thermal Processes, John Wiley, New York, 1991.
5. Wan, K.K., Li, D.H., Liu, D., Lam, J.C., Future trends of building heating and cooling loads and energy consumption in different climates, Build. Environ. 46 (1) (2011) 223–234.
6. Varun, Saini, R.P. and Singal, S.K. A review of roughness geometry used in solar air heaters. Sol Energy 2007; 81:1340–50.
7. Han, J.C., Zhang, Y.M. and Lee, C.P., 1991, Augmented heat transfer in square channels with parallel, crossed, and V shaped angled ribs, Trans. ASME Journal of Heat Transfer, Vol. 113, pp. 590-596.
8. Saini, S.K. and Saini, R.P., 2008, Development of correlations for Nusselts number and friction factor for solar air heater with roughened duct having arc-shaped wire as artificial roughness, Solar Energy, Vol. 82, pp. 1118-1130.
9. Lau, S. C., McMillan, R.D., Han, J.C., "Turbulent heat transfer and friction in a square channel with discrete rib tabulators", Trans. ASME J. Heat Transfer, Vol. 113, pp. 360 - 366, 1991.
10. Karwa, R. Solanki, S.C. and Saini, J.S., "Heat transfer coefficient and friction factor correlation for the transitional flow regime in rib-roughened rectangular duct", Int. Journal of Heat and Mass Transfer, Vol. 42, pp. 1597-1615, 1999.
11. Mahmood, G.I., Ligrani, P.M., Chen, K., Variable property and temperature ratio effects on Nusselts number in a rectangular channel with 45° angled rib turbulators, Journal of Heat Transfer, Vol. 125, pp. 769-778, 2003.
12. Ridouane, E.I.H., Campo, A., 2007, Heat transfer and pressure drop characteristics of laminar air flows moving in a parallel-plate channel with transverse hemi-cylindrical cavities, International Journal of Heat and Mass Transfer, Vol. 50, pp. 3913-3924.
13. Gupta, D., Solanki, S.C., Saini, J.S., Thermohydraulic performance of solar air heaters with roughened absorber plates. Solar Energy, Vol. 61, pp. 33–42, 1997.

14. Gupta, D., Solanki, S.C., Saini, J.S., Heat and fluid flow in rectangular solar air heater ducts having transverse rib roughness on absorber plate, Solar Energy, Vol. 51, pp. 31-37, 1993.
15. Momin, A. M. E., Saini, J.S., Solanki, S.C., 2002, Heat transfer and friction in solar air heater duct with V-shaped rib roughness on absorber plate, International Journal of Heat and Mass Transfer, Vol. 45, pp. 3383-3396.
16. Wongcharee, K. Changcharoen, W., Eiamsa-ard, S., 2011, Numerical investigation of flow friction and heat transfer in a channel with various shaped ribs mounted on two opposite ribbed walls, International Journal of Chemical Reactor Engineering, Vol. 9, pp. 1-21.
17. Skullong, S., Promvongse, P., Experimental Investigation on Turbulent Convection in Solar Air Heater Channel Fitted with Delta Winglet Vortex Generator. Fluid dynamics and transport phenomena, Chinese Journal of Chemical Engineering, 22(1)1-10(2014).
18. Pandey, N.K., Bajpai, V.K., Varun, Experimental investigation of heat transfer augmentation using multiple arcs with gap on absorber plate of solar air heater. Solar Energy 134 (2016) 314–326.
19. Kumar, V., Prasad, L., Experimental investigation on heat transfer and fluid flow of air flowing under three sides concave dimple roughened duct. International Journal of Mechanical Engineering and Technology (IJMET), Volume 8, Issue 11, November 2017, pp. 1083–1094, Article ID: IJMET\_08\_11\_110.
20. Kumar, V., Prasad, L., Thermal performance investigation of one and three sides concave dimple roughened solar air heaters. International Journal of Mechanical Engineering and Technology (IJMET) Volume 8, Issue 12, December 2017, pp. 31–45, Article ID: IJMET\_08\_12\_004.
21. Kumar, V., Prasad, L., Performance Analysis of three sides concave dimple shape roughened solar air heater, J. sustain. dev. energy water environ. syst., 6(4), pp 631-648, 2018.
22. Kumar, V., Nusselt number and friction factor correlations of three sides concave dimple roughened solar air heater, Renewable Energy 135 (2019) 355-377.
23. ASHRAE Standard 93-97, "Methods of testing to determine the thermal performance of solar collectors", American Society of Heating, Refrigerating and Air-conditioning Engineers Inc., Atlanta Ga., 1977.
24. Kline, S.J., McClintock, F.A., Describing uncertainties in single sample experiments. Mech Eng 1953; 75:3–8.

**Nomenclatures**

Parameters	Symbol	Unit
Surface area of absorber	A <sub>p</sub>	m <sup>2</sup>
Area of orifice of orifice	A <sub>o</sub>	m <sup>2</sup>
Specific heat capacity of air	C <sub>p</sub>	J/kgK
Length of SAH duct	L	m
Width of SAH duct	W	m
Height of SAH duct	H	m
Acceleration due to gravity	g	m/s <sup>2</sup>
Mass flow rate of air	ṁ	Kg/s
Thermal conductivity of air	k	W/mK
Test section pressure drop	ΔP <sub>d</sub>	N/m <sup>2</sup>
Orifice meter pressure drop	ΔP <sub>o</sub>	N/m <sup>2</sup>
Useful heat gain	Q <sub>u</sub>	W
Rise in air temperature	ΔT	°C
Outlet air temperature	T <sub>o</sub>	°C
Air Inlet Temperature	T <sub>i</sub>	°C
Ambient temperature	T <sub>a</sub>	°C
Intensity of global solar radiation (Insolation)	I	W/m <sup>2</sup>
Mean absorber plate temperature	T <sub>pm</sub>	°C
Mean air temperature in the	T <sub>fm</sub>	°C

duct		
Average velocity of air through the duct	V	m/s
Wind velocity	W <sub>v</sub>	m/s
Coefficient of discharge	C <sub>d</sub>	-
Hydraulic diameter of duct	D <sub>h</sub>	mm
Roughness pitch	p	mm
Roughness or ball's height	e	mm
Diameter of spherical ball	d <sub>b</sub>	mm
Angle of attack	α	°
Diameter of orifice	D	mm
Solar air heater	SAH	-
Cross-section	c/s	-
versus	v/s	-

Dimensionless Parameters

Name of parameter	Symbol
Relative roughness pitch	p/e
Relative roughness height	e/D <sub>h</sub>
Spherical ball height to diameter ratio	e/d <sub>b</sub>
Relative angle of attack	α/55
Friction factor	f
Friction factor for smooth surface	f <sub>s</sub>
Friction factor for roughened duct	f <sub>r</sub>
Nusselt number	Nu
Nusselt number for roughened duct	Nu <sub>r</sub>
Prandtl number	Pr
Reynolds number	Re
Aspect ratio of collector duct	W/H

Greek symbols

Name of Parameters	Symbol	Unit
Dynamic viscosity of air	μ	N s/m <sup>2</sup>
Air density	ρ	Kg/m <sup>3</sup>
Density of manometric fluid (water)	ρ <sub>m</sub>	Kg/m <sup>3</sup>
Angle of attack	α	
Kinematic viscosity of air	ν	m <sup>2</sup> /s
Relative angle of attack	α/55	
Ratio of orifice diameter (D <sub>2</sub> ) to pipe internal diameter (D <sub>1</sub> ).	β	-

Suffix

r	Roughened
s	Smooth
i	Inlet
o	Outlet
f	Fluid
a	Air

APPENDIX-A  
Uncertainty Analysis

Measurement Uncertainty

The experimental data recorded during investigation often differ from the actual data due to a lot of unaccountable factors while performing experiments. This deviation of the recorded data from actual data is called as uncertainty. The uncertainty prevailing in the measurement of various parameters has been calculated following a simple procedure suggested by Klein and McClintock [23]. The procedure for the evaluation of uncertainty has been discussed below:

Let a parameter be calculated using certain measured quantities as,

$$y = y(x_1, x_2, x_3, \dots, x_n)$$

Then uncertainty in measurement of y is given as follows:

$$\delta_y = \left[ \left( \frac{\delta_1}{\delta_1} \delta_1 \right)^2 + \left( \frac{\delta_2}{\delta_2} \delta_2 \right)^2 + \left( \frac{\delta_3}{\delta_3} \delta_3 \right)^2 + \dots + \left( \frac{\delta_n}{\delta_n} \delta_n \right)^2 \right]^{0.5} \tag{1}$$

Where  $\delta_1, \delta_2, \delta_3, \dots, \delta_n$  are the possible errors in measurements of  $x_1, x_2, x_3 \dots x_n$ .

$\delta_y$  is absolute uncertainty and  $\frac{\delta_y}{y}$  is relative uncertainty.

Uncertainty in the measurement of various parameters:

1. Area of flow, plate and orifice meter

$$\frac{\delta A_p}{A_p} = \left[ \left( \frac{\delta L}{L} \right)^2 + \left( \frac{\delta W}{W} \right)^2 \right]^{0.5} \tag{2}$$

Area of absorber plate (A<sub>p</sub>):

$$A = W \times L$$

$$\begin{aligned} \frac{\delta A_p}{A_p} &= \left[ \left( \frac{1}{1200} \right)^2 + \left( \frac{0.05}{330} \right)^2 \right]^{0.5} \\ &= 8.469 \times 10^{-4} \\ &= 0.0008469 \end{aligned} \tag{3}$$

$$\frac{\delta A_{flow}}{A_{flow}} = \left[ \left( \frac{\delta H}{H} \right)^2 + \left( \frac{\delta W}{W} \right)^2 \right]^{0.5}$$

Cross sectional area of air flow duct (A):

$$\begin{aligned} \frac{\delta A_c}{A_c} &= \left[ \left( \frac{\delta H}{H} \right)^2 + \left( \frac{\delta W}{W} \right)^2 \right]^{0.5} \\ \frac{\delta A_c}{A_c} &= \left[ \left( \frac{0.05}{30} \right)^2 + \left( \frac{0.05}{330} \right)^2 \right]^{0.5} \\ &= 1.67 \times 10^{-3} \\ &= 0.001671 \end{aligned}$$

Area of orifice meter (A<sub>o</sub>):

$$\begin{aligned} \frac{\delta A_o}{A_o} &= \left[ \left( \frac{\pi D_o \times \delta D_o}{2} \right)^2 + \left( \frac{\pi D_o^2}{4} \right)^2 \right]^{0.5} \\ \frac{\delta A_o}{A_o} &= \left[ \frac{2 \delta D_o}{D_o} \right] \\ \frac{\delta A_o}{A_o} &= \left[ \frac{2 \times 0.05}{38} \right] \\ &= 2.631 \times 10^{-3} \\ &= 0.002631 \end{aligned} \tag{4}$$

2. Hydraulic diameter

$$\begin{aligned} \frac{\delta D_h}{D_h} &= \left[ \left( \frac{\delta D_h \delta W}{W} \right)^2 + \left( \frac{\delta D_h \delta H}{H} \right)^2 \right]^{0.5} \\ &= \left[ \frac{2(330 \times 30)(330 + 30)}{2(W \times H)(W + H)} \right]^{-1} \\ \frac{\delta D_h}{D_h} &= \left[ \left( \frac{0.05 \times 0.05}{330} \right)^2 + \left( \frac{0.05 \times 0.05}{30} \right)^2 \right]^{0.5} \\ &= \left[ \frac{2(330 \times 30)(330 + 30)}{2(330 \times 30)(330 + 30)} \right]^{-1} \\ &= 3.731 \times 10^{-3} \\ &= 0.003731 \end{aligned} \tag{5}$$

3. Density

$$\begin{aligned} \frac{\delta \rho_a}{\rho_a} &= \left[ \left( \frac{\delta P_a}{P_a} \right)^2 + \left( \frac{\delta T_a}{T_a} \right)^2 \right]^{0.5} \\ \frac{\delta \rho_a}{\rho_a} &= \left[ \left( \frac{0.2}{101} \right)^2 + \left( \frac{0.41}{39} \right)^2 \right]^{0.5} \\ &= 0.00106 \end{aligned} \tag{6}$$

**4. Mass flow rate**

$$\frac{\delta \dot{m}}{\dot{m}} = \left[ \left( \frac{\delta C_d}{C_d} \right)^2 + \left( \frac{\delta A_v}{A_v} \right)^2 + \left( \frac{\delta \rho_a}{\rho_a} \right)^2 + \left( \frac{\delta \Delta P_a}{P_a} \right)^2 \right]^{0.5} \quad (7)$$

$$\frac{\delta \dot{m}}{\dot{m}} = \left[ \left( \frac{0.005}{0.62} \right)^2 + (0.002631)^2 + (0.00106)^2 + \left( \frac{0.14}{354} \right)^2 \right]^{0.5}$$

$$= 8.411 \times 10^{-3}$$

$$= 0.008411$$

**5. Velocity of air through test section**

$$V = \frac{\dot{m}}{\rho(WH)} \quad (8)$$

$$\frac{\delta V}{V} = \left[ \left( \frac{\delta \dot{m}}{\dot{m}} \right)^2 + \left( \frac{\delta \rho}{\rho} \right)^2 + \left( \frac{\delta W}{W} \right)^2 + \left( \frac{\delta H}{H} \right)^2 \right]^{0.5}$$

$$\frac{\delta V}{V} = \left[ (0.008411)^2 + (0.00106)^2 + \left( \frac{0.05}{330} \right)^2 + \left( \frac{0.05}{30} \right)^2 \right]^{0.5}$$

$$= 7.63 \times 10^{-3}$$

$$= 0.00763$$

**6. Reynolds Number (Re)**

$$\text{Re} = \frac{\rho V D_h}{\mu} \quad (9)$$

$$\frac{\delta \text{Re}}{\text{Re}} = \left[ \left( \frac{\delta V}{V} \right)^2 + \left( \frac{\delta \rho}{\rho} \right)^2 + \left( \frac{\delta D_h}{D_h} \right)^2 + \left( \frac{\delta \mu}{\mu} \right)^2 \right]^{0.5}$$

$$\frac{\delta \text{Re}}{\text{Re}} = \left[ (0.00763)^2 + (0.00106)^2 + (0.003731)^2 + \left( \frac{0.002}{1.89} \right)^2 \right]^{0.5}$$

$$= 8.051 \times 10^{-3}$$

$$= 0.008051$$

**7. Useful heat gain**

$$\frac{\delta Q_u}{Q_u} = \left[ \left( \frac{\delta \dot{m}}{\dot{m}} \right)^2 + \left( \frac{\delta C_p}{C_p} \right)^2 + \left( \frac{\delta \Delta T}{\Delta T} \right)^2 \right]^{0.5} \quad (10)$$

$$\frac{\delta Q_u}{Q_u} = \left[ (0.008411)^2 + \left( \frac{1.4}{1005} \right)^2 + \left( \frac{0.68}{24.48} \right)^2 \right]^{0.5}$$

$$= 0.03753$$

**8. Heat transfer co-efficient (h)**

$$\frac{\delta h}{h} = \left[ \left\{ \frac{\delta Q}{Q} \right\}^2 + \left\{ \frac{\delta A_p}{A_p} \right\}^2 + \left\{ \frac{\delta (T_{pm})}{(T_{pm})} \right\}^2 \right]^{0.5} \quad (11)$$

$$\frac{\delta h}{h} = \left[ \{0.03753\}^2 + \{0.0008469\}^2 + \left\{ \frac{0.29}{(29.77)} \right\}^2 \right]^{0.5}$$

$$= 0.04865$$

**9. Nusselt number (Nu)**

$$\frac{\delta Nu}{Nu} = \left[ \left\{ \frac{\delta h}{h} \right\}^2 + \left\{ \frac{\delta D_h}{D_h} \right\}^2 + \left\{ \frac{\delta (k)}{(k)} \right\}^2 \right]^{0.5} \quad (12)$$

$$\frac{\delta Nu}{Nu} = \left[ \{0.04865\}^2 + \{0.003731\}^2 + \left\{ \frac{\delta (0.00001)}{(0.02652)} \right\}^2 \right]^{0.5}$$

$$= 0.04357$$

**10. Friction factor (f)**

$$\frac{\delta f}{f} = \left[ \left\{ \frac{\delta (\Delta P_d)}{(\Delta P_d)} \right\}^2 + \left\{ \frac{\delta D_h}{D_h} \right\}^2 + \left\{ \frac{\delta (L)}{L} \right\}^2 + \left\{ \frac{\delta (V)}{V} \right\}^2 + \left\{ \frac{\delta (\rho)}{\rho} \right\}^2 \right]^{0.5} \quad (13)$$

$$\frac{\delta f}{f} = \left[ \left\{ \frac{(0.01)}{(10)} \right\}^2 + \{0.003731\}^2 + \left\{ \frac{(0.67)}{1200} \right\}^2 + \{0.00763\}^2 + \{0.00106\}^2 \right]^{0.5}$$

$$= 0.04871$$

The uncertainty analysis has been carried out for the entire set of parameter investigated within the operating range and the uncertainty variation of various parameters obtained is presented in Table 2.

# OPTIMIZATION OF RC ONE WAY SLAB USING GENETIC ALGORITHMS

**Fayaz Basha Shaik Bepari<sup>1</sup>**

Assistant Professor,  
Department of civil Engineering,  
Chaitanya Bharathi Institute of  
Technology,  
Proddatur, Andhra Pradesh, India,  
fayazbasha768@gmail.com

**S.Mahaboob Basha<sup>2</sup>**

Assistant Professor,  
Department of civil Engineering,  
Chaitanya Bharathi Institute of  
Technology,  
Proddatur, Andhra Pradesh, India,  
basha.myd@gmail.com

**Y.Dasthagir<sup>3</sup>**

Assistant Professor,  
Department of civil Engineering,  
Chaitanya Bharathi Institute of  
Technology,  
Proddatur, Andhra Pradesh, India,  
dasthagir.y@gmail.com

## ABSTRACT

*Design Optimization is the process of finding best design parameters that satisfy the project requirements both in terms of strength and serviceability criteria. In the present paper this optimization is carried out for Reinforced Concrete (RC) slabs using Genetic Algorithms (GA), an iterative procedure which is based on theory of natural selection and evolutionary biology. The reinforced concrete slabs considered in particular for the design of simply supported one way slab. The design of the slabs is based on IS: 456-2000 code specifications. The objective is to include the cost of concrete, the cost of reinforcement and the cost of formwork respectively with their volume of materials.*

*This genetic algorithm iterative values are developed using MATLAB and the codes are used for optimization. The results obtained are compared with the known published results.*

*Further, the changes in the optimum values are studied by the variation of several constraints such as the number of generations, population size and mutation rate. Also by changing the fixed parameters i.e., the characteristic cube strength of concrete and characteristic yield strength of steel, the effect on the optimum cost for a particular loading condition and also for various loading conditions is studied.*

**Keywords:** Design optimization, Genetic Algorithm, One way slab, Reinforced Concrete

## 1. INTRODUCTION

In the construction stream of civil engineering, in particular the construction of reinforced concrete structures, optimization is playing a vital role in terms of economy as well as safety considerations. The overall cost of the reinforced concrete structure including the cost of concrete, reinforcement steel and cost of formwork are considered for optimization<sup>[1]</sup>. The optimum solution obtained by using conventional methods face some difficulties while solving problems related to executing same moment of resistance exhibited by slab measurements and percent of reinforcement steel. To avoid the difficulty, the Genetic Algorithm (GA) method of optimization of RC simply supported one way slab according to IS 456:2000<sup>[2]</sup> is studied in the present paper.

### 1.1. OPTIMUM DESIGN OF STRUCTURE

Optimum design indicates the most economical design that is practically possible which should also satisfy the safety requirements as per IS code. Optimum structural design indicates maximum utilisation of the existing material sources.

## 1.2. OBJECTIVE OF THE STUDY

The main objective of the study is minimization of total cost of the RC simply supported slab and using Genetic Algorithm optimization program<sup>[3]</sup> in MATLAB software with IS 456:2000 code as a constraint.

## 1.3. APPROACH OF THE STUDY

After the detailed inspection of the preceding related works, genetic algorithm optimization programs are established and the efficiency of the optimization programs are verified by applying illustrative problems on RC simply supported one way slab. The design results obtained from MATLAB are compared with the previous works. Also the known parameters are changed and the variation of optimum values as influenced by the variation of the constraint is studied

## 2. METHODOLOGY OF THE STUDY

Design of any member indicates the determination of dimensions of the structure which fulfil the requirements of the code and should be most economical and safe. The present study is conducted on slabs which are the reinforced concrete elements transferring the transverse loads which creates the bending moments and shear forces<sup>[4]</sup>.

The basic design begins by selecting the cross section dimensions which should withstand the bending moment and also selecting the necessity of steel reinforcement. Then the slab dimensions should be checked for shear and deflection.

### 2.1. DESIGN PREVIEW FOR SLABS

The programs developed in the thesis for the optimization of simply supported and cantilever slab follows certain provisions of IS 456:2000, which include the clear cover to the steel, trial sections for depth, maximum moment coefficients of slabs, requirements for reinforcing steel, shear reinforcement and deflection control.

#### 2.1.1. SIMPLY SUPPORTED ONE WAY SLAB

The loading diagram and the geometry of simply supported one way slab are shown in fig.1 and fig.2 respectively.

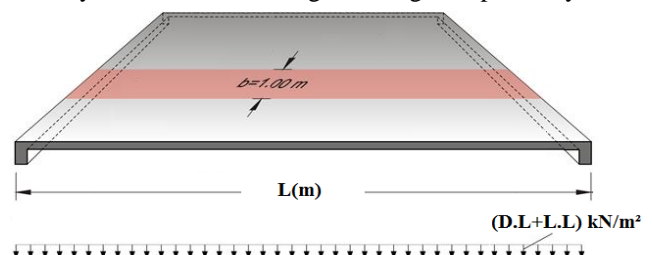


Figure 1: Typical simply supported RC one way slab with distributed load<sup>[5]</sup>

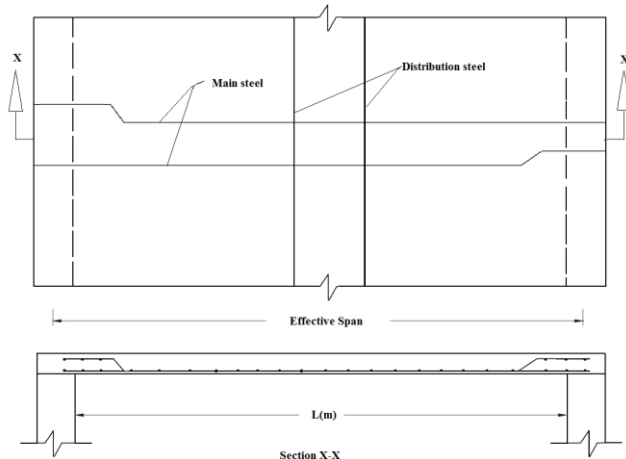


Figure 2: Geometry of a RC one way slab <sup>[6]</sup>

2.1.2. CONSTANT PARAMETERS

The constant values considered for the reinforced concrete one way slab model are Span length of the slab, Span to depth ratio, The characteristic compressive cube strength of the concrete, The characteristic strength of the steel, The uniformly distributed super imposed loads, The cost of the quantity of concrete, The cost of required steel reinforcement, The cost of the required formwork.

2.1.3. DESIGN VARIABLES

The following variables are treated in the simply supported one way slab problem are:  $d$  = effective depth of slab ( $x_1$ ),  $p_t$  = percentage of steel ( $x_2$ ),  $s_v$  = spacing of reinforcement bars( $x_3$ ).

2.1.4. DESIGN CONSTRAINTS

The design constraints used in the study include the span to depth ratio, minimum depth constraint, constraints to be considered in flexural design, minimum and maximum spacing between reinforcement bars, deflection constraints and the constraints for shear design according to IS 456:2000

2.1.5. OBJECTIVE FUNCTION

The objective function in this RC one way slab in which the total cost including the cost of concrete, the cost of reinforcement steel and the cost of formwork is defined as follows:

$$f(x) = C_c [width * (x(1) + d') * breadth - (x(2) * 0.01 * width * x(1) * x(3) * (\frac{width}{x(2)} + 1) * breadth) (0.0012 * width * (x(1) + d'))] + C_s [(x(2) * 0.01 * width * x(1) * x(3) * (\frac{width}{x(2)} + 1) * breadth) + (0.0012 * width * (x(1) + d'))] + C_f [breadth * (x(1) + d')]$$

Where,

$x(1)$  = effective depth of the slab,  $d$

$x(2)$  = percentage reinforcement ratio of steel,  $p_t$

$$p_t = \frac{100 f_{ck}}{2 f_y} * \left( 1 - \sqrt{1 - \frac{4.598 * w_u * l^2}{b d^2 * f_{ck} * 8}} \right)$$

$x(3)$  = spacing of reinforcement,  $s_v$

$$s_v = \frac{78.5398 * \phi^2}{b * d * p_t}$$

$C_c$  = cost of concrete including labour charges(Rs./m<sup>3</sup>)

$C_s$  = cost of steel including bending of bars (Rs./m<sup>3</sup>)

$C_f$  = cost of formwork(Rs./m<sup>2</sup>)

$d'$  = effective nominal cover to the reinforcement (mm)

$f_{ck}$  = characteristic compressive strength of the concrete in N/mm<sup>2</sup>

$f_y$  = characteristic yield strength of the steel in N/mm<sup>2</sup>

$l$  = effective span of the slab in metre.

$M_u$  = bending moment due to super imposed load and self-weight in kN-m

$w_u$  = design load in kN/m<sup>2</sup> = 1.5(dead load +live load)

$b$  = width of the slab = 1000 mm

$\phi$  = diameter of the reinforcing bar (mm)

3. GENETIC ALGORITHM

Genetic algorithms are the search algorithms that have been evolved from the evolution observed in nature, namely the process of natural selection, genetic and survival of the fittest. The main operators include:selection, fitness function, reproduction, crossover, mutation<sup>[8]</sup> etc.,

3.1 IMPLEMENTATION OF GENETIC ALGORITHM IN MATLAB

MATLAB, an acronym for MAT-rix LAB-oratory, is a very effective technical language for mathematical programming. It offers a broad form of options that are useful to a designer who utilises GA and to those who want to experiment with optimization using genetic algorithms to learn about possible applications.

4. RESULTS

Reinforced concrete simply supported one way slab and cantilever slab are studied by making valid generated GA programs, the results obtained are compared with the previous work.

4.1. REINFORCED CONCRETE ONE WAY SLAB PROBLEM

The loading diagram considered for the slab is as shown in fig. 3

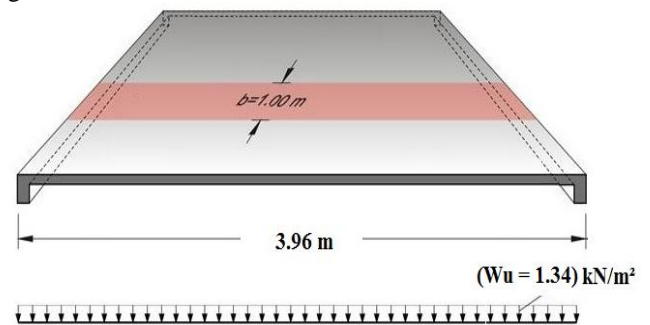


Figure 3: The RC one way slab numerical example

4.1.1. THE FIXED PARAMETERS

- 1) Span of the slab is 3.96 m
- 2) Uniformly distributed load of 1.34 kN/m<sup>2</sup>
- 3) Characteristic cube strength of the concrete  $f_{ck}$ = 20.68 MPa
- 4) Cost of concrete,  $C_c$  = 610 (Rs. /m<sup>3</sup>)
- 5) Characteristic strength for the steel  $f_y$  = 275.8 MPa
- 6) Cost of steel bars,  $C_s$  =95.2809 (Rs. /kg).

SOLUTION:

The above problem is solved using Genetic algorithm coding and the results obtained are as follows:

Cost = 1650.34 Rs. /m

$d$  = 167.80 mm

$p_t$  = 0.3738%

$s_v$  = 262.9 mm

This study is compared with one of the previous works

Cost = 1770.36 Rs. /m

$d = 158.75 \text{ mm}$

$p_t = 0.42\%$

$s_v = 220 \text{ mm}$

The optimum cost obtained by genetic algorithm coding is compared with the optimal cost obtained by one of the previous works and it is observed that former showed a reduction of 6.78% in total cost.

#### 4.2. EFFECT OF CHANGE OF MUTATION, GENERATION AND POPULATION:

##### Input data for design problem

- 1) Span of the slab is 4 m
- 2) Uniformly distributed live load of  $3 \text{ kN/m}^2$
- 3) The characteristic cube strength for concrete  $f_{ck} = 20 \text{ MPa}$
- 4) The characteristic yield strength of steel  $f_y = 415 \text{ MPa}$ .

**Output:** For 100 generation, 100 population size, and 0.01 mutation.

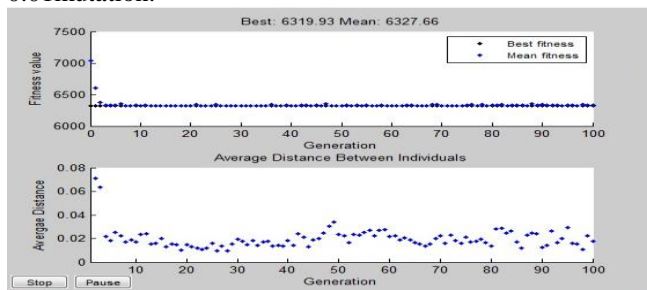


Figure 4: showing the optimum cost value for one way slab

##### 4.2.1 THE NUMBER OF GENERATIONS:

A study is carried out by changing the number of generations while making the other values as unchanged as follows:

The number of population size = 100, and the mutation rate = 0.01, the method of selection is selected as Roulette Wheel function.

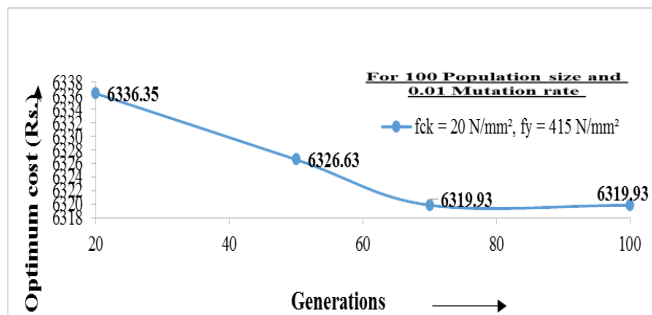


Figure 5: No. of generations vs. Optimum cost for one way slab

##### 4.2.2 THE POPULATION SIZE:

A study is carried out by changing the population size while making the other values as unchanged as follows:

The number of generations = 100, and the mutation rate = 0.01, the method of selection is selected as Roulette Wheel function.

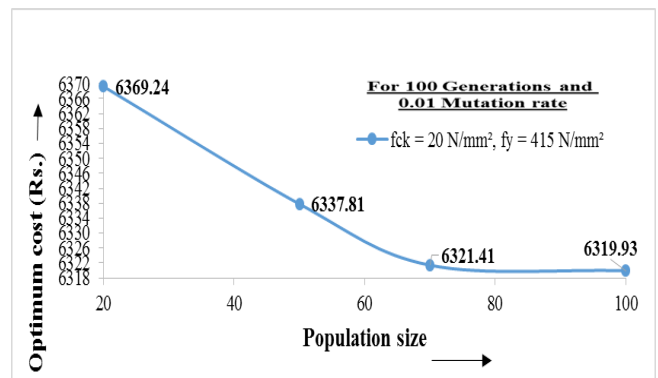


Figure 6: Population size vs. Optimum cost for one way slab

##### 4.2.3 MUTATION RATE

A study is carried out by changing the mutation rate while making the other values as unchanged as follows:

The number of generations = 100, and the number of population size = 100, the method of selection is selected as Roulette Wheel function.

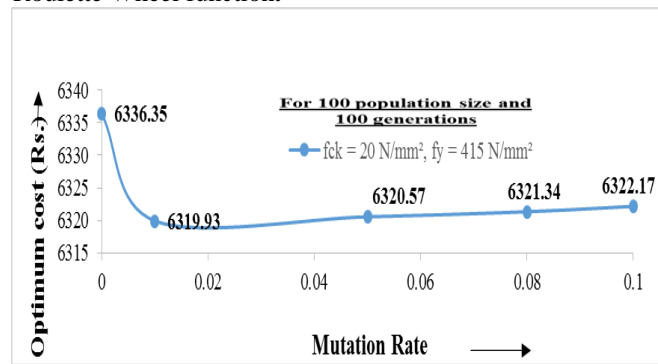


Figure 7: Mutation rate vs. Optimum cost for one way slab

#### 4.3 EFFECT ON OPTIMUM COST BY CHANGING THE CONSTANT PARAMETERS

The effect on the optimum cost value by changing the constant parameters is observed using illustrated problems of the RC one way.

##### 4.3.1 EFFECT OF VARIATION IN GRADE OF CONCRETE AND STEEL:

By changing the value of the compressive cube strength of the concrete and for the steel, there will be correspondingly change in the unit cost of the concrete and steel. In this region genetic algorithm programs are applied for different values of the compressive cube strength of the concrete and for the steel and the respective obtained optimum values of the solution is studied. The changing values of concrete are 20 and 25 MPa and for steel the changing values are 415 and 500 MPa for the RC one way slab.

The results of the illustrated problems shown in fig. subsequently for a particular load is studied and by changing loading values the effect of variation in grade of concrete and steel is studied for simply supported RC one way slab.

##### INPUT DATA FOR DESIGN PROBLEM

- 1) Span of the slab is 4 m
- 2) Uniformly distributed live load of 3,5 and  $7 \text{ kN/m}^2$

- 3) The characteristic cube strength for concrete  $f_{ck} = 20$  and 25 MPa
- 4) The characteristic yield strength of steel  $f_y = 415$  and 500 MPa.

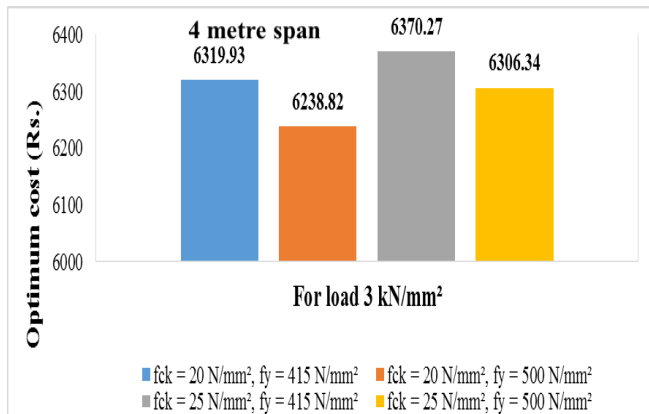


Figure 8: Effect of variation of grade of concrete and steel (RC one way slab)

## 5. CONCLUSIONS

- 1) It was observed that when the no. of generations and population size is smaller the obtained value of the GA codes for the both the slabs show far away from the optimum value of the solution and the best optimum value is obtained by changing the generation value to 100 after this value also there is no change in this best solution.
- 2) Mutation rate plays an important role in the genetic algorithm process. It was shown that without and with larger values of mutation rate the obtaining solution is far away from the best obtained solution and at value of 0.01 mutation rate the optimum solution is obtained.
- 3) In this study the illustrated examples are accomplished which shows that the total cost of slab increases when there is increase in characteristic strength of concrete, while fixing the applied load and grade of steel.
- 4) In this study the illustrated examples are applied which shows that while there is increase in grade of the steel, there will be decrease in the optimum cost value while fixing the applied load and compressive strength of concrete.
- 5) The optimum cost for the slab is achieved by M20 grade of concrete and Fe500 grade of steel.
- 6) On comparison with an earlier literature related to cost optimization of reinforced concrete slabs, it was concluded that there was cost reduction of 6.78% for the RC one way slab.

## 6. REFERENCES

1. **Chakrabarty, B.K.**, (1992), "A model for optimal design of reinforced concrete beams", Asian Journal of Civil Engineering, Vol. 118, pp. 3238-3242.
2. **IS 456-2000**, "Code of Practice for Plain and Reinforced Concrete", Bureau of Indian Standards, New Delhi.
3. **Saini, B., Sehgal, V.K., and Gambhir, M.L.**, (2006), "Genetically optimized artificial neural network based optimum design of singly and doubly reinforced

- concrete beams", Asian Journal of Civil Engineering, Building and Housing, Vol.7, pp. 82-97.
4. **Sahab, M.G., Ashaour, A.F., and Toropov, V.V.**, (2004), "Cost optimization of reinforced concrete flat slab buildings", Engineering Structures, Vol.12, pp. 124 - 256.
5. <http://www.buildinghow.com/enus/Products/Books/VolumeB/Slabs/Cantilevers-one-way-slabs>.
6. **Krishna Raju, N., and Pranesh, R.N.**, (2003), Reinforced Concrete Design, Second Edition, New Age International Limited, Publishers.
7. **Dutta, B.N.**, (1992), Estimation and Costing in Civil Engineering, Twenty fourth Edition, UBS Publishers and Distributors Pvt.Ltd.
8. **Whitely, D.**, (1994), "A genetic algorithm tutorial", Statistics and computing, Vol.4, pp. 65-85.
9. **Alqedra, M., Arafa, M., and Ismail, M.**, (2011), "Optimum cost of prestressed concrete beams using genetic algorithms", Journal of Artificial Intelligence, Vol.4, pp.76-88.
10. **Behrouz, A.N., and Hesam, V.**, (2011), "Minimum cost design of concrete slabs using Particle Swarm Optimization", World Applied Sciences Journal, Vol. 13, pp.2484-2494.
11. **Gunaratnam, D.J., and Sivakumaran, N.S.**, (1978), "Optimum design of reinforced concrete slabs ", Structural Engineering, Vol.3, pp. 61 – 67.
12. **Camp, C.V., Pezeshk, S., and Hansso, H.**, (2003), Flexural design of reinforced concrete frames using a genetic algorithm", Asian Journal of Civil Engineering, Vol.23, pp. 733 – 944.

# WEAR BEHAVIOUR OF ALUMINIUM MATRIX COMPOSITES

Vijayakumar. K

Lecturer, Department of Mechanical Engineering, TPEVR Government Polytechnic College, Vellore- 632002, Tamilnadu.

E-mail: kvtpdevr@gmail.com

## ABSTRACT

Aluminium based metal matrix composites have low density, relatively low price, available in large quantities, superior strength to weight ratio and corrosion resistance. So it is extensively used in automotive and aerospace industries for drums, brake callipers, disc brake rotors, transmission casing, connecting rods and oil pumps, where adhesive wear are predominant in these components. For adhesive wear, the influence of applied load, sliding speed, wearing surface hardness, reinforcement content and morphology are critical parameters in relation to the wear rate encountered by the material. The reinforcements added to an alloy lead to variation in properties and improve the composite wear resistance. In this present work, it is to fabricate and study the wear behaviour of Aluminium matrix composites. Aluminium alloy reinforced with B<sub>4</sub>C particles with various weight percentage will be fabricated their wear behaviour will be studied using computerized Pin-on-disc wear testing machine.

Keywords :Adhesive wear, Pin-on-disc, wear parameters, Aluminium Matrix Composites (AMCs)

## 1. INTRODUCTION

Today searches in finding new materials superior than the conventional ones have an increasing demand. In these studies, Aluminium Matrix Composites (AMCs) have gained great attention especially in the industries such as aviation, space and automotive. Recently, AMCs have been used for the automobile products, such as engine piston, cylinder liner, brake drum, brake disc due to their light weight, high strength, high specific modulus, low co-efficient of thermal expansion and good wear resistance properties.

An important issue in the production of Metal Matrix Composites (MMCs) is the chemical compatibility between the matrix and the reinforcement, particularly when using liquid metal process. Casting of MMCs is an attractive processing method since it is relatively inexpensive and offers a wide selection of materials and processing conditions. But poor wetting between Al and B<sub>4</sub>C below 1100°C means that it is difficult

to produce Al - B<sub>4</sub>C composites by mixing particles into the liquid phase. In order to enhance the wettability of ceramics and improve their incorporation behaviour into Al metals, particles are often heat treated or coated.

Therefore, K<sub>2</sub>TiF<sub>6</sub> flux is used in order to increase the wetting between Al and B<sub>4</sub>C and facilitate the incorporation of B<sub>4</sub>C particles into molten aluminium. To avoid insufficient reaction phase at the interface and to lower the processing cost, no additional processes except the traditional casting method were used in this study.

## 2. EXPERIMENTAL PROCEDURE

### 2.1 MATERIAL SELECTION

Material has been selected based on the properties, cost and application. The boron carbide particles are added as reinforcement with Aluminum cast alloy to improve the wear characteristics of the composite material.

Matrix Phase : ALUMINUM ALLOY LM25

Reinforcement : BORON CARBIDE (B<sub>4</sub>C)

### 2.1.1 SPECIFICATION OF ALUMINIUM ALLOY LM 25

Table 1 Chemical Composition of Aluminium Alloy LM 25

Contents	Chemical composition
Copper (Cu)	0.01
Silicon (Si)	6.86
Magnesium (Mg)	0.37
Iron (Fe)	0.159
Nickel (Ni)	< 0.001
Tin (Sn)	< 0.005
Zinc (Zn)	0.01
Titanium (Ti)	0.02
Lead (Pb)	< 0.002
Aluminum (Al)	Balance

### 2.1.2 APPLICATIONS OF ALUMINIUM ALLOY LM 25

- Used in Automobile engine blocks and liner.

- Hydraulic cylinders and pressure vessels.
- Intricate components
- In Automotive braking system.

### 2.1.3 BORON CARBIDE (B<sub>4</sub>C)

Boron Carbide is an extremely hard ceramic material. Boron Carbide is one of the hardest materials known, ranking third behind diamond and cubic boron nitride. It is the hardest material produced in tonnage quantities. Boron carbide powder is mainly produced by reacting carbon with B<sub>2</sub>O<sub>3</sub> in an electric arc furnace, through carbo – thermal reduction or by gas phase reactions. For commercial use B<sub>4</sub>C powders usually need to be milled and purified to remove metallic impurities.

### 2.1.4 PROPERTIES OF B<sub>4</sub>C

- Extreme hardness
- Difficult to sinter to high relative densities without the use of sintering aids.
- Good chemical resistance
- Good nuclear properties
- Low density
- Light weight
- Erosion resistance

**Table 2 Typical Properties of Boron Carbide**

Density (g / cm <sup>3</sup> )	2.52
Melting Point (°C)	2445
Hardness (Knoop 100g) (Kg / mm <sup>2</sup> )	2900-3580
Fracture Toughness (MPa.m <sup>-1/2</sup> )	2.9-3.7
Young's Modulus (GPa)	450-470
Electrical Conductivity (at 25°C) (S)	140
Thermal Conductivity (at 25°C) (W/m.K)	30-42
Thermal Expansion Co – eff. X 10 <sup>-6</sup> (°C)	5
Thermal neutron capture cross section ( barn)	600

### 2.1.5 APPLICATIONS OF BORON CARBIDE (B<sub>4</sub>C)

- Used as an abrasive in polishing and lapping applications
- Used for dressing diamond tools.
- Ceramic tooling dies applications.
- Used for precision tool parts.

## 2.2 PROCESSING OF THE COMPOSITE

Liquid state fabrication of Metal Matrix Composites involves incorporation of dispersed

phase into a molten matrix metal, followed by its Solidification. In order to provide high level of mechanical properties of the composite, good interfacial bonding (wetting) between the dispersed phase and the liquid matrix should be obtained. The simplest and the most cost effective method of liquid state fabrication is Stir Casting. Stir Casting is a liquid state method of composite materials fabrication, in which a dispersed phase ( ceramic particles, short fibers) is mixed with a molten matrix metal by means of mechanical stirring. The liquid composite material is then cast by conventional casting methods and may also be processed by conventional Metal forming technologies.

Stir Casting is characterized by the following features:

- Content of dispersed phase is limited (usually not more than 30 Vol.%)
- Distribution of dispersed phase throughout the matrix is not perfectly homogeneous.
- There are local clouds (clusters) of the dispersed particles ( fibers).
- There may be gravity segregation of the dispersed phase due to a difference in the densities of the dispersed and matrix phase.
- The technology is relatively simple and low cost.

## 2.3 WEAR TEST

A pin-on-disc test apparatus was used to investigate the dry sliding wear characteristics of the fabricated AMCs. ASTM G99 – 05 a standard test method for wear testing using a pin-on-disc apparatus was followed. The wear specimen (pin) of 6 mm diameter and 40 mm height was machined from the cast AMC samples. The disc material was chosen as AISI 4140 (EN 19) steel alloy. The disc specimen of 55 mm diameter and 10 mm thickness was cut from the steel rod and heat treated to achieve the hardness of 55 HRC. The contact surfaces of the pin and disc material were surface grinded and polished metallographically in order to achieve the surface roughness of 0.8 μm or below. Surface roughness was ensured using contact surface roughness tester SurfCorder SE3500 and the R<sub>a</sub> values are found to be less than 0.8 μm. During the test the pin was pressed against the rotating counter part by applying the load. LVDT on the lever arm helps determine the wear at any point of time by monitoring the movement of the arm. Applied load helps to maintain the pin in contact with the disc. This movement of the arm generates a signal which is used to determine the maximum wear and the coefficient of friction is monitored continuously as wear occurs. The initial

weight of the pin material is measured in a single pan electronic weighing machine with least count of 0.0001 g. After running through a fixed sliding distance the specimen was removed, cleaned with acetone, dried and weighed to determine the weight loss due to wear. The difference in the weight measured before and after the test gave the sliding wear of the composite specimen and then the volume loss was calculated.

### 3. RESULTS AND DISCUSSION

The experimental plan is designed to find the factors influencing the wear process to achieve the minimum wear rate and maximum coefficient of friction. The experiments were developed by involving the following factors, sliding speed, sliding distance, load and weight percentage reinforcement of the material. These parameters are helpful in determining the composite performance.

15	1.5	1000	45	6	0.003402355	0.4032
16	2.0	1000	15	6	0.004108788	0.4631
17	2.0	1000	30	6	0.003412572	0.4235
18	2.0	1000	45	6	0.002272722	0.3912
19	1.5	1000	15	9	0.001859952	0.5336
20	1.5	1000	30	9	0.002616557	0.4812
21	1.5	1000	45	9	0.003347977	0.4436
22	2.0	1000	15	9	0.001861809	0.5032
23	2.0	1000	30	9	0.002246064	0.4712
24	2.0	1000	45	9	0.002981587	0.4335

Table 3 Results of AMCs

S l. No	Sliding speed (m/s)	Sliding Distance (m)	Load (N)	% reinforcement	Wear rate (mm <sup>3</sup> /m)	COF
1	1.5	1000	15	Base Alloy	0.002217161	0.4065
2	1.5	1000	30	Base Alloy	0.00339448	0.3811
3	1.5	1000	45	Base Alloy	0.003699875	0.3334
4	2.0	1000	15	Base Alloy	0.004077313	0.4045
5	2.0	1000	30	Base Alloy	0.001889111	0.3672
6	2.0	1000	45	Base Alloy	0.004087481	0.3372
7	1.5	1000	15	3	0.002355	0.4568
8	1.5	1000	30	3	0.002973514	0.3929
9	1.5	1000	45	3	0.003854201	0.437
10	2.0	1000	15	3	0.003476429	0.4451
11	2.0	1000	30	3	0.003350712	0.4040
12	2.0	1000	45	3	0.00380004	0.4445
13	1.5	1000	15	6	0.0020522	0.4735
14	1.5	1000	30	6	0.002272276	0.4513

Figure 1 Wear Rate Vs Load

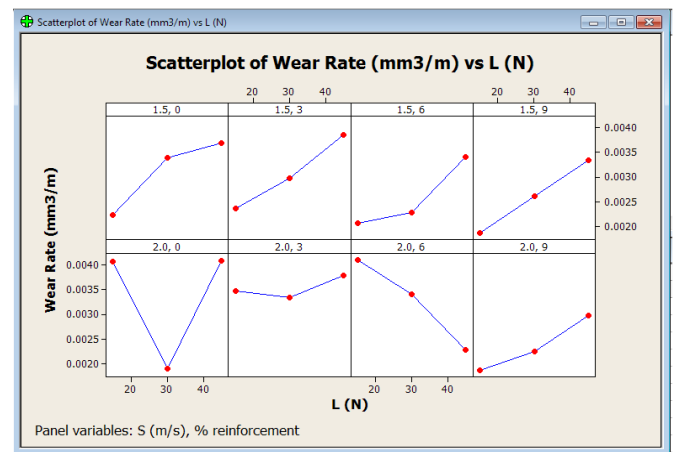
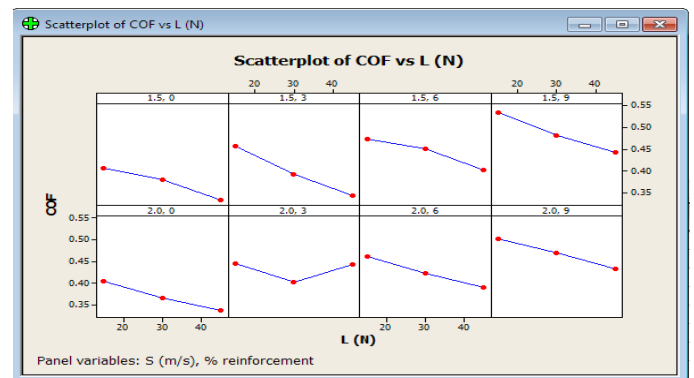


Figure 2 COF Vs Load



### 4. CONCLUSION

The experimental study reveals following conclusions:

1. For a given load, the cumulative wear volumes of composites and pure aluminium pins increase linearly under dry sliding
2. The wear rate increases linearly with the increase in normal load
3. The average co-efficient of friction decreases with increase in load in both pure aluminium and composites. However the composites show a higher co-efficient of friction than that observed in pure aluminium

## REFERENCES

1. Topcua, H.O Gulsoyb, N. Kadioglu, A.N. Gulluoglu, (2009) 'Processing and mechanical properties of B<sub>4</sub>C reinforcement Al matrix composites', Journal of Alloys and Compounds, Vol.482 pp.516-521
2. GursoyArslan, AyseKalemtas, (2009) Processing of silicon carbide – boron carbide – aluminum composites, 'Journal of the European Ceramic Society, Vol.29, pp.473-480.
3. Surappa.M.K., (2003) 'Aluminum matrix composites: Challenges and opportunities', Sadhnan, Vol.28, Parts 1& 2 pp. 319-334.
4. Shorowordi K.M., Laoui. T, Haseeb A.S.M.A, Celis J.P., Froyen .L, (2003) 'Microstructure and interface characteristics of B<sub>4</sub>C, SiC and Al<sub>2</sub>O<sub>3</sub> reinforced Al matrix composites: a comparative study', Journal of Materials Processing Technology, Vol.142,pp. 738-743.
5. R.Ipek (2005) 'Adhesive wear behavior of B<sub>4</sub>C and SiC reinforced 4147 Al matrix composites (Al/ B<sub>4</sub>C – Al/SiC)', Journal of material processing technology, Vol.162-163,pp.71-75.
6. Hashim.J.,L.Looney, M.S.J. Hashmi, (1999) Metal matrix composites: production by the stir casting method', Journal of Materials Processing Technology Vol. 92-93 pp. 1-7
7. Ramachandra.M., K. Radhakrishna, 'Effect of reinforcement of flyash on sliding wear, slurry erosive wear and corrosive behavior of aluminum matrix composite', Wear Vol.262 pp.1450-1462.
8. Deuis.R.L.,C.Subramanian& J.M. Yellupb, 'DRY SLIDING WEAR OF ALUMINUM COMPOSITES -A REVIEW', Composites Science and Technology, Vol.57,pp.415-435.
9. Pasto.A.E., D.N Braski, T.R. Watkins, W.D. Porter, E. Lara- Curzio, S.B.McSpadden, (1999) Characterization techniques for composites and other advanced materials', Composites: Part B, Vol.30, pp.631-646
10. Kok.M., K.O zdin, (2007) 'Wear resistance of aluminum alloy and its composites reinforced by Al<sub>2</sub>O<sub>3</sub> particles'. Journal of Materials Processing Technology, Vol. 183, pp.301-309
11. Sathyabalan, P.V. Selladurai and P.Sakthivel (2009) ANN Based Prediction of Effect of Reinforcements on Abrasive Wear Loss and Hardness in a Hybrid MMC', American J. of Engineering and Applied Sciences 2 (1) pp. 50-53
12. Shorowordi.K.M., A.S.M.A Haseeb, J.P. Celis, (2006) 'Tribo-surface characteristics of Al- B<sub>4</sub>C and Al-SiC composites worn under different contact pressures', Wear, Vol.261, pp.634-641
13. Hosking.F.M., F.Folgar Portillo, R.Wunderlin T,R. Mehrabian, (1982) Composites of aluminium alloys: fabrication and wear behaviour', Journal Of Materials Science, Vol. 17 pp. 477 – 498
14. IsilKerti, FatihToptan, (2008) 'Microstructural variations in cast B<sub>4</sub>C reinforced aluminium matrix composites (AMCs)', Materials Letters, Vol.62pp. 1215-1218

# *THERMAL ANALYSIS OF VARIOUS FRICTION SURFACING MATERIALS USING ANSYS*

Sivanesh A R

*Department of Mechanical Engg  
Sri Ranganathar Institute of Engineering  
and Technology  
Coimbatore, India  
sivaneshravi@gmail.com*

Aravind Kumar R

*Department of Mechanical Engg  
Sri Ranganathar Institute of Engineering  
and Technology  
Coimbatore, India  
aravindrano@gmail.com*

Arivazhakan.D

*Department of Mechanical Engg  
Sri Ranganathar Institute of Engineering  
and Technology  
Coimbatore, India  
arivu0678@gmail.com*

**Abstract**— Surface engineering techniques are increasingly being used in manufacturing industries to extend the life of components. Friction surfacing is an advanced process of great potential, especially in the field of repair and reclamation of worn and damaged components. The temperature field of consumable rod in friction surfacing, as a kind of thermal processing technology, is an important factor in the successful implementation of the process. In this paper, the heat source model of various consumable rods (Aluminum, Brass, and Zinc) is coated on low carbon steel using friction surfacing process. And we do analysis for each component using ANSYS. From the obtained results we identify the best suitable material for low carbon steel combination.

**Keywords**— Friction surfacing, Temperature field, Thermal analysis

## I. INTRODUCTION

Friction surfacing is an advanced technique in surface modification. Its typical process is illustrated in Fig. 1 in which a consumable-rod rotates at a high spindle speed. The symbol  $n$  represents rotations per minute, and a certain axial force  $F$  is applied on the consumable-rod from the top to allow the consumable-rod to press against the substrate tightly. As a result, intense friction heat is produced from the friction generated at the rubbing surface between the substrate and the consumable-rod. Later, the contact end of the consumable rod becomes plasticized, and the preheating phase is then

accomplished. The substrate begins to move relative to the consumable-rod at traverse speed  $v$ , and the coating material transfers from the end of the consumable-rod to the substrate to form a coating.

Due to its advantages, such as its clean, high efficiency, and good qualities, friction surfacing has become a potential “green” manufacturing technology. It opens up a new area of repair and reclamation of worn and damaged components. In fact, the technique has attracted a number of researchers in the recent decade.

With friction surfacing employed primarily in the field of engineering, most studies conducted on it have focused on its technical characteristics. Vitanov and co-workers (Vitanov et al., 2000, 2001; Vitanov and Voutchkov, 2005) developed a neurofuzzy model-based decision support system to speed up the parameter selection process. Verevkin et al. (2003) calculated the parameters of friction surfacing regimes on the basis of mathematical modeling. Batchelor et al. (1996) attempted to identify the feasibility of various consumable materials (aluminum, zinc and brass) on

substrates under, studied the effects of metal type on friction surfacing. Studied the interfacial phenomena during the friction surfacing of low carbon steel.

Apart from technical characteristics, many studies dwelled on identifying the mechanisms of the process. Bedford et al.(2001) discussed the mechanism of auto-hardening of the surfacing layer in friction surfacing. Fukakusa (1996, 1997) put forward the concept of real rotational contact plane in friction surfacing, together with in friction welding. The surfacing materials transferred from the consumable rod to the substrate does not pass through the whole rotational plane, but only the center of the rotational plane, that is called real rotational contact plane.

Focus on the utilization of aluminum zinc and brass bars for the coating layer employed hollow rods composed of to get uniformly distributed M.M.C. coatings. Coated aluminum, zinc and brass bars onto substrate (low carbon), and studied the effects of surfacing conditions on the structure and mechanical properties of both the monolayer and multilayer. In the present study, thermal analysis was employed to simulate the consumable-rod’s temperature field. The temperature field in friction surfacing, especially of the consumable-rod, is considered an important element in analyzing the process’ mechanism and in the proper choice of key process parameters. The result from this study can provide theoretical guidance in analyzing the feasibility and choosing key parameters in similar endeavors.

## II. EXPERIMENTAL

The experimental apparatus is modified based on a driller, wherein the substrate’s motion relative to the consumable-rod is achieved by moving the working platform of the driller.

Temperatures at certain points of the consumable-rod were measured using a thermocouple. The temperature distribution up to preheat at the consumable-rod were distributed evenly along the axial side with of the interval of 10mm. The temperature of the point at the rubbing surface was measured through the method referred to as “semi-thermal couple” (Du et al., 1996).

The experimental work on micro friction surfacing was conducted by adapting a friction surfacing machine for the purpose. The rotational speed (rpm), the feed rate of mechtrode ( $V_z$ ) and the traverse rate of the substrate ( $V_x$ ) were the essential machine input parameters. The normal force which is set directly on dedicated machines (for friction surfacing) was represented by the feed rate  $V_z$  of the mechtrode because of the specific requirements of the

friction surfacing machine. Normal force ( $F_n$ ) and substrate temperatures at specific locations were the measurable in process parameters. And temperature distribution of mechtrode is the process output that measured. The substrate geometry and its dimensions (mm) are shown in Fig. 1.

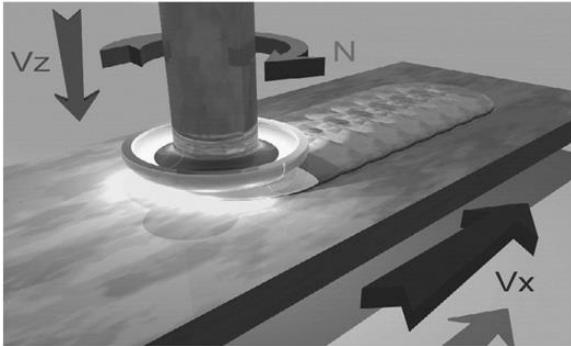
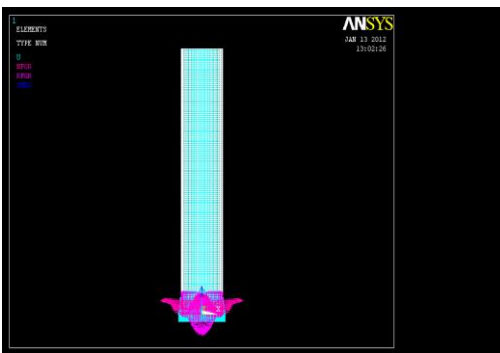


FIG.1.Friction Surfacing Process

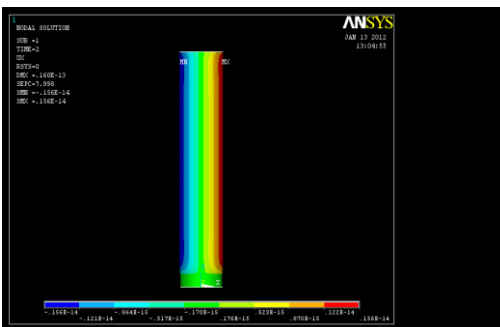
### III. COUPLED FIELD ANALYSIS

#### A.MATERIAL OF ALUMINIUM

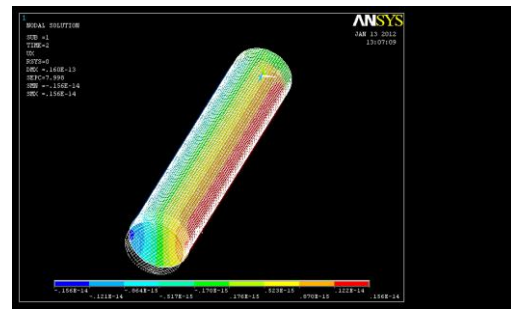
a)Meshed with load model



b)Deformed shape only

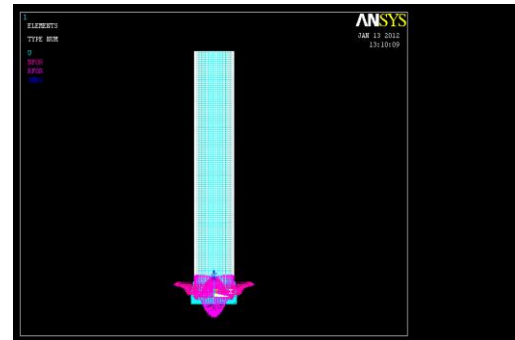


c)Deformed with un-deformed shape

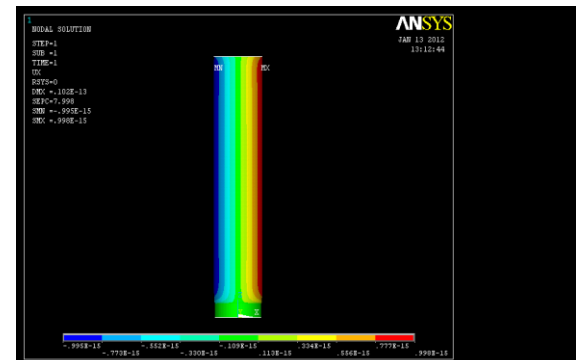


#### B.MATERIAL OF ZINC

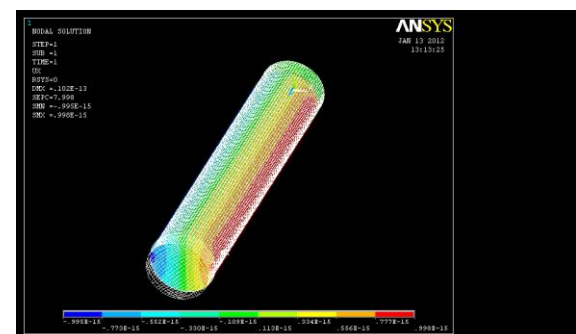
a)Meshed with load model



b)Deformed shape only

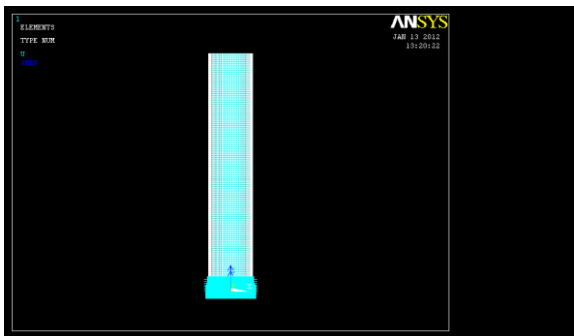


c)Deformed with un-deformed shape

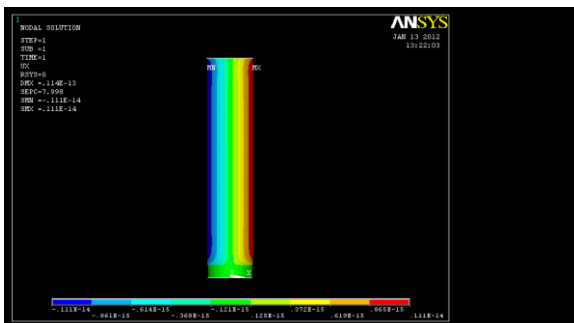


C. MATERIAL OF BRASS

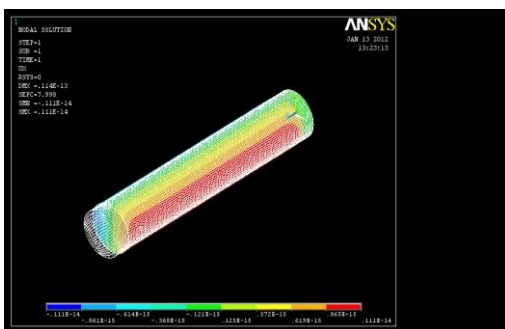
a) Meshed with load model



b) Deformed shape only

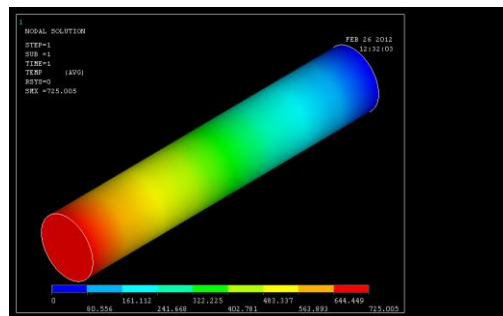


c) Deformed with un-deformed shape

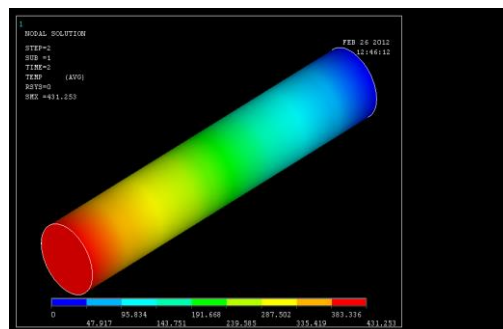


V. THERMAL ANALYSIS

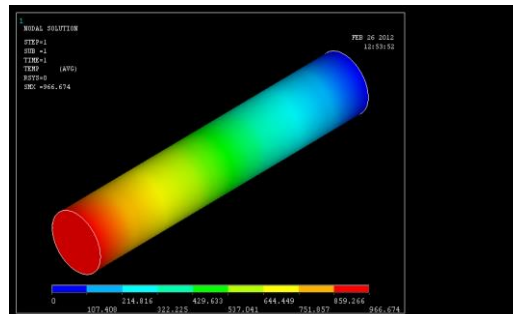
A. Temperature distribution in Aluminium



B. Temperature distribution in Zinc



C. Temperature distribution in Brass



VI. OPTIMIZATION OF SPEED

IV. DESIGN CALCULATION

Power (or) heat flux =  $2\pi nt/60$

Torque (t) =  $(\pi/16) \times fs \times d^3$

$t/j = g\theta/l = \tau/r$

Torque = force x distance (or) length

t = torque

n = speed

g = young's modulus

l = length

r = radius

fs = shear stress

j = polar moment of inertia

MATERIALS	OPTIMIZED SPEED (RPM)	TEMPERATURE RANGE (°C)
ALUMINIUM	1500	644.44 - 725.00
ZINC	450	383.33 - 431.25
BRASS	1000	859.26 - 966.67

## VII. DIMENSION OF MATERIALS

Substrate (low carbon steel)

Length=150 mm

Breath=100 mm

Thickness=18 mm

Consumable rod or mechtrode (Al, B, Zn)

Length=100 mm

Diameter=18 mm

## VIII. MELTING POINT OF MATERIALS

Low carbon steel = (1464-1536<sup>0</sup>C)

Al = 660<sup>0</sup>C

B = 940<sup>0</sup>C

Zn = 419<sup>0</sup>C

## IX. CONCLUSION

- Based on the existing research work we have studied the friction surfacing process. From that going to select three mechtrode (aluminium, brass and zinc) with the friction surfacing process is going to done on low carbon steel substrate.
- Finally analysis results to identify the best suitable material for low carbon steel combination.
- Finally zinc is the best suitable material for low carbon steel combination in friction surfacing process

## X. REFERENCES

- [1]. H. Khalid Rafi, et al. ``Friction surface tool steel (H13) coating on low carbon steel: A study on the effects of process parameters on coating characteristics and integrity`` Surface and Coatings Technology 205 (2010) 232-242.
- [2]. Xuemei Liua,\*, Junshan Yaob, Xinhong Wang, Zengda Zoua, Shiyao Qua `` Finite difference modeling on the temperature field of consumable-rod in friction surfacing`` journal of materials processing technology 209 (2009 ) 1392–1399.
- [3]. V.I. Vitanov,et al `` Application of response surface methodology for the optimization of micro friction surfacing process`` Surface & Coatings Technology 204 (2010) 3501–3508.
- [4]. H. Khalid Rafi , G.D. Janaki Ram, G. Phanikumar, K. Prasad Rao `` Micro structural evolution during friction surfacing of tool steel H13`` Materials and Design (2010).
- [5]. Mehmet Eroglu ``Boride coatings on steel using shielded metal arc welding electrode: Microstructure and hardness. Surface & Coatings Technology`` 203 (2009) 2229–2235.
- [6]. X. M. Liu , Z.D. Zou , S.Y.Qu`` Finite Difference Modeling on The Temperature Field of Substrate in Friction

Surfacing`` Second International Conference on Computer Modeling and Simulation (2010)

[7]. M.L.Herring,J.I.Mardel, B.l.fox ``The effect of material selection and manufacturing process on the surface finish of composites`` journal of material processing technology 210(2010)926-940.

[8]. V.I.Vitanov,N.Javaid ``investigation of the thermal field in micro friction surfacing`` surface & coating technology 204 (2010) 2624-2631.

# EFFECT OF IMMERSION DEPTH OF A SWIRLING FLOW TUNDISH SEN ON MULTIPHASE FLOW AND HEAT TRANSFER IN MOLD

Siddappa Nyamagoud<sup>1</sup>

Assistant professor  
Dept of Mech Engg,  
Mrce,Hyd,INDIA.

<sup>1</sup>siddappanyamagoud@gmail.com,

J Sudha pallavi<sup>2</sup>

Assistant professor  
Dept of Mech Engg,  
Mrce,Hyd,INDIA.

<sup>2</sup>sudhapallavi24@gmail.com

M Veerareddy<sup>3</sup>

Assistant professor  
Dept of Mech Engg,  
Mrce,Hyd,INDIA.

<sup>3</sup>mudelveera@gmail.com,

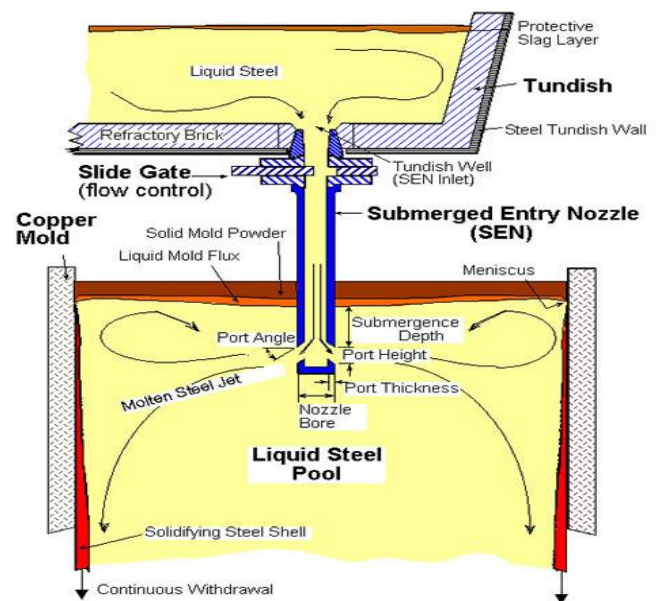
**Abstract**—The effect of the immersion depth of a new swirling flow tundish SEN (Submerged Entry Nozzle) on the multiphase flow and heat transfer in a mold was studied using numerical simulation. The RSM (Reynolds Stress Model) and the VOF (Volume of Fluid) model were used to solve the steel and slag flow phenomena. The results show that the SEN immersion depth can significantly influence the steel flow near the meniscus. Specifically, an increase of the SEN immersion depth decreases the interfacial velocity, and this reduces the risk for the slag entrainment. The calculated Weber Number decreases from 0.8 to 0.2 when the SEN immersion depth increases from 15 cm to 25 cm. The temperature distribution has a similar distribution characteristic for different SEN immersion depths. The high temperature region is located near the solidification front. Temperature near the meniscus was slightly decreased when the SEN immersion depth was increased, due to an increased steel moving distance from the SEN outlet to the meniscus.

**Keywords**—swirling tundish; heat transfer; submerged entry nozzle; flow pattern; contineous casting mold.

## I. INTRODUCTION

Multiphase flow and heat transfer are very important phenomena in the continuous casting mold. These phenomena include steel-slag flow, inclusion motion, solidification, and so on. They can significantly influence the quality of the semifinal steel product. The basis for a good control on multiphase flow and heat transfer is a desirable steel flow in mold. In the past, many studies have been carried out to optimize the multiphase flow and heat transfer in mold. In the past, many studies have been carried out to optimize the multiphase flow and heat transfer in mold. The optimization investigations firstly focused on the structure of the SEN (Submerged Entry Nozzle), such as the SEN type (straight or bifurcated), SEN port design (shape, angle, thickness), and SEN immersion depth. Argon injection in SEN was also a widely investigated method to improve the continuous casting process, with the aim to reduce the nozzle clogging, reduce the steel reoxidation and increase the inclusion floatation in mold. Recently, swirling flow SEN has been considered to be a promising method to further modify the steel flow in mold. The significant improvement with this method is that it can directly change

the steel flow characteristics before the steel flows into the mold for example, the prevention of an impingement jet flow from a straight SEN. It was found that the heat and mass transfer near the meniscus can be remarkably activated, and a uniform velocity distribution can be obtained within a short distance from the SEN outlet .Furthermore, the penetration depth of the SEN outlet flow is remarkably decreased in a billet mold. Industrial trial results show that the swirling flow SEN effectively improved the steel product quality and reduced the clogging problem of the SEN side ports.



## II. MODEL DESCRIPTION

A three-dimensional mathematical model has been developed to describe the multiphase flow and heat transfer in a billet mold during the continuous casting of steel. The geometry and the dimension of the billet mold model is shown

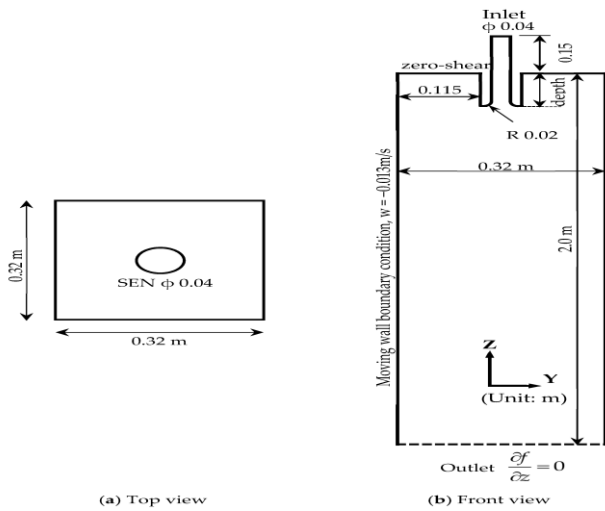


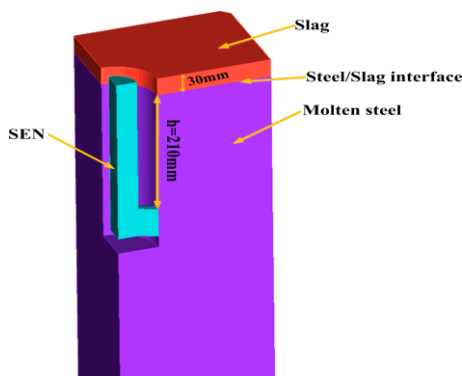
Figure 1. geometry of casting mold(top view and front view)

**A. Model assumption**

The numerical model is based on the following assumptions:

- Steel and slag behave as incompressible Newtonian fluids
- Solidification in the mold is not considered;
- A constant molecular viscosity for steel and slag was assumed. This is due to the fact that the maximum temperature difference in the mold is only 30 K between 1788 K and 1818 K as the superheat of the steel. The viscosity change in this temperature range is not significant, and this can be seen from a previous study.
- A constant steel and slag density was used. The temperature influence on the steel density change was accounted for in the source term of the momentum equation.

Full geometrical models are taken for all cases. For



example, the meshed computational model equipped with the two-port SEN is shown in Figure 2, where the technology of local grid refinement is applied to simulate the behavior of the initial solidified shell more accurately. The meshes of FLUENT computational domain include non-uniform grids with approximately 1,700,000 cells.

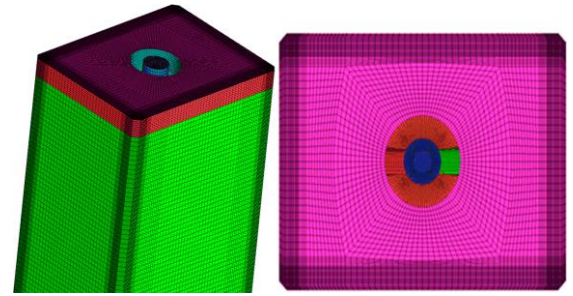


Table 1 Thermal properties of the steel and slag.

Parameters	Symbols	Steel	Slag
Density,kg/m <sup>3</sup>	$\rho_o$	7000	2600
Viscosity,kg(m-s)	$\mu$	.006	.09
Thermal conductivity,w(m-k)	K	35	1.1
Specific heat,j/(kg-k)	$C_p$	628	1200

**B. Boundary Conditions**

The velocity profile on the cross section of the cylindrical tundish SEN, which has been solved in a previous study, was used as the inlet boundary condition for the current simulation of the mold flow. This steel flow velocity at the inlet in figure 1, has been presented in a previous study and, thus, it is not repeated here. A nonslip boundary condition was imposed on the SEN wall. A zero-shear slip wall boundary condition was used at the mold surface. For the mold wall, a moving wall boundary condition with the velocity of 0.013 m/s in Z or downwards direction was used to account for the movement of the solidified shell in a real casting process. A fully developed flow condition is adopted at the mold outlet, where the normal gradients of all variables are set to zero. A constant steel temperature of 1818 K was used at the inlet, with a superheat of 30 K. A constant temperature of 1788 K was imposed on the solidified shell. An adiabatic condition was used both at the SEN wall and at the free surface.

**C. Solution method**

The numerical model was solved using the commercial software ANSYS FLUENT 18.0. The numerical simulations were carried out based on 1.4 million grid cells to guarantee the grid-independent solution. A fine grid was used in the near-wall region, with the  $y^+$  value of the first grid layer

around 1. The PISO (Pressure-Implicit with Splitting of Operators) scheme was used for the pressure-velocity coupling. Furthermore, the PRESTO method was adopted to discretize the pressure. The governing equations were discretized using a second order upwind scheme. The convergence criteria were as follow: The residuals of all dependent variables were smaller than  $1 \times 10^{-3}$  at each time step.

### III. SIMULATION RESULTS AND DISCUSSION

#### A. Steel flow phenomena

Figure shows the steel flow path in the mold with different SEN immersion depths. It can be observed that the steel flow pattern in mold was similar for different SEN depths. It delivers the steel into the mold along the periphery of the SEN, which is in  $360^\circ$ . The SEN outlet flow moves towards the solidified shell after it flows out from the straight SEN due to the swirling flow effect, inducing a rotational steel flow momentum. After the steel stream reaches the solidified shell, a part of the steel flows downwards along the solidified shell with a horizontally rotational flow momentum, and another part of the steel moves upwards and towards the meniscus. Due to the difference in SEN immersion depth, the top rotational flow region near the meniscus was large when a large immersion depth of SEN was used. This should be beneficial for the decrease of the steel flow velocity, since the steel from SEN outlet needs a long distance to reach the steel-slag interface. Therefore, the current swirling flow tundish SEN can deliver high temperature steel uniformly distributed towards the solidified shell, no matter the change of the SEN depth.

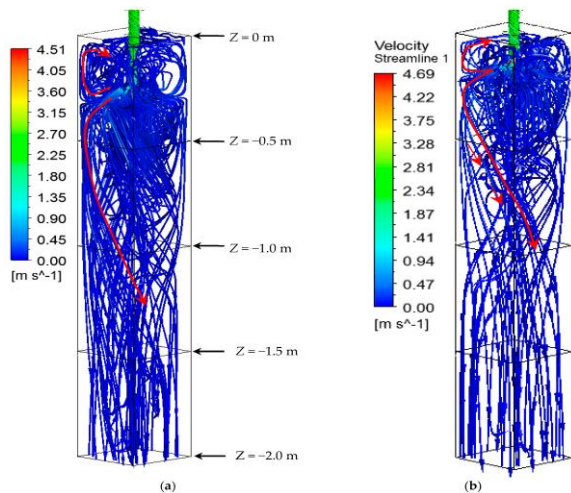


Figure 2. comparison of steel path flow in mold, SEN immersion depth of 25(a) cm and 15(b) cm

The velocity on the vertical plane located at the middle of the mold for different SEN immersion depths. It can be seen that the high velocity region was located at the solidification front in the mold. Steel moves downwards at the region near the solidified shell and it flows upwards in the center of the mold. The effect of the SEN depth is mainly on the steel flow velocity at the top of the mold. It can be seen that the region with a high steel flow velocity was reduced when a

large SEN immersion depth was used. This is expected to reduce the risk of the slag entrainment at the steel-slag interface. When a large SEN immersion depth was used, the length of the SEN was increased. The dissipation of the rotational momentum was expected due to the friction of the SEN wall. However, it did not show significant influence on the steel flow in the mold below the height of the SEN outlet.

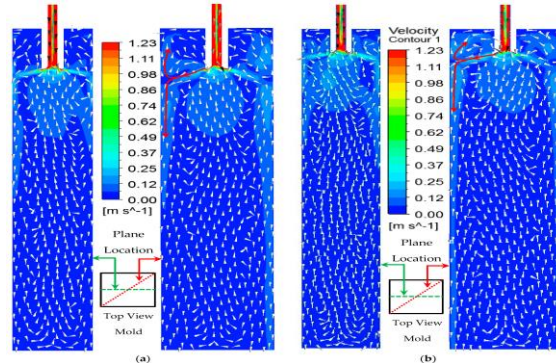


Figure 3. Steel flow velocity in vertical middle plane of the mold both 15 cm and 25 cm of immersion.

Comparison of vertical velocity distributions along the line, with the mold depth of 1.5 m, for different SEN immersion depths. It can be seen that a large velocity with a magnitude of 0.03 m/s exists in the solidification front. This may be helpful to shear off the dendrites from the solidification interface and promotes the nucleate, which results in an enhancement of the transition from a columnar to equiaxed solidification.

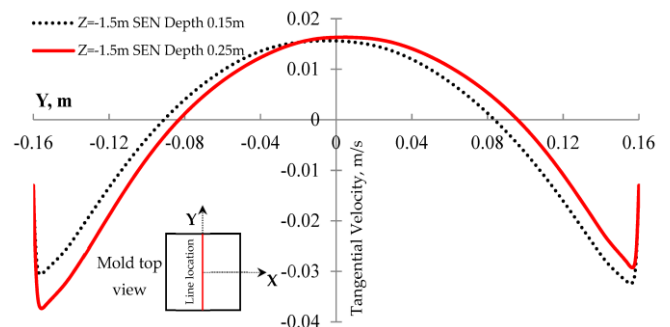


Figure 4. Vertical steel flow velocity along with horizontal lines in different depths.

#### B. Steel-slag interface phenomena

One of the most important concerns about the swirling flow SEN is about the steel flow and heat transfer near the meniscus. Due to the existence of the swirling flow, the impingement jet flow in a conventional tundish casting disappeared. The steel flow moves towards the solidification front, the induced steel flow in the meniscus region was increased, and this led to the heat transfer near the meniscus accelerating. However, a large steel flow velocity near the meniscus region also illustrates a high risk of the slag entrainment. Therefore, it is very important to investigate the effect of the SEN immersion depth on the steel-slag interface behavior.

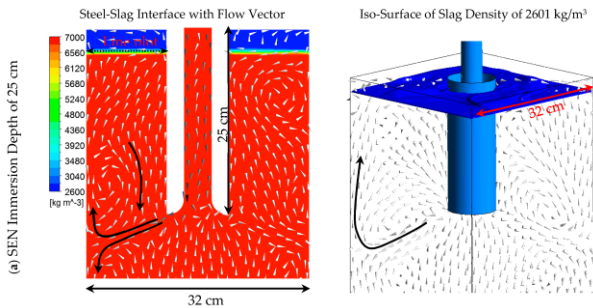


Figure 5. Steel slag interface with steel flow vectors.

A. Temperature fields

Steel temperature in the mold is very important, since it significantly influences the solidification structure, which in turn determines the product quality. The swirling flow SEN has proven that it can accelerate steel superheat removal. This is good for the formation of equiaxed crystals. It can be seen that similar temperature distribution characteristics were observed for different SEN immersion depths. Due to the swirling flow effect, steel with a high temperature flows towards the solidified shell. It increased the temperature near the solidified shell as well as the temperature gradient there, while the core temperature of the billet was low. On the cross section at a depth of 0.5 m in the mold, the maximum temperatures for the immersion depths of 25 cm and 15 cm are 1806 and 1804 K, respectively. It can be seen that the high temperature region is not located in the center of the mold. These values decrease to 1796 K and 1795 K at the mold depth of 1.5 m, respectively.

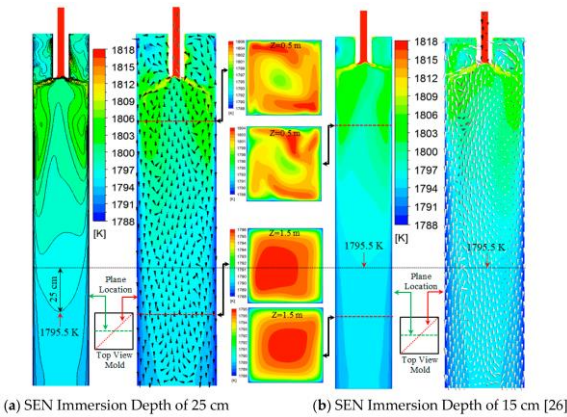


Figure 6. Temperature distribution in mold for different SEN immersion depths.

Here, the high temperature region was located in the mold center. This is due to the fact that the superheat of the steel near the solidification front can be removed fast, while that in the mold center cannot be easily dissipated. In addition, there are some differences induced by the increase of the immersion depth. The first issue is about the temperature near the meniscus, where a low temperature was observed when a large immersion depth was used.

The velocity magnitude distribution along different lines in mold depth direction. Figure 7a is the velocity distribution at

Location A with 1 cm away from the solidification shell. At the top of the mold, it can be seen that the velocity magnitude with a large SEN immersion depth is smaller than that with a small SEN immersion depth. This is helpful to reduce the risk of the slag entrainment. In the low part of the mold, the velocity near the solidification front is larger with a larger SEN immersion depth, and this is helpful for the formation of equiaxed crystals. In Figure 7b, the velocity distribution at Location B, which is close to the mold center, was presented. It can be seen that the major difference exists at the top of the mold, with a smaller velocity when a larger SEN depth was used. Furthermore, the velocity was similar at the location in deep mold. In summary, the general trend of the flow change when the SEN immersion depth was increased is that the velocity in the top mold decreased while the velocity at the low part of the mold increased.

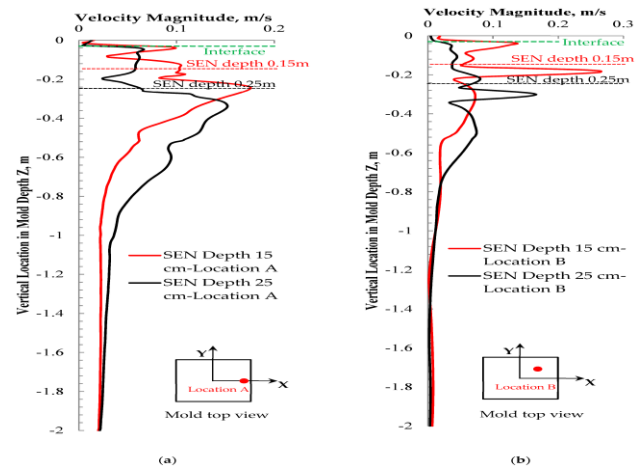


Figure 7. Total velocity distribution.

IV. CONCLUSION

The effects of the SEN immersion depth on the multiphase flow and heat transfer in a mold with a new cylindrical tundish design for continuous casting were investigated using numerical simulations. The main conclusions were the following:

Steel flow patterns are similar for different SEN immersion depths, with the flow direction towards the solidification front.

An increase in the SEN immersion depth decreases the interfacial velocity and this reduces the risk of slag entrainment. The calculated Weber Number is 0.8 and 0.2 for the SEN depth of 15 cm and 25 cm, respectively. The steel flow velocity near the solidification front below the SEN outlet is increased with a large SEN immersion depth.

The temperature distribution has a similar distribution characteristic. The high temperature region is located near the solidification front. Temperature near the meniscus was slightly decreased when the SEN immersion depth was increased.

A large SEN immersion depth was recommended in order to reduce the slag entrainment. This will not reduce the steel

flow velocity near the solidification front, nor will it significantly reduce the temperature near the meniscus.

#### A. SCOPE OF THE PRESENT WORK

Based on the literature review, the baseline geometric model of the tundish will be created by using the ANSYS Design Modeller. The geometry was meshed using the pre-processor tool ANSYS Meshing. Flow behaviour of the baseline model was done in FLUENT and validated against available literature with Volume fraction contours. Finally study the tundish container with swirl chamber with dams to improve the performance of the tundish container.

#### B. OBJECTIVE

To study the alternative configurations at transient state working conditions to identify the “best available” solution which allows equalization of the liquid metal through-time from the inlet to the different outlets, which is necessary to guarantee homogeneous thermo-chemical characteristics of the metal feeding the different casting lines

#### REFERENCES

- [1] Y. Sahai, R. Ahuja: *Steelmaking Proc.*, vol.69, (1986) pp.677-687
- [2] J.W. Han, K.J. Bai, J.K.Yoon: *J. Korean Inst. Met.*, vol. 25, (1987)pp.778-789.
- [3] H. Nakajima, F. Sebo, S. Tanaka, L. Dumitru, D.J. Harris, R.I.L. Guthrie: *Tundish Metallurgy*, Vol. I , Warrendale, PA, pp.101-112
- [4] J. Knoepke, J. Mastervich: *Tundish Metallurgy*, Vol. I , Warrendale, PA, pp.113- 124
- [5] C.J. Dobson, R. Serje, K. Gregory: *Proc. Of 4th International Conference Continuous Casting*,Vol. 2, (1988)pp.682-693
- [6] K. M. Godiwalla, S. K. Sinha, C. S. Sivaramakrishnan: *Steel Res.* vol.65,( 1994) , pp.267-272
- [7] L. K. Chiang: *Steelmaking Proc.*, vol.75,(1992),pp.437-450.
- [8] Y.He and Y.Sahai: *Metal. Trans. B*, vol.18B,( 1987) pp.81.
- [9] J.Szekely and N. El-kaddah: *Steelmaking Proc.*, vol.69,(1986) pp.761-765.
- [10] S.M.Lee, Y.S.Koo, T.Kang et.al: *Proc. 6th Int. Iron & Steel Cong., ISIJ, Tokyo, 1990: pp.239*
- [11]Wondrak, Th.; Eckert, S.; Galindo, V.; Gerbeth, G.; Stefani, F.; Timmel, K.; Peyton, A.J.; Yin, W.; Riaz, S. Liquid metal experiments with swirling flow submerged entry nozzle. *Ironmak. Steelmak.* 2012,
- [12]Szekely, J.; Yadoya, R.T. The physical and mathematical modelling of the flow field in the mold region of continuous casting systems. Part II. The mathematical representation of the turbulence flow field. *Metall. Mater. Trans.*1973,

# Vibration Analysis of Two Wheeler Suspension System under Various Loading Conditions (An Analytical Approach)

**Mr. Vinodkumar Reddy.B<sub>1</sub>, Mr J.Chandra sekhar<sub>2</sub>, Mr. K.Venkat Siva<sub>3</sub>**

*<sub>1</sub>Assistant Professor In Mechanical Engineering, MallaReddy College of Engineering, Hyderabad, India*

*<sub>2</sub>Assistant Professor In Mechanical Engineering, MallaReddy College of Engineering, Hyderabad, India*

*<sub>3</sub>Assistant Professor In Mechanical Engineering, MallaReddy College of Engineering, Hyderabad, India*

**Abstract** - - *It is evident that there is a constantly growing interest in providing acceptable system performances of vehicle suspension systems, especially in the past two decades as vehicle suspension systems have many vital functions: for instance, to support the vehicle weight, to provide effective isolation of the chassis from road excitations, to keep tyre contact with the ground, and to maintain the wheels in appropriate position on the road surface. Vehicle suspension systems play an important role in guaranteeing the stability and improving suspension performances of vehicles. In this Research a Suspension System is Analyzed by considering load. Vibration Analysis is done to validate the strength of suspension system. The Deformation of suspension system is checked under various loading conditions. Acceleration and Velocity of Suspension system is checked under various Road Conditions. For the Analysis purpose, Honda Passion is Chosen as a Base Model.*

**Key Words:** Suspension System, Vibration Analysis, Deformation, Acceleration, Velocity, Road Condition, Honda Passion

**NOMENCLATURE:**

A	Amplitude
C	Spring Index
C	Damping co efficient
C <sub>c</sub>	Critical Damping Co efficient
D	Mean Diameter of coil
D	Wire Diameter
D <sub>o</sub>	Outer Diameter of spring
G	Modulus of rigidity
h	Height of spring

\*\*\*

K	Spring stiffness
L <sub>s</sub>	Solid Length
m	Mass
n	Number of Turns
r	Frequency ratio
V	Velocity
ω	Frequency
ω <sub>n</sub>	Natural Frequency
X <sub>1</sub>	Displacement
$\dot{X}_1$	Velocity of Vehicle
$\ddot{X}_1$	Acceleration
Z	Damping ratio
$\frac{X_1}{Y}$	Amplitude Ratio

**1. INTRODUCTION**

Vehicle suspension systems play an important role in guaranteeing the stability and improving suspension performances of vehicles. It is worth noting that the problem of control design for active suspension systems should be paid considerable attention[1]. In addition, the vehicle suspension systems can provide as much comfort as possible for the passengers and ensure the other suspension performance by serving the basic function of isolating passengers from road-induced vibration and shocks. Hence, the control design problem of proper active suspension systems is always an important research topic for achieving the desired vehicle suspension performances.

Several performance characteristics should be considered and need to be optimized for designing a good performance suspension system[3]. It is widely accepted that three main suspension performances should be taken into account when designing a suspension controller, namely, ride comfort (i.e., directly related to acceleration sensed by passengers), road handling (i.e., associated with the contact forces of tires and road surface), and suspension deflection (i.e., referred to the displacement between the sprung mass and unsprung mass) However, it is difficult to minimize all three parameters simultaneously as these performances are often conflicting with each other, For example, the minimization of suspension travel cannot be accomplished simultaneously with the maximization of the ride comfort. In other words, enhancing ride comfort performance results in larger suspension stroke and smaller damping in the wheel-hop mode[4]. Hence, how to derive an appropriate trade-off between these performances is the main task for successfully designing a vehicle suspension control system.

### 1.1 TYPES OF SUSPENSION SYSTEM

Most modern motorcycle suspensions are still based on a telescopic cartridge fork design, which houses both the spring and damper unit. This design proved to be lightweight, inexpensive, and sturdy enough to handle the loads of today's motorcycles. Damper technology, however, has continuously evolved. Mono-tube dampers have given way to twin tube dampers, while fixed orifice damper valving has been replaced by rider adjustable compression and rebound adjusters. The end goal has been to provide the rider with better ride performance while maintaining comfort[7].

- 1) Active Suspension system
- 2) Passive Suspension System
- 3) Semi active Suspension system
- 4) Adjustable suspension system

A passive suspension system is one in which the characteristics of the components (springs and dampers) are fixed. These characteristics are determined by the designer of the suspension, according to the design goals and the intended application. Passive suspension design is a compromise between vehicle handling and ride comfort. In an active suspension, the passive damper or both the passive damper and spring are replaced with a force actuator. In this type of system, the conventional spring element is retained, but the damper is replaced with a controllable damper.

### 1.2 LITERATURE SURVEY

The literature survey was mainly focus on the design of spring of the suspension system to increase the performance of the two wheeler suspension system. The design of the spring was varied depending upon the parameters of the springs, like wire diameter, outer diameter, pitch, number of active turns etc. material for the spring has also its advantages. Current trends have focused on the design of

springs using various materials. Then the springs would be checked under various conditions. Stress and deflection would be checked of the springs under various materials and under various conditions to check the efficiency of the springs of the suspension systems. Analyses have been carried out by using software and efficient design would be carried out for the suspension system. Experimental set up have also been used to check the property and efficiency of the suspension systems.

## 2. DESIGN CALCULATION FOR HELICAL SPRING OF SUSPENSION SYSTEM (HONDA PASSION)

The vibration Analysis was carried out to check the suspension system under various road conditions. For the Analysis purpose, Honda Passion is chosen. According to the standard specification of Rear Suspension system, the design calculation was carried out. The standard dimension of Honda Passion is Describe Below.

Material: Structural Steel

- modulus of rigidity  $G = 79300 \text{ MPa}$
- Mean Coil Diameter  $D=42\text{mm}$
- Diameter of wire  $d = 8\text{mm}$
- Number of Active Turns  $n_1= 17$
- Height  $h = 220\text{mm}$
- Outer diameter of spring  $DO= D + d =50\text{mm}$
- Kerb Weight = 116kgs
- Let weight of 1 person = 60Kgs
- Weight of 2 persons =  $60 \times 2 = 120\text{Kgs}$
- Weight of bike + 2 persons = 236Kgs

Now, Let us Assume that the Rear Suspension system can carry the load of 60% Of Overall Vehicle Weight.

So, 60% of 236 = 142 Kgs = 1394

$N C = \text{spring index} = 5.25 = 5.3$

Solid length,  $L_s = n_1 \times d = 17 \times 8 = 136\text{mm}$

### 2.1 VIBRATION ANALYSIS OF SUSPENSION SYSTEM

Here, we carried out Vibration Analysis of Rear Suspension System by Analytical. This Analysis was carried out to check the various Parameters of Two Wheeler Suspension System. For the Analysis purpose, we choose Rear Suspension of Honda Passion and Analysis was carried out under various Road Conditions. Vehicle has Mass of 236 Kgs including Bike Kerb Weight and considering 2 persons. The spring stiffness (Force required per Unit Deflection) was calculated by using Online spring Stiffness Calculator. We Analyze the suspension system under various Road conditions by varying speed of 50 Km/hr and 80 Km/hr. we assume that road surface varied sinusoidal with Amplitude 0.04 m and considering Wavelength 6m. Whole body vibration (WBV) occurs when workers sit or stand on vibrating seats or foot

pedals. Prolonged Exposure to high levels of WBV causes motion sickness, fatigue and headaches. WBV is one of the strongest risk factors for low back disorders. Vibrations with less than 0.315 m/s<sup>2</sup> are found to be comfortable between 0.315m/s<sup>2</sup> and 2.5m/s<sup>2</sup> are found to be uncomfortable greater than 2.5m/s<sup>2</sup> are found to be extremely uncomfortable. Typical whole -body vibration exposure levels of heavy vehicle drivers are in the range 0.4 to 2.0 m/s<sup>2</sup>.

**Table 1** ISO standard with respect to the vibration exposure and its effect on health of driver[2].

Exposure Duration in Hrs	Likely Health Risk	Caution Zone	Comfort Level
8	0.8	0.5	0.315
12	0.7	0.4	0.315

Now, we want to find out the Spring stiffness value of the Helical Spring. The spring stiffness value was carried out by using the Online Spring Stiffness Calculator.

**Table 1** www.tribology-abc.com [5].

The screenshot shows a web-based calculator for round wire helical springs. It includes a diagram of a spring with force F applied, and the following formulas:

$$F = \frac{\pi d^3}{16 r} \tau$$

$$f = \frac{64 n r^3 F}{d^4 G}$$

The input parameters and their values are:

- Diameter of spring wire d: 8 (10<sup>-3</sup> m)
- Mean coil diameter D: 42 (10<sup>-3</sup> m)
- Number of active coils n: 17
- Shear modulus G = E / (2 (1+v)): 79.3 (10<sup>9</sup> Pa)
- Spring force F: 1394 (N)

The calculated results are:

- Spring outer diameter Dout = D + d: 50 (10<sup>-3</sup> m)
- Spring radius r = D / 2: 21 (10<sup>-3</sup> m)
- Spring length closed (solid) Lc = n d: 136 (10<sup>-3</sup> m)
- Spring deflection f: 43.24 (10<sup>-3</sup> m)
- Energy stored W = F f / 2: 30.14 (J)
- Spring stiffness k = dF / df = F / f: 32.24 (10<sup>3</sup> N/m)
- Spring length free LO > Lc + f: 179.24 (10<sup>3</sup> N/m)
- Pitch of lead s = LO / n: 10.54 (10<sup>-3</sup> m)
- Shear stress τ: 291.19 (10<sup>6</sup> Pa)

www.tribology-abc.com

Now, Vibration Analysis Carried out by Analytically[6]. Natural Frequency:- the frequency at which a system oscillates when not subjected to a continuous or repeated external force.

$$\text{Natural Frequency } \omega_n = \sqrt{\frac{k}{m}} \quad \text{Eq. (1)}$$

$$\omega_n = 15.06 \text{ rad/sec}$$

Frequency of the Object:- the rate at which something occurs over a particular period of time or in a given sample.

$$\text{Frequency } \omega = 2\pi f = \frac{(V \times 1000)}{3600} \frac{1}{6} \quad \text{Eq. (2)}$$

$$= 0.290889 \times V$$

Now, We find out Frequency of the object at Various Speed. For the Analysis Purpose, we choose speed at 50 Km/hr and 80 Km/hr.

$$\text{For 50Km/hr} = 0.290889 \times 50 = 14.54 \text{ rad/sec}$$

$$\text{For 80Km/hr} = 0.290889 \times 80 = 23.27 \text{ rad/sec}$$

Frequency Ratio:- Frequency Ratio is defined as the Ratio of Frequency of the object to the Natural Frequency.

$$\text{Frequency Ratio (r)} = \frac{\omega}{\omega_n} \quad \text{Eq. (3)}$$

$$(r)_{50\text{km/hr}} = \frac{\omega}{\omega_n} = 0.965$$

$$(r)_{80\text{km/hr}} = \frac{\omega}{\omega_n} = 1.545$$

Now, for the Analysis purpose we want to carry out two different cases. The Analysis was carried out to check the different parameters. We done the Analysis at two different speeds. First case was consider the speed at 50 Km/hr and second case consider the speed at 80 Km/hr.

**Case 1:-** At speed 50 Km/hr

Here, we consider a Simple Harmonic Motion (S.H.M). According to Simple Harmonic Motion, the Acceleration is directly Proportional to displacement and always directed towards the mean position from the point. As we assume the Analysis was carried out At sinusoidal Amplitude of 0.04m and considering the Wavelength 6m[3].

Displacement, Velocity and Acceleration at Amplitude A(0.04m,0.08m,0.12m,0.16m).

Displacement, Velocity and Acceleration at Amplitude A(0.04m,0.08m,0.12m,0.16m)

Displacement:- Displacement is defined as the distance travelled per unit time. Displacement is carried out at various Amplitude According to the sinusoidal manner.

$$X_1 = A_1 \sin \omega t = 0.0043 \text{ m At time period } t = \frac{2\pi}{\omega} = 0.432 \text{ sec}$$

$$X_1 = A_2 \sin \omega t = 0.0086 \text{ m At time period } t = \frac{2\pi}{\omega} = 0.432 \text{ sec}$$

$$X_1 = A_3 \sin \omega t = 0.0130 \text{ m At time period } t = \frac{2\pi}{\omega} = 0.432 \text{ sec}$$

$$X_1 = A_4 \sin \omega t = 0.0173 \text{ m At time period } t = \frac{2\pi}{\omega} = 0.432 \text{ sec}$$

Eq. (4)

Velocity:- Velocity is defined as the rate of change of Displacement per Unit time. For the different Amplitude, velocity has been encountered as Following.

$$\dot{X}_1 = A_1 \omega \cos \omega t = 0.243 \text{ m/s}$$

$$\dot{X}_1 = A_2 \omega \cos \omega t = 0.486 \text{ m/s}$$

$$\dot{X}_1 = A_3 \omega \cos \omega t = 0.729 \text{ m/s}$$

$$\dot{X}_1 = A_4 \omega \cos \omega t = 0.972 \text{ m/s} \quad \text{Eq. (5)}$$

Acceleration:- Acceleration is defined as the Rate of change of velocity per Unit time. According to the Amplitude, acceleration was carried out at S.H.M.

$$\ddot{X}_1 = -\omega^2 \times X_1 = 0.909 \text{ m/s}^2$$

$$\ddot{X}_1 = -\omega^2 \times X_1 = 1.691 \text{ m/s}^2$$

$$\ddot{X}_1 = -\omega^2 \times X_1 = 2.748 \text{ m/s}^2$$

$$\ddot{X}_1 = -\omega^2 \times X_1 = 3.593 \text{ m/s}^2 \quad \text{Eq. (6)}$$

Now, after finding out the Velocity and Acceleration value, we want to find out the Damping Factor or Damping Ratio. Damping Ratio is a Dimensionless Parameter measure describing how oscillations in a system decay after a disturbance. Many systems exhibit oscillatory behavior when they are disturbed from their position of Static Equilibrium. A mass suspended from a spring, for example, might if pulled and released, it will bounce up and down.

Damping co efficient:-

$$c = \frac{F}{X} \quad c = 5736.62 \text{ Ns/m} \quad \text{Eq. (7)}$$

Critical Damping Co efficient:-

$$C_c = 2m\omega_n \quad C_c = 1993.68 \text{ Ns/m} \quad \text{Eq. (8) Damping Ratio:-}$$

$$\zeta = \frac{C}{C_c} \quad \text{Eq. (9)}$$

$$\zeta = 2.87$$

Amplitude Ratio:-

$$\left( \frac{X_1}{Y} \right)_{40 \text{ km/hr}} = \left[ \frac{1 + (2\zeta r)^2}{(1-r^2)^2 + (2\zeta r)^2} \right]^{1/2} = 1.0324$$

$$\left( \frac{X_1}{Y} \right)_{60 \text{ km/hr}} = \left[ \frac{1 + (2\zeta r)^2}{(1-r^2)^2 + (2\zeta r)^2} \right]^{1/2} = 0.988 \quad \text{Eq. (10)}$$

Above Analysis was carried out by considering the speed of Vehicle as a 50 Km/hr. now same Vibration Analysis carried out by using Vehicle speed as a 80 Km/hr.

**Case 2:-** At speed 80 Km/hr

Displacement, Velocity and Acceleration at Amplitude A(0.04m,0.08m,0.12m,0.16m)

$$X_1 = A_1 \sin \omega t = 0.0042 \text{ m At time period } t = \frac{2\pi}{\omega} = 0.270 \text{ sec}$$

$$X_1 = A_2 \sin \omega t = 0.0084 \text{ m At time period } t = \frac{2\pi}{\omega} = 0.270 \text{ sec}$$

$$X_1 = A_3 \sin \omega t = 0.0127 \text{ m At time period } t = \frac{2\pi}{\omega} = 0.270 \text{ sec}$$

$$X_1 = A_4 \sin \omega t = 0.0169 \text{ m At time period } t = \frac{2\pi}{\omega} = 0.270 \text{ sec}$$

Now find out the Velocity,

$$\dot{X}_1 = A_1 \omega \cos \omega t = 0.230 \text{ m/s}$$

$$\dot{X}_1 = A_2 \omega \cos \omega t = 0.461 \text{ m/s}$$

$$\dot{X}_1 = A_3 \omega \cos \omega t = 0.692 \text{ m/s}$$

$$\dot{X}_1 = A_4 \omega \cos \omega t = 0.923 \text{ m/s}$$

Second phase is Acceleration. Acceleration is finding out by considering the Amplitude Value.

$$\ddot{X}_1 = -\omega^2 \times X_1 = 2.274 \text{ m/s}^2$$

$$\ddot{X}_1 = -\omega^2 \times X_1 = 4.548 \text{ m/s}^2$$

$$\ddot{X}_1 = -\omega^2 \times X_1 = 6.876 \text{ m/s}^2$$

$$\ddot{X}_1 = -\omega^2 \times X_1 = 9.151 \text{ m/s}^2$$

### 3. RESULTS AND DISCUSSION

Above Analysis was carried out to check which parameters were directly affected the vehicle comfort ride and also the efficiency of the Vehicle suspension system. From the above Analysis, the value of Velocity and Acceleration were calculated at sinusoidal Amplitude of 0.04 m. the results from the Analysis was discussed below by using the table and graphs.

**Table 2** Result of Velocity at various Amplitude

Speed (Km/hr)	Road One Velocity (m/s)	Road Two Velocity (m/s)	Road Three Velocity (m/s)	Road Four Velocity (m/s)
50	0.243	0.486	0.729	0.972
80	0.230	0.461	0.692	0.923

**Table 4** Result of Acceleration at various Amplitude

Speed (Km/hr)	Road One Acceleration (m/s <sup>2</sup> )	Road Two Acceleration (m/s <sup>2</sup> )	Road Three Acceleration (m/s <sup>2</sup> )	Road Four Acceleration (m/s <sup>2</sup> )
50	0.909	1.691	2.748	3.593
80	2.274	4.548	6.876	9.151

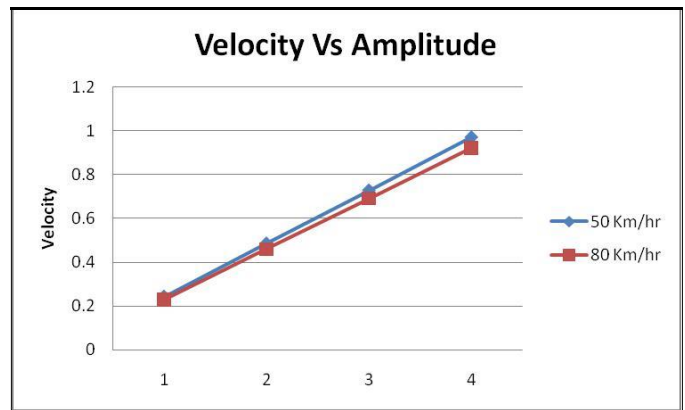


**Chart -1:** Amplitude Vs Velocity

Above Analysis shows the relation between Amplitude and Velocity at different conditions. From the Analysis we show that as the Amplitude increases, the Velocity is also increased. So we can say that Velocity is directly proportional to the Amplitude.

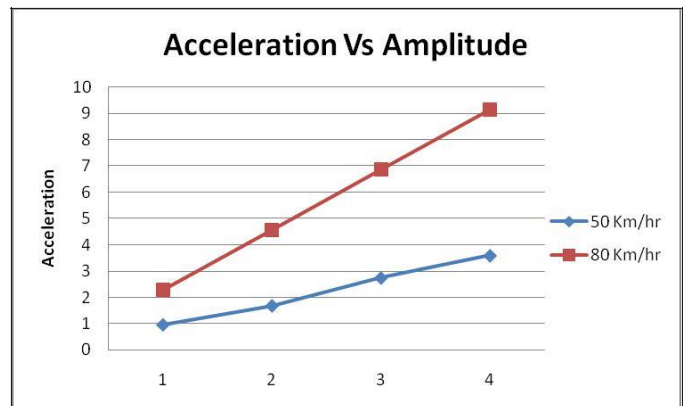


**Chart -2:** Amplitude Vs Acceleration

From Analytical analysis it was observed that as amplitude of road or road roughness raises acceleration may also going to be rise. Here through graph we can observe that acceleration is to be occurring is more than comfort level or as per international standard notified in above table. The nature of vibration present in a vehicle depends upon the dynamic characteristics of the two wheeler and road surface characters. From the results it is found that, for the given acceleration of two wheeler and human body the ideal operating conditions is more than comfort level that is mean above 0.315 m/s<sup>2</sup> or above total acceleration i.e. 0.8 m/s<sup>2</sup> as a safety standard level of vibration.

### 3. CONCLUSIONS

Acceleration because of is a physical disturbance that occurs in vehicles. Its effect on the human body depends mainly on the acceleration, frequency, magnitude, direction of vibration, area of contact and duration of exposure. From the above analysis it is found that for the given acceleration of two wheeler and human body the ideal operating condition is more than standard level. According to standard level, vibration less than  $0.315 \text{ m/s}^2$  are found comfortable. vibration between  $0.315 \text{ m/s}^2$  and  $2.5 \text{ m/s}^2$  are found to be uncomfortable. Vibration greater than  $2.5 \text{ m/s}^2$  are found to be extremely uncomfortable. so from above analysis we conclude that rise of speed or rise of amplitude may directly affect the Acceleration of vehicle. Hence we have scope to redesign the suspension system to reduce its vibration as possible.

### 4. ACKNOWLEDGEMENT

We are thankful to all those who have directly or indirectly helped us in preparing this paper. We are also thankful to our colleagues' faculty members who had given their help directly or indirectly to convert my ideas and information into paper, which propose to present. I also thankful to acknowledge Dr. Kartikeyan A, Head of the Mechanical Engineering Dept., Mallareddy college of Engineering, Hyderabad. At last I would like to thank all those real and virtual factors that have helped me to put for this presentation.

### REFERENCES

- [1] Achyut P. Banginwar ,Nitin D. Bhusale, Kautuk V. Totawar "Design and analysis of shock absorber using FEA tool" International Journal of Engineering Research and Development. Volume 10, Issue 2 (February 2014).
- [2] Bridger R S "Introduction to ergonomics" McGraw- hill International editions.
- [3] Mukesh Hadpe, Dr.D.S.Deshmukh, P.M.Solanki " Vibration Analysis of Two Wheeler (ANALITICALLY) International Journal of Innovative Research in Science,Engineering and Technology.
- [4] Pinjarla.Poornamohan, Lakshmana Kishore.T "design and analysis of a shock absorber" International Journal of Research in Engineering and Technology,Journal of Management in Engineering, January 4, 2013.
- [5] [www.tribology-abc.com](http://www.tribology-abc.com)
- [6] Divyarajsinh Rathod and Dr Chinmay Desai "Design and Analysis of Two wheeler suspension system" NCRAES, May 2015.
- [7] Divyarajsinh Rathod "Design and Analysis of test rig to check the performance of suspension system" Thesis, June July 2015.

# **THERMAL ANALYSIS OF DISC BRAKE TO MINIMIZING THE TEMPERATURE BY USING ANSYS**

**Praksh .D.Chavan**

Assistant Professor  
Department of Mechanical Engg  
Malla Reddy College Of Engineering  
Email:pakuchavan625@gmail.com

**Mahadev.Godamagave**

Assistant Professor  
Department of Mechanical Engg  
Malla Reddy College Of Engineering  
Email:mahadev.godamagave@gmail.com

**Abhishek kulkarni**

Assistant Professor  
Department of Mechanical Engg  
Malla Reddy College Of Engineering  
Email:kulkarnithermal@gmail.com

\*\*\*

**Abstract** – These day technologies go beyond us. For automotive field, the technology of engine develops very fast even the system of the bike, car, luxury or comforts everything that develops by the innovation of engineer. Thus, safety is the first important thing we must focus. This paper is presented with “Design and Thermal analysis of disc brake for minimizing temperature” which studies about on disc brake rotor by analysis of different shapes of slot of different vehicles Disc brake rotor. Therefore, we can optimize number of shapes of slot to estimate the good thermal conductivity of the disc brake rotor. In this paper, Thermal analysis done on real model of disc brake rotor of Bajaj Pulsar 220 and Thermal analysis of disc brake rotor. Different shapes of slot are because of to reduce the weight of disc rotor and for good thermal conductivity. Hopefully this paper will help everyone to understand Thermal analysis of disc brake rotor and how disc brake work more efficiently, which can help to reduce the accident that may happen in each day. Modeling was done using CATIA V5R21 software and Static and Transient Thermal Analysis was done using ANSYS 15 software.

**Key Words:** Disc brake rotor, Thermal analysis etc

## **1.INTRODUCTION**

A brake is a device used to generate an artificial frictional which is applied to moving member of machine, for stopping motion. For execution of braking operation, the brakes pad and disc absorb the kinetic energy from wheel. The energy absorbed by brake is generating heat. This heat is passing in to the atmosphere and stops the vehicle, so the braking system should have the following ability;

1. The brake disc having ability to transfer heat to atmosphere and maintain constant temperature to improve performance of disc.
2. Anti-wear property of the brakes must be good.
3. The driver must have have proper control on the vehicle during brake applied and the vehicle should not skid.

4. The brakes must be having enough power to stop the vehicle with in a minimum distance in case emergency.

## **1.1 CLASSIFICATION OF BRAKES**

The classification of mechanical braking system in 2 subgroups according to the direction of acting forces are

Axial brake

Radial brake

**Axial brake:** In this brake, the force acting on the braking system is only in the axial direction to the brake. For example, Disc brake is acting in axial direction.

**Radial brake:** In this brake, the force acting on the braking system is in perpendicular to axial direction. The radial brakes subdivided into internal and external brake.

## **2. PROBLEM DEFINATION AND OBJECTIVES**

Extreme thermal environments are an important issue in the design of sliding contact systems such as brakes and clutches. Thermal stresses due to high temperatures may induce a number of unfavorable conditions such as surface cracks and permanent distortions. Frictional heating, thermal deformation and elastic contact in sliding contact systems affect the contact pressure and temperature on the friction surfaces. If the sliding speed is excessively high, these coupled thermal and mechanical behaviors can be unstable leading to localized high temperature contact regions called “hot spots” on the sliding interface.

The appearance of these hot spots is known as frictionally excited thermo elastic instability or TEI and is observed in many practical applications, especially brakes and clutches. Hot spots can cause material damage and thermal crack, and induce an undesirable frictional vibration known as “hot judder” in automotive disk brake systems.

## OBJECTIVES

- Design of the disc for a disc brake system using load analysis, stress analysis and thermal analysis system approach.
- The disc brake rotor is to be rigidity and stability.
- Heat absorption and dispersion.
- Federal safety requirements.
- Increase the rotor and pad life.

## 3. LITERATURE REVIEW

Before starting with actual working, it's always helpful to study literature and work already carried out in similar field. This study helps to decide project outline and flow. Some research papers, articles are available in which similar type of issues, case studies have discussed. In this chapter, summary of such papers and literature published by various researchers is described.

**1.N. Balasubramanyam, Smt. G. Prasanthi** In this project, three-dimensional modeling and meshing Structural & thermal analysis using the simulation program ANSYS were successfully implemented. This has allowed for greater flexibility and accuracy in the results achieved. They were taken 3 different materials of disc brake using constant hydraulic pressure 1 Mpa at time of running condition & analysis. On the basis of various results gathered from the analysis, it is decided that grey Cast Iron is the suitable material for disc brake.

**2. Subhasis Sarkar, Pravin P. Rathod** In automobile brake system ventilated disc brake is the art of technology. This research paper reviews work of previous investigators on transient thermal analysis on the design rotor and ventilated rotor disc is to compare and evaluate their performance. The aim of this research paper review work is to study various research done in past to improve heat transfer rate of ventilated disc brake by changing material and vane geometry. If vane is angled and of alternate length other than straight radial vane. Contact time between air flow and vanes (time between air inlet and outlet flow through vanes) is also important factor in heat transfer from Disc rotor. There is also scope of research in improvement of heat transfer of rotor by increasing the contact time between vanes and air flow by design modification of vanes in such way that fulfils the requirement.

**3. Atul Sharma and M. L. Aggarwal** This research paper explains the design and finite element analysis (FEA) model of brake disc by which deflections in X, Y, Z direction and Von mises stress can be calculated by applying boundary conditions. The FEA outcomes are correlated with

experimental data. The model is safe under the practical loading condition and our factor of safety is 20.34.

**4. Ameer Fareed Basha Shaik, Ch. Lakshmi Srinivas** The paper presented here is a study of model of a disc brake of Honda Civic. In this paper Structural & Thermal analysis was done in the brake disc. After changing the design of disc brake analysis was done. The material used as Cast Iron. Actual disc brake has no holes, changing the design of the disc brake by giving certain holes for more heat dissipation. Modelling was done in Catia and Analysis is done in ANSYS. Study the amount of deformation due to pressure loading and tangential Force. The modular brake was then analysed using a nodal temperature of 300°F. These results were used to study the increase in deformation in the caliper at high temperatures. The displacement increased as compared with the previous case. Since race cars brakes always operate at high temperature the thermal deformation/displacement results are important.

**5. Zheng han** In this final year project, three-dimensional modeling and meshing using the simulation program ANSYS were successfully implemented. This has allowed for greater flexibility and accuracy in the results achieved. The mechanical performances of a conventional disc brake system and the Perimetria disc brake system under three different simulation environments were studied and compared. Under torsional strength simulation, the Perimetria disc brake performs better with its maximum values of First Principal Stress and Von Mises Stress being significantly lower than those in the conventional brake-disk. Under lateral strength simulation, the Perimetria brake-disk yielded almost similar results to that of the conventional brake-disk. For both the static tests mentioned, the maximum stresses (weak points) in the Perimetria brake-disk occur at the mounting holes. These maximum stresses occur at the holes. This is due to the design of the brake-disk which concentrates the stress on the inner diameter during expansion and contraction. This indicates that the number of potential points for crack initiation is higher.

**6. Daniel Das.A, Christo Reegan Raj.V, Preethy.S,Ramya Bharani.G** The aim of this paper was to investigate the temperature fields and also structural fields of the solid disc brake during short and emergency braking with four different materials. The distribution of the temperature depends on the various factors such as friction, surface roughness and speed. The effect of the angular velocity and the contact pressure induces the temperature rise of disc brake. The finite element simulation for two-dimensional model was preferred due to the heat flux ratio constantly distributed in circumferential direction. We will take down the value of temperature, and deformation for different pressure condition using analysis software with four materials. The Disc brakes are made up of cast iron.

#### 4. DESIGN PARAMETERS OF DISC BRAKE

Standard parameters of two-wheeler in Bajaj 220cc are Brake rotor material = Grey cast iron (ASTM grade 25) Brake rotor dimension = 240mm  
 Yield stress of grey cast iron = 110 Mpa  
 Pad brake area =  $2000 * 10^{-6} \text{ m}^2$   
 Maximum pressure = 1 Mpa  
 Maximum temperature = 250°C

#### 5. ANALYSIS OF DISC BRAKE

In this paper we analyzed static and transient thermal analysis of disc brake system. In material section of disc brake is to be Grey cast iron. Both analysis has done using ANSYS 15 software.

##### STATIC STRUCTURE ANALYSIS

Static structure analysis is the most common application in FEM. Static analysis determines the displacement, stress, strain, force in structure or component caused by loads that do not induce inertia and damping effects. This project deals with the study of stress, deformation on rotor disc under static condition. After completion of finite element model it must constrain and load must be applied to the model. User can define constrain and load in various way. The following figure shows the result of static analysis.

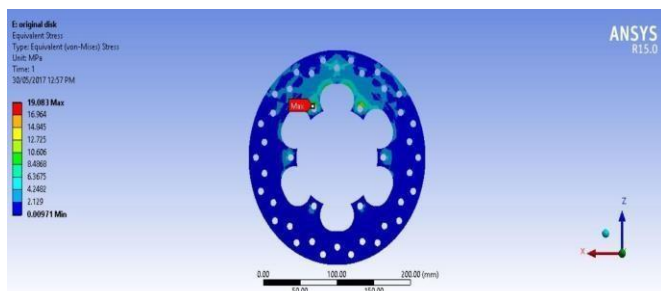


Fig 5.1 Original disc brake

From the above figure shows stress distribution of original disc brake, it is observed that maximum stress is 19.03 Mpa.

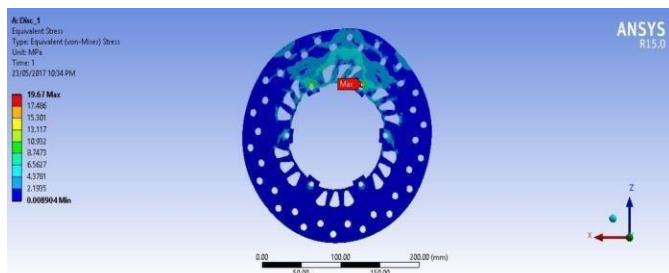


Fig 5.2 New disc 1

Above figure shows the stress distribution of new disc 1, it is observed that maximum stress is 19.67 Mpa.

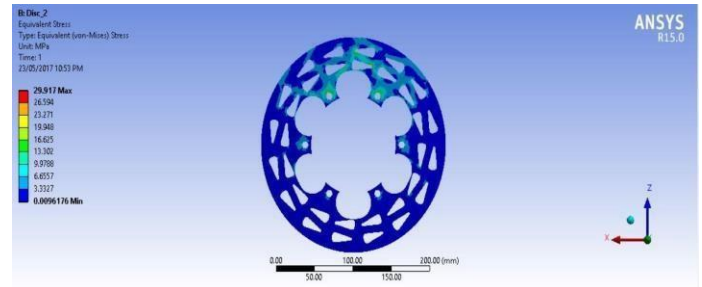


Fig 5.3 New disc 2

Above figure shows the stress distribution of new disc 2, it is observed that maximum stress is 29.917 Mpa.

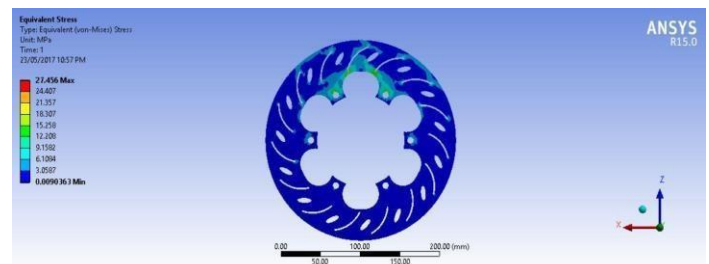


Fig 5.4 New disc 3

Above figure shows the stress distribution of new disc 3, it is observed that maximum stress is 27.456 Mpa.

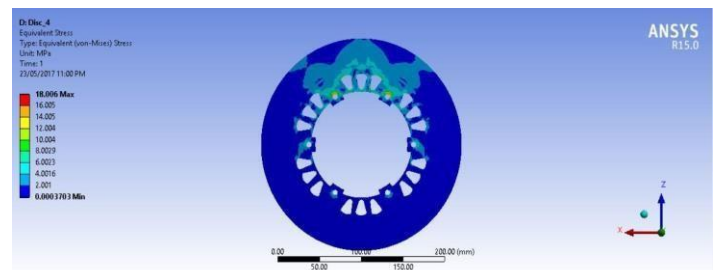


Fig 5.5 New disc 4

Above figure shows the stress distribution of new disc 4, it is observed that maximum stress is 18 Mpa.

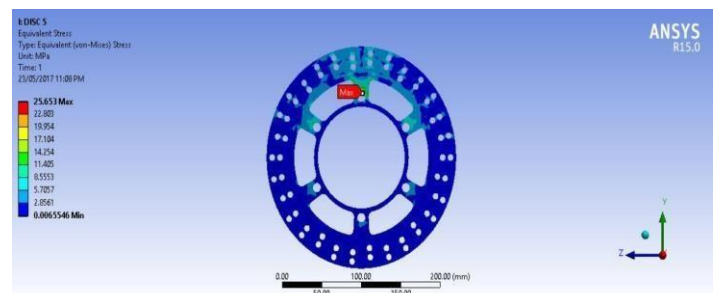


Fig 5.6 New disc 5

Above figure shows the stress distribution of new disc 5, it is observed that maximum stress is 25.653 Mpa.

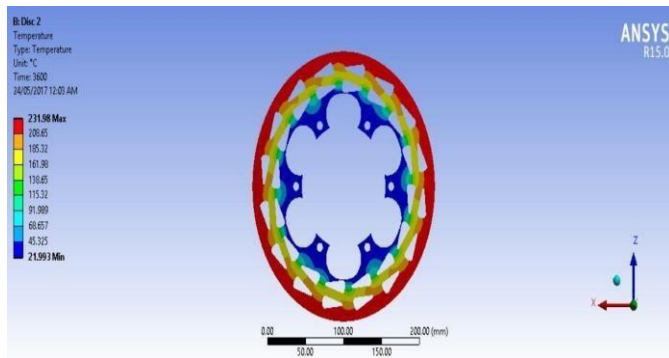


Fig 5.9 Transient thermal analysis on new disc 2

As shown in above figure transient thermal analysis was

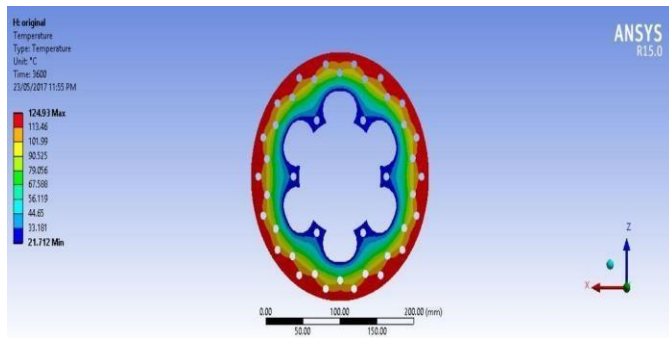


Fig 5.7 Transient thermal analysis on original disc

As shown in above figure transient thermal analysis was conducted on the disc and maximum temperature observed is 124.93°C and minimum temperature observed is 21.712°C.

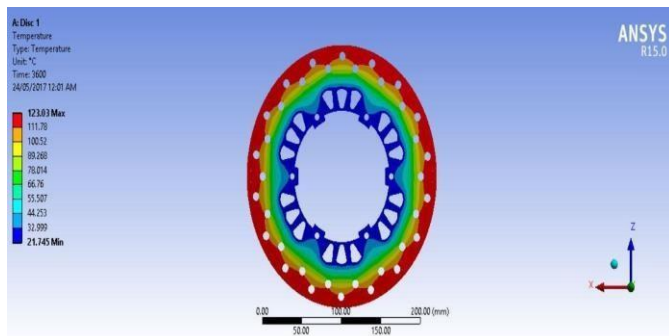


Fig 5.8 Transient thermal analysis on new disc 1

As shown in above figure transient thermal analysis was conducted on the disc and maximum temperature observed is 123.03°C and minimum temperature observed is 21.745°C.

conducted on the disc and maximum temperature observed is 238.98°C and minimum temperature observed is 21.99°C.

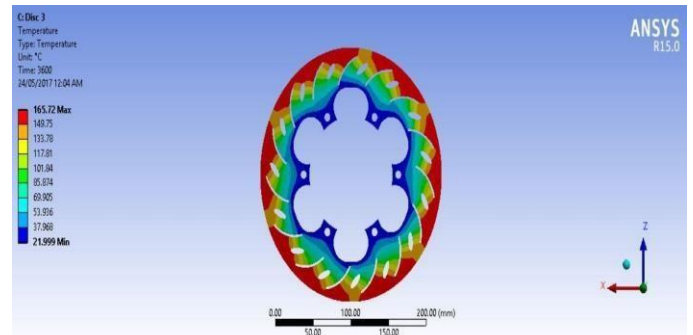


Fig 5.10 Transient thermal analysis on new disc 3

As shown in above figure transient thermal analysis was conducted on the disc and maximum temperature observed is 165.72°C and minimum temperature observed is 21.99°C.

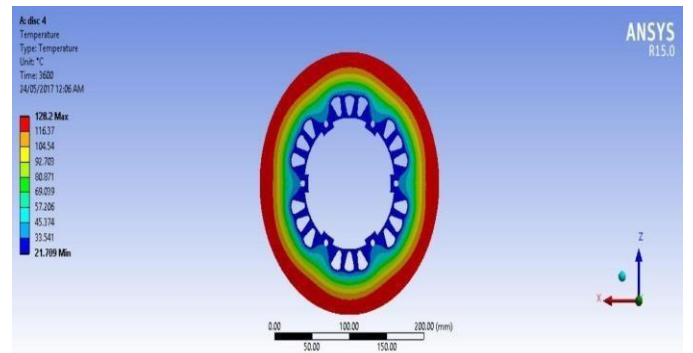


Fig 5.11 Transient thermal analysis on new disc 4

As shown in above figure transient thermal analysis was conducted on the disc and maximum temperature observed is 128.2°C and minimum temperature observed is 21.70°C.

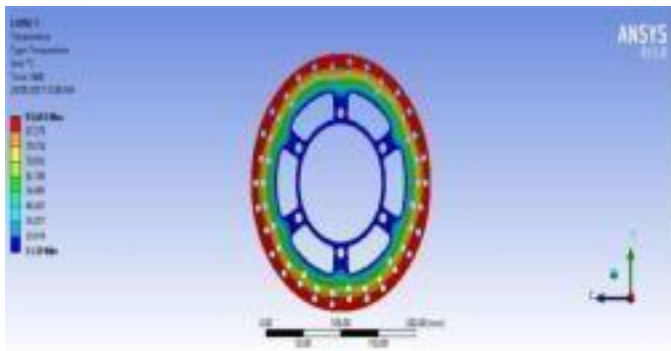


Fig 5.12 Transient thermal analysis on new disc 4

As shown in above figure transient thermal analysis was conducted on the disc and maximum temperature observed is 95.603°C and minimum temperature observed is 21.59°C

From transient thermal analysis for different design it shows that the new disc 5 generates the minimum temperature 95.603°C. Hence new disc 5 is the best among all.

## 6. RESULT AND COMPARISON

### STATIC STRUCTURE

Table 6.1 comparison of stress and deformation for different discs

	Stress	Deformation
Original disc	19.083	0.003695
New disc 1	19.67	0.003829
New disc 2	29.917	0.00568
New disc 3	27.456	0.005342
New disc 4	18.006	0.003519
New disc 5	25.653	0.00585

Above table shows the comparison of stresses between different discs where the maximum stresses developed in original disc is 19.083 Mpa while that in the new disc 5 is 25.653 Mpa which is well below the yield limit of 110 Mpa. Hence the design is safe.

### TRANSIENT THERMAL ANALYSIS

Table 6.2 Comparison of temperature and weight for different discs

	Temperature(°C)	Weight (kg)
Original disc	124.93	0.985
New disc 1	123.03	1.0811
New disc 2	231.98	0.877

New disc 3	165.72	0.965
New disc 4	128.2	1.148
New disc 5	95.603	0.895

Above table 6.2 shows the comparison of temperature and weight in different discs as shown the temperature maximum generated in original disc is 124.93°C while that in new disc 5 is 95.603°C. As it seen the weight of original disc is 0.985kg while that of new disc 5 is 0.895kg.

## 7. CONCLUSIONS

The above study can provide a useful design and help to improve the brake performance of disc brake system. From the above result, we can say that minimum temperature distribution occurs in modify (new disc 5) as compare to actual standard Bajaj pulsar 2wheeler and other new discs. Also for structural analysis result of computational we found the new brake disc design is safe based on strength and rigidity criterion. On the basis of various results gathered from the analysis, it is decided that grey cast iron is the suitable material for disc brake. New disc 5 is good brake disc compared to original brake disc of Bajaj pulsar of two-wheeler and other new disc brake for heat dissipation. New disc 5 carrying high brake force during running condition without any cracks, buckling.

## REFERENCES

- [1] Smt. G. Prasanthi, N. Balasubramanyam, "Design and Analysis of Disc Brake for a Two-Wheeler", International Journal of Mechanical and Industrial Technology (IJMIT) Vol. 1, Issue ,October 2013- March 2014.
- [2] Subhasis Sarkar, Pravin P. Rathod, "Review paper on Thermal Analysis of Ventilated Disc Brake by varying Design parameter", International Journal of Engineering Research and Technology (IJERT) Vol. 2, Issue 12, December – 2013.
- [3] M. L. Aggarwal, Atul Sharma, "Deflection and stress Analysis of Brake Disc using Finite Element Method", Oct 19-20, 2012.
- [4] Ch. Lakshmi Srinivas, Ameer Fareed Basha Shaik, "Structural and Thermal Analysis of Disc Brake with and without cross drilled rotor of race car", International Journal of Advanced Engineering Research and Studies IJAERS/ Vol. 1/Issue 4 / July-sept., 2012.
- [5] Daniel Das. A, Christo Reegan Raj. V, Preethy. S, Ramya Bharani. G, "Structural and Thermal Analysis of Disc Brake in Automobile", International Journal of Latest Trends in Engineering and Technology (IJLTET) Vol. 2, Issue 3 May 2013.

# Design and experimental study on Solar dish collector for stirling engine

<sup>1</sup>B. Simran, <sup>2</sup>Dr. Vikash Kumar

<sup>1</sup>Student, MTech, <sup>2</sup> Associate Professor, MTech, Ph.d

<sup>1,2</sup>Mallareddy college of Engineering, Secunderabad

<sup>1</sup>chinna.2k17@gmail.com, <sup>2</sup>vikash\_mech@mrce.in

---

## Abstract:

Solar energy is the most promising energy in today's world as it is most abundant and ecofriendly. It is an important source of renewable energy resource. To utilize such energy, we require a concentrating solar collector. It optically reflects and focuses the sun's incident solar energy onto a small receiving area using mirrors or lenses is called a **Solar Dish Collector**. The Parabolic Dish Solar Collector technology is very useful as it is used for approximately all solar energy applications such as steam and power generation, water heating, air heating etc. In this paper, design of a parabolic solar dish collector is accomplished and performs experimental study of concentrating solar collector used in Stirling engine.

**Keywords:** Solar energy, solar dish collector, stirling engine.

## 1. INTRODUCTION

The world energy requirements are now completely depend on non-renewable energy resources such as oil, coal and natural gas. As these were going to depleted in near future, we need to search for an alternative energy resources such as renewable energy sources. Renewable resources are an important aspect of sustainability, the most frequently used renewable resources are biomass, water, geothermal, wind and solar. Unlike fossil fuels, we can regenerate or replenish these resources. The selection of type of energy source depends on economic, environmental and safety considerations. Solar energy is considered to be more suitable on the basis

of environmental and safety considerations. The solar energy is the most abundant, permanent and free of cost. The energy from the sun cannot be used directly such as for air heating, hot water generation, electricity and in drying applications. Solar collector is one of the main components in a solar thermal system. It absorbs the solar radiation as heat and transfers it to the heat transport fluid. The collected solar energy will be transferred either for hot water generation or space heating or to a thermal storage tank etc.

Based on the way of solar collection, the solar collectors are classified into non concentrated or stationary solar collector and concentrated type. A non-concentrated solar collector has the same area for intercepting and absorbing solar radiation. They are permanently fixed in position and do not track the sun, three set of collectors fall in this category: the flat plate collectors (FPC), compound parabolic collectors (CPC), and the evacuated tube collectors (ETC) single axis tracking and two axis tracking. While concentrated type will have a concave shaped reflective surface for intercepting radiation and it will be focused to a small area and thus increases radiation flux. Another advantage of concentrated collectors is that higher temperature can be achieved than that of non-concentrated collectors.

The three main types of concentrated collectors are parabolic dish, parabolic trough and tower receiver. Among them, parabolic dish collector is one of the developing technologies. Since it has small absorber area, it has less radiation losses.

Stirling engines are a type of reciprocating external heat engine that

uses one or more pistons to achieve useful work through some input of heat from an external source. Stirling engines use the same gas over and over, unlike internal combustion engines which constantly intake and exhaust the gas. Also, they do not use explosions like normal gasoline engines, therefore they are very quiet.

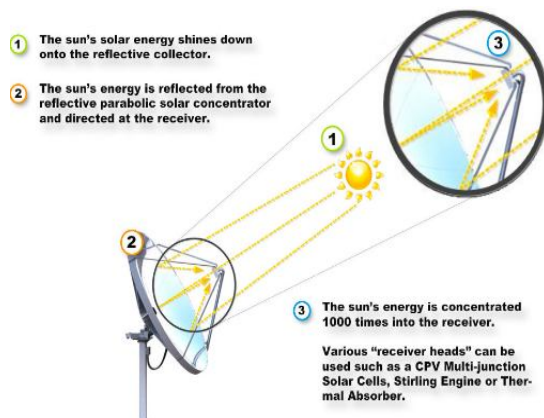


Figure 1 Parabolic concentrating solar collector

Solar energy collectors are special kind of heat exchangers that transform solar radiation energy to internal energy of the transport medium, it is the major component of any solar energy systems. Using parabolic dishes is a well-tested approach to concentrate solar radiation, and was an early experimental tool at many locations worldwide. The optical efficiency of parabolic dishes is considerably higher than that of parabolic trough, Linear Fresnel reflector or Power tower systems because the mirror is always pointed directly at the sun. In this study, the reflector for the parabolic concentrator is made of a mirror; the interior of the parabolic concentrator is covered with the reflective mirrors, which reflect the solar rays on the face of a receiver placed at the focal position of the parabolic concentrator.

## 2. A REVIEW OF INVESTIGATIONS

**Lifang Li et al. [1]** developed a new concept for designing and fabricating large parabolic dish. The dish mirror was

formed from several optimal-shaped thin flat metal petals with highly reflective surfaces. Attached to the rear surface of the mirror petals were several thin layers whose shapes optimized to reflective petals form into a parabola when their ends were pulled toward each other by cables or rods.

**B. Ricardo, V. Nicolas, E. C. Alma, S. Daniel and P. Guillermo [2]** (2012) developed a mathematical model of a system consisting of parabolic dish collector with cavity receiver and Stirling engine at its focal point.

**Atul [3]** (2012) had performed an experimental study of parabolic dish solar water heater with coated and non-coated receiver. The system consists of parabolic dish of 1.4m diameter with aluminium mirrors and cone shaped helical coil made of copper and is coated with nickel chrome is placed at its focal point. The experimental results showed that with the increase in mass flow rate, the total heat loss increased and thus the efficiency of the system also reduced. In this paper a parabolic dish collector system was designed for hot water generation and simulation of dish collector was also done.

**El Ouederni et al [4]** presented an experimental study of a parabolic solar concentrator, the solar flux and temperature distribution on the receiver was carried out, the results describe correctly the awaited physical phenomena.

**Saleh Ali et al. [5]** have presented an interesting study that aims to develop a 3-D static solar concentrator that can be used as a low cost technology for production of portable hot water in rural India. They used the ray tracing software for evaluation of the optical performance of a static 3-D elliptical hyperboloid concentrator

**Pavlović et al. [6]** presented a mathematical and physical model of the new offset type parabolic concentrator with a spiral coil absorber for calculating its optical performance. The designed parabolic concentrator is a low cost solar concentrator for medium temperature applications.

**G. Shiva, G. Barat, H. T. Teymour and B. Ahmad [7]** calculated the thermal efficiency of a point focus parabolic dish steam generating system under varying climatic conditions. A parabolic dish collector with cylindrical receiver was used for steam or hot water generation. A performance analysis was done over an entire year and it was found that as the absorber temperature was increased from 150 to 200<sup>0</sup>C, the convective heat loss coefficient was increased by about 25 to 41%

**M. R. A. Ghani, A. Rosnani, G. K. Chin, R.H. Siti and Z. Jano [8]** (2014) had done an analysis to determine about influence of material reflectivity and aperture size on the heat transfer rate from concentrator to receiver in parabolic dish systems. Among the different reflective materials, silver has highest reflectivity (96%) followed by aluminium (92%), iron sheet (87%) and stainless steel (67%).

**Eswaramoorthy et al. [9]** conducted an experiment on small scale solar parabolic dish thermoelectric generator. They fabricated solar parabolic dish collector using an unused satellite dish antenna fitted with polished aluminum sheet as concentrator surface. The concentrated solar radiation and water cooled heat sink was the driving potential to generate electricity; they studied various operating parameters like receiver plate temperature, power output and conversion efficiency with respect to solar radiation. From the experiment it was found that the receiver plate temperature was significantly affecting the power output.

**Yadav et al. [10]** investigated a solar powered air heating system using parabolic trough collector using different reflectors. In this experiment, the reflected solar radiations were focused on absorber tube which was placed at focal length of the parabolic trough. In this setup, air was used as working fluid which collects the heat from absorber tube. He used three different reflectors for analysis and they observed that performance of Aluminum sheet is

excellent as compare to steel sheet and Aluminum foil as reflector.

### 3. DESIGN OF PARABOLIC SOLAR COLLECTOR

In a parabola, all the incoming solar rays from a light source are reflected back to the focal point of the parabola. The solar concentrator was developed using a semi-spherical surface covered with many small sections of mirrors to form a segmented, spherical concentrator. The frame of the parabola was made from a mini dish satellite receiver plate. The solar concentrator takes advantage of all incoming solar radiation and concentrates it at the focus.

Figure 2 shows the parabolic dish concentrator parameters. The equation for the parabola in cylindrical coordinates is given by:

$$Z = \frac{r^2}{4f} \text{ -----(1)}$$

The diameter of the opening parabolic surface is d, and the focal distance of the parabola is f. the surface of this parabola is given by :

$$S = \left\{ \left[ 1 + \left( \frac{d}{4f} \right)^2 \right]^{\frac{3}{2}} - 1 \right\} \text{ ----- (2)}$$

The cross-section of the opening is:

$$A = \frac{\pi d^2}{4} \text{ -----(3)}$$

To calculate the focal distance, the following equation is used

$$f = \frac{d^2}{16h} \text{ -----(4)}$$

Where

- h is the height of the dish
- d is the diameter of the dish
- f is the focal point
- F is the load
- r is the radius

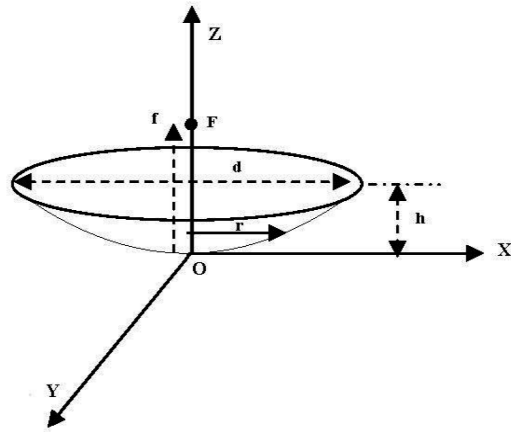


Figure 2 parameters of parabolic dish collector

The geometric concentration of this model is

$$C_g = \frac{S_0}{S_a} \text{-----(5)}$$

Characteristics of the solar concentrator

Diameter of opening of the parabola	2.2m
Surface collecting of the parabola	3.8m <sup>2</sup>
Depth of the parabola	0.4m
Focal distance, f	0.75m

Table 1 characteristics of solar concentrator

#### 4. USE OF SOLAR DISH COLLECTOR IN STIRLING ENGINE

Stirling engines are a type of reciprocating external heat engine that uses one or more pistons to achieve useful work through some input of heat from an external source. Stirling engines use the same gas over and over, unlike internal combustion engines which constantly intake and exhaust the gas. Also, they do not use explosions like normal gasoline engines, therefore they are very quiet.

Solar energy is one of the famous renewable energy sources that can be used as an input energy source for Stirling engine. Solar Stirling systems convert the thermal energy in solar radiation to mechanical energy and then to electrical energy. Solar Stirling systems have demonstrated the highest efficiency of any solar power generation system by converting nearly 30% of direct-normal incident solar radiation into electricity after accounting for power losses. Solar Stirling system produces electricity by using parabolic collector and Stirling engine. Dish/Stirling concentrating solar power (CSP) converts solar heat into electricity by focusing solar radiation onto a receiver containing a heat-engine known as a Stirling engine.

#### 4.1 Thermodynamics of stirling engine

The cycle consist of four processes namely isothermal compression and expansion and isentropic heat addition and rejection processes in the sequence. The below Figure 3 shows the PV and TS diagrams and Figure 4 shows the operating cycles of the stirling engine schematically.

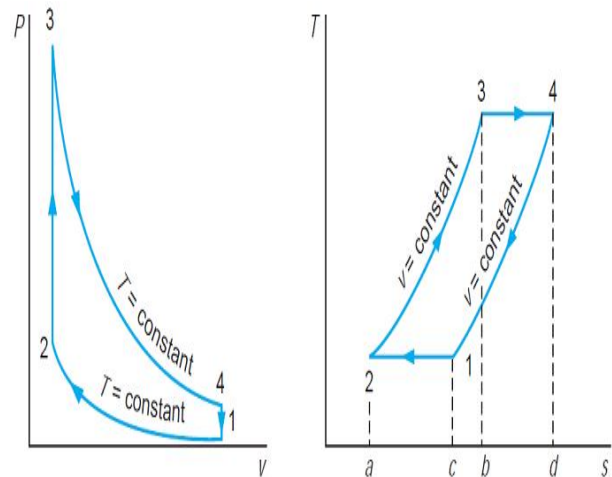


Figure 3 PV and TS diagrams

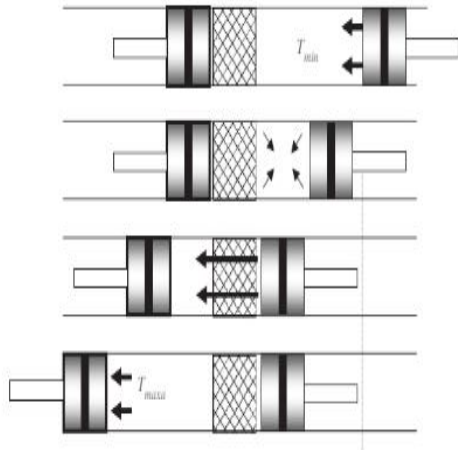


Figure 4 Operating cycles of Stirling engine

### 4.2 Efficiency of Stirling engine

The efficiency of Stirling engine for an ideal gas  $Pv=nRT$  is as follows

The mechanical work is

$$\Delta W_{12} = - \int_{V_1}^{V_2} p(V)dV = -nRT_2 \ln \frac{V_2}{V_1}$$

$$\Delta W_{23} = \Delta W_{41} = 0$$

$$\Delta W_{34} = -nRT_1 \ln \frac{V_1}{V_2}$$

On the isothermal curves the change in the internal energy  $\Delta U = \Delta W + \Delta Q$  is zero.

$$\Delta Q_{12} = -\Delta W_{12} > 0$$

$$\Delta Q_{34} = -\Delta W_{34} < 0$$

On the isochoric curve the heat quantities are

$$\Delta Q_{23} = C_V(T_1 - T_2) < 0$$

$$\Delta Q_{41} = C_V(T_2 - T_1) > 0$$

The efficiency is then

$$\eta = \frac{-\Delta W}{\Delta Q} \text{ -----(6)}$$

So final efficiency in terms of temperature and volume is

$$\eta = \frac{T_2 - T_1}{T_2 + \frac{C_V(T_2 - T_1)}{nR \ln V_2/V_1}} \text{ -----(7)}$$

It is smaller than the efficiency of the Carnot cycle. But it should be equal to it if all processes are done reversibly. The efficiency of Stirling engine lies between 15% to 25% if it is run with motors. Stirling engines have the advantage to use any heat source (i.e., renewable energy sources, especially solar), to be quieter and to be more reliable and with less maintenance costs depending of their design.

### 4.3 Solar Stirling engine

Solar collectors include a special type of solar engine built into the solar receiver. This so called heat engine, is driven by the solar thermal energy converting it into rotational mechanical output by the cyclic compression of the engine's working gas, which is usually helium or hydrogen. The mechanical power that is produced is then used to drive an electrical generator or alternator producing a significant amount of AC electrical power. These types of solar heat engines are commonly called a Stirling Engine.

Stirling engines belong to the group of closed-loop hot-gas machines that work on the basic principal that a gas will change its volume when subjected to a heat change producing an isothermal compression of the cold and isothermal expansion of the hot gas at a constant volume. This temperature change, and thus the continuous operation of the engine, is produced by moving the gas between two different chambers producing a constantly high and a constantly low temperature.

The efficiency and operation of the Stirling heat engine is determined by the operating temperature of the gas which is kept between 650°C and 750°C. To constantly keep the reflected solar radiation at the correct focal point and temperature during the whole of the day, a two-axis sun tracking system is used with the dish which continuously rotates the solar concentrator.



Figure 5 Solar Stirling components

## 5. SUMMARY

The solar Stirling engine dish convert sunlight in most climates, however they have proven to be most effective in hot and dry climates, where the system converts one third of the solar energy into electricity. It is an efficient solar Stirling engine technology that combines a both low environmental impact and low Levelized Cost of Energy, making it very competitive with all alternative electrical energy technologies. Ripasso energy AB is the company from Sweden, designed a Solar Stirling dish module that set a new efficiency world record of 32% when compared to normally operated Stirling engine. Considering that recent reports and negotiations point towards the need to reduce carbon emissions, solar Stirling engine.

Today we are moving toward the use of natural resource for the energy generation. Stirling engine is one of the effective and efficient device to convert solar energy into mechanical work. It is the best device as compare to other solar device in power generation.

## 6. RESULT

Today worldwide concerns about the best way of utilization of the natural energy and developing technique to reduce

pollution. Stirling engine is one of the best example of heat engine which convert heat energy into mechanical work. Stirling engine is also operated by heat from sunrays. The solar Stirling have better efficiency than that of other solar device like photovoltaic cell, solar panel etc.

## REFERENCES

1. Lifang Li, Steven Dubowsky "A new design approach for solar concentrating parabolic dish based on optimized flexible petals", *Mechanism and Machine Theory* 46(2011) pp 1536-1548
2. B. Ricardo, V .Nicolas, E. C. Alma, S.Daniel and P. Guillermo, "Mathematical model for the study and design of a solar dish collector with cavity receiver for its application in Stirling engines," *Journal of Mechanical Science and Technology*, vol.26, pp.3311-3321, May 2012.
3. A. S. Atul, "Experimental Investigation of variation of mass flow rate on the performance of parabolic dish collector with nickel chrome coated receiver," *International Journal of Sustainable Energy Development*, vol.1, pp.29-35, December 2012.
4. A.R. El-Ouederni, et al., *Experimental Study of a parabolic solar concentrator*. *Revue des Energies Renouvelables* 2009. 12(3): p. 395-404.
5. Saleh Ali, I. M., et al., *An Optical Analysis of a Static 3-D Solar Concentrator*, *Solar Energy*, 88 (2013), Feb., pp. 57-70
6. Pavlović, S., et al., *Optical Model and Numerical Simulation of the New Offset Type Parabolic Concentrator with Two Types of Solar Receivers*, *Facta Universitatis, Series: Mechanical Engineering*, 13 (2015), 2, pp. 169-180
7. G. Shiva, G. Barat, H. T. Teymour and B. Ahmad, "Thermal performance of a point-focus solar steam generating system" *Annual International*

Conference on Mechanical Engineering,  
May 2013.

8. M. R. A. Ghani, A. Rosnani , G.K. Chin, R.H. Siti and Z. Jano, “The Influence of concentrator size, reflective material and solar irradiance on the parabolic dish heat transfer,” Indian Journal of Science and Technology, vol.7, pp.1454-1460, September 2014.
9. M.Eswaramoorthy<sup>1</sup>, .Shanmugam<sup>2</sup>, A R. Veerappan “Experimental Study on Solar Parabolic Dish Thermoelectric Generator”, International Journal of Energy Engineering (IJEE) Jun. 2013, Vol. 3 Iss. 3, PP. 62-66.
10. Avadhesh Yadav, Manoj Kumar, Balram “Experimental Study and Analysis of Parabolic trough Collector with Various Reflectors” International Journal of Mathematical, Computational, Physical and Quantum Engineering Vol:7 No:12, 2013 pp1161-1165

# NATURAL CONVECTIVE HEAT TRANSFER FROM INCLINED NARROW PLATES

R.Swapna  
Mechanical Engineering  
Malla reddy college of engg  
Hyderabad, India  
Email: [swapna3094@gmail.com](mailto:swapna3094@gmail.com)

Mr.V.Ravinder(M.tech)  
Mechanical Engineering  
Malla reddy college of engg  
Hyderabad, India  
Email: [vankudothravinder@gmail.com](mailto:vankudothravinder@gmail.com)

**Abstract**— *Natural Convection flow in a vertical channel with internal objects is encountered in several technological applications of particular interest of heat dissipation from electronic circuits, refrigerators, heat exchangers, nuclear reactors fuel elements, dry cooling towers, and home ventilation etc.*

*In this thesis the air flow through vertical narrow plates is modeled using CREO design software. The thesis will focus on thermal and CFD analysis with different Reynolds number ( $2 \times 10^6$  &  $4 \times 10^6$ ) and different angles ( $0^\circ, 30^\circ, 45^\circ$  &  $60^\circ$ ) of the vertical narrow plates. Thermal analysis done for the vertical narrow plates by steel, aluminum & copper at different heat transfer coefficient values. These values are taken from CFD analysis at different Reynolds numbers.*

*In this thesis the CFD analysis to determine the heat transfer coefficient, heat transfer rate, mass flow rate, pressure drop and thermal analysis to determine the temperature distribution, heat flux with different materials.*

*3D modeled in parametric software Pro-Engineer and analysis done in ANSYS.*

**Keywords**— *Types of convection, Natural convection, inclined plates, copper material.*

## I. INTRODUCTION

### Natural Convection

In natural convection, the fluid motion occurs by natural means such as buoyancy. Since the fluid velocity associated with natural convection is relatively low, the heat transfer coefficient encountered in natural convection is also low.

### Mechanisms of Natural Convection

Consider a hot object exposed to cold air. The temperature of the outside of the object will drop (as a result of heat transfer with cold air), and the temperature of adjacent air to the object will rise. Cons

equently, the object is surrounded with a thin layer of warmer air and heat will be transferred from this layer to the outer layers of air. The temperature of the air adjacent to the hot object is higher, thus its density is lower. As a result, the heated air rises. This movement is called the natural convection current. Note that in the absence of this movement, heat transfer would be by conduction only and its rate would be much lower. In a gravitational field, there is a net force that pushes a light fluid placed in a heavier fluid upwards. This force is called the buoyancy force.

**Natural convection** is a mechanism, or type of heat transport, in which the fluid motion is not generated by any external source (like a pump, fan, suction device, etc.) but only by density differences in the fluid occurring due to temperature gradients. In natural convection, fluid surrounding a heat source receives heat, becomes less dense and rises. The surrounding, cooler fluid then moves to replace it. This cooler fluid is then heated and the process continues, forming convection current; this process transfers heat energy from the bottom of the convection cell to top. The driving force for natural convection is buoyancy, a result of differences in fluid density. Because of this, the presence of a proper acceleration such as arises from resistance to gravity, or an equivalent force (arising from acceleration, centrifugal force or Coriolis effect), is essential for natural convection. For example, natural convection essentially does not operate in free-fall (inertial) environments, such as that of the orbiting International Space Station, where other heat transfer mechanisms are required to prevent electronic components from overheating.

### Natural Convection from a Vertical Plate

In this system heat is transferred from a vertical plate to a fluid moving parallel to it by natural convection. This will occur in any system wherein the density of the moving fluid varies with position.

$$Nu_m = 0.478(Gr^{0.25})$$

Mean Nusselt Number =  $Nu_m = h_m L / k$

Where

$h_m$  = mean coefficient applicable between the lower edge of the plate and any point in a distance L (W/m<sup>2</sup>. K)

L = height of the vertical surface (m)

k = thermal conductivity (W/m. K)

GrashoffNumber =  $Gr = \frac{g L^3 (t_s - t_\infty)}{\nu^2 T}$

Where

g = gravitational acceleration (m/s<sup>2</sup>)

L = distance above the lower edge (m)

$t_s$  = temperature of the wall (K)

$t_\infty$  = fluid temperature outside the thermal boundary layer (K)

$\nu$  = kinematic viscosity of the fluid (m<sup>2</sup>/s)

T = absolute temperature (K)

## II. LITERATURE REVIEW

In 1972, Aung et al. [12] presented a coupled numerical experimental study. Under isothermal conditions at high Rayleigh numbers their experimental results were 10% lower than the numerical ones. This difference has also been observed between Bodoia's and Osterle's numerical results [8] and Elenbaas' experimental ones [7]. They ascribed the discrepancies to the assumption of a flat velocity profile at the channel inlet.

In 2004, Olsson [17] presented a similar study. He worked on the different existing correlations, including those of Bar-Cohen and Rohsenow, and compared them with experimental results. Finally he proposed some corrected correlations that are valid for a wide range of Rayleigh numbers.

In 1989, Webb and Hill [18] studied the laminar convective flow in an experimental asymmetrically heated vertical channel. They worked on isoflux heating with a modified Rayleigh number (see eq. 13) changing from 500 to 107. Their temperature measurements performed in horizontal direction on the heated wall showed variations of ± 1.5%, and the flow was assumed to be 2D. They studied correlations for local, average and higher channel Nusselt numbers and compared them to previous works ([9], [10] and [11]). Their correlations were calculated for pure convective flow and the radiation losses were estimated and subtracted from

the heat input. They found that constants C1 and C2 were strongly dependent on modified Rayleigh numbers below  $Ra_b < 105$  but that they were independent for higher Rayleigh numbers. Good agreement was seen between their results for high Rayleigh numbers and the flat plate solution of Sparrow and Gregg [10].

## III. PROCEDURE:

Air flow through vertical narrow plates is modeled using CREO design software. The thesis will focus on thermal and CFD analysis with different Reynolds number ( $2 \times 10^6$  &  $4 \times 10^6$ ) and different angles ( $0^\circ, 30^\circ, 45^\circ$  &  $60^\circ$ ) of the vertical narrow plates. Thermal analysis done for the vertical narrow plates by steel, aluminum & copper at different heat transfer coefficient values.

Reynolds numbers	Angle of plate	material
$2 \times 10^6$	$0^\circ, 30^\circ, 45^\circ$ & $60^\circ$	Copper
$4 \times 10^6$		aluminum
		steel

## INTRODUCTION TO CAD

Computer-aided design (CAD) is defined as the application of computers and graphics software to aid or enhance the product design from conceptualization to documentation. CAD is most commonly associated with the use of an interactive computer graphics system, referred to as a CAD system. Computer-aided design systems are powerful tools and in the mechanical design and geometric modeling of products and components.

There are several good reasons for using a CAD system to support the engineering design

Function:

- To increase the productivity
- To improve the quality of the design
- To uniform design standards
- To create a manufacturing data base
- To eliminate inaccuracies caused by hand-copying of drawings and inconsistency between
- Drawings

## INTRODUCTION TO CREO

PTC CREO, formerly known as Pro/ENGINEER, is 3D modeling software used in mechanical engineering, design, manufacturing, and in CAD drafting service firms. It was one of the first 3D CAD modeling applications that used a rule-based parametric system. Using parameters, dimensions and features to capture the behavior of the product, it can optimize the development product as well as the design itself.

#### **ADVANTAGES OF CREO PARAMETRIC SOFTWARE**

1. Optimized for model-based enterprises
2. Increased engineer productivity
3. Better enabled concept design
4. Increased engineering capabilities
5. Increased manufacturing capabilities
6. Better simulation
7. Design capabilities for additive manufacturing

#### **CREO parametric modules:**

- Sketcher
- Part modeling
- Assembly
- Drafting

#### **ANSYS Software:**

ANSYS is an Engineering Simulation Software (computer aided Engineering). Its tools cover Thermal, Static, Dynamic, and Fatigue finite element analysis along with other tools all designed to help with the development of the product. The company was founded in 1970 by Dr. John A. Swanson as Swanson Analysis Systems, Inc. SASI. Its primary purpose was to develop and market finite element analysis software for structural physics that could simulate static (stationary), dynamic (moving) and heat transfer (thermal) problems. SASI developed its business in parallel with the growth in computer technology and engineering needs. The company grew by 10 percent to 20 percent each year, and in 1994 it was sold. The new owners took SASI's leading software, called ANSYS®, as their flagship product and designated ANSYS, Inc. as the new company name.

#### **Benefits of ANSYS:**

- The ANSYS advantage and benefits of using a modular simulation system in the design process are well documented
- The ANSYS advantage is well-documented.
- ANSYS is a virtual prototyping and modular simulation system that is easy to use and

extends to meet customer needs; making it a low-risk investment that can expand as value is demonstrated within a company.

#### **Structural analysis :**

Structural analysis is probably the most common application of the finite element method. The term structural (or structure) implies not only civil engineering structures such as ship hulls, aircraft bodies, and machine housings, as well as mechanical components such as pistons, machine parts, and tools.

#### **Types of Structural Analysis:**

Different types of structural analysis are:

- Static analysis
- Modal analysis
- Harmonic analysis
- Transient dynamic analysis
- Spectrum analysis
- Buckling analysis
- Explicit dynamic analysis

#### **Static Analysis:**

Static analysis calculates the effects of steady loading conditions on a structure, while ignoring inertia and damping effects, such as those caused by time varying loads. Static analysis is used to determine the displacements, stresses, strains, and forces in structural components caused by loads that do not induce significant inertia and damping effects. Steady loading and response are assumed to vary slowly with respect to time.

The kinds of loading that can be applied in a static analysis include:

- Externally applied forces and pressures
- Steady-state inertial forces (such as gravity or rotational velocity)
- Imposed (non-zero) displacements
- Temperatures (for thermal strain)

A static analysis can be either linear or non-linear. All types of non-linearities are allowed-large deformations, plasticity, creep, stress, stiffening, contact (gap) elements, hyper elastic elements, and so on.

#### **Over-view of steps in a static analysis:**

The procedure for a modal analysis consists of three main steps:

1. Build the model.
2. Apply loads and obtain the solution.
3. Review the results.

**Basic Steps in ANSYS:**

**Pre-Processing (Defining the Problem):** The major steps in pre-processing are given below

- Define key points/lines/ areas/volumes.
- Define element type and material/geometric properties
- Mesh lines/ areas/volumes as required.

The amount of detail required will depend on the dimensionality of the analysis (i.e., 1D, 2D, axis-symmetric, 3D).

**Solution (Assigning Loads, Constraints, And Solving):** Here the loads (point or pressure), constraints (translational and rotational) are specified and finally solve the resulting set of equations.

**Post Processing:** In this stage, further processing and viewing of the results can be done such as:

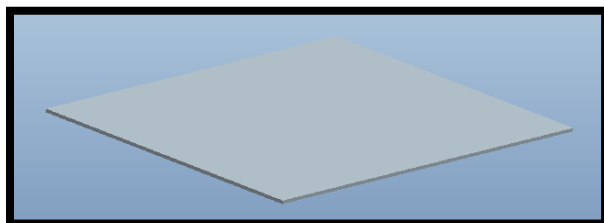
- Lists of nodal displacements
- Element forces and moments
- Deflection plots
- Stress contour diagrams

**Advanced Post-Processing:**

ANSYS provides a comprehensive set of post-processing tools to display results on the models as contours or vector plots, provide summaries of the results (like min/max values and locations). Powerful and intuitive slicing techniques allow getting more detailed results over given parts of your geometries. All the results can also be exported as text data or to a spreadsheet for further calculations. Animations are provided for static cases as well as for nonlinear or transient histories. Any result or boundary condition can be used to create customized charts.

**IV . MODELLING AND ANALYSIS**

**Vertical narrow plate 3D model**



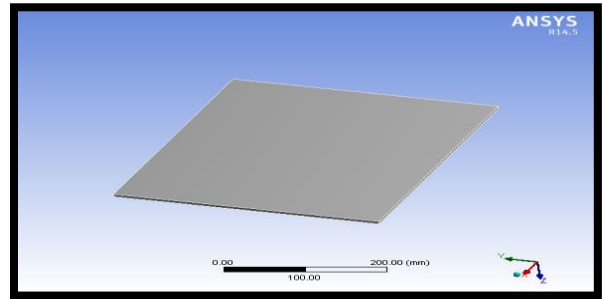
**MATERIAL PROPERTIES OF AIR**

Thermal conductivity =0.024w/m-k

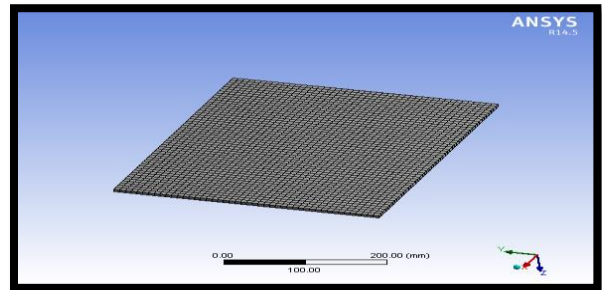
Density =1.225kg/m<sup>3</sup>

Viscosity =1.98×10<sup>-5</sup> kg/m-s

**IMPORTED MODEL**

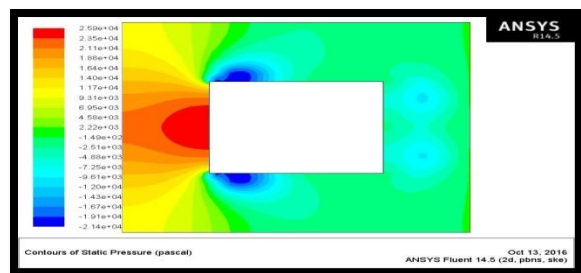


**MESHED MODEL**



**VERTICAL NARROW PLATE AT 0°**

**REYNOLDS NUMBER - 2×10<sup>6</sup>**



**Mass flow rate**

Mass Flow Rate	(kg/s)
inlet	79.311481
interior_trm_srf	196.93365
outlet	-79.3256
wall_trm_srf	0
<b>Net</b>	<b>-0.014198383</b>

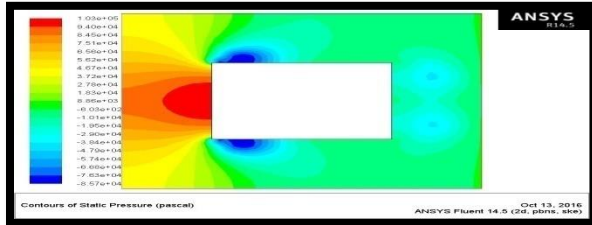
**Heat transfer rate**

Total Heat Transfer Rate		(w)
inlet	5974630.5	
outlet	-6031706	
wall_trn_srf	0	
-----		
Net	-57075.5	

**Mass flow rate**

Mass Flow Rate		(kg/s)
inlet	99.139221	
interior_trn_srf	-54.444607	
outlet	-99.00412	
wall_trn_srf	0	
-----		
Net	0.13510132	

**REYNOLDS NUMBER -  $4 \times 10^6$**



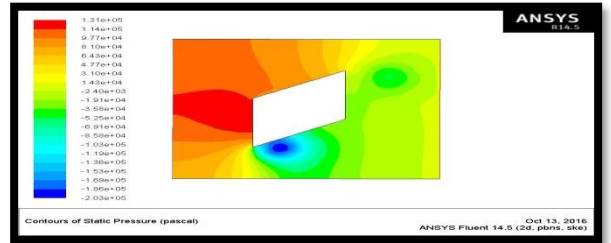
**Heat transfer rate**

Total Heat Transfer Rate		(w)
inlet	1481683.6	
outlet	-1479661.3	
wall_trn_srf	0	
-----		
Net	2022.375	

**MASS FLOW RATE**

Mass Flow Rate		(kg/s)
inlet	158.63991	
interior_trn_srf	393.53253	
outlet	-158.66556	
wall_trn_srf	0	
-----		
Net	-0.025650024	

**REYNOLDS NUMBER -  $4 \times 10^6$**



**HEAT TRANSFER RATE**

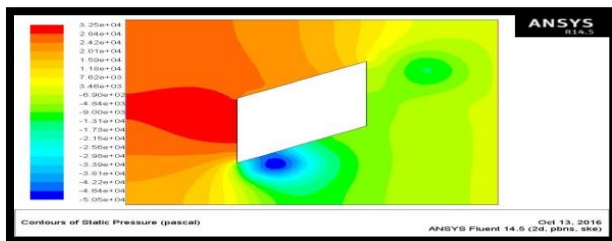
Total Heat Transfer Rate		(w)
inlet	11950556	
outlet	-12070637	
wall_trn_srf	0	
-----		
Net	-120081	

**Mass flow rate**

Mass Flow Rate		(kg/s)
inlet	198.29997	
interior_trn_srf	-105.51134	
outlet	-197.43877	
wall_trn_srf	0	
-----		
Net	0.86120605	

**VERTICAL NARROW PLATE AT 30°**

**REYNOLDS NUMBER -  $2 \times 10^6$**

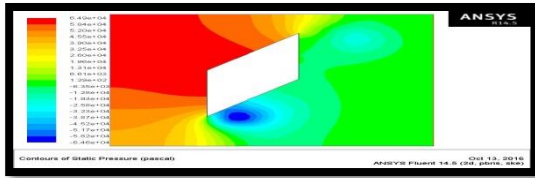


**Heat transferrate**

Total Heat Transfer Rate		(w)
inlet	2963688.3	
outlet	-2950814	
wall_trn_srf	0	
-----		
Net	12874.25	

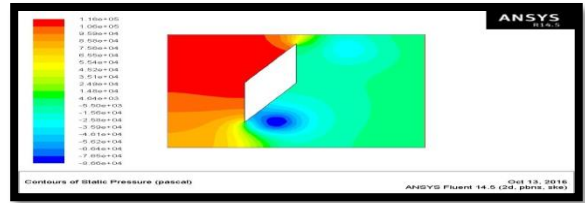
**VERTICAL NARROW PLATE AT 45°**

**REYNOLDS NUMBER -  $2 \times 10^6$**



Mass flow rate

Mass Flow Rate (kg/s)	
inlet	99.139221
interior_trm_srf	1081.3646
outlet	-98.893143
wall_trm_srf	0
Net	0.24607849



Mass flow rate

Mass Flow Rate (kg/s)	
inlet	99.139221
interior_trm_srf	1325.8466
outlet	-99.647263
wall_trm_srf	0
Net	-0.50804138

Heat transfer rate

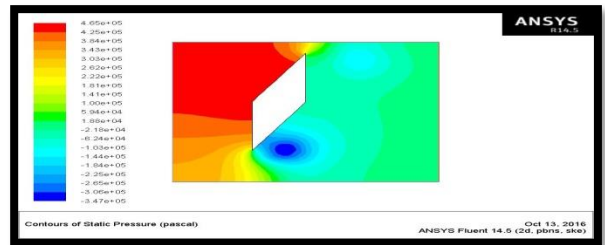
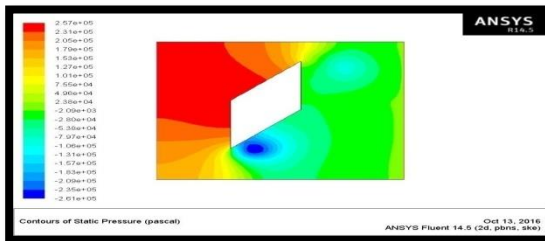
Total Heat Transfer Rate (w)	
inlet	1481683.6
outlet	-1478005.8
wall_trm_srf	0
Net	3677.875

Heat transfer rate

Total Heat Transfer Rate (w)	
inlet	1481683.6
outlet	-1491557.3
wall_trm_srf	0
Net	-9873.625

REYNOLDS NUMBER -  $4 \times 10^6$

REYNOLDS NUMBER -  $4 \times 10^6$



Mass flow rate

Mass Flow Rate (kg/s)	
inlet	198.29997
interior_trm_srf	2164.0718
outlet	-197.68851
wall_trm_srf	0
Net	0.61146545

Mass flow rate

Mass Flow Rate (kg/s)	
inlet	198.29997
interior_trm_srf	2652.6765
outlet	-199.35345
wall_trm_srf	0
Net	-1.0534821

Heat transfer rate

Total Heat Transfer Rate (w)	
inlet	2963688.3
outlet	-2954559.3
wall_trm_srf	0
Net	9129

Heat transfer rate

Total Heat Transfer Rate (w)	
inlet	2963688.3
outlet	-2983982.5
wall_trm_srf	0
Net	-20294.25

VERTICAL NARROW PLATE AT  $60^\circ$

REYNOLDS NUMBER -  $2 \times 10^6$

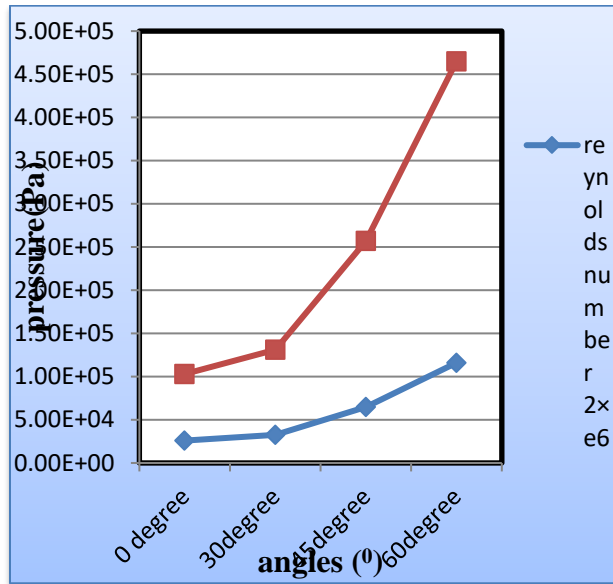
**CFD ANALYSIS RESULT TABLE**

Reynolds number	Models	Pressure (Pa)	Velocity (m/s)	Heat transfer coefficient (w/m <sup>2</sup> -k)	Mass flow rate (kg/s)	Heat transfer rate (W)
2×10 <sup>6</sup>	0 <sup>0</sup>	2.59e+04	2.22e+02	3.14e+02	0.0141983	57075.5
	30 <sup>0</sup>	3.25e+04	2.80e+02	3.39e+02	0.13510132	2022.375
	45 <sup>0</sup>	6.49e+04	3.40e+02	4.06e+02	0.246078	3677.875
	60 <sup>0</sup>	1.16e+05	5.01e+02	4.93e+02	0.50804138	9873.625
4×10 <sup>6</sup>	0 <sup>0</sup>	1.03e+05	4.44e+02	5.52e+02	0.02565	120081
	30 <sup>0</sup>	1.31e+05	5.60e+02	5.96e+02	0.86120605	12874.25
	45 <sup>0</sup>	2.57e+05	6.80e+02	7.09e+02	0.611465	9129
	60 <sup>0</sup>	4.65e+05	1.00e+03	8.55e+02	1.05348	20294.25

**THERMAL ANALYSIS RESULT TABLE**

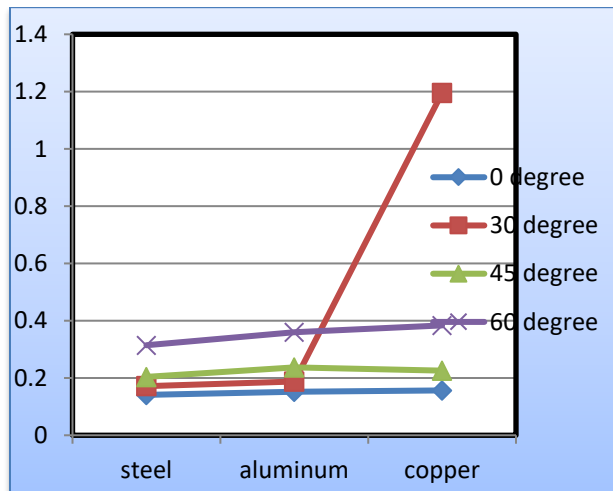
Models	Materials	Temperature (°C)		Heat flux (w/mm <sup>2</sup> )
		Max.	Min.	
0 <sup>0</sup>	Steel	343	333.99	0.14103
	Aluminum	343	339.2	0.15159
	Copper	343	341.76	0.15657
30 <sup>0</sup>	Steel	343	331.7	0.17153
	Aluminum	343	338.22	0.18744
	Copper	343	341.41	1.1951
45 <sup>0</sup>	Steel	343	329.74	0.20385
	Aluminum	343	341.08	0.23701
	Copper	343	337.26	0.22608
60 <sup>0</sup>	Steel	343	325.73	0.3144
	Aluminum	343	335.2	0.35993
	Copper	343	340.34	0.38359

**CFD ANALYSIS GRAPHS**



**THERMAL ANALYSIS**

**HEAT FLUX**



**CONCLUSION**

In this thesis the air flow through vertical narrow plates is modeled using CREO design software. The thesis will focus on thermal and CFD analysis with different Reynolds number ( $2 \times 10^6$  &  $4 \times 10^6$ ) and different angles ( $0^\circ, 30^\circ, 45^\circ$  &  $60^\circ$ ) of the vertical narrow plates. Thermal analysis done for the vertical narrow plates by steel, aluminum & copper at different heat transfer coefficient values. These values are taken from CFD analysis at different Reynolds numbers.

By observing the CFD analysis the pressure drop & velocity increases by increasing the inlet Reynolds numbers and increasing the plate angles. The heat transfer rate increasing the inlet Reynolds numbers, more heat transfer rate at  $0^\circ$  angles.

By observing the thermal analysis, the taken different heat transfer coefficient values are from CFD analysis. Heat flux value is more for copper material than steel & aluminum.

So we can conclude the copper material is better for vertical narrow plates.

**REFERENCES**

1. Arpaci, V. S., 1995, "Buoyant Turbulent Flow Driven by Internal Energy Generation," Int. J. Heat Mass Transfer, Vol. 38, pp. 2761-2770.
2. Asfia, F. J., and Dhir, V. K., 1994, "An Experimental Study of Natural Convection in a Volumetrically Heated Spherical Pool With Rigid Wall," ASME Paper 94-WA/HT-26.
3. Cheung, F. B., 1980a, "Heat Source-Driven Thermal Convection at Arbitrary Prandtl Numbers," J. Fluid Mech., Vol. 97, pp. 743-758.
4. Cheung, F. B., 1980b, "The Boundary Layer Behaviour in Transient Turbulent Thermal Convection Flow," ASME Journal of HEAT TRANSFER Vol. 102, pp. 373-375.
5. Cheung, F. B., 1978, "Turbulent Thermal Convection in a Horizontal Fluid Layer With Time Dependent Volumetric Energy Sources." AIAA/ASME Thermophysics and Heat Transfer Conf., 78-HT-6, Palo Alto.
6. Cheung, F. B., 1977, "Natural Convection in a Volumetrically Heated Fluid Layer at High Rayleigh Numbers," Int. J. Heat Mass Transfer, Vol. 20, pp. 499-506.
7. Cheung, F. B., Shiah, S. W., Cho, D. H., and Tan, M. J., 1992, "Modelling of Heat Transfer in a Horizontal Heat Generating Layer by an Effective Diffusivity Approach," ASME/HTD, Vol. 192, pp. 55-62.
8. Dinh, T. N., and Nourgalier, R. R., 1997, "On Turbulence Modelling in Large Volumetrically Heated Liquid Pools," Nucl. Engng. Design, in press.
9. Fan, T. H., 1996, "Heat Transport Phenomena of Turbulent Natural Convection in a Melt Layer With Solidification," M.S. thesis, The Pennsylvania State University, University Park, PA.
10. Fielder, H. E., and Wile, R., 1970, "Turbulent Free Convection in a Horizontal Fluid Layer with a Volumetric Heat Source," Paper NC 4.5, Proc. Fourth Int. Heat Transfer Conf., Vol. IV, pp. 1-12.

# MODELING AND MANUFACTURING OF A CENTRIFUGAL BLOWER

Velpula.Srinu<sup>1</sup>, N.Kishorekumar<sup>2</sup>, K.Veerawamy<sup>3</sup>

1, 2, 3.Asst.Proff. Mechanical Engineering Dept Malla Reddy College of Engineering

**Abstract:** Diffusive blowers are utilized widely for on-board maritime applications have high clamor levels. The commotion delivered by a pivoting segment is fundamentally because of irregular stacking power on the cutting edges and intermittent cycle of approaching are with the edges of the rotor. The contemporary cutting edges in maritime applications are comprised of aluminum or steel and create commotion that makes unsettling influence the general population working close to the blower.

The present work goes for analyzing the selection of composites as a choice to metal for better vibration control. Composites, known for their prevalent damping attributes are all the more encouraging in vibration decrease contrasted with metals. The demonstrating of the blower was finished by utilizing strong displaying programming, CATIA V5 R19. The blower is fit with a three dimensional hex8 work is done using HYPERMESH 10

**Keywords:** centrifugal blower Aluminium and steel

CATIA V5 R21 ANSYS hypermesh10

## 1. Introduction

Blowers are one of the components utilized consistently in submarines. They are introduced in ventilation and cooling frameworks in every submarine compartment. Ventilation frameworks ordinarily introduced by focal frameworks incorporate supply and fumes fans, serve for ventilation of settlement and other than convenience territories with air with concurrent ventilation of capacity batteries and for air cooling and cleaning from unsafe and smelling pollutions. Cooling frameworks are introduced by nearby, compartment gathering and single pipe frameworks. These frameworks are utilized to give agreeable conditions as far as

air temperature and stickiness for the team in settlement territories and other convenience regions, air cleaning in galleys, arrangement rooms, and sterile zones and furthermore for air blending in compartments.

All blowers planned for submarine establishment vary from mechanical ones not just for their high unwavering quality and quality under powerful effects yet additionally for low clamor

and vibration levels. As blower speaks to an expansive piece of submarine instruments, they should normally meet the accompanying necessary prerequisites for all systems:

1.Minimum weight-dimensional parameters. Dependable activity at submarine movements. Vibration and effect opposition.

2.Convenience of mountings, fixes and simple access to oil focuses. Keeping of administration life at transportation and changes in atmosphere.

### 1.1 CAUSES OF NOISE GENERATION IN CENTRIFUGAL BLOWER

Tonal clamor caused by rotational recurrence and fan sharp edge passing recurrence (BPF) and their sounds. These are generally the prevailing clamor source. Broadband streamlined clamor created via wind stream at the channel and outlet of the cooling fan. Mechanical clamor caused by erosion in heading and seals, vibration because of engine fan static and dynamic lopsided turning masses, resounding vibration of engine fan housings, engine fan mounting and misalignment, and so forth. Electromagnetically created clamor caused by changing of electromagnetic field in the electric engine.radiating machines, ill-advised establishment of couplings frequently causes mechanical clamor at twice siphon speed (misalignment). In the event that siphon speed is close or goes through the parallel basic speed, commotion can be created by high vibrations

coming about because of awkwardness or by rubbing of heading, seals, or impellers. In the case of rubbing happens, it might be portrayed by a sharp screeches. Wind age commotion might be created engine fans, shaft keys, and coupling jolts.

As a rule, throb sources are of four kinds

1. Discrete-recurrence parts created by the impeller.

2. Broad-band violent vitality coming about because of high stream speeds.

3. Impact commotion comprising of discontinuous blasts of expansive band clamor caused by cavitation, blazing, and water pound.

4. Flow-instigated throb caused by intermittent vortex arrangement when stream is past impediments and side branches in the funneling framework.

## 1.2 NOISE CONTROL TECHNIQUES

Ecological commotion generally does not exude straightforwardly from the vitality source rather, it transmitted along mechanical or fluid ways before it at last emanates from some vibrating surface into the encompassing condition. The ways to deal with treating siphon clamor by and large incorporate the accompanying: Modify the basic design or operating condition to minimize the generation of acoustic energy.

1. Prevent sources from creating airborne commotion by interfering with the way between the vitality source and the audience. This methodology may extend from separation mounts at the source to physically evacuating the audience.

## 1.3 ROLE OF COMPOSITE MATERIALS IN NOISE SIGNATURE CONTROL

Composite material is a framework that is made by the engineered gathering of at least two materials. The material comprises of fiber of high quality and modulus inserted in a pitch with unmistakable interfaces between them. They create a blend of properties that can't be accomplished with both of the constituents acting alone. Composite materials have high quality, modulus.

The most widely recognized frame in which strengthened composites are utilized in basic application is known as a cover and it is acquired by stacking various thin layers of strands and lattice and solidifying them into the ideal thickness. Fiber introduction in each layer and stacking grouping of different

layers can be controlled to get an extensive variety of physical and mechanical properties for the composite overlay. These materials are found to have high damping co-effective. The damping property of a material speaks to its ability to diminish transmission of vibration caused by mechanical unsettling influences to a structure. The proportion of damping of a material is its damping factor. Expanding the estimation of  $\eta$  is alluring for decreasing the reverberation adequacy of vibration in a structure. Damping factor esteem relies upon various elements, including fiber and gum types, fiber introduction edge, and stacking arrangement.

## 1.4 SCOPE OF THE PROJECT

The extent of the venture is as per the following:

- a) To break down the relocation and worries of composite blower and contrasted and Aluminum blower.
- b) Comparing common frequencies of both Aluminum and composite blower.
- c) To think about the vibration decrease because of composite blower rather than Aluminum blower.

## 1.5 APPROACH OF THIS PROJECT

Limited component strategy is the most flexible of every single numerical system accessible. Consequently the blowers have been broke down by the Finite Element Analysis system (FEA). With the end goal of limited component examination, the economically accessible limited component bundle, ANSYS 11.0 has been utilized. The investigation of diffusive blowers incorporates displaying and examination. The accompanying examination has been completed on the blower

1. Static examination
2. Modular examination

## 1.6 CAUSES OF NOISE GENERATION IN CENTRIFUGAL BLOWER

In outward machines, inappropriate establishment of couplings regularly causes mechanical commotion at twice siphon speed (misalignment). On the off chance that siphon speed is close or goes through the parallel basic speed, clamor can be produced by high vibrations coming about because of irregularity or by rubbing of orientation, seals, or impellers. In

the case of rubbing happens, it might be portrayed by a piercing screeches. Wind age commotion might be created engine fans, shaft keys, and coupling bolts. When weight vacillations are delivered specifically by fluid movement, the sources are liquid dynamic in character. Potential liquid powerful sources incorporate choppiness, stream partition (vorticity), cavitation, water-mallet, blazing, and impeller communication with the siphon outwater. The subsequent weight and stream throbs might be either intermittent or expansive band in recurrence and for the most part energize either the funneling or the siphon itself into mechanical vibration.

## 2. Literature Survey

Because of their various applications, examines on blowers and their issues have been pulling in the scientists. Huang Chen-Kang and Hsieh Mu-En [1] gave a short presentation about the blowers and diverse kinds of blowers. They focused on divergent blowers which are generally utilized for ventilation and cooling frameworks and clarified about the execution investigation and advanced plan of in reverse bended airfoil radial blower. Amid his investigation, the CFD bundle FLUENT is utilized to reenact four in reverse bended airfoil radiating blowers. At that point the reenactment results are contrasted and the deliberate outcomes for validation. J.B. Moreland [2] clarifies the lodging impact of divergent blower. The sound power range for a radial blower working at free conveyance is described by upgrade at different frequencies inferable from acoustical resonances in the blower lodging. The most reduced reverberation recurrence compares to the Helmholtz reverberation was depicted by methods for a lumped parameter relationship from which both the reverberation recurrence and the level of upgrade is processed and Higher request resonances recurrence and the level of improvement is likewise figured which are additionally unmistakable in blower clamor spectra. Renjing Cao and Jun HU [3] proposed a bunch configuration way to deal with accomplish a decent streamlined and acoustic execution of a ventilation framework and a propelled estimation framework

was embraced to test the streamlined and acoustic execution of the unit which depended on a pipe test fix with non-reflection acoustic limit and was intended to isolate the mechanical and wind stream produced commotion. This estimation gadget was situated at the ventilation room supply diffuser and the outcomes demonstrated that the group radiating blower gives a higher mass stream rate and a lower sound weight level than a regular mechanical ventilation framework.

[Prezelj Jurij](#) and [Carudina Mirko](#) [4]

clarified about the distinguishing proof of commotion sources on outward blower which was performed with an acoustic camera at the structure and off-plan task conditions and reasoned that the rotational clamor wins at the structure purpose of activity, and that the non-rotational commotion wins at off-structure activity. The principle wellspring of commotion inside a suction unit can be credited to the efficiently created clamor, at the plan and in addition at off-structure activity.

## 3. CENTRIFUGAL BLOWERS

### 3.1 TYPES OF BLOWERS

Blowers can accomplish a lot higher weights than fans, as high as 1.20 kg/cm<sup>2</sup>. They are likewise used to create negative weights for modern vacuum frameworks. The divergent blower and the positive dislodging blower are two fundamental sorts of blowers, which are portrayed beneath. ers look more like divergent siphons than fans. The impeller is commonly outfit driven and turns as quick as 15,000 rpm. In multi-arrange blowers, air is quickened as it goes through every impeller. In single-organize blower, air does not take numerous turns, and consequently it is increasingly proficient. Outward blowers conventionally neutralize weights of 0.35 to 0.70 kg/cm<sup>2</sup>, however can accomplish higher weights. One trademark is that wind current will in general drop definitely as framework weight builds, which can be a detriment in material passing on frameworks that rely upon a relentless air volume. Along these lines, they are frequently utilized in applications that are not inclined to stopping up.

### 3.2 POSITIVE-DISPLACEMENT BLOWERS

Positive relocation blowers have rotors, which "trap" air and push it through lodging. These blowers give a consistent volume of air regardless of whether the framework weight fluctuates. They are particularly reasonable for applications inclined to obstructing, since they can deliver enough weight (normally up to 1.25 kg/cm<sup>2</sup>) to blow stopped up materials free. They turn much slower than radiating blowers (e.g. 3,600 rpm) and are regularly belt headed to encourage speed changes. An outward blower with rearwardly bended impeller cutting edges situated in lodging between two lodging faces that are divided separated along the impeller pivot. One of the lodging faces characterizes a lodging channel. The lodging is considerably stopped except for the channel and an outlet.

### 3.3 PRINCIPLE OF CENTRIFUGAL BLOWER

Working guideline is a mix of two impacts: Centrifugal power which creates increasingly static weight and again diversion of the wind current by the cutting edges, yet here the redirection is from a radially outward bearing into a winding stream design. If there should be an occurrence of forward bended sharp edges the air redirections impact the stream design and on the execution.

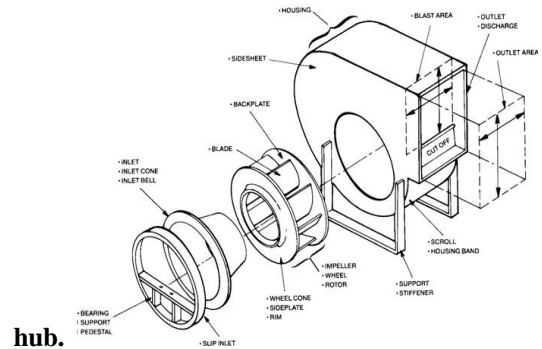


**Centrifugal blower**

### 3.4 FLOW PATTERN IN CENTRIFUGAL BLOWER

The wind stream enters the blower unit pivotally, equivalent to in a hub stream fan, yet then spreads out in a channel molded example, transforming 900 into different radially outward headings previously meeting the cutting edges. The cutting edges at that point redirect these individual air streams into a winding example to a relatively circumferential bearing. All these air streams are at last gathered by parchment lodging and

are brought together into a solitary air stream that leaves the unit at a correct point to the



**hub.**

**Parts of centrifugal blower**

### 3.5 DISADVANTAGES OF BLOWER

Most noise problems can be modeled as source path receiver systems. It is most desirable to reduce the strength or number of the sources. For example, replacing one or both of the metal contacts with softer material such as nylon or strong durable plastic might reduce the noise from the impact of two metal machine parts in punch press. However, it is sometimes difficult to reduce the noise at a source without extensive redesign. Sound waves have an effective range in water greater by several orders of magnitude than electromagnetic waves. These characteristics are primarily responsible for the present large scale use of underwater sound in commercial as well as military applications. Underwater sound is generated by many types of sources, both within and outside the medium, natural and artificial. Natural sounds are usually considered noise and are primary constituents of the important category of ambient noise.

### 3.6 OVERVIEW OF COMPOSITE MATERIALS

Fiber strengthened composite material comprises of strands of high quality and modulus installed in or clung to a lattice with particular interfaces between them. In this frame, the two strands and network hold their physical and compound characters, yet they deliver a blend of properties that can't be accomplished with both of the constituents acting alone. When all is said in done,

filaments are the central load conveying individuals; while the encompassing grid keeps them in wanted area and introduction, goes about as a heap exchange medium among them and shields them from ecological harms because of lifted temperatures and moistness. Hence, despite the fact that the strands give fortification to the network, the last additionally serves various valuable capacities in a fiber strengthened composite material. The most widely recognized frame in which fiber fortified composites are utilized in auxiliary applications is known as an overlay. Stacking various thin layers of strands and grid and merging them into wanted thickness. Fiber introduction in each layer has a swell as the stacking grouping of different layers can be controlled to create an extensive variety of physical and mechanical properties for the composite cover The present blower is a multi layered sinewy composite blower. Each layer or lamina is a solitary layer composite and in this manner introduction is differed by plan. Each layer is thin (thickness 0.3 mm) and can't be straightforwardly utilized. A few indistinguishable layers are reinforced together to frame a multi layer overlays of thickness equivalent to 3, 5, 6, 8 mm. Each layer may vary from the other in

### 3.7 CLASSIFICATION OF COMPOSITES

Composite materials are ordinarily grouped at following two unmistakable dimensions:

The primary dimension of grouping is typically made concerning the lattice constituent. The real composite classes incorporate Organic Matrix Composites (OMCs), Metal Matrix Composites (MMCs) and Ceramic Matrix Composites (CMCs). The term natural framework composite is commonly accepted to incorporate two classes of composites, to be specific Polymer Matrix Composites (PMCs) and carbon network composites regularly alluded to as carbon-carbon composites. The second dimension of grouping alludes to the support shape - fiber fortified composites, laminar composites and particulate composites. Fiber Reinforced composites (FRP) can be additionally isolated into those containing

intermittent or constant filaments. Fiber Reinforced Composites are made out of filaments inserted in network material. Such a composite is viewed as an irregular fiber or short fiber composite if its properties differ with fiber length. Then again, when the length of the fiber is with the end goal that any further increment long does not further expand, the versatile modulus of the composite, the composite is viewed as persistent fiber fortified. Filaments are little in measurement and when pushed pivotally, they twist effectively in spite of the fact that they have great elastic properties. These strands must be bolstered to shield singular filaments from twisting and clasping.

Laminar Composites are made out of layers of materials held together by grid. Sandwich structures fall under this class. Particulate Composites are made out of particles dispersed or implanted in a grid body. The particles might be chips or in powder shape. Cement and wood molecule sheets are instances of this classification.

### 3.8 ELASTIC PROPERTIES OF ALMINA UNIDIRECTIONAL CONTINUOUS FIBER 0° LAMINA

$$\text{Longitudinal modulus} = E_{11} = E_f V_f + E_m V_m$$

$$\text{Major Poisson's proportion} = \mu_{12} = \mu_f V_f + \mu_m V_m$$

Relative volumes of the constituent

$$\text{Transverse Modulus} = E_{22} =$$

$$\text{Minor Poisson's proportion} = \mu_{12} =$$

$$\text{Shear Modulus} = G_{12} =$$

## 4. INTRODUCTION OF CAD

PC Aided Design (CAD) is a strategy in which man and machine are mixed in to critical thinking group, personally coupling the best qualities of each. The consequence of this blend works superior to either man or machine would work alone , and by utilizing a multi discipline approach, it offers the upsides of incorporated cooperation.

The advances in Computer Science and Technology brought about the rise of amazing equipment and programming apparatus. It offers scope for use in the whole structure process bringing about enhancement in the nature of plan. The crisis of CAD as a field of specialization will assist the architect with acquiring the learning and aptitudes required in the utilization of these apparatuses in a productive and compelling path on the structure procedure. CATIA-V5 is the business' accepted standard 3D mechanical plan suit. It is the world's driving CAD/CAM/CAE programming, gives an expansive scope of incorporated answers for cover all parts of item structure and assembling. Quite a bit of its prosperity can be ascribed to its innovation which goads its client's to all the more rapidly and reliably improve another strong, parametric, highlight based model. Since that CATIA-V5 is unmatched in this field, in all procedures, in all nations, in all sort of organizations along the supply chains. Catia-v5 is likewise the ideal answer for the assembling venture, with cooperative applications, strong responsiveness and web availability that make it the perfect adaptable building answer for quicken developments. Catia-v5 gives simple to utilize arrangement custom fitted to the requirements of little medium estimated endeavors and also substantial mechanical organizations in all enterprises, customer products, creations and get together. Electrical and gadgets merchandise, car, aviation, shipbuilding and plant structure. It is easy to understand strong and surface displaying should be possible effectively.

#### **4.1.PRODUCTDEVELOPMENTTHROUGH CAD PROCESS:**

The item starts with a need that is distinguished dependent on costumer and market's requests . The item experiences two fundamental procedures from the thought conceptualization to the completed item the plan procedure and the assembling procedure. Item advancement through CAD item. Union and examination are the fundamental sub forms that establish the condescend procedure. Amalgamation is vital to plan an investigation. completed item the structure procedure and the assembling procedure. Item improvement through CAD item. Combination and investigation are the principle sub forms that

establish the condescend procedure. Amalgamation is essential to plan an investigation.

#### **4.2 CATIA**

There are distinctive modules in CATIA utilizing which diverse undertakings can be performed. The primary window and modules of CATIA appeared in figure:

catia-v5 Interface

The primary modules are:-

- Sketcher Design
- Part Design
- Assembly
- Drafting
- Wireframe and Surface Design
- Sheet Metal Design

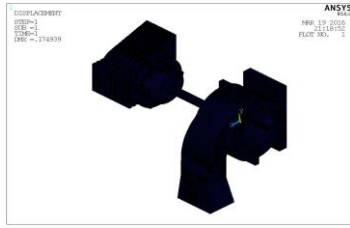
#### **4.3 PART MODELING**

The **Version 5 Part Design** application makes it possible to design precise 3D mechanical parts with an intuitive and flexible user interface, from sketching in an assembly context to iterative detailed design. **Version 5 Part Design** application will enable you to accommodate design requirements for parts of various complexities, from simple to advanced.

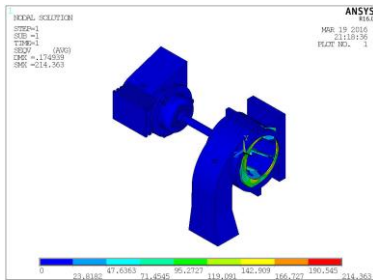
Select Start -> Mechanical Design -> Part Design from the menu bar

## 6. RESULT

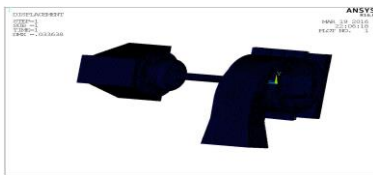
### 6.1 STATIC ANALYSIS OF ALUMINIUM ALLOY BLOWER



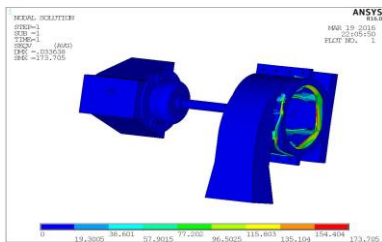
Deformation of Aluminium alloy blower



Vanishes stress of blower



Deformation of stainless steel alloy blower



Vanishes stress of stainless steel alloy blower

	Aluminum Blower	Stainless steel alloy
Deformation in mm	0.1749 mm	0.3363mm
Vonmisse tress N/mm <sup>2</sup>	214.363N/mm <sup>2</sup>	173.705 /mm <sup>2</sup>

### CONCLUSIONS

The stresses of **stainless steel alloy** obtained in static analysis 173.705 N/mm<sup>2</sup> are within the allowable stress limits (600 N/mm<sup>2</sup>).

### FUTURE SCOPE OF WORK

In present work the harmonic analysis is carried out for both aluminum and c stainless steel blower and response is compared. The aerofoil blade profile may be used for impeller blade and further solution is required.

### References:

1. Huang Chen-Kang and Hsieh Mu-En, "Execution investigation and advanced structure of Backward bended airfoil divergent blowers", American culture of Heating, Refrigerating and Air Conditioning Engineers, May 1, 2009
2. Prezelj Jurij and Carudina Mirko, "Recognizable proof of commotion sources in divergent blower with acoustic camera", The Journal of Acoustical Society of America, Volume 123, Number 5, p. 3824, May 2008.
3. J.B. Moreland, "Lodging impact on diffusive blower commotion", Journal of Sound and Vibration, Volume 36, Number 2, pp. 191-205, 22 September 1974.
4. G. H. Koopmann and W. Neise, "The utilization of Resonators to quietness outward blower", Journal of Sound and Vibration, Volume 82, Number 1, pp. 17-27, 8 May 1982.

# DESIGN OF ABSORPTION REFRIGERATION SYSTEM DRIVEN BY ENGINE EXHAUST GAS FOR VEHICLES

## -A REVIEW PAPER

P.Pavan Kumar  
Mechanical Engineering dept  
Malla reddy college of Engg  
Hyderabad, India  
email: [pavansmachine@gmail.com](mailto:pavansmachine@gmail.com)

Dr. Ananth ,professor  
Mechanical Engineering dept  
Malla reddy college of Engg  
Hyderabad,India  
email: [subramaniananth@gmail.com](mailto:subramaniananth@gmail.com).

**Abstract**— As we tend to all recognize that absorption refrigeration has no moving elements, Air conditioning is that the method of sterilisation the properties of air (primarily temperature and humidity) to additional favorable conditions. additional usually, air con will talk to any style of technological cooling, heating, ventilation, or medical care that modifies the condition of air. it's a widely known indisputable fact that an outsized quantity of warmth energy related to the exhaust gases from Associate in Nursing engine is wasted.

In this thesis, energy from the exhaust gas of an internal combustion engine is used to power an absorption refrigeration system to air-condition an ordinary passenger car. All the required parts for the absorption refrigeration system is designed and modeled in 3D modeling software CREO parametric software. Thermal analysis is done on the main parts of the refrigeration system to determine the thermal behavior of the system.

**Keywords**—refrigeration, vapour, absorption, refrigerant, CAD, CREO

### I. INTRODUCTION

Refrigeration is the process of casting off warmth from an enclosed or controlled space, or from a substance, and transferring it to an area in which it's miles unobjectionable. The number one cause of refrigeration is lowering the temperature of the enclosed area or substance after which keeping that decrease temperature as evaluate to surroundings. Cold is the absence of heat, therefore on the way to lower a temperature, one "removes warmth", rather than "including cold." The basic objective of growing a vapour absorption refrigerant system for vehicles is to cool the distance inside the automobile through making use of waste heat and exhaust gases from engine. The air con gadget of motors in these days's world makes use of "Vapour Compression Refrigerant System" (VCRS) which absorbs and gets rid of heat

from the interior of the car that's the space to be cooled and in addition rejects the heat to be somewhere else. Now to increase a performance of vehicle past a sure restriction vapour compression refrigerant device resists it because it can't employ the exhaust gases from the engine. The heat required for running the Vapour Absorption Refrigeration System can be obtained from that which is wasted into the atmosphere from an IC engine. G. Vicatos[4] observed that in the exhaust gases of motor vehicles, there is enough heat energy that can be utilized to power an air conditioning system. Once a secondary fluid such as water or glycol is used, the aqua ammonia combination appears to be a good candidate as a working fluid for an absorption car air conditioning system. In the paper, the waste heat from gas engine turbine can be used as the heat source for the absorption refrigeration system. The experimental analysis showed that performance of the integrated refrigerating system was greatly improved by using the waste heat of gas engine. Colbourne [5] summarized a study analyzing over 50 published technical documents comparing the performance of fluorinated refrigerants and HCs. A significantly higher number of tests showed an increase in performance when using HCs as compared to using fluorinated refrigerants (Colbourne and Suen,)[6]. Similarly, Colbourne and Ritter[7] investigated the compatibility of non-metallic materials with HC refrigerant and lubricant mixtures. They performed experiments in compliance with European standards for the testing of elastomeric materials and ASHRAE material compatibility test standards. Setaro et al. [8] tested and compared the heat transfer and pressure drop through a brazed plate heat exchanger and a tube-and-fin coil for two different refrigerants, R22 and R290 in an air-to-water heat pump system. Qin et al. [9] developed an exhaust gas driven automotive air conditioning working on a new hydride pair. The results showed that cooling power and system coefficient of performance increase while the minimum refrigeration temperature decreases with growth of the heat source temperature. System heat transfer properties still needed to be

improved for better performance. Koehler et al. [10] designed, built and tested a prototype of an absorption refrigeration system for truck refrigeration using heat from the exhaust gas. The refrigeration cycle was simulated by a computer model and validated by test data.

## II.COMPONENTS OF AIR COOLED ABSORPTION SYSTEM INTRODUCTION TO CAD AND CREO

The components are condenser, evaporator in tis paper we are designing the condenser and evaporator for that we used cad and creo.

S.N	Engine Type	Power Output (kW)	Waste Heat
1.	Small air cooled diesel engine	35	30-40 % of energy waste loss from IC engines
2.	Water air cooled engine	35-150	
3.	Earth moving machineries	520-720	
4.	Marine applications	150-220	
5.	Trucks and road engines	220	

### A. INTRODUCTION TO CAD

Computer-aided layout (CAD) is using laptop structures (or workstations) to useful resource within the creation, change, evaluation, or optimization of a layout. CAD software is used to increase the productivity of the fashion designer, enhance the best of design, improve communications through documentation, and to create a database for manufacturing. CAD output is often within the form of digital files for print, machining, or other production operations. The time period CADD (for Computer Aided Design and Drafting) is also used.

Its use in designing digital systems is referred to as electronic design automation, or EDA. In mechanical layout it's far referred to as mechanical design automation (MDA) or computer-aided drafting (CAD), which incorporates the technique of creating a technical drawing with using pc software program.

CAD software for mechanical layout uses either vector-based totally photos to depict the objects of conventional drafting, or might also produce raster portraits showing the overall appearance of designed items. However, it includes greater than simply shapes. As inside the manual drafting of technical and engineering drawings, the output of CAD need to bring statistics, along with substances, approaches, dimensions, and tolerances, consistent with application-unique conventions.

CAD may be used to design curves and figures in two-dimensional (2D) area; or curves, surfaces, and solids in 3-dimensional (3D) space.

### B. INTRODUCTION TO CREO

PTC CREO, previously known as Pro/ENGINEER, is 3-d modeling software utilized in mechanical engineering, design, production, and in CAD drafting carrier firms. It changed into one of the first 3D CAD modeling applications that used a rule-primarily based parametric gadget. Using parameters, dimensions and features to capture the behavior of the product, it could optimize the improvement product as well as the layout itself.

The name become changed in 2010 from Pro/ENGINEER Wildfire to CREO. It become introduced by using the company who evolved it, Parametric Technology Company (PTC), all through the launch of its suite of design products that consists of programs inclusive of assembly modeling, 2D orthographic perspectives for technical drawing, finite detail analysis and more.

PTC CREO says it can provide a more efficient layout experience than different modeling software program due to its unique functions such as the mixing of parametric and direct modeling in one platform. The entire suite of applications spans the spectrum of product development, giving designers alternatives to apply in every step of the manner. The software also has a greater user friendly interface that provides a better revel in for designers. It also has collaborative capacities that make it clean to proportion designs and make changes.

There are limitless advantages to using PTC CREO. We'll check them in this -component series.

First up, the largest advantage is improved productiveness due to its green and flexible design competencies. It changed into designed to be less difficult to use and have functions that allow for design procedures to transport more quickly, making a designer's productivity degree increase.

A particular feature is that the software program is available in 10 languages. PTC is aware of they have people from all around the world the usage of their software program, so they offer it in multiple languages so almost all people who wants to use it is able to achieve this.

### C. ADVANTAGES OF CREO PARAMETRIC SOFTWARE

1. Optimized for model-based totally organizations
2. Increased engineer productivity
3. Better enabled concept layout
- four. Increased engineering competencies
- five. Increased manufacturing talents
6. Better simulation
7. Design abilities for additive manufacturing

### D. CREO parametric modules:

- Sketcher
- Part modeling
- Assembly
- Drafting

### E. FINAL DIMENSIONS

Dimensions of the designed pre-heater

Outside Diameter of the tube,  $D_0 = 0.012$  m

Inside Diameter of the tube,  $D_j = 0.01$  m

Length of the tube,  $L = 2$  m

By using comparable calculations additionally findout the

Dimensions of the following Generator

It is the place wherein the exhaust gas tube is surpassed via the field and the tube emperature is assumed to be a regular.

Dimensions of the designed generator

Outside Diameter of the exhaust gas tube,

$D_0 = 0.04$  m

Taking interior diameter of the exhaust gasoline tube,  $D_i =$

0.038 m

Length of the tube required for the desired warmth

switch,  $L = 1$  m

Condenser:

Assume circular cross segment of the condenser coil of

thickness,  $a = 5$  mm & Diameter  $d = 18$  mm.

Dimensions of the designed condenser

Diameter of the tube,  $d = 0.018$  m Thickness of the

tube,  $a = 0.1/2$  m Length of the tube,  $L = 7.45$  m

Evaporator

The evaporator is of circular go segment and should

be manufactured from copper tubes to have maximum heat

switch from the environment to the refrigerant. The

tube is coiled to accommodate it inside the car.

Dimensions of the designed evaporator

Outside Diameter of the tube,  $D_0 = 0.01$  m Inside

Diameter of the tube,

$D_j = 0.008$  m Length of the tube,  $L = 6.26$  m

Absorber

Dimensions of the designed absorber

Outside diameter of the absorber,  $D_0 = 76$  mm Total

length of the absorber,

$L = 205$  mm Outer diameter of the fins,

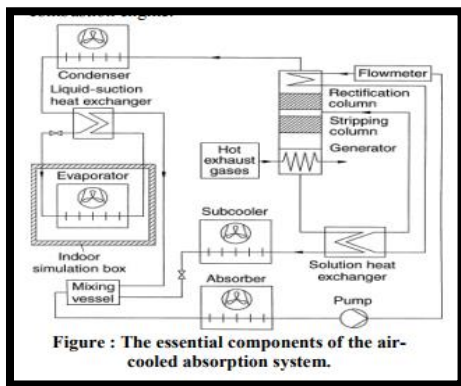
$D_f = 109$  mm, No. Of fins,  $n = 7$

### III. WORKING PRINCIPLE

Absorption cycles produce cooling and/or heating with thermal input and minimal electric input, by using heat and mass exchangers, pumps and valves. The absorption cycle is based on the principle that absorbing ammonia in water causes the vapor pressure to decrease. The basic operation of an ammonia-water absorption cycle is as follows. Heat is applied to the generator, which contains a solution of ammonia water, rich in ammonia. The heat causes high pressure ammonia vapor to absorb the solution. Heat can either be from combustion of a fuel such as clean-burning

natural gas, or waste heat from engine exhaust, other industrial processes, solar heat, or any other heat source. The high pressure ammonia vapor flows to a condenser, typically cooled by outdoor air. The ammonia vapor condenses into a high pressure liquid, releasing heat which can be used for product heat, such as space heating. The high pressure ammonia liquid goes through a restriction, to the low pressure side of the cycle. This liquid, at low pressures, boils or evaporates in the evaporator. This provides the cooling or refrigeration product. The low pressure vapor flows to the absorber, which contains a water-rich solution obtained from the generator. This solution absorbs the ammonia while releasing the heat of absorption. This heat can be used as product heat or for internal heat recovery in other parts of the cycle, thus unloading the burner and increasing cycle efficiency. The solution in the absorber, now once again rich in ammonia, is pumped to the generator, where it is ready to repeat the cycle [13].

**Vapour absorption refrigeration device**



1.	Engine Make	Kirloskar
2.	Engine Type	Single Cylinder
3.	Power	3.7 kW
4.	Speed	1500 rpm
5.	Bore Diameter	80 mm

6.	Stroke Length	110 mm
7.	Room Temperature	29 °C
8.	Exhaust Gas Temperature Range	125°C to 260°C

**Table : IC Engine specifications.**

**IV. LITERATURE REVIEW**

**Li-Ting Chen, 1988,** Modified ejector-absorber absorption refrigeration cycle is presented and analyzed. From the results it is observed that a considerable improvement in COP is obtained with the present cycle when compared with that of the conventional cycle[1] .

**George Vicatos, 1995,** The author studied the absorption refrigeration system and Heat and Mass correlation and simulate the system and then designed the system. This study has developed a methodology which could be adopted in designing an absorption refrigeration plant, given a refrigeration requirement[2] .

**Shiyi Wang, 1996,** In this thesis S Wang designed the system, simulated it at different loads, manufactured it, carried out bench test and road test. In the exhaust gases of motor vehicles, there is enough heat energy which can be utilized to power an air-conditioning system “free” from any energy requirements [3].

**P. Sriksirin et al., 2001,** This paper provided a literature review on absorption refrigeration technology. A doubleeffect absorption systems using lithium bromide/water seem to be the only high performance system which is available commercially [4].

**J Gryzagoridis et al.,2008,** The theoretical design is verified by a unit that is tested under both laboratory and road-test conditions. The evaluation of the COP, with and without the heat exchanger also proves that unless there is a high purity refrigerant, the effect of the heat exchanger to the generator’s heat is small [5].

**Andre Aleixo Manzela et al., 2010,** This work presented an experimental study of an ammonia-water absorption refrigeration system using the exhaust of an internal combustion engine as energy source. Overall, carbon monoxide emission was decreased when the absorption refrigerator was installed in the exhaust gas, while hydrocarbon emissions increased [6].

**Khaled S. AlQdah, 2011,** This work presented an experimental study of an aqua-ammonia absorption system used for automobile air conditioning system. It is evident that COP strongly

depends on working conditions such as generator, absorber, condenser and evaporating the of temperature [7].

**Isaac Mathew Pavoodath**, 2012, In this paper study of absorption refrigeration is done. Such a system would vastly help take of the compressor load of the vehicle engine and would prove a great percentile of power saving for small capacity engines [8].

**Christy V Vazhappilly et al.**, 2013, A breadboard prototype of an absorption system for refrigeration using heat from the exhaust-gases is to be designed, built and tested. The heating coil generator system of absorption refrigeration system has been replaced by plate frame type heat exchanger, there by utilizing the exhaust gases of the IC engine [9].

**Janardhanan.k et al.**, 2014, This work presented a theoretical study of an aqua-ammonia absorption system used for automobile air conditioning system. Using a vapor absorption refrigeration system within an automobile as an air conditioner will not only reduce the fuel consumption of the vehicle while working but will also reduce the environmental pollution [10].

**S. Manoj prabhakar et al.**, 2014, This work presented an experimental study refrigeration system, using vapor absorption system. The coefficient of performance of the system is low, that means that the system is expected to use a lot of energy with respect to the cooling it offers [11].

**J.P. Yadav et al.**, 2014, In this paper study of an experimental set up is designed and fabricated. Using heat exchangers, analyzer, and pre-heater the COP of the system further improves. Even by using two evaporators the effectiveness of the system can be increased [12].

**Paul Cedric Agra et al.**, 2014, This paper simulated the performance of the system using waste heat, a Bunsen burner was used which was attached to a propane tank via a rubber hose with a regulator. The small scale model with maximum COP 0.3685 at evaporator temperature 28 degree Celsius was achieved. In order to improve the performance of the system it is suggested to use high concentration of aqua ammonia solution [13].

**S. Thanga mohan raja et al.**, 2015, In this paper study of absorption refrigeration is done. The waste heat energy available in exhaust gas is directly proportional to the engine speed and exhaust gas flow rate [14].

**Tambe. Y.D et al.**, 2015, In this paper the more focus was given to the design and manufacturing of the system with 80 cc internal combustion petrol engine. The experiments conducted on the system, prove that the concept is feasible and could be used for refrigeration in traction and non traction application of engine [15].

**K L Rixon et al.**, 2015, In this paper study, design and fabrication of absorption refrigeration is done and result are obtained accordingly. Using a vapor absorption refrigeration system within an automobile as an air conditioner will not only reduce the fuel consumption of the vehicle but will also provide many other advantages like the efficiency of the engine is not decreased considerably [16].

**N. Chandana reddy et al.**, 2015, In this paper, an overview of utilization of waste heat with a brief literature of the current related research is studied. A maximum power consumption of 42.38 percent is saved using proposed system compared to existing system [17].

**Atishey Mittal et al.**, 2015, In this paper study of comparison of absorption refrigeration and compression refrigeration system is done. Waste heat recovery system is the best way to recover waste heat and saving the fuel [18].

**Dinesh Chandrakar et al.**, 2016, In this paper designing of absorption refrigeration is done and results are obtained. As power output increase, the heat recovered from exhaust gas also increase difficulty may occur when the vehicles at rest or in very slow moving traffic conditions [20].

#### V.GAPS IDENTIFIED

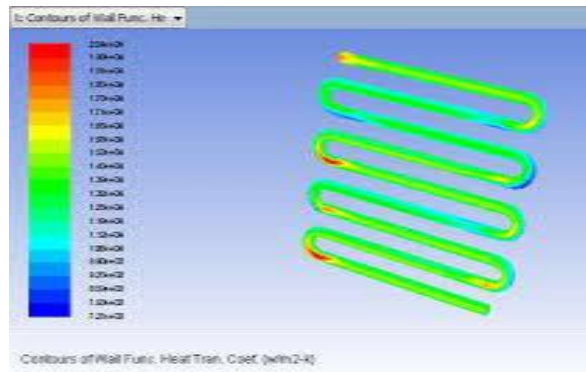
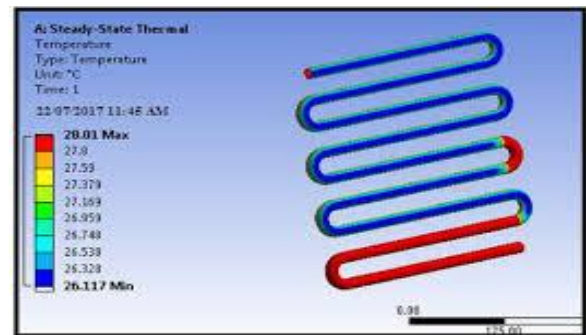
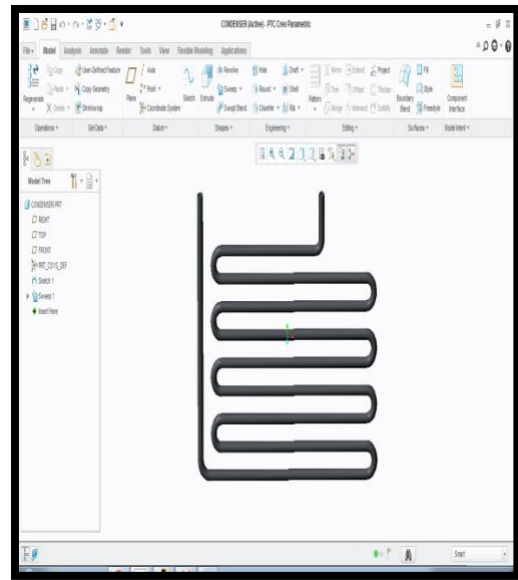
There are some gaps identified

1. The exhausted waste heat from the running coach engine is well-established by simulation calculation. The calculative results have fine coincidence with the tested data.

2. On the basis of the quantitative analysis of the exhausted gas parameters, the main devices are determined in the absorption compression hybrid cycle driven respectively by the waste heat of exhaust gases and power from the coach engine. One dimensional steady distribution parameter model in the generator and lumped parameters model in the other heat exchangers are established, for coupling heat transfer in the unit.

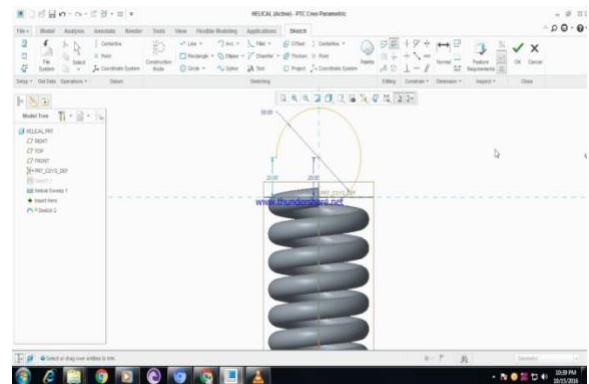
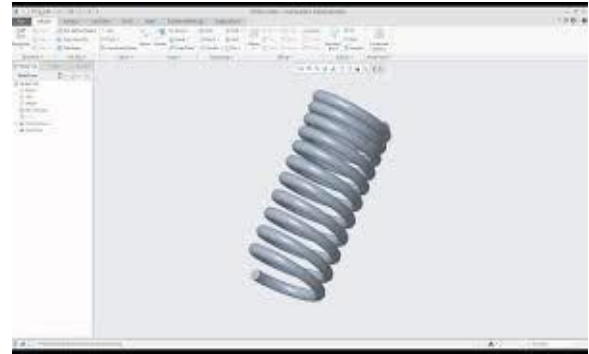
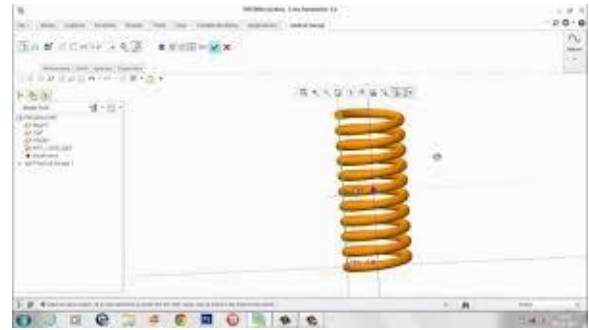
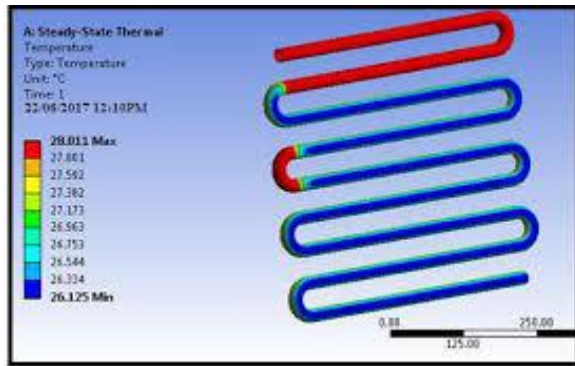
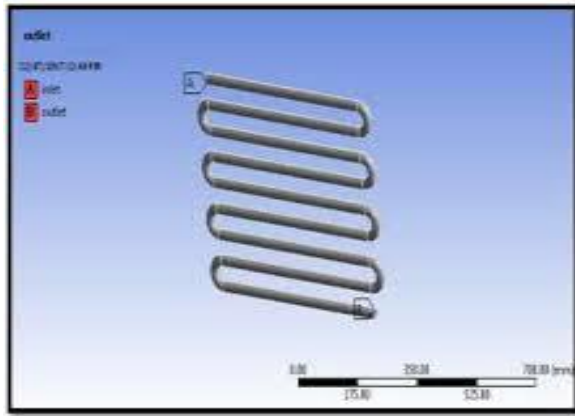
3. The ARSC can completely meet the demand of coach space cooling, when the running speed ( $u$ ) is greater than 100 km/h; the ARSC together with the CRSC supplies the cooling capacity for the coach, when  $u$  is between 40 and 100 km/h; When  $u$  is lower than 40 km/h, the ARSC has no cooling effect, and the cooling demand for the coach is fully supplied by the CRSC. The characteristics of the ARSC are analyzed under different ambient temperatures. The performance of the ARSC drops with the rise in ambient temperature.

4. The ACHRC have advantages of meeting coach cooling demands by recovering the waste heat from engine and consuming less fuel oil. The compact and light weight structures are considered to apply into the key devices in the ACHRC

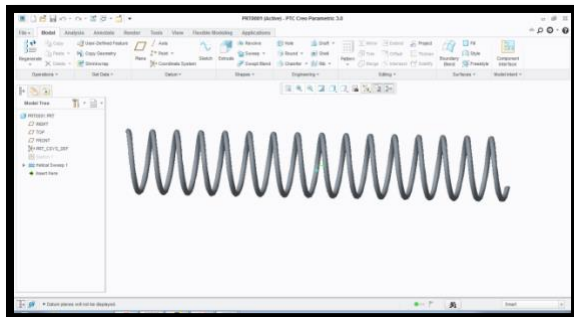


## VI. MODELING OF CONDENSOR AND EVAPORATOR IN CAD AND CREO

### Condenser model



Evaporator version



Advantages

Uses Engine warmth as supply of energy for this reason enhances the efficiency of engine. Moving parts are handiest within the pump, that's a small detail in the machine therefore operation becomes smooth and also carrying and tearing is decreased. The system works at low evaporator pressures with out affecting the COP of the machine. Environmental friendly, no launch of CFC derivatives. Helps in shielding OZONE layer from depletion. Helps engine to cool, as it extracts warmth from engine. Low jogging value. Higher engine electricity performance.

## VII.CONCLUSION

1. In the exhaust gases of motor vehicles, there is enough heat energy that can be utilised to power an air-conditioning system. Therefore, if air-conditioning is achieved without using the engine's mechanical output, there will be a net reduction in fuel consumption and emissions.
2. Once a secondary fluid such as water or glycol is used, the aqua-ammonia combination appears to be a good candidate as a working fluid for an absorption car air-conditioning system. This minimises any potential hazard to the passengers.
3. The low COP value is an indication that improvements to the cycle are necessary. A high purity refrigerant would give a higher refrigeration effect, while the incorporation of a solution heat exchanger would reduce the input heat to the generator. The present system has both a reflux condenser and a heat exchanger. However, the reflux condenser is proved inadequate to provide high purity of the refrigerant and needs to be re-addressed. The evaluation of the COP, with and without the heat exchanger also proves that unless there is a high purity refrigerant, the effect of the heat exchanger to the generator's heat is small.

## VIII.REFERENCES

- [1]. Andy Pearson (2008) refrigeration with ammonia and hydrocarbons, *Int journal of refrigeration*, 545-551.
- [2]. I. Horuz (1999) vapor absorption in road transport vehicles, *Journal of energy engineering*, Vol. 125, No. 2, 48-58
- [3]. Jabnithflame (2011) Development of an A/C system using waste heat of an I.C engine
- [4]. G Victos, J Gryzagoridis & S Wang, "A car air conditioning system based on an absorption refrigeration cycle using energy from exhaust gas of an internal combustion engine", *journal of energy in southern Africa*, Vol 19, issue 4, November 2008, pp.6-11.
- [5] Colbourne, D., 2000. An overview of hydrocarbons as replacement refrigerants in commercial refrigeration and air conditioning. Refrigeration Northern Ireland Centre for Energy Research and Technology.
- [6] Colbourne, D., Suen, K.O., 2000. Assessment of performance of hydrocarbon refrigerants. In: *Proceedings of the Fourth IIRGustav Lorentzen Conference on Natural Working Fluids*, Purdue, USA.
- [7] Colbourne, D., Ritter, T.J., 2000. Compatibility of Non-Metallic Materials with Hydrocarbon Refrigerant and Lubricant Mixtures. IIF-IIR- Commission B1, B2,E1 and E2 – Purdue University, USA
- [8] Setaro, T., Boccardi, G., Corberan, J.M., Urchueguia, J., Gonzalez, J., 2000. Comparative study of evaporation and condensation of propane and R22 in a brazed plate heat exchanger and a tube and fins coil. In: *Proceedings of the Fourth IIR Gustav Lorentzen Conference of Natural Working Fluids*, Purdue, USA, pp. 233–238
- [9] Qin F, Chen J, Lu M, Chen Z, Zhou Y, Yang K. Development of a metal hydride refrigeration system as an exhaust gas-driven automobile air conditioner. *Renewable Energy* 2007;32:2034–52.
- [10] Koehler J, Tegethoff WJ, Westphalen D, Sonnekalb M. Absorption refrigeration system for mobile applications utilizing exhaust gases. *Heat Mass Transfer* 1997;32:333–40.
- [11]. William H Severens and Jullian R. Fellows, *Air Conditioning & Refrigeration* (Willey International-1958)
- [12]. Richard G. Jordan and Gayle B. Priester *Refrigeration & Air Conditioning* (Prentice Hall Of India Pvt Ltd.,New Delh-1965).
- [13] A. Mittal, D. Shukla, and K. Chauhan, "A refrigeration system for an automobile based on vapor absorption refrigeration cycle using waste heat energy from the engine", *International Journal of Engineering Science and Research Technology*, vol. 4, no. 4, 2015.
- [14] G. Vicatos, "Heat and mass transfer characteristics: Design and optimization of absorption refrigeration machines", PhD thesis, University of Cape Town, South Africa, 1995.
- [15] S. Wang, *Motor vehicle air-conditioning utilizing the exhaust gas energy to power an absorption refrigeration cycles*, University of Cape Town, South Africa, 1996.

# HEAT TRANSFER ENHANCEMENT

Md Nizam Raza  
Mechanical Engineering  
Malla reddy college of engg  
Hyderabad,India  
Email:nizamraza93@gmail.com

Vikas Kumar  
Mechanical Engineering  
Malla reddy college of engg  
Hyderabad,India

**Abstract**—Heat Transfer enhancement used to enhance the heat transfer rate. It is categorized into passive and active methods. Active methods require external power while passive methods do not require any external power to improve the thermohydraulic performance of the system. Passive methods are widely used in both experimental and numerical applications. Passive methods include various components which are located in the fluid flow path such as twisted tapes, coiled wires.

**Keywords**—heat transfer enhancement, coiled wire, thermohydraulic, heat transfer, twisted tape.

## I. INTRODUCTION

Heat transfer enhancement is a process of increasing heat transfer rate and thermohydraulic performance of the system using various methods. Heat transfer enhancement technique are commonly used in areas such as process industries, heating and cooling in evaporators, refrigerators, radiators, automobiles etc.

Heat transfer enhancement methods are classified into three categories which include active method, passive method, and compound method. Active method require external power to input the process while passive method don't require any external power. Two or more active and passive method can be compound together that is called compound method which is used to produce a higher enhancement.

### Active Techniques

Active technique is used to enhance the heat transfer transfer rate by using an external power source to adjust the flow field so as to obtain an improvement in thermal efficiency. Providing an external power in most application is not easy for this reason use of active techniques is limited.

### Passive techniques

Passive techniques does not require any external power; rather geometry or surface of the flow channel is modified to increase the thermohydraulic performance of the systems.

The inserts, ribs, and rough surface are utilized to promote fluid mixing and turbulence flow, which results in an increment of the overall heat transfer rate.

### Compound technique

A compound technique consist of the combination of more than one heat transfer enhancement method to increase the thermohydraulic performance of heat exchangers. It can be employed simultaneously to generate an augmentation that promotes the performance of the system either of the techniques operating independently.

### Passive technique

#### Rough surface

They may be either integral to the base surface or made by placing a roughness adjacent to the surface.

Integral roughness is formed by machining or restructuring the surface. For single phase flow the configuration is generally chosen to promote mixing in the boundary layer near the surface, rather than to increase the heat transfer surface area.

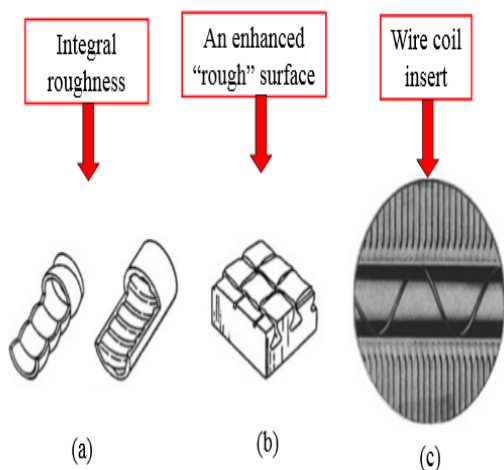


Fig. 1.2 (a) Tube-side roughness for single-phase or two-phase flow, (b) "rough" surface for nucleate boiling, (c) wire-coil insert.

### Extended Surfaces

They are routinely employed in many heat exchangers.

Thermal resistance may be reduced by increasing the heat transfer coefficient or the surface area of both heat transfer coefficient and surface area. Use of plain fin may provide only area increase. However, formation of a special shape extended surface may also provide increased  $h$ .

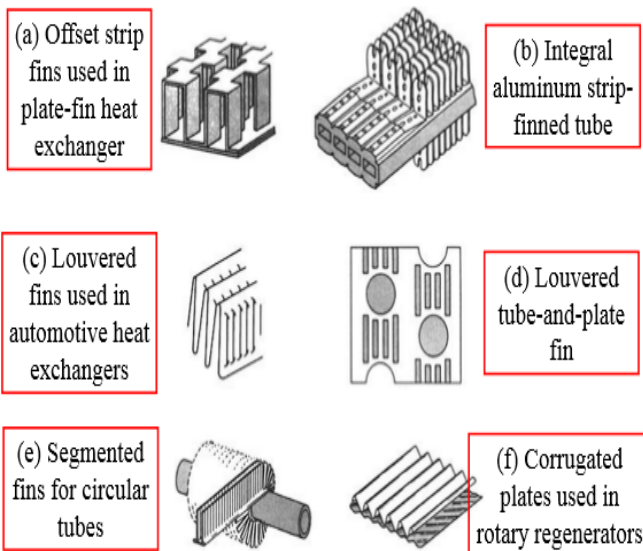
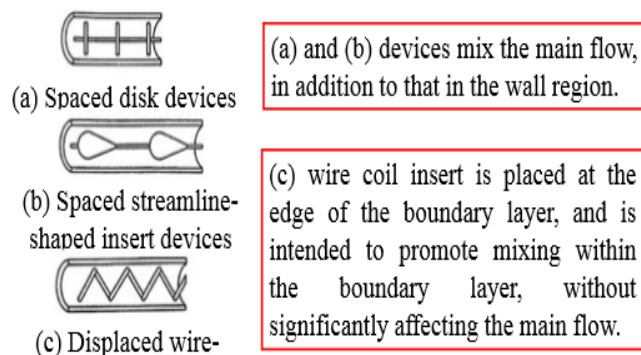


Fig. 1.3 Enhanced surfaces for gases

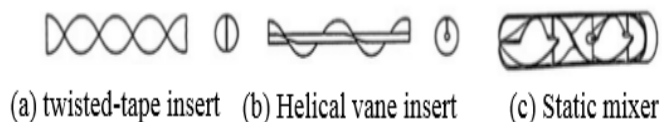
### Displaced inserts

Displaced insert devices are devices inserted into the flow channel to improve energy transport at the heated surface indirectly.



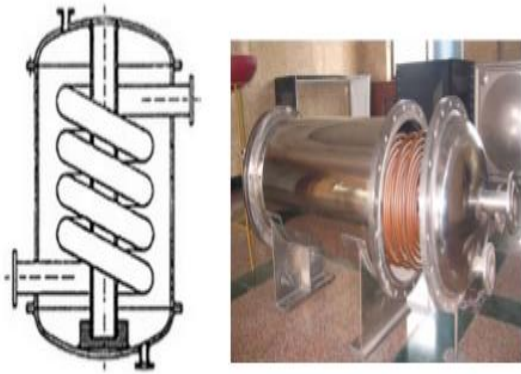
### Swirl flow device

Swirl flow device include number of geometrical arrangements or tube inserts for forced flow that create rotating or secondary flow.



### Coiled tubes

They may provide more compact heat exchangers secondary flow in the coiled tube produces higher single phase coefficients and improvement in most boiling regimes.



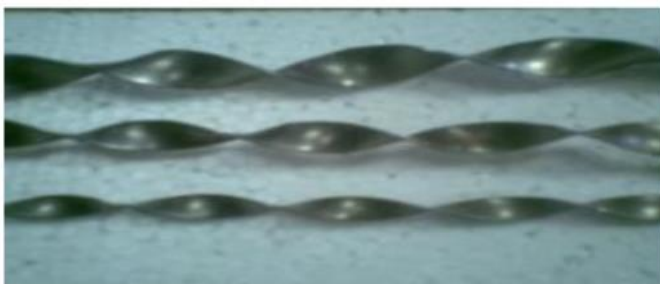
this a many researchers have been done by experimentally and numerically to investigate the desired design to achieve the better thermal performance with less frictional losses. The heat transfer enhancement of twisted tapes inserts depends on the Pitch and Twist ratio.

### Experimental Section

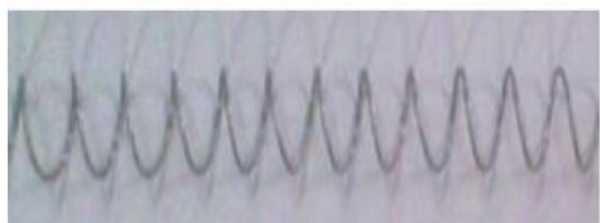
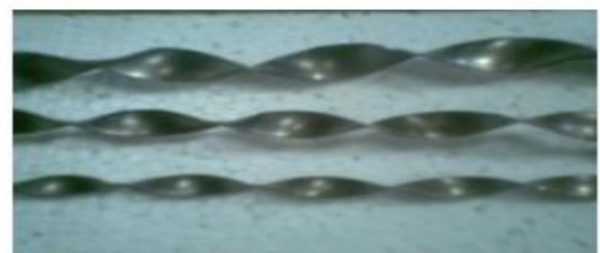
#### Twisted tapes

Twisted tapes are the metallic strips twisted using some of the suitable techniques as per the required shape and dimension, which are inserted in the flow to enhance the heat transfer. The twisted tape inserts are most suitable and widely used in heat exchangers to enhance the heat transfer.

The twisted tapes are made of mild steel and have tape width ( $w$ ) of 10 mm, 15 mm & 20mm. Tape thickness ( $d$ ) of 0.8 mm, and tape length ( $l$ ) of 900 mm. Also a wire coil having pitch of 30 mm is used to generate co-swirl. All tapes were prepared with different twist ratios,  $y/w = 3.5, 2.66$  and  $2.25$  respectively where twist ratio is defined as twist length ( $l$ ) to tape width ( $w$ ). Schematic view of twisted tape & wire coil is shown in Fig. On the other hand, to avoid an additional friction in the system that might be caused the thicker tape. To produce the twisted tape, one end of a straight tape was clamped while another end was carefully twisted to ensure a desired twist length. As shown in Fig these twisted tapes are fixed one by one inside the pipe having wire coil to generate co-swirl



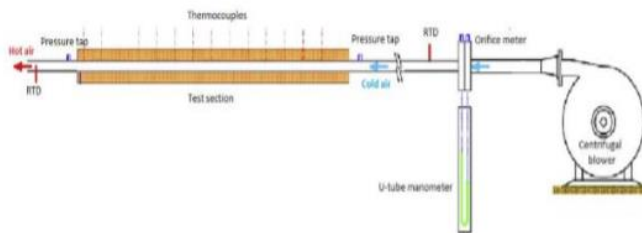
Twisted tape inserts increase heat transfer rates with less friction factor. The use of twisted tapes in a tube gives simple passive technique for enhancing the convective heat transfer by making swirl into the heavy flow which disrupting the boundary layer at the tube surface due to rapidly changes in the surface geometry. Which means to say that such type of tapes induce turbulence and swirl flow which induces inside the boundary layer and which gives better results of heat transfer coefficient and Nusselt number due to the changes in geometry of twisted tape inserts. Simultaneously, the pressure drop inside the tube will be increases when using twisted-tape as an insert. For



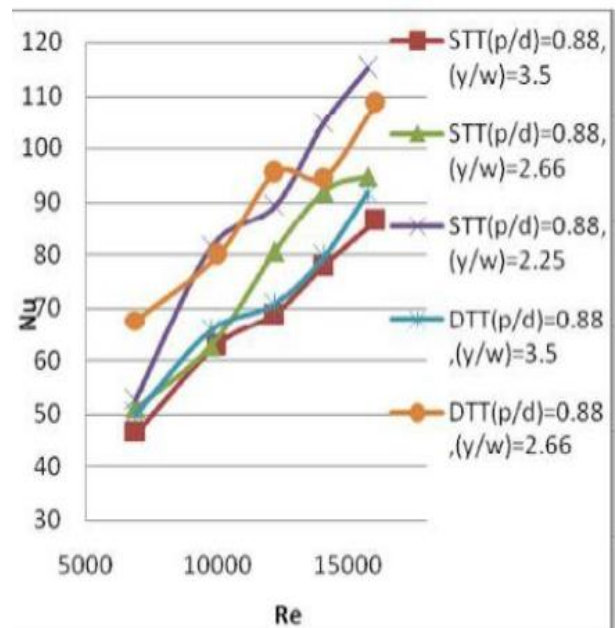
The test section is surrounded by nichrome heating wire, which is wrapped around the test section with a

pitch distance of 5 mm. This pitch is good enough to provide a nearly uniform heating on the outer surface of the test section tube. The heating wire was powered by a variable AC power supply. The overall electrical power added to the heating section,  $Q$ , was calculated by measuring the voltage (0–200 V) and the electrical current (0–2 A). To control the convection losses from the test section and other components, foam insulation and glass wool used. Four thermocouples are to be embedded on the test section to measure surface temperature of pipe and two thermocouples are placed in air stream at entrance and exist of test section to measure air temperature. To avoid floating voltage effects, the thermocouple bead is insulated from the electrically heated tube wall surface with a very thin sheet of mica between the thermocouple and the tube surface so as not to be effected from electricity.

Fig shows the schematic view of experimental set-up.



Experimental results show that the Nusselt number (therefore, the heat transfer coefficient) increases with increasing Reynolds number for the conventional turbulent tube flow. This is the most likely caused by a stronger turbulence and better contact between fluid and heating.



The variations of Nusselt number with Reynolds number for three different twist ratios ( $y/w = 3.5, 2.66, 2.25$ ) with wire coil of pitch ratio ( $p/d = 0.88$ ) shown in figure 6.1. Nusselt number increases with the decrease of twist ratio and the increase of Reynolds number. The highest Nusselt number is achieved for twist ratio ( $y/w = 2.25$ ) and pitch ratio ( $p/d = 0.88$ ).

### Conclusions:

We know the heat transfer enhancement can be done by using treated surfaces, using inserts, using extended surfaces which are the most important passive methods to enhance the heat transfer

The twisted tape inserts are most suitable and widely used in heat exchanger to enhance the heat transfer. Twisted tape inserts increase heat transfer rate with less friction factor. The coiled circular wire should be applied instead of smooth one to obtain higher heat transfer.

## References

1. Prabhakar Ray, Dr. Pradeep Kumar Jhinge, "A review paper on heat transfer rate enhancement by wire coil inserts in the tube", International journal of engineering sciences & research technology (2014), Vol.3(6) pp. 238-243.
2. G. D. Gosavi, S.V. Prayagi and V.S. Narnaware, "Use of perforated fins as a natural convection heat transfer-A Review", International Journal Of Core Engineering & Management (2014),
3. Allan Harry Richard.T.L, Agilan.H, "Experimental Analysis of Heat Transfer Enhancement Using Fins in Pin Fin Apparatus (2015), Vol. 2.
4. N. C. Kanojiya, V. M. Kriplani, P. V. Walke, "Heat Transfer Enhancement in Heat Exchangers With Inserts: A Review", International Journal of Engineering Research & Technology (2014), Vol. 3
5. Nikhil S Shrikhande, V. M. Kriplani, "Heat Transfer Enhancement in Automobile Radiator using Nanofluids: A Review", International Journal of Engineering Research & Technology (2014), Vol. 3

# ANALYTICAL INVESTIGATION OF HEAT TRANSFER ENHANCEMENT IN A MICRO TUBE USING NANO FLUIDS

-A REVIEW PAPER

Sanketh m  
Mechanical Engineering dept  
Malla reddy college of Engg  
Hyderabad, India  
email:sunnym191@gmail.com

Dr.Vikash Kumar  
Mechanical Engineering dept  
Malla reddy college of Engg  
Hyderabad,India  
email: vikash\_mech@mrce.in

## ABSTRACT

In the last few years, the fast growth of research in the heat transfer area was improved by using new kind of heat transfer fluids called nanofluids which have nanosized particles. Forced convective laminar flow of different types of nanofluids such as (TiCand MgO), with different volume fractions 0.4 and 0.5 using water as base fluids was investigating by using CFD analysis.

The Micro tube (MT) with 0.01 cm diameter and 20 cm length is using in this investigation. This investigation covers Reynolds number in the range of 90 to 800.

CFD analysis to determine the heat transfer coefficient, heat transfer rate, pressure drop and mass flow rate at different NANO fluids(MgO and TiC) at different volume fractions 0.4 &0.5.

Thermal analysis to determine the temperature distribution and heat flux with different materials. present used material for micro tube copper, replaced with composite materials.

## INTRODUCTION TO CAD

**Computer-aided design (CAD)** is the use of computer systems (or workstations) to aid in the creation, modification, analysis, or optimization of a design. CAD software is used to increase the productivity of the designer, improve the quality of design, improve communications through documentation, and to create a database for manufacturing. CAD

output is often in the form of electronic files for print, machining, or other manufacturing operations. The term **CADD** (for Computer Aided Design and Drafting) is also used.

Its use in designing electronic systems is known as electronic design automation, or **EDA**. In mechanical design it is known as mechanical design automation (**MDA**) or **computer-aided drafting (CAD)**, which includes the process of creating a technical drawing with the use of computer software.

CAD software for mechanical design uses either vector-based graphics to depict the objects of traditional drafting, or may also produce raster graphics showing the overall appearance of designed objects. However, it involves more than just shapes. As in the manual drafting of technical and engineering drawings, the output of CAD must convey information, such as materials, processes, dimensions, and tolerances, according to application-specific conventions.

CAD may be used to design curves and figures in two-dimensional (2D) space; or curves, surfaces, and solids in three-dimensional (3D) space.

## INTRODUCTION TO CREO

PTC CREO, formerly known as Pro/ENGINEER, is 3D modeling software used in mechanical engineering, design, manufacturing, and in CAD drafting service firms. It was one of the first 3D CAD modeling

applications that used a rule-based parametric system. Using parameters, dimensions and features to capture the behavior of the product, it can optimize the development product as well as the design itself.

The name was changed in 2010 from Pro/ENGINEER Wildfire to CREO. It was announced by the company who developed it, Parametric Technology Company (PTC), during the launch of its suite of design products that includes applications such as assembly modeling, 2D orthographic views for technical drawing, finite element analysis and more.

PTC also offers comprehensive training on how to use the software. This can save businesses by eliminating the need to hire new employees. Their training program is available online and in-person, but materials are available to access anytime.

A unique feature is that the software is available in 10 languages. PTC knows they have people from all over the world using their software, so they offer it in multiple languages so nearly anyone who wants to use it is able to do so.

The time saved by using PTC CREO isn't the only advantage. It has many ways of saving costs. For instance, the cost of creating a new product can be lowered because the development process is shortened due to the automation of the generation of associative manufacturing and service deliverables.

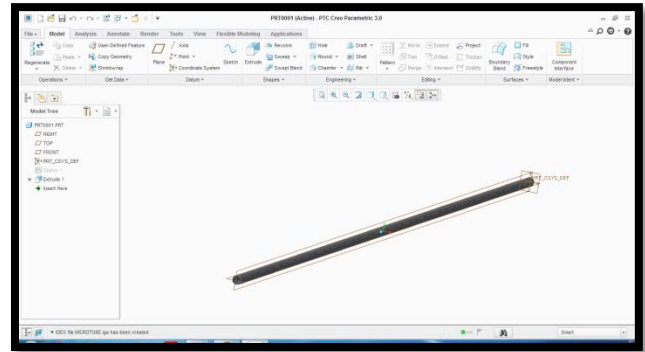
### ADVANTAGES OF CREO PARAMETRIC SOFTWARE

1. Optimized for model-based enterprises
2. Increased engineer productivity
3. Better enabled concept design
4. Increased engineering capabilities
5. Increased manufacturing capabilities
6. Better simulation
7. Design capabilities for additive manufacturing

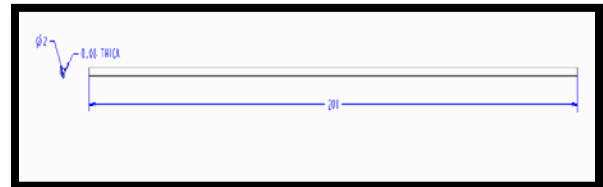
### CREO parametric modules:

- Sketcher
- Part modeling
- Assembly
- Drafting

### 3D MODEL OF MICRO TUBE



### 2d model of micro tube



### INTRODUCTION TO FEA

Finite Element Analysis (FEA) was first developed in 1943 by R. Courant, who utilized the Ritz method of numerical analysis and minimization of variational calculus to obtain approximate solutions to vibration systems. Shortly thereafter, a paper published in 1956 by M. J. Turner, R. W. Clough, H. C. Martin, and L. J. Top established a broader definition of numerical analysis. The paper centered on the "stiffness and deflection of complex structures".

By the early 70's, FEA was limited to expensive mainframe computers generally owned by the aeronautics, automotive, defense, and nuclear industries. Since the rapid decline in the cost of computers and the phenomenal increase in computing power, FEA has been developed to an incredible precision. Present day

supercomputers are now able to produce accurate results for all kinds of parameters.

FEA consists of a computer model of a material or design that is stressed and analyzed for specific results. It is used in new product design, and existing product refinement. A company is able to verify a proposed design will be able to perform to the client's specifications prior to manufacturing or construction. Modifying an existing product or structure is utilized to qualify the product or structure for a new service condition. In case of structural failure, FEA may be used to help determine the design modifications to meet the new condition.

There are generally two types of analysis that are used in industry: 2-D modeling, and 3-D modeling. While 2-D modeling conserves simplicity and allows the analysis to be run on a relatively normal computer, it tends to yield less accurate results. 3-D modeling, however, produces more accurate results while sacrificing the ability to run on all but the fastest computers effectively. Within each of these modeling schemes, the programmer can insert numerous algorithms (functions) which may make the system behave linearly or non-linearly. Linear systems are far less complex and generally do not take into account plastic deformation. Non-linear systems do account for plastic deformation, and many also are capable of testing a material all the way to fracture.

A wide range of objective functions (variables within the system) are available for minimization or maximization:

- Mass, volume, temperature
- Strain energy, stress strain
- Force, displacement, velocity, acceleration
- Synthetic (User defined).

There are multiple loading conditions which may be applied to a system. Some examples are shown:

- Point, pressure, thermal, gravity, and centrifugal static loads

- Thermal loads from solution of heat transfer analysis
- Enforced displacements
- Heat flux and convection
- Point, pressure and gravity dynamic loads.

### Types of Engineering Analysis

**Structural** analysis consists of linear and non-linear models. Linear models use simple parameters and assume that the material is not plastically deformed. Non-linear models consist of stressing the material past its elastic capabilities. The stresses in the material then vary with the amount of deformation as in.

**Vibrational** analysis is used to test a material against random vibrations, shock, and impact. Each of these incidences may act on the natural vibrational frequency of the material which, in turn, may cause resonance and subsequent failure.

Fatigue analysis helps designers to predict the life of a material or structure by showing the effects of cyclic loading on the specimen. Such analysis can show the areas where crack propagation is most likely to occur. Failure due to fatigue may also show the damage tolerance of the material.

**Heat Transfer** analysis models the conductivity or thermal fluid dynamics of the material or structure. This may consist of a steady-state or transient transfer. Steady-state transfer refers to constant thermo properties in the material that yield linear heat diffusion.

### CALCULATIONS TO DETERMINE PROPERTIES OF NANO FLUID BY CHANGING VOLUME FRACTIONS

Volume fraction= 0.4 & 0.5(taken from journal paper)

#### MATERIAL PROPERTIES

MAGNESIUM OXIDE

Density = 3560 kg/m<sup>3</sup>

Thermal conductivity =45 W/m-k

Specific heat = 955 J/kg-k

**TITANIUM CARBIDE**

Density = 4930 kg/m<sup>3</sup>

Thermal conductivity =330 W/m-k

Specific heat = 711 J/kg-k

**WATER**

Density = 998.2 kg/m<sup>3</sup>

Thermal conductivity = 0.6 W/m-k

Specific heat = 4182 J/kg-k

Viscosity = 0.001003kg/m-s

**NOMENCLATURE**

$\rho_{nf}$  = Density of nano fluid (kg/m<sup>3</sup>)

$\rho_s$  = Density of solid material (kg/m<sup>3</sup>)

$\rho_w$  = Density of fluid material (water) (kg/m<sup>3</sup>)

$\phi$  = Volume fraction

$C_{pw}$  = Specific heat of fluid material (water) (j/kg-k)

$C_{ps}$  = Specific heat of solid material (j/kg-k)

$\mu_w$  = Viscosity of fluid (water) (kg/m-s)

$\mu_{nf}$  = Viscosity of Nano fluid (kg/m-s)

$K_w$  = Thermal conductivity of fluid material (water) (W/m-k)

$K_s$  = Thermal conductivity of solid material (W/m-k)

**NANO FLUID CALCULATIONS**

**MAGENSIUM OXIDE**

**DENSITY OF NANO FLUID**

At  $\phi =0.4$

$$\rho_{nf} = \phi \times \rho_s + [(1-\phi) \times \rho_w]$$

$\rho_{nf} = 2022.92 \text{ kg/m}^3$

At  $\phi =0.5$

$\rho_{nf} = 2025.94 \text{ kg/m}^3$

**SPECIFIC HEAT OF NANO FLUID**

$$C_{p\text{ nf}} = \frac{\phi \times \rho_s \times C_{ps} + (1-\phi)(\rho_w \times C_{pw})}{\phi \times \rho_s + (1-\phi) \times \rho_w}$$

At  $\phi =0.4$

$C_{p\text{ nf}} = 1910.408 \text{ j/kg-k}$

At  $\phi =0.5$

$C_{p\text{ nf}} = 1900.404 \text{ j/kg-k}$

**VISCOSITY OF NANO FLUID**

$$\mu_{nf} = \mu_w (1+2.5\phi)$$

At  $\phi =0.4$

$\mu_{nf} = 0.002006 \text{ kg/m-s}$

At  $\phi =0.5$

$\mu_{nf} = 0.002256 \text{ kg/m-s}$

**THERMAL CONDUCTIVITY OF NANO FLUID**

$$K_{nf} = \frac{K_s + 2K_w + 2(K_s - K_w)(1+\beta)^3 \times \phi}{K_s + 2K_w - (K_s - K_w)(1+\beta)^3 \times \phi} \times k_w$$

At  $\phi =0.4$

$\beta=0.1$  taken from journal

$K_{nf} = 0.1.84577 \text{ (W/m-k)}$

At  $\phi =0.5$

$\beta=0.1$  taken from journal

$K_{nf} = 0.2015 \text{ (W/m-k)}$

**TITANIUM CARBIDE**

### DENSITY OF NANO FLUID

$$\rho_{nf} = \phi \times \rho_s + [(1-\phi) \times \rho_w]$$

VOLUME FRACTION 0.4

$$\rho_{nf} = 2570.92 \text{ kg/m}^3$$

VOLUME FRACTION 0.5

$$\rho_{nf} = 2964.1 \text{ kg/m}^3$$

### SPECIFIC HEAT OF NANO FLUID

$$C_{p \text{ nf}} = \frac{\phi \times \rho_s \times C_{ps} + (1-\phi)(\rho_w \times C_{pw})}{\phi \times \rho_s + (1-\phi) \times \rho_w}$$

At  $\phi = 0.4$

$$C_{p \text{ nf}} = 5357.01 \text{ j/kg-k}$$

At  $\phi = 0.5$

$$C_{p \text{ nf}} = 4069.1 \text{ j/kg-k}$$

### VISCOSITY OF NANO FLUID

$$\mu_{nf} = \mu_w (1 + 2.5\phi)$$

At  $\phi = 0.4$

$$\mu_{nf} = 0.002006 \text{ kg/m-s}$$

At  $\phi = 0.5$

$$\mu_{nf} = 0.00225675 \text{ kg/m-s}$$

### THERMAL CONDUCTIVITY OF NANO FLUID

$$K_{nf} = \frac{K_s + 2K_w + 2(K_s - K_w)(1 + \beta)^3 \times \phi}{K_s + 2K_w - (K_s - K_w)(1 + \beta)^3 \times \phi} \times K_w$$

$\beta = 0.1$  taken from journal

At  $\phi = 0.4$

$$K_{nf} = 2.625 \text{ W/m-k}$$

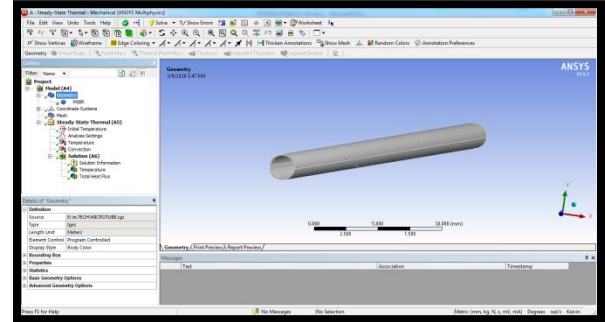
At  $\phi = 0.5$

$$K_{nf} = 4.12 \text{ W/m-k}$$

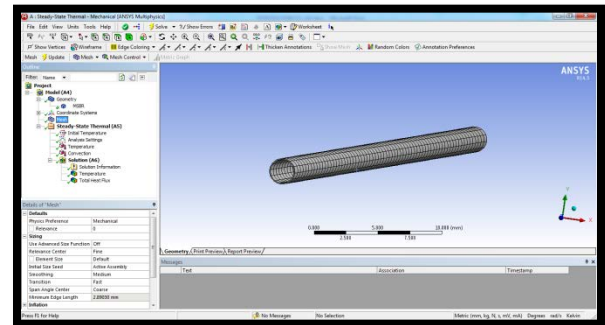
### THERMAL ANALYSIS OF MICRO TUBE

#### MATERIAL-COPPER

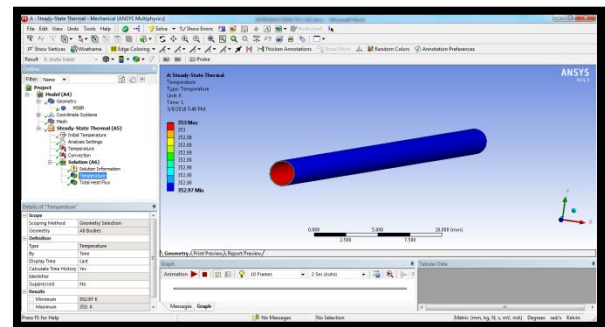
#### IMPORTED MODEL



#### MESHED MODEL.



#### TEMPERATURE DISTRIBUTION



### DISCUSSION

Various authors have performed the experimental investigation related to heat transfer enhancement and its affecting factors by using Al<sub>2</sub>O<sub>3</sub>, CuO, TiO<sub>2</sub>, ZrO<sub>2</sub>, Ag, SiC and Diamond nanoparticle. Amongst all CuO and Al<sub>2</sub>O<sub>3</sub> are frequently used for higher thermal

conductivity, but many type of nanoparticle using to enhance the heat transfer rate at different application, and discussed many factor affecting the heat transfer rate of Nano fluid. Mixing is important for enhancement of heat transfer rate, so ultrasonic mixture is suitable for enhance thermal conductivity of nanoparticle.

## CONCLUSIONS

Heat transfer rate increases with increasing concentration of nanoparticle. Heat transfer rate is directly proportional to the Reynolds number and Peclet number of Nano fluid. The fine grade of Nano particles increases the heat transfer rate but it's having poor stability. Clustering and collision of nanoparticles is main factor to affect the heat transfer rate of Nano fluid. Concentration of nanoparticles increases the pressure drop of Nano fluid. Spherical shaped nanoparticles increases the heat transfer rate of Nano fluid compared with other shaped nanoparticles. Boiling was to reduce the enhancement of heat transfer rate. Spiral pipe having higher heat transfer rate compared with the circular plain tube. Inclined tube possess the low pressure drop compared with horizontal tube.

## REFERENCES

- [1] L.B.Mapa, Sana Mazhar, Heat transfer in mini heat exchanger using Nano fluids. IL/IN sectional conference.
- [2] J.Koo, C.Kleinstrecker, Laminar Nano fluid flow in micro heat sink. International journal of heat and mass transfer 48(2005).
- [3] Shung-Wei Kang, Wei-Chiang Wei, Sheng-Hong Tsai, Shih-Yu YANG, Experimental investigation of silver Nano fluid on heat pipe thermal performance, Applied thermal engineering 26(2006).
- [4] Shuichi Torii, Experimental study on convective heat transfer of aqueous suspension of Nano diamond particle, International symposium on Eco Topia science 07 (2007).
- [5] S.J.Kim, I.C. Bang, J.Buongiorno, and L.N.Hu, Study of pool boiling and critical heat

flux enhancement in Nano fluid. bulletin of the polish academy of sciences technical science. vol55, no 2, 2007.

[6] Yanuar, N.Putra, Gunawan S.M.Bagi, Flow and convective heat transfer characteristic of spiral pipe for Nano fluid. IJRRAS 7(3). June 2011.

[7] Nawaf H. Saeid and Tan HengChaia, Investigation of thermal performance of air to water heat exchanger using Nano fluid, IIUM Engineering journal special issue mechanical engineering, 2011.

[8] E.Ebrahimiinia- Bajestan, H.Niazmand, Convective heat transfer of Nano fluid flow through an isothermally heated curved pipe. Iranian journal of chemical engineering vol.8 no.2, (2011).

[9] Manay E, Salein B, Yilmaz M, Gelis Thermal performance analysis of Nano fluid in micro channel heat sinks. World academy of Science, Engineering and Technology vol. 67 (2012).

[10] Anchupogu Praveen, penugonda Suresh babu, Venkata Ramesh Manila, Analysis on heat transfer in Nano fluid for alumina-water. International journal of advanced scientific research and technology issue 2, volume 2 (April 2012).

## HEAT TRANSFER ALONG VERTICAL CHIMNEY

K. Rajanikanth (M.tech)  
 Mechanical Engineering  
 Malla reddy college of engg  
 Hyderabad, India  
 Email: [rajani.kaithoju@gmail.com](mailto:rajani.kaithoju@gmail.com)

D.r. T.V.Reddy. Ph.D  
 Mechanical Engineering  
 Malla reddy college of engg  
 Hyderabad,India  
 Email: [viceprincipal@mrce.in](mailto:viceprincipal@mrce.in)

### Abstract—

Chimney, which form the last component of a system using a flue gas such as boiler, play a vital role in maintaining efficiency, draft, etc, of a system and also in minimizing the atmospheric pollution. Steel chimneys are also known as steel stacks. The steel chimneys are made of steel plates and supported on foundation. The steel chimneys are used to escape and disperse the flue gases to such a height that the gases do not contaminate surrounding atmosphere. The hot gases occupy. For the purpose of the structural design of steel the chimney, the height and diameter of chimney. Chimneys are required larger volume than before. The weight of gases per cubic meter becomes less to carry vertically and discharge, gaseous products of combustion, chemical waste gases, and exhaust air from an industry to the atmosphere. In this thesis, chimney materials (concrete used for the design of the chimney. The chimney was considered as a cantilever beam with annular will be designed considering with insulation and without insulation. The Bureau of Indian Standards (BIS) design codes procedures will be the chimney is done in CREO Parametric software and fluid- structural and thermal analysis is done on the chimney in ANSYS software. A simplified model of chimneys with various insulation cross section. 3D model of and carbon epoxy). Static analysis is to determine the deformation, stress and strain for chimney with insulation and without insulation. Thermal analysis to determine the heat flux of the chimney with different materials to different models. CFD analysis to determine the pressure drop, velocity, heat transfer coefficient, mass flow rate and heat transfer rate.

**Keywords:** Combustion,insulation,CFD,Heat transfer coefficient

### I. INTRODUCTION

A chimney is a structure that provides ventilation for hot flue gases or smoke from a boiler, stove, furnace or fireplace to the outside atmosphere. Chimneys are typically vertical, or as near as possible to vertical, to ensure that the gases flow smoothly, drawing air into the combustion in what is known as the stack, or chimney effect. The space inside a chimney is called a flue. Chimneys may be found in buildings, steam locomotives and ships. In the United States, the term

smokestack (colloquially, stack) is also used when referring to locomotive chimneys or ship chimneys, and the term funnel can also be used. The height of a chimney influences its ability to transfer flue gases to the external environment via stack effect. Additionally, the dispersion of pollutants at higher altitudes can reduce their impact on the immediate surroundings. In the case of chemically aggressive output, a sufficiently tall chimney can allow for partial or complete self-neutralization of airborne chemicals before they reach ground level. The dispersion of pollutants over a greater area can reduce their concentrations and facilitate compliance with regulatory limits.

**RESIDENTIAL FLUE LINERS:** A flue liner is a secondary barrier in a chimney that protects the masonry from the acidic products of combustion, helps prevent flue gas from entering the house, and reduces the size of an oversized flue. Newly built chimneys have been required by building codes to have a flue liner in many locations since the 1950s. Chimneys built without a liner can usually have a liner added, but the type of liner needs to match the type of appliance it is servicing. Flue liners may be clay tile, metal, concrete tiles, or poured in place concrete. Clay tile flue liners are very common in the United States. However, this is the only liner which does not meet Underwriters Laboratories 1777 approval and frequently have problems such as cracked tiles and improper installation. Clay tiles are usually about 2 feet (0.61 m) long, various sizes and shapes, and are installed in new construction as the chimney is built. A refractory cement is used between each tile. Metal liners may be stainless steel, aluminum, or galvanized iron and may be flexible or rigid pipes. Stainless steel is made in several types

### History:



A smoke hood in the Netherlands. Image: Cultural Heritage Agency of the Netherlands

### CHIMNEY POTS, CAPS AND TOPS:

A chimney pot is placed on top of the chimney to expand the length of the chimney inexpensively, and to improve the

chimney's [draft](#). A chimney with more than one pot on it indicates that there is more than one fireplace on different floors sharing the chimney. A chimney [cowl](#) is placed on top of the chimney to prevent birds and other animals from nesting in the chimney. They often feature a rain guard to prevent rain or snow from going down the chimney. A metal wire mesh is often used as a [spark arrestor](#) to minimize burning debris from rising out of the chimney and making it onto the roof. Although the masonry inside the chimney can absorb a large amount of moisture which later evaporates, rainwater can collect at the base of the chimney. Sometimes weep holes are placed at the bottom of the chimney to drain out collected water.



A chimney cowl or wind directional cap is a helmet-shaped chimney cap that rotates to align with the wind and prevent a backdraft of smoke and wind back down the chimney.

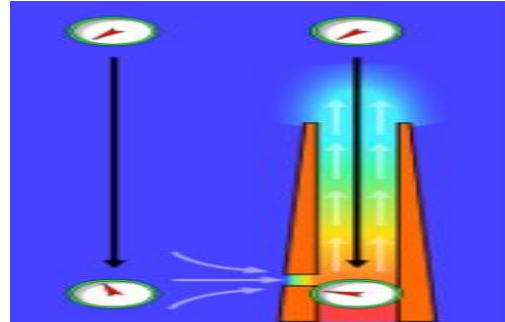


**A H-style cowl:**

An H-style cap (cowl) is a chimney top constructed from chimney pipes shaped like the letter H. (Its image is included in cowl (chimney).) It is an age-old method of regulating draft in situations where prevailing winds or turbulences cause downdraft and backpuffing. Although the H cap has a distinct advantage over most other downdraft caps, it fell out of favor because of its bulky design. It is found mostly in marine use but has been regaining popularity due to its energy-saving functionality. The H-cap stabilizes the draft rather than increasing it. Other downdraft caps are based on the Venturi effect, solving downdraft problems by increasing the updraft constantly resulting in much higher fuel consumption. A chimney damper is a metal plate that can be positioned to close off the chimney when not in use and prevent outside air from entering the interior space, and can be opened to permit hot gases to exhaust when a fire is burning. A top damper or cap damper is a metal spring door placed at the top of the chimney with a long metal chain that allows one to open and close the damper from the fireplace. A throat damper is a metal plate at the base of the chimney, just above the firebox, that can be

opened and closed by a lever, gear, or chain to seal off the fireplace from the chimney. The advantage of a top damper is the tight weatherproof seal that it provides when closed, which prevents cold outside air from flowing down the chimney and into the living space—a feature that can rarely be matched by the metal-on-metal seal afforded by a throat damper.

**CHIMNEY DRAUGHT OR DRAFT:**



The stack effect in chimneys: the gauges represent absolute air pressure and the airflow is indicated with light grey arrows. The gauge dials move clockwise with increasing pressure.

Main article: Flue gas stack When coal, oil, natural gas, wood, or any other fuel is combusted in a stove, oven, fireplace, hot water boiler, or industrial furnace, the hot combustion product gases that are formed are called flue gases. Those gases are generally exhausted to the ambient outside air through chimneys or industrial flue gas stacks (sometimes referred to as smokestacks). The combustion flue gases inside the chimneys or stacks are much hotter than the ambient outside air and therefore less dense than the ambient air. That causes the bottom of the vertical column of hot flue gas to have a lower pressure than the pressure at the bottom of a corresponding column of outside air. That higher pressure outside the chimney is the driving force that moves the required combustion air into the combustion zone and also moves the flue gas up and out of the chimney. That movement or flow of combustion air and flue gas is called "natural draught/draft", "natural ventilation", "chimney effect", or "stack effect". The taller the stack, the more draught or draft is created. There can be cases of diminishing returns: if a stack is overly tall in relation to the heat being sent out of the stack, the flue gases may cool before reaching the top of the chimney. This condition can result in poor drafting, and in the case of wood burning appliances, the cooling of the gases before emission can cause creosote to condense near the top of the chimney. The creosote can restrict the exit of flue gases and may pose a fire hazard. Designing chimneys and stacks to provide the correct amount of natural draft involves a number of design factors, many of which require iterative trial-and-error methods. As a "first guess" approximation, the following equation can be used to estimate the natural draught/draft flow rate by assuming that the molecular mass (i.e., molecular weight) of the flue gas and the external air are equal and that the frictional pressure and heat losses are negligible:

where:

- Q** = chimney draught/draft flow rate, m<sup>3</sup>/s  
**A** = cross-sectional area of chimney, m<sup>2</sup> (assuming it has a constant cross-section)  
**C** = discharge coefficient (usually taken to be from 0.65 to 0.70)  
**G** = gravitational acceleration, 9.807 m/s<sup>2</sup>  
**H** = height of chimney, m  
**T<sub>i</sub>** = average temperature inside the chimney, K  
**T<sub>e</sub>** = external air temperature, K.

#### MAINTENANCE AND PROBLEMS:



Chimneys on the Parliamentary Library in Wellington, New Zealand.

A characteristic problem of chimneys is they develop deposits of creosote on the walls of the structure when used with wood as a fuel. Deposits of this substance can interfere with the airflow and more importantly, they are combustible and can cause dangerous chimney fires if the deposits ignite in the chimney. Heaters that burn natural gas drastically reduce the amount of creosote buildup due to natural gas burning much cleaner and more efficiently than traditional solid fuels. While in most cases there is no need to clean a gas chimney on an annual basis that does not mean that other parts of the chimney cannot fall into disrepair. It is now possible to buy "faux-brick" facades to cover these modern chimney structures. Other potential problems include: "spalling" brick, in which moisture seeps into the brick and then freezes, cracking and flaking the brick and loosening mortar seals, shifting foundations, which may degrade integrity of chimney masonry nesting or infestation by unwanted animals such as squirrels, or chimney swifts chimney leaks drafting issues, which may allow smoke inside building issues with fireplace or heating appliance may cause unwanted degradation or hazards to chimney

#### Cooling tower used as an industrial chimney

At some power stations, which are equipped with plants for the removal of sulfur dioxide and nitrogen oxides, it is possible to use the cooling tower as a chimney. Such cooling towers can be seen in Germany at the Power Station Staudinger Grosskrotzenburg and at the Power Station Rostock. At power stations that are not equipped for removing sulfur dioxide, such usage of cooling towers could result in serious corrosion problems which are not easy to prevent.

#### LITERATURE REVIEW:

##### 1. Seismic Analysis And Design Of Industrial

**Chimneys** This paper describes a simplified method that allow obtaining the fundamental period of vibration, lateral displacement, shear force and bending moment through a set of equations, obtaining for all cases studied an error below 10%. The results obtained in this study were applied to a total of 9 real chimneys (4 of steel and 5 of reinforced concrete) built in Chile, with the objective of calibrating founded expressions. During the stage of the analysis, it was verified that the criterion of consistent masses provide better results than the criterion of lumped masses, and as a very important conclusion a discrete analysis of the model in twenty segments of the beam is satisfactory. The most representative variables that define the model with which it is possible to carry out a parametric analysis of the chimney. As important parameters we could refer to: slenderness ratio  $H/D_{inf}$ , radius ratio  $R_{sup}/R_{inf}$ , thickness ratio  $E_{sup}/E_{inf}$  and thickness diameter ratio  $D_{inf}/E_{inf}$ . Later, by varying each one of the chosen parameters several analysis of representative chimneys of this great family, could be carried out. As seismic loads, the spectrums of accelerations recommended by the code of seismic design for structures and industrial installations in Chile, have been considered. Modal responses were combined using the combination rule CQC. In all the cases studied in this investigation, the influence of the P-Δ effect, the soil structure interaction, and the influence on responses that provoke the inclusion of lining, have been disregarded.

##### 2. Analysis Of Self Supported Steel Chimney As Per Indian Standard

Most of the industrial steel chimneys are tall structures with circular cross-sections. Such slender, lightly damped structures are prone to wind-excited vibration. Geometry of a self supporting steel chimney plays an important role in its structural behaviour under lateral dynamic loading. This is because geometry is primarily responsible for the stiffness parameters of the chimney. However, basic dimensions of industrial self supporting steel chimney, such as height, diameter at exit, etc., are generally derived from the associated environmental conditions. To ensure a desired failure mode design code (IS-6533: 1989 Part 2) imposes several criteria on the geometry (top-to-base diameter ratio and height-to-base diameter ratio) of steel chimneys. The objective of the present study is to justify the code criteria with regard to basic dimensions of industrial steel chimney.

##### 3. Analysis of Tall RC Chimney as per Indian Standard Code

Reinforced chimneys are used in Power plants to take the hot and poisonous flue gas to a great height. They are tall and slender structures, designed mainly to resist the lateral forces like wind and earthquake as well as the thermal stresses of the flue gas. An attempt is done to understand the variation of lateral deflection at the top of the chimney, by varying the height of chimney above 275 m. CED 38:7892 Code of practice for design of reinforced concrete chimney (Third revision of IS 4998:1992 [Part I]) is used for the analysis. The location selected for the study is Bellary in Karnataka. Along wind and temperature are only considered for this study. Sufficient amount of reinforcement is provided to

resist the bending moment in the vertical direction and horizontal loops are provided to cater for the horizontal shear and temperature gradient. A total of five models are selected for five different heights and the analysis and design are done. ANSYS software was used to do the analysis. All the models were analyzed and the lateral deflection was calculated.

#### 4. Analysis and Computational Study of a High Chimney Tower for Solar Energy

**Abstract:** A Solar Chimney Power Plant consists of central chimney that is surrounded by a transparent canopy located a few meters above ground level. An analysis of solar chimneys has been developed, aimed particularly to study stability and structural strength of a model of cylindrical reinforced concrete tower with 500m in tall and 50m in diameter. The design of this tower has several technical challenges. This model is subjected to its own weight, the effects of wind and the pressure due to the flow of air inside the chimney. In this study, the effect of these loads on the stability and strength of the chimney has been examined. The rings stiffened are necessary to prevent ovalisation of the structure. In addition, the influence of various designs of rings-stiffened is taken into consideration in the mechanical behaviour of this tower. Numerical simulation modeling method based on finite element method is adopted using the "Autodesk Robot structural analysis professional" software.

#### 5. Nonlinear Dynamic Analysis Of Chimney-Like Towers

In this study the most important problem i.e. earthquake behaviour of the structures, hysteric behaviour of material and section properties are studied. The significance of this study is mainly concentrated on model simplification that provides sufficient accuracy based on a nonlinear discrete model. Tous power plant chimney is investigated numerically as an example. The nonlinear dynamic analysis essentially needed for seismic assessment in evaluation of actual performance of complicated structures during earthquakes than the damage indices of structure had to be calculated using appropriate damage models.

#### 6. Dynamic Soil-Structure Interaction Analysis of Tall Multi-Flue Chimneys Under Aerodynamic And Seismic Force.

The present paper proposes a semi analytic mathematical model based on which both seismic and aerodynamic response of such a tall chimneys are studied for various soil stiffness and are compared with fixed base conventional method as per UBC 97 (for seismic load) and CICIND (for wind loading). Soil Structure interaction also has an important effect on seismic forces of tall chimneys. Although for tall chimneys rested on firm soil, earthquake loads decreased as a result of increasing in period values, seismic forces may amplify by using different response spectra in calculation. This means that the soil structure interaction effects are reliant on characteristic of the seismic excitation in addition to chimneys properties. JEEVAN T, SOWJANYA G. V (2014)



#### INTRODUCTION TO CREO :

PTC CREO, formerly known as Pro/ENGINEER, is 3D modeling software used in mechanical engineering, design, manufacturing, and in CAD drafting service firms. It was one of the first 3D CAD modeling applications that used a rule-based parametric system. Using parameters, dimensions and features to capture the behavior of the product, it can optimize the development product as well as the design itself. The name was changed in 2010 from Pro/ENGINEER Wildfire to CREO. It was announced by the company who developed it, Parametric Technology Company (PTC), during the launch of its suite of design products that includes applications such as assembly modeling, 2D orthographic views for technical drawing, finite element analysis and more. PTC CREO says it can offer a more efficient design experience than other modeling software because of its unique features including the integration of parametric and direct modeling in one platform. The complete suite of applications spans the spectrum of product development, giving designers options to use in each step of the process. The software also has a more user friendly interface that provides a better experience for designers. It also has collaborative capacities that make it easy to share designs and make changes. There are countless benefits to using PTC CREO. We'll take a look at them in this two-part series. First up, the biggest advantage is increased productivity because of its efficient and flexible design capabilities. It was designed to be easier to use and have features that allow for design processes to move more quickly, making a designer's productivity level increase. The time saved by using PTC CREO isn't the only advantage. It has many ways of saving costs. For instance, the cost of creating a new product can be lowered because the development process is shortened due to the automation of the generation of associative manufacturing and service deliverables. PTC also offers comprehensive training on how to use the software. This can save businesses by eliminating the need to hire new employees. Their training program is available online and in-person, but materials are available to access anytime. A unique feature is that the software is available in 10 languages. PTC knows they have people from all over the world using their software, so they offer it in multiple languages so nearly anyone who wants to use it is able to do so.

#### ADVANTAGES OF CREO PARAMETRIC SOFTWARE :

1. Optimized for model-based enterprises

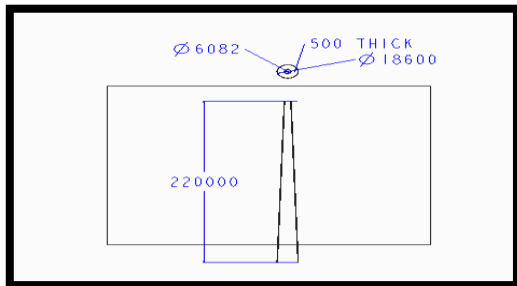
2. Increased engineer productivity
3. Better enabled concept design
4. Increased engineering capabilities
5. Increased manufacturing capabilities
6. Better simulation
7. Design capabilities for additive manufacturing

### CREO PARAMETRIC MODULES:

- Sketcher
- Part modeling
- Assembly
- Drafting



**2D MODEL OF CHIMNEY**



### INTRODUCTION TO FEA:

Finite element analysis is a method of solving, usually approximately, certain problems in engineering and science. It is used mainly for problems for which no exact solution, expressible in some mathematical form, is available. As such, it is a numerical rather than an analytical method. Methods of this type are needed because analytical methods cannot cope with the real, complicated problems that are met with in engineering. For example, engineering strength of materials or the mathematical theory of elasticity can be used to calculate analytically the stresses and strains in a bent beam, but neither will be very successful in finding out what is happening in part of a car suspension system during cornering. One of the first applications of FEA was, indeed, to find the stresses and strains in engineering components under load. FEA, when applied to any realistic model of an engineering component, requires an enormous amount of computation and the development of the method has depended on the availability of suitable digital computers for it to run on. The method is now applied to

problems involving a wide range of phenomena, including vibrations, heat conduction, fluid mechanics and electrostatics, and a wide range of material properties, such as linear-elastic (Hookean) behavior and behavior involving deviation from Hooke's law (for example, plasticity or rubber-elasticity). Many comprehensive general-purpose computer packages are now available that can deal with a wide range of phenomena, together with more specialized packages for particular applications, for example, for the study of dynamic phenomena or large-scale plastic flow. Depending on the type and complexity of the analysis, such packages may run on a microcomputer or, at the other extreme, on a supercomputer. FEA is essentially a piece-wise process. It can be applied to one-dimensional problems, but more usually there is an area or volume within which the solution is required. This is split up into a number of smaller areas or volumes, which are called finite elements. Figure 1 shows a two-dimensional model of a spanner that has been so divided: the process is called discretisation, and the assembly of elements is called a mesh.

### INTRODUCTION TO ANSYS:

ANSYS is general-purpose finite element analysis (FEA) software package. Finite Element Analysis is a numerical method of deconstructing a complex system into very small pieces (of user-designated size) called elements. The software implements equations that govern the behaviour of these elements and solves them all; creating a comprehensive explanation of how the system acts as a whole. These results then can be presented in tabulated, or graphical forms.

### Generic Steps to Solving any Problem in ANSYS:

Like solving any problem analytically, you need to define (1) your solution domain, (2) the physical model, (3) boundary conditions and (4) the physical properties. You then solve the problem and present the results. In numerical methods, the main difference is an extra step called mesh generation. This is the step that divides the complex model into small elements that become solvable in an otherwise too complex situation. Below describes the processes in terminology slightly more attune to the software.

**Build Geometry:** Construct a two or three dimensional representation of the object to be modeled and tested using the work plane coordinate system within ANSYS.

**Define Material Properties:** Now that the part exists, define a library of the necessary materials that compose the object (or project) being modeled. This includes thermal and mechanical properties.

**Generate Mesh:** At this point ANSYS understands the makeup of the part. Now define how the modeled system should be broken down into finite pieces.

**Apply Loads:** Once the system is fully designed, the last task is to burden the system with constraints, such as physical loadings or boundary conditions.

**Present the Results:** After the solution has been obtained, there are many ways to present ANSYS' results, choose from many options such as tables, graphs, and contour plots.

## SPECIFIC CAPABILITIES OF ANSYS:

### Structural

Static Analysis - Used to determine displacements, stresses, etc. under static loading conditions. ANSYS can compute both linear and nonlinear static analyses. Nonlinearities can include plasticity, stress stiffening, large deflection, large strain, hyper elasticity, contact surfaces, and creep. Transient Dynamic Analysis - Used to determine the response of a structure to arbitrarily time-varying loads. All nonlinearities mentioned under Static Analysis above are allowed. Buckling Analysis - Used to calculate the buckling loads and determine the buckling mode shape. Both linear (eigenvalue) buckling and nonlinear buckling analyses are possible.

### Thermal:

ANSYS is capable of both steady state and transient analysis of any solid with thermal boundary conditions. Steady-state thermal analyses calculate the effects of steady thermal loads on a system or component. Users often perform a steady-state analysis before doing a transient thermal analysis, to help establish initial conditions. A steady-state analysis also can be the last step of a transient thermal analysis; performed after all transient effects have diminished. ANSYS can be used to determine temperatures, thermal gradients, heat flow rates, and heat fluxes in an object that are caused by thermal loads that do not vary over time. Such loads include the following:

- Convection
- Radiation
- Heat flow rates
- Heat fluxes (heat flow per unit area)
- Heat generation rates (heat flow per unit volume)

### Fluid Flow:

The ANSYS/FLOTRAN CFD (Computational Fluid Dynamics) offers comprehensive tools for analyzing two-dimensional and three-dimensional fluid flow fields. ANSYS is capable of modeling a vast range of analysis types such as: airfoils for pressure analysis of airplane wings (lift and drag), flow in supersonic nozzles, and complex, three-dimensional

flow patterns in a pipe bend. In addition, ANSYS/FLOTRAN could be used to perform tasks including:

- Calculating the gas pressure and temperature distributions in an engine exhaust manifold
- Studying the thermal stratification and breakup in piping systems
- Using flow mixing studies to evaluate potential for thermal shock
- Doing natural convection analyses to evaluate the thermal performance of chips in electronic enclosures
- Conducting heat exchanger studies involving different fluids separated by solid regions

### COUPLED FIELD:

A coupled-field analysis is an analysis that takes into account the interaction (coupling) between two or more disciplines (fields) of engineering. A piezoelectric analysis, for example, handles the interaction between the structural and electric fields: it solves for the voltage distribution due to applied displacements, or vice versa. Other examples of coupled-field analysis are thermal-stress analysis, thermal-electric analysis, and fluid-structure analysis. Some of the applications in which coupled-field analysis may be required are pressure vessels (thermal-stress analysis), fluid flow constrictions (fluid-structure analysis), induction heating (magnetic-thermal analysis), ultrasonic transducers (piezoelectric analysis), magnetic forming (magneto-structural analysis), and micro-electro mechanical systems (MEMS).

**Modal Analysis** - A modal analysis is typically used to determine the vibration characteristics (natural frequencies and mode shapes) of a structure or a machine component while it is being designed. It can also serve as a starting point for another, more detailed, dynamic analysis, such as a harmonic response or full transient dynamic analysis. Modal analyses, while being one of the most basic dynamic analysis types available in ANSYS, can also be more computationally time consuming than a typical static analysis. A reduced solver, utilizing automatically or manually selected master degrees of freedom is used to drastically reduce the problem size and solution time.

**Harmonic Analysis** - Used extensively by companies who produce rotating machinery, ANSYS Harmonic analysis is used to predict the sustained dynamic behavior of structures to consistent cyclic loading. Examples of rotating machines which produced or are subjected to harmonic loading are:

- Turbines
- Gas Turbines for Aircraft and Power Generation
- Steam Turbines
- Wind Turbine
- Water Turbines
- Turbopumps
- Internal Combustion engines
- Electric motors and generators
- Gas and fluid pumps

- Disc drives

A harmonic analysis can be used to verify whether or not a machine design will successfully overcome resonance, fatigue, and other harmful effects of forced vibrations.

## INTRODUCTION TO CFD:

Computational fluid dynamics, usually abbreviated as CFD, is a branch of fluid mechanics that uses numerical methods and algorithms to solve and analyze problems that involve fluid flows. Computers are used to perform the calculations required to simulate the interaction of liquids and gases with surfaces defined by boundary conditions. With high-speed supercomputers, better solutions can be achieved. Ongoing research yields software that improves the accuracy and speed of complex simulation scenarios such as transonic or turbulent flows. Initial experimental validation of such software is performed using a wind tunnel with the final validation coming in full-scale testing, e.g. flight tests.

## METHODOLOGY:

In all of these approaches the same basic procedure is followed.

- During preprocessing
- The geometry (physical bounds) of the problem is defined.
- The volume occupied by the fluid is divided into discrete cells (the mesh). The mesh may be uniform or non-uniform.
- The physical modeling is defined – for example, the equations of motion + enthalpy + radiation + species conservation
- Boundary conditions are defined. This involves specifying the fluid behaviour and properties at the boundaries of the problem. For transient problems, the initial conditions are also defined.
- The simulation is started and the equations are solved iteratively as a steady-state or transient.
- Finally a postprocessor is used for the analysis and visualization of the resulting solution.

## CONCLUSION:

Chimney, which form the last component of a system using a flue gas such as boiler, play a vital role in maintaining efficiency, draft, etc, of a system and also in minimizing the atmospheric pollution. The ease of thermal control by means of air natural convection stimulates the investigation of configurations with the aim at improving the thermal performance. The steel chimneys are used to escape and disperse the flue gases to such a height that the gases do not contaminate surrounding atmosphere. The hot gases occupy. For the purpose of the structural design of steel the chimney, the height and diameter of chimney. Chimneys are required larger

volume than before. A chimney, which is an unheated extension of a flow passage, enhances the flow acceleration through buoyancy. It acts like a shroud so that the merged thermal plumes (Thermal boundary layers) inside the pipe are accelerated along the duct without scattering. The height of the chimney determines the acceleration distance of the hot plume, and the heat transfer is enhanced as the flow rate increases.

## REFERENCES:

1. Heat transfer effects of chimney height, diameter, and Prandtl number
2. International Communications in Heat and Mass Transfer, Volume 66, 2015, pp. 196-202
3. Enhanced natural convection heat transfer of a chimney-based radial heat sink
4. Energy Conversion and Management, Volume 108, 2016, pp. 422-428
5. Experimental investigation of chimney-enhanced natural convection in hexagonal honeycombs
6. Theoretical and Applied Mechanics Letters, Volume 4, Issue 3, 2014, Article 032005
7. Heat transfer enhancement by the chimney effect in a vertical isoflux channel
8. Auletta A., Manca O., Morrone B., Naso V.
9. (2001) International Journal of Heat and Mass Transfer, 44 (22) , pp. 4345-4357.
10. HEAT TRANSFER ENHANCEMENT FROM A VERTICAL, ISOTHERMAL CHANNEL GENERATED BY THE CHIMNEY EFFECT  
 a. *G. Straatman, J. D.Tarasuk and J. MFloryan*
11. J. Heat Transfer 115(2), 395-402 (May 01, 1993) (8pages)doi:10.1115/1.2910691

## PERFORMANCE ANALYSIS OF BOILER IN POWER PLANT -A REVIEW PAPER

P.Papi reddy  
Mechanical Engineering dept  
Malla reddy college of Engg  
Hyderabad, India  
email:papireddy97@rediffmail.com

Dr. Ananth ,professor  
Mechanical Engineering dept  
Malla reddy college of Engg  
Hyderabad,India  
email: subramaniananth@gmail.com.

**Abstract— In India, coal is the dominant source of energy generation. Efficiency of any conventional coal fired unit ranges from 34-38%. This paper presents the efficiency calculation of boiler, turbine and condenser of a 210 MW unit. The study focuses on evaluation of various parameters like dry flue gas loss, wet flue gas loss, moisture in fuel and hydrogen, condenser back pressure, turbine cylinder efficiency, soot formation, etc. and some optimization techniques are mentioned to minimize the same. The benefits of these techniques are considerable fuel saving, emission reduction, heat rate improvement, cost minimization, increased equipment life cycle, etc. Cost analysis through heat rate deviation has been done to determine annual fuel savings. Lastly various critical parameters are mentioned for further improvement of plant performance**

**Index Terms— Coal fired power plant, rankine cycle, boiler efficiency, turbine efficiency, condenser efficiency, heat rate**

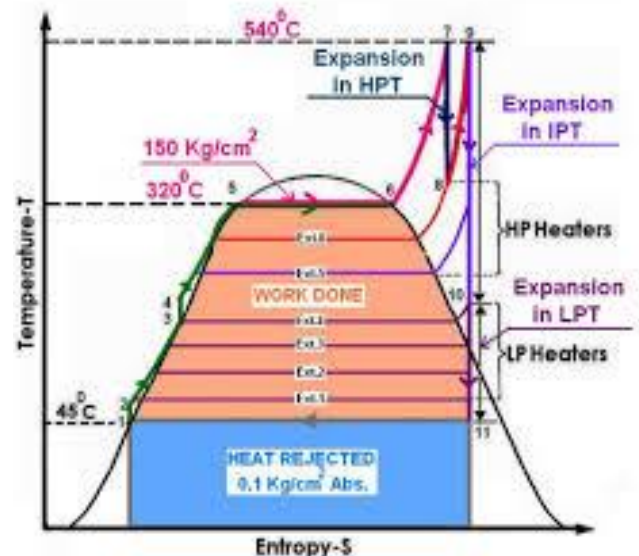
### I. INTRODUCTION

A boiler is an enclosed vessel that provides a means for Combustion heat to be transferred into water until it becomes heated water or steam. The hot water or steam under pressure is then usable for transferring the heat to a process. Water is a useful and cheap medium for transferring heat to a process. When water is boiled into steam its volume increases about 1,600 times, producing a force that is almost as explosive as gunpowder. This causes the boiler to be extremely dangerous equipment that must be treated with utmost care. The process of heating a liquid until it reaches its gaseous state is called evaporation. Heat is transferred from one body to another by means of radiation, which is the transfer of heat from a hot body to a cold body without a conveying medium, convection, the transfer of heat by a conveying medium, such as air or water and conduction,

transfer of heat by actual physical contact, molecule to molecule.

**Boiler Specification:** The heating surface is any part of the boiler metal that has hot gases of combustion on one side and water on the other. Any part of the boiler metal that actually contributes to making steam is heating surface. The amount of heating surface of a boiler is expressed in square meters. The larger the heating surface a boiler has, the more efficient it becomes. The quantity of the steam produced is indicated in tons of water evaporated to steam per hour. Maximum continuous rating is the hourly evaporation that can be maintained for 24 hours. F & A means the amount of steam Generated from water at 100 0C to saturated steam at 100

This condensate is then sent back to boiler through boiler feed pump via low pressure and high pressure heaters.



It works on the principle of modified rankine

cycle. The function of thermal power plant is to generate steam in boiler which is used to drive turbine and generator mounted on the same shaft to produce electricity. The exhaust from low pressure turbine is condensed in condenser and the resultant condensate is extracted through condensate extraction pump.

The CEA in India uses power station heat rate as a proxy for calculating plant efficiency. The heat rate of a power plant is the amount of chemical energy that must be supplied to produce one unit of electrical energy. Some of the heat rate factors that affect power plant performance are ageing of machine, coal quality, plant load factor, operating margins, initial plant design, etc

The basic purpose of a boiler is to turn water into steam, in this case saturated steam. This operation sounds relatively simple but is actually more complicated. Other components and processes such as the deaerator and economizer are necessary to help the overall operation run more efficiently. The boilers utilized on campus are of the stack drum type, which means there are drums within the boilers stacked one above the other. In these particular boilers there are two drums. The upper drum is called a steam drum and is where saturated steam leaves the boiler. While the lower drum is called the mud drum and is where liquid feed water enters. It is also where sediment carried into the boiler settles. Tubes called risers and down comers are used to connect the two drums.

All of the energy required within the boiler is produced by the combustion of a fuel. The burner acts very similar to the gas stove at home, just more complicated. It is comprised of a wind box, igniter, fuel manifold and/or atomizing gun, observation port and flame safety scanner. Currently the boilers can burn either fuel oil or natural gas. Fluctuating prices of fuel can raise or lower the cost to produce steam. Having the choice between two different fuels gives the option of burning the lower cost fuel.

Operation of the boiler begins with feed water entering the mud drum where it is heated. The combustion of fuel within the furnace provides the required energy which is imparted by a combination of convection and radiation. A two-phase water mixture forms within the riser and begins to ascend to the steam drum due to its decreasing density. Boiling to 100% quality in the tubes is undesirable because water vapour has different heat transfer characteristics than liquid

water. This can lead to high wall temperatures and eventual tube burnout. Once it reaches the steam drum the majority of saturated vapour will be removed from the two-phase mixture; there by increasing the remaining mixtures density. The increase in density will initiate its descent in the down comers back to the mud drum. This natural circulation continuously allows for a constant flow of saturated steam exiting the boiler.

Combustion occurs when fossil fuels, such as natural gas, fuel oil, coal or gasoline, react with oxygen in the air to produce heat. The heat from burning fossil fuels is used for industrial processes, environmental heating or to expand gases in a cylinder and push a piston. Boilers, furnaces and engines are important users of fossil fuels. Fossil fuels are hydrocarbons, meaning they are composed primarily of carbon and hydrogen. When fossil fuels are burned, carbon dioxide (CO<sub>2</sub>) and water (H<sub>2</sub>O) are the principal chemical products, formed from the reactants carbon and hydrogen in the fuel and oxygen (O<sub>2</sub>) in the air. The simplest example of hydrocarbon fuel combustion is the reaction of methane (CH<sub>4</sub>), the largest component of natural gas, with O<sub>2</sub> in the air.

When this reaction is balanced, or stoichiometric, each molecule of methane reacts with two molecules of O<sub>2</sub> producing one molecule of CO<sub>2</sub> and two molecules of H<sub>2</sub>O. When this occurs, energy is released as heat. The combining of oxygen (in the air) and carbon in the fuel to form carbon dioxide and generate heat is a complex process, requiring the right mixing turbulence, sufficient activation temperature and enough time for the reactants to come into contact and combine.

Unless combustion is properly controlled, high concentrations of undesirable products can form. Carbonmonoxide (CO) and soot, for example, result from poor fuel and air mixing or too little air. Other undesirable products, such as nitrogen oxides (NO, NO<sub>2</sub>), form in excessive amounts when the burner flame temperature is too high. If a fuel contains sulphur, sulphur dioxide (SO<sub>2</sub>) gas is formed. For solid fuels such as coal and wood, ash forms from incombustible materials in the fuel.

## II. METHODOLOGY

### Performance of Boiler

Boiler is an enclosed pressure vessel where heat generated by combustion of fuel is transferred to water to become steam. Boiler efficiency is defined as the heat added to the working fluid expressed as a percentage of heat in the fuel being burnt

### Direct Method

The energy gain of the working fluid (water and steam) is compared with the energy content of the boiler fuel.

$$\eta = \frac{(hg - hf) * Q}{q * GCV} * 100$$

Where,

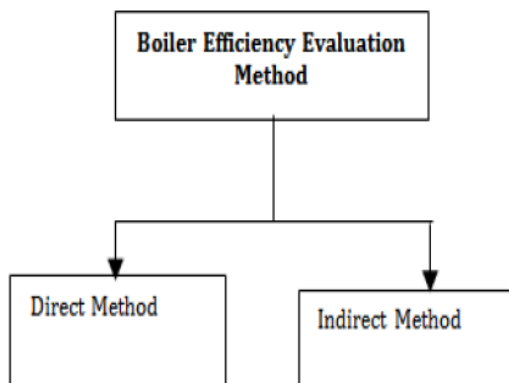
hg – Enthalpy of saturated steam in kCal/kg of steam

hf – Enthalpy of feed water in kCal/kg of water

Q – Quantity of steam generated per hour (Q) in kg/hr.

q – Quantity of fuel used per hour (q) in kg/hr

GCV – gross calorific value of the fuel in kCal/kg of fuel



### Indirect Method or Heat Loss Method:

The efficiency is the difference between the

losses and the energy input.

The main advantage of indirect method is that the errors obtained from this method do not make any major change in the efficiency.

Thus if boiler efficiency is 90% an error of 1% in direct method will result in significant change in efficiency, i.e.

$$90C \pm 0.9 = 89.1 \text{ to } 90.9$$

Whereas in indirect method, 1% error in measurement of losses will result in;

$$\begin{aligned} \text{Efficiency} &= 100 - (10 \pm 0.1) \\ &= 90 \pm 0.1 = 89.9 \text{ to } 90.1 \end{aligned}$$

Accountable losses in coal fired boilers are:

- Heat loss due to dry flue gas as sensible heat (L1)
- Un-burnt losses in bottom ash as carbon (L2).
- Heat loss due to moisture in the coal (L3).
- Heat loss due to moisture from burning of hydrogen in coal (L4).
- Heat loss due to moisture in air (L5).
- Heat loss due to incomplete combustion of carbon (L6)
- Loss due to surface radiation and convection (L7).

Theoretical air requirement=

$$= \frac{[(11.6 * C) + \{34.8 * (H_2 - O_2/8)\}] + (4.35 * S)}{100}$$

$\frac{kg}{kg}$  of fuel

Excess air supplied

$$= \frac{O_2\%}{21 - O_2\%} * 100$$

Actual mass of air supplied/kg of fuel (AAS) =

$$\left\{ 1 + \frac{EA}{100} \right\} * \text{Theoretical air}$$

1) Percentage heat loss due to dry flue gas

$$= \frac{m * cp * (T_f - T_a)}{GCV \text{ of fuel}} * 100$$

Where;

m = mass of dry flue gas in kg/kg of fuel  
 Cp = Specific heat of flue gas (0.23 kcal/kg 0C)

2) Percentage heat loss due to unburnt carbon in bottom ash =

$$= \frac{\text{Total ash collected} / \text{kg of fuel burnt} * \text{GCV of bottom ash}}{\text{GCV of fuel}} * 100$$

3) Percentage heat loss due to evaporation of moisture present in fuel

$$= \frac{M * \{584 + cp * (Tf - Ta)\}}{\text{GCV of fuel}} * 100$$

Where,

M – kg of moisture in 1kg of fuel  
 Cp – Specific heat of superheated steam (0.45 kcal/kg)0C  
 \* 584 is the latent heat corresponding to the partial pressure of water vapour.

4) Percentage heat loss due to evaporation of water formed due to H2 in fuel

$$= \frac{9 * H2 * \{584 + cp * (Tf - Ta)\}}{\text{GCV of fuel}} * 100$$

Where,

H2 – kg of H2 in 1 kg of fuel  
 Cp – Specific heat of superheated steam (0.45 kcal/kg 0C)

5) Percentage heat loss due to moisture present in air

$$= \frac{\text{AAS} * \text{humidity factor} * cp * (Tf - Ta)}{\text{GCV of fuel}} * 100$$

Where,

Cp – Specific heat of superheated steam (0.45 kcal/kg 0C)

6) Percentage heat loss due to incomplete combustion

$$L_6 = \frac{\% \times C \times 5744}{(\% CO + \% CO_2) \times \text{GCV of coal}} \times 100$$

Where,

L5 = % Heat loss due to partial conversion of C to CO  
 CO = Volume of CO in flue gas leaving economizer (%)  
 CO2 = Actual Volume of CO2 in flue gas (%)  
 C = Carbon content kg / kg of fuel

7) Percentage heat loss due to radiation and other unaccounted loss

Unaccounted losses include losses from boiler casing to surrounding, loss due to combination of carbon and water, heat carried away in ash, losses due to unburnt volatile matter, heat loss due to bottom seal water. Radiation loss depends on the effectiveness of the boiler casing insulation.

In a relatively small boiler, with a capacity of 10 MW, the radiation and unaccounted losses could amount to between 1% and 2% of the gross calorific value of the fuel, while in a 500 MW boiler, values between 0.2% to 1% are typical. The loss may be assumed appropriately depending on the surface condition.

Boiler efficiency ( $\eta$ ) = 100 – (1 + 2 + 3 + 4 + 5 + 6 + 7)

**Table 1 Losses in boiler by indirect method**

Sl. No.	Heat losses (%)	Design	Corrected
1.	L1	4.46	5.38
2.	L2	0.49	0.63
3.	L3	2.64	2.68
4.	L4	3.49	3.54
5.	L5	0.13	0.16
6.	L6	0.02	0.02
7.	L7	1.21	1.06
	$\eta$ of boiler	87.56	86.53

**Performance of Turbine**

**Table 2 Heat rate deviation of different parameters**

Sl.No.	Particulars	Unit	Design	Operation	UHR Loss (Kcal/Kwh)
1.	Partial loading	%		0	0
2.	LPT. Exhaust steam temp Cond. Backpressure	°C Ksc	43.2 0.089	43.5 0.91	-2
3.	D.M. make up	T/Hr		6.25	-11
4.	Final F.W. temp.	°C	247	251.44	0
5.	R.H. spray	T/Hr	0	15.75	-12
6.	Main steam press.	KSC	129	124.57	-9
7.	Main steam temp.	°C	537	533.36	-1
8.	HRH steam temp.	°C	537	537.15	0
9.	oxygen	%	3.5	2.73	0
10.	F1.gas temp. at RAH O/L[left] F1.gas temp. at RAH O/L[right]	°C °C		146.23 146.57	-8
11.	Turbine cycle eff. Loss (Other than Ageing)	%	0		-18
12.	Carbon in bottom ash	%	2	2.1	0

### Performance of Condenser

Condensers are devices in which cooling water is used to condensate the exhaust steam from the steam turbine.

The primary objective of a condenser is to maintain a very low back pressure on the exhaust side low pressure turbine. This enables the steam to expand to a greater extent which results in an increase in available energy for converting into mechanical work. [Shende M.B. *et al*, 2015]. Following formula is used for calculating condenser efficiency:

Condenser efficiency = rise in temperature of cooling water [Saturation temp corresponding to the absolute pressure in the condenser] - [inlet temp of cooling of water

Steam turbine is a mechanical device that extracts thermal energy from pressurized steam, and converts it to useful mechanical work. The steam turbines are split into three separate stages, High Pressure (HP), Intermediate Pressure (IP) and Low Pressure (LP) stage, which are mounted on the same shaft along with generator. [Kumar *et al*, 2013].

Turbine efficiency is defined as the ratio of mechanical work output in kcal (or KJ) to the total heat available across the turbine in kcal (or kJ) expressed as a percentage.

Following formulas are used for calculating turbine efficiency

1) Total accountable losses+ Design heat rate= Unit heat rate

2) Accountable losses of turbine + Design turbine heat rate= Turbine heat rate

3) Turbine cycle efficiency

$$= \frac{860}{\text{turbine heat rate}} * 100$$

**Table 3** Condenser performance parameters

Sl.No.	Particulars	Unit	Design	Operational
1.	Vacuum	Ksc	0.91	0.909
2.	CW O/L Temp	°C	38.4	39.45
3.	CW I/L Temp	°C	30	28.9
4.	LPT Exhaust Temp	°C	43.2	43.5
5.	CW temp. rise	°C	10	10.54

### III. EFFICIENCY CALCULATION

Step- 1)

DTCHR of 210 MW is 2021 kcal/kwh.

GTCHR=24+2021

$$= 2045 \text{ kcal /kwh}$$

Step-2)

$$\text{Turbine } \eta = \frac{860}{\text{turbine heat rate}} * 100$$

Turbine  $\eta$ = 42.05%

Step -3)

UHR=GTCHR/Boiler Efficiency

$$=2045/86.53$$

=2363 kcal/kwh

Step -4)

Condenser  $\eta$

= Rise in cooling water temperature

LPT exhaust temp – Inlet temp. of c.w

= 0.7219

Step-5)

$$\text{Plant } \eta = \frac{860}{\text{Unit heat rate}} * 100$$

$$= 35.9\%$$

#### IV. COST BENEFIT ANALYSIS

Heat rate is helpful in determining how efficiently any unit is being operated, as lower is the heat rate higher will be the operational efficiency. For identifying the performance of either any unit or unit equipments, heat rate deviation is used instead of heat rate. This heat rate deviation can be converted into cost for calculating annual fuel cost. Cost calculation using heat rate instead of heat rate deviation is often overlooked in a thermal power plant.

Heat rate deviation in helpful in identifying the problem in any equipment or auxiliary, and its magnitude is helpful in assigning priority level to these problems. Since, heat rate deviations can be converted into cost, it is helpful in solving the highest priority problems first so as to minimize the amount of fuel consumption.

Cost of heat rate deviation = heat rate deviation\*net generation\* fuel cost

An increase in heat rate results in increasing the fuel consumption whereas any decrease in heat rate results in reduction of fuel requirement for producing a given number of KWH of energy. Heat rate also plays a key role in any purchasing decision, be it fuel, oil, or any equipment, etc.

**Table 4 Cost of heat rate deviation**

Sl. No.	Particulars	Unit	UHR Loss (Kcal/kWh)	Cost of heat rate deviation (Rs)
1.	Partial loading	%	0	0
2.	LPT. exhaust steam temp	Deg C		
	Cond. backpressure	Ksc	-2	-34.06
3.	D.M. make up	T/Hr	-11	-187.33
4.	Final F.W. temp.	Deg C	0	0

In above table, cost of heat rate deviation of each parameter has been calculated where,

Net generation= gross generation-auxiliary power consumption  
= 195.41MW

Fuel cost = Rs 610/ton or Rs 87.2/106 kcal

-ve sign of heat rate deviation indicates the better performance of plant and +ve sign indicates poor performance of plant.

From table, we get cost of heat rate deviation= Rs -1038.83

(-) sign indicates the cost saving in fuel.

Annual cost of heat rate deviation

= heat rate fuel cost

\* unit rating \* PLF

\* hrs in a year

$$=2452 * \frac{87.2}{10^6} * 210 * 1000 * 1.01 * 8760$$

$$=Rs 397,266,299.9 /yr$$

$$=2452 * \frac{87.2}{10^6} * 210 * 1000 * 1.01 * 8760$$

$$=Rs 271,399,749.5 /yr$$

If 1% heat rate is reduced then annual cost of fuel would be

Annual cost of heat rate deviation

$$=2452 * \frac{87.2}{10^6} * 210 * 1000 * 1.01 * 8760 * 0.01$$

$$=Rs 3,972,662.99 /yr$$

$$=Rs 3,972,662.99 /yr$$

Annual cost of heat rate deviation

$$2452 * \frac{87.2}{10^6} * 210 * 1000 * 1.01 * 8760 * 0.69$$

$$= 2,713,997.49 /yr$$

$$= 2,713,997.49 /yr$$

This is the annual saving in fuel cost just by 1% improvement in heat rate.

Some the areas where heat rate improvement can result in tremendous improvement of overall heat rate are mentioned below.

- By giving heat rate awareness training to operation staff:- 0.5% to 1%
- Heat rate information availability to plant personnel:- 0.5% to 1.5%
- By proper utilization of controllable losses information by operation staff:- 0.75% to 1%
- By conducting routine testing program at regular intervals:- 0.7% to 2%
- By increasing the routine monitoring of feed water heater performance:- 0.3% to 0.6%
- By optimizing soot blower operation:- 0.7%

Maximum improvement in heat rate ranges from approximately 3 to 5% for this unit. This could save annual cost of fuel from Rs 8,141,992.48 /yr to Rs 13,569,987.48 /yr (for 2015-16 financial year).

## V. DISCUSSION

### Dry flue gas loss optimization

The dry flue gas loss depends on two factors. They are excess air and air heater gas outlet temperature.

#### Excess air control

For every 1% reduction in excess air there is approximately 0.6% rise in efficiency. Excess air is monitored by CO<sub>2</sub> and O<sub>2</sub> measurements at air heater inlet.

Air infiltration should be controlled to limit this loss. Various methods like oxygen analyzers, draft gauges and stack damper control can be used to calculate readings of excess air.

#### 5.1.2 Air heater gas outlet temperature optimization:-

It should be lowest from overall efficiency point of view, whereas should be high on account of corrosion problem. For Indian coals having low percentage (approx

(0.5%)) of Sulphur, this specified temperature is of the order . A rise in air heater gas outlet temperature reduces boiler efficiency by some of the causes of his gas outlet temperature are lack of soot blowing, high excess air, low final feed water temperature, improper combustion, poor milling, air in leakage before the combustion chamber, etc. Though in the short run, low air heater gas outlet temperature improves efficiency; in the long run it can result in low boiler efficiency because of deposition on its elements and corrosion.

Most obvious cause of low air heater gas outlet temperature is lighting and firing a cold boiler. Its remedy is to bypass the air heater until the gas temperature is high enough to permit normal operation. It's another reason is air leakage across air heater seals. The rate of air leakage varies with the square root of the differential pressure across the air heater.

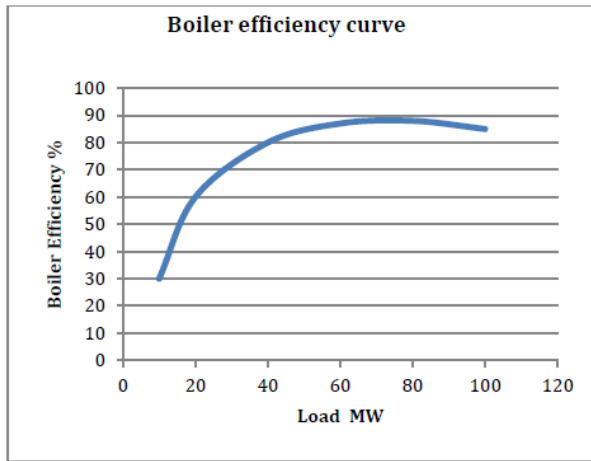
### Wet flue gas loss optimization

Losses due to moisture in fuel, hydrogen in fuel and moisture in combustion air depends on final gas outlet temperature. These losses decrease slightly with fall in boiler output.

Power plant waste heat can be used to remove moisture before pulverization process which can provide heat rate and emission benefits, reduce maintenance cost and it will also be reducing cooling water makeup requirement.

### Carbon in ash loss optimization

This loss depends on the fineness of pulverized fuel, excess air and combustion condition. If combustion is not monitored properly the loss which is normally about 1% may be as high as 4-5%. Some of the causes of high carbon content in ash are coarse grinding, mal adjustment of flame, unequal loading of different mills, incorrect primary air temperature, etc.



pressure (i.e. lower condenser vacuum) for a design specified cooling water temperature rise and terminal temperature difference. Hence low inlet temperature values must be maintained.

Reduced cooling water flow rate shall increase the cooling water temperature rise, which leads to higher saturation temperature at design terminal temperature difference and corresponding saturation pressure.

Condensate level in the hot well if gets more than design value, will lead to improper heat transfer because it will cover some of the cooling water tubes thereby making them unavailable for condensation.

**Turbine efficiency optimization**

Turbine cylinder efficiency is around 85%, 92% and 80-85% for HP, IP and LPT respectively. Some of the losses that occur in stem path are loss due to solid particle erosion of moving blades, solid particle erosion and roughness of diaphragm blades and damage of the fins of shaft blades.

Optimization of these losses can help in turbine cylinder efficiency improvement. It can be done by taking measures like increasing the turbine exit annulus area, lowering the kinetic energy of the steam as it leaves the last stage blade, steam blowing should be done after boiler Overhauling, Replacement of all Tip Seals, Inter stage & Gland Seals in every capital overhauling, Strict & vigilant control on water chemistry, using additives in feed water to reduce surface tension due to formation of water droplets, etc.

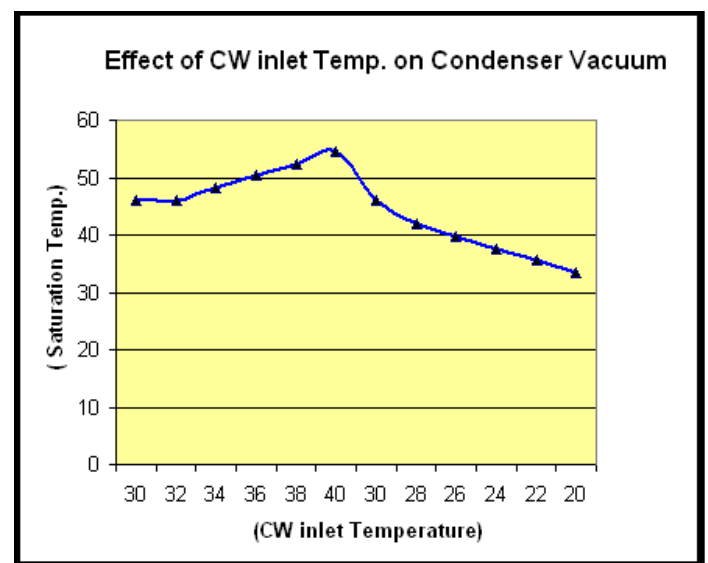
**Condenser vacuum optimization**

Heat loss from thermal power plant is mainly due to heat rejection through the condenser. A difference of 5% in cooling water inlet temperature changes unit heat consumption by around 1%. It can be done by following ways:

- High cooling water inlet temperature leads to higher saturation temperature and corresponding rise in condenser saturation

Internal and external tube deposit causes high terminal temperature difference which can be minimized by on-line condenser tube cleaning and better de-mineralized water quality management respectively.

Air ingress results in poor heat transfer coefficient which increases condensing temperature in order to get heat across air barrier, this makes the vacuum worst. It can be avoided by frequent leak detection test and effective steam sealing of low pressure turbine.



### Steam temperature control

One of the techniques used to prevent excessively high steam temperatures at the inlets to the high pressure and intermediate pressure turbines is to spray liquid H<sub>2</sub>O into the steam. Referred to as attemperating spray, these liquid flows are taken from the turbine cycle and result in an increase in heat rate.

Consequently, attemperating spray flow rates should be the minimum flow rates needed to control steam temperatures to the design levels. If main steam and hot reheat steam were at lower than desired temperatures, while both main steam and hot reheat attemperating sprays were in operation, then it will result in heat rate penalties due to low steam temperatures and to use of attemperation when it was not needed. Thus an upgrade to the steam temperature controls and perhaps repair of leaking flow control valves would be needed to prevent this type of loss.

### Scaling and soot abatement

Factors favoring soot formation are high temperature and shortage of oxygen. Elevated stack temperature indicates soot deposition as well as scaling on the water side. With every 22% C increase in stack temperature, 1% efficiency loss occurs in boilers. Practices like periodic off-line cleaning of radiant furnace surfaces, boiler tube banks, economizers and air heaters are necessary to remove scaling and soot formation.

## VI. RESULTS

Following results have been concluded

- 5% change in excess air changes dry flue gas loss by 1%.
- Radiation and convection losses are around 0.4 to 1%
- A difference of 5% in cooling water temperature changes the unit heat consumption by 1%.
- Condenser vacuum should be maintained at 0.89 to 0.9 ksc.
- By combustion optimization heat rate reduction in the range of 0.5% to 1 % can be achieved.

- By upgrading steam turbine generators and enhancement of auxiliary component can lead to improvement of 2 to 4%.
- By reducing steam, water and internal leakage heat rate can be improved by 0.5%.

## VII. CONCLUSION

Also following critical parameters must be observed so as to further increase the plant performance:

- Main steam temperature and pressure should be increased
- Re-heater spray should be decreased
- Condenser vacuum should be decreased
- Turbine cylinder efficiency should be increased
- Dry flue gas loss should be decreased
- Un-burnt carbon percentage should be decreased
- Moisture in fuel should be decreased
- Moisture in combustion air should be decreased
- Heat rate should be decreased
- Plant should be operated at full load for maximum efficiency.

## VIII. FUTURE SCOPE

By regular heat rate improvement program, efficiency can be increase to an extent. Following aspects can be further studied to improve plant efficiency. They are-

Air ingress deteriorates the heat transfer coefficients. There by increasing the condensing temperature in order to get heat across air barrier. This makes the vacuum worse.

Re heater pressure drop adversely affect the HPT exhaust pressure, thereby affecting the IPT inlet pressure

## IX. REFERENCES

- [1] Dhanre G.T, Dhanre U.T. and Mudafale K., (2014), Review Paper on Energy Audit of a Boiler in Thermal Power Plant, IJSR, vol.2, issue 6, Oct-Nov 2014.
- [2] Kurkiya R and Chaudhary S (2012), Energy Analysis of Thermal Power Plant , International Journal of Science & Engineering Research Volume (IJSER), VOL-3, ISSUE-7, July-2012
- [3] Kumar, C. K. and G. S. Rao (2013). Performance analysis from the energy audit of a thermal power plant, International Journal of Engineering trends and Technology (IJETT), ISSN: 2231-5381.
- [4] Shende M.B, Shinde N. N., Desai S. B.and Wagh M.M., (2015), Performance of Thermal Power Plant on System Based, IRJET, vol.2, issue.4, july-2015
- [5] Robert J.Tramel (2000), Heat rate improvement guidelines for Indian Power Plants, volume 1, 2United States Tennessee Valley Authority , June 2000
- [6] Palo Alto (2014), Range and Applicability of heat rate improvements, EPRICA:2014, 3002003457
- [7] Vinchurkar A.G, Lakhe R.R and Shrivastava R.L (2014). Energy efficiency analysis of thermal plant boilers, IJRME, vol 2,issue 3,May-June-2014.
- [8] Singh, S. P., Philip G., Singh S.K. (2014), Effect of condenser vacuum on performance of a Reheat Regenerative 210 MW Fossil-Fuel based Power Plants, IJETAE, vol 4,issue 1,Feb-2014.

## Improvement of an Automobile Radiator using Thermal Analysis

**S.Vinay (M.Tech)**  
**Mechanical Engineering**  
**Malla Reddy College of Engineering**  
**Hyderabad, India**  
**Email:vinaysonnaitenkam@gmail.com**

**Dr.Karthikeyan, Ph.d**  
**Mechanical Engineering**  
**Malla Reddy College of Engineering**  
**Hyderabad, India**  
**Email:karthirajme@gmail.com**

**Abstract:** Radiators are used to transfer thermal energy from one medium to another for the purpose of cooling. Radiators are used for cooling internal combustion engines, mainly in automobiles but also in pistonengine aircraft, railway locomotives, motorcycles, stationary generating plant. The radiator transfers the heat from the fluid inside to the air outside, thereby cooling the fluid, which in turn cools the engine. Research is being carried out for several decades now, in improving the performance of the heat exchangers, having high degree of surface compactness and higher heat transfer abilities in automotive industry. These compact heat exchangers have fins, louvers and tubes. In this project we are designing a radiator without louver fins and with louver fins. The original radiator has no louver fins, we are modifying that by giving louver fins. 3D model is done in Pro/Engineer.  
**Keywords:** Ansys Milling, Taguchi, H13 Steel.

Notwithstanding that such devices tend to transfer heat mainly by convection and might logically be called convectors. The term "convector" refers to a class of devices in which the source of heat is not directly exposed.



**Fig.1. Water-air convective cooling radiator.**

### I. INTRODUCTION

#### A. Introduction to Automobile Radiator

Radiators are heat exchangers used to transfer thermal energy from one medium to another for the purpose of cooling and heating. The majority of radiators are constructed to function in automobiles, buildings, and electronics. The radiator is always a source of heat to its environment, although this may be for either the purpose of heating this environment, or for cooling the fluid or coolant supplied to it, as for engine cooling. Despite the name, radiators generally transfer the bulk of their heat via convection, not by thermal radiation, though the term "convector" is used more narrowly; see radiation and convection, below. The Roman hypocaust, a type of radiator for building space heating, was described in 15 AD. The heating radiator was invented by Franz San Galli, a Polish-born Russian businessman living in St. Petersburg, between 1855 and 1857.

#### B. Radiation and Convection

One might expect the term "radiator" to apply to devices that transfer heat primarily by thermal radiation (see: infrared heating), while a device which relied primarily on natural or forced convection would be called a "convector". In practice, the term "radiator" refers to any of a number of devices in which a liquid circulates through exposed pipes (often with fins or other means of increasing surface area),

#### C. Introduction To Pro/Engineer

Pro/ENGINEER, PTC's parametric, **integrated** 3D CAD/CAM/CAE solution, is used by discrete manufacturers for mechanical engineering, design and manufacturing. Created by Dr. Samuel P. Geisberg in the mid-1980s, Pro/ENGINEER was the industry's first successful parametric, 3D CAD modeling system as shown in Fig.1. The parametric modeling approach uses parameters, dimensions, features, and relationships to capture intended product behavior and create a recipe which enables design automation and the optimization of design and product development processes. This powerful and rich design approach is used by companies whose product strategy is family-based or platform-driven, where a prescriptive design strategy is critical to the success of the design process by embedding engineering constraints and relationships to quickly optimize the design, or where the resulting geometry may be complex or based upon equations. Pro/ENGINEER provides a complete set of design, analysis and manufacturing capabilities on one, integral, scalable platform. These capabilities, include Solid Modeling, Surfacing, Rendering, Data Interoper-

ability, Routed Systems Design, Simulation, Tolerance Analysis, and NC and Tooling Design.

Companies use Pro/ENGINEER to create a complete 3D digital model of their products. The models consist of 2D and 3D solid model data which can also be used downstream in finite element analysis, rapid prototyping, tooling design, and CNC manufacturing. All data is associative and interchangeable between the CAD, CAE and CAM modules without conversion. A product and its entire bill of materials(BOM) can be modeled accurately with fully associative engineering drawings, and revision control information. The associativity in Pro/ENGINEER enables users to make changes in the design at any time during the product development process and automatically update downstream deliverables. This capability enables concurrent engineering design, analysis and manufacturing engineers working in parallel and streamlines product development processes. Pro/ENGINEER is an integral part of a broader product development system developed by PTC. It seamlessly connects to PTC's other solutions including Windchill, ProductView, Mathcad and Arbortext.

**II. DIFFERENT MODULES IN PRO/ENGINEER**

- Part Design
- Assembly
- Drawing
- Sheetmetal
- Manufacturing



**Fig.2. Model of Radiator.**

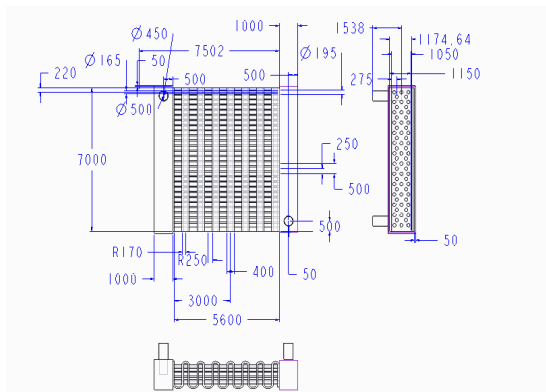


**Fig.3. 2D Drawing.**

**III. THERMAL ANALYSIS**

**A. Without Louver FINS**

Set Units - /units,si,mm,kg,sec,k  
 File- change Directory-select working folder  
 File-Change job name-Enter job name  
 Select element-Solid-20node 90

**B. Material Properties – Aluminum Alloy 6061**

Density – 0.0000027 Kg/mm<sup>3</sup>  
 Thermal Conductivity – 180W/mK  
 Specific Heat – 896 J/Kg K

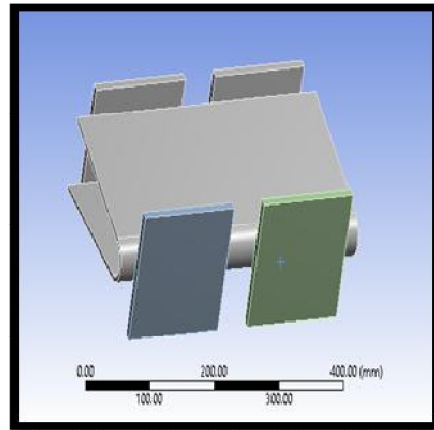


**Fig.4. Imported Model.**

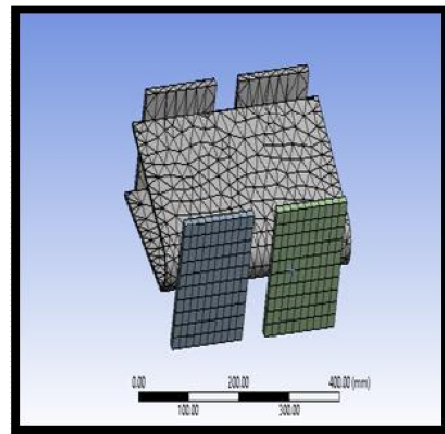


**Fig.5. Meshed model.**

Apply Thermal-Temperature- on Area=353K

Convections – on Area-Film Co-efficient– 0.034 W/mm<sup>2</sup> K

Bulk Temperature – 303 K

**Performance Improvement of an Automobile Radiator using CFD Analysis**

**IV. RESULTS**

Results of this paper is as shown in Figs.6 to 12.

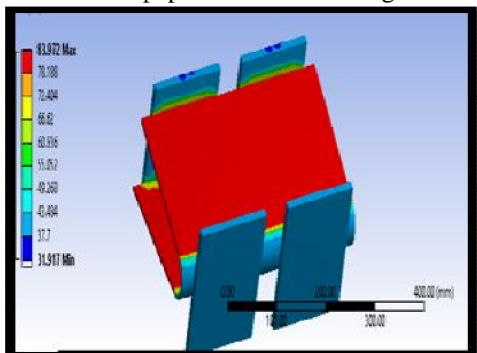


**Fig.6. Temperature.**

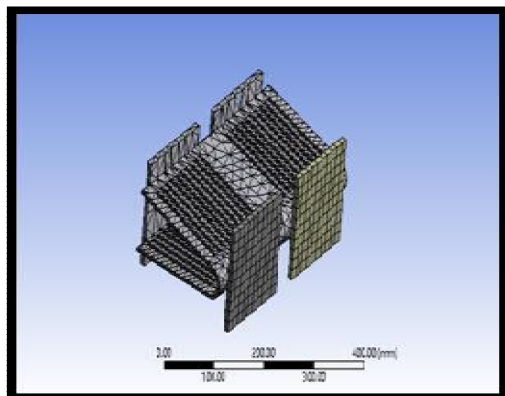


**Fig.9. Meshed model.**

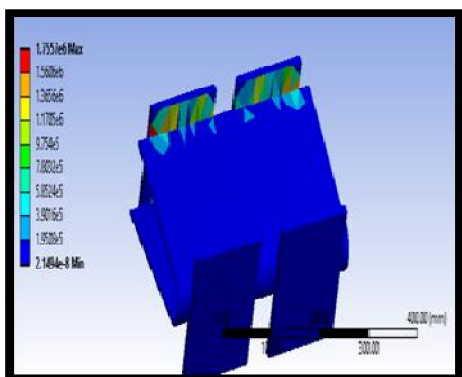


**Fig.7. Thermal error.**

**Loads:**

Apply Thermal-Temperature- on Area=353K  
 Convections – on Area-Film Co-efficient – 0.034 W/mm<sup>2</sup>  
 K  
 Bulk Temperature – 303 K

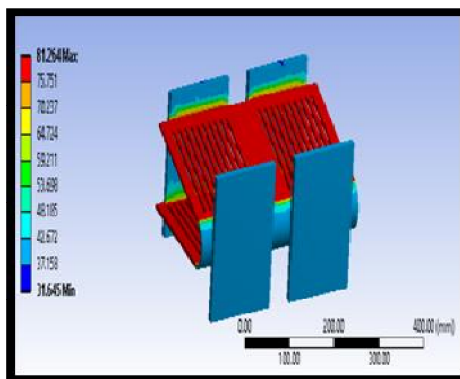


**Fig.10. Temperature.**

**A. Heat Flux**

**With Louver FINS:**

Set Units - /units,si,mm,kg,sec,k  
 File- change Directory-select working folder  
 File-Change job name-Enter job name  
 Select element-Solid-20node 90  
 Material Properties  
 Youngs Modulus =

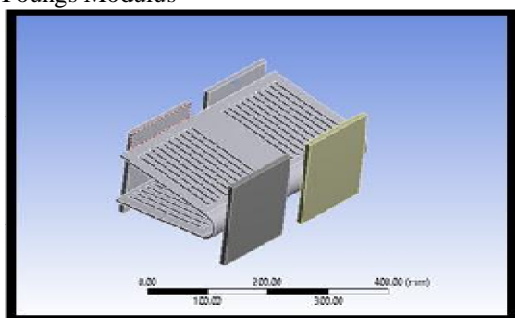


**Fig.8. Imported.**

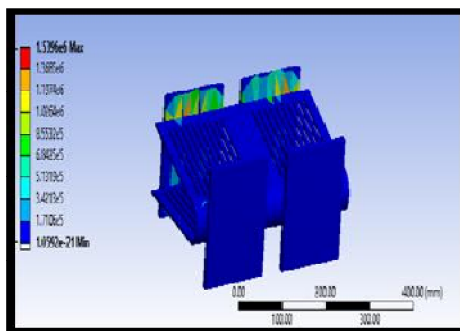


**Fig.11. Thermal error**

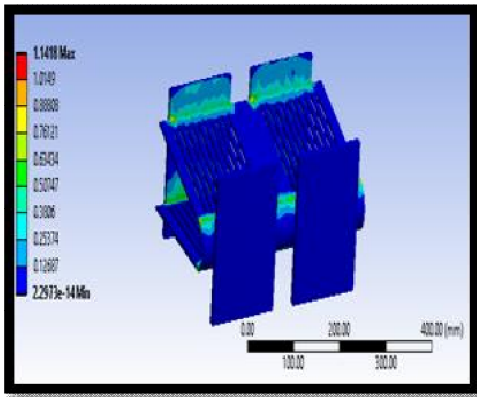


Fig.12. Heat flux.

**B. Results Table CFD Analysis**

**TABLE I: Original Model**

	Mass flow rate (Kg/sec)			
	0.08 kg/sec	0.140 kg/sec	0.210 kg/sec	0.280 kg/sec
Pressure (Pa)	1.56e+01	2.82e+01	4.35e+01	5.94e+01
Velocity (m/s)	1.02e+00	1.77e+00	2.64e+00	3.51e+00
Temperature (K)	3.53e+02	3.53e+02	3.53e+02	3.53e+02
Mass Flow Rate (Kg/S)	1.147e-06	9.8341e-07	2.5331e-07	5.3644e-07
Total Heat Transfer rate at wall (W)	2749	3011	3149	3225

**TABLE II: With Louver FINS**

	Mass flow rate (Kg/sec)			
	0.08 kg/sec	0.140 kg/sec	0.210 kg/sec	0.280 kg/sec
Pressure (Pa)	1.17e+02	2.14e+02	3.37e+02	4.68e+02
Velocity (m/s)	1.44e+00	2.50e+00	3.73e+00	4.94e+00
Temperature (K)	3.53e+02	3.53e+02	3.53e+02	3.53e+02
Mass Flow Rate (Kg/S)	4.616e-06	2.920e-06	2.840e-06	3.069e-06
Total Heat Transfer rate at wall (W)	5961	7463	8346	8872

**TABLE III: Thermal Results**

	With louvers	Without louvers
Temperature (°C)	81.264	83.972
Thermal Error	1.5396e6	1.7557e6
Heat Flux (W/mm <sup>2</sup> )	1.1418	0.98837

**V. CONCLUSION**

In this project a radiator is designed without louver fins and with louver fins. The original radiator has no louver fins, it has been modified by specifying louver fins. 3D model is designed in Pro/Engineer. The analysis tool ANSYS is used to perform CFD analysis on radiator at different mass flow rates. By observing the analysis results, the velocity is increased by 29.16%, pressure is increased by 86.66% and heat transfer rate at walls is increased by 53.88% for the modified model than the original that is the radiator with louvered fins.

performed to analyze the heat transfer rate to determine the thermal flux. The material taken is Aluminum alloy 6061 for thermal analysis. By observing the thermal analysis results, thermal flux is increased by 13.43% for the modified model. So it can be concluded that modifying the radiator model with louver fins yields better results. Ultimately it can be summarized that by providing louvers for the radiator and increasing the louver pitch helped in reducing the pumping power requirements with increase in heat transfer rate. This will help in increasing the power output per unit mass of the radiator. Hence it is recommended to increase the louver spacing for the geometry under consideration.

**VI. REFERENCES**

[1] Performance Improvement of a Louver-Finned Automobile Radiator Using Conjugate Thermal CFD Analysis by Junjanna G.C.

[2] Performance Investigation of an Automotive Car Radiator Operated With Nanofluid as a Coolant by Durgesh kumar Chavan and Ashok T. Pise Sahin.

[3] Heat Transfer Enhancement of Automobile Radiator with TiO<sub>2</sub>/Water Nanofluid by Paresh Machhar, Falgun Adroja.

[4] Wolf, I., Frankovic, B., Vilicic, I., A numerical and experimental analysis of neat transfer in a wavy fin and tube heat exchanger, Energy and the Environment (2006) pp.91-101.

[5] Wang, C.C., Lo, J, Lin, Y.T. Wei, C.S., Flow visualization of annular and delta winlet vortex generators in fin and tube heat exchanger application, International Journal of Heat and Mass Transfer, 45, (2002), pp.3803-3815.

[6] Leu, J.S., Wu, Y.H., Jang, J.Y., Heat transfer and fluid flow analysis in plate-fin and tube heat exchangers with a pair of block shape vortex generators, International Journal of Heat and Mass Transfer, 47 (2004), pp. 4327-4338.

## DESIGN AND CFD ANALYSIS OF HAIR PIN HEAT EXCHANGER AT DIFF NANO FLUIDS

M.Renuka  
Mechanical Engineering dept  
Malla reddy college of Engg  
Hyderabad, India  
email:mathangirenuka94@gmail.com

Dr. Velmurugan  
Mechanical Engineering dept  
Malla reddy college of Engg  
Hyderabad,India  
email: velmurugan\_mech@mrce.in

### ABSTRACT

Heat exchanger is a device used to transfer heat between one or more fluids. The fluids may be separated by a solid wall to prevent mixing or they may be in direct contact. In this thesis, glycerin(40%) fluid is mixed with base fluid water(60%) are calculated for their combination properties. The nano fluid is titanium carbide, magnesium Oxide and silver nano particle for weight percentage 0.2%, 0.5%, 0.7% & 1.0%. Theoretical calculations are done determine the properties for nano fluids and those properties are used as inputs for analysis. Hair pin Exchangers are available in single tube(double pipe) or multiple tubes within a hairpin shall (multi tube),bare tubes,finned tubes,U-tubes,straight tubes,fixed tube sheets and removable bundle.

### INTRODUCTION

Heat exchangers are one of the mostly used equipment in the process industries. Heat Exchangers are used to transfer heat between two process streams. One can realize their usage that any process which involve cooling, heating, condensation, boiling or evaporation will require a heat exchanger for these purpose. Process fluids, usually are heated or cooled

before the process or undergo a phase change. Different heat exchangers are named according to their application. For example, heat exchangers being used to condense are known as condensers, similarly heat exchanger for boiling purposes are called boilers Usually, there is lots of literature and theories to design a heat exchanger according to the requirements.

Heat exchangers are of two types:-

Where both media between which heat is exchanged are in direct contact with each other is Direct contact heat exchanger, Where both media are separated by a wall through which heat is transferred so that they never mix, Indirect contact heat exchanger.

A typical heat exchanger, usually for higher pressure applications up to 552 bars, is the shell and tube heat exchanger. Shell and tube type heat exchanger, indirect contact type heat exchanger. It consists of a series of tubes, through which one of the fluids runs. The shell is the container for the shell fluid. Generally, it is cylindrical in shape with a circular cross section, although shells of different shape are used in specific applications. For this

particular study shell is considered, which a one pass shell is generally. A shell is the most commonly used due to its low cost and simplicity, and has the highest log-mean temperature-difference (LMTD) correction factor. Although the tubes may have single or multiple passes, there is one pass on the shell side, while the other fluid flows within the shell over the tubes to be heated or cooled. The tube side and shell side fluids are separated by a tube sheet.

### 1.1 TUBULAR HEAT EXCHANGERS

A tubular heat exchanger can either consist of a smaller-diameter tube mounted inside a larger diameter tube (“double-pipe exchanger”, see Figure 1) or, more commonly, a tube bundle inside a shell (“shell-and-tube exchanger”, see Figure 1.1). Thus, heat transfer surfaces are plain or enhanced tubes. Additionally, shell-and-tube heat exchangers can contain multiple-pass tube bundles, i.e., for double-pass we have a bundle of U-tubes, for triple-pass the tubes in the bundle bend twice, etc. Multiple-pass shells are common as well. Baffles, either segmental or doughnut and disc ones, present in the shell direct fluid flow in shell-side, support the tubes, and limit possible tube vibrations.



Figure 1: Countercurrent double-pipe heat exchanger

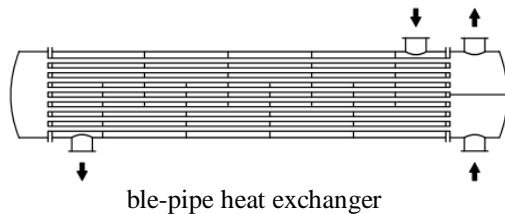
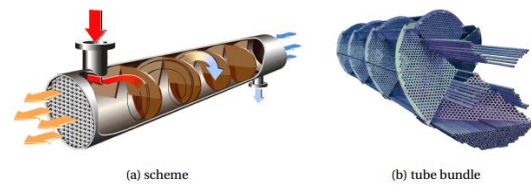


Figure 1.1: Shell-and-tube heat exchanger

Figure 1.1: Segmentally baffled one-pass shell and two-pass tube shell-and-tube heat exchanger

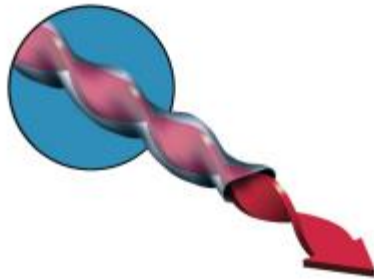
Flow in shell-side can be improved by suitable adjustments of baffle design as is done in helixchangers (Král et al., 1996) – see Figure 1.2. Such an arrangement also increases the heat transfer rate vs. pressure drop ratio, reduces leakages (baffle bypass effect), flow-induced vibrations, and limits creation of stagnation zones thus decreasing fouling rate (CB&I Lummus Technology, 2012).



The Helixchanger: shell-and-tube heat exchanger with helical baffles (CB&I Lummus Technology, 2012, reprinted with permission).

Another sub-type of shell-and-tube heat exchangers is the lamella exchanger employing hollow lamellae instead of tubes while no baffle plates are present. This, combined with pure countercurrent and highly turbulent flow, guarantees a high heat transfer rate and low pressure drop (Hewitt et al., 1994, Sec. 4.2.5). It is obvious that a smaller tube diameter will yield higher heat transfer surface area. The lower limit on tube outer diameter, however, is around 20 mm to ensure cleaning can be performed (Hewitt et al., 1994, Sec. 6.2.3). Considering shell-side, the minimum recommended tube pitch is approximately 1.25 times the tube diameter (Hewitt et al., 1994, Sec. 6.2.5). As for thermal expansion, it can be dealt with by using a U-tube bundle, a toroidal expansion joint on the shell, or a floating head. Generally, pure countercurrent flow arrangement is preferred (Hewitt

et al., 1994, sec. 3.7). If necessary, heat transfer can be intensified by using twisted tubes (see Figure 2.5), twisted tube inserts, enhanced tube surfaces, etc. Of course, such enhancements should be avoided when fouling is a real possibility. Figure 2.5. Twisted tube (K)



The above figure Twisted tube (Koch Heat Transfer Company, LP, 2012, reprinted with permission); this design is reported to improve shell-side distribution and increase tube-side heat transfer coefficient by 40 % compared to plain tubes

The advantages of tubular exchangers are the ease of manufacturing and maintenance and the possibility of using tube enhancements. As for disadvantages, these units provide relatively small heat transfer surface area per unit volume.

### 1.2 Plate Heat Exchangers

In plate heat exchangers fluids flow alternately between stacked plain or cross-corrugated, Plates that can be sealed and held together in two different ways. Either gasket are placed, Near the plate edges as shown in Figure and the stack is held together by a frame or, the plates are brazed or welded thus forming a single element. Spiral heat exchangers (see Figure being fundamentally identical, generally contain only

two coiled plates.

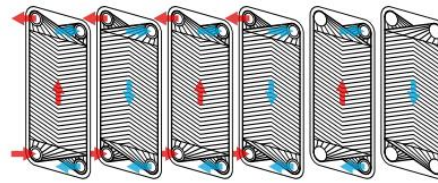


Figure 1.3 : Gasketed plates; flow directions of hot and cold fluids are marked by arrows and gaskets by a thick line (the two rightmost plates are end plates – one for the hot fluid and one for the cold fluid)

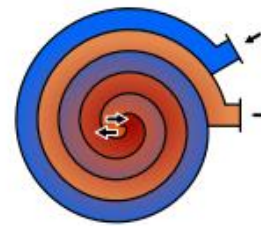


Figure 1.4: Cross-section of a spiral heat exchanger – hot stream inlet and cold stream outlet are near the exchanger axis while cold stream inlet and hot stream outlet are on the outer wall

With plate exchangers we are able to reach very high compactness, that is, a very large Heat transfer area with a small exchanger footprint. Also, heat transfer tends to be more Efficient than in shell-and-tube exchangers due to more complex flow passage geometry Leading to higher degree of turbulence (Hewitt et al., 1994, Sec. 7.2.1). Since flow arrangement of these heat exchangers can be considered to be almost pure countercurrent, with a certain Temperature difference we get higher heat duty than for a shell-and-tube exchanger under Equivalent conditions. Alternatively, to get the same heat duty as in case of a shell-and-tube Exchanger a lower temperature difference is necessary.

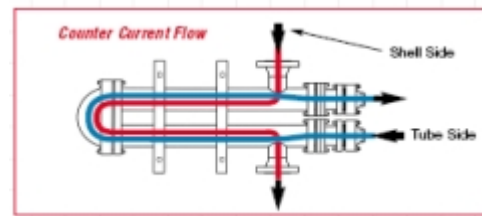
### 1.3 Air-Cooled Heat Exchangers

Air-cooled heat exchangers, commonly employed e.g. for condensing vapours, have several major advantages. They are cheap and very simple, thus little maintenance is necessary. No intricate piping or pumping system is required and, in most cases, fouling or corrosion do not occur at a significant rate (Hewitt et al., 1994, Sec. 9.2.1). On the other hand, there are disadvantages that must be considered, namely heat transfer coefficient being relatively low and hence these exchangers tend to be larger (Hewitt et al., 1994, Sec. 9.2.2). We must also bear in mind that embedded fans may be noisy and that temperature difference available for cooling may be lower in some locations due to warmer climate.

Figure shows two common arrangements of these exchangers – forced draft and induced draft. In both cases, air passes over tubes in a tube bundle in which cooled fluid is flowing. These arrangements can be either horizontal as shown in the figure, vertical, or inclined. Additionally, tubes may be finned to enhance air-side heat transfer. With induced draft we obtain a more uniform air distribution while with forced draft less electrical power is required by the fan (cooler air has lower density; Hewitt et al., 1994, Sec. 9.3.1.1).

Hairpin heat exchangers utilize true counter-current flow. Unlike multi-pass shell-and-tube designs where correction factors are used to account for inefficiencies resulting from co-current passes, this process maximizes temperature differences between shellside and tubeside fluids. When a process calls for a temperature cross (hot fluid outlet temperature is below cold fluid outlet temperature), a hairpin heat exchanger is the most efficient design, with fewer sections and less surface area. Double-

pipe heat exchangers utilize a single pipe-within-a-pipe design and are commonly used for high fouling services such as slurries where abrasive materials are present, and for smaller duties. Standard shell diameters range from 2" (50,8 mm.) to 6" (152,4 mm.). Multi-tube heat exchangers are used for larger duties with standard designs for shell diameters up to 30" (762 mm.) and surface areas in excess of 10,000 ft<sup>2</sup> (930 m<sup>2</sup>) per section. BROWN FINTUBE® range of products includes a variety of unique enhancement devices for different process conditions.



#### Advantages of Hairpin-Style Heat Exchangers

- Offers smaller footprint for compliance with overall length restrictions.
- Able to be stacked via special supports.
- Accommodates differential thermal expansion without the need for an integrated expansion joint.
- Withstands high terminal temperature gradients, preventing potential failure due to thermal stresses.
- Able to handle a temperature cross between the cold- and hot-side fluids because of the pure countercurrent flow design.
- Offers a more thermally efficient design with a smaller shell than traditional shell-and-tube heat exchangers.

This article will provide a closer look at each of these features.

**Differential Thermal Expansion.** When differential thermal expansion is a concern, a traditional fixed-tube heat exchanger may not be suitable for the service. Expansion joints commonly are needed in such applications, which add cost to the heat exchanger, especially if higher pressures or high alloy materials are required.

**High Terminal Temperature Gradients.**

Hairpin exchangers can accommodate high terminal temperature gradients (terminal ends are decoupled). The hairpin dual-tubesheet design also handles large temperature swings from inlet to outlet. The single-tubesheet design of a TEMA U-type would have a large temperature gradient across the single tubesheet between the hot and cold sides of the tube-side fluid. This can lead to warpage and potential failure due to thermal stresses.

**Pure Counter current Flow.** When a large temperature cross exists between the process streams, pure counter current flow is necessary. A temperature cross is defined by the outlet temperature of each fluid crossing over each other; that is, the hot-side outlet temperature is lower than the cold-side outlet temperature.

**Thermally Efficient.**

Special closure styles are available when the tube-side design pressure is high. In many of these cases, the hairpin design can be more thermally efficient than a traditional shell and tube. Additionally, the design typically results in a smaller shell.

**Basco Hairpin Heat Exchangers**

A hairpin design is often more thermally efficient than a traditional shell and tube, which

results in a lower up-front cost and lower overall weight

**PERFORMANCE NOTES.**

- Ideal for applications that require high thermal performance and a compact footprint
- All connections are at one end of the heat exchanger
- Sizes up to 60 in. (150 cm) in diameter and 480 in. (1200 cm) in length
- Materials include carbon steel, 300 series stainless steel, Duplex stainless steel, copper alloy, chrome-moly alloys, Hastelloy, Inconel, Monel, 254 SMO, alloy clad/weld overlay
- Designed and fabricated per ASME, TEMA, CRN, PED, CML.

**LITERATURE SURVEY**

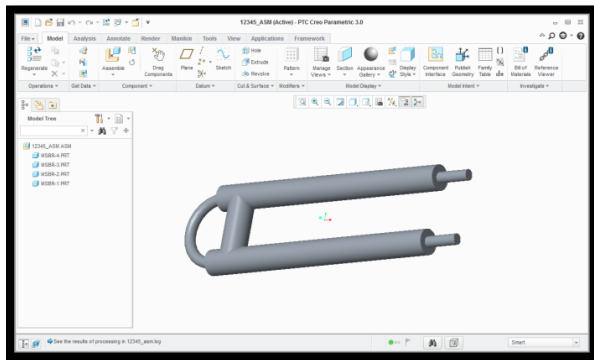
**DESIGN AND ANALYSIS OF DOUBLE PIPE HEAT EXCHANGER USING COMPUTATIONAL METHOD**

Heat transfer equipment is defined by the function it fulfills in a process. On the similar path, Heat exchangers are the equipment used in industrial processes to recover heat between two process fluids. They are widely used in space heating, refrigeration, air conditioning, power plants, chemical plants, petrochemical plants, petroleum refineries, and natural gas processing. The operating efficiency of these exchangers plays a very key role in the overall running cost of a plant. So the designers are on a trend of developing heat exchangers which are highly efficient compact, and cost effective. A common problem in industries is to extract maximum heat

from a utility stream coming out of a particular process, and to heat a process stream.

### DESIGN AND EXPERIMENTAL ANALYSIS OF SPIRAL TUBE HEAT EXCHANGER

Spiral tube heat exchangers are known as excellent heat exchanger because of far compact and high heat transfer efficiency. An innovative spiral tube heat exchanger is designed for particular process engineering. A new arrangement for flow of hot and cold fluids is employed for design, hot fluid flows in axial path while the cold fluid flows in a spiral path. To measure the performance of the spiral tube heat exchanger, its model is suitably designed and fabricated so as to perform experimental tests. The paper gives analysis of spiral tube



### INTRODUCTION TO FEA

Finite Element Analysis (FEA) was first developed in 1943 by R. Courant, who utilized the Ritz method of numerical analysis and minimization of variational calculus to obtain approximate solutions to vibration systems. Shortly thereafter, a paper published in 1956 by M. J. Turner, R. W. Clough, H. C. Martin, and L. J. Top established a broader definition of numerical analysis. The paper centered on the "stiffness and deflection of complex structures".

FEA consists of a computer model of a material or design that is stressed and analyzed for specific results. It is used in new product design, and existing product refinement. A company is able to verify a proposed design will be able to perform to the client's specifications prior to manufacturing or construction. Modifying an existing product or structure is utilized to qualify the product or structure for a new service condition. In case of structural failure, FEA may be used to help determine the design modifications to meet the new condition.

There are multiple loading conditions which may be applied to a system. Some examples are shown:

- Point, pressure, thermal, gravity, and centrifugal static loads
- Thermal loads from solution of heat transfer analysis
- Enforced displacements
- Heat flux and convection
- Point, pressure and gravity dynamic loads

Each FEA program may come with an element library, or one is constructed over time. Some sample elements are:

- Rod elements
- Beam elements
- Plate/Shell/Composite elements
- Shear panel
- Solid elements
- Spring elements
- Mass elements
- Rigid elements
- Viscous damping elements

Many FEA programs also are equipped with the capability to use multiple materials within the structure such as:

- Isotropic, identical throughout
- Orthotropic, identical at 90 degrees
- General anisotropic, different throughout

### Types of Engineering Analysis

**Structural** analysis consists of linear and non-linear models. Linear models use simple parameters and assume that the material is not plastically deformed. Non-linear models consist of stressing the material past its elastic capabilities. The stresses in the material then vary with the amount of deformation as in.

**Vibrational** analysis is used to test a material against random vibrations, shock, and impact. Each of these incidences may act on the natural vibrational frequency of the material which, in turn, may cause resonance and subsequent failure.

Fatigue analysis helps designers to predict the life of a material or structure by showing the effects of cyclic loading on the specimen. Such analysis can show the areas where crack propagation is most likely to occur. Failure due to fatigue may also show the damage tolerance of the material.

**Heat Transfer** analysis models the conductivity or thermal fluid dynamics of the material or structure. This may consist of a steady-state or transient transfer. Steady-state transfer refers to constant thermo properties in the material that yield linear heat diffusion

### Results of Finite Element Analysis.

#### FLUID- TITANIUM CARBIDE

Mass Flow Rate (kg/s)	
cold_inlet	0.049999997
cold_outlet	-0.32807608
contact_region-contact_region_3-contact_region_2-contact_region_3-src	-0.55263227
contact_region-contact_region_3-contact_region_2-contact_region_3-trg	0.55263826
contact_region_4-src	0.010181041
contact_region_4-trg	-0.01018121
hot_inlet	0.49999997
hot_outlet	-0.44418025
interior-16	-0.55263825
interior-5	0.010180908
interior_nsbr	-16.106001
wall-14	0
wall-15	0
wall-17	0
wall-18	0
wall_nsbr	0
Net	-0.022258495

#### FLUID- TITANIUM CARBIDE

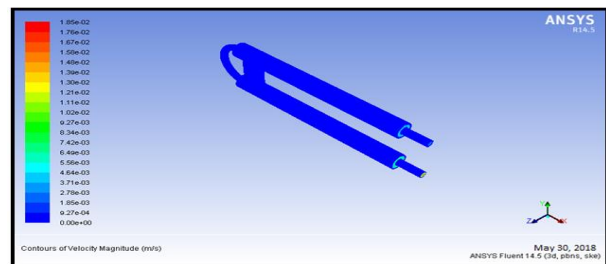
#### HEAT TRANSFER RATE

Total Heat Transfer Rate (w)	
cold_inlet	2985.0381
cold_outlet	-70495.189
contact_region-contact_region_3-contact_region_2-contact_region_3-src	0
contact_region-contact_region_3-contact_region_2-contact_region_3-trg	0
contact_region_4-src	0
contact_region_4-trg	0
hot_inlet	150220.63
hot_outlet	-86969.914
wall-14	0
wall-15	0
wall-17	0
wall-18	0
wall_nsbr	0
Net	-3249.3610

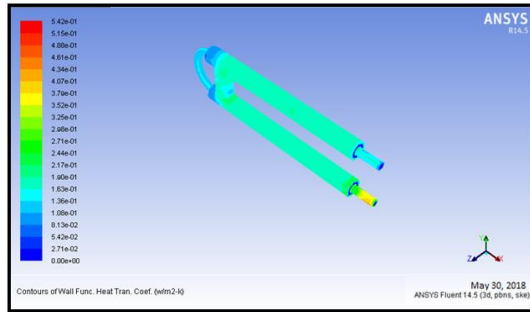
#### AT 0.5%

#### PRESSURE VELOCITY

Total Heat Transfer Rate (w)	
cold_inlet	2580.425
cold_outlet	-63756.617
contact_region-contact_region_3-contact_region_2-contact_region_3-src	0
contact_region-contact_region_3-contact_region_2-contact_region_3-trg	0
contact_region_4-src	0
contact_region_4-trg	0
hot_inlet	133434.72
hot_outlet	-73759.672
wall-14	0
wall-15	0
wall-17	0
wall-18	0
wall_nsbr	0
Net	-1501.1453



## HEAT TRANSFER COEFFICIENT



## CONCLUSION

In this thesis, glycerin(40%) fluid is mixed with base fluid water(60%) are calculated for their combination properties. The nano fluid is titanium carbide, magnesium Oxide and silver nano particle for weight percentage 0.2%, 0.5%, 0.7% & 1.0%. Theoretical calculations are done determine the properties for nano fluids and those properties are used as inputs for analysis. Hairpin Exchangers are available in single tube (Double Pipe) or multiple tubes within a hairpin shell (Multitude), bare tubes, finned tubes, U-tubes, straight tubes (with rod-thru capability), fixed tube sheets and removable bundle.

By observing the CFD analysis results the heat transfer rate value more at silver nano particle weight percentage 1.0%.

So it can be concluded the silver nano particle nano fluid at weight percentage 0.2% fluid is the better fluid for hair pin heat exchanger.

## REFERENCES

1. A.O. Adelaja, S. J. Ojolo and M. G. Sobamowo, "Computer Aided Analysis of Thermal and Mechanical Design of Shell and Tube Heat Exchangers", Advanced Materials Vol. 367 (2012) pp 731 -737 © (2012) Trans Tech Publications, Switzerland.
2. Yusuf Ali Kara, Ozbilen Guraras, "A computer program for designing of Shell and tube heat exchanger", Applied Thermal Engineering 24(2004) 1797-1805

3. Rajagopal THUNDIL KARUPPA RAJ and Srikanth GANNE, "Shell side numerical analysis of a shell and tube heat exchanger considering the effects of baffle inclination angle on fluid flow", Thundil Karuppa Raj, R., et al: Shell Side Numerical Analysis of a Shell and Tube Heat Exchanger, THERMAL SCIENCE: Year 2012, Vol. 16, No. 4, pp. 1165-1174.

4. S. Noie Baghban, M. Moghiman and E. Salehi, "Thermal analysis of shell-side flow of shell-and tube heat exchanger using experimental and theoretical methods" (Received: October 1, 1998 -Accepted in Revised Form: June 3, 1999).

5. A. Gopi Chand, Prof. A. V. N. L. Sharma, G. Vijay Kumar, A. Srividya, "Thermal analysis of shell and tube heat exchanger using mat lab and floefdsoftware", Volume: 1 Issue: 3 276 -281, ISSN: 2319 -1163.

6. Hari Haran, Ravindra Reddy and Sreehari, "Thermal Analysis of Shell and Tube Heat ExChanger Using C and Ansys"

## **ANALYSIS OF HEAT TRANSFER RATE BY VARYING COOLING FLUID FOR ENGINE CYLINDER FINS**

**Mr.RANJITH AAVULA**  
M-Tech Student,  
Department of Mechanical Engineering,  
Malla Reddy College of Engineering,  
Maisammaguda, Medchal dist. TS  
Email id:ranjith.education02@gmail.com

**Mr.VIKASH KUMAR (Ph.D)**  
Professor,  
Department of Mechanical Engineering,  
Malla Reddy College of Engineering,  
Maisammaguda, Medchal dist. TS  
Email id:vikash-mech@mrce.in

### **ABSTRACT:**

The Engine cylinder is one of the major automobile components, which is subjected to high temperature variations and thermal stresses. In order to cool the cylinder, fins are provided on the cylinder to increase the rate of heat transfer. By doing thermal analysis on the engine cylinder fins, it is helpful to know the heat dissipation inside the cylinder.

The principle implemented in this project is to increase the heat dissipation rate by using the invisible working fluid, nothing but air. We know that, by increasing the surface area we can increase the heat dissipation rate, so designing such a large complex engine is very difficult. The main purpose of using these cooling fins is to cool the engine cylinder by air.

The main aim of the project is to analyze the thermal properties by varying cooling fluid, material and thickness of cylinder fins.

Parametric models of cylinder with fins have been developed to predict the thermal behavior. The models are created by the geometry, rectangular and also by varying thickness of the fins for both geometries. Cooling fluids used in this thesis is air, oil. The 3D modeling software used is Pro/Engineer.

Thermal analysis is done on the cylinder fins to determine variation in temperature

distribution. The analysis is done using ANSYS. Transient thermal analysis determines temperatures and other thermal quantities that vary over time.

### **KEY WORDS:**

FINS, CYLINDER, AIR, LIQUID-OIL, TEMPERATURE, CFD MODELING, ANSYS

### **Introduction:**

Internal combustion engine cooling uses either air or a liquid to remove the waste heat from an internal combustion engine. For small or special purpose engines, air cooling makes for a lightweight and relatively simple system. The more complex circulating liquid-cooled engines also ultimately reject waste heat to the air, but circulating liquid improves heat transfer from internal parts of the engine. Engines for watercraft may use open-loop

cooling, but air and surface vehicles must recirculate a fixed volume of liquid.

The main aim of the project is to design cylinder with fins for a 150cc engine, by changing the thickness of the fins, changing the cooling fluid and to analyze the transient thermal properties of the fins. Analyzation is also done by varying the materials of fins. Present used material for cylinder fin body is Aluminum alloy 204 which has thermal conductivity of 110 – 150 w/mk.

Our aim is to change the material for fin body by analyzing the fin body with other materials and also by changing the thickness.

Geometry of fins – Rectangular

Thickness of fin – 3mm ,2.5mm

Materials – Aluminum Alloy A204,Al- 6061

Cooling Fluid – Air, Oil

STEPS INVOLVED IN THE PROJECT:

1. MODELING
2. THEORETICAL CALCULATIONS
3. TRANSIENT THERMAL ANALYSIS

### BASIC PRICIPLE:

Most internal combustion engines are fluid cooled using either air (a gaseous fluid) or a liquid coolant run through a heat exchanger (radiator) cooled by air. Marine engines and some stationary engines have ready access to a large volume of water at a suitable temperature. The water may be used directly to cool the engine, but often has sediment, which can clog coolant passages, or chemicals, such as salt, that can chemically damage the engine. Thus, engine coolant may be run through a heat exchanger that is cooled by the body of water.

Most liquid-cooled engines use a mixture of water and chemicals such as antifreeze and rust inhibitors. The industry term for the antifreeze mixture is *engine coolant*. Some antifreezes use no water at all, instead using a liquid with different properties, such as propylene glycol or a combination of propylene glycol and ethylene glycol. Most "air-cooled" engines use some liquid oil cooling, to maintain acceptable temperatures for both critical engine parts and the oil itself. Most "liquid-cooled" engines use some air cooling, with the intake stroke of air cooling the combustion chamber. An exception is Wankel engines, where some parts of the combustion chamber are never cooled by intake, requiring extra effort for successful operation.

### Air-cooling

Cars and trucks using direct air cooling (without an intermediate liquid) were built over a long period from the very beginning and ending with a small and generally unrecognized technical change.

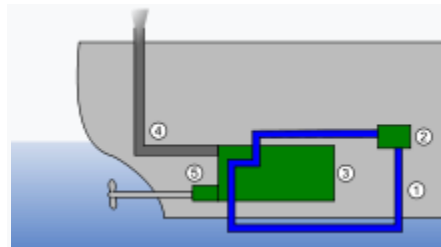
For many years air cooling was favored for military applications as liquid cooling systems are more vulnerable to damage by shrapnel.

Air-cooled engines have may be an advantage from a thermodynamic point of view due to higher operating temperature. The worst problem met in air-cooled aircraft engines was the so-called "Shock cooling".

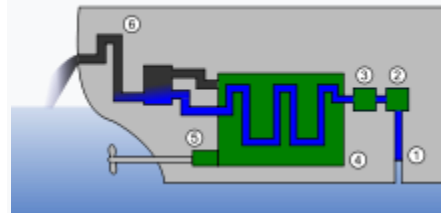
### Liquid cooling

*Main article: Radiator (engine cooling)*

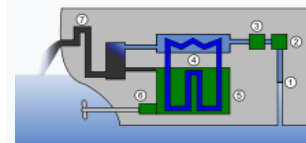
Today, most automotive and larger IC engines are liquid-cooled.



A fully closed IC engine cooling system



Open IC engine cooling system



Semiclosed IC engine cooling system

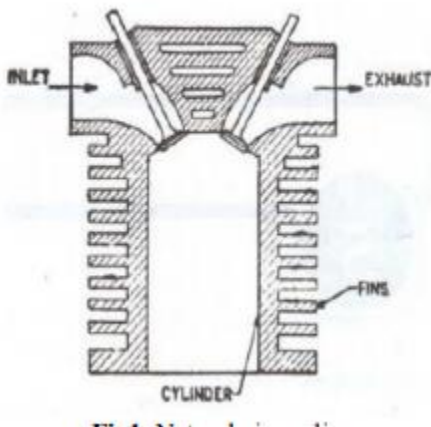
Liquid cooling is also employed in maritime vehicles (vessels). For vessels, the seawater itself is mostly used for cooling. In some cases, chemical coolants

are also employed (in closed systems) or they are mixed with seawater cooling.

### Natural Air Cooling:

In normal cause, larger parts of an engine remain exposed to the atmospheric air. When the vehicles run, the air at certain relative velocity impinges upon the engine, and sweeps away its heat. The heat carried-away by the air is due to natural convection, therefore this method is known as natural air-cooling. Engines mounted on 2-wheelers are mostly cooled by natural air.

As the heat dissipation is a function of frontal cross-sectional area of the engine, therefore there exists a need to enlarge this area. An engine with enlarge area will becomes bulky and in turn will also reduce the power by weight ratio. Hence, as an alternative arrangement, fins are constructed to enhance the frontal cross-sectional area of the engine. Fins (or ribs) are sharp projections provided on the surfaces of cylinder block and cylinder head. They increase the outer contact area between a cylinder and the air. Fins are, generally, casted integrally with the cylinder. They may also be mounted on the cylinder.



### Natural air cooling

#### Fins:

A fin is a surface that extends from an object to increase the rate of heat transfer to or from the environment by increasing convection. The amount of conduction, convection, radiation of an object

determines the amount of heat it transfers. Increasing the temperature difference between the object and the environment, increasing the convection heat transfer coefficient, or increasing the surface area of the object increases the heat transfer. Sometimes it is not economical or it is not feasible to change the first two options. Adding a fin to the object, however, increases the surface area and can sometimes be economical solution to heat transfer problems. Circumferential fins around the cylinder of a motor cycle engine and fins attached to condenser tubes of a refrigerator are a few familiar examples.



Fernando Illan simulated the heat transfer from cylinder to air of a two-stroke internal combustion finned engine. The cylinder body, cylinder head (both provided with fins), and piston have been numerically analyzed and optimized in order to minimize engine dimensions. The maximum temperature admissible at the hottest point of the engine has been adopted as the limiting condition. Starting from a zero-dimensional combustion model developed in previous works, the cooling system geometry of a two-stroke air cooled internal combustion engine has been optimized in this paper by reducing the total volume occupied by the engine. A total reduction of 20.15% has been achieved by reducing the total engine diameter  $D$  from 90.62 mm to 75.22 mm and by increasing the total height  $H$  from 125.72 mm to 146.47 mm aspect ratio varies from 1.39 to 1.95. In parallel with the total volume reduction, a slight increase in engine efficiency has been achieved. G. Babu and M. Lavakumar analyzed the thermal properties by varying geometry, material and thickness of cylinder fins.

The models were created by varying the geometry, rectangular, circular and curved shaped fins and also

by varying thickness of the fins. Material used for manufacturing cylinder fin body was aluminum Alloy 204 which has thermal conductivity of 110-150W/mk and also using aluminum alloy 6061 and Magnesium alloy which have higher thermal conductivities. They concluded that by reducing the thickness and also by changing the shape of the fin to curve shaped, the weight of the fin body reduces thereby increasing the efficiency.

After these verifications the effects of parameters such as thickness ratio,  $\alpha$ , dimensionless fin semi thickness,  $\delta$ , length ratio,  $\lambda$ , thermal conductivity parameter,  $\beta$ , Biot number,  $Bi$ , on the temperature distribution are illustrated and explained.

## LITERATURE SURVEY

### COOLING SYSTEM OF IC ENGINES

Heat engines generate mechanical power by extracting energy from heat flows, much as a water wheel extracts mechanical power from a flow of mass falling through a distance. Engines are inefficient, so more heat energy enters the engine than comes out as mechanical power; the difference is waste heat which must be removed. Internal combustion engines remove waste heat through cool intake air, hot exhaust gases, and explicit engine cooling.

Engines with higher efficiency have more energy leave as mechanical motion and less as waste heat. Some waste heat is essential: it guides heat through the engine, much as a water wheel works only if there is some exit velocity (energy) in the waste water to carry it away and make room for more water. Thus, all heat engines need cooling to operate.

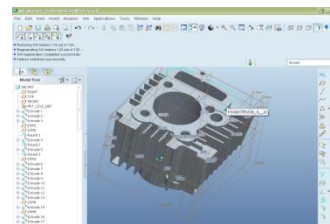
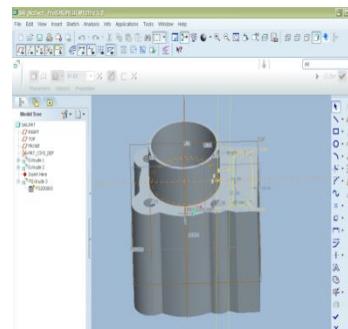
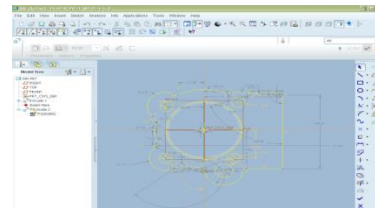
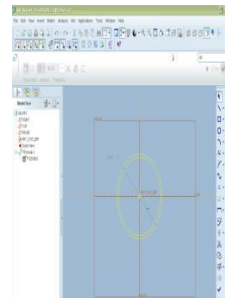
Cooling is also needed because high temperatures damage engine materials and lubricants. Internal-combustion engines burn fuel hotter than the melting temperature of engine materials, and hot enough to set fire to lubricants. Engine cooling removes energy fast enough to keep temperatures low so the engine can survive.

Some high-efficiency engines run without explicit cooling and with only accidental heat loss, a design

called adiabatic. For example, 10,000 mile-per-gallon "cars" for the Shell economy challenge are insulated, both to transfer as much energy as possible from hot gases to mechanical motion, and to reduce reheat losses when restarting. Such engines can achieve high efficiency but compromise power output, duty cycle, engine weight, durability, and emissions.

## MODELS OF CYLINDER FIN BODY

### ORIGINAL FIN BODY



### 2D DRAWINGS



**Effectiveness of fin**

$\epsilon = 48$

**THERMAL FLUX CALCULATIONS**

THICKNESS-2.5mm

**Heat flux**

Heat flow  $q = UA\Delta T$

=0.001285

**COOLING FLUID - OIL**

**ALUMINUM ALLOY 204 – Thickness 3mm**

Length of fin (L)=130mm=0.13m

Width of fin (b)=130mm=0.13m

Thickness y=3mm

$$m = \sqrt{\frac{hp}{kA_c}} = \sqrt{\frac{0.266 \times 50}{120 \times 0.00078}} = 11.92 \text{ m}^{-1}$$

$\Theta_o = 273.67\text{K}$

**Heat lost by fin**

$Q_{fin} = 279.65\text{W}$

**Maximum heat transferable by fin when if entire fin at base temperature**

$Q_{max} = 1135.62\text{W}$

$\eta = (Q_{fin}/Q_{max}) = (279.65/1135.62) \times 100 = 24.62$

**Effectiveness of fin**

$$\epsilon = \frac{\text{heat lost with fin}}{\text{heat lost without fin}} = 40$$

Effectiveness should be more than 1

**ALUMINUM ALLOY 6061 – Thickness 2.5mm**

Length of fin (L)=130mm=0.13m

Width of fin (b)=130mm=0.13m

Thickness y=2.5mm

$$m = \sqrt{\frac{hp}{kA_c}} = \sqrt{\frac{0.265 \times 50}{180 \times 0.000325}} = 47.68 \text{ m}^{-1}$$

$\Theta_o = 3209.69\text{K}$

**Heat lost by fin**

$Q = 8952.64\text{W}$

**Maximum heat transferable by fin when if entire fin at base temperature**

$Q_{max} = 19978.39\text{W}$

$\eta = (Q_{fin}/Q_{max}) = (3209.69/19978.39) \times 100 = 44.81$

**Effectiveness of fin**

$$\epsilon = \frac{\text{heat lost with fin}}{\text{heat lost without fin}}$$

$$\epsilon = \sqrt{(pk/hA)} = \sqrt{(2k/hy)} = \sqrt{\{(2 \times 180)/(50 \times 0.0025)\}}$$

= 48

**THERMAL FLUX CALCULATIONS**

**THICKNESS – 3mm**

Contact area A = 1775.62 mm<sup>2</sup>

Fin area = 865.447mm<sup>2</sup>

Cylinder outside area = 4436.44mm<sup>2</sup>

Over all surface area = 4436.44+1775.62 = 6212.06mm<sup>2</sup>

**Heat flux**

Heat flow  $q = UA\Delta T$

$q/a = 11.813/6212.06 = 0.001901 \text{ W/mm}^2$

**THICKNESS – 2.5mm**

Contact area A = 1910.85 mm<sup>2</sup>

Fin area = 1195.83mm<sup>2</sup>

Cylinder outside area = 4436.44mm<sup>2</sup>

**Heat flux**

Heat flow  $q = UA\Delta T$

$$h = q/a = 8.1615/6347.29 = 0.00257 \text{ W/mm}^2$$

**THERMAL ANALYSIS OF FIN BODY**

**COOLING FLUID – AIR**

**ALUMINUM ALLOY 204 –3mm THICKNESS**

Set Units - /units,si,mm,kg,sec,k

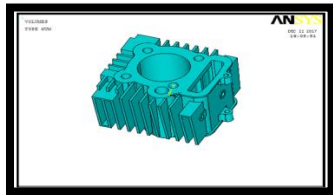
File- change Directory-select working folder

File-Change job name-Enter job name

Preferences-Thermal

\preprocessor-Element type-add/edit/delete-Select Add-Solid 20 node 90

**MODEL IMPORTED FROM PRO/ENGINEER**



Material properties -material Models –Thermal Conductivity -isotropic

**MATERIAL PROPERTIES**

Thermal Conductivity – 120 w/mk

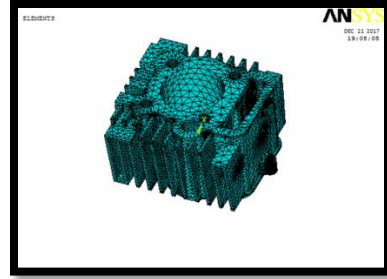
Specific Heat – 0.963 J/g °C

Density – 2.8 g/cc

**MESHED MODEL**

Select Mesh Tool Icon – Select Smart Size –On Pick All-ok

Select Mesh Tool Window –Select All Areas-pick all



Finite element analysis or FEA representing a real project as a “mesh” a series of small, regularly shaped tetrahedron connected elements, as shown in the above fig. And then setting up and solving huge arrays of simultaneous equations. The finer the mesh, the more accurate the results but more computing power is required

**LOADS**

Define Loads -Apply Thermal-Temperature- on Area-Select inside area=5585K

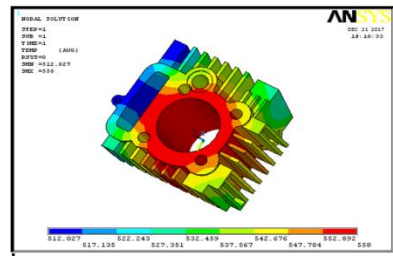
Convections – on Areas (select Remaining areas-Film Co-efficient – 25 W/mmK

Bulk Temperature – 313 K

Solution – Solve - Current LS file – Ok

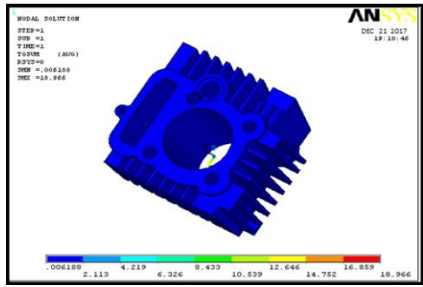
**RESULTS**

**General post processor- contour plot- nodal solution- Nodal Temperature**



According to the contour plot, the temperature distribution maximum temperature at bore because the operating temperature passing inside of the bore. So we applied the temperature inside of the bore and applied the convection to fins. Then the maximum temperature at bore and its distributed to outer surface of the fins.

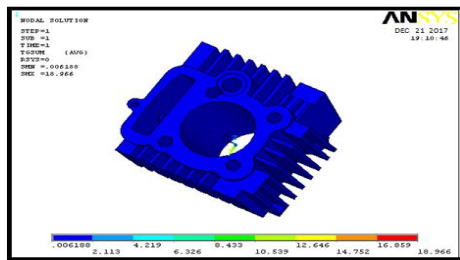
**General post processor- contour plot- Thermal Gradient-Thermal Gradient Vector Sum**



According to the contour plot, the thermal gradient maximum at bore because the operating temperature passing inside of the bore. So we applied the temperature inside of the bore and applied the convection to fins. Then the minimum gradient at fins.

According to the above contour plot, the maximum gradient is 18.966 k/m and minimum gradient is 0.006188 k/m.

**General post processor- contour plot-Thermal Flux –Thermal Flux Vector Sum**



According to the contour plot, the thermal flux maximum at bore because the operating temperature passing inside of the bore. So we applied the temperature inside of the bore and applied the convection to fins. Then the minimum thermal flux at fins.

According to the above contour plot, the maximum thermal flux is 18.966 k/m and minimum thermal flux is 0.006188 k/m.

**ALUMINUM ALLOY 6061 – 2.5mm**

**THICKNESS**

**MATERIAL PROPERTIES**

Thermal Conductivity – 180 w/mk

Specific Heat – 0.896 J/g °C

Density – 2.7 g/cc

**LOADS**

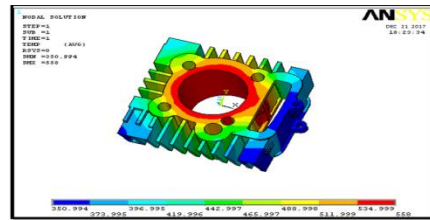
Temperature -558 K

Film Coefficient – 50 w/m<sup>2</sup> K

Bulk Temperature – 313 K

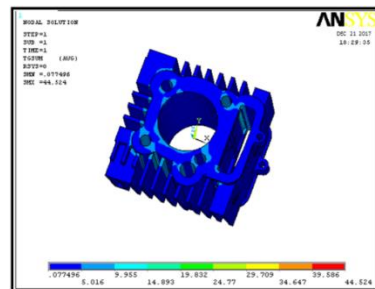
**RESULTS**

**NODAL TEMPERATURE MODEL**



According to the contour plot, the temperature distribution maximum temperature at bore because the operating temperature passing inside of the bore. So we applied the temperature inside of the bore and applied the convection to fins. Then the maximum temperature at bore and its distributed to outer surface of the fins.

**THERMAL GRADIENT SUM MODEL**

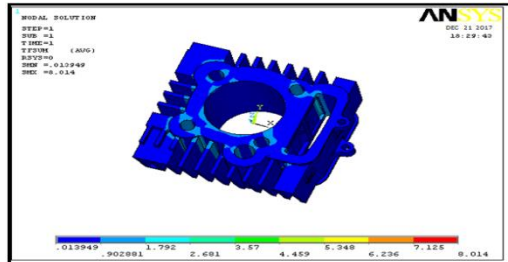


According to the contour plot, the thermal gradient maximum at bore because the operating temperature passing inside of the bore. So we

applied the temperature inside of the bore and applied the convection to fins. Then the minimum gradient at fins.

According to the above contour plot, the maximum gradient is 44.524 k/m and minimum gradient is 0.077496 k/m.

**THERMAL FLUX SUM MODEL**



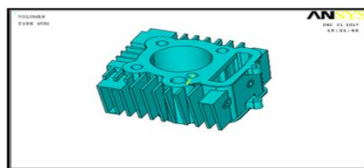
**THERMAL ANALYSIS OF FIN BODY**

**COOLING FLUID - OIL**

According to the contour plot, the thermal flux maximum at bore because the operating temperature passing inside of the bore. So we applied the temperature inside of the bore and applied the convection to fins. Then the minimum thermal flux at fins. This condition applied all model of Proe

**ALUMINUM ALLOY 204 –3mm THICKNESS**

**MODEL IMPORTED FROM PRO/ENGINEER**



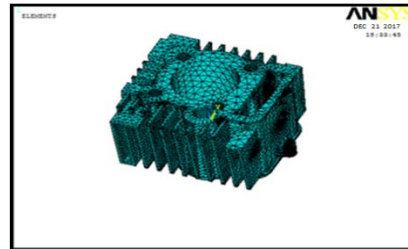
**MATERIAL PROPERTIES**

Thermal Conductivity – 120 w/mk

Specific Heat – 0.963 J/g °C

Density – 2.8 g/cc

**MESHED MODEL**



**LOADS**

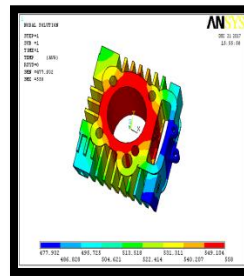
Temperature -558 K

Film Coefficient – 50 w/m<sup>2</sup> K

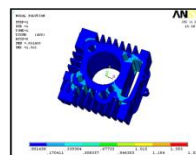
Bulk Temperature – 313 K

**RESULTS**

**NODAL TEMPERATURE**



**THERMAL FLUX SUM MODEL**



maximum thermal flux is 1.522 k/m and minimum thermal flux is 0.001433 k/m.

**ALUMINUM ALLOY 6061 – 2.5mm THICKNESS**

**MATERIAL PROPERTIES**

Thermal Conductivity – 180 w/mk

Specific Heat – 0.896 J/g °C

Density – 2.7 g/cc

**LOADS**

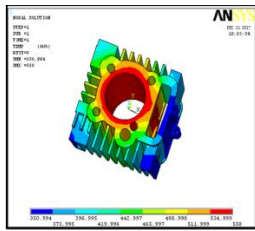
Temperature -558 K

Film Coefficient – 50 w/m<sup>2</sup> K

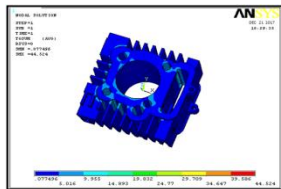
Bulk Temperature – 313 K

**RESULTS**

**NODAL TEMPERATURE MODEL**

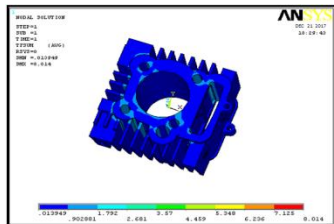


**THERMAL GRADIENT SUM MODEL**



maximum gradient is 44.524 k/m and minimum gradient is 0.077496 k/m.

**THERMAL FLUX SUM**



maximum thermal flux is 8.014 k/m and minimum thermal flux is 0.013949 k/m.

**COOLING FLUID – AIR:**

**THEORETICAL RESULTS TABLE**

		THICKNESS (mm)	HEAT LOSS (W)	EFFECTIVENESS	EFFICIENCY
<b>RECTANGULAR</b>	A	3	132.369	56.56	15.35
	L				
	-				
	204				
	A	2.5	135.09	75.89	8.8
	L				
	-				
	6061				

**THERMAL ANALYSIS RESULTS TABLE**

	Al-204,3mm	Al-6061,2.5mm
Nodal Temperature (K)	558	558
Thermal Gradient (K/mm)	18.966	2.694
Thermal Flux (w/mm <sup>2</sup> )	2.276	0.484947

**THEORETICAL THERMAL FLUX (W/mm<sup>2</sup>) RESULTS TABLE**

	3mm	2.5mm
ALLUMINIUM		
AIR	0.0009508	0.001285

**COOLING FLUID - OIL**

**THEORETICAL RESULTS TABLE**

		THICKNESSES (mm)	HEAT LOSS (W)	EFFECTIVENESS	EFFICIENCY
RECTANGULAR	AL-204	3	279.65	40	24.62
	AL-6061	2.5	895.264	48	44.81

**THERMAL ANALYSIS RESULTS TABLE**

	Al-204,3mm	Al-6061,2.5mm
Nodal Temperature (K)	558	558
Thermal Gradient (K/mm)	12.685	44.524
Thermal Flux (w/mm <sup>2</sup> )	1.522	8.014

**THEORETICAL THERMAL FLUX (W/mm<sup>2</sup>)**

**RESULTS TABLE**

	3mm	2.5mm
ALLUMINIUM		
OIL	0.001901	0.00257

**CONCLUSION**

In this thesis, a cylinder fin body for a 150cc motorcycle is modeled using parametric software Pro/Engineer. The original model is changed by changing the thickness of the fins. The thickness of the original model is 3mm, it has been reduced to 2.5mm. By reducing the thickness of the fins, the overall weight is reduced Present used material for fin body is Aluminum Alloy 204.. The material for the original model is changed by taking the consideration of their densities and thermal conductivity.

By observing the thermal analysis results, thermal flux is more for Aluminum alloy 6061 and also by reducing the thickness of the fin, the heat transfer rate is increased.

Thermal flux is also calculated theoretically. By observing the results, heat transfer rate is more when the thickness of the fin is 2.5mm.

**FUTURE SCOPE**

The shape of the fin can be modified to improve the heat transfer rate and can be analyzed. The use of Aluminum alloy 6061 as per the manufacturing aspect is to be considered. By changing the thickness of the fin, the total manufacturing cost is extra to prepare the new component.

**REFERENCES**

1. Thermal Engineering by I. Shvets, M. Kondak
2. Thermal Engineering by Rudramoorthy
3. Thermal Engineering by R.K. Raj put
4. Thermal Engineering by Sarkar
5. Online Materials

# DESIGN AND ANALYSIS OF HEAVY VEHICLE CHASSIS FOR DIFFERENT ALLOY MATERIALS

Md Akhil

Department of Mechanical Engg.  
Malla Reddy College of Engineering,  
Maisammaguda, Dhulapally, Kompally,  
Secunderabad, Telangana-500100, India  
Email:  
[mohammed.akhil786@gmail.com](mailto:mohammed.akhil786@gmail.com)

Mohd Imran

Department of Mechanical Engg.  
Malla Reddy College of Engineering  
Maisammaguda, Dhulapally, Kompally,  
Secunderabad, Telangana-500100, India  
Email: [mohdimrana392@gmail.com](mailto:mohdimrana392@gmail.com)

A. Karthikeyan

Professor, Department of Mechanical  
Engg. Malla Reddy College of  
Engineering Maisammaguda,  
Dhulapally, Kompally, Secunderabad,  
Telangana-500100, India  
Email: [karthirajme@gmail.com](mailto:karthirajme@gmail.com)

**Abstract:-**The chassis forms the main structure of the modern automobile. A large number of designs in pressed-steel frame form a skeleton on which the engine, wheels, axle assemblies, transmission, steering mechanism, brakes, and suspension members are mounted. During the manufacturing process the body is flexibly bolted to the chassis. For vehicles, chassis consists of an assembly of all the essential parts of a truck (without the body) to be ready for operation on the road.

**Keyword:** heavy vehicle chassis, Static analysis

## 1. INTRODUCTION TO CHASSIS

The chassis forms the main structure of the modern automobile. A large number of designs in pressed-steel frame form a skeleton on which the engine, wheels, axle assemblies, transmission, steering mechanism, brakes, and suspension members are mounted. During the manufacturing process the body is flexibly bolted to the chassis.

This combination of the body and frame performs variety of functions. It absorbs the reactions from the movements of the engine and axle, receives their action forces of the wheels in acceleration and braking, absorbs aerodynamic wind forces and road shocks through the suspension, and absorbs the major energy of impact in the event of an accident. There has been a gradual shift in modern small car designs. There has been a trend toward combining the chassis frame and the body into a single structural element. In this grouping, the steel body shell is reinforced with braces that make it rigid enough to resist the forces that are applied to it. To achieve better noise-isolation characteristics, separate frames are used for other cars. The presence of heavier-gauge steel components in modern separate frame designs also tends to limit intrusion in accidents.

Layout of Chassis and Its Main Components:

The following main components of the Chassis are

1. Frame: it is made up of long two members called side members riveted together with the help of number of cross members.
2. Engine or Power plant: It provides the source of power

3. Clutch: It connects and disconnects the power from the engine flywheel to the transmission system.

4. Gear Box
5. U Joint
6. Propeller Shaft
7. Differential

Functions of the Chassis Frame:

1. To carry load of the passengers or goods carried in the body.
2. To support the load of the body, engine, gear box etc.
3. To withstand the forces caused due to the sudden braking or acceleration
4. To withstand the stresses caused due to the bad road condition.
5. To withstand centrifugal force while cornering

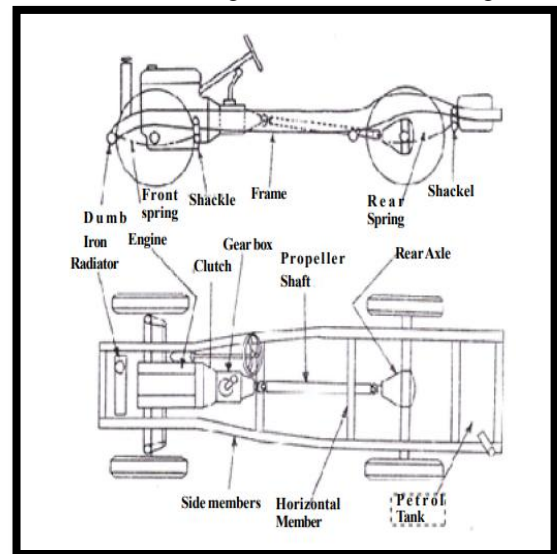


Fig:1. Line diagram

The loads acting on the chassis frame are as follow

1. Stationary loads namely the loads of permanent attachment like all the parts of the chassis, body etc.
2. Short duration loads while turning, braking etc.
3. Momentary loads while quick acceleration, sudden braking etc.

4. Loads applied while crossing roads of irregular and uneven surfaces
  5. Loads caused by sudden accidents, head on collisions etc
  6. Loads caused by irregular and overloading of vehicle.
- The loads acting on the chassis frame are as follow



Fig:2. Conventional chassis

In this type of chassis the body is made as a separate unit and then joined with ladder frame. It supports all the systems in a vehicle such as the Engine, Transmission system, Steering system, Suspension system.

## 2. LITERATURE REVIEW

Design & analysis of automobile chassis by A.harikumar, v. deepanjali, The objective of paper is to find out best material and most suitable cross-section for an Eicher E2 TATA Truck ladder chassis with the constraints of maximum shear stress, equivalent stress and deflection of the chassis under maximum load condition. In present the Ladder chassis which are uses for making buses and trucks are C and I cross section type, which are made of Steel alloy (Austenitic). In the present work, we have taken higher strength as the main issue, so the dimensions of an existing vehicle chassis of a TATA Eicher E2 (Model no.11.10) Truck is taken for analysis with materials namely ASTM A710 Steel, ASTM A302 Alloy Steel and Aluminum Alloy 6063-T6 subjected to the same load.

Design and analysis of chassis frame of TATA 2516TC by R. L. PATEL<sup>1</sup>, K.R.Gawande<sup>2</sup>, D.B.Morabiya<sup>3</sup> Automotive chassis is an important part of an automobile. The chassis serves as a frame work for supporting the body and different parts of the automobile. Also, it should be rigid enough to withstand the shock, twist, vibration and other stresses. Along with strength, an important consideration in chassis design is to have adequate bending and torsional stiffness for better handling characteristics. So, strength and stiffness are two important criteria for the design of the chassis. This report is the work performed towards the analysis of the automotive chassis with constraints of stiffness, strength and natural frequency.

Design and analysis of chassis frame by Ianurag, Iamrendra kumarsingh, Iakash tripathi, Iaditya prataptiwari, Iinitish upadhyay, 2 shyambiharilal Truck chassis is the structural ba

ckbone of any vehicle. The main function of the truck chassis is to carry the goods and payload placed upon it. The chassis frame has to bear the stresses developed and deformation occurs in it and that should be within a limit. This paper presents the study of the stress developed in chassis as well as deformation of chassis frame. The stress and deformation has been calculated for the chassis frame and the analysis has been done for the validation on the chassis frame. The model of the chassis has been developed in Creo (Pro-E) 2.0 and static structural analysis has been done in ANSYS WORKBENCH 15.0.

## 3. DESIGN CALCULATIONS FOR CHASSIS FRAME

Material and Geometry of Eicher E2 (Model No.11.10) Truck

Side bar of the chassis are made from "C" Channels with 210mm x 76 mm x 6 mm

Material of the chassis is ASTM A710 Steel

Front Overhang (a)	= 935 mm
Rear Overhang (c)	= 1620 mm
Wheel Base (b)	= 3800 mm
Modulus of Elasticity, E	= 2.10 x 10 <sup>5</sup> N / mm <sup>2</sup>
Poisson Ratio	= 0.28
Capacity of Truck	= 8 tons = 8000kg = 78480 N
Capacity of Truck with 1.25 %	= 98100 N
Weight of the body and engine	= 2 ton = 2000 kg = 19620 N
Total load acting on chassis	= Capacity of the Chassis + Weight of body and engine = 98100 + 19620 = 117720 N

Chassis has two beams. So load acting on each beam is half of the Total load acting on the chassis.

$$\text{Load acting on the single frame} = \frac{117720}{2} = 58860 \text{ N / Beam}$$

*Calculation for Reaction Beam* is simply clamp with shock absorber and leaf spring. So, beam is considered as a simply supported beam supported at C and D with uniformly distributed load.

Load acting on the entire span of the beam	= 58860 N
Length of the beam	= 6355 mm

$$\text{Uniformly Distributed Load} = \frac{58860}{6355} = 9.26 \text{ N/dm}$$

For getting the load at reaction *C* and *D*, taking the moment about *C* and we get the reaction load generate at the support *D*. Calculation of the moment are as under.

Moment about C:

$$9.26 \times 935 \times 935 / 2 = (9.26 \times 3800 \times 3800 / 2) - (R_d \times 3800) + (9.26 \times 1620 \times 4610)$$

$$R_d = 34727.65 \text{ N}$$

$$\text{Total load acting on the beam} = 9.26 \times 6355 = 58847.3 \text{ N}$$

$$R_c + R_d = 58847.3$$

$$R_c = 24119.65 \text{ N}$$

**SPECIFICATION OF MATERIAL**

Properties	ASTM A 710	ASTM A 310	ASTM A 27	STEEL ST 37
Density(g/cm <sup>3</sup> )	7.85	7.79	7.89	7.8
Young's modulus (MPa)	80000	78000	190000	20000
Poisson's ratio	0.29	0.33	0.29	0.29

**FATIGUE ANALYSIS OF CHASSIS**

Fatigue is the weakening of a material caused by repeatedly applied loads. It is the progressive and localized structural damage that occurs when a material is subjected to cyclic loading. The nominal maximum stress values that cause such damage may be much less than the strength of the material typically quoted as the ultimate tensile stress limit, or the yield stress limit.

Life Damage Safety factor FATIGUE ANALYSIS OF CHASSIS Fatigue is the

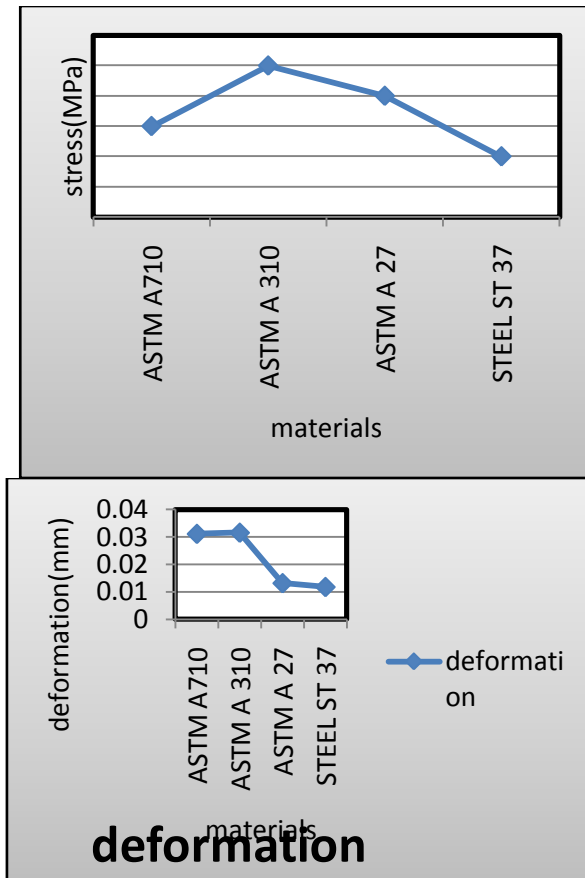
Material	Deformation(mm)	Stress (MPa)	Strain
ASTM A710	0.45562	11.098	0.00013903
ASTM A310	0.46208	11.1	0.00014264
ASTM A27	0.19188	11.099	0.000058546
STEEL ST 37	0.17352	11.097	0.000052959

weakening of a material caused by repeatedly applied loads. It is the progressive and localized structural damage that occurs when a material is subjected to cyclic loading. The nominal maximum stress values that cause such damage may be much less than the strength of the material typically quoted as the ultimate tensile stress limit, or the yield stress limit.

STATIC ANALYSIS RESULTS TABLE Here, from comparison of steel chassis with steel alloy chassis as shown in above table, it can be seen that the maximum deflection 0.4

MATERIALS	MODE SHAPES	DEFORMATION (mm)	Frequency (Hz)
ASTM A 710	1	11.481	38.422
	2	11.369	40.081
	3	7.8979	42.022
ASTM A 310	1	11.562	38.053
	2	11.45	39.677
	3	7.9576	41.612
ASTM A 27	1	11.458	59.102
	2	11.343	61.661
	3	7.886	64.663
STEEL ST 37	1	11.524	62.495
	2	11.408	65.202
	3	7.9319	68.377

6208 mm on ASTM A 310 chassis and corresponding deflection in ASTM A 710, ASTM A 27 and STEEL ST 37 are 0.45562 mm, 0.19188 mm and 0.17352 mm. Also the von-mises stress in the ASTM A 310 chassis is 11.1 MPa while in ASTM A 710, ASTM A 27 and STEEL ST 37 the von-mises stresses are 11.098 MPa, 11.099 MPa and 11.097 MPa respectively.



MODAL ANALYSIS RESULTS TABLE

MATERIALS	MODE SHAPES	DEFORMATION (mm)	Frequency (Hz)
ASTM A710	1	6.4982	53.844
	2	6.4945	54.262
	3	6.1459	57.975
ASTM A310	1	6.5207	53.278
	2	6.5177	53.688
	3	6.1603	57.419
ASTM A27	1	6.488	82.779
	2	6.4777	83.421
	3	6.1305	89.129
STEEL ST 37	1	6.5187	87.529
	2	6.515	88.207
	3	6.1658	94.242

IMPORTED MODEL

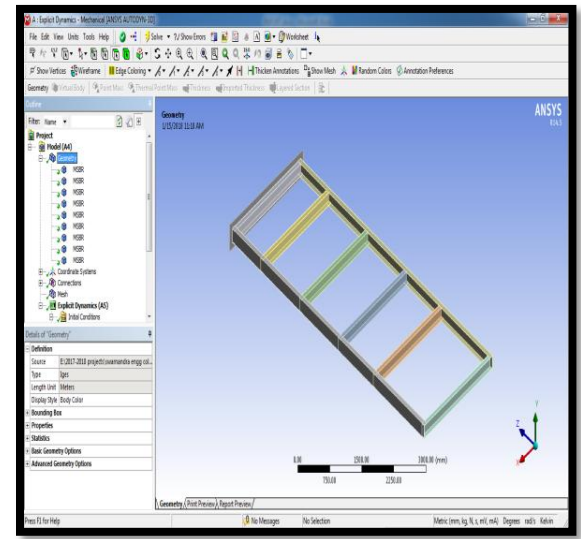
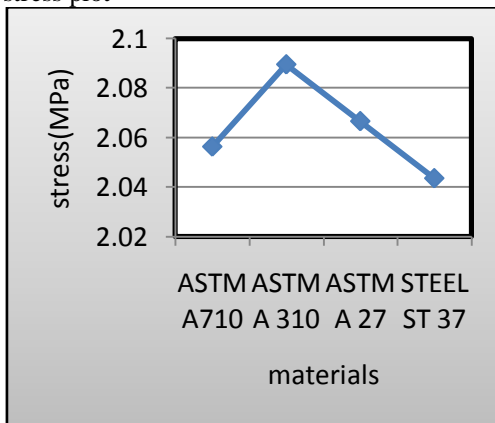


Fig:4 MESHED MODEL

STATIC ANALYSIS RESULTS TABLE

DEFORMATION PLOT

stress plot



FATIGUE ANALYSIS RESULTS

Material	Life		Damage	Safety factor
	Max.	Min.		
ASTM A710	$1 \times 10^6$	23151	43195	0.41919
ASTM A310	$1 \times 10^6$	21826	45816	0.41251

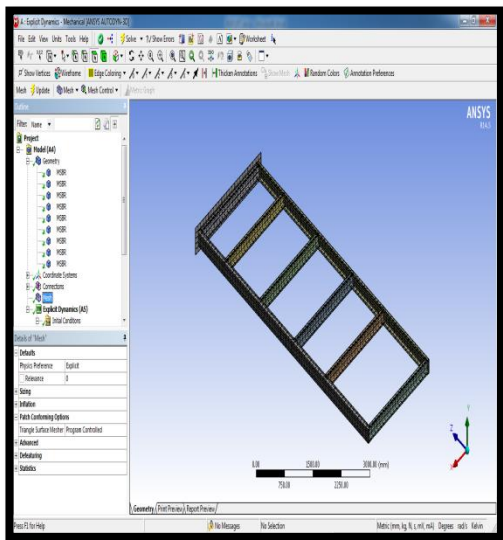


Fig:5 BOUNDARY CONDITIONS

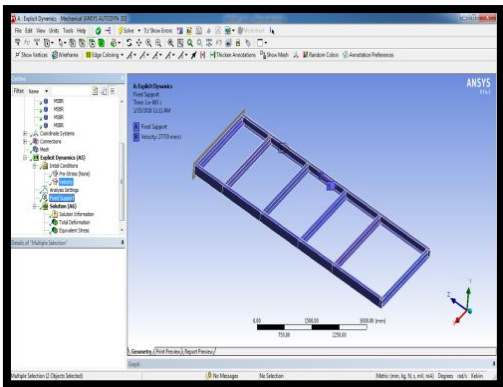


Fig:6 Deformation

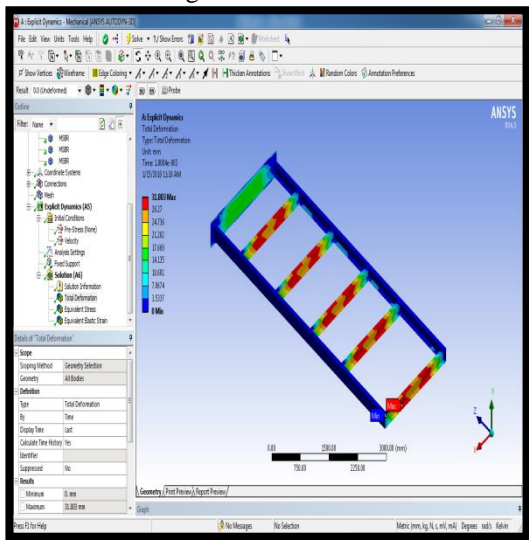


Fig:7 Stress

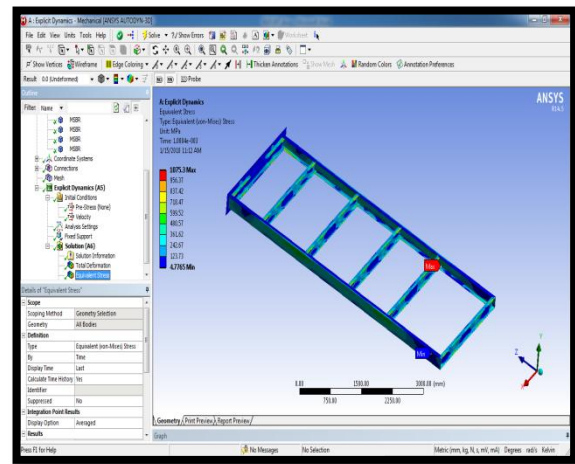


Fig:8 Strain

Material	Deformation(mm)	Stress (M Pa)	Strain
ASTM A 710	31.803	1075.3	0.013441
ASTM A 310	31.777	1061.5	0.013609
ASTM A 27	32.441	1735.4	0.0091565
STEEL S T 37	31.112	482.15	0.024171

Here, from comparison of steel chassis with steel alloy chassis as shown in above table, it can be seen that the maximum deflection 32.441 mm on ASTM A 27 chassis and corresponding deflection in ASTM A 710, ASTM A 310 and STEEL ST 37 are 31.803 mm, 31.777 mm and 31.112 mm. Also the von-mises stress in the ASTM A 27 chassis 1735.4 MPa while in ASTM A 710, ASTM A 310 and STEEL ST 37 the von-mises stresses are 1075.3 MPa, 1061.5 MPa and 482.15 MPa respectively.

Material	Deformation (mm)	Stress (MPa)	Strain
ASTM A710	30.983	958.36	0.01198
ASTM A 310	31.041	939.35	0.012043
ASTM A 27	33.481	1659.2	0.0087329
STEEL ST 37	31.932	449.99	0.022499



from the above results the rectangular section chassis having less stress when we compare the c-section chassis and having less stress ASTM A 27 steel.

**FUTURE SCOPE OF WORK**

Analysis can be done on chassis by changing the fiber orientation of composite material. It can be obtained by doing the analysis with metal matrix composite chassis.

**5. REFERENCES**

[1] Abhishek Singh, et al, "Structural Analysis of Ladder Chassis for Higher Strength", International Journal of Emerging Technology and Advanced Engineering, ISSN: 2250-2459, Volume 4, Issue 2, February 2014.

[2] Patel Vijaykumar, et al, "Structural Analysis of Automotive Chassis Frame and Design Modification for Weight Reduction", International Journal of Engineering Research & Technology, ISSN: 2278-0181, Volume 1, Issue 3, May 2012.

[3] Vishal Francis, et al, "Structural Analysis of Ladder Chassis Frame for Jeep Using Ansys", International Journal of Modern Engineering Research, ISSN: 2249-6645, Volume 4, Issue 4, April 2014.

[4] Monika S. Agarwal, et al, "Finite Element Analysis of Truck Chassis", International Journal of Engineering Sciences & Research, ISSN: 2277-9655, December 2013.

[5] Vijaykumar V. Patel and R.I. Patel, "structural analysis of ladder chassis frame", ISSN 2231 2581, Mechanical department, Government engineering college, Gujrat.

[6] Sairam Kotari and V. Gopinath, "Static and dynamic analysis on tatra chassis", vol 2, ISSN: 2249-6645 department of mechanical engineering, QIS college of engineering, Andhra Pradesh.

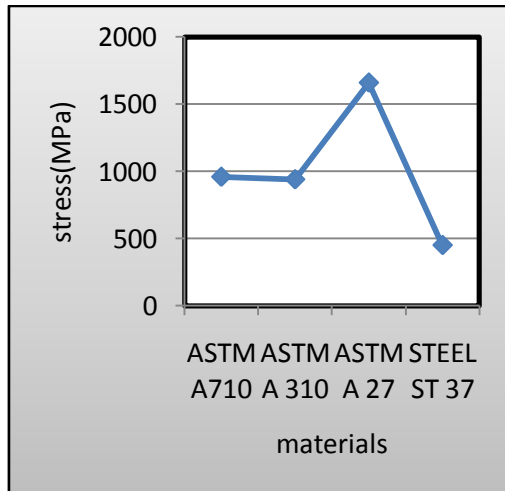
[7] Introduction to chassis design, by Keith J. Wakeham, Memorial University of Newfoundland And Labrador.

[8] Chetan J. Choudhury and akashlodhi, "Static load analysis of TATA-407 chassis" -an approach, ISSN 2231-5063, Mechanical department, K.D.K. college of engineering, Maharashtra.

[9] PSG Design Data Book for Standard Data-M/sKalaikathir Achchagam, Coimbatore 2004

**STATIC ANALYSIS RESULTS TABLE**

Here, from comparison of steel chassis with steel alloy chassis as shown in above table, it can be seen that the maximum deflection 33.481 mm on ASTM A 27 chassis and corresponding deflection in ASTM A 710, ASTM A 310 and STEEL ST 37 are 30.983 mm, 31.041 mm and 31.932 mm. Also the von-mises stress in the ASTM A 27 chassis is 1659.2 MPa while in ASTM A 710, ASTM A 310 and STEEL ST 37 the von-mises stresses are 958.36 MPa, 939.35 MPa and 449.99 MPa respectively.



**4. CONCLUSION**

The design and static structural analysis of steel alloy chassis has been carried out. Comparison has been made between c-section and rectangular section chassis having same materials and same load carrying capacity. The stress and displacements have been calculated using theoretically as well as using ANSYS for steel alloy (ASTM A 27, ASTM A 710, ASTM A 310 and STEEL ST 37) chassis. A comparative study has been made between c-section and rectangular section with respect to strength and weight.

# DESIGN AND ANALYSIS OF PRESSURE VESSEL WITH FRP MATERIAL

Sukruthi Priya

Department of Mechanical Engg.  
Malla Reddy College of Engineering,  
Maisammaguda, Dhulapally, Kompally,  
Secunderabad, Telangana-500100, India  
Email: [priya.sukruthi92@gmail.com](mailto:priya.sukruthi92@gmail.com)

Ravi Chandra

Department of Mechanical Engg.  
Malla Reddy College of Engineering  
Maisammaguda, Dhulapally, Kompally,  
Secunderabad, Telangana-500100, India  
Email: [pelimeli09@gmail.com](mailto:pelimeli09@gmail.com)

V. Ravinder

Asst. Prof. Department Mechanical  
Engg.  
Malla Reddy College of Engineering  
Maisammaguda, Dhulapally, Kompally,  
Secunderabad, Telangana-500100, India  
Email: [vankudothravinder@gmail.com](mailto:vankudothravinder@gmail.com)

## Abstract

**Long life of component is paramount. Today's lot of money is wasted to prevent the component from corrosion. The present project work is aimed at designing pressure vessel using composite material by which it is protected from corrosion and to increase life time. The present project work aimed at establishing design, analysis and manufacturing process for making pressure vessel with FIBER RENFORCED PLASTIC. Design process consists of implementing FEM for the selection design. Analyzing design is done using CATIA-V5 software. As the pre component design and development requires use investments in the design of die and break ever number of components to be manufactured is very high. To come out of this problems as to reduce the project cost the advanced FRP based manufacturing technique were adopted to reduce the break ever batch number of components a thorough investigation in the form of pilot project report for the product development. Present project work is aimed at advanced composite material for the component manufacturing so as to exploit the advantage of failure behavior of FRP for Presents Design and Establishing a Design and Manufacturing Process for the Created Component.**

KEY WORDS: Pressure vessel, FRP material.

## 1. INTRODUCTION

Composites are able to meet diverse design requirements with significant weight savings as well as "high strength –to-weight ratio" as compared to conventional materials.

Composite material is a material system composed of two or more dissimilar materials, differing in forms and insoluble in each other, physically distinct and chemically inhomogeneous. The resulting product properties are much different from the properties of constituent materials.

Composite are combination of two materials in which one of the materials, called reinforce, is in the form of fiber sheets, or particles, and is embedded in the

other materials called matrix. There in forcing material and matrix material ceramic or polymer. Composites are used because overall properties of the composite are superior are used because overall properties of the composite are superior to those of the individual components. For example: polymer ceramic composite have a great modulus than the polymer component, but are not as ceramics.

## 2. LITERATURE REVIEW

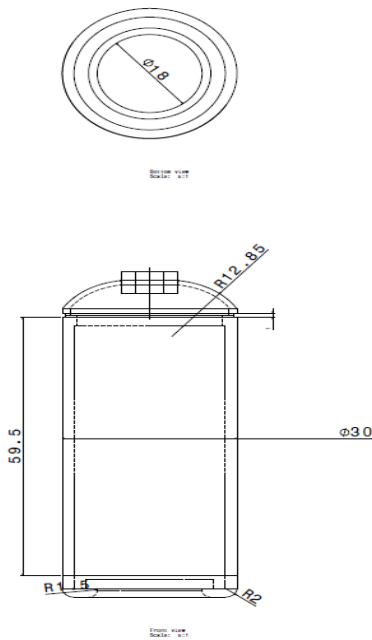
### 2.1 MOISTURE ABSORPTION BEHAVIOR FOR GLASS-FIBER COMPOSITES

Weitzman recently gave a comprehensive review on this subject. In general, the moisture absorption behavior of composite materials can be categorized into several types. Glass fiber reinforced plastic (gfrp) exhibit such behavior under specified conditions. For instance, e-glass/vinyl ester with acryl-silant or epoxy Silone surface treatment follows linear fickianbehavior for water absorption up to 80 c .in fact periodic change in the aforementioned environments will results in many such jumps. For example fiber/matrix debones and matrix cracking which is often irreversible? Also an irreversible process causes of leaching out of the material from the bulk following chemical or physical breakdown. Sorption process involving severe circumstances such as elevated temperatures external load and high solvent concentration will often results in behavior. In general the moisture absorption behavior depends on temperature, applied load type of media time and material system and is inseparable from other performance aspects concerning durability.

Moisture absorption will results in development of residual stress plasticizing the resin and accelerate time-dependent behavior .data on visco elastic behavior for pultruded gfrp under the influence of fluid absorption are rare, although there are data on creep-rupture of the material in fluids (i.e., stress corrosion ). As pointed out by some investigators that moisture absorption level in history –dependent, and therefore sorption behavior under temperature cycles is not the same as under constant humidity and temperature level. However, for pultruded gfrp this kind of data does not exist.

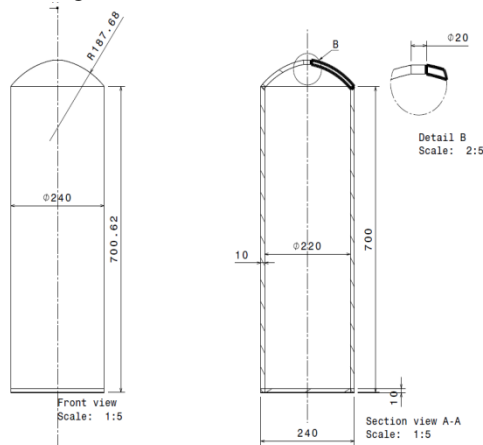
### 3. PROBLEM DESCRIPTION

Proposed design-1:



Design 1 consists of number of grooved profiles. The design was proposed in view of enhancing moment of inertia when comparing to the existing design. But the improving of MOI is sufficient enough as per our expectations. The design 2 has proposed.

Proposed design-2:



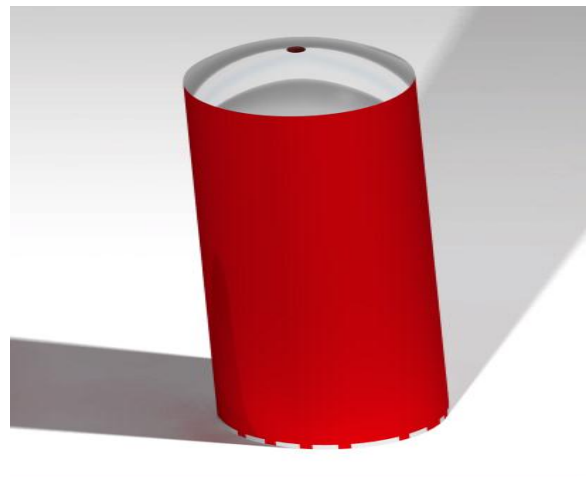
Design 2 was better when compared to design1, as the geometrical profile is a almost to a box type cross section. With this considerable improvement is achieved as per our discussions as we decided to improve the design. Hence design 2 has been selected for fabrication.

### 4. Modelling and Analysis:

Design is a continuous process to better components with improved performance than the existing ones. A new or better component is one which is more economical in all respects such as cost, performances, and aesthetics and so on. The present work also focuses on establishing a manufacturing process suitable for small scale industry in the view of generating new kind of employment. Through consensus the finalized design has been adopted for manufacturing.

In the present work the PVC made oxygen cylinder is studied thoroughly. During this process the design of oxygen cylinder has been studied to FEM analysis making use of ANSYS 13.0 and CATIA-V5 modeling

With simulated loads the stress levels in the structure very high when compare to the yield strength of the component which leads to the failure of the component. The test results were published.



Isometric view of oxygen cylinder

### 5. RESULTS

From the FEM analysis and basic stiffness calculation it is clearly evident from the results that flexural rigidity of the polymer glass reinforced construction with foam core has 51 times greater than compared to PVC

Even though the cost of the component is slightly higher than the break even number of components is to produced is very very low, which is the important concern in this project and apart for that the paramount objective to prevent the oxygen cylinder from corrosion.

As the stiffness of the component is 29 times greater than the exiting oxygen cylinder made by steel.

Capacity of FRP oxygen cylinder is comparatively high when compare with the oxygen cylinder manufactured with steel.

Form Break ever analysis it is clearly evident that the large sized batch production is required in case of steel made pressure vessel. The size of the break ever batch number with FRP sandwich construction made it comparable for small scale production. Basic objective of this project is generating a new market with new type of employment opportunities and also to achieve flexibility in design i.e.as per the customer requirements design can be changed design can be introduced very easily and the Break ever size very low.

The product cost is comparatively low and quality of the component is 50 times in view of stiffness is considered As the scope of a product has constraints towards the duration project time the impact energy calculations were not performed definitely the internal energy with stand will be high as the pressure vessel roll is to protect content from the outer atmosphere.

## 6. CONCLUSION

For further improvement, in case strength is to be increased glass epoxy or carbon epoxy and kevel or epoxy based fibers can be utilized for further enhancement and built in color can be achieved by mold design.

## REFERENCES

- 1) An Introduction to Composites Materials by Hull, D. and T.W.Clyne at Cambridge University
- 2) Ashby M.F (1989) on the Engineering design properties of GPS,British plastics federation, London.
- 3) Dingle,M.F.(1987) aligned discontinuous carbon fiber composites.
- 4) ALLEN, H.G., Analysis and Design of Structural Sandwich Panels,Pregamon
- 5) Chawal K (1987) Composite material-science and engineering, Material research and Engineering series by Springer Verlag
- 6) HOLISTER, G.S. & THOMAS, C,F., Fiber Reinforced Materials, Elsevier(1966)
- 7) PLANTEMA, F.J., Sandwich Construction.
- 8) Stanley L. E., S.S. Gharpure, and D. O. Adams (2000). MechanicalProperty Evaluation of Sandwich Panels.

International SAMPESymposium and Exhibition, 45(2): 1650-1661.

- 9) Harrington, Ron; Hock Kathy(1991). Flexible Polyurethane Forms, Mildland: The Dow Chemical Company.

# Evaluation of Overall Heat Transfer Coefficient for a Composite 3d Panel Using FEM

D Shekhar

Department of Mechanical Engg.  
Malla Reddy College of Engineering,  
Maisammaguda, Dhulapally, Kompally,  
Secunderabad, Telangana-500100, India  
Email: dshekarnaik@gmail.com

B. Sadanand

Department of Mechanical Engg.  
Malla Reddy College of Engineering  
Maisammaguda, Dhulapally, Kompally,  
Secunderabad, Telangana-500100, India  
Email: sadanandbijje@gmail.com

Dr. P. Velmurugan

Professor, Department of Mechanical Engg.  
Malla Reddy College of Engineering  
Maisammaguda, Dhulapally, Kompally,  
Secunderabad, Telangana-500100, India  
Email: velmurugan\_mech@mrce.in

**Abstract-** The overall heat transfer coefficient (overall) of an object is a measure of heat ability to flow taking into consideration both conductive part of material and convective part of liquid surrounded. The value of overall indicates how much heat can enter the system from the surroundings. Evaluating the overall heat transfer coefficient is very easy for 2D planes with simple heat transfer equations, but when two or three materials are sandwiched to form a complex object, it is difficult to evaluate the overall heat transfer coefficient by hand calculations and simplifying the system from 3D to 2D plane also involves more generalization and assumptions there by ending up with inaccurate results of overall heat transfer coefficient. This paper throws a light on how to accurately and easily evaluate the overall of system through FEM concepts using Solid Works Simulation.

**Keywords-** Overall Heat Transfer Coefficient, Solid Works, Solid Works Simulation, Thermal Analysis, FEM

## I. INTRODUCTION

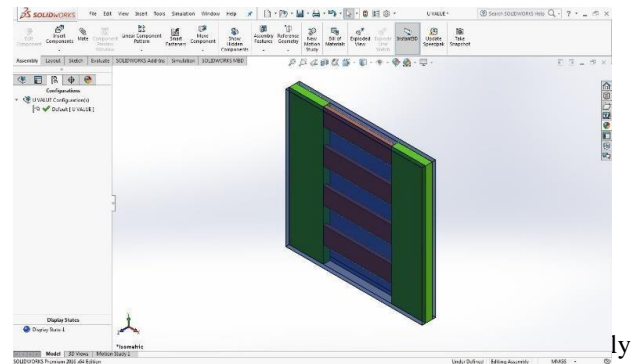
[1]The overall heat transfer coefficient represents the total resistance to heat transfer from one fluid to another. SI units of Overall Heat transfer Coefficient is  $W/m^2K$ . In a control flow system [2] Both the overall heat transfer coefficient (OHTC) and local heat transfer coefficient (LHTC) of increase with increasing inlet mass flow rates. The general heat transfer equation which relates heat flux ( $Q'$  in  $W/m^2$ ), overall heat transfer coefficient ( $U_{overall}$  in  $W/m^2K$ ) and temperature difference ( $\Delta T$  in Kelvin) is

$$Q' = U_{overall}\Delta T$$

In this paper a composite panel of 200 mm x 200 mm X 20 mm is considered, the panel is made up of three metals, for finding out the overall heat transfer coefficient, air of convective heat transfer coefficient of  $25 W/m^2K$  is considered as fluid medium on both sides of the panel.

## II. MODELLING

S.No	Material	Colour
1	Steel (Top and bottom covers)	Blue
2	Aluminium (Vertical brackets)	Green
3	Copper (Horizontal brackets)	Brown



CAD software Solid Works, the deigned model and is detailed in 1a and its components with material are detailed in table 1.

### III. THERMAL SIMULATION-FEM ANALYSIS

Modelling of Composite Panel is followed by Thermal analysis, to evaluate the overall heat transfer coefficient .

The following steps are followed in analysis: Solid

Works initial settings and methodology:

- Open solid works and select Thermal under simulation as shown in Fig 2a.
- Now from thermal loads select temperature , assign 25 °c for one face of model and on opposite face assign a temperature of 26 °C as shown in Fig 2b.(therefor  $\Delta t= 1K$ )
- Now from same loads select convective load and on both sides of model assign a convective heat transfer of 25 W/m<sup>2</sup>Kas shown in fig 2c, generally this convective heat transfer coefficient of air varies from 5 to 100 depending on geometry and flow, here a value of 25 is considered.
- Now using Solid work default mesh parameters discretization/meshing of model is done and is shown in Fig 2d.
- Now run the Simulation and the results get automatically gets loaded in the results column of simulation tree as shown in Fig 2e.
- Now right click on results and export the heat flux along Z axis , the values of heat flux of all elements are obtained in a excel file.get the average of the all.

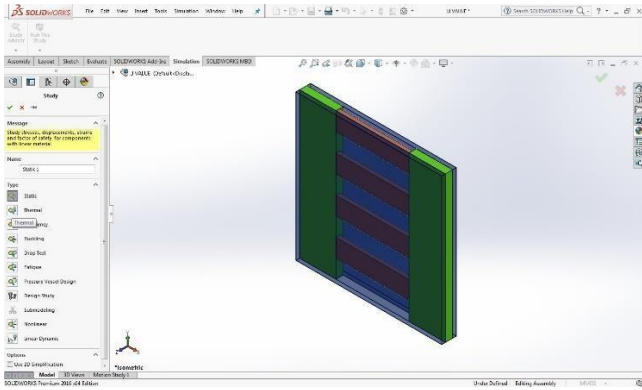


Fig.2a- Initializing Thermal Simulation

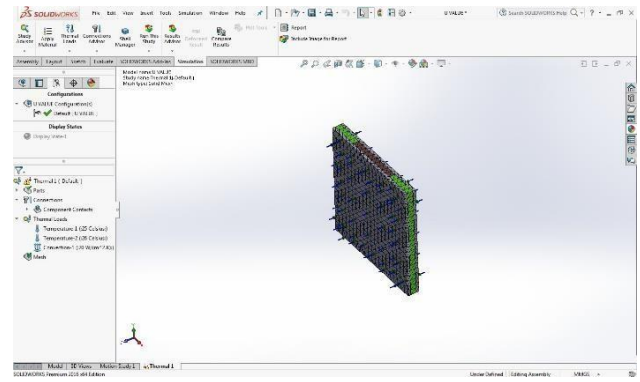


Fig 2 d : Meshing of Composite Panel

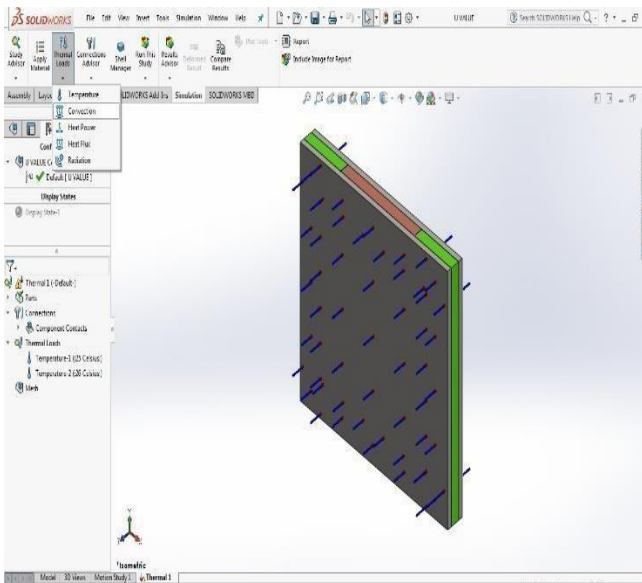


Fig.2b:Defining temperature in thermal loads

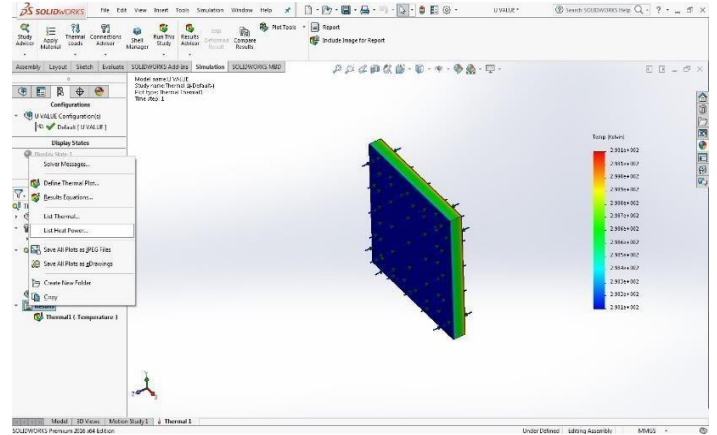


Fig 2 e :Results of Thermal simulation

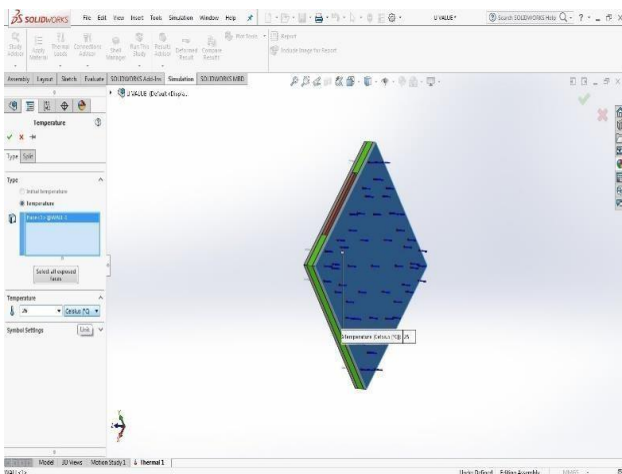


Fig.2c- Defining convective constant in Thermal loads

Node	X (mm)	Y (mm)	Z (mm)	HFLUX (W/m <sup>2</sup> )
6	5077	88.6296	58.4601	164.42 3.06E+03
7	4428	88.6296	198.46	164.42 3.04E+03
8	5044	88.6296	148.46	164.42 3.02E+03
9	6309	88.6296	48.4601	164.42 2.99E+03
10	4920	3.62961	173.46	164.42 2.96E+03
11	4929	8.62961	123.46	164.42 2.93E+03
12	5105	3.62961	148.46	164.42 2.96E+03
13	4488	3.62961	198.46	164.42 2.96E+03
14	5549	8.62961	123.46	164.42 2.96E+03
15	4448	88.6296	198.46	164.42 2.96E+03
16	5086	33.6296	148.46	164.42 2.95E+03
17	5628	88.6296	123.46	164.42 2.95E+03
18	4482	8.62961	198.46	164.42 2.95E+03
19	5100	13.6296	148.46	164.42 2.95E+03
20	6357	23.6296	48.4601	164.42 2.95E+03
21	4483	13.6296	198.46	164.42 2.95E+03
22	6382	8.62961	73.4601	164.42 2.95E+03
23	4489	33.6296	198.46	164.42 2.95E+03

Fig 2 f : Exported Results of Thermal simulation

#### IV. CONCLUSION

- The modeling of Composite Panel is done using solid works followed by thermal analysis using solid works simulation.
- The overall heat transfer coefficient along Z-axis is found out indirectly by using heat flux results (refer equation 1) for a temperature difference of 1 degree and its value is 2900W/m<sup>2</sup>K.

## REFERENCES

- [1] EOTA.ETAG 016: Guideline for European Technical Approval of Self-Supporting Composite Lightweight Panels, 2003.
- [2] ABAQUS, Standard Users Manual Ver. 6.10, Hibbitt, Karlsson & Sorensen, Inc. 2011.
- [3] ARTIFHEAT v.2.1, User Documentation, Gdańsk, 2001.
- [4] Polish Ministry of Infrastructure, Executive regulations of Buildings Technical Requirements, Warsaw, 2010.

[1]

*(PDF) EVALUATION OF OVERALL HEAT  
TRANSFER COEFFICIENT FOR  
ACOMPOSITE 3D PANEL USING FEM .*

Available from:

<https://www4.ncsu.edu/doster/NE400/Text/HeatExchangers/HeatExchangers.PDF>

# EFFECT OF WELDING SPEED AND GROOVE ANGLE ON STRENGTH OF BUTT WELD JOINT USING TIG WELDING

B. Dileep Kumar  
Department of Mechanical Engg.  
Malla Reddy College of  
Engineering, Maisammaguda,  
Dhulapally, Kompally,  
Secunderabad, Telangana-500100,  
India

Email:  
[dileepkumar4228@gmail.com](mailto:dileepkumar4228@gmail.com)

Mr. Vikash Kumar  
Assistant Professor  
Department of Mechanical Engg.  
Malla Reddy College of  
Engineering Maisammaguda,  
Dhulapally, Kompally,  
Secunderabad, Telangana-500100,  
India

Email: [vikashism2012@gmail.com](mailto:vikashism2012@gmail.com)  
Orcid Id: <https://orcid.org/0000-0002-5015-2761>

Dr. S. Ananth  
Professor, Department of  
Mechanical Engg.  
Malla Reddy College of  
Engineering Maisammaguda,  
Dhulapally, Kompally,  
Secunderabad, Telangana-500100,  
India

Email:  
[subramaniananth@gmail.com](mailto:subramaniananth@gmail.com)

**Abstract:** Welding is the metal joining process in which two or more metal having same material or different can be joined by heating to a plastic state. It is mostly used for joining metals in process industry, in fabrication, maintenance, repair of parts and structures. The metal plates and pipes used in process industry and they have welding strength as their important parameter. In this thesis, the welding speed and geometry to find out tensile and impact strength in case of butt weld joint will be done. For V-groove geometry different models of plate with various included angles from  $35^{\circ}$ ,  $45^{\circ}$ ,  $50^{\circ}$  will be made from structural steel (A633 Grade E). Currently different welding speeds are used in precision welding applications such as nuclear reactor pressure vessels, boilers etc. where welding accuracy as well as quality with strength is an important parameter. So in this project experimentation will be done on different welding speed such as 0.4 cm/sec, 0.8 cm/sec and 1.20cm/sec to prepare a V-groove butt weld joint. Generally the V-groove geometry with included angle up to  $60^{\circ}$  is in use.

**Keywords:** metal, welding, joint

## 1. INTRODUCTION:

Welding is, at its center, merely the way of bonding 2 objects of metallic. Whereas there are opportunity approaches in which to affix metallic (riveting, brazing and bonding, as an example), attachment has turn out to be the strategy of selection for its electricity, potency and flexibility.

There are loads of completely special attachment methods, and a number of are being unreal all of the time. Some methods use warmth to generally melt 2 objects of metal along, commonly including 'filler steel' into the joint to behave as a binding agent. Opportunity methods deem pressure to bind metal along, and still others use a mixture of each heat and stress. No longer like bonding and brazing, anywhere the metal gadgets being joined stay unaltered, the approach of attachment continually adjustments the work items. This may appear to be a trivial

reason; however it is certainly vital to know-how why attachment Produces such robust bonds. In the approaches of soldering and brazing, portions of steel are joined with the aid of introducing a third material (with a decrease melting factor) into the mixture. Melting this 0.33 material among the surfaces of the unique portions binds the portions together. The bond, but, is handiest as robust as the becoming a member of material. Welding, then again, cuts out the intermediary and joins the original portions immediately to each other. The result is a strong, cohesive bond that's regularly as strong as the fabric itself.

## 2.METHODOLOGY:

Objective of the work In this thesis, materials V-groove geometry distinct models of plate with diverse included angles from 35, 45, 50 will be crafted from structural metal (A633 Grade E). Currently special welding speeds are including zero.Four cm/sec, zero.Eight cm/sec and 1.20cm/sec to put together a V-groove butt weld joint. Effect of method current on the tensile power of weld joint may be analyzed.

**EXPERIMENTAL PROCEDURE:** In this thesis, experiments are made to understand the effect of TIG welding parameters welding speed and groove angle on output parameters such as hardness of welding, tensile strength of welding.



Finished components For the experiment, welding parameters selected are shown in table.

The welding current and electrodes considered are

PROCESS PARAMETERS	LEVEL1	LEVEL2	LEVEL3
WELDING SPEED ( cm/s)	0.4	0.8	1.20
GROOVE ANGLE( <sup>0</sup> )	35	45	50

GROOVE ANGLE( <sup>0</sup> )	WELDING SPEED ( cm/s)
35	0.4
35	0.8
35	1.2
45	0.4
45	0.8
45	0.6
50	0.4
50	0.8
50	1.2

GROOVE ANGLE( <sup>0</sup> )	WELDING SPEED ( cm/s)	ULTIMATE TENSILE STRENGTH (MPa)
35	0.4	375
35	0.8	410
35	1.2	451.197
45	0.4	403
45	0.8	440.581
45	1.2	372
50	0.4	375.287
50	0.8	369
50	1.2	378

**INTRODUCTION TO TAGUCHI TECHNIQUE:** Taguchi defines Quality Level of a product because the Total Loss

incurred by means of society due to failure of a product to perform as desired when it deviates from the added goal overall performance degrees.

This consists of fees associated with negative overall performance, operating prices (which adjustments as a product ages) and any added charges due to dangerous facet consequences of the product in use.

**Taguchi Methods:** Help businesses to perform the Quality Fix! Quality troubles are because of Noises inside the product or manner machine Noise is any unwanted impact that will increase variability. Conduct tremendous. Problem Analyses Employ Inter-disciplinary Teams. Perform Designed Experimental Analyses. Evaluate Experiments using ANOVA and Signal-to noise strategies

**Defining the Taguchi Approach:** Noise Factors Cause functional variation they fall into three “classes” outer noise – environmental conditions inner noise – lifetime deterioration three. between product noise – piece to piece variation the point then is to produce processes or products the are robust against noises: don’t spend the money to put off all noise, build designs (product and manner) that may perform as desired – low variability – within the presence of noise! we say: robustness = high quality to reliably meet our design goals means: designing quality in! we locate that taguchi taken into consideration three levels of design: stage 1: system design degree 2: parameter design degree three:

**TOLERANCE DESIGN :** All About Innovation – New Ideas, Techniques, Philosophies . Application Of Science And Engineering Knowledge Includes Selection Of: Material Processes Tentative Parameter Values : Parameter Design: Tests For Levels Of Parameter Values. Selects "Best Levels" For Operating Parameters to be Least Sensitive to Noises, Develops Processes Or Products That Are Robust A Key Step To Increasing Quality Without Increased Cost. Tolerance Design: A "Last Resort" Improvement Step. Identifies Parameters Having the greatest Influence On Output Variation. Tightens Tolerances On These Parameters. Typically Means Increases In Cost .Selecting Parameters for Study and Control. Select The Quality Characteristic. Define The Measurement Technique. Enumerate, Consider, And Select The Independent Variables And Interactions. Brainstorming .Shannon’s approach in which they’re decided via looking at the goods. FMEA – failure mode and results evaluation. Preliminary Steps in Improvement Studies. To Adequately Address The Problem At Hand We Must: Understand Its Relationship With The Goals We Are Trying To Achieve. Explore/Review Past Performance compare to favored Solutions three. Prepare An 80/20 Or Pareto Chart Of These Past Events: Develop A "Process Control" Chart -- This Helps To Better See The Relationship among Potential Control And Noise Factors. A Wise Person Can Say: A Problem Well Defined Is Already Nearly Solved!!

**TAGUCHI PARAMETER DESIGN FOR TURNING PROCESS:**

In order to pick out the system parameters affecting the selected device exceptional characteristics of turning, the subsequent process parameters are selected for the present work: reducing pace (A), feed fee (B) and intensity of reduce (C). The selection

of parameters of interest and their tiers is based totally on literature evaluate and a few initial experiments conducted. Selection of Orthogonal Array: The procedure parameters and their values are given in table. It was also decided to look at the 2 – factor interaction outcomes of technique parameters on the selected traits at the same time as turning. These interactions had been taken into consideration among slicing speed and feed charge (AXB), feed price and depth of reduce (BXC), cutting velocity and depth of cut (AXC).

PROCESS PARAMETERS	LE VEL1	LEVEL2	LEVEL3
WELDING SPEED ( cm/s)	0.4	0.8	1.20
GROOVE ANGLE(°)	35	45	50

1.Effect of welding geometry parameter on hardness for aisi304 tig. Welding is an area wherein technological tendencies out match the tendencies in its technology base that's generally driven with the aid of the outstanding industrial demand for welded structure. Reliability, Reproducibility and Viability necessities are forcing Technologists to take a look at weld defects consisting of distortion, warm cracking, in a systematic and logical technique than on experimental basis. Distortion is an unwanted bodily trade from specs in a fabricated structures is as a result of non-uniform growth and contraction of the weld metal at some stage in heating and cooling cycle of the welding manner many factors viz., fabric houses, welding system and strategies followed make accurate prediction of distortion hard. Groove perspective, Root gap and root face become taken to analyze Hardness in butt weld joints.

A overview paper on impact of welding pace and groove angle on Strength of butt weld joint the usage of tig welding.

Welding is most critical operation in any enterprise. It is crucial to optimize the diverse parameters of welding process in order that we can achieve the reliability, productivity and great of the goods. So industries are forcing the engineers to take a look at the welding manner parameters including electrodes, inert fuel, present day, voltage and so forth. The ojective of any industry is manufacturing of excessive quality merchandise at low fee and increase the manufacturing fee. TIG welding system is versatile and normally used operation for joining of materials with the software of warmth and /or strain or fillet material to increase the production with much less time and price.The upgoing examine is performed to analyze the impact of welding speed, groove angle and bevel top on strength of mechanical residences along with tensile check, effect take a look at. Also the current examine purpose to investigate the impact of welding speed on hardness of HAZ(Heat Affected Zone) and longitudinal and transver distortion of butt weld joint. Mechanical testings are performed to discover the mechanical houses of butt weld joint.

3.Studies on Effects of Welding Parameters on the Mechanical Properties of Welded Low-Carbon Steel.

In this work, the impact of warmth input at the mechanical homes of low-carbon metallic became studied the use of welding approaches: Oxy-Acetylene Welding (OAW) and Shielded Metal Arc Welding (SMAW). Two special edge preparations on a particular size, 10-mm thick low-carbon

metallic, with the following welding parameters: twin welding voltage of 100 V and 220 V, various welding currents at 100, one hundred twenty, and 150 Amperes and unique slight metal electrode gauges of 10 and 12 were investigated. The tensile power, hardness and effect electricity of the welded joint had been carried out and it changed into found that the tensile energy and hardness lessen with the increase in heat input into the weld. However, the effect power of the weldment increases with the increase in heat enter. Besides it was additionally found that V-grooved aspect training has higher mechanical properties as compared with directly part training under the equal situations. Microstructural examinations carried out discovered that the cooling charge in specific media has substantial impact on the microstructure of the weldment. Pearlite and ferrite have been located within the microstructure, however the proportion of ferrite to pearlite various below distinct situations.

Results: Using randomization technique, specimen was turned and cutting forces were measured with the three – dimensional dynamometer. The experimental data for the cutting forces have been reported in Tables. Feed and radial forces being ‘lower the better’ type of machining quality characteristics, the S/N ratio for this type of response was and is given below:

Where  $y_1, y_2, \dots, y_n$  are the responses of the machining characteristics for each parameter at different levels.

TAGUCHI ORTHOGONAL ARRAY

GROOVE ANGLE(°)	WELDING SPEED ( cm/s)
35	0.4
35	0.8
35	1.2
45	0.4
45	0.8
45	1.2
50	0.4
50	0.8
50	1.2

OBSERVATION : The following are the observations made by running the experiments. The ultimate tensile strength observed.

GROOVE ANGLE(°)	WELDING SPEED ( cm/s)	ULTIMATE TENSILE STRENGTH (MPa)
35	0.4	375

35	0.8	410
35	1.2	451.197
45	0.4	403
45	0.8	440.581
45	1.2	372
50	0.4	375.287
50	0.8	369
50	1.2	378

**3. RESULTS:**

Taguchi technique stresses the significance of reading the response variant the usage of the sign-to-noise (S/N) ratio, resulting in minimization of great characteristic variation due to uncontrollable parameter. The slicing pressure is taken into consideration because the quality feature with the idea of “the larger-the-better”. The S/N ratio for the larger-the-higher is

$$S/N = -10 * \log(\Sigma(Y^2)/n)$$

Where n is the range of measurements in a tribulation/row, in this case, n=1 and y is the measured value in a run/row. The S/N ratio values are calculated by means of taking into account above Eqn. With the help of software program Minitab 17.

The pressure values measured from the experiments and their corresponding S/N ratio values are listed in Table

↓	C1	C2	C3	C4	C5	C6
	GROOVE ANGLE	WELDING SPEED	TENSILE STRENGTH	TENSILE STRENGTH1	SNRA1	MEAN1
1	35	0.4	375.000	376.00	51.4922	375.500
2	35	0.8	410.000	409.00	52.2451	409.500
3	35	1.2	451.197	450.90	53.0845	451.048
4	45	0.4	403.000	403.01	52.1062	403.005
5	45	0.8	440.581	441.21	52.8867	440.895
6	45	1.2	372.000	372.10	51.4120	372.050
7	50	0.4	375.287	375.26	51.4870	375.274
8	50	0.8	369.000	368.00	51.3287	368.500
9	50	1.2	378.000	379.00	51.5613	378.500

**CONCLUSION:**

The experiment designed by Taguchi method fulfills the desired objective. Fuzzy interference system has been used to find out the ultimate tensile strength .The all possible values of have been calculated by using MINITAB 17.0 software. Analysis of variance (ANOVA) helps to find out the significance level of the each parameter. The optimum value was predicted using

MINITAB-17 software. The welding parameters are Welding speed, and groove angle for TIG welding of work piece steel. In this work, the optimal parameters of welding speed are 0.4cm/s, 0.8 cm/s & 1.2 cm/s, groove angle 35,45 and 50 degrees. Experimental work is conducted by considering the above parameters. Ultimate tensile strength validated experimentally. The experimental results confirmed the validity of the used Taguchi method for enhancing the welding performance and optimizing the welding parameters in TIG welding at welding speed 1.2 cm/s , and groove angle 35.

**REFERENCES:**

[1] N.S. Rajkumar, Srihari, “A examine of impact of groove perspective on angular distortion& impact strength in butt weld”,International convention on mechanical engineering, December,2001. [2] N,Ren,M.Zan, “Constructing effect of weld & warmness affected zone on deformation behavior of welded tubes in numerical manipulate bending procedure”, Journal on material processing era(2012). [3] Rossi ,E. Boniface, “Welding engineering”, Mc Grow-Hill Book company New York,2012. [4] I. Sattari-Far ,M.R Farahani, “Effect on weld groove form& bypass range on residual stresses in butt weld pipes”, International magazine of strain vessel & piping (2009) .[5] D.Akbari,I. Sattari-Far, “Effect of welding heat input on residual stresses in butt weld of assorted pipe joints”, International magazine of stress vessel & piping (2009) .[6] T. H. Hyde, J. A. Williams, W. Sun, “Factors, Defined from Analysis, Contributing to the Creep Performance of Weld Repairs”, Creep Performance of Weld Repairs OMMI (Vol. 1, Issue three) December 2002. [7] T. H. Hyde, J. A. Williams, A. A. Becker,W. Sun, “A overview of the finite detail evaluation of repaired welds under creep conditions”, Review of FE evaluation of repaired welds OMMI (Vol. 2, Issue 2) Aug. 2003.[8] Tseng, K. H., & Hsu, C. Y. (2011). Performance of activated TIG system in austenitic stainless steel welds. Journal of Materials Processing Technology, 211(3), 503-512. [9] Narang, H. K., Singh, U. P., Mahapatra, M. M., & Jha, P. K. (2011). Prediction of the weld pool geometry of TIG arc welding by means of using fuzzy common sense controller. International Journal of Engineering, Science and Technology, 3(nine), 77-85.

## *EXPERIMENTAL INVESTIGATIONS OF TUBE CONFIGURATION IN HORIZONTAL SURFACE CONDENSER*

N RAGHAVAN  
nraghavan.swastik@gma il.com

LANKA PRIYANKA  
Lohilakshmi.lakshmi@g mail.com

SAI DEEPIKA  
suryabogaram14@gmail. com

Assistant professor<sup>1,2,3</sup>, Malla Reddy College of Engineering, Hyderabad, INDIA

### ABSTRACT

*This study presents the analyses of the effect of the arrangement of tubes in a tube bundle in a horizontal, two-pass condenser on the amount of heat transferred to the circulating water in the tubes. The tube bundle is assumed to act as a staggered tube bank in cross- flow with downward superheated steam flow. The saturated circulating water is assumed to be turbulent flow. Previously defined relationships for heat transfer through tube banks, including condensate inundation, vapor shear, and the effect of tube surface geometry are used in analyzing six tube configurations to determine the largest change in temperature of the circulating water. The heat flux in the system is defined as a function of the condenser and tube material properties, tube geometry, tube spacing, condensate inundation and steam velocity. Numerical modeling of the six tube configurations using a Reynolds- averaged Navier-Stokes (RANS) approach is presented to confirm the analytical results. Analyses of the analytical and numerical results from the six configurations examined provide the optimal tube arrangement for maximum heat transfer to the circulating water. It is found that the circulating water temperature is dependent. tubes rows where the steam-air mixture velocities are the highest. Furthermore, the magnitude of the velocity profile is proportional to the magnitude of the change in circulating water temperature.*

*Keywords: condenser; boiler; CFD.*

### 1. INTRODUCTION RANKINE CYCLE

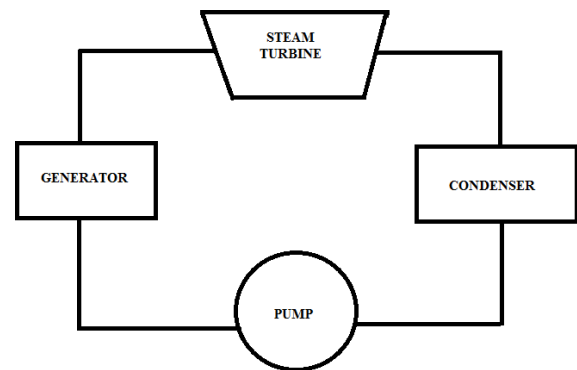


Fig.1.1 Rankine cycle

**FUNCTION OF STEAM CONDENSER** The function of a surface condenser is to create the lowest possible turbine or process operating back pressure while condensing steam. The condensate generated is usually recirculated back into the boiler and reused. Both of these operations are accomplished at the best efficiency consistent with the ever- present problem of economy. Surface Condenser also provides a convenient point for make up water entry and expelling point for non condensable gases.

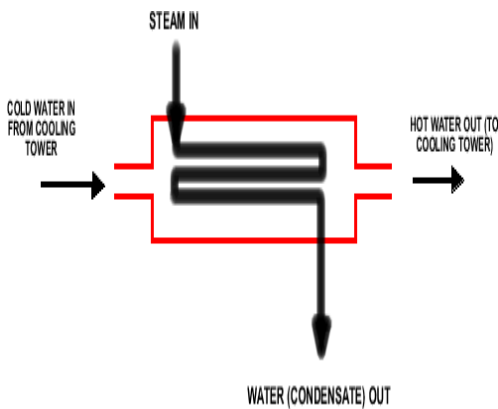


Fig.1.2 Function of Steam Condenser

**CLASSIFICATION OF CONDENSERS** Heat removed from a product during the refrigeration process must be disposed of. This heat can be dumped as waste or reused for space, water, or process heating. The section of a refrigeration system that accomplishes heat rejection is the condenser. Two types of condensers are currently available:

- Direct Type Condenser
- Surface Condenser

## 2. LITERATURE REVIEW

Several papers have been written providing heat transfer, vapor velocity, film condensation and pressure drop correlations over horizontal tube banks based on experimental results and detailed simulations using computational fluid dynamics (CFD) models.

An analysis of a two-pass condenser is performed by **Malin [1]** using a CFD model simulating flow and heat transfer. In Malin's work, a single-phase approach for the steam-air mixture flow within the condenser is used to calculate the performance of a condenser with a superheated steam supply.

The simulated condenser employs the use of two tube bundles of parallel staggered tubes with the first-pass entering the lower bundle and exiting the condenser through the upper tube bundle.

Browne and Bansal [2] examined variations in experimental observations made in over 70 papers to provide an overview of condensation heat transfer on horizontal tube bundles for downward flowing condensing vapor. The effects of surface geometry, condensate inundation, vapor shear and gravity are studied.

Wilson and Bassiouny [3] provided results for laminar and turbulent flow of air across a single tube row as well as staggered and in-line tube banks. The effects of flow and tube geometry on the Nusselt number, friction factor, velocity and turbulence kinetic energy profiles are presented therein.

Mehrabian [4] evaluated the heat transfer and pressure drop of air over a single, circular tube and over a tube bank based on experimental results. Additionally, a relationship between the velocity distribution of air in cross flow and pressure drop over horizontal tubes is provided.

## 3. PROBLEM DESCRIPTION:

The objective of this project is to analyze different tube configurations in a tube bundle to determine the best arrangement for the maximum amount of heat transferred to the circulating water in a horizontal, two-pass condenser. The six configurations shown below will be examined.

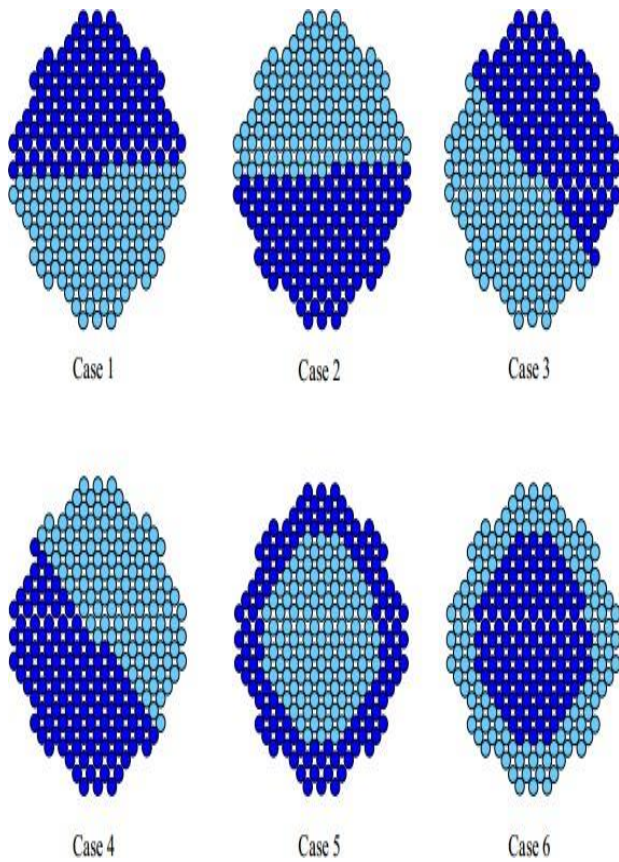


Fig. 2.1 Cross-Sectional View of Tube Configurations

The dark blue and light blue portions of the cross-sectional views in Fig. 2.1 represent the cold first-pass and warmer second-pass in the tube bundle, respectively.

#### 4. NUMERICAL ANALYSIS - MODELING USING RANS SOLVER

FLOW3D, CFD software developed by Flow Science Inc., is used to simulate the condenser for each of the six cases. The condenser geometry, initial conditions, operating parameters and assumptions made in the heat and mass transfer algorithm, are used to create the FLOW3D models. Analyzing the condenser and tube bundle using FLOW3D generated a steam-air

mixture velocity profile, which is used to confirm the velocity profile created in the heat and mass transfer algorithm.

A numerical mesh is created for each of the six cases. A large grid is generated that included the entire cross-section of the condenser. A smaller, denser grid embedded within the larger grid is created for the tube bundle. This nested grid permitted greater resolution around the individual tubes. The first-pass tubes and second-pass tubes are grouped into separate subcomponents within the nested grid. These tube regions are further arranged into separate subcomponents for Cases 3 through 6 in order to group together the tubes exhibiting similar heat fluxes and circulating water temperatures, which varied as a result of the tube configurations. Since the subcomponents are treated as having the same properties, smaller subcomponents had properties closer to the actual properties of the individual tubes that made up each subcomponent. The average circulating water temperature and overall heat transfer coefficient is calculated for each subcomponent. In order for FLOW3D to treat the tubes as having a constant circulating water inlet temperature, fixed surface heat transfer coefficients are applied to the tubes, thus assuming the tubes are maintained at a constant temperature. This is necessary to prevent the tube inlet circulating water temperature from converging to a higher temperature with the steam inlet temperature, preventing any heat transfer from occurring.

#### 5. ANALYTICAL DISCURSION

The six tube configurations presented and analyzed to determine the outlet circulating water temperature using the mathematical model described. Since the tube bundle contains an odd number of tubes, the

	Temperature (°C)	
	Mehrabian	FLOW3D
First-Pass Outlet	24.872	22.380
Second-Pass Outlet	29.657	23.147
T Between Passes	4.786	0.767
Overall ΔT	8.547	2.037

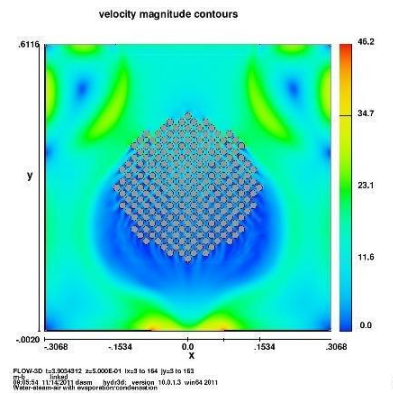
number of tubes has been divided as equally as possible in the first and second-passes to prevent the number of tubes in a particular pass from influencing the circulating water temperature.

The mathematical model, based on the work of Malin [1], employs an iterative solution method to solve for the heat flux, and subsequently for the outlet circulating water temperature. Applying the algorithm to the six cases yielded values for the heat flux from the steam-air mixture to the circulating water, the outer tube wall temperature, the interface temperature and the circulating water temperature for every row of tubes in the tube bundle. The heat flux distribution through the tube bundle is analyzed by graphing the change in circulating water temperature for each row along the length of the tubes in the first and second-passes. The six cases are compared by evaluating the average circulating water temperatures of the first-pass and second-pass tubes.

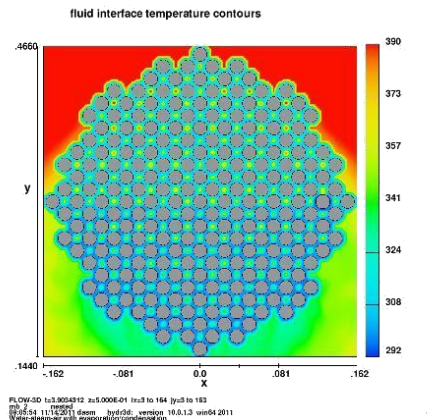
An energy balance is performed for each case to validate the algorithm results. The results of the energy balance for Case 1 are provided and are representative of the results obtained from each case since the methodology presented in followed for all six cases.

The six tube configurations are modeled in FLOW3D, which provided the velocity of the steam-air mixture. The FLOW3D velocity profiles are used in the algorithm to calculate circulating water temperatures. Comparisons between the initial results from the algorithm using velocity profiles based on Mehrabian [4] and those obtained using FLOW3D data are presented.

FLOW3D Velocity Magnitude Contours



FLOW3D Mixture Temperature Contours



CONCLUSION

Table.5.1 Steam-Air Mixture Velocity Profiles

Steam-Air Mixture Velocity Profiles (m/s)								
	Mehrabn		FLOW3D					
Row	Cases 1-6	Case 1	Case 2	Case 3	Case 4	Case 5	Case 6	
1	48.20	26.74	26.74	26.77	26.72	26.82	26.68	
2	68.16	26.93	26.80	26.79	26.81	26.76	26.85	
3	83.48	25.58	25.84	25.84	25.84	25.79	25.87	
4	96.40	23.26	23.57	23.58	23.57	23.52	23.59	
5	107.78	25.33	30.17	30.14	30.12	30.18	30.24	
6	118.06	24.33	24.37	24.31	24.32	24.36	24.31	
7	127.52	24.01	24.04	24.01	24.01	24.07	24.10	
8	136.33	19.41	19.62	19.61	19.64	19.64	19.72	
9	144.60	18.92	17.43	17.34	17.38	17.33	17.08	
10	152.42	18.71	18.76	18.82	18.75	18.87	18.84	
11	159.86	13.71	13.93	13.98	13.91	14.03	13.98	
12	166.97	13.77	13.75	13.78	13.70	14.00	13.94	
13	173.78	10.49	10.57	10.46	10.48	10.72	10.69	
14	180.34	10.98	11.05	10.96	10.96	10.94	10.87	
15	186.67	9.79	9.90	9.72	9.74	9.75	9.62	
16	192.80	9.56	9.64	9.53	9.51	9.34	9.27	
17	198.73	7.64	7.80	7.60	7.61	8.23	8.23	
18	204.49	7.19	7.93	7.82	7.80	8.35	8.34	
19	210.09	6.19	6.77	6.54	6.55	6.87	6.81	
20	215.55	6.04	6.16	6.01	6.03	6.63	6.27	
21	220.87	5.28	5.85	5.53	5.49	5.97	5.93	
22	226.07	4.63	5.37	5.16	5.14	5.73	5.37	
23	231.15	4.77	5.12	4.72	4.67	5.18	5.12	
24	236.13	4.39	4.72	4.37	4.33	5.05	4.65	
25	240.99	4.64	5.08	4.49	4.48	5.18	4.90	

Six unique tube configurations in a horizontal, two-pass condenser are analyzed in an iterative heat and mass transfer algorithm to determine the outlet circulating water temperature through the tubes. The algorithm considers the heat transferred from the steam-air mixture to the interface

between the mixture and condensate, through the condensate, through the tube wall and into the circulating water. The algorithm also takes into account the latent heat produced by the condensate forming around the tubes. A steam-air mixture velocity profile is established using the approach taken by Mehrabian. The outlet circulating water temperature for each first-pass row is calculated and using a weighted average, a new inlet circulating water temperature is created for the second-pass tubes, from which an exit circulating water temperature is calculated.

The results using the assumed Mehrabian-based steam-air mixture velocity profile in the heat and mass transfer algorithm show that all six cases has higher outlet circulating water temperatures for the second-pass tubes than for the first-pass tubes. More heat is transferred to the first-pass tubes when these tubes are located on the bottom of the tube bundle, such as in Cases 2 and 4. Case 2 resulted in the most heat transferred to the first-pass tubes, resulting in the warmest circulating water at the outlet of the first-pass, with a temperature of 25.996°C. Case 1 resulted in the largest change in circulating water temperature from the first-pass to the second-pass with a change of 4.786°C. Overall, Case 3 resulted in the most heat transferred to the circulating water, with an average second-pass outlet temperature of 29.758°C.

The Mehrabian steam-air mixture velocity profile that is used in the algorithm could be more accurate and closer to the actual velocity in the condenser, similar to the velocity profile seen in the FLOW3D simulations, by using a different correction factor. The Mehrabian [4] approach directly increases the pressure drop, and consequently, the row velocity with each

successive row, which significantly increases the velocity at higher rows. The steam-air mixture velocity profiles obtained from FLOW3D simulations of the six cases decrease as the steam-air mixture moves downward through the tube bundle, due to the tubes obstructing the mixture flow path. This velocity profile is opposite from the assumed profile based on Mehrabian. The FLOW3D velocity profiles obtained for each of the six cases are relatively similar and exhibit symmetry. Comparable to the results using the Mehrabian-based velocity profile, the results using FLOW3D data shows an increase in circulating water temperature in both the first and second-passes. Case 1 has the hottest circulating water temperature of 22.380°C at the outlet of the first-pass tubes. Case 2 has the largest change in temperature between the first and second-passes of 1.322°C. Case 5 has the hottest second-pass circulating water temperature of 23.216°C.

In comparing results calculated from the Mehrabian and FLOW3D steam-air mixture velocity profiles in the algorithm, the heat flux and circulating water temperature are found to be proportional to the velocity. As the velocity increases, the heat flux and circulating water temperature increases, consistent with thermodynamic principles. The first-pass tubes that experience the highest velocity, which are the lowest tube rows with a Mehrabian-based velocity profile (Cases 2 and 4) and the highest tube rows with a FLOW3D-based velocity profile (Cases 1 and 3), has the most heat transfer to the tubes. The tubes where the highest velocities result in the highest outlet circulating water temperature. Therefore, the velocity is proportional to the circulating water temperature.

The FLOW3D models may be refined to more accurately compare the results of the

algorithm with those employing the Mehrabian approach to the steam-air mixture velocity. The FLOW3D grid that is generated is relatively coarse and the flow is assumed laminar in order to expedite simulating all six cases. A higher grid resolution and assuming a turbulent steam-air mixture flow through the bundles would each increase the predicted maximum velocity through the tubes. A grid sensitivity and/or closure model sensitivity analysis could be performed to further validate the results obtained herein.

## REFERENCES

- A. Behzadmehr, N. Galanis and A. Laneville, Low Reynolds number mixed convection in vertical tubes with uniform wall heat flux, *International Journal of Heat and Mass Transfer* **46** (2003), pp. 4823–4833.
- A. E. Bergles and W. J. Marnar Augmentation of Highly Viscous Laminar Heat Transfer Inside Tubes with Constant Wall Temperature, *Experimental Thermal and Fluid Science* 1989; 2:252-267.
- A.E. Saad, A.E. Sayed, E.A. Mohamed, M.S. Mohamed, Experimental study of turbulent flow inside a circular tube with longitudinal interrupted fins in the stream wise direction, *Experimental Thermal Fluid Science* 15 (1) (1997) 1–15.
- Alam, P.S. Ghoshdastidar, A study of heat transfer effectiveness of circular tubes with internal longitudinal fins having tapered lateral profiles, *International Journal of Heat and Mass Transfer* 45 (6) (2002) 1371–1376.
- Bergles, A. E., and Joshi, S. D., Augmentation Techniques for Low Reynolds Number In-Tube Flow, in *Low Reynolds Number Flow Heat Exchangers*, S. Kakac, R. K. Shah, and A. E. Bergles, Eds. Hemisphere, Washington, D.C., pp. 695-720, 1983.
- B. Yu, J.H. Nie, Q.W. Wang, W.Q. Tao, Experimental study on the pressure drop and heat transfer characteristics of tubes with internal wave-like longitudinal fins, *Heat Mass Transfer* 35 (1999) 65–73.
- C.P.Kothandaraman.S.Subramanyan. Heat and Mass transfer Data book  
New age international publisher sixth edition.
- C.R. Friedrich, S.W. Kang, Micro heat exchangers fabricated by diamond machining, *Precision Engineering* 16 (1994) 56–59.
- D.A. Olson, Heat transfer in thin, compact heat exchangers with circular, rectangular, or pin-fin flow passages, *ASME Journal of Heat Transfer* **114** (1992), pp. 373–382.
- D Q kern design of process heat transfer.D.Q. Kern, *Process Heat Transfer*, McGraw-Hill, New York, 1950.
- Ebru Kavak Akpinar Evaluation of heat transfer and exergy loss in a concentric double pipe exchanger equipped with helical wires. *Energy Conversion and Management* 47 (2006). 3473-3486.
- e. r. g. eckert, r. j. goldstein, w. e. ibele, s. v. patankar, t. w. simon, n. a. decker, s. l. girshick, p. j. strykowski, k. k. tamma, a. bar-cohen, j. v. r. heberlein and d. l. hofeldt Heat transfer-a review of 1990 literature *Int.J Heat Mass Trans.* Vol. 34, No. 12, pp. 2931-3010, 1991.
- Edited by Chang S. Hsu Exxon Mobil Research and Engineering Company Baton Rouge, Louisiana, And Paul R. Robinson PQ Optimization Services Katy, Texas, USA *Practical Advances in Petroleum Processing Volume 2*
- G. Fabbri, A genetic algorithm for fin profile optimization, *Int. J. Heat Mass Transfer* 40 (9) (1997) 2165–2172.
- G. Fabbri, Heat transfer optimization in internally finned tubes under laminar flow conditions, *Int. J. Heat Mass Transfer* 41 (10) (1998) 1243–1253.
- John H. Lienhard IV / John H. Lienhard V. A heat transfer textbook third edition.
- Kuehn, T. H. and Goldstein, R. J. An experimental and theoretical study of natural convection in the annulus between horizontal concentric cylinders. *Journal of Fluid Mechanics*, 1976, 74, 695-719.

# Effect of Geometrical and Roughness Parameters on Artificially Roughened Solar Air Heater

Md. Ahmad Kamal Hassan  
 Department of Mechanical Engg.  
 Jamia Millia Islamia, New Delhi, India  
 Email: [ahmadkamalpatna@gmail.com](mailto:ahmadkamalpatna@gmail.com)

Dr. M. Muzaffarul Hasan  
 Assistant Professor  
 Department of Mechanical Engg.  
 Jamia Millia Islamia, New Delhi, India  
 Email: [mmhasan@jmi.ac.in](mailto:mmhasan@jmi.ac.in)

## ABSTRACT

Artificial roughness employed on the absorber plate of SAHs is the most effective method to augment the rate of heat transfer to flowing fluid in the roughened duct of solar air heater. Artificial roughness provided is of various forms like ribs, dimples, baffles, wire mesh, delta winglets, etc. The objective of this paper is to analyze the various roughness geometries used on absorber plate in order to improve the heat transfer and friction characteristics. Augmentation in heat transfer for roughened SAHs is obtained by destroying laminar sub-layer in the vicinity of the absorbing surface. However, this gain is accomplished at the expense of increase in pressure drop. The main aim of this paper is to determine the optimum roughness geometry parameter at which maximum heat transfer is obtained at minimum frictional losses.

**Keywords:** Solar air heater, Artificial roughness, roughness pitch, roughness height

## 1. INTRODUCTION

Solar air heaters works on solar thermal technology in which the energy from the sun is captured by an absorbing medium and used to heat air. Solar air heating is a renewable energy heating technology used to heat or condition air for buildings or process heat applications. It is typically the most cost-effective out of all the solar technologies, especially in commercial and industrial applications, and it addresses the largest usage of building energy in heating climates, which is space heating and industrial process heating [34]. The value of heat transfer coefficient and heat capacity for air is low which reduces the heat transfer rate and thus increases the heat loss to the surroundings. A large number of researchers have used solar air heaters of different configurations to remove these drawbacks associated with solar air heaters to better serve the purpose of air heating [35]. Simple flat plate collector is the simplest and most commonly used type of collector. It is composed of one, two or three glazing over a flat plate which is backed by insulation. In flat plate collectors, the area absorbing the solar radiation is the

same as the area capturing solar radiation. The collector are oriented towards the equator facing north in the southern hemisphere and facing south in the northern hemisphere [21]. Different types of artificially roughened solar collectors used are shown in Fig. 1.

### 1.1 Artificially roughened solar air heaters

In order to attain higher convective heat transfer coefficient, turbulent flow at the heat transfer surface is required. The artificial roughness has been used extensively for the enhancement of forced convective heat transfer coefficient in solar air heaters. It is found that the use of artificial roughness on heat transferring surface breaks the viscous sub-layer in the proximity of the surface. However, creating turbulence requires energy that comes from the fan or the blower. Hence, it is desirable to create the turbulence very close to the surface only where the heat transfer takes place and the core of the flow is not disturbed to avoid excessive losses. This can be achieved by using roughened surfaces on the air side. Use of artificial roughness seems to be an attractive proposition for improving the heat transfer coefficient [55]. The artificial roughness is one of the most effective methods considering heat

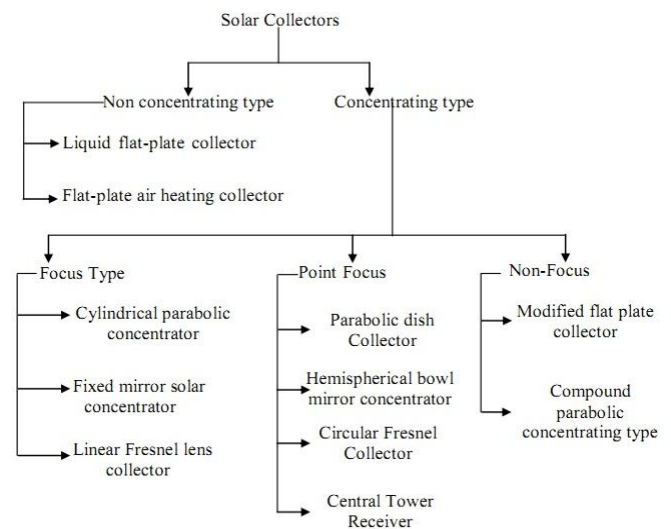


Fig. 1. Different types of solar collectors

transfer coefficient enhancement with limited frictional losses. Several investigators have used different

geometries of artificial roughness on the underside of the absorber plate to study the augmentation of heat transfer with corresponding increase in the pumping power. The major thermal resistance in a solid-fluid interaction is due to the formation of a boundary layer and efforts for enhancing heat transfer have been directed towards artificially destroying or disturbing the boundary layer [56]. In order to attain higher heat transfer co-efficient, it is desirable that the flow at the heat transferring surface is to be made turbulent. However, excessive turbulence leads to increase power requirement from the fan or blower to make the air flow through the duct. It is therefore desirable that the turbulence must be created only in the region very close to the heat transferring surface i.e. laminar sub-layer only. To minimize the friction losses, special care should be taken while selecting the dimension for the roughness geometries like height of the roughness element should be kept small in comparison with the duct dimensions. This has been achieved by active, passive or some combination of active and passive methods.

### 1.2 Active methods

These methods require additional external energy. Some of the most commonly used active methods are mentioned below:

- (i) Mixing or scrubbing of the fluid from the heat transferring surface by mechanical means.
- (ii) Vibrating or rotating the hot surface which causes the boundary layer thickness to decrease significantly.
- (iii) Flow subjected to acoustic waves of 1 Hz to ultrasonic frequency.
- (iv) Suction of heated fluid through porous surface.

### 1.3 Passive methods

In case of the passive techniques, the direct input of external power is not required. They generally use surface or geometrical modifications to the flow channel, or incorporate an insert, material, or additional device. The artificial roughness is one of passive techniques of enhancement of heat transfer. In this technique, the surface is modified by using different types of roughness that promotes turbulence in the flow field, primary in single phase flow and does not increase the area of heat transferring surface. These include:

- (i) Use of extended heat transfer surfaces.
- (ii) Use of swirl flow devices such as twisted tap inserts to create rotating flow.
- (iii) Turbulence promoters or roughened heating surfaces to reduce the thickness of the laminar sub-layer or to break the laminar sub-layer.

## 2. ANALYSIS OF ARTIFICIALLY ROUGHENED SURFACE

An extensive experimental study of turbulent flow of fluids in rough pipes with various degrees of relative roughness heights ( $e/D_h$ ) with a range of Reynolds number from 600 to  $10^6$  was carried out by Nikuradse [57]. The roughness was obtained by sand grains cemented to the walls of the pipes. It was found that the friction factor decreases as Reynolds number increases. Based on the law of wall similarity, a correlation for friction factor for flow over sand grain roughness was developed. His data, covering a wide range of roughness heights were correlated by the friction similarity function as given below:

$$f = 2 \left[ A + B \ln \left( V^* e / \bar{u} \right) - 2.456 \ln \left( 2e / D_h \right) \right]^2 \quad (1)$$

where, 'A' and 'B' are parameters depending upon the regimes of flow discussed below and ' $\bar{u}$ ' is the mean velocity. The term  $V^*$  is the friction velocity, defined mathematically as:

$$V^* = \sqrt{(\tau_o / \rho)} \quad (2)$$

where, ' $\tau_o$ ' is the wall shear stress and ' $\rho$ ' is the density of the flowing fluid.

Here, a term called Roughness Reynolds number ( $e^+$ ) is defined as given below:

$$e^+ = V^* / (e / \bar{u}) \quad (3)$$

The roughness Reynolds number ( $e^+$ ) defined in terms of  $e/D_h$ , Re, f and is expressed as follows:

$$e^+ = \text{Re} \left( e / D_h \right) \sqrt{f / 2} \quad (4)$$

Eq. (1) can be rewritten as:

$$f = 2 \left[ A + B \ln \left( e^+ \right) - 2.456 \ln \left( 2e / D_h \right) \right]^2 \quad (5)$$

The law of wall similarity was proposed by Nikuradse by correlating his experimental data for different roughened tubes is as follows:

$$U^+ = \frac{\bar{u}}{V^*} = 2.5 \ln \left( \frac{Y}{e} \right) + A \quad (6)$$

He found that a plot of parameter "A" as a function of  $\log \left( V^* e / \bar{u} \right)$  is very similar to the curve for the resistance

law obtained by plotting  $\left( \frac{1}{(2/f)^{0.5}} \right) + 2 \log \left( 2e / D_h \right)$  vs.  $\left( V^* e / \bar{u} \right)$

From this the value of "A" was deduced as:

$$A = \sqrt{\frac{2}{f}} + 2.5 \ln \left( \frac{2e}{D_h} \right) + 3.75 \quad (7)$$

Thus,

$$A = U^+ - 2.75 \ln \left( \frac{Y}{e} \right) = \sqrt{\frac{2}{f}} + 2.5 \ln \left( \frac{2e}{D_h} \right) + 3.75 \quad (8)$$

The non-dimensional parameter "A" is named differently by different investigators as the roughness parameter by (Han et al.) [58] or momentum transfer function (Han et al.) [59]

or roughness function (Lau et al.) [60] and is commonly denoted by  $R(e^+)$ . The relation for  $R(e^+)$  is given as:

$$R(e^+) = \sqrt{\frac{2}{f}} + 2.5 \ln\left(\frac{2e}{D_h}\right) + E \tag{9}$$

where,  $E$  is geometric parameter and depends on the configuration of the duct. The value of ‘ $E$ ’ was reported by Nikuradse as 3.75 for pipe.

The plot of the roughness function,  $R(e^+)$ , against roughness Reynolds number ( $e^+$ ) obtained by Nikuradse is shown in Figure. 2.1 The three flow regions shown in Figure 2.2 are explained as under:

**2.1 Hydraulically Smooth Flow ( $0 < e^+ < 5$ )**

In this flow region of low surface roughness, there is no effect of roughness on the friction factor. The values of the friction factor coincide with those for a smooth pipe for all values of relative roughness height ( $e/D_h$ ). Nikuradse [1952] correlated the measured of pressure loss data in this regime in the form of  $R(e^+)$ .

$$R(e^+) = 5.5 + 2.5 \ln(e^+) \tag{10}$$

**2.2 Transitionally Rough Flow ( $5 \leq e^+ \leq 70$ )**

In transition zone, the surface roughness becomes noticeable and increase in friction factor with increase in roughness Reynolds number ( $e^+$ ) can be observed. This zone reveals that the resistance factor depends on the Reynolds number and relative roughness height. The roughness height ( $e$ ) and the projection extends through the boundary layer creates vortices which produce an additional loss of energy. Increase in the roughness Reynolds number, the projections passing above the viscous sub-layer increases due to reduced viscous sub-layer thickness with increase in Reynolds number. With increase in the roughness Reynolds number the energy loss is high.

**2.3 Fully Rough Region ( $e^+ > 70$ )**

In fully rough region, the roughness Reynolds number attains a constant value and roughness function is independent of the roughness Reynolds number. Energy loss due to the vortices attains a constant value and an increase in the roughness Reynolds number no longer increases the friction factor.

Law of the wall as proposed by Nikuradse has been represented in Figure. 2.2 which depicts dimensionless velocity ( $U^+$ ) as a function of dimensionless distance ( $Y^+$ ). The different zones of the velocity profile are represented as under:

$$U^+ = Y^+, \text{ for laminar sub-layer, } 0 < Y^+ < 5 \tag{11}$$

$$U^+ = 5.0 \ln Y^+ - 3.5, \text{ for buffer zone, } 5 \leq Y^+ < 30 \tag{12}$$

$$U^+ = 2.5 \ln Y^+ + 5.5, \text{ for turbulent zone, } Y^+ > 30 \tag{13}$$

The different flow regimes velocity profile and law of wall similarity for flow under rough surface as observed by Nikuradse is shown in Figure 2.1 and 2.2 respectively.

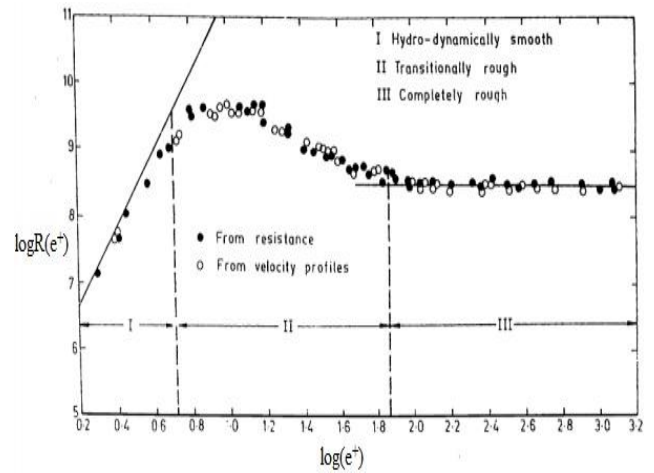


Fig. 1 Relation between roughness function  $R(e^+)$  and roughness Reynolds number

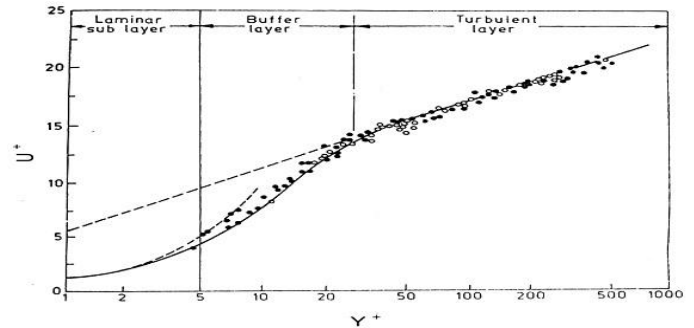


Fig. 2 Velocity profile for flow in circular smooth tubes at high Reynolds number

Fig. 2.3 shows the flow patterns downstream of a rib as the rib height and pitch are changed. Separation occurs at the rib, forming a widening free shear layer which reattaches 6-8 rib heights downstream from the separation point. For value of relative roughness pitch less than 10, the reattachment will not occur thus reducing the heat transfer. While, an increase in roughness pitch beyond 10 also results in decreasing the enhancement, Prasad and Saini [61]. Therefore there exists an optimum arrangement of pitch and height that will result in maximum heat transfer enhancement.

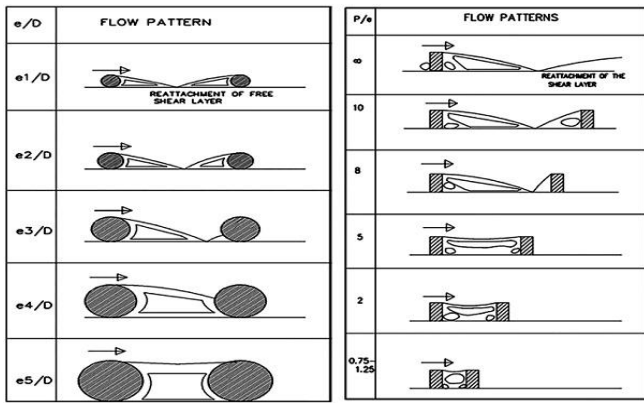


Fig. 3 Effect of rib height and pitch on flow

Prasad and Mullick [62] suggested the use of artificial roughness in the form of small diameter wires in a solar air heater to improve the thermal performance of the collector. Gupta et al. [63-64] investigated the friction factor and heat transfer characteristics of the inclined wires used as the artificial roughness as shown in Fig. 2.4. The investigated parameters are relative roughness height in the range of 0.018 to 0.052, aspect ratio in the range of 6.8 to 11.5, angle of attack varies from 40° to 90° and flow Reynolds number ranges from 3000 to 18000. They reported that angle of attack of 60° produces maximum heat transfer where as the angle of attack of 70° showed the highest friction factor.

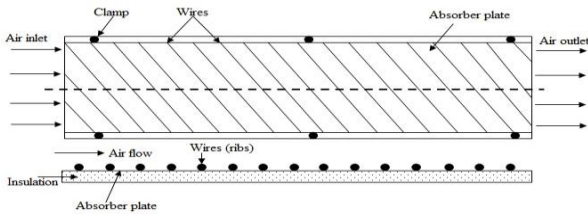


Fig. 4 Roughened absorber plate with inclined wire (Gupta et al. [1997])

Han et al. [65] investigated the effect of rib pitch to height ratio, and rib height to equivalent hydraulic diameter on friction factor and heat transfer coefficient for Reynolds number range of 7,000 to 90,000, relative roughness pitch range of 10 to 40, and relative roughness height range of 0.021 to 0.063 as shown in Fig. 2.5 (a to i). He found that the maximum values of friction factor and the Stanton number occur at a relative roughness pitch of 10. Both the average friction factor and Stanton number increased with increasing relative roughness height.

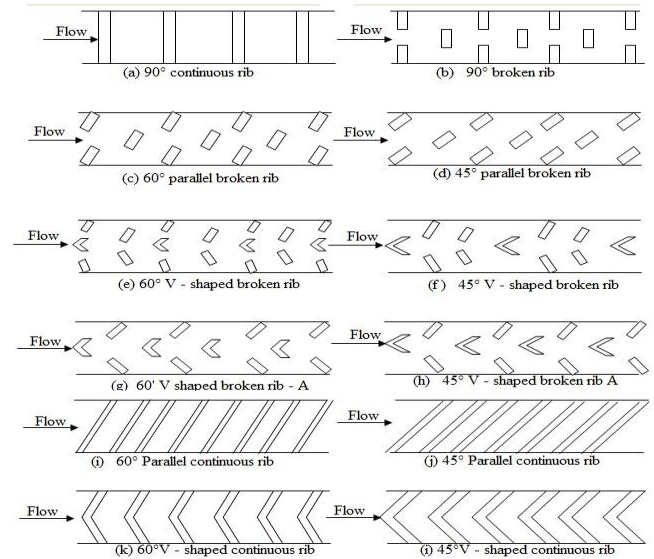


Fig. 5 Top view of rib configuration

Prasad and Saini [61] develops an empirical correlations for heat transfer coefficient and friction factor for a solar air heater duct artificially roughened by small diameter wires of various relative roughness heights ranging from 0.020 to 0.033 and relative roughness pitch varying from 10 to 20 for Reynolds numbers range between 5000 to 50,000. The results showed that the average friction factor and Nusselt number increased with increase in relative roughness height. The average Nusselt number of the roughened duct was about 2.10, 2.24 and 2.34 times than that of the smooth duct for relative roughness height of 0.020, 0.027 and 0.033 respectively. The average friction factor of the roughened duct was about 3.08, 3.67, and 4.26 times than that of the smooth duct. The increase in the average Nusselt number and average friction factor for relative roughness pitch of 10, 15 and 20 in the roughened duct was about 2.38, 2.14, 2.01 and 4.25, 3.39. Solar energy can be used to supply energy demand in the form of thermal energy (solar thermal systems) as well as in the form of electricity (solar photovoltaic systems). The important applications of solar energy are: Water heating, Space heating and cooling, Solar cooking, Solar crop drying, Solar distillation, Solar refrigeration, Green houses, Solar power (Electric) generation, Solar furnace, Solar water pumping etc. In order to make the solar energy utilization economically viable, its efficient collection and conversion to thermal energy at the absorber surface are very essential. The most important component of solar energy utilization system is the solar collector.

### 3. PERFORMANCE OF SOLAR AIR HEATER DUCT

#### 3.1. Thermal performance

Thermal performance of SAH duct is expressed as the convective heat transport between the absorber and the working medium i.e. air (Fig. 1). The thermal efficiency of a typical SAH duct is low due to low value of convective heat transfer coefficient (h) due to laminar sub-layer formation close to the absorber plate. The rate of useful energy gain by

the air flowing through SAH duct may also be calculated by using the following equation [7]:

$$Q_u = \dot{m} C_p (T_o - T_i) = h A_p (T_{pm} - T_{fm}) \quad (14)$$

Nusselt number for a smooth duct can be obtained by Dittus-Boelter Equation [8]:

$$Nu = 0.023 Re^{0.8} Pr^{0.4} \quad (15)$$

The heat transfer coefficient (h) can be increased by the application of artificial roughness on the air flow side of absorber plate and thereby cause increase in the thermal efficiency given by [9].

$$\eta_{th} = \frac{Q_u}{IA_c} \quad (16)$$

### 3.2. Hydraulic performance

The air flowing through the SAH duct undergoes frictional losses and hence accounts for the extra energy in form of mechanical power that has to be supplied to the blower to circulate air properly in the duct. The hydraulic performance for the fully developed turbulent flow can be represented by friction factor which is given by:

$$f = \frac{\Delta p_d D_h}{2 \rho L v_d^2} \quad (17)$$

Further using above equations mechanical power can be computed by [10]:

$$P = \frac{\dot{m} \Delta p_d}{\rho} \quad (18)$$

A basic layout of solar flat plate collector is depicted below [11]:

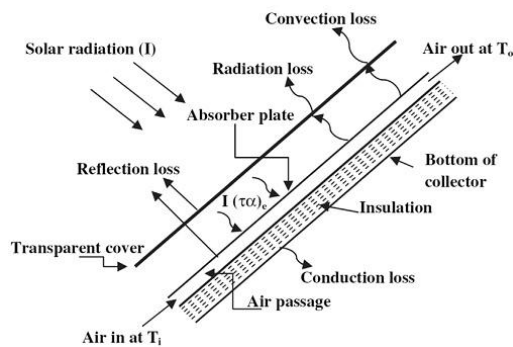


Fig. 6 Basic layout of solar flat plate collector

### 3.3. Thermo-hydraulic performance

The overall enhancement in the performance of a roughened SAH duct can be determined by considering thermal and hydraulic characteristics simultaneously in contrast to the SAH with smooth duct. A thermohydraulic performance parameter given by [7] is used to compare the roughened and smooth surfaces in terms of Nusselt number and friction

factor ratios. Therefore, thermohydraulic performance of a SAH is determined by [12]:

$$\eta_{thp} = \frac{(Nu / Nu_s)}{(f / f_s)^{1/3}} \quad (19)$$

## 4. CONCEPT OF ARTIFICIAL ROUGHNESS

In conventional flat plate SAH's the laminar sub layer has to be disturbed for enhancing the heat transfer by inducing turbulence adjacent to the absorber plate surface. This can be effectively done by the employment of artificial ribs on the air flow side of the absorber. However, the use of artificial roughness may result in high pressure loss due to friction and hence more power requirements for pumping of fluid [13-16]. For the investigation of the effect of artificial roughness elements, SAH is usually modeled as rectangular channel with one wall comprising ribs on the air flow side while other three walls are kept smooth. The provision of roughness has extended to three walls instead of one wall as used by most of the researchers [17-18].

The key geometrical factors used to characterize the geometry of artificial roughness includes the rib height, rib pitch, inclination, rib cross-section etc. and flow parameter namely Reynolds number. The influence of these parameters on thermal and hydraulic performance of SAH duct is discussed below:

### 4.1. Effect of rib height (e).

The viscous sub layer breaks due to presence of ribs which creates local wall turbulence and enhances the rate of heat transfer. If the ribs project beyond the viscous sub-layer thickness, this will increase the turbulence and heat transfer rate, consequently there will be high friction losses. Prasad & Saini reported that the optimum thermo hydraulic performance will be achieved where roughness height is slightly higher than the transition sub-layer thickness [19].

### 4.2. Effect of rib pitch (p).

The air flow pattern in the inter-rib region is affected with the change in the rib pitch. Reattachment occurs only if the rib elements are separated properly. For effective use of the ribs, the flow should separate and reattach in the inter-rib space; and then again separate. It may be noted that the flow reattachment followed with attached flow is not desirable as it results in re-formation of the laminar sub-layer in the attached length. The pitch of the roughness elements is expressed in non-dimensional form as ratio of pitch to height ratio (p/e) [20].

### 4.3 Effect of rib cross section.

The flow pattern close to the roughened absorber plate also depends on the cross-section of the rib whereas the re-attachment profile also varies among different cross-sections. Circular cross-section has low heat transfer properties as compared to square, triangular or trapezoidal cross-section [20]. Whereas the pressure drop is lower in circular rib as there is more streamlined flow in contrast to square or triangular ribs which has sharp edges. Other cross-sections like chamfered, L-shaped, trapezoidal etc. were also investigated but generally circular or square cross-

section rib is preferred as these provide better thermohydraulic performance and are easily available avoiding machining complications.

4.4. Effect of inclination.

Apart from the effect of rib height and pitch, the parameter that has been found to be most influential is the angle of attack ( $\alpha$ ) of the flow with respect to the rib position. It is to be pointed out that whereas the two fluid vortices upstream and downstream of a transverse rib are essentially stagnant relative to the mainstream flow which raises the local fluid temperature in the vortices and wall temperatures near the rib resulting in low heat transfer. The vortices move along the rib to subsequently join the main stream i.e. the fluid enters at the leading end of the rib and comes out near the trailing end as shown in Fig. 2.41. The moving vortices bring the cooler channel fluid in contact with leading end, raising heat transfer rate while at the trailing end heat transfer is relatively low [21].

4.5 Effect of Reynolds number (Re).

The influence of Reynolds number on the flow pattern is illustrated in Fig. 6. At lower Reynolds number, the reattachment distance is relatively large and the flow reattached length is thereby small. The region before the reattachment point comprises low heat transfer rate and is maximum at the reattachment point and drops along the reattached length. So, it can be evidently seen from the Fig. 6 that the reattachment profile changes with the increasing Reynolds number and reattachment distance keeps on decreasing. The flow re-circulation zone behind the rib decreases in the region before the reattachment point. Thus, the low heat transfer region behind the rib is reduced which results in enhancement in overall heat transfer.

Table 1 shows the various roughness geometries and the range of operating and flow parameters used by researchers.

5. DISCUSSIONS

Applications of solar energy, most prominent renewable source available, are likely to expand in near future. The conversion of solar energy involves heat exchange process which makes it essential to design more efficient heat exchanger. The artificial rib roughness method is generally preferable for enhancement of heat transfer by breaking laminar sub-layer near the absorbing surface. Numerous rib roughness geometries employed in solar air heaters have been investigated till now (Table 1). Started with the simplest transverse ribs [11,12], the other forms like inclined ribs [18], v-shaped ribs [21] and arc shaped ribs [30–32] were investigated experimentally. Arc shaped ribs offered lower friction penalty as compared to others. Apart from these geometries, investigation has also been made on other geometries like broken transverse ribs [15], inclined ribs with gap [19], dimple shaped elements [42], expanded metal mesh [20], chamfered ribs [13], s-shaped ribs [35], broken arc ribs [32], w-shaped ribs [37,38], discrete v-down ribs [27,28]. All these investigations reported the thermal performance enhancement with some increase in pumping requirements. Prasad and Mullick [11] initiated the concept of artificial roughness using small diameter wires on the

absorber surface on one wall aimed to enrich the thermal performance of the SAH. The wire diameter of 0.84mm,  $e/D = 0.019$  and  $P/e = 12.7$  were the parameters used in this study. The outcome of this study reported the enhancement in the efficiency from 62% to 72% at  $Re = 40,000$ .

Prasad and Saini [12] explored the influence of small wires applied as roughness elements on the absorber plate to study their effect on thermal and friction factor performance in fully developed region. The study was carried out for  $P/e = 10, 15$  and  $20$ ,  $e/D = 0.020, 0.027$  and  $0.033$  and Reynolds number ranging  $5000-50,000$ . They concluded that with the increase in  $e/D$ , both Nusselt number and friction factor increase, but the rate of heat transfer enhancement diminishes while the rate of friction factor increase was almost even. The application of rib roughness reported the enhancement of the Nusselt number and friction factor as 2.38 and 4.35 times over a smooth duct. The optimum values of  $P/e$  and  $e/D$  were found to be 10 and 0.027 respectively. The study also suggests that rib height must be equal to laminar sub-layer thickness.

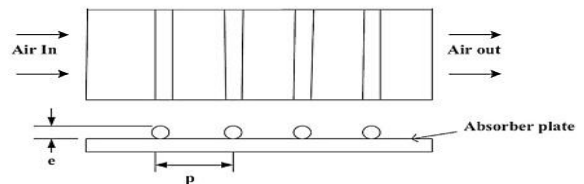


Fig. 7 Transverse rib roughness used by Prasad and Saini

Karwa et al. [13] carried out an experimental study to determine the influence of chamfered ribs applied in transverse direction as artificial roughness for predicting the thermo-hydraulic performance of the roughened SAH duct

Table 1: Different roughness geometry used by different researchers

Authors	Roughness element	Reynolds No.	Non-dimensional parameters and values		
			p/e	e/D <sub>h</sub>	Other parameters
Prasad and Saini	Transverse ribs	5000	10–20	0.020–0.033	
Saini and Saini	Expanded metal mesh	1900–13,000	15	0.012–0.039	W/H=11, L/e=25–71.87
Gupta et al.	Small diameter traverse rib	4000–18,000	10	0.02–0.05	$\alpha = 60^\circ$
Karwa et al.	Machined Ribs	3000–20,000	4.5–8.5	0.014–0.032	d/w=0.167–0.5 W/H=5.87
Bhagoria et al.	Wedge shaped ribs	3000–18000	10	0.015–0.033	$\Phi=8-15$
Sahu and Bhagoria	Broken integral transverse ribs	3000–12,000	6.67–20	0.0338	W/H=8
Jaurker et al.	Rib and groove combination		4.5–10	0.018–0.0363	g/p= 0.3–0.7

Karmare and Tikekar	Wire ribs-grid shape	3600–17,000	12.5–36	0.035–0.044	$\alpha = 60^\circ$ $l/s=1.72-1$
Varun et al.	Inclined and transverse wire	2000–14,000	10	0.030	
Saini and Verma.	Dimple protrusions	2000–17,000	8–12	0.018–0.037	
Layek et al.	Chamfered compound rib	3000–21000	10	0.03	$\alpha = 5^\circ-30^\circ$ $g/p=0.5$
Karmare et al.	Metal grit rib	17,000–40,000	15–17.5	0.035–0.044	$l/s=1.72$
Kumar et al.	Discretized W-shape rib	3000–15,000	10	0.0168–0.0338	$\alpha = 30^\circ-75^\circ$ $W/H = 8$
Bopche and Tandale	U shaped rib	3800–18,000	6.67–57.14	0.0186–0.03986	$\alpha = 90^\circ$
Hans et al.	Multiple V shape rib	2000–20000	6–12	0.019–0.043	$\alpha = 30^\circ-75^\circ$ $W/w = 1-10$
Lanjewar et al.	W shaped rib	2300–14,000	10	0.018–0.03375	$\alpha = 30^\circ-75^\circ$ $W/H = 8$
Lanjewar et al.	W shape with different orientations	2300–14,000	10	0.03375	$\alpha = 30^\circ-75^\circ$ $W/H = 8$
Sethi et al.	Dimple shape in arc shape	3600–18,000	10–12	0.021–0.036	
Kumar et al.	Multi V shape with gap rib	2000–20,000	6–12	0.022–0.043	$\alpha = 30^\circ-75^\circ$ $W/w = 1-10$
Yadav et al.	Circular protrusion in arc shape	3600–18,100	12–24	0.015–0.03	$\alpha = 45^\circ-75^\circ$ $W/H = 11$

(Fig. 8). The parameters range were taken as duct aspect ratio from 4.8 to 12,  $e/D$  from 0.0141 to 0.0328,  $P/e$  from 4.5 to 8.5, Rib chamfer angle from  $-15^\circ$  to  $18^\circ$  and  $Re$  from 3000 to 20,000. The augmentation in Stanton number and friction factor was highest at the chamfer angle of  $15^\circ$  and was of the order of 2 and 3 times respectively.

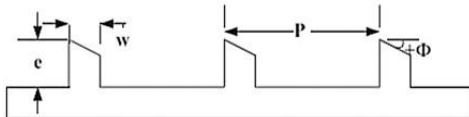


Fig. 8. Chamfered Rib roughness geometry by Karwa et al.

Verma and Prasad [14] experimentally evaluated the outcome of the application of transverse wires in SAH duct in actual outdoor conditions and studied its optimum performance. The investigation range of Reynolds number from 5000 to 20,000,  $P/e$  from 10 to 40, roughness Reynolds number from 8 to 42 and  $e/D$  from 0.01 to 0.03 were investigated. Maximum thermo-hydraulic performance of 71% has been obtained at roughness Reynolds number of 24.

Sahu and Bhagoria [15] investigated the thermal performance of roughened SAH duct using broken transverse rib arrangement as shown in Fig. 9. Investigation

was done for  $Re$  from 3000 to 12,000,  $P/e$  from 10 to 30 and  $e/D = 0.0338$ . Nusselt number attained its maximum value at  $P/e$  of 10 and after that it decreases. The heat transfer coefficient of the roughened absorber plate was 1.25–1.4 times higher than the smooth plate.

Yadav and Bhagoria [17] performed a 2-D investigation on equilateral triangular section transverse rib (Fig. 10) by using CFD code ANSYS FLUENT 12.1. Parameters ranges were taken as  $P/e$  from 7.14 to 35.71,  $e/D$  from 0.021 to 0.042 and Reynolds number from 3800 to 18,000. Maximum improvement in Nusselt number of 3 times and friction factor enhancement of 3.56 times over the smooth duct was obtained corresponding to the  $p/e$  of 7.14, Reynolds number of 15,000 and  $e/D$  of 0.042.

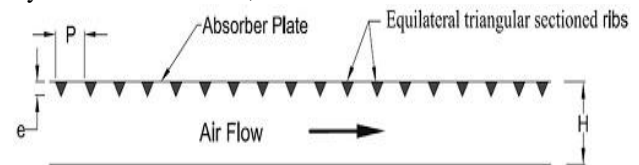


Fig. 9. Equilateral triangular sectioned ribs used by Yadav and Bhagoria

Gupta et al. [18] presented a study on the application of the inclined circular transverse ribs (Fig. 11.) as artificial roughness to investigate the fluid flow characteristics of a roughened SAH duct. The study encompassed the range of Reynolds number from 3000 to 18,000, duct aspect ratio from 6.8 to 11.5,  $e/D$  from 0.018 to 0.052, and fixed  $P/e = 10$ . The study reported the maximum augmentation in Nusselt number and friction factor as 1.8 and 2.7 times of smooth duct at  $\alpha = 60^\circ$  and  $e/D = 0.033$ . Further the best thermohydraulic performance of roughened duct was obtained at  $e/D = 0.033$  corresponding to  $Re = 14,000$ . The authors also studied the performance of Stanton number in transitional flow and fully developed flow. Stanton number was seen to be increasing up to  $Re = 12,000$  and thereafter it decreased.

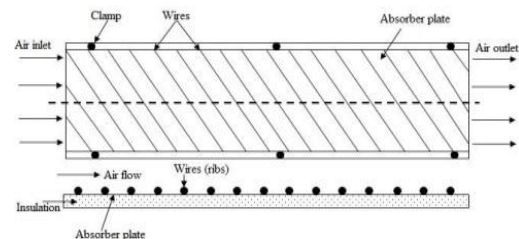


Fig. 10. Roughened absorber plate with inclined wire used by Gupta et al.

Aharwal et al. [19] performed experimentation on a SAH duct with square cross-section inclined ribs with a gap (Fig. 12). The duct has a  $W/H = 5.84$ ,  $P/e = 10$ ,  $e/D = 0.0377$ , and  $\alpha = 60^\circ$ . The gap width ( $g/e$ ), gap position ( $d/w$ ) and Reynolds number was varied in the range of 0.5–2, 0.1667–0.667 and 3000–18,000 respectively. The maximum augmentation of Nusselt number and friction factor over the smooth duct was 2.59 and 2.87 times respectively. The thermo-hydraulic performance parameter was obtained for the  $g/e = 1.0$  and  $d/w = 0.25$ .

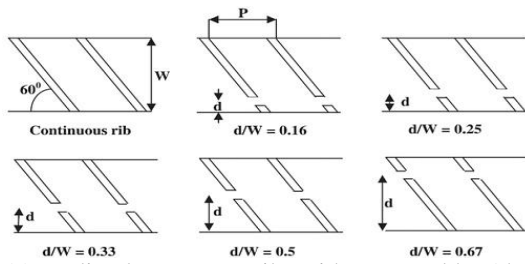


Fig. 11. Inclined transverse ribs with gap used by Aharwal et al.

Saini and Saini [20] determined the performance of a SAH duct roughened with expanded metal mesh geometry (Fig. 13). As an alternative to transverse ribs, authors suggested the use of commercially available metal matrix which can be easy to fix on absorber plate. They investigated the effect of roughness parameters viz.  $L/e$  from 25 to 71.87,  $S/e$  from 15.62 to 46.87,  $e/D$  from 0.12 to 0.039 and  $Re$  from 1900 to 13,000. The highest Nusselt number was attained at  $L/e = 46.87$  and  $S/e = 25$  at  $\alpha = 61.9^\circ$ . The friction factor was registered maximum corresponding to  $\alpha = 72^\circ$  for  $L/e = 71.87$ . The maximum enhancement in heat transfer coefficient was 4 and 5 times respectively over the smooth duct.

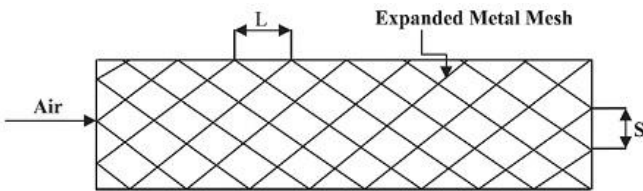


Fig. 12. Expanded metal mesh geometry used by Saini and Saini

Hans et al. [22] presented a study of multiple V-ribs roughness (Fig. 15) considering the parameters as Reynolds number from 2000 to 20,000,  $e/D$  from 0.019 to 0.043,  $P/e$  from 6 to 12,  $\alpha$  from  $30^\circ$  to  $75^\circ$  and  $W/w$  from 1 to 10. The investigation revealed that with the increase in  $W/w$ , heat transfer attains maximum value at  $W/w$  of 6 and is lower on both sides. Nusselt number and friction factor enhancement was attained as 6 and 5 times that of smooth duct.

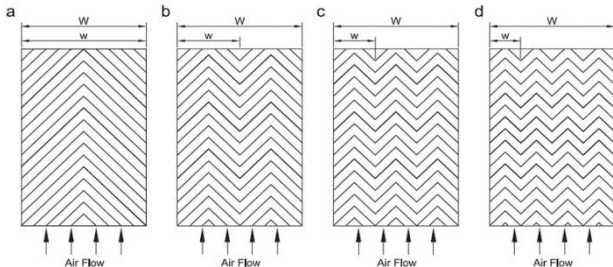


Fig. 13. Multiple V-rib roughness used by Hans et al.

Saini and Saini [30] evaluated the performance of SAH duct roughened with arc shaped wires as rib elements as shown in Fig. 20. Heat transfer coefficient and friction factor were studied for Reynolds number from 2000 to 17,000,  $e/D$  from 0.0213 to 0.0422 and  $\alpha/90$  from 0.3333 to 0.6666. The application of arc shaped roughness geometry resulted in the maximum Nusselt number improvement of 3.80 and

friction factor boost of 1.75 times corresponding to parameters as  $\alpha/90 = 0.3333$  and  $e/D = 0.0422$ .

Yadav et al. [31] employed arc shaped dimple roughness (Fig. 21) for parameter range as  $Re$  from 3600 to 18,100,  $P/e$  from 12 to 24,  $e/D$  from 0.015 to 0.03 and  $\alpha$  from  $45^\circ$  to  $75^\circ$ . They found that the maximum boost in Nusselt number and friction factor was 2.89 and 2.93 times respectively for the  $e/D = 0.03$ ,  $P/e = 12$ , and  $\alpha = 60^\circ$ .

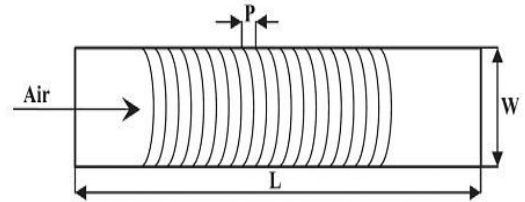


Fig. 14. Arc shaped roughness used by Saini and Saini

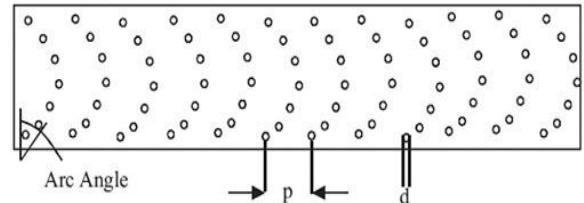


Fig. 15. Arc shaped dimple roughness used by Yadav et al.

Pandey et al. [35] carried out study on multiple arc ribs with gap (Fig. 24) used as roughness in SAH absorber plate. The investigation considered rib parameters as  $P/e$  from 4 to 16,  $e/D$  from 0.016 to 0.044,  $W/w$  from 1 to 7,  $\alpha$  from  $30^\circ$  to  $75^\circ$ ,  $d/x$  from 0.25 to 0.85 and  $g/e$  from 0.5 to 2.0. The maximum increment found in heat transfer was 5.85 and pumping power increment was 4.96 times at  $P/e = 8$ ,  $W/w = 5$ ,  $g/e = 1$ ,  $d/x = 0.65$  and  $e/D = 0.044$  at  $Re = 21,000$ .

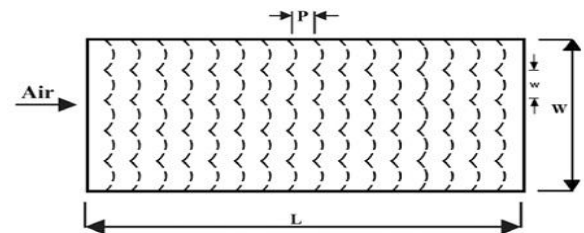


Fig. 16. Multiple broken arc rib used by Pandey et al.

Kumar et al. [36] studied the influence of the arc shape wire ribs arranged in 'S' shape on the heat transfer and friction factor characteristics of solar air heater as shown in Fig. 25. The experimentation considered  $Re$  from 2400 to 20,000 and rib parameters as  $P/e$  from 4 to 16,  $e/D$  from 0.022 to 0.054,  $W/w$  from 1 to 4 and  $\alpha$  from  $30^\circ$  to  $75^\circ$ . Experimentation shows the maximum enhancement in Nusselt number and friction factor of 4.64 and 2.71 times over the smooth duct at  $W/w = 3$ ,  $P/e = 8$  and  $\alpha = 60^\circ$ .

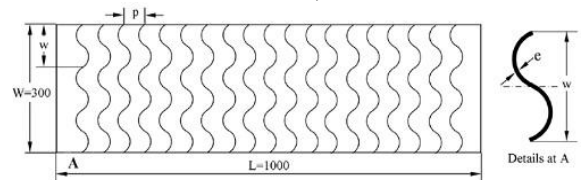


Fig. 17. S-shaped ribs arrangement used by Kumar et al.

Thakur et al. [33] performed 2-D computational simulations of SAH duct roughened with hyperbolic ribs as shown in Fig. 33. The investigation encompassed the parameter range as  $e = 0.5\text{--}2\text{mm}$  and  $P = 10\text{--}20\text{mm}$ . The optimum thermohydraulic performance of the order of 2.16 was achieved for  $e = 1\text{mm}$  and  $P = 10\text{mm}$  at  $Re = 6000$ . Performance of hyperbolic rib was compared with rectangular, triangular and semicircular rib geometries and was found to be best among all up to  $Re = 10,000$ .

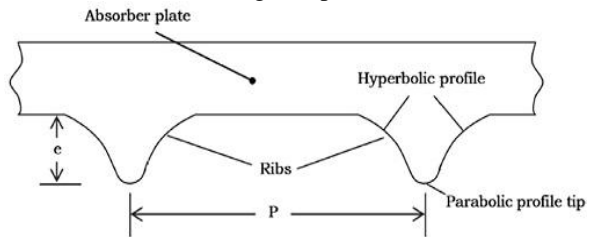


Fig. 18. Hyperbolic rib geometry used by Thakur et al.

## 6. CONCLUSIONS

Applications of solar energy, most prominent renewable source available, are likely to expand in near future. The conversion of solar energy involves heat exchange process which makes it essential to design more efficient heat exchanger. The artificial rib roughness method is generally preferable for enhancement of heat transfer by breaking laminar sub-layer near the absorbing surface. Numerous rib roughness geometries employed in solar air heaters have been investigated till now (Table 1). Started with the simplest transverse ribs [11,12], the other forms like inclined ribs [18], v-shaped ribs [21] and arc shaped ribs [30–32] were investigated experimentally. Arc shaped ribs offered lower friction penalty as compared to others. Apart from these geometries, investigation has also been made on other geometries like broken transverse ribs [15], inclined ribs with gap [19], dimple shaped elements [42], expanded metal mesh [20], chamfered ribs [13], s-shaped ribs [35], broken arc ribs [32], w-shaped ribs [37,38], discrete v-down ribs [27,28]. All these investigations reported the thermal performance enhancement with some increase in pumping requirements. Creation of gap in the rib have shown improved performance over the continuous rib. Further the ribs in multiples such as multiple v-ribs [22], multiple arc ribs [33–35] have resulted in remarkable enhancement in heat transfer coefficient. Economically, the wire fixation method is the most feasible method among other methods; as it does not involve any machining operations and is simple. But it may be a tedious task in large scale production. Therefore, a suitable geometry of artificial roughness must be selected which is not only easily available, but should also be simple to fix on the absorber plate and also offers substantial augmentation in heat transfer coefficient at low pumping power penalty. For better understanding and optimizing of the heat transfer and flow mechanism, attempt have been made to study the effect of various influencing roughness and flow parameters on the thermal and hydraulic performance of solar air heater

through the flow visualization. Attempt have been made towards understanding the in-depth flow phenomena related to the heat transfer process. This may be beneficial for the further improvement in this field as the specific locations in the solar air heater can be targeted for improvement in the future.

In this article, a comprehensive review of different rib roughness geometries reported for conventional solar air heater has been conducted. Effect of various shapes and size of artificial ribs are reported in literature. Substantial heat transfer enhancement has been achieved using ribs of various design accompanied by some pressure losses. Heat transfer and friction characteristics and the correlations reported by the investigators have been summarized. Computational Fluid Dynamics (CFD) analysis has been carried out to visualize and study the effect of various geometrical and flow parameters for the optimum design of solar air heater. Based on the comprehensive literature survey, the following conclusions have been drawn:

1. Application of artificial rib roughness improves the thermo-hydraulic performance of conventional solar air heater. The rib roughness improves the thermal performance due to breaking of laminar sub layer. The friction factor penalty is small as the flow is disturbed in the laminar sub layer only.
2. The thermal and fluid flow characteristics of numerous rib roughness geometries have been investigated for various roughness parameters viz., relative rib pitch, relative rib height, relative rib width, attack angle etc. For most rib geometries, the thermo-hydraulically optimum values of relative rib pitch ( $P/e$ ), relative rib height ( $e/D$ ), relative rib width ( $W/w$ ) and attack angle ( $\alpha$ ) have been reported to be 10, 0.043, 6 and  $60^\circ$  respectively.
3. The thermohydraulic performance of inclined ribs is better than transverse ribs due to creation of secondary flow cells. The V-shape ribs further improve the thermo-hydraulic performance due to more number of secondary flow cells. The arrangement of ribs in multiples, such as multiple V, multiple arc, further enhance the thermohydraulic performance.
4. A gap in rib of the order of rib height substantially improves the thermohydraulic performance of roughened duct. The improvement in Nusselt number in the range of 1.1–1.3 times and pumping power penalty of 1–1.4 times were reported due to introduction of gap.
5. The maximum augmentation in heat transfer and pumping power was 6.74 and 6.37 times for multiple V-ribs with gap, which is followed by multiple V-ribs with augmentation of 6 and 5 times respectively.
6. From thermo-hydraulic considerations, the arc arrangement has lesser pressure losses than V

arrangement, which may be due to curved secondary flow and consequently results in better thermohydraulic performance. Therefore, multiple arc ribs and multiple arc ribs with gap are recommended for better overall thermo-hydraulic performance.

#### **FUTURE SCOPE**

For future developments, experimental approach used for the analysis of rib roughened SAH duct should be accompanied with Computational Fluid Dynamics (CFD) method which provides fast, non-expensive and in-depth analysis for the optimization of SAH's. More studies can be conducted using sun tracking systems and reflectors. Double pass solar air heaters should be investigated using artificial rib roughness as very few studies are reported in this aspect. Compound heat transfer enhancement techniques may be employed for further improvement in thermal performance of SAH's. Combined with the surface enhancement methods, other reported methods in literature viz. selective coatings, arched or corrugated absorber plate, fluid additive methods can be tested in future for combined heat transfer enhancement in solar air heaters.

## REFERENCES

1. Duffie, J. A., Beckman, W. A., Solar Engineering Thermal Processes, John Wiley, New York, 1991.
2. Gawande VB, Dhoble AS, Zodpe DB, Chamoli S. A review of CFD methodology used in literature for predicting thermo-hydraulic performance of a roughened solar air heater. *Renew Sustain Energy Rev* 2016; 54:550–605.
3. Sharma SK, Kalamkar VR. Computational fluid dynamics approach in thermo-hydraulic analysis of flow in ducts with rib roughened walls – a review. *Renew Sustain Energy Rev* 2016; 55:756–88.
4. Alam T, Kim M-H. A critical review on artificial roughness provided in rectangular solar air heater duct. *Renew Sustain Energy Rev* 2017; 69:387–400.
5. Yadav, A.S., Bhagoria, J.L., A CFD based thermo-hydraulic performance analysis of an artificially roughened solar air heater having equilateral triangular sectioned rib roughness on the absorber plate. *International Journal of Heat and Mass Transfer* 70 (2014) 1016–1039.
6. Tiwari, R.C., Kumar, A., Gupta, S.K., Sootha, G.D., Thermal performance of flat-plate solar collectors manufactured in India. *Energy Conversion and Management*, Volume 31, Issue 4, 1991: 309-313.
7. Sethi, M., Varun, Thakur, N.S., Correlations for solar air heater duct with dimpled shape roughness elements on absorber plate. *Sol Energy*. 2012; 86: 2852–61.
8. Karwa, R., Chitoshiya, G., Performance study of solar air heater having v-down discrete ribs on absorber plate. *Energy* 2013; 55:939–55.
9. Patil, A.K., Saini, J.S. and Kumar, K., 2011, Effect of Gap Position in Broken V rib Roughness Combined with Staggered Rib on Thermohydraulic Performance of Solar Air Heater, *Green*, Vol. 1 (4), 329–338.
10. Singh, I., Singh S., A review of artificial roughness geometries employed in solar air heaters, *Renewable and Sustainable Energy Reviews* 92 (2018) 405–425.
11. Prasad, B.N., Saini, J.S., "Thermohydraulic optimization of artificially roughened solar air heaters", *Proc. NSC, Solar Energy Society of India, Hyderabad (India)*, 1988.
12. Verma S.K., Prasad B.N., Investigation for the optimal thermohydraulic performance of artificially roughened solar air heaters, *Renewable Energy*, Vol. 20, 9-36, 2000.
13. Bopche, S.B., Tandale, M.S., Experimental investigations on heat transfer and friction characteristics of a turbulators roughened solar air heater, *International Journal of Heat and Mass Transfer*, Vol. 52 (11-12), 2834-2848, 2009.
14. Lanjewar, A., Bhagoria, J.L., Sarviya, R.M., Heat transfer and friction in solar air heater duct with W-shaped rib roughness on absorber plate, *Energy*, Vol. 36, 4531-4541, 2011.
15. Kumar, A., Saini., RP, Saini, JS., 2012, Experimental investigation on heat transfer and fluid flow characteristics of air flow in a rectangular duct with Multi V-shaped rib with gap roughness on the heated plate, *Solar Energy*, Vol. 86, pp. 1733–49.
16. Singh, I., Singh, S., A review of artificial roughness geometries employed in solar air heaters, *Renewable and Sustainable Energy Reviews* 92 (2018) 405–425
17. Kumar, V., Prasad, L., Experimental investigation on heat transfer and fluid flow of air flowing under three sides concave dimple roughened duct. *International Journal of Mechanical Engineering and Technology (IJMET)*, Volume 8, Issue 11, November 2017, pp. 1083–1094, Article ID: IJMET\_08\_11\_110.
18. Kumar, V., Prasad, L., Thermal performance investigation of one and three sides concave dimple roughened solar air heaters. *International Journal of Mechanical Engineering and Technology (IJMET)* Volume 8, Issue 12, December 2017, pp. 31–45, Article ID: IJMET\_08\_12\_004.
19. Prasad B.N., Saini J.S., Effect of artificial roughness on heat transfer and friction factor in a solar air heater, *Solar Energy*, Vol. 41(6), 555–560, 1988.
20. Hans VS, Saini RP, Saini JS. Performance of artificially roughened solar air heaters-a review. *Renew Sustain Energy Rev* 2009; 13: 1854–69.
21. Alam, T., Kim, M.H., A critical review on artificial roughness provided in rectangular solar air heater duct. *Renewable and Sustainable Energy Reviews* 69 (2017) 387–400.
22. Taslim, M.E., Li T., Krecher D.M, Experimental heat transfer and friction in channels roughened with angled, V-shaped and discrete ribs on two opposite walls, *Transactions of ASME Journal of Turbo-machinery*, Vol. 118, 20-28, 1996.
23. Gupta, D., Solanki, S. C., Saini, J. S., 1997, Thermohydraulic performance of solar air heaters with roughened absorber plates. *Solar Energy*, Vol. 61, pp. 33–42.
24. Gupta, D., Solanki, S.C. and Saini, J.S., 1993, Heat and fluid flow in rectangular solar air heater ducts having transverse rib roughness on absorber plate, *Solar Energy*, Vol. 51, pp. 31-37.
25. Han, J.C., Zhang, Y.M. and Lee, C.P., 1991, Augmented heat transfer in square channels with parallel, crossed, and V shaped angled ribs, *Trans. ASME Journal of Heat Transfer*, Vol. 113, pp. 590-596.
26. Saini, S.K. and Saini, R.P., 2008, Development of correlations for Nusselts number and friction factor for solar air heater with roughened duct having arc-shaped wire as artificial roughness, *Solar Energy*, Vol. 82, pp. 1118-1130.

27. Tanda, C., 2004, Heat transfer in rectangular channels with transverse and V-shaped broken ribs, *International Journal of Heat and Mass Transfer*, Vol. 47, pp. 229-243.
28. Aharwal, K.R., Gandhi, B.K., Saini, J.S., 2008, Experimental investigation on heat transfer enhancement due to a gap in an inclined continuous rib arrangement in a rectangular duct of solar air heater, *Renewable Energy*, Vol. 33, pp. 585-596.
29. Saini, R.P., Verma, J., 2008, Heat transfer and friction correlations for a duct having dimple shape artificial roughness for solar air heater, *Energy*, Vol. 33, pp. 1277-1287.
30. Prasad K., Mullick S.C., Heat transfer characteristics of a solar air heater used for drying purposes, *Applied Energy*, Vol. 13, 83-93, 1985.
31. Prasad B.N., Saini J.S., Effect of artificial roughness on heat transfer and friction factor in a solar air heater, *Solar Energy*, Vol. 41(6), 555–560, 1988.
32. Karwa, R., Solanki, S. C. and Saini, J. S., Heat transfer coefficient and friction factor correlation for the transitional flow regime in rib-roughened rectangular duct, *Int. Journal of Heat and Mass Transfer*, Vol. 42, pp. 1597-1615, 1999.
33. Sahu MM, Bhagoria JL. Augmentation of heat transfer coefficient by using 90° broken transverse ribs on absorber plate of solar air heater. *Renew Energy* 2005; 30:2057–73.
34. Yadav, A.S., Bhagoria, J.L., A CFD based thermo-hydraulic performance analysis of an artificially roughened solar air heater having equilateral triangular sectioned rib roughness on the absorber plate. *International Journal of Heat and Mass Transfer* 70 (2014) 1016–1039.
35. Hans VS, Saini RP, Saini JS. Heat transfer and friction factor correlations for a solar air heater duct roughened artificially with multiple v-ribs. *Sol Energy* 2010; 84:898–911.
36. Yadav S, Kaushal M, Varun, Siddhartha. Nusselt number and friction factor correlations for solar air heater duct having protrusions as roughness elements on absorber plate. *Exp Therm Fluid Sci* 2013; 44:34–41.
37. Pandey NK, Bajpai VK, Varun. Experimental investigation of heat transfer augmentation using multiple arcs with gap on absorber plate of solar air heater. *Sol Energy* 2016; 134:314–26.
38. Kumar, V., Prasad, L., Experimental investigation on heat transfer and fluid flow of air flowing under three sides concave dimple roughened duct. *International Journal of Mechanical Engineering and Technology (IJMET)*, Volume 8, Issue 11, November 2017, pp. 1083–1094, Article ID: IJMET\_08\_11\_110.
39. Kumar, V., Prasad, L., Thermal performance investigation of one and three sides concave dimple roughened solar air heaters. *International Journal of Mechanical Engineering and Technology (IJMET)* Volume 8, Issue 12, December 2017, pp. 31–45, Article ID: IJMET\_08\_12\_004.
40. Kumar, V., Prasad, L., Performance Analysis of Three-sides Concave Dimple Shape Roughened Solar Air Heater, *J. sustain. dev. energy water environ. syst.*, 6(4), pp 631-648, 2018.
41. Kumar, V., Nusselt number and friction factor correlations of three sides concave dimple roughened solar air heater, *Renewable Energy* 135, (2019), 355-377.

# ANALYSIS OF SINGLE STRAP HYBRID BUTT JOINT IN LAMINATED FRP COMPOSITES

I.Prasanna<sup>1</sup>, A.Happy<sup>2</sup>, K.Sandhya<sup>3</sup>

<sup>1,2,3</sup> Assistant Professor, Mechanical Engg. Dept, Malla Reddy College of Engineering, Hyderabad, India.

prasannabobba81@gmail.com<sup>1</sup>, happy.angelika5@gmail.com<sup>2</sup>, sandi.sandhya123@gmail.com<sup>3</sup>

**ABSTRACT**

*The present investigation deals with the static analysis of adhesively bonded single strap hybrid butt joint in laminated FRP composites using three-dimensional theory of elasticity based finite element method. The finite element model is validated and is extended for the analysis of a single strap hybrid butt joint made of generally and specially orthotropic laminates subjected to longitudinal load with C-F end condition. The stresses are computed in adherends and adhesive. The results of the present analysis reveals that the three-dimensional stress analysis is required for the analysis of single strap hybrid butt joint in laminated FRP composites.*

*Keywords: SSHBJ, FEM, FRP, C-F*

**1. INTRODUCTION**

Fiber reinforced plastic (FRP) materials have proven to be very successful in structural applications. They are widely used in the aerospace, automotive and marine industries. FRP materials or composites behave differently than typical metals such as steel or aluminum. A typical composite contains layers of aligned fibers oriented at different angles held together by a resin matrix, giving high strength and stiffness in different directions. This anisotropy can cause difficulties when joining two parts together, especially if the two pieces have different stiffness and strength characteristics. The joint can potentially become the weakest link in the structure due to the large amount of load it must transfer. There are wide varieties of ways to join different parts together. Two major methods include mechanical fastening and adhesive bonding. Adhesive bonding of structures has significant advantages over conventional fastening systems. Bonded joints are considerably more fatigue resistant than mechanically fastened

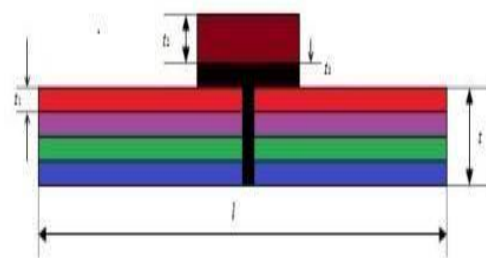
structures because of the absence of stress concentrations that occur at fasteners. Joints may be lighter due to the

Roy et.al (4) employed shear specimens and butt-joint specimens to measure the shear and tensile strengths of five types of adhesive bonds for brittle and Homalite polymers. In order to examine the possible stress singularities, they have employed two optical techniques, photo elasticity and coherent gradient sensing to record fringe pattern until specimens failed.

**2. PROBLEM MODELING**

Geometry.

The geometry of the single strap hybrid butt joint used for the validation is as shown in Fig.1. Where the dimensions are taken as  $t = 20$  mm,  $t_1 = 5$  mm,  $t_2 = 5$  mm,  $t_3 = 2$  mm,  $l = 100$  mm. The width of the plate in the Z-direction is taken as 25 mm.



All dimensions are in mm  
Fig. 1 Geometry of the single strap hybrid butt joint

**Finite Element Model**

The finite element mesh is generated using a three-dimensional brick element 'SOLID 45' of ANSYS [8]. This element (Fig. 2) is a structural solid element designed based on three-dimensional elasticity theory and is used to model thick orthotropic solids. The element is defined by 8

nodes having three degrees of freedom per node: translations in the nodal x, y, and z directions.

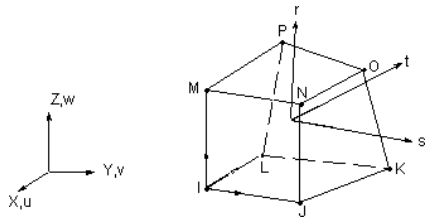


Fig. 2 SOLID 45 Elements

**Loading**

The following types of loads are applied for validation and prediction of the response of the structure for the present analysis.

- i) A longitudinal uniform pressure of 10MPa is applied for the validation purpose
- ii) A uniform longitudinal load of 10 MPa is applied for the present analysis

**Boundary Conditions**

one end of the joint is clamped and the other end is restricted to move in the transverse direction (C-F). A uniform longitudinal load of 10 MPa is applied.

**Material Properties**

The following mechanical properties are used for the validation and analysis of single strap hybrid butt joint (7).

**i) Graphite/epoxy FRP (adherend)**

$E_L = 172.72$  GPa;  $E_T = 6.909$  GPa;  
 $\nu_{LT} = \nu_{LZ} = 0.25$ ;  
 $G_{LT} = 3.45$  GPa;  $G_{TT} = 1.38$  Gpa

**ii) Epoxy (adhesive)**

$E = 5.171$  GPa;  $\nu = 0.35$

**iii) Strap**

$E = 200$  GPa;  $\nu = 0.25$

**Laminate sequence**

- i) Two  $+ \theta^0 / - \theta^0 / - \theta^0 / + \theta^0$  laminated FRP composite plates are used as adherends for the present analysis. The value of  $\theta$  is measured from the longitudinal direction of the structure (x-axis) and varied from  $0^0$  to  $90^0$  in steps of  $15^0$ .

**3. RESULTS**

**Validation**

Fig. 3 Shows Finite element mesh on the overlap region of the single strap hybrid butt joint.

The finite element mesh divisions on the non-overlap region are same as that given for overlap region across thickness, but along the length a course mesh is considered to limit the number of nodes without losing the accuracy of the solution. Table3. 1 shows the values of the stresses at the free surfaces where the stresses should be zero and close agreement is found. Later this model is used for the analysis of single strap hybrid butt joint made of specially and generally orthotropic laminates subjected to longitudinal loading.

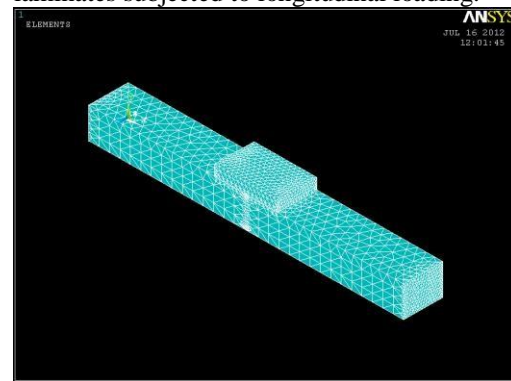


Fig. 3 Finite element mesh on the overlap region of the single strap hybrid butt joint

**Table 1.** values of the stresses at the free surfaces where the stresses should be zero.

NODE NUMER	STRESS IN MPA		
1393	-0.0299	-0.133	0.025
1451	0.043	-0.12	-0.008
1526	0.04779	0.0945	-0.0772
1469	0.11365	-0.405	-0.0485
1493	-0.1251	-0.0801	0.053
1475	-0.0886	0.0175	0.023
1422	-0.0704	-0.4421	-0.0536
1444	0.0128	0.0853	0.0782
1432	0.06672	-0.19424	0.0465
1462	0.0314	0.1223	0.0186

Variation of maximum stresses in the Laminates with respect to the fiber angle  $\theta$ :

The variation of stresses is due to the variation in internal stiffness in the adherends due to the change in fiber angle. The inter laminar effects at the interfaces of adherends also influences the stresses.

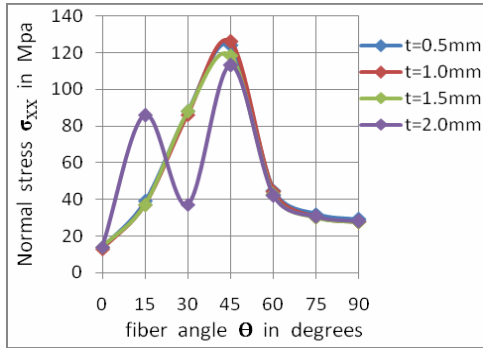


Fig.4 Variation of  $\sigma_{xx}$  in the Laminate

This Fig shows that the stress increases with increase in fiber angle  $\theta$  upto  $45^\circ$  and decreases with increase in angle. For the adhesive thickness  $t=2.0$  mm the stress increases upto  $15^\circ$  and decreases with increase in angle. The maximum stress is at  $45^\circ$  and minimum stress is at  $0^\circ$  for all adhesive thicknesses.

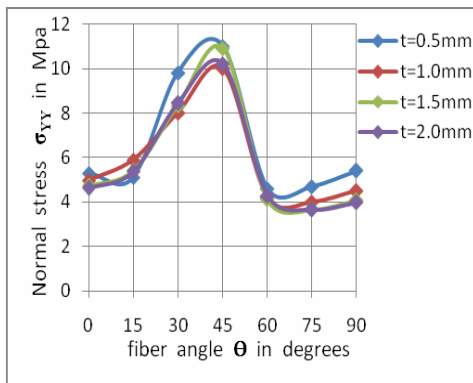


Fig. 5 Variation of  $\sigma_{yy}$  in the Laminate

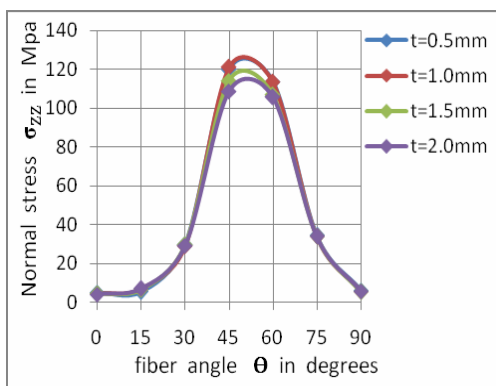


Fig. 6 Variation of  $\sigma_{zz}$  in the Laminate

Fig.5 and 6 shows that the stress value is low between 0 to  $15^\circ$  and gradually increases upto  $45^\circ$  where the stress is maximum. Thereby it is followed with decrease in stress value with increase in fiber angle. The minimum stress value is found to be at  $75^\circ$ . The induced stress is very low in magnitude for

the adhesive thickness  $t=2.0$  mm compared to others.

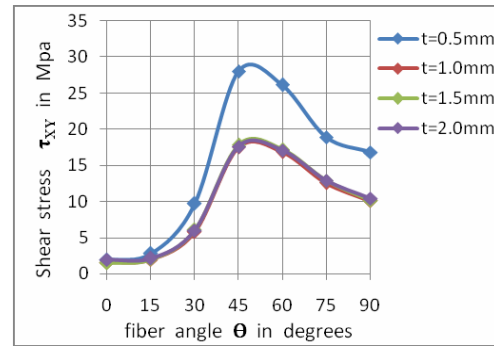


Fig. 7 Variation of  $\tau_{xy}$  in the Laminate

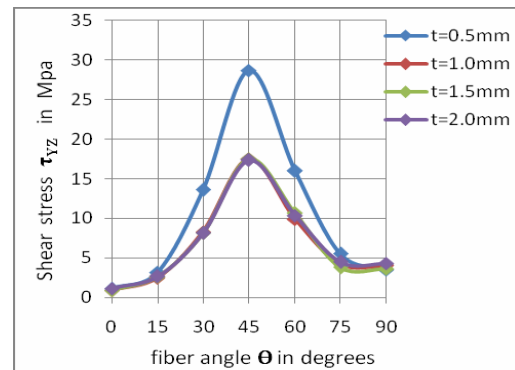


Fig. 8 Variation of  $\tau_{yz}$  in the Laminate

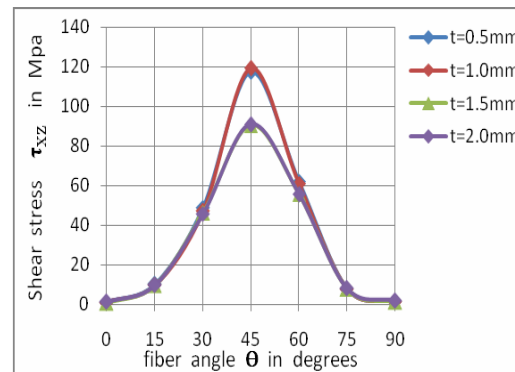


Fig.9 Variation of  $\tau_{zx}$  in the Laminate

Fig.7, 8 and 9 depicts the variation of shear stress  $\tau_{xy}$ ,  $\tau_{yz}$  and  $\tau_{xz}$  with respect to fiber angle  $\theta$ . The induced shear stress is observed to be maximum at  $45^\circ$  and minimum in between 0 to  $15^\circ$ . The stress is high for thickness  $t=0.5$ mm.

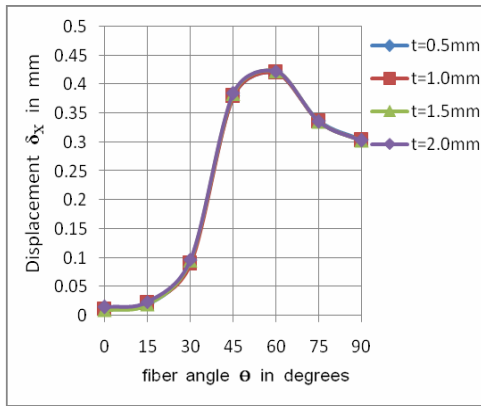


Fig.10 Variation of  $\delta_x$  in the Laminate

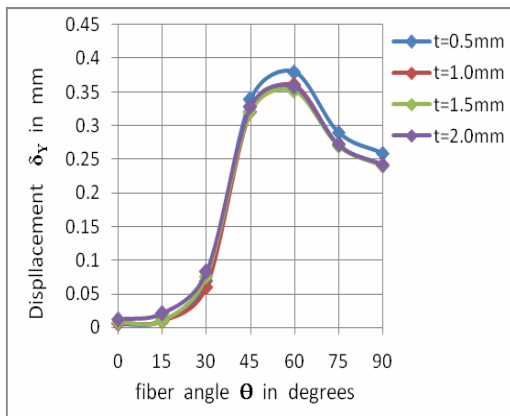


Fig. 11 Variation of  $\delta_y$  in the Laminate  
 Fig.10 and 11 shows the variation of displacement  $\delta_x$  and  $\delta_y$  with respect to fiber angle  $\theta$ . The curve gradually increases with increase in angle and the displacement is observed to be maximum at  $60^\circ$  followed by decrease in value with increase in angle. The stress is minimum at  $0^\circ$ .

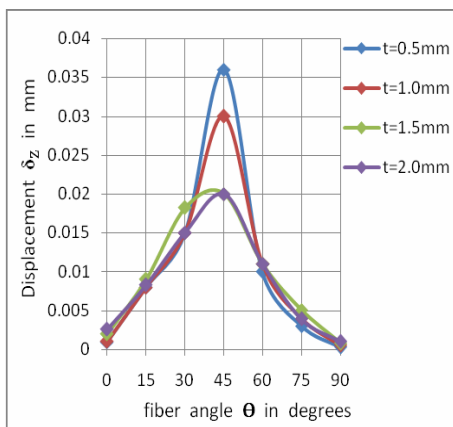


Fig. 12 Variation of  $\delta_z$  in the Laminate

Fig. 12 depicts the variation of displacement  $\delta_z$  with respect to fiber angle  $\theta$ . The displacement increases with increase in fiber angle upto  $45^\circ$  and thereby it decreases with increase in

angle. The maximum displacement is more for adhesive thickness  $t=0.5\text{mm}$  when compared to other thicknesses.

**Variation of maximum stresses in the Vertical Adhesive with respect to the fiber angle  $\theta$ :**

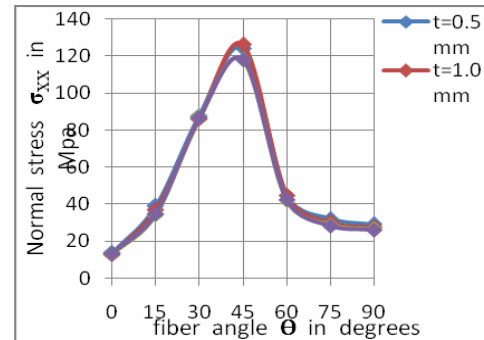


Fig. 13 Variation of  $\sigma_{xx}$  in the adhesive  
 This fig. shows that with increase in fiber angle  $\theta$  the stress also increases and is maximum at  $45^\circ$  and decreases with increase in angle.

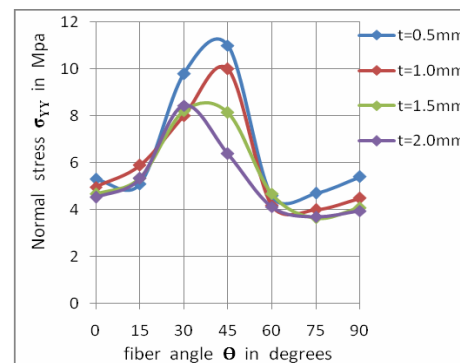


Fig. 14 Variation of  $\sigma_{yy}$  in the adhesive

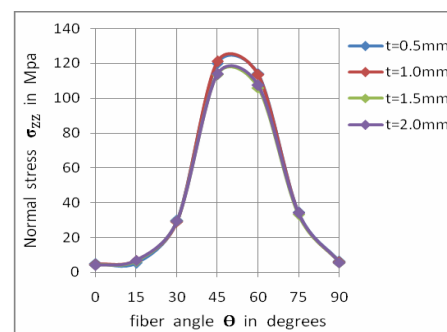


Fig. 15 Variation of  $\sigma_{zz}$  in the adhesive

Fig. 14 and 15 depicts the variation that stress increases with increase in fiber angle  $\theta$ . The maximum stress is observed to be at an angle of  $45^\circ$ . The induced stress is maximum for the adhesive thickness  $t=0.5\text{mm}$ .

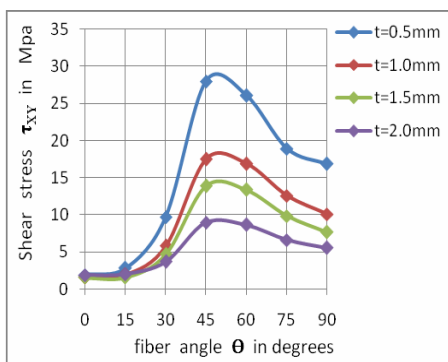


Fig. 16 Variation of  $\tau_{xy}$  in the adhesive

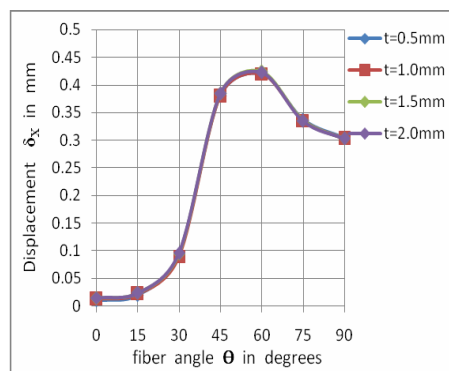


Fig. 19 Variation of  $\delta_x$  in the adhesive

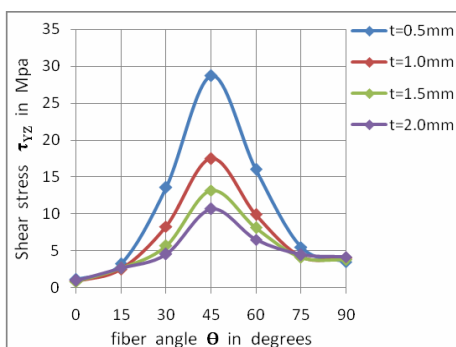


Fig. 17 Variation of  $\tau_{yz}$  in the adhesive

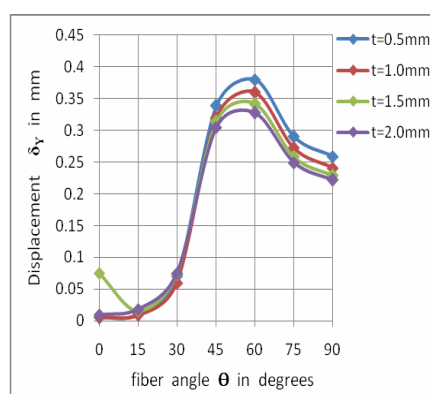


Fig. 20 Variation of  $\delta_y$  in the adhesive

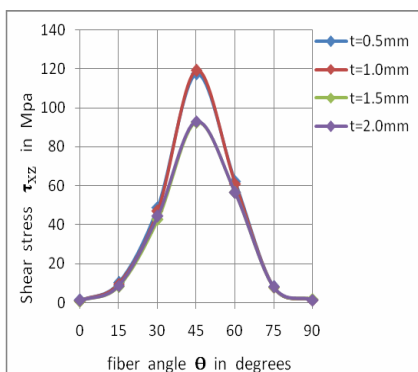


Fig. 18 Variation of  $\tau_{zx}$  in the adhesive

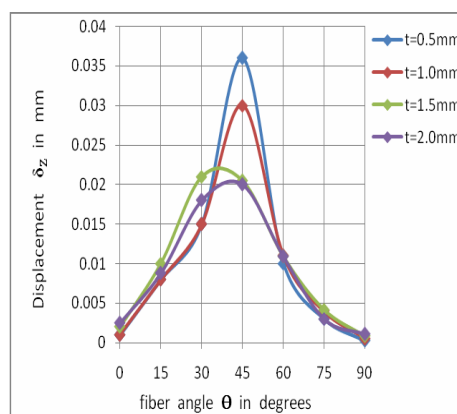


Fig. 21 Variation of  $\delta_z$  in the adhesive  
 This fig shows that the displacement is maximum at 45° and minimum at 0 and 90°. The maximum displacement decreases with increase in all adhesive thickness.

Fig. 16,17 and 18 shows the variation of shear stress  $\tau_{xy}$ ,  $\tau_{yz}$  and  $\tau_{zx}$  with respect to fiber angle  $\theta$ . The shear stress is minimum at 0° and increases with increase in angle. The shear stress is observed to be maximum at an angle of 45° and decreases with increase in angle. The induced shear stress is minimum for the adhesive thickness  $t=2.0\text{mm}$  when compared to other thicknesses.

Variation of maximum stresses in the Horizontal Adhesive with respect to the fiber angle  $\theta$ :

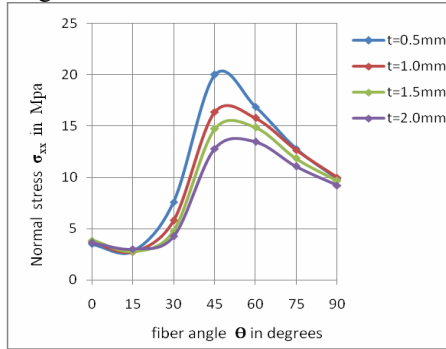


Fig. 22 Variation of  $\sigma_{xx}$  in the adhesive

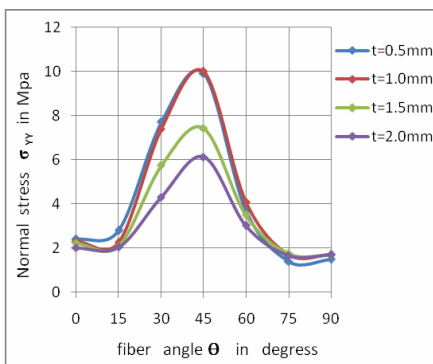


Fig. 23 Variation of  $\sigma_{yy}$  in the adhesive

Fig. 22 and 23 depicts the variation of Normal stress  $\sigma_{xx}$  and  $\sigma_{yy}$  with respect to fiber angle  $\theta$ . The stress increases with increase in fiber angle  $\theta$  followed by decrease with increase in angle. The stress is maximum at  $45^\circ$  and minimum in between  $0$  to  $15^\circ$ .

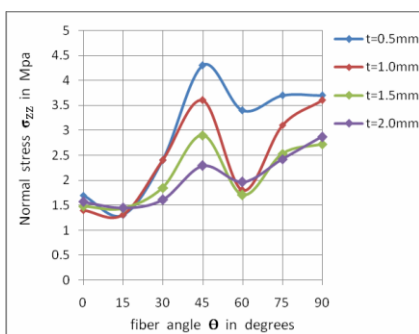


Fig. 24 Variation of  $\sigma_{zz}$  in the adhesive

This Fig. shows that the stress increases with increase in fiber angle  $\theta$  upto  $45^\circ$  and decreases upto  $60^\circ$  followed by increase with increase in angle. The induced stress is maximum for the adhesive thickness  $t=0.5\text{mm}$ .

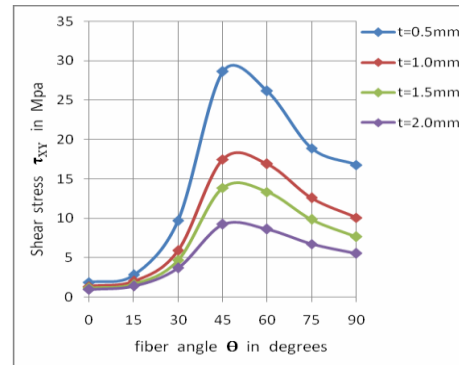


Fig. 25 Variation of  $\tau_{xy}$  in the adhesive

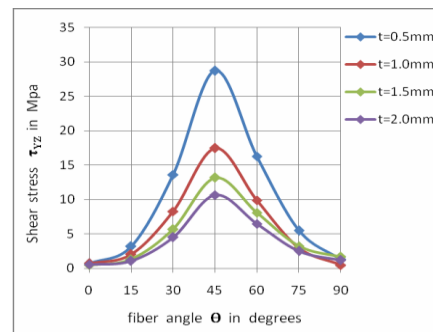


Fig. 26 Variation of  $\tau_{yz}$  in the adhesive

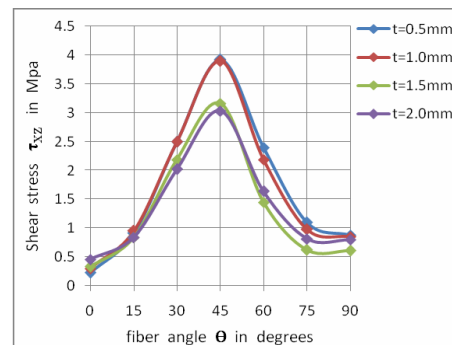


Fig. 27 Variation of  $\tau_{zx}$  in the adhesive

Fig. 25, 26 and 27 shows the variation of shear stress  $\tau_{xy}$ ,  $\tau_{yz}$  and  $\tau_{zx}$  with respect to fiber angle  $\theta$ . The induced shear stress is maximum at  $45^\circ$  and minimum in between  $0$  to  $15^\circ$  and  $75$  to  $90^\circ$ . The induced shear stress is minimum for the adhesive thickness  $t=2.0\text{mm}$

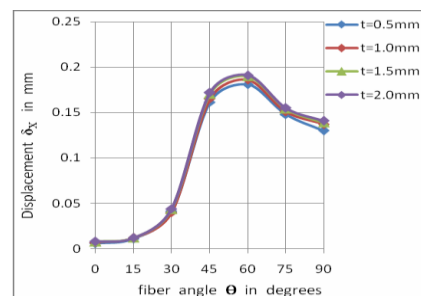


Fig.28 Variation of  $\delta_x$  in the j adhesive

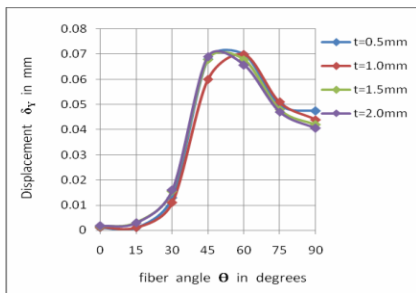


Fig.29 Variation of  $\delta_y$  in the adhesive

Fig.28 and 29 shows the variation of displacement  $\delta_x$  and  $\delta_y$  with respect to fiber angle  $\theta$ . The displacement increases with increase in fiber angle followed by decrease in value with increase in angle. The maximum displacement is at an angle  $60^\circ$  and minimum at  $0^\circ$ .

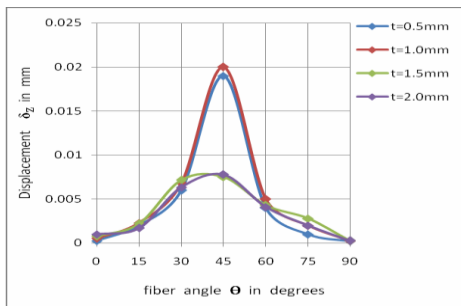


Fig.30 Variation of  $\delta_z$  in the adhesive

Fig.30 shows the variation of displacement  $\delta_z$  with respect to fiber angle  $\theta$ . The displacement is maximum at  $45^\circ$  and minimum at  $0$  and  $90^\circ$ . The maximum displacements are observed to be more for the adhesive thickness  $t=1.0\text{mm}$

**CONCLUSIONS:**

Three-dimensional finite element analysis has been taken up for the evaluation of the stresses in the adherends and adhesive of single strap hybrid butt joint made of FRP laminates of generally and specially orthotropic nature subjected to longitudinal load with C-F end conditions. The following conclusions are drawn:

- The normal stresses  $\sigma_{xx}$  and  $\sigma_{zz}$  in laminate and vertical adhesive are very high in magnitude between  $30^\circ$  and  $55^\circ$ . The fiber angle range i.e.,  $0^\circ-15^\circ$  and  $75^\circ-90^\circ$  is recommended in order to avoid the failure of fibers due to tearing or substrate failure.
- The displacements in adherends and adhesive are observed to be almost same and minimum between the fiber angles  $0^\circ$  and  $15^\circ$ .

- Maximum value of  $\tau_{xz}$  is found in vertical adhesive for longitudinal loading. Hence interfacial failure between the adhesive and the adherend or cohesive failure may likely to occur. This stress is observed to be minimum between  $0^\circ-15^\circ$  and  $75^\circ-90^\circ$ . Fiber angle orientation  $0^\circ-15^\circ$  or  $75^\circ-90^\circ$  is preferable to avoid the interfacial failure and cohesive failure.

- Magnitude of all the stresses is very less in the horizontal adhesive when the structure is subjected to longitudinal loading
- Variation of the stresses in the width direction is significant and therefore three-dimensional analysis is necessary.

**REFERENCES**

1. Reedy, E.D., and Guess, T.R., ‘Interface corner stress states: plasticity effects’, Int. journal of Fracture, V.81, No.3, 1996, p269-282.
2. Reedy, E.D., and Guess, T.R., ‘Comparison of butt tensile strength data with interface corner stress intensity factor prediction’, Int. J. Solids & Structures, 30, 1993, 2929.
3. Reedy, E.D., and Guess, T.R., ‘Interface corner failure analysis of joint strength: Effect of Adherend Stiffness’, Int. J. of Fracture, V.88, 4, 1993, p305-314.
4. Roy Xu, L., Sreeparna Sengupta., and Huacheng Kuai., ‘An experimental and numerical investigation of adhesive bonding strengths of polymer materials’, International Journal of Adhesion & Adhesives, 24, 2004, p455-460.
5. Fassio, F., Santini, S., and Vallee, T., ‘Tensile tests on bonded double strap joints between pultruded GFRP profiles’, Proceedings of the international symposium on bond behaviour of FRP in structures, (BBFS 2005).
6. Mitra, A.K., and Ghosh, B., ‘Interfacial stresses and deformations of an adhesive bonded double strap butt joint under tension’, computers & structures V.55, 4, 1995, p687-694.
7. Tungikar, V.B., and Rao, K.M., ‘Three dimensional exact solution of thermal stresses in rectangular composite laminate’, Composite Structures, 27, 1994, p419-430.
8. ANSYS reference manuals (2006)
9. Mallick, P.K., ‘Fiber-reinforced Composites’, MARCEL DEKKER, INC, 1988, P159-162.
10. Jones, R.M., ‘Mechanics of Composite Material’, Scripta book company, Wasington D.C, 1975.
11. Isaac, M.D., and Ishai Ori., ‘Engineering Mechanics of Composite Materials’, Oxford University Press, 1994.

# EFFECT OF BIODIESEL BLENDS AND NANO-PARTICLES ON ENGINE PERFORMANCE

**Md. Ashfaque Alam**

Research Scholar

Department of Mechanical Engineering,

NIT Jamshedpur, Jharkhand-831014, India India,

Email: [mdashfaque502@gmail.com](mailto:mdashfaque502@gmail.com)

**Dr. A. K. Prasad**

Associate Professor,

Department of Mechanical Engineering,

NIT Jamshedpur, Jharkhand-831014, India India,

Email: [akprasad.me@nitjsr.ac.in](mailto:akprasad.me@nitjsr.ac.in)

## Abstract

As a renewable, sustainable and alternative fuel for compression ignition engines, biodiesel instead of diesel has been increasingly fueled to study its effects on engine performances and emissions in the recent 10 years. But these studies have been rarely reviewed to favor understanding and popularization for biodiesel so far. In this work, reports about biodiesel engine performances and emissions, published by highly rated journals in scientific indexes, were cited preferentially since 2000 year. From these reports, the effect of biodiesel on engine power, economy, durability and emissions including regulated and non-regulated emissions, and the corresponding effect factors are surveyed and analyzed in detail. The use of biodiesel leads to the substantial reduction in PM, HC and CO emissions accompanying with the imperceptible power loss, the increase in fuel consumption and the increase in NO<sub>x</sub> emission on conventional diesel engines with no or fewer modification. And it favors to reduce carbon deposit and wear of the key engine parts. Therefore, the blends of biodiesel with small content in place of petroleum diesel can help in controlling air pollution and easing the pressure on scarce resources without significantly sacrificing engine power and economy. However, many further researches about optimization and modification on engine, low temperature performances of engine, new instrumentation and methodology for measurements, etc., should be performed when petroleum diesel is substituted completely by biodiesel.

**Keywords:** Biodiesel, Diesel engine, Performance, Emission

## INTRODUCTION

Innovations that lead to ozone friendly technology, biodegradable plastics, recycled waste, renewable energy sources and fuel efficient appliances using alternative fuels are included in sustainable development. Sustainable development, in a broader sense, implies the utilization of present resources in a proficient manner. In the long term, renewable energies will dominate the world's energy supply system. The reason is very simple and imperative: there is no

alternative. Mankind cannot indefinitely continue to base its activities on the consumption of finite energy resources. Renewable sources of energy are in line with an overall strategy of sustainable development.

To sustain the steady rate of progress, the developing countries like India, require much higher level of energy. In future, with the problem of increasing population and for the better quality of life, the demand of energy is going to increase rapidly. From the last ten to fifteen years, people around the world are getting aware about the environmental pollution. Today, globally, the top priority is getting clean and affordable energy. In India, petroleum is the second largest source of energy after coal. But still large amount of crude petroleum is imported. The petroleum derived products are being used by almost all transport sectors, agriculture sector, etc. As per the estimates, oil reserves in India will last for next twenty to thirty years.

Increased use of fossil fuels in various areas lead to anthropogenic degradation of the environment due to emission of harmful gases like carbon monoxide (CO), hydrocarbons (HC), Polyaromatic hydrocarbons (PAH), oxides of nitrogen (NO<sub>x</sub>), aldehydes and particulate matter (PM), benzene (C<sub>6</sub>H<sub>6</sub>), oxides of sulphur (SO<sub>x</sub>). The earnest attempts have been made in recent past to reduce vehicular pollution by improving fuel quality and vehicle technology. But there is little scope in this area. Therefore, we need to develop and promote appropriate technology for utilizing non-traditional renewable energy sources to satisfy energy requirements. Proliferation of fuel prices, exhausting hydrocarbon reserves of the world, increase in pollution and shortage of conventional petroleum-based products have forced everyone to look for the new technology and alternative fuels to fulfill the ever-increasing demands of energy. The various alternative fuels that have been either experimented or used commercially in engines include Methanol, Hydrogen, Compressed Natural Gas (CNG), Ethanol, Liquefied Petroleum Gas (LPG) and transesterified vegetable oils (Bio-diesel). Vegetable oil in its raw is very difficult to be used in engines. It has to be converted to a more engine friendly fuel called bio-diesel.

The post petroleum crisis has shifted the focus of energy planners towards renewable, alternative energy resources which could match the convenient features of oil at a relatively low price. It has been realized that the internal combustion (IC) engines form an indispensable part for the

industrial growth and development and it is not possible to stay away from IC engines at this exigency. Hence, it is highly required to seek alternative fuels for the safe survival of the existing engines. Bio-fuels like Ethanol and Bio-diesel appear to be more feasible options for meeting such criterion. The use of such bio-fuels in blends with petroleum based liquid fuels also does not require any major changes in the infrastructure for supply and distribution.

### 1.1 Need for Alternative Fuels

The oil prices are hiking due to severe shortage of oil and increased use of conventional fuels directly contributes to the crisis of global warming. Trends in the recent past shows that the demand for oil will exceed than supply and this gap will continue to grow, which can cause an energy crisis by the year 2020. Despite the improvements been made in lowering dangerous tailpipe exhaust emissions, automobile is still the single biggest source of air pollution till now. The use of diesel engines is continuously increasing due to its higher efficiency and higher power output. On the other hand, awareness on diesel vehicle has also increased due to higher noise level compared to gasoline engines. Noise emission from diesel engines is important, similar to exhaust emissions. Whenever the fuel quality varies, it affects the engine emissions and performance characteristics [5, 57, 58, 63, 64]. Lot of research has been done all over the world on combustion and exhaust emission from diesel engines fueled with alternative fuels [1-4, 6-19, 21-32, 34-56, 59-65, 111]. However a very little work has been reported in terms of noise generated from diesel engine fueled with alternative fuels [1-4, 6, 29]. The present work was taken up considering the importance of simultaneous study of noise, fuel economy and exhaust emissions on diesel engine fueled with alternative fuel. A general discussion and literature survey is presented here on the following lines: Vegetable oil as diesel substitute *Jatropha Curcas*, Source of alternative fuel, Bio-diesel as diesel substitute, Engine noise, Noise studies on diesel engines with alternative fuels.

## 2. BIODIESEL AS DIESEL SUBSTITUTE

Pure vegetable oils when used as CI engine fuel pose problems when subjected to prolonged usage. Therefore the best way to use vegetable oil as fuel is to convert it to biodiesel [8]. Bio-diesel is defined as mono alkyl-ester made up from renewable sources such as vegetable oils, animal fats and waste cooking oil. Bio-diesel can be used in neat form or blended with diesel without engine modifications. Main characteristic of bio-diesel are quite similar to diesel and can be blended with diesel to create a stable bio-diesel blend. The properties of some of the bio-diesel are shown in Table 1.7 [8].

Properties	Bio-diesel (vegetable oil methyl-ester)					
	Pea nut	Soya bean	Palm	Sunflower	Linseed	Tallow
Kinematic viscosity at 37.8 °C	4.9	4.5	5.7	4.6	3.59	-
Cetane number	54	45	62	49	52	-
Lower heating value (MJ/l)	33.6	33.5	33.5	33.5	35.3	-
Cloud point (°C)	5	1	13	1	-	12
Pour point (°C)	-	-7	-	-	-15	9
Flash point (°C)	176	178	164	183	172	96
Density (g/ml)	0.883	0.885	0.88	0.86	0.874	-
Carbon residue (wt%) at 40 °C	-	1.74	-	-	1.83	-

Bio-diesel contains 10-11% of oxygen by weight which leads to lower heating value than diesel on weight basis but due to higher density than diesel the overall reduction in energy content is less on volume basis. Presence of oxygen in the molecule results in its better combustion, hence better thermal efficiency. Cetane number of bio-diesel is also higher which means smoother combustion. Some of the advantages of bio-diesel are as follows [7, 32, 33]:

- ❖ Bio-diesel degrades faster than diesel.
- ❖ Bio-diesel is more lubricating than diesel.
- ❖ Bio-diesel is non toxic.
- ❖ Bio-diesel is an oxygenated fuel, thus implying that its oxygen content plays a role in making fatty compounds suitable as diesel by cleaner burning.
- ❖ Bio-diesel runs in any conventional, unmodified diesel engine.
- ❖ Bio-diesel has a high flash point compared to diesel. This means it is safer to transport.
- ❖ Provide a domestic, renewable energy supply.
- ❖ Bio-diesel does not produce green house effects, because the balance between the amount of CO<sub>2</sub> emissions and the amount of CO<sub>2</sub> absorbed by the plants producing vegetable oil is equal.
- ❖ Bio-diesel contains no sulfur.
- ❖ 90% reduction in cancer risks, according to Ames Mutagenicity.
- ❖ Cetane number of bio-diesel is greater than diesel.

Bio-diesel also has some disadvantages which are listed below [7, 32, 33]:

- ❖ Higher nitrogen oxide emissions.
- ❖ Lower energy content than diesel.

- ❖ Lower engine speed and power.
- ❖ More expensive.
- ❖ Higher cloud point and pour point.
- ❖ Fuel pumping difficulty from higher viscosity.
- ❖ Cold start problem.

### 2.1 Bio-Diesel Standard

Bio-diesel standard identifies the parameters the pure bio-diesel must meet before being used as a fuel for the diesel engine. Specifications of pure bio-diesel as per ASTM D 6751-02 standard are given in Table 1.8 [33].

Table 1.9 Pure bio-diesel specification (ASTM D 6751-02)

Property	Method	Limits	Units
Flash point	D 93	130 min	°C
Water and sediment	D 2709	0.050 max	% volume
Kinematic viscosity at 40 °C	D 445	1.9-6.0	mm <sup>2</sup> /s
Sulfated ash	D 874	0.020 max	Wt %
Total sulfur	D 5453	0.05 max	-
Copper strip corrosion	D 130	No. 3 max	-
Cetane number	D 613	47 min	-
Cloud point	D 2500	Report	°C
Carbon residue	D 4530	0.050 max	Wt %
Acid number	D 664	0.80 max	mg KOH/g
Free glycerin	D 6584	0.020	Wt %
Total glycerin	D 6584	0.240	Wt %
Phosphorus	D 4951	0.0010	Wt %
Vacuum distillation end point	D 1160	360 °C max, at 90% distilled	°C

### 2.2 Spray Characteristic of Bio-Diesel

Physical properties such as density, viscosity and isothermal compressibility strongly affect injection process such as injection pressure, injection rate and spray characteristics. Variations in the injection process affect combustion characteristics which in turn affects engine performance and emissions. Yamane et al. [34] conducted a study to evaluate

the influence of the physical properties of the fuel on the injection characteristics. The experiments were carried out on a single cylinder, horizontal-type, four stroke direct injection diesel engine. In the experiments, two kind of bio-diesel and two neat fatty acids: methyloleate and methyl-linoleate were tested. In the study, it was concluded that in case of bio-diesel the injection pressure rises and the injection timing advances with a decrease in fuel temperature whereas at higher fuel temperature, difference in injection timing and injection pressure between bio-diesel and diesel disappears. It was found in the study that the spray penetration for the bio-diesel was shorter than that of diesel thus resulting in poor air-fuel mixing. In case of bio-diesel substantial fuel rich mixture was formed at the center of the combustion chamber and a portion of this mixture that failed to burn was emitted as soluble organic fraction. Szybist and Boehman [35] conducted experiment to measure the effect of bio-diesel on fuel injection timing and combustion. In the experiment, fuel injection timing was measured by digital imaging, laser attenuation, and fuel line pressure. It was found that bio-diesel advances the fuel injection timing and advance in fuel injection timing increases with increasing bio-diesel content in diesel. It was also found that the advance in fuel injection timing resulted in an earlier ignition. The same results were also found by Alam et al. [36]. Szybist and Boehman [35] also concluded that the start of premixed combustion advances with increasing bio-diesel content which results in a higher combustion pressure and temperature. Higher temperature and pressure in the cylinder during combustion result in an increase in NOx. It was concluded in the study that the reason for the dynamic advance in fuel injection timing for bio-diesel is the increase in the bulk modulus of compressibility. He et al. [37] conducted a study to investigate the spray properties of bio-diesel. It was concluded that the spray tip penetration and cone angles of bio-diesel increases with increasing injection duration. It was also concluded that under the same injection duration and ambient pressure, bio-diesel can result in a higher injection pressure due to higher viscosity, density and bulk modulus. Spray tip penetrations of bio-diesel were found to be smaller than that of diesel at the beginning of injection and grows quickly to become bigger than that of diesel at the end of the injection. It was also concluded that the use of bio-diesel increases the spray angle as compared to diesel.

### 3. PERFORMANCE, EMISSIONS AND COMBUSTION CHARACTERISTICS OF BIO-DIESEL AS DIESEL SUBSTITUTE

Several investigations have shown that when bio-diesel and its blends are used as compression ignition engine fuel, there is reduction in smoke opacity particulates, un-burnt hydrocarbons, carbon mono oxide and slight increase in NOx emissions. Rickeard et al. [38] reported that bio-diesel reduces emissions, notably HC, CO, and particulates; however, reduction in the emissions depends upon engine design, adjustment and test conditions. As per U.S. EPA, bio-diesel has been comprehensively evaluated in terms of

emissions and potential health effects under the clean Air Act Section 211(b). These programs include stringent emissions testing protocols required by EPA for certification of fuels in the USA. The data gathered through these tests include thorough inventory of the environmental and human health effect's attributes that current technology will follow [20]. The results of emission tests for pure bio-diesel and blend of 20% bio-diesel compared to diesel are given in Table 1.9.

Scholl and Sorenson [39] conducted a study to investigate the effects of load, fuel injection timing and injector orifice diameter on the engine performance and emissions running on soybean methyl-ester and diesel. It was found that the overall rate of heat release of soybean oil methyl-ester was similar to diesel. Combustion related parameters such as ignition delay, peak pressure, peak rate of pressure rise, and instantaneous combustion rate were close to that of diesel at the same load, speed, injection timing and nozzle diameter. It was also found that ignition delay period of soybean oil methyl-ester was more sensitive to change in injection timing and nozzle diameter than diesel. Injection timings found to have pronounced effect on the engine performance and emissions for both the fuels. Smaller diameter nozzle gave higher cylinder pressure, maximum rate of pressure rise and higher premixed burning for both the fuels. It was also found that soybean methyl-ester gave lower HC emission and smoke. NO<sub>x</sub> emissions were higher for soybean methyl-ester as compared to diesel. It was concluded in the study that in terms of combustion behavior and exhaust emission characteristics, soybean oil methyl-ester can basically be regarded as interchangeable with diesel.

Song and Zhang [40] also found that with soybean oil methyl-ester HC and smoke emissions were reduced; whereas, NO<sub>x</sub> emissions were increased. It was found that soybean oil methyl-ester and its blends have on average, a reduction of 20.04% for smoke, a reduction of 41.07% of HC emissions, a reduction of 36.67 % for CO emissions and an increase of 23.21% for NO<sub>x</sub>. An average increase in brake power of 5.19% and torque of 5.26% were also found with soybean methyl-esters and its blends. 20wt% of bio-diesel blend was found to be an optimum compromise between NO<sub>x</sub> and smoke emissions.

Ozsezen et al. [19] conducted a study to evaluate the performance and combustion characteristics of a direct injection diesel engine fueled with bio-diesels such as waste (frying) palm oil methyl-ester (WPOME) and canola oil methyl-ester (COME). It was found in the study that when the test engine was fueled with WPOME or COME, the engine performance slightly weakened and the combustion characteristics slightly changed when compared to that of diesel. The bio-diesels caused reduction in carbon monoxide (CO), unburned hydrocarbon (HC) emissions and smoke opacity, but they led to increase in nitrogen oxide (NO<sub>x</sub>) emissions.

Table 1.9 Bio-diesel emissions compared to conventional diesel [20]

Emissions	B100	B20
<b>Regulated Emissions</b>		
Total Unburned Hydrocarbons	-93%	-30%
Carbon Monoxide	-50%	-20%
Particulate Matter	-30%	-22%
NO <sub>x</sub>	+13%	+2%
<b>Non-Regulated Emissions</b>		
Sulphates	-100%	-20%*
Polycyclic Aromatic Hydrocarbons (PAH)**	80%	--13%
NPAH (Nitrated PAHs)	-90% **	-50%***
Ozone potential of Speciated HC	-50%	-10%
Life-Cycle Emissions		
Carbon Dioxide (LCA)		
Sulphur Dioxide (LCA)		
*Estimated from B100 results. **Average reduction across all compounds measured. ***2-nitroflourine results were within test method variability		

Babu [41] investigated the effect of injection pressure and injection timing on the performance and exhaust emission characteristics of a direct injection, naturally aspirated diesel engine operating on diesel and diesel-Biodiesel blends. It was concluded in the study that the engine performance and exhaust emission characteristics of the engine operating on the ester fuels at advanced injection timing were better than when operating at increased injection pressure. It was also found that the engine performance deteriorated in an attempt to retard the injection timing and reduced injection pressure. Kumar et al. [42] conducted a study on DI diesel engine running on karanja oil methyl-ester. It was found in the investigation that the addition of bio-diesel to diesel has significantly reduced CO, unburned hydrocarbons (HC) and smoke emissions but it increases the NO<sub>x</sub> emissions slightly. It was also found that there was no significant power reduction in the engine operation when operated with blends of bio-diesel and diesel.

Kim et al. [43] conducted experimental investigation to study the effect of engine speed, exhaust gas recirculation (EGR) and intake pressure on the particulate size distribution and exhaust gas emissions on a compression ignition engine fueled with bio-diesel derived from soybean. It was found that bio-diesel had higher maximum injection rate compared to diesel. Premixed combustion and

combustion pressure were also lower with bio-diesel. It was found that particulate size distribution was increased by increasing engine speed for bio-diesel as well as for diesel. The use of bio-diesel found to have shifted the particulate size concentration to the side of smaller particulate diameter. With EGR, significant increase in particulate number density was found for diesel when compared to bio-diesel. Boosting intake pressure significantly shifted particulate distribution to a smaller size.

Senatore et al. [44] observed that in case of bio-diesel, heat release always takes place in advance as compared to diesel. This behavior determines consistently higher peaks in the mean temperature in the combustion chamber and, hence higher concentrations of nitrogen oxides in the exhaust. It was also found that CO and smoke emissions were lower for the rapeseed methyl-ester as compared to diesel. It was concluded in the study that the reasons for the advances in the injector lift and instantaneous injection pressure for bio-diesel were different density and different quantity of mass injected.

Nwafor [45] found that CO emissions with rapeseed methyl-ester were similar, CO<sub>2</sub> emissions were higher and HC emissions were lower as compared to diesel. It was also concluded that fuel consumption increased proportionally to the amount of RME added in the blend. Exhaust temperature was also found to be same for RME and diesel.

Selim et al. [46] investigated the effect of speed, load, injection timing and compression ratio on the engine performance on a Ricardo E6 indirect injection diesel engine fueled with jojoba methyl-ester. It was found that variation of maximum cylinder pressure and maximum pressure rise rate with engine speed for jojoba methyl-ester was almost similar to that of gas oil. Jojoba methyl-ester, however exhibited slightly lower pressure rise rate than gas oil. It was concluded that advancing the injection timing generally increases the maximum pressure and maximum pressure rise rate. Maximum pressure rise rate for jojoba methyl-ester was found to be similar to that of gas oil in mid range of injection timing, whereas at very early injection and late injection jojoba methyl-ester had higher rate of pressure rise. Rate of pressure rise was reduced with the increase in compression ratio. Power and torque produced by jojoba methyl-ester were close to that of gas oil. It was concluded in the investigation that jojoba methyl-ester can be a good replacement of gas oil from the point of view of torque, power produced, and combustion noise and also in terms of cyclic variability.

Leung [47] carried out investigations on three types of diesel engines, using blends of waste cooking oil based bio-diesel. It was found in the investigation that when bio-diesel was used, there was reduction in CO, HC and smoke level. But, there was a slight increase in NO<sub>x</sub> emissions and fuel consumption with increasing percentage of bio-diesel in the blends. Leung et al. [48] conducted a study, on a single cylinder diesel engine fueled with bio-diesel to investigate the effect of injection timing, plunger diameter and injection pressure on NO<sub>x</sub>, PM and HC emissions. It was concluded in the study that the retarded timing and rapid diffusion

combustion is a suitable strategy to improve bio-diesel combustion performance.

In developing countries like India, production of bio-diesel from edible oil is not feasible. Non edible oils such as Pongamia (karanja), Jatropha, Madhuca (mahua), Azadirachta indica A Jeuss (neem) etc. are best suited for bio-diesel production in India because plenty of wasteland is available in India, which can be utilized for growing such non-edible oil seed crops.

Raheman and Phadatare [50] conducted a study to evaluate the performance and emission characteristics of a diesel engine working on karanja methyl-ester. It was found that CO, smoke and NO<sub>x</sub> emissions were reduced on an average of 80%, 50% and 26% respectively whereas Bose et al. [51] found that CO emissions of karanja methyl-ester were higher than diesel. It was also found that esterified karanja oil had higher brake thermal efficiency than diesel. The reason concluded for higher efficiency was higher injection pressure of karanja methyl-ester, which leads to improvement in performance.

Raheman and Ghadge [52] conducted a study on Ricardo E6 engine fueled with mahua bio-diesel and its blends. They observed that brake specific fuel consumption increased and brake thermal efficiency decreased with increase in content of mahua bio-diesel in the blends. Smoke and HC emissions were found to be lowered whereas NO<sub>x</sub> emissions increased with increase in bio-diesel content in the blends. It was concluded that blends upto 20% mahua bio-diesel can be used as compression engine fuel without significantly affecting engine performance and emissions.

Sinha and Agarwal [53] carried out experimental investigations to evaluate combustion characteristics of rice bran oil methyl-ester and its blends on a direct injection transportation diesel engine. Tests were performed at different loads and at constant speed. Different combustion related parameters such as combustion pressure, rate of pressure rise, instantaneous heat release, cumulative heat release and mass fraction burned were analyzed. It was found in the investigation that peak pressure was higher for bio-diesel blends at low loads but at higher load, peak pressure of diesel was higher. Maximum rate of pressure rise was also lower for the bio-diesel blends as compared to that of diesel. After carrying out the heat rate analysis, it was found that the combustion starts earlier for bio-diesel blends because of shorter ignition delay and earlier injection timing. The premixed combustion heat release of bio-diesel blends was lower than diesel because of shorter ignition delay. Due to shorter ignition delay of bio-diesel, less fuel accumulates in the combustion chamber leading to lower heat release. It was found in the study that cumulative heat release decreases with the increase of bio-diesel content in the blends owing to the lower heating value of the bio-diesel. However, it was concluded in the investigation that rice bran methyl-ester and its blends can be used in the engine without any modifications.

Tziourtzioumis et al. [54] conducted a study on a common-rail high pressure injection passenger car diesel engine fueled with B70 bio-diesel. The aim of the study was to

understand that how the electronic control unit of engine respond to different fuel qualities. Bio-diesel employed in the test was a FAME based on 40% rapeseed oil, 30% soybean oil and 30% waste cooking oil as raw material. In the study, effect of the B70 blend on the main fuel injection parameters such as common-rail pressure, pilot and main injection advance were measured and they found to be increased with bio-diesel. It was concluded that increase in rail pressure was due to a lower heating value of bio-diesel because for producing same power more fuel needs to be injected in the cylinder, which causes a higher fuel delivery. It was observed in the study that reduction in NO<sub>x</sub> was only at medium to high load where as there was sharp reduction in CO and HC emissions at all loads.

Agarwal et al. [55] found that bio-diesel and EGR both can be employed together in CI engine to reduce NO<sub>x</sub> and smoke simultaneously. In the investigation, HC and CO emissions also found to be decreased. It was concluded in the study that 20 % bio-diesel blend with 15% EGR is optimum for bio-diesel to improve thermal efficiency and to reduce exhaust emissions.

Ghosh et al. [56] conducted a study to evaluate the prospects of Jatropha methyl-ester in India. It was concluded in the study that jatropha methyl-ester is safer because of high flash point, has less exhaust emissions and has comparable mileage with diesel. They found that Jatropha plants on Gopalpur (Orissa) field station withstood the Orissa super cyclone in 1999. The plant also survived two successive years of drought. They also found that Jatropha is suited to varied climatic conditions, prevalent throughout India. It was concluded that Jatropha methyl-ester is the important part of the solution to the energy challenges faced by India or the world, especially when it not only stretches finite supplies of conventional fuel but restores the land it grows on, does not displace more viable agricultural land, and improves the environment both through the cultivation process and cleaner burning of the fuel.

Sahoo et al. [59] conducted a study on a three cylinder water cooled tractor engine fueled with Jatropha, karanja and polanga based methyl-esters. In the study, maximum increase in power was observed for 50% Jatropha methyl-ester. Smoke emissions were also found to be lower with all bio-diesels and their blends. Noticeable reduction in HC and PM was also seen with bio-diesel and their blends, however slight increase in CO and NO<sub>x</sub> was observed. Among all the tested fuels, best brake specific fuel consumption was observed for blend of 20% Jatropha methyl-ester. It was also concluded that no hardware modifications were required for handling the fuels tested in the existing engine. In another study [60] on the combustion analysis of Jatropha, karanja and polanga based bio-diesel it was found that the maximum cylinder pressure has occurred for pure polanga bio-diesel. Ignition delays of different bio-diesels and their blends were also lower than that of diesel which causes lower premixed combustion rate for bio-diesel and their blends. Among the different bio-diesels and their blends, ignition delays of pure Jatropha methyl-ester were consistently shorter varying

between 5.9° and 4.2° crank angles lower than diesel at different loads.

#### 4. Conclusions and further researches

Biodiesel, produced from renewable and often domestic sources, represents a more sustainable source of energy and will therefore play an increasingly significant role in providing the energy requirements for transportation. Therefore, more and more researches are focused on the biodiesel engine performances and its emissions in the past 10 years. Although there have always been inconsistent trends for biodiesel engine performances and its emissions due to the different tested engines, the different operating conditions or driving cycles, the different used biodiesel or reference diesel, the different measurement techniques or instruments, etc., the following general conclusions could be drawn according to analysis and summary of the massive related literatures in this work:

1. The use of biodiesel will lead to loss in engine power mainly due to the reduction in heating value of biodiesel compared to diesel, but there exists power recovery for biodiesel engine as the result of an increase in biodiesel fuel consumption. Especially for the blend fuel including a portion of biodiesel, it is not easy for drivers to perceive power losses during practical driving.
2. The vast majority of literatures agree that NO<sub>x</sub> emissions will increase when using biodiesel. This increase is mainly due to higher oxygen content for biodiesel. Moreover, the cetane number and different injection characteristics also have an impact on NO<sub>x</sub> emissions for biodiesel.
3. It is accepted commonly that CO emissions reduce when using biodiesel due to the higher oxygen content and the lower carbon to hydrogen ratio in biodiesel compared to diesel.
4. It is predominant viewpoint that HC emissions reduce when biodiesel is fueled instead of diesel. This reduction is mainly contributed to the higher oxygen content of biodiesel, but the advance in injection and combustion of biodiesel also favor the lower THC emissions.
5. There exist the inconsistent conclusions, some researches indicated that the CO<sub>2</sub> emission reduces for biodiesel as a result of the low carbon to hydrocarbons ratio, and some researchers showed that the CO<sub>2</sub> emission increases or keeps similar because of more effective combustion. But in any event, the CO<sub>2</sub> emission of biodiesel reduces greatly from the view of the life cycle circulation of CO<sub>2</sub>.
6. Most of researches showed that aromatic and polyaromatic compounds emissions for biodiesel reduce with regard to diesel. Carbonyl compounds emission shave discordant results for biodiesel, although it is widely accepted that, biodiesel increases these oxidants emissions because of higher oxygen content.

7. It can be concluded that the blends of biodiesel with small content by volume could replace diesel in order to help in controlling air pollution and easing the pressure on scarce resources to a great extent without significantly sacrificing engine power and economy.

## References

1. Spessert, B.M., Arendt, L. and Schleicher, A., "Influence of fuel quality on exhaust gas and noise emissions of small industrial diesel engines", 03SETC-38, SETC Congress, 2003, Madison, USA.
2. Spessert, B.M., Arendt, L. and Schleicher, A., "Influence of RME and vegetable oils on exhaust gas and noise emissions of small industrial diesel engines", 04SETC-3, SETC Congress, 2004, Graz, Austria.
3. Schleicher, A., Spessert, B.M., Gehrke, S. and Pohl, M., "Influence of alternate fuels on exhaust gas and noise emissions of small industrial diesel engines", 05SETC-32, SETC Congress, 2005, Bangkok, Thailand.
4. Patro, T.N. and LaRue, D.A., "Alternate Fueled Powertrain - An Insight into its Combustion Related NVH issues", SAE Paper No. 1999-01-1758, 1999.
5. Anderton, D. and Waters, P.E., "Effect of fuel Composition on Diesel Engine Noise and Performance", SAE Paper No. 820235, 1982.
6. Chan, C.M.P., Moncrieff, I.D. and Pettitt, R.A., "Diesel Engine Combustion Noise with Alternative Fuels", SAE Paper No. 820236, 1982.
7. Babu, A.K. and Devaradjane, G., "Vegetable Oils and Their Derivatives As Fuels For CI Engines: An Overview", SAE Paper No. 2003-01-0767, 2003.
8. Agarwal, A.K., "Biofuels (alcohols and biodiesel) applications as fuels for internal combustion engines", *Progress in Energy and Combustion Science*, 2007, Vol. 33, pp. 233-271.
9. Srivastava, A. and Prasad, R., "Triglycerides-based diesel fuels", *Renewable and Sustainable Energy Reviews*, 2000, Vol. 4, pp. 111-133.
10. Ma, F. and Hanna, M.A., "Biodiesel production: a review". *Bioresource Technology*, 1999, Vol. 70, pp. 1-15.
11. Murayama, T., Oh, Y., Miyamoto, N. and Chikahisa, T., "Low Carbon Flower Buildup, Low smoke and Efficient Diesel Operation with vegetable Oils by Conversion to Mono-Ester and Blending with Diesel Oil or Alcohols", SAE Paper No. 841161, 1984.
12. Bari, S., Yu, C.W. and Lim, T.H., "Effect of fuel injection timing with waste cooking oil as a fuel in a direct injection diesel engine", *Proc. Instn Mech. Engrs Part D: J. Automobile Engineering*, 2004, Vol. 218, pp. 93-104.
13. Subramanian, K.A., Singal, S.K., Saxena, M. and Singhal, S., "Utilization of liquid biofuels in automotive diesel engines: An Indian perspective", *Biomass and Bio-energy*, 2005, Vol. 29, pp. 65-72.
14. Lance, D.L. and Anderson, J.D., "Emissions Performance of Pure Vegetable Oil in Two European Light Duty Vehicles", SAE Paper No. 2004-01-1881, 2004.
15. Hemmerlein, N., Korte, V. and Richter, H., "Performance, Exhaust Emissions and Durability of Modern Diesel Engines Running on Rapeseed Oil", SAE Paper No. 910848, 1991.
16. Barsic, N.J., and Hun, ke, A.L., "Performance and Emission Characteristic of a Naturally Aspirated Diesel Engine with Vegetable oil fuels", SAE Paper No. 810262, 1981.
17. Rakopoulos, C.D., Antonopoulos, K.A., Rakopoulos, D.C., Hountalas, D.T. and Giakoumis, E.G., "Comparative performance and emissions study of a direct injection Diesel engine using blends of Diesel fuel with vegetable oils or bio-diesels of various origins", *Energy Conversion and Management*, 2006, Vol. 47, pp. 3272-3287.
18. Wang, Y.D., Al-Shemmeri, T., Eames, P., McMullan, J., Hewitt, N., Huang, Y. and Rezvani, S., "An experimental investigation of the performance and gaseous exhaust emissions, of a diesel engine using blends of a vegetable oil", *Applied Thermal Engineering*, 2006, Vol. 26, pp. 1684-1691.
19. Ozsezen, A.N., Canakci, M., Turkcan, A. and Sayin, C., "Performance and combustion characteristics of a DI diesel engine fueled with waste palm oil and canola oil methyl esters", *Fuel*, 2009, Vol. 88, pp. 629-636. "Report of the committee on development of Bio-fuel", Planning commission, Government of India, 2003, New Delhi.
20. Achten, W.M.J., Verchot, L., Franken, Y.J., Mathijs, E., Singh, V.P., Aerts, R. and Muys, B., "Review: Jatropha bio-diesel production and use", *Biomass and Bioenergy*, 2008, Vol. 32, pp. 1063-1084.
21. Prasad, C.M.V, Krishna, M.V.S.M, Reddy, C.P. and Mohan, K.R., "Performance evaluation of non-edible vegetable oils as substitute fuels in low heat rejection diesel engines", *Proc Instn Mech Engrs Part D*, 2000, Vol. 214, pp. 181-187

# Cost and Time Effectiveness through Six Sigma's ECRS Technique – Experimental Study at an Automobile Assembly Plant

R.Saravanan<sup>\*1</sup>, T.Malyadri<sup>2</sup>, Nagasrisaihari Sunkara<sup>3</sup>, M.S.Srinivasa Rao<sup>4</sup>

<sup>\*1</sup>Dean Academics & Professor of Mech. Engg., Ellenki College of Engg. and Tech., Hyderabad, TS.

<sup>2,3,4</sup>Assistant Professors of Mech. Engg., VNR Vignana Jyothi Institute of Engg. and Tech., Hyderabad,

<sup>\*</sup> e-mail of Corresponding Author: dr.saravanan@gmail.com

## ABSTRACT

*Even though the technology upgraded day by day, many of the industrial operations were not upgraded till completion their depreciation period due to either unaware of cost and time savings or negligence or unnoticed. A scientific proposal not only needs to highlight such need for up gradation but also attracts the industrial management to form Small Group Activity team to identify such losses and countermeasures. Here the case study which belongs to a proposal of replacement machines as their depreciation period got over in an assembly plant of a largest and leading automobile manufacturer. The objective this research is to suggest the valid proposal and procure the equipment with proposed improvements. The six sigma's ECRS methodology majorly govern this experimental investigation. This study included the process evaluation, conceptual design, basic engineering design, computer aided design and validation, cost analysis. The effectiveness is verified and presented in this paper. The proposed machine reduced 70.27% of processing time, 39.02% of equipment cost and 70.25% cost per piece.*

## 1. INTRODUCTION

The feasibility investigation plays vital role in industries, in particularly introducing new systems, renovation of existing facilities, making replacement policies. The utility is the prime objective of those studies [1]. This research focuses to prepare a valid engineered report with experimental confirmation. The engineered part is carried out with computer aided conceptual design and analysis. In the literature many approaches have proposed to achieve the cost effectiveness. [2] used ECRS method to achieve cost effectiveness and achieved 50% scrap reduction. [3,4] suggested the simulation to achieve the cost effectiveness in the shop floor, [5] suggested new equipment design based on the specific requirements to achieve high

cost effectiveness, this research considered this suggestion and designed new tool for meeting the specific requirement. [6] suggested the genetic algorithm based line balancing to achieve cost effectiveness in assembly shops. [7] used the Single Minute Exchange of die systems (SMED) to reduce the Set-Up time Reduction. Such ideas considered in this study to coalesce of two stage operations into single stage. [8,9] advised to validate proposal through the computer aided design by static and dynamic analysis. Here such computer aided conceptual design and stability analysis were included. Hence this research is unique.

## 2. MATERIALS AND METHODS

The ECRS methods can be defined by following

E - Eliminate non value adding time (Tool changing time, axes movement, indexing)

C - Combine operation (Combination cutting tools)

R - Reduce value adding time (Optimize parameters)

S - Simplify operation (Programming – Multiple to single pass)

### 2.1 Problem

The case study organization is one of the largest heavy automobile manufacturers in India. This paper deals the problem concerned with wheel and assembly shop. In the assembly line of the wheel and assembly shop the wheel and assembly shop operation of wheel hub racer and bolts are carried at separate machines which includes set up times, unloading times transport times, additional man power etc. the Figure 1 illustrates the wheel hub assembly, sequence of assembly and Racer press operation after the stud pressed. the Figure 2 illustrates the the conventional bolt pressing machine, racer pressing machine



Figure 1 (L) Wheel hub (M) Assembly Sequence (c) Racer press operation



Figure 2 bolt pressing machine (L) Racer pressing machine (R)

### 3. PROPOSED SOLUTION

#### 3.1 Perception

The simultaneous engineering and work integrating concepts are powerful in reduction of cycle time and improving the productivity rapidly. The two operations are performed at different machines. Hence, the two operations are to be carried out in single machine without changing the order of operation by means of telescopic cylinder.

#### 3.2 Conceptualization

The contemplation is a mechanism that provides dual movement to the ram. The first movement for pressing the racer on the hub and then the pressing bolts in next. This design of compound tool consists

of a ram which is used to provide a dual movement with the help of tandem cylinder. The compound tool has a tool bunk in the centre to press the racer bearing into the wheel hub and the outer part of the tool presses the bolt into the hub. The figure 3 illustrates the conceptual design and telescopic cylinder.

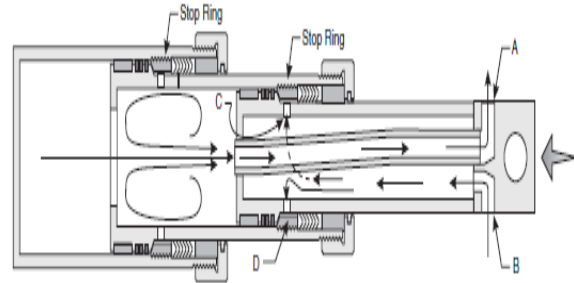
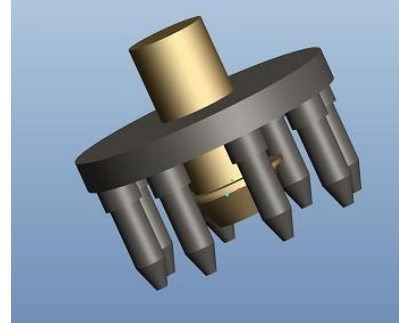


Figure 3 Conceptual design of tool head with ram (L) and Telescopic cylinder (R).

The telescopic cylinders provide an exceptionally long stroke which extends stage by stage in a compact initial package. The collapsed length of typical telescopic cylinders varies from 20% to 40% of their extended length. Thus, when mounting space is limited and the application needs a long stroke, a telescopic cylinder is a natural solution.

The construction of the system must consist of principle parts like Sliding ram, Plunger setup, Base and fixture and Hub lifter. The sliding ram is used to move the plunger setup up and down by means of hydraulic system. The plunger setup is mounted on the sliding ram to press (with eighty ton of pressure) the bolt and bearing racer in the wheel hub. The mild steel base and Fixture are strong enough to bear the compression load. An adapter is fixed on the centre of the base. The pneumatic cylinder is fixed with base. The Hub lifter is used to lift wheel hub after completion of press operation.

#### 3.3 Press Requirement:

Component specification is: Racer made up of High Carbon Chromium Steel (permissible stress ( $\sigma_2$ ) is 550 N/mm<sup>2</sup>) and the stud made by SG iron (permissible stress ( $\sigma_1$ ) is 230 N/mm<sup>2</sup>). The Racer OD and ID are 130 and 125 mm respectively,

**Diameter of Piston to press Stud**

The stud diameter is 36 mm.  
 Contact area of bolt ( $A_1$ ) =  $\pi/4*d^2*n$  = 8143.01mm<sup>2</sup>  
 Load ( $F_1$ ) = stress\*contact area = 187.289187 kN = 191 ton-force  
 The Pressure required for pressing the racer ( $P_1$ ) = 1.9 kN/mm<sup>2</sup>  
 Hence required diameter of the piston ( $d_1$ ) =  $\sqrt{\frac{4 \times \text{load}}{\pi \times \text{pressure}}} = 35.43 \text{ mm} \cong 36 \text{ mm}$ .

**Diameter of Piston to press Racer**

The Contact area of racer ( $A_2$ ) =  $\pi/4*(d_1^2 - d_2^2)$  = 1001.38 mm<sup>2</sup>  
 Required Load ( $F_2$ ) = stress\*area = 550759 N  $\cong$  56 ton-force  
 Pressure required for pressing the racer( $P_2$ ) = 1.5 kN/mm<sup>2</sup>  
 Hence required diameter of the piston ( $d_2$ ) =  $\sqrt{\frac{4 \times \text{load}}{\pi \times \text{pressure}}} = 21.62 \text{ mm} \cong 22 \text{ mm}$ .  
 If the FOS is 1.5 means the maximum force required is 286.5  $\cong$  300 ton-force

**3.4 Computer Aided Design and Validation**

The computer aided design of compound tool with wheel hub (left) and compound tool alone (middle) and Wheel Hub Assembly (Right) are shown in Figure 4. The Figure 5 illustrates the compound tool to before and press positions. The necessary stability investigations were made like stress (Refer top left of Figure 6), strain (Refer bottom left of Figure 6), and displacement (Refer top right of Figure 6) analysis and plotted graph for path-length graph (Refer bottom right of Figure 6) and ensured the fulfillment of requirements and safety.

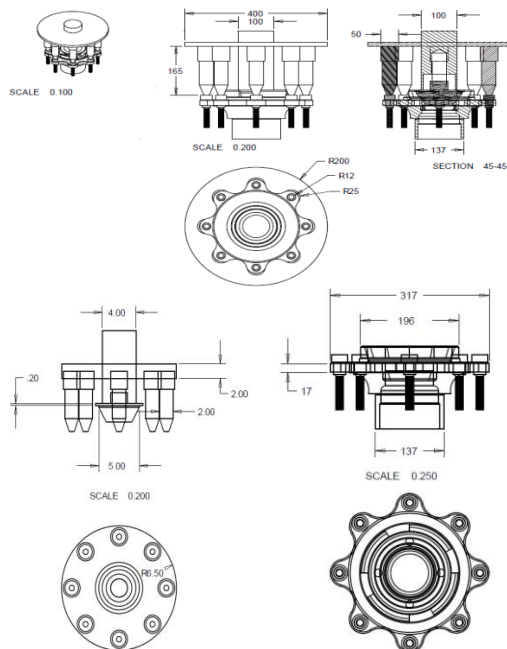


**Figure 4** compound tool with wheel hub (left) and compound tool alone (middle) and Wheel Hub Assembly (Right)

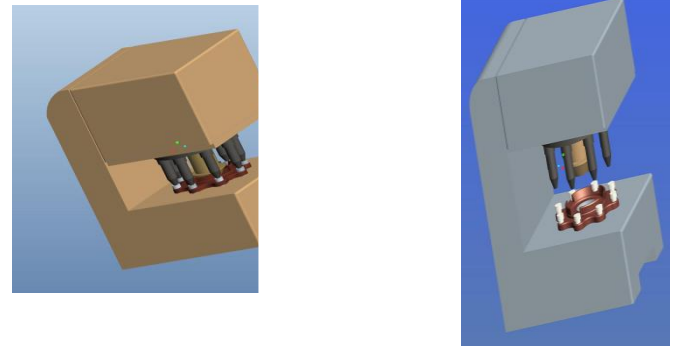


**Figure 5** the compound tool to before and press positions

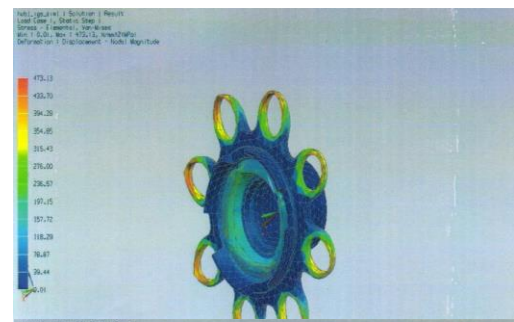
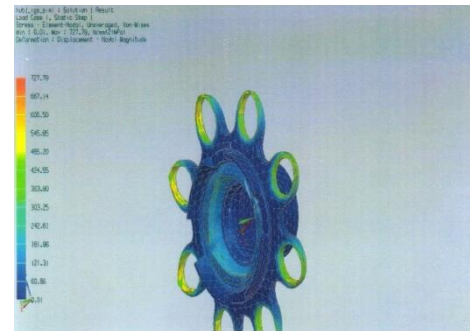


**Figure 6:** Results of Stress (TL), displacement (TR) and strain (BL) analysis and Stress v/s Path-length relationship (BR)

**3.5 Procedure of Proposed Method**

Initially the hub is brought to the hydraulic press machine. Hub is inserted into the fixture such that it holds the hub firmly during the entire process. Now the hub is pulled down by the pneumatic power to perform the operation. Then the inner bearing racer is inserted in the lower ram and the outer bearing

racer is inserted in the hub. Then the bolts are inserted in the hub. Now by means of hydraulic pressing machine the racer is installed into the hub. The center plunger rams and the lower ram presses the inner and the outer bearing racer respectively. After finishing the entire process the ram is moved to its initial position and the hub is ejected from fixture by pneumatic power.

4. RESULTS AND DISCUSSIONS

The equipment ordered with proposed requirement and trails study were made for validation of actual effectiveness. The following topic discussed such effectiveness in detail.

4.1 Benefits

**Tangible Benefits:** these benefits can be quantified. The proposed method viz. Reduced manpower, space requirement, Production cost, Material movement, buffer and power consumption. It increases the production, productivity and profits. The Figure 7 illustrates the reduction of processing time span, equipment cost and cost of processing per piece by the proposed machine.

**Intangible Benefits:**

The intangible benefits are qualitative and measured them from the employee opinion in about the proposed method. The employ gained knowledge in quality, cost saving, time saving and safety in an industry. The team spirit, motivation and morale improved the creativity and motivation towards innovation increased. The workers get motivated in problem solving and participation in Small group activities.

4.2 Cost Analysis]

Initially the proposal based on the combined operations was accepted by the management and ordered new equipment based on the proposal submitted. The exact cost analysis was carried out after took the trail with new equipment. The detailed cost analysis presented in the table 1 for conventional case and the Table 2 for new equipment that is proposed case.

Table 1 Cost Involved in Conventional Process

Previous Process	Specifica	Cost		Total Cost
<b>Machine Cost</b>				<b>20,50,000.00</b>
Racer Pressing Machine	100 Ton	8,000,00.00		
Bolt Pressing Machine	200 Ton	12,50,000.00		
<b>Process Cost</b>			<b>Cost/Part</b>	<b>Cost/Day</b>
Press Machine Cost	1hr	350		<b>539.50</b>
Cycle Time For Racer Pressing	27 Sec	2.63	131.50	
Set Up Time(Includes Loading/Unloading)	24 Sec	2.33	116.50	
Cycle Time For Bolt Pressing	20 Sec	1.94	97.00	
Set Up Time(Includes Loading/Unloading)	40 Sec	3.89	194.50	
<b>Over Heads</b>				
Operation Wages	2	20,000	666.67	
Per Hour Unit In Kwh	=Hp*0.746*Power Factor			
Current Consumption-Racer Pressing	30hp	21 Unit/Hr	104.00	<b>882.67</b>
Current Consumption-Bolt Pressing	20hp	14 Unit/Hr	112.00	
<b>Total Cost</b>				<b>20,51,422.17</b>

Table 2 Cost Involved in Proposed Process

Current Process	Speci tion	Cost	Total Cost	
<b>Machine Cost</b>			<b>12,50,000.00</b>	
Combined Pressing Machine	200 Ton	12,50,000.00		
<b>Process Cost</b>			<b>160.50</b>	
Press Machine Cost	1hr	350		
Cycle Time For Racer & Bolt Pressing	24 Sec	2.33		11
Set Up Time(Includes Loading/Unloading)	9 Sec	0.88		44
<b>Over Heads</b>			<b>882.67</b>	
Operation Wages	2	20,000		66.67
Per Hour Unit In Kwh	=Hp*0.746*Power Factor			
Current Consumption For Combined Pressing	30hp	21 Unit /Hr		168
<b>Total Cost</b>			<b>12,51,043.17</b>	

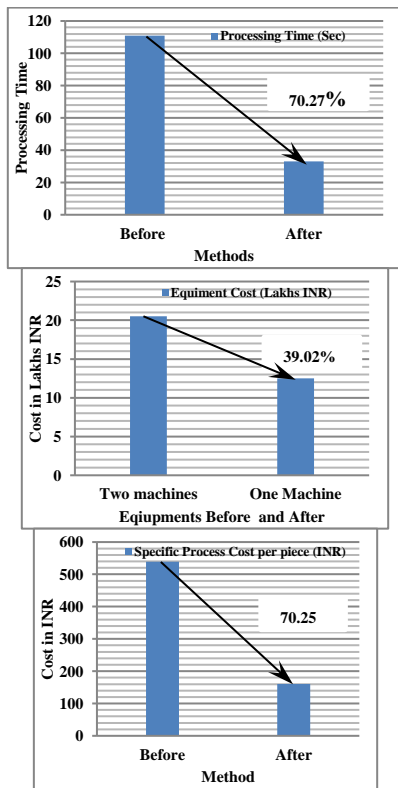


Figure 7 Time and Cost Effectiveness of Proposed Method

## CONCLUSION

The Proposal of replacing equipments is prepared by analyzing through ECRS methodology. The time and cost effectiveness were achieved significantly and discussed well. The ECRS suggested the new press of maximum compression capacity with single stage operation with help of newly designed tool head. The telescopic cylinder employed for performing the operations in the sequence. The designed compound tool yielded many Tangible and intangible benefits. After excrementally proved, formed SGA team to identify chance to implement their innovation. The basic training was given on QC tools, management Tools, SMED etc. through one point lesson methodology by considering the continuous improvement in that assembly unit.

## REFERENCES

1. C Gnanavel, R Saravanan, M Chandrasekaran and R Pugazhenti, 'Case Study of Cycle Time Reduction by Mechanization in Manufacturing Environment', International Conference on Emerging Trends in Engineering Research IOP Publishing IOP Conf. Series: Materials Science and Engineering 183 (2017) 012023 doi:10.1088/1757-899X/183/1/012023. pp. 1-7.
2. T Gopalakrishnan and R Saravanan, 'Cast Off expansion plan by rapid improvement through Optimization tool design, Tool Parameters and using Six Sigma's ECRS Technique' International Conference on Emerging Trends in Engineering Research IOP Publishing IOP Conf. Series: Materials Science and Engineering 183 (2017) 012016 doi:10.1088/1757-899X/183/1/012016. Pp 1-10.
3. R. Pugazhenti, R Saravanan, M. Chandrasekaran, R Franklin Issac and P. Vivek, Optimization of Wheel Axle Plant Manufacturing Environment by Simulation, ARPN Journal of Engineering and Applied Sciences, Vol. 12, No. 8, April 2017, pp. 2412-2418
4. Saravanan Rathinasamy and Raju R, 2010 Sequencing and scheduling of non-uniform flow pattern in parallel hybrid flow shop International Journal of Advanced Manufacturing Technology 49(1) 213-225.
5. C Gnanavel, R Saravanan, M Chandrasekaran and J J Jayakanth, 'Improvement of Productivity in TIG Welding Plant by Equipment Design in Orbit', International Conference on Emerging Trends in Engineering Research IOP Publishing IOP Conf. Series: Materials Science and Engineering 183 (2017) 012020 doi:10.1088/1757-899X/183/1/012020
6. Rajeshkumar S and Saravanan R., "An approach for balancing the assembly line using genetic algorithms' International Journal of Advanced and Innovative Research, Vol. 2(3), pp 573-579.

7. R.Saravanan and K.Mothilal, 'Coalesce of Automation and SMED to Enhance SUR – a Case Study' International Journal of Science and Research, Vol. 6, No.5, 2017, pp.1287 - 1291.
8. R.Saravanan and G.Vinoth Reddy, "Investigation On Influence of Cooling Design In Structural Stability Of Cmsx-4 Made Gas Turbine Guide Vanes" International Journal of Science and Research, Volume 6 Issue 4, 2017, pp. 2522-2526. .
9. R.Saravanan and M.Karuppasamy, 'Investigation on the influence of CMSX4 and Nimonic 901 for Fixed blades of Gas Turbine with Impingement Cooling', International Journal of Recent Innovation in Engineering and Research, Vol. 2(5), 2017, pp. 107-111

# STUDY ON SCOPE OF EMERGING TREND OF ORGAN PRINTING BY USING 3D PRINTING TECHNOLOGY

K prakash<sup>1</sup> A vetrivel<sup>2</sup> L.shri hari<sup>3</sup>, M sakthivel<sup>4</sup>

<sup>1,2,3,4</sup>Assistant professor, Mechanical Department, SNS College of Technology, , Coimbatore-641035  
prakasktg@gmail.com<sup>1</sup>

**Abstract**— Organ transplantation faces a major problem of shortage of donors, disparity between supply and demand, greater morbidity and mortality on waiting list and transplanting the organ from the donor to the recipient every 17minutes patient dies waiting for transplant and every 13 minutes someone is added to the waiting list. The expected solution for this issue is 3D printing[1]. The 3D printer prints layer by layer known as Additive manufacturing of a particular organ structure to form a cell scaffold. The printer uses 3D slash, Sketch up software for printing the organs even free hand sketching can also be printed using 3D printers, It is achieved by the process of cell seeding in which cells of interest are pipetted directly onto the scaffold structure, Materials for 3D printing usually consist of Alginate or fibrin polymers that have been integrated with cellular adhesion molecules that supports physical attachment of the cells. It uses cell culture method for producing cells as a filler material for the 3D printer; this printer uses the patient's tissue[2] for printing the organs, so it can suit in the patient's body. The possible organs that can be printed using 3D printers are Ears, nose, hands, legs, liver and even Heart. The advantage of 3D printers it will replace organ donors, it may solve the organ donation shortage, it may reduce the transportation risk. In this paper the working principle of organ bio printer, the tissue culture and vascularisation methods are illustrated.

**Keywords**— Future of Organ Transplantation, Kidney & Heart Printing, Additive Manufacturing

## I. INTRODUCTION

A printable organ is an artificially constructed device designed for organ replacement, produced using 3D printing techniques. The primary purpose of printable organs is in transplantation. Research is currently being conducted on artificial heart, kidney, and liver structures, as well as other major organs. For more complicated organs, such as the heart, smaller constructs such as heart valves have also been the subject of research. Some printed organs are approaching functionality requirements for clinical implementation, and primarily include hollow structures such as the bladder, as well as vascular structures such as urine tubes 3D printing allows for the layer-by-layer construction of a particular organ structure to form a cell scaffold. This can be followed by the

process of cell seeding, in which cells of interest are pipetted directly onto the scaffold structure. Additionally, the process of integrating cells into the printable material itself, instead of performing seeding afterwards, has been explored. Modified inkjet printers have been used to produce three- dimensional biological tissue. Printer cartridges are filled with a suspension of living cells and a smart gel, the latter used for providing structure. Alternating patterns of the smart gel and living cells are printed using a standard print nozzle, with cells eventually fusing together to form tissue. When completed, the gel is cooled and washed away, leaving behind only live cells

## II. NECESSITY

There is a global shortage of organs available for lifesaving transplants; the organ transplantation faces common problems like organ shortage, Disparity between supply and demand, Greater morbidity and mortality on waiting list. In India around 6000 people die every day waiting for organ transplant, Every 17 minutes someone dies waiting for transplant, Every 13 minutes someone is added to a waiting list. The demand is simply endless.

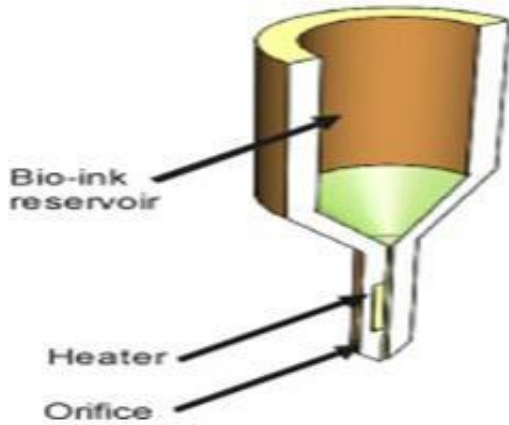
## III. 3DPRINTING TECHNIQUES

Organ printing using 3D printing can be conducted using a variety of techniques, each of which confers specific advantages that can be suited to particular types of organ production. Two of the most prominent types of organ printing are drop-based bioprinting and extrusion bioprinting. Numerous other ones do exist, though are not as commonly used, or are still in development [3].

### A. Drop-based bioprinting (Inkjet)

Drop-based bioprinting creates cellular constructs using individual droplets of a designated material, which has oftentimes been combined with a cell line. Upon contact with the substrate surface, each droplet begins to polymerize, forming a larger structure as individual droplets begin to

coalesce. Polymerization is instigated by the presence of calcium ions on the substrate, which diffuse into the liquefied



bioink and allow for the formation of a solid gel. Drop-based[4] bio printing is commonly used due to its efficient

speed, though this aspect makes it less suitable for more complicated organ structures. In fig 1 the image illustrates the cut section of a thermal inkjet bioprinter.

Fig.1 Image of Inkjet Bioprinter

#### B. Extrusion bioprinting

Extrusion bioprinting involves the constant deposition of a particular printing material and cell line from an extruder, a type of mobile print head. This tends to be a more controlled and gentler process for material or cell deposition, and allows for greater cell densities to be used in the construction of 3D tissue or organ structures. However, such benefits are set back by the slower printing speeds entailed by this technique. Extrusion bioprinting is often coupled with UV light, which photopolymerizes the printed material to form a more stable, integrated construct. In fig 2 the image illustrates the cut section of a extrusion bioprinter.

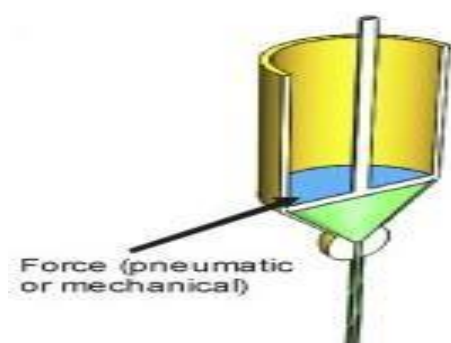


Fig.2 Image of extrusion bioprinter

#### IV. PROCESS

The organ 3D printing consists of two major steps. The first step is taking biopsy of the patient's body, and then it is followed with vascularization.

##### Biopsy

A biopsy is a procedure to remove a piece of tissue or a sample of cells from your body so that it can be analyzed in a laboratory.

##### A. Bone marrow biopsy

Bone marrow is the spongy material inside some of your larger bones where blood cells are produced. During a bone marrow biopsy, your doctor draws a sample of bone marrow out of the back of your hipbone using a long needle

##### B. Endoscopic biopsy

During endoscopy, your doctor uses a thin, flexible tube (endoscope) with a light on the end to see structures inside your body. Special tools are passed through the tube to take a small sample of tissue to be analyzed.

##### C. Needle biopsy

During a needle biopsy, your doctor uses a special needle to extract cells from a suspicious area.

Needle biopsy procedures include:

**Fine-needle aspiration.** During fine-needle aspiration, a long, thin needle is inserted into the suspicious area. A syringe is used to draw out fluid and cells for analysis[6].

**Core needle biopsy.** A larger needle with a cutting tip is used during core needle biopsy to draw a column of tissue out of a suspicious area.

**Vacuum-assisted biopsy.** During vacuum-assisted biopsy, a suction device increases the amount of fluid and cells that is extracted through the needle. This can reduce the number of times the needle must be inserted to collect an adequate sample

**Image-guided biopsy.** Image-guided biopsy combines an imaging procedure such as X-ray, computerized tomography (CT), magnetic resonance imaging (MRI) or ultrasound with a needle biopsy.

##### D. Skin biopsy

A skin (cutaneous) biopsy removes cells from the surface of your body.

**Shave biopsy.** During a shave biopsy, the doctor uses a tool similar to a razor to scrape the surface of your skin.

**Punch biopsy.** During a punch biopsy, the doctor uses a circular tool to remove a small section of your skin's deeper layers.

**Incisional biopsy.** During an incisional biopsy, the doctor uses a scalpel to remove a small area of skin. Whether you receive stitches to close the biopsy site depends on the amount of skin removed.

**Excisional biopsy.** During an excisional biopsy, the doctor removes an entire lump or an entire area of abnormal skin.

You'll likely receive stitches to close the biopsy site. In Fig 3: the image illustrates the process of bone marrow biopsy.

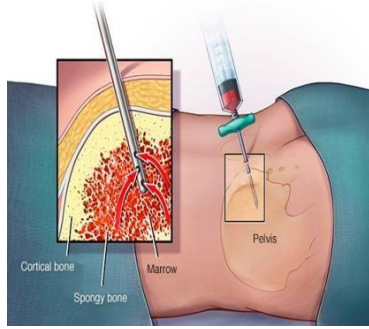


Fig.3 the process of bone marrow biopsy

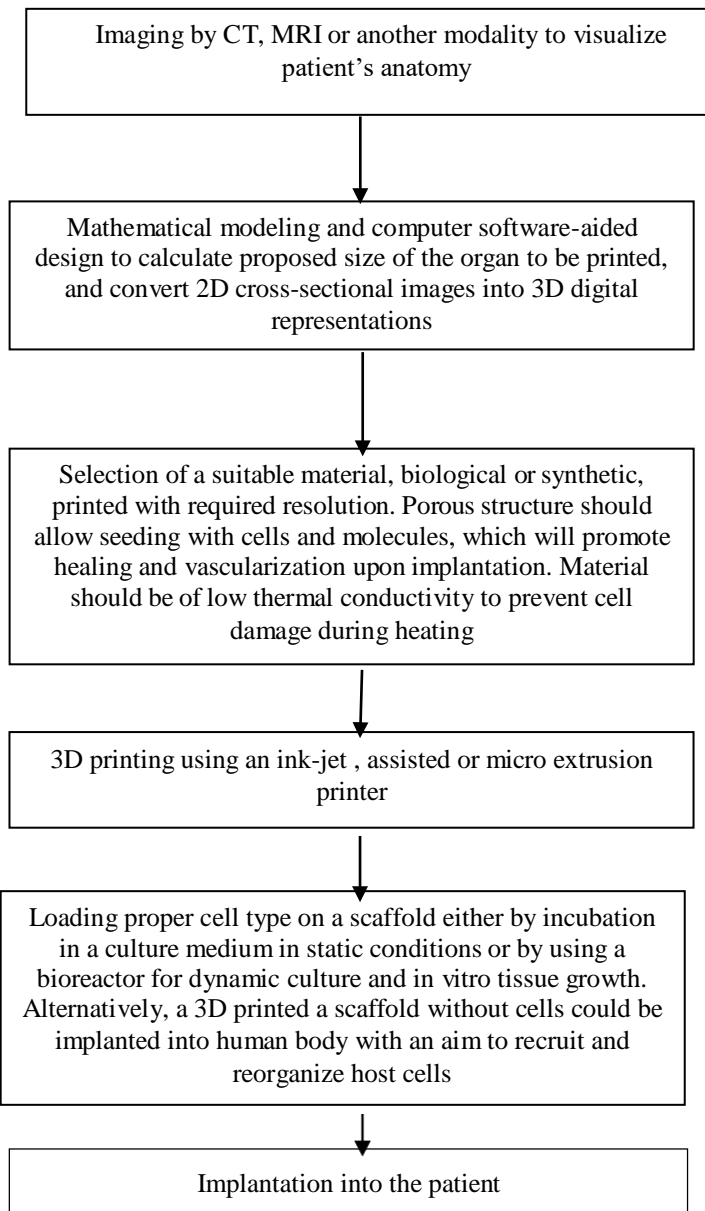


Fig. 4 various steps followed in 3D printing

In Fig.4, the flow chart illustrates various steps involved in 3D printing process.

### Vascularization

The transfer of nutrients and oxygen to cells throughout a printed organ is essential for its function. In very small or thin tissues of less than a millimeter in thickness, cells can receive nutrients through diffusion. However, larger organs require the transportation of nutrients to cells deeper inside the tissue, which requires that the tissue be vascularized, and thus able to receive blood for the exchange of cargo like oxygen and cell wastes. Early organ printing techniques created solid tissues that were unable to vascularize, or vascularized only slowly as host blood vessels entered the transplant, leading to issues like necrosis inside the tissue that can threaten the health and successful recovery of a transplant recipient. More recently developed techniques allow printed organs to be created with a more complex 3D structure, including preexisting internal vasculature, that permits faster integration of the transplant into the host circulatory system. There are multiple techniques for creating vascular systems currently under development. One method is the separate extrusion printing of vessels that are then incorporated into a larger tissue. Another method is sacrificial printing, in which the entire tissue is printed at once, and a dissolvable or otherwise removable bioink is used to form the interior of the vessels[4]. Once this sacrificial scaffolding is removed, usually by a chemical or thermal method, the rest of tissue then contains a vascular pattern. Fig.4 illustrates the various steps involved in 3D organ printing process. A bioreactor for dynamic culture and in vitro tissue growth. Alternatively, a 3D printed a scaffold without cells could be implanted into human body with an aim to recruit and reorganize host cell.

### V.PRINTING MATERIALS

Materials for 3D printing usually consist of alginate or fibrin polymers that have been integrated with cellular adhesion molecules, which support the physical attachment of cells. Such polymers are specifically designed to maintain structural stability and be receptive to cellular integration. The term "bioink" has been used as a broad classification of materials that are compatible with 3D bioprinting. Printing materials must fit a broad spectrum of criteria, one of the foremost being biocompatibility. The resulting scaffolds formed by 3D printed materials should be physically and chemically appropriate for cell proliferation. Biodegradability is another important factor, and insures that the artificially formed structure can be broken down upon successful transplantation, to be replaced by a completely natural cellular structure. Due to the nature of 3D printing, materials used must be customizable and adaptable, being suited to wide array of cell types and structural conformations. Hydrogel alginates have emerged as one of the most commonly used materials in organ printing research, as they are highly customizable, and can be fine-tuned to simulate certain mechanical and biological properties characteristic of natural

tissue. The ability of hydrogels to be tailored to specific needs allows them to be used as an adaptable scaffold material, which is suited for a variety of tissue or organ structures and physiological conditions. A major challenge in the use of alginate is its stability and slow degradation, which makes it difficult for the artificial gel scaffolding to be broken down and replaced with the implanted cells' own matrix. Alginate hydrogel that is suitable for extrusion printing is also often less structurally and mechanically sound; however, this issue can be mediated by the incorporation of other biopolymers, such as Nano cellulose, to provide greater stability. The properties of the alginate or mixed-polymer bioink are tunable and can be altered for different applications and types of organs[5]. In fig 5 the image of stem cell or cells taken from a biopsy of a patient are put into a growth medium to multiply and are used to form the bioink

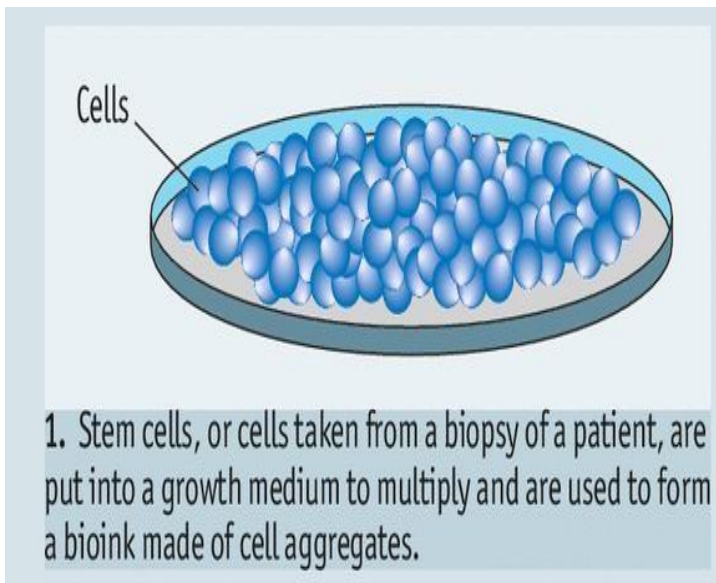


Fig.5 Stem Cells

#### CONCLUSION

From the dawn of human history, medicine has been a key field of research. It is important because it affects everyone. From the common cold to kidney failure, everyone faces illness at some point in their life. With the development of medical technology, people have been living longer. This trend can continue with the use of 3D printers to create organs, which are very heavily demanded and very much under-supplied. The use of 3D printed organs will be beneficial not just for transplant reasons, but also for research and experimentation purposes. This move will also decrease the demand for black market organs, which will thus improve world security and human safety, however marginal the change may be. In the short term, organ-printing can be used for bio fabrication in vitro model for drug toxicity, drug discovery and modeling human diseases. In the long term, organ-printing technology can solve the problem of human organ shortage for transplantation once and forever.

#### REFERENCES

- [1] Cooper-White, Macrina. "How 3D Printing Could End The Deadly Shortage Of Donor Organs" Huffington Post. Retrieved 27 March 2015.
- [2] Auger, François A.; Gibot, Laure; Lacroix, Dan. "The Pivotal Role of Vascularization in Tissue Engineering". Annual Review of Biomedical Engineering 2013.
- [3] Bajaj, Piyush; Schweller, Ryan M.; Khademhosseini, Ali; West, Jennifer L.; Bashir, Rashid. "3DBiofabrication Strategies for Tissue Engineering and Regenerative Medicine" Annual Review of Biomedical Engineering. 2014.
- [4] Boland, Thomas. "Patent US7051654: Ink-jet printing of viable cells" Retrieved 31 March 2015.
- [5] Kesti, Matti; Müller, Michael; Becher, Jana; Schnabelrauch, Matthias; d'Este, Matteo; Eglin, David; Zenobi-Wong, Marcy "A versatile bioink for three-dimensional printing of cellular scaffolds based on thermally and photo-triggered tandem gelation" Acta Biomaterialia. 2015.
- [6] Anderson JB, Webb AJ "Fine-needle aspiration biopsy and the diagnosis of thyroid cancer". The British Journal of Surgery 1987.